PPAR Research

The Role of Peroxisome Proliferator-Activated Receptors (PPARs) in Disease and Targeted Treatments

Lead Guest Editor: Sainan Li
Guest Editors: Jingjing Li, Jianhua Wang, Xiaoming Fan, and Xiaojie Lu

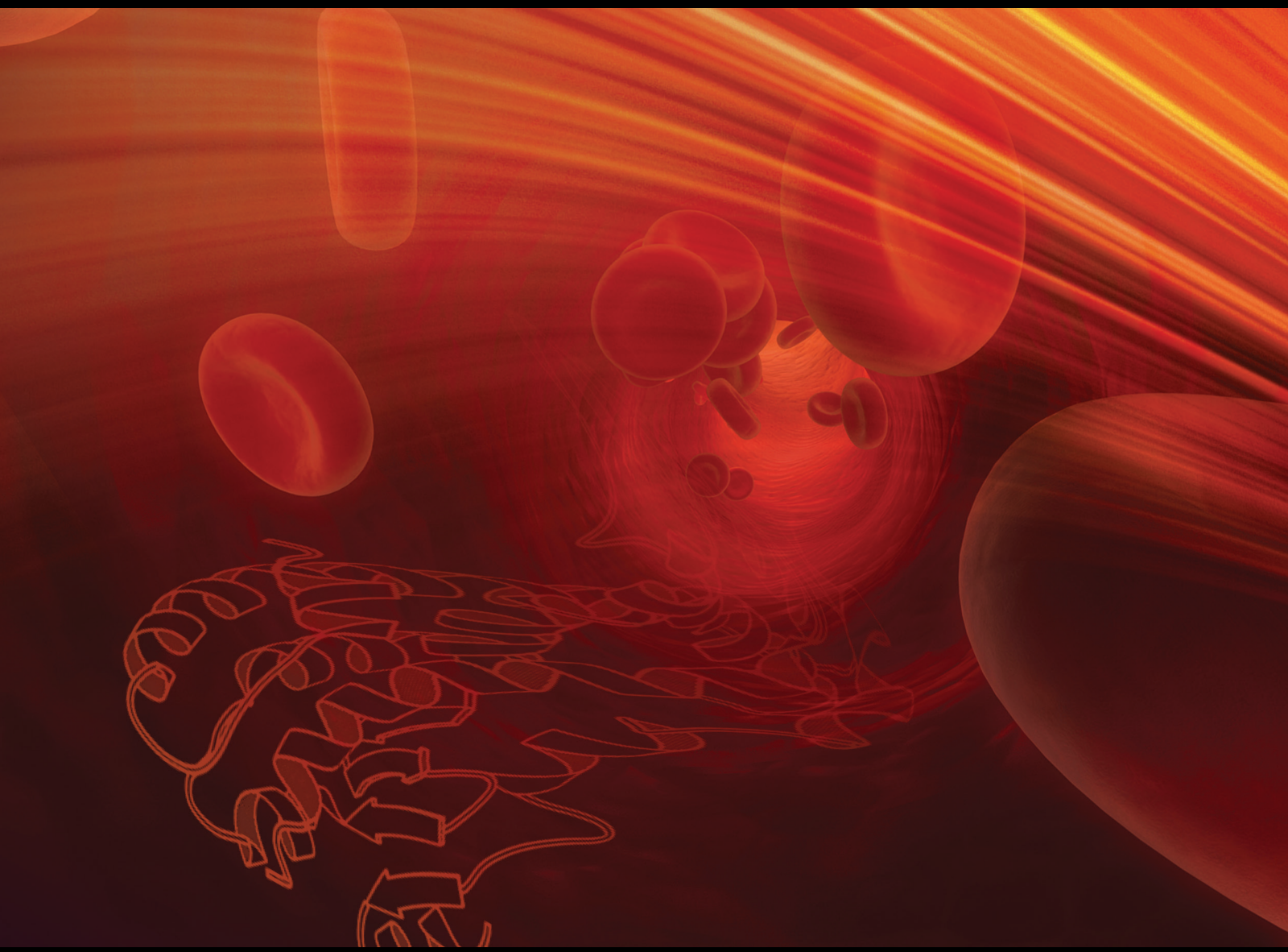

The Role of Peroxisome Proliferator-Activated Receptors (PPARs) in Disease and Targeted Treatments

PPAR Research

The Role of Peroxisome Proliferator-Activated Receptors (PPARs) in Disease and Targeted Treatments

Lead Guest Editor: Sainan Li
Guest Editors: Jingjing Li, Jianhua Wang, Xiaoming Fan, and Xiaojie Lu

Contents

Hindawi
PPAR Research
Volume 2021, Article ID 6626295, 15 pages
https://doi.org/10.1155/2021/6626295

Research Article

PPARγ Plays an Important Role in Acute Hepatic Ischemia-Reperfusion Injury via AMPK/mTOR Pathway

Liwei Wu,[1] **Qiang Yu**,[1] **Ping Cheng**,[2] **and Chuanyong Guo**[1]

[1]*Department of Gastroenterology, Shanghai Tenth People's Hospital, Tongji University School of Medicine, Shanghai 200072, China*
[2]*Department of Gerontology, Shanghai Minhang District Central Hospital, Shanghai 201100, China*

Correspondence should be addressed to Ping Cheng; cppipi123@163.com and Chuanyong Guo; guochuanyong@hotmail.com

Received 14 October 2020; Accepted 10 June 2021; Published 5 July 2021

Academic Editor: Christopher Lau

Background. Hepatic ischemia-reperfusion (IR) injury is one of the severe complications associated with liver surgery and leads to liver dysfunction. PPARγ is always linked with various physiologic pathways, and it can alleviate liver damage in IR injury. *Aim*. In this study, we explored the potential mechanism of PPARγ in the pathogenesis of hepatic IR injury by mice model. *Methods*. After treated with si-PPARγ or rosiglitazone, mice were subjected to hepatic ischemia-reperfusion. Liver tissue and blood samples were collected to evaluate liver injury and detected relative mRNA and protein expressions. *Results*. The expression of PPARγ was increased after reperfusion. And the alleviation of PPARγ aggravated the liver damage in IR; at the same time, upregulation of the expression of PPARγ released the liver damage. And these effects of PPARγ in IR were related to the AMPK/mTOR/autophagy signaling pathway. *Conclusion*. PPARγ plays an important role in hepatic IR injury at least partly via the AMPK/mTOR/autophagy pathway.

1. Introduction

Ischemia-reperfusion (IR) is a phenomenon occurring after the restoration of arterial blood flow to a specific organ or tissue [1]. The pathophysiology of IR injury is mainly the induction of oxidative stress and inflammatory cascade reaction. Thus, the reperfusion of blood flow may result in oxidative damage and inflammation rather than recovery. Hepatic IR injury is one of the severe complications associated with liver surgery and leads to liver failure or primary nonfunction, thus, increasing morbidity and mortality after liver surgery [2–4]. Since hepatectomy or liver transplantation is the most effective method for the treatment of end-stage liver diseases, it is essential to detect the possible preoperative and perioperative interventions for minimizing IR-induced hepatocellular damage, especially in patients with cirrhosis.

As a member of the family of nuclear receptors, peroxisome proliferator-activated receptor-γ (PPARγ) acts as heterodimers with DNA response elements and can regulate various metabolism responses [5, 6]. PPARγ has an important role in regulating the inflammatory response and oxidative stress in hepatic IR injury [7–9]. The protecting effects of PPARγ agonists, such as telmisartan [10], irbesartan [11], darglitazone [12], rosiglitazone [13], and pioglitazone [14], in IR injury have been reported [15]. And these evidences suggested that PPARγ agonists can modulate inflammatory responses, oxidative stress, and metabolism in IR. The adenosine monophosphate-activated protein kinase/mammalian target of rapamycin (AMPK/mTOR) signaling pathway has been confirmed that it is a critical regulator of cellular processes, including cell growth, viability, differentiation, survival, and metabolism [16–18]; mTOR has been also identified as a key modulator of autophagy [19]; and its dysregulation has been implicated in a variety of pathological disorders, including playing critical roles in regulating liver IR injury. And PPARγ can modulate the mTOR pathway. In this study, we downregulated and upregulated the expression of PPARγ and explored the function of PPARγ in hepatic IR injury, and we treated mice with mTOR inhibitor, rapamycin (Rapa), to make sure PPARγ showed its effects in hepatic IR injury via AMPK/mTOR pathway.

2. Methods

2.1. Animal Preparation. This project was approved by the Animal Care and Use Committee of Shanghai Tongji University and Shanghai Tenth People's Hospital (SHDSYY-2021-4990), China. And all animal experiments complied with the guidelines of the China National Institutes of Health. Six-week-old male Balb/c mice (Shanghai SLAC Laboratory Animal, Shanghai, China) were used in our experiments. All mice weighed 23-28 g and housed in a standard environment. All efforts have been done to minimize the suffering of mice in this research.

The animals underwent either sham surgery or ischemia-reperfusion (IR) operation. Partial warm hepatic ischemia was induced as described previously [20]. After anesthetized with 1.25% sodium pentobarbital (Nembutal, St. Louis, MO, USA), the blood supply to the left lateral and median lobes of the liver was interrupted, causing 70% ischemia. After 45 minutes of hepatic ischemia, we restored blood supply and initiated reperfusion. We performed the same operation protocol in sham control mice without vascular occlusion. Mice were sacrificed after 2, 6, 12, and 24 hours of ischemia-reperfusion, and blood and liver were collected for further analysis.

Rapamycin (S1039, Selleck) was dissolved in dimethyl sulfoxide (DMSO) at 25 mg/ml before administration. In the rapamycin-treated groups, animals have received rapamycin at a dose of 1.5 mg/kg per day before injury through intraperitoneal injection.

2.2. In Vivo Transfection with PPARγ Short Interfering RNA (siRNA). Firstly, siRNA PPARγ (guide: 5′UCAGCUCCG UGGAUCUCUCCGUAAU′, passenger: 5′AUUACGGAG AGAUCCACGGAGCUGA′) or siRNA control (GenePharma, Suzhou, China) was bought from Genema. Then, according to the producer instruction, siRNA PPARγ or siRNA control was dissolved in RNase-free water to the concentration of 1 μg/μL. Then, 5 μL PPARγ siRNA or 5 μL control siRNA and 5 μL in vivo transfection reagent (18668-11, Engreen, Co., Beijing, China) were, respectively, diluted with 5 μL 10% glucose. Finally, the mixtures were injected into the tail vein of mice.

2.3. Animal Experiment Design. According to our experiment plan, mice were distributed into the following groups:

(1) Natural group ($n = 3$): mice without any treatment

(2) Sham group ($n = 5$): mice underwent sham surgery

(3) Vehicle group ($n = 5$): mice were treated with methylcellulose orally once a day for 5 days without operation

(4) Drug group ($n = 5$): mice were treated with 10 mg/kg rosiglitazone orally once a day for 5 days without operation

(5) Si-control group ($n = 5$): mice were injected from the tail vein with control siRNA once a day for 2 weeks without operation

(6) Si-PPARγ group ($n = 5$): mice were injected from the tail vein with PPARγ siRNA once a day for 2 weeks without operation

(7) IR groups ($n = 20$): mice underwent IR operation and sacrificed at 2, 6, 12, and 24 hours after reperfusion

(8) IR + Rosi groups ($n = 20$): after treated with 10 mg/kg rosiglitazone orally once a day for 5 days, mice underwent IR operation and sacrificed at 2, 6, 12, and 24 hours after reperfusion

(9) IR + si-PPARγ groups ($n = 20$): after injected with PPARγ siRNA once a day for 2 weeks, mice underwent IR operation and sacrificed at 2, 6, 12, and 24 hours after reperfusion

(10) IR + si-PPARγ+Rosi groups ($n = 20$): after treated with both PPARγ siRNA and 10 mg/kg rosiglitazone, mice underwent IR operation and sacrificed at 2, 6, 12, and 24 hours after reperfusion

(11) IR + Rapa ($n = 5$): after intraperitoneally injected with the mTOR inhibitor rapamycin for 5 days, mice underwent IR operation and sacrificed at 12 hours after reperfusion

(12) IR + si-PPARγ+Rapa ($n = 5$): after treated with both PPARγ siRNA and rapamycin, mice underwent IR operation and sacrificed at 12 hours after reperfusion

2.4. Serum Enzyme Analysis. Serum was separated by centrifugation at 1,500 g for 10 min and stored at -80°C. Serum levels of aspartate aminotransferase (AST) and alanine aminotransferase (ALT) were measured by kits bought from Jiancheng Co. (Nanjing, China).

2.5. Histology, Immunohistochemical(IHC) Staining, and Terminal Deoxynucleotidyl Transferase dUTP Nick End Labeling (TUNEL) Assay. Liver tissue samples were fixed and embedded in the following standard steps. Liver sections were cut and stained with hematoxylin and eosin. For IHC, the slices were dewaxed and rehydrated; and after an antigen retrieval process and blocking, slices were incubated with primary antibodies described in western blot analysis part overnight. For the TUNEL, the slices were treated according to the instruction and then incubated in the TUNEL reaction mixture (Roche, Mannheim, Germany) at room temperature for 1 h.

2.6. Western Blot Analysis. Western blotting was performed as standard protocol. Protein was extracted from frozen liver samples. A total of 80 ng protein was loaded onto 6%, 10%, and 12.5% SDS-polyacrylamide gels, and the separated proteins were transferred to PVDF membranes. The membranes were incubated overnight at 4°C with primary antibodies followed by incubation with a secondary antibody (1 : 2,000). Finally, the blots were scanned using an Odyssey two-colour infrared laser imaging system (Li-Cor, Lincoln, NE, USA). Western blots were performed using the following

Table 1: Sequences of primer pairs used for amplification of mRNA by real-time PCR.

	Forward	Reverse
β-Actin	GGCTGTATTCCCCTCCATCG	CCAGTTGGTAACAATGCCATGT
Bax	AGACAGGGGCCTTTTTGCTAC	AATTCGCCGGAGACACTCG
TNF-α	CAGGCGGTGCCTATGTCTC	CGATCACCCCGAAGTTCAGTAG
PPARγ	GTCTTGGATGTCCTCGATGGG	TTATGGAGCCTAAGTTTGAGTTTGC

antibodies; PPARγ (Cell Signaling Technology), mTOR (Cell Signaling Technology), p-mTOR (Cell Signaling Technology, Ser2448), AMPKα (Cell Signaling Technology), p-AMPKα (Cell Signaling Technology, Thr172), TNF-α (Cell Signaling Technology), IL-1β (Cell Signaling Technology), Bax (Proteintech), cleaved caspase-9 (Proteintech), Beclin1 (Proteintech), LC3 (Proteintech), and β-actin (Abcam).

2.7. RNA Extraction and Quantitative Real-Time- (qRT-) PCR Analysis. The total RNA was isolated from tissues according to the standard protocol. The first strand of cDNA was synthesized using a reverse transcription kit (TaKaRa Biotechnology) and was used to analyse the indicator expression. Real-time PCR experiments were performed according to the protocol of the real-time PCR kit (Takara, Otsu, Shiga, Japan). The ratio of each gene compared to β-actin was calculated by standardizing the ratio of each control to the unit value. The primer sequences for qRT-PCR were shown in Table 1.

2.8. Statistics. All experiments were conducted three times and were analyzed using Graph Pad Prism 5.0 software. Data are expressed as means ± SD. The differences between before and after IR of mice, with or without si-PPAR injection, and with or without TZDs administration were evaluated using two-way ANOVA with the Student's t-test to compare between the two groups. p value of less than 0.05 was considered statistically significant.

3. Results

3.1. The Expression of PPARγ in IR Injury. To confirm the activation of PPARγ during the hepatic ischemia-reperfusion injury, we detected the expression of PPARγ by western blot and qRT-PCR. In Figures 1(a) and 1(b), both the protein and mRNA expression of PPARγ were increased after reperfusion, especially after 6 hours. Following, we did a histopathological analysis for IR injury (Figure 1(c)). Obvious necrosis could be seen after 6 hours, and the rate of necrosis was over 50% after 12 hours after reperfusion. Figure 1(d) exhibited the immunohistochemical staining of PPARγ in collected liver tissues, and the number of positive cells changed almost in parallel with the above results. We hypothesized that this change was due to the protective mechanism of PPARγ on damaged hepatocytes. And we compared natural group, sham group, vehicle group, drug group, and siRNA-control groups to exclude their influence on the following results (Supplementary Figure 1).

3.2. Alleviation the Expression of PPARγ Aggravated the Liver Damage in IR. Si-PPARγ was injected into mice via the tail vein to downregulate its expression, and the pathological alteration after reperfusion was compared with that in normal mice. Serum levels of ALT and AST were measured after reperfusion (Figure 2(a)), and we found that the downregulation of PPARγ aggravated the damage of hepatocytes. And then we evaluated the damage in terms of inflammation and apoptosis.

We detected the level of inflammation through proinflammatory cytokine TNF-α and IL-1β. The circulating levels of them were indeed upregulated by PPARγ downregulation (Figure 2(b)). Consistent with the former, the expression of TNF-α and IL-1β was higher in the si-PPARγ group (Figures 2(c) and 2(e)). Apoptosis is a prominent feature of IR injury, and its participation was confirmed. Bax is a famous proapoptotic family member, and we detected its mRNA expression firstly. The graph in Figure 2(d) showed that with the increase of Bax expression during IR injury, PPARγ downregulation made this increase more obvious. Then, we used western blot to measure the protein expression of Bax and caspase9, whose results (Figure 2(e)) exhibited that the injection of si-PPARγ increased the occurrence of apoptosis during IR injury. Thus, the alleviation of PPARγ aggravated the liver damage in IR.

3.3. Upregulation of the Expression of PPARγ Released the Liver Damage in IR. Rosiglitazone is a typical PPARγ agonist and is widely used in clinics. A group of mice were treated with 10 mg/kg rosiglitazone orally for 5 days before IR, and we also compared their pathological alteration after reperfusion with that in normal mice. Figure 3(a) showed the serum levels of ALT and AST, and we found that the upregulation of PPARγ reduced the damage of hepatocytes. And then we evaluated the damage in the same way we used it before.

We detected the level of TNF-α and IL-1β. The circulating levels of them were downregulated by rosiglitazone (Figure 3(b)). Consistent with the former, the expression of TNF-α and IL-1β was lower in the rosiglitazone treatment group (Figures 3(c) and 3(e)). The graph in Figures 3(d) and 3(e) showed that the increased expression of Bax and caspase9 during IR injury was relieved by the treatment of rosiglitazone, that is, the occurrence of apoptosis during IR injury was reduced. Thus, the upregulation of PPARγ mitigated liver damage in IR.

3.4. The Influence of PPARγ in IR May Be Linked with AMPK/mTOR/Autophagy Signaling Pathway. To make sure the effect of PPARγ in IR injury, those mice, which were injected with si-PPARγ, were treated with Rosi. And we detected the index of apoptosis and inflammation in these mice after reperfusion for 12 hours, which were exhibited

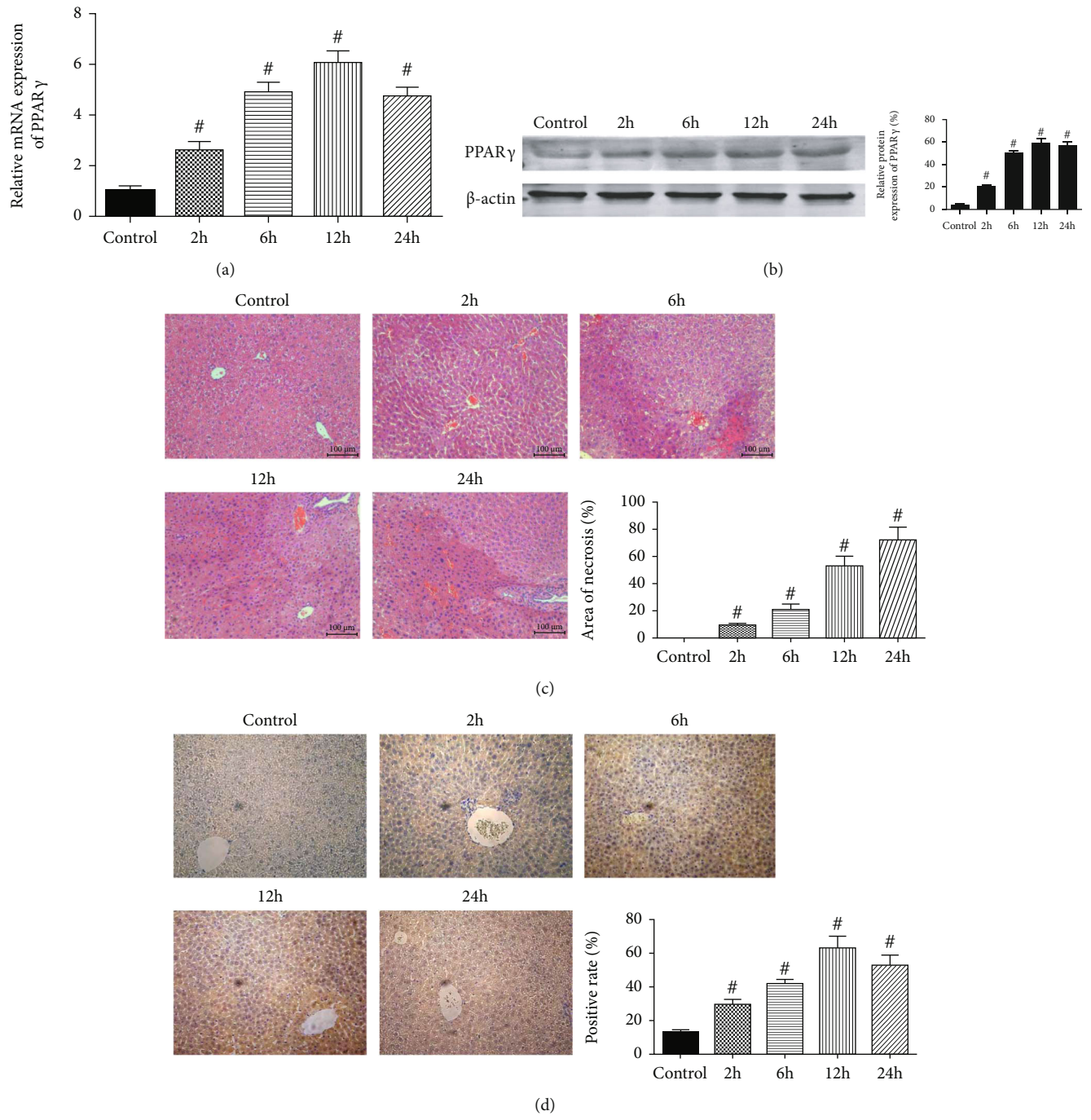

Figure 1: The expression of PPARγ in IR injury. Notes: (a) relative mRNA expression of PPARγ ($n = 5$, # means $p < 0.05$ for IR versus control after 2, 6, 12, and 24 h); (b) protein expression of PPARγ ($n = 3$, # means $p < 0.05$ for IR versus control after 2, 6, 12, and 24 h); (c) representative H&E stained sections of the liver (original magnification, ×200). The ratio of necrosis area to total area was analyzed with Image-Pro Plus 6.0 ($n = 5$, # means $p < 0.05$ for IR versus control after 2, 6, 12, and 24 h); (d) Immunohistochemistry staining (×200) showing the expression of PPARγ. The ratio of brown area to total area was analyzed with Image-Pro Plus 6.0 ($n = 5$, # means $p < 0.05$ for IR versus control after 2, 6, 12, and 24 h).

in Figures 4(a)–4(d). These results showed that liver damage during IR injury, including hepatocyte apoptosis and inflammation responses, was definitely related to the expression of PPARγ. Besides, we also detected the changes of pyroptosis in our study, which were exhibited in Supplementary Figure 2.

As an important kinase in energy hemostasis, AMPK is an upstream target and negative regulator of mTOR, which is a major negative regulator of autophagy. Autophagy plays a vital role in various liver damage. Combined with previous reports, we speculated that the effects of PPARγ during IR injury may be related to the AMPK/mTOR/autophagy

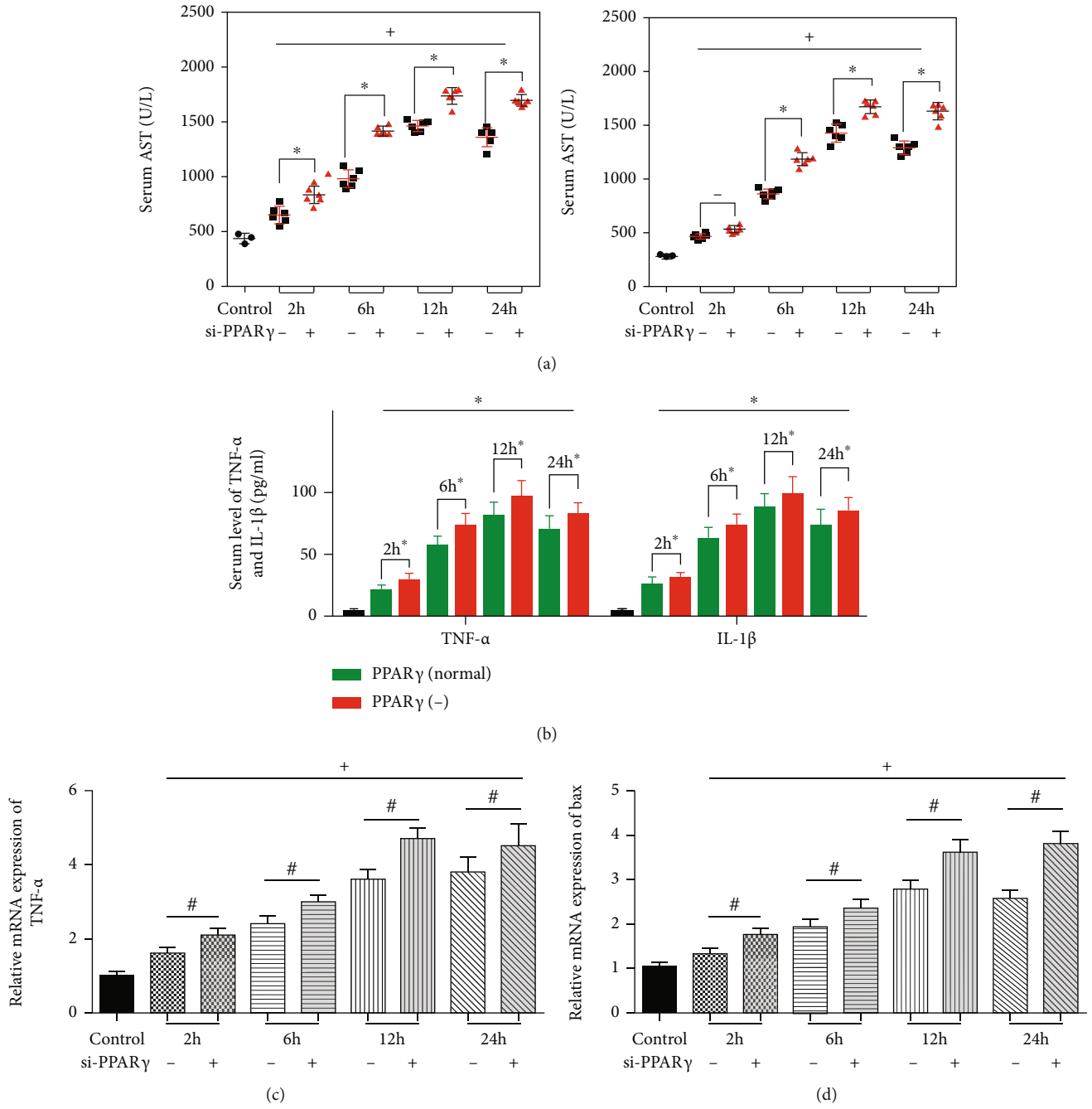

Figure 2: Continued.

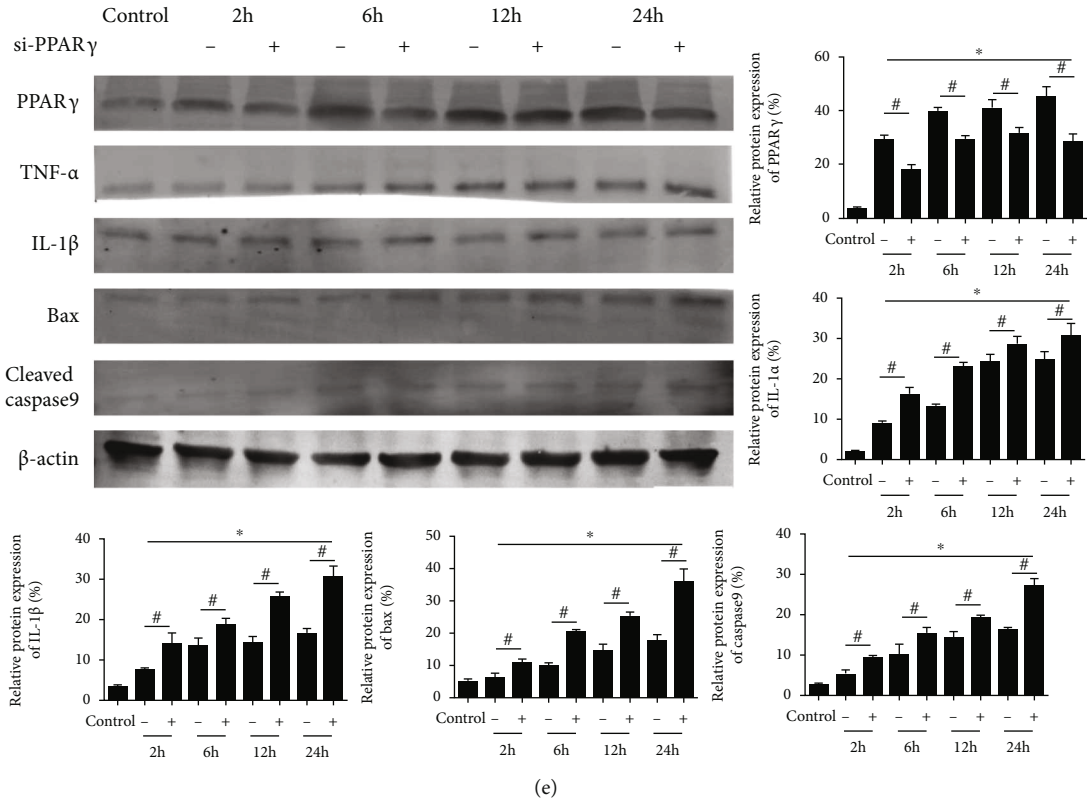

Figure 2: Effect of PPARγ alleviation on liver function and pathology of mice in IR. Notes: (a) the levels of serum ALT and AST ($n = 5$, $*$ means $p < 0.05$ for si-PPARγ versus IR after 2, 6, 12, and 24 h, + means $p < 0.05$ for IR verse control); (b) the levels of serum TNF-α and IL-1β ($n = 5$, $*$ means $p < 0.05$ for si-PPARγ versus IR after 2, 6, 12, and 24 h, + means $p < 0.05$ for IR verse control); (c) relative mRNA expression of TNF-α ($n = 5$, # means $p < 0.05$ for si-PPARγ versus IR after 2, 6, 12, and 24 h, + means $p < 0.05$ for IR verse control); (d) relative mRNA expression of Bax ($n = 5$, # means $p < 0.05$ for si-PPARγ versus IR after 2, 6, 12, and 24 h, + means $p < 0.05$ for IR verse control); (e) protein expression of PPARγ, TNF-α, IL-1β, Bax, and cleaved caspase9 ($n = 3$, # means $p < 0.05$ for si-PPARγ versus IR after 2, 6, 12, and 24 h, $*$ means $p < 0.05$ for IR verse control).

signaling pathway. Thus, we measured the protein expression of p-AMPK, p-mTOR, and autophagy-related proteins, LC3, P62, and Beclin1, whose expressions were changed along with PPARγ (Figures 4(e) and 4(f)). The treatment of Rosi obviously promoted AMPK phosphorylation and reduced the phosphorylated form of mTOR, which contributed to the suppression of autophagy in mouse livers. And si-PPARγ leads to opposite effects. Furthermore, we detected the above changes in mice treated with both si-PPARγ and Rosi, and the results were in agreement with those mentioned above. Thus, the effects of PPARγ in IR injury were linked with the AMPK/mTOR/autophagy signaling pathway.

To make sure our conclusion, we treated mice with rapamycin to inhibit the function of mTOR and detected changes in inflammation response and apoptosis, whose results were shown in Figure 5. We measured the expression of TNF-α, Bax, and Beclin1, and we found that effects caused by si-PPARγ were blocked by rapamycin. Accordingly, we confirmed the relationship between PPARγ and AMPK/mTOR.

4. Discussion

In the liver, IR injury can occur in several clinical situations, for example, liver trauma, resection, and transplantation. The pathogenesis of IR is closely related to oxidative stress, energy metabolism disorders, inflammatory response, and cell apoptosis and autophagy [21]. As is known to all, PPARγ demonstrated significant functions in the tissue protection and repair [22–24]. And advances in PPAR ligands and agonists renew opportunities for drug development [25]. Here, in our present study, we found that the activation of PPARγ could confer hepatoprotective effects against hepatic IR injury and also investigated the therapeutic potential of PPARγ agonists for the protection of hepatic injury. The major findings of this study include (1) the expression of PPARγ were increased after reperfusion, which hinted the protective role of PPARγ in hepatic IR injury; (2) alleviation the expression of PPARγ could aggravate the liver damage in IR; otherwise, the upregulation released liver damage; (3) the protective effects of PPARγ may involve anti-inflammatory and antiapoptosis activity as demonstrated in vivo; (4) the underlying mechanism of PPARγ in IR injury may be linked with AMPK/mTOR/autophagy signaling pathway.

PPARγ is a ligand-activated transcription factor of the nuclear hormone receptor superfamily known to modulate target genes involved in the regulation of various inflammatory responses, cell growth and apoptosis, metabolism, fibrosis, and tissue repair [26, 27]. Several studies have indicated

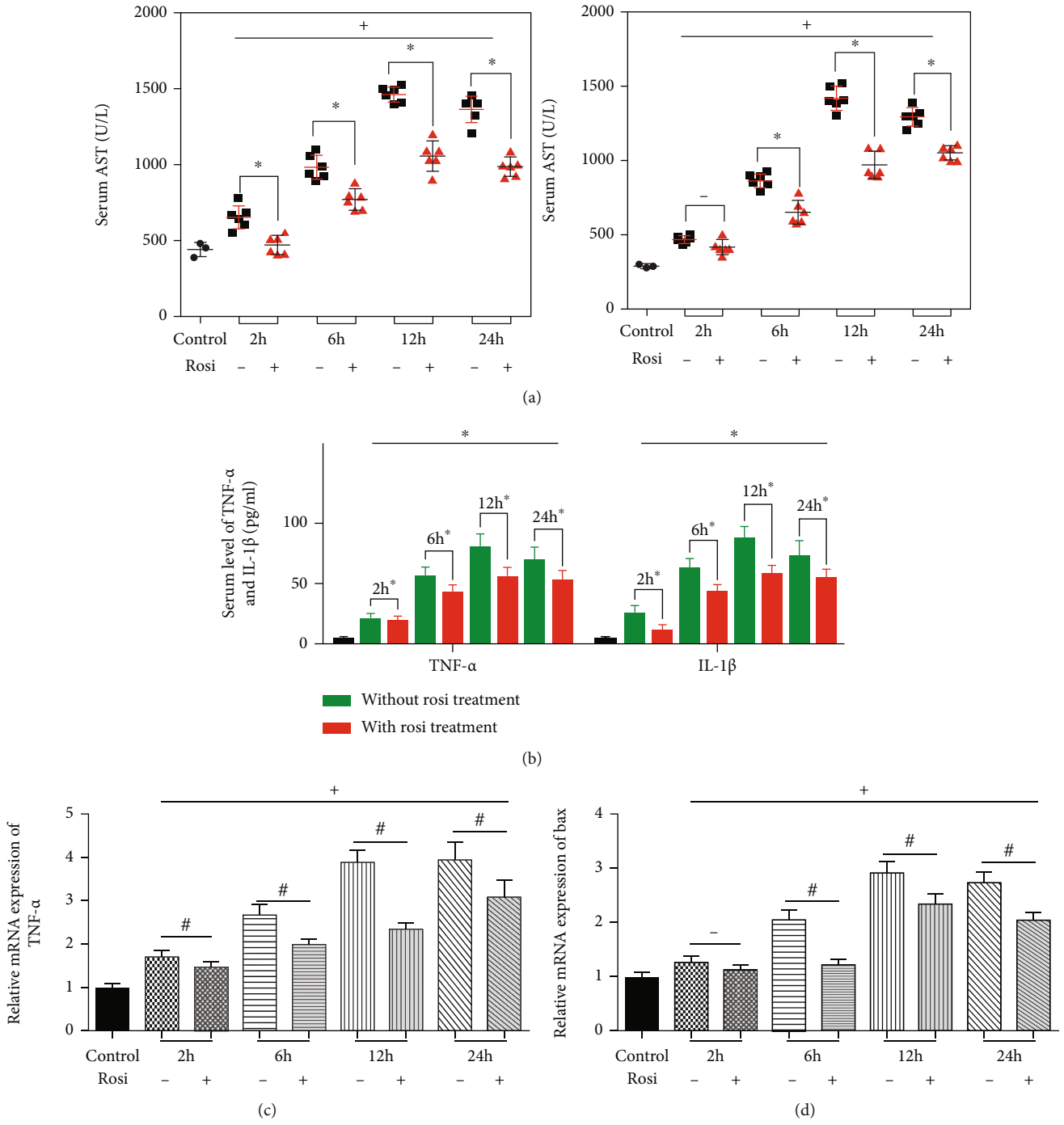

Figure 3: Continued.

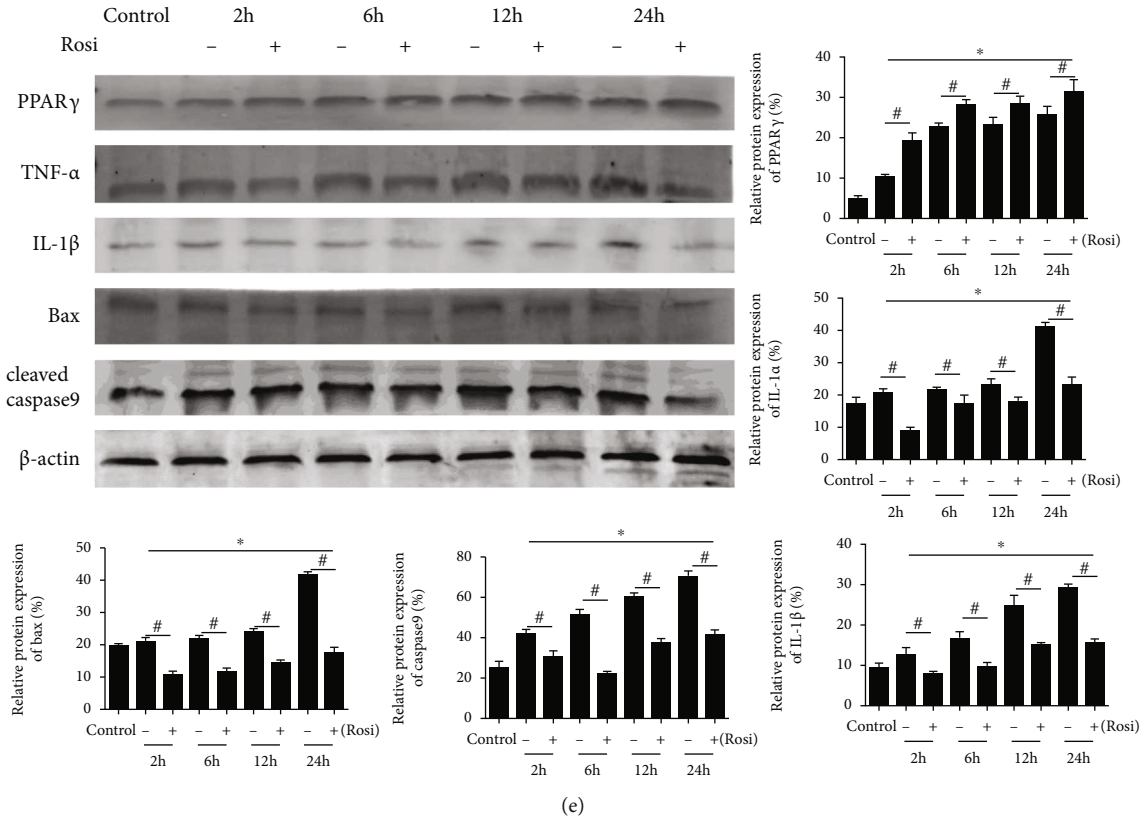

Figure 3: Effect of PPARγ upregulation on liver function and pathology of mice in IR. Notes: (a) the levels of serum ALT and AST ($n = 5$, $*$ means $p < 0.05$ for Rosi versus IR after 2, 6, 12, and 24 h, + means $p < 0.05$ for IR verse control); (b) the levels of serum TNF-α and IL-1β ($n = 5$, $*$ means $p < 0.05$ for Rosi versus IR after 2, 6, 12, and 24 h, + means $p < 0.05$ for IR verse control); (c) relative mRNA expression of TNF-α ($n = 5$, # means $p < 0.05$ for Rosi versus IR after 2, 6, 12, and 24 h, + means $p < 0.05$ for IR verse control); (d) relative mRNA expression of Bax ($n = 5$, # means $p < 0.05$ for Rosi versus IR after 2, 6, 12, and 24 h, + means $p < 0.05$ for IR verse control); (e) protein expression of PPARγ, TNF-α, IL-1β, Bax, and cleaved caspase9 ($n = 3$, # means $p < 0.05$ for si-PPARγ versus IR after 2, 6, 12, and 24 h, $*$ means $p < 0.05$ for IR verse control).

that the activation of PPARγ is a therapeutic target for acute hepatic IR injury [7, 15, 28]. Additionally, agonists of PPARγ exhibited anti-inflammation and antiapoptosis properties both in vitro and in vivo and could impart protection from IR in mice models [29, 30]. In the present experiment, our results demonstrated that the expression of PPARγ was increased during reperfusion. Combined with the previous researches, we hypothesized that this change was due to the spontaneous protective mechanism of PPARγ on damaged hepatocytes.

To clarify our hypothesis, we regulated the expression of PPARγ by injection of si-PPARγ or administration of rosiglitazone, a typical PPARγ agonist. After the above treatment, serum liver enzymes ALT and AST showed the same changes as expected. And then we detected the liver damage in terms of inflammation and apoptosis. Excessive inflammatory response and hepatocyte apoptosis are recognized as key mechanism of liver IR injury. We detected the level of inflammation through proinflammatory cytokines TNF-α and IL-1β. The circulating levels of them were obviously upregulated by si-PPARγ and downregulated by rosiglitazone. Results of qRT-PCR and western blot exhibited that when compared with the IR group, the expression of TNF-α and IL-1β was higher in the si-PPARγ group and lower in the rosiglitazone group. Apoptosis is a prominent feature of IR injury, and its participation was confirmed. Bax and caspase9 are famous proapoptotic indices, and we detected their mRNA and protein expression. With the increase of Bax and caspase9 expression during IR injury, PPARγ downregulation exacerbated this increase; however, the treatment of rosiglitazone relieved it. Thus, the alleviation of PPARγ aggravated the liver damage in IR; and at the same time, the upregulation of PPARγ mitigated the liver damage. Further, it has been reported that rosiglitazone is protective on a variety of injuries, including IR injury of many organs. Our results indicated that rosiglitazone may reduce, although do not ablate, hepatic damage after IR injury.

When further elucidating the potential mechanism of the effects of PPAR in IR, we focused on the pathway, AMPK/mTOR mediated autophagy. AMPK exists in all eukaryotic cells as a highly conserved protein kinase. It is a major regulator of energy homeostasis that balances energy supply and demand and ultimately modulates cellular and organ growth [31, 32]. AMPK can be activated by a variety of stresses including poisonous metabolites and pathological precursors such as starvation, ischemia, and hypoxia [33]. mTOR, a 289

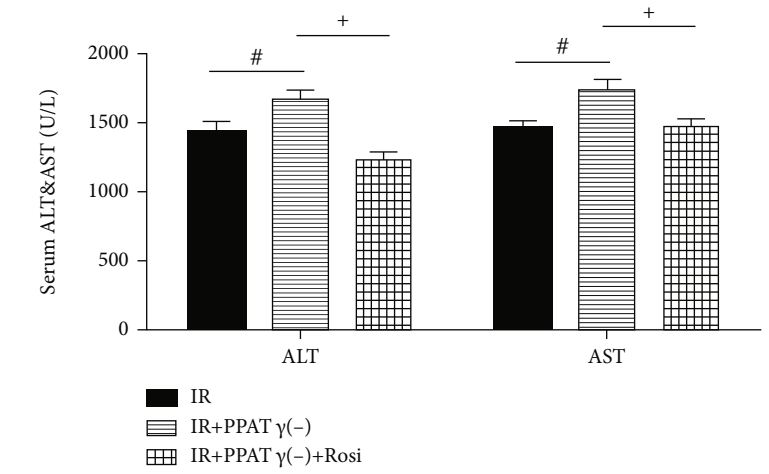

(a)

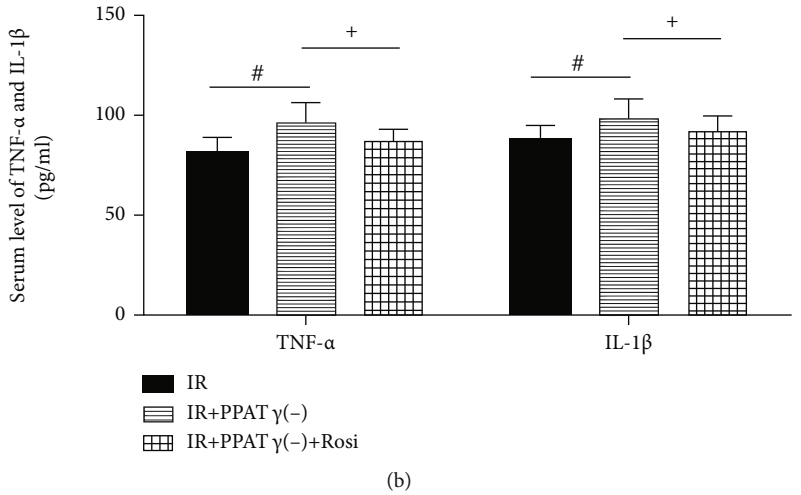

(b)

Figure 4: Continued.

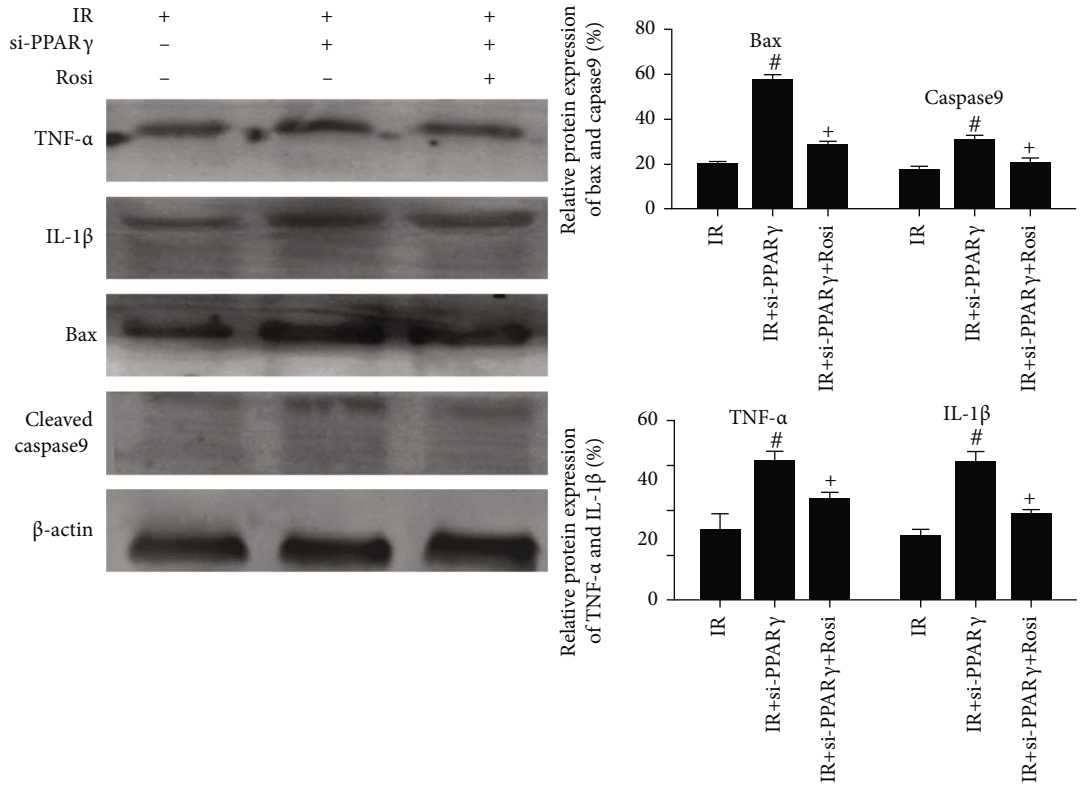

(c)

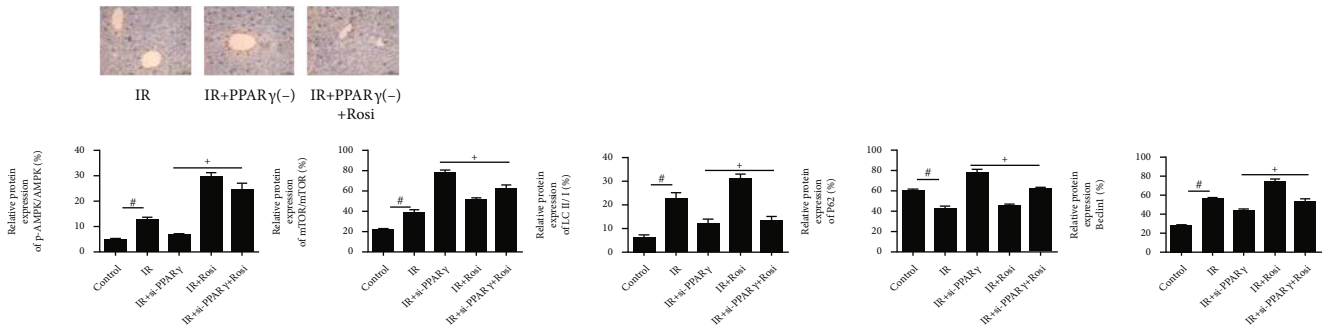

(d)

Figure 4: Continued.

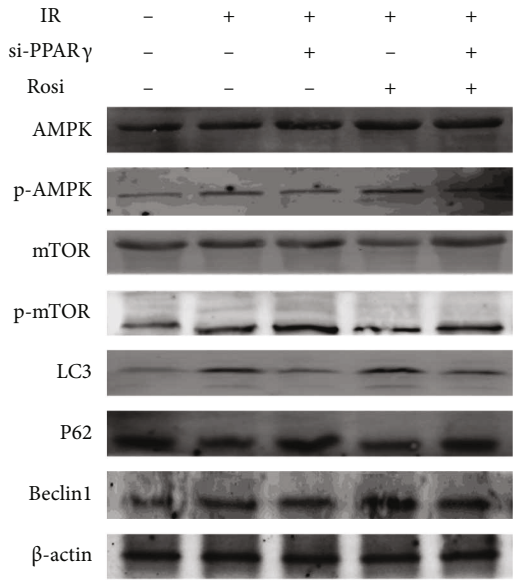

(e)

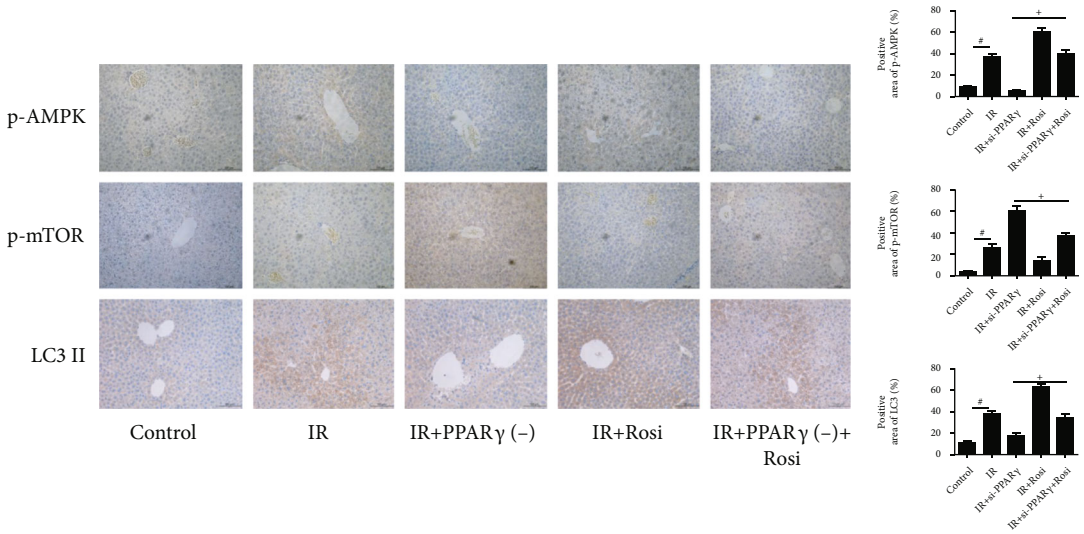

(f)

Figure 4: The influence of PPARγ in IR may be linked with the AMPK/mTOR/autophagy signaling pathway. Notes: (a) the levels of serum ALT and AST for IR after 12 h ($n = 5$, # means $p < 0.05$ for si-PPARγ versus IR, + means $p < 0.05$ for si-PPARγ+Rosi versus si-PPARγ); (b) the levels of serum TNF-α and IL-1β for IR after 12 h ($n = 5$, # means $p < 0.05$ for si-PPARγ versus IR, + means $p < 0.05$ for si-PPARγ+Rosi versus si-PPARγ); (c) protein expression of TNF-α, IL-1β, Bax, and cleaved caspase9 for IR after 12 h ($n = 3$, # means $p < 0.05$ for si-PPARγ versus IR, + means $p < 0.05$ for si-PPARγ+Rosi versus si-PPARγ); (d) TUNEL staining (×200) showed apoptotic cells in mice liver for IR after 12 h; (e) protein expression of AMPK, p-AMPK, mTOR, p-mTOR, LC3, and Beclin1 for IR after 12 h ($n = 3$, # means $p < 0.05$ for IR versus control, + means $p < 0.05$ for IR ± si-PPARγ±Rosi versus IR); (f) immunohistochemistry staining (×200) showing the expression of p-AMPK, p-mTOR, and LC3 for IR after 12 h ($n = 3$, # means $p < 0.05$ for IR versus control, + means $p < 0.05$ for IR ± si-PPARγ±Rosi versus IR).

kDa serine/threonine kinase, is a master negative regulator of autophagy, modulating cell growth, cell proliferation, cell cycle, and cell motility [16]. Autophagy plays a key role in the modulation of inflammation, cellular homeostasis and dysregulation, and cell death or survival. It has been proved associated with various liver disorders, including hepatitis, liver fibrosis, fatty liver, and acute IR injury [34–37]. It has been accepted that AMPK inhibits mTORC1 through phosphorylation, thus, inducing autophagy in response to cellular stress cues.

The relationship between PPARγ and AMPK/mTOR pathway has been discussed before [17, 38]. Jimenez-Flores et al. [39] and Zhong et al. [40] reported that p-AMPK and PPAR-γ expression levels are significantly reduced in diabetic mouse livers and the increase of the expression of alleviated liver damage. Zhong et al. [41] found db/db mice showed significantly decreased PPAR-γ and p-AMPK expression levels and increased p-mTOR expression, and the expression of Atg7, Beclin-1, and LC3 was also decreased. Micheliolide reversed these effects and alleviated the

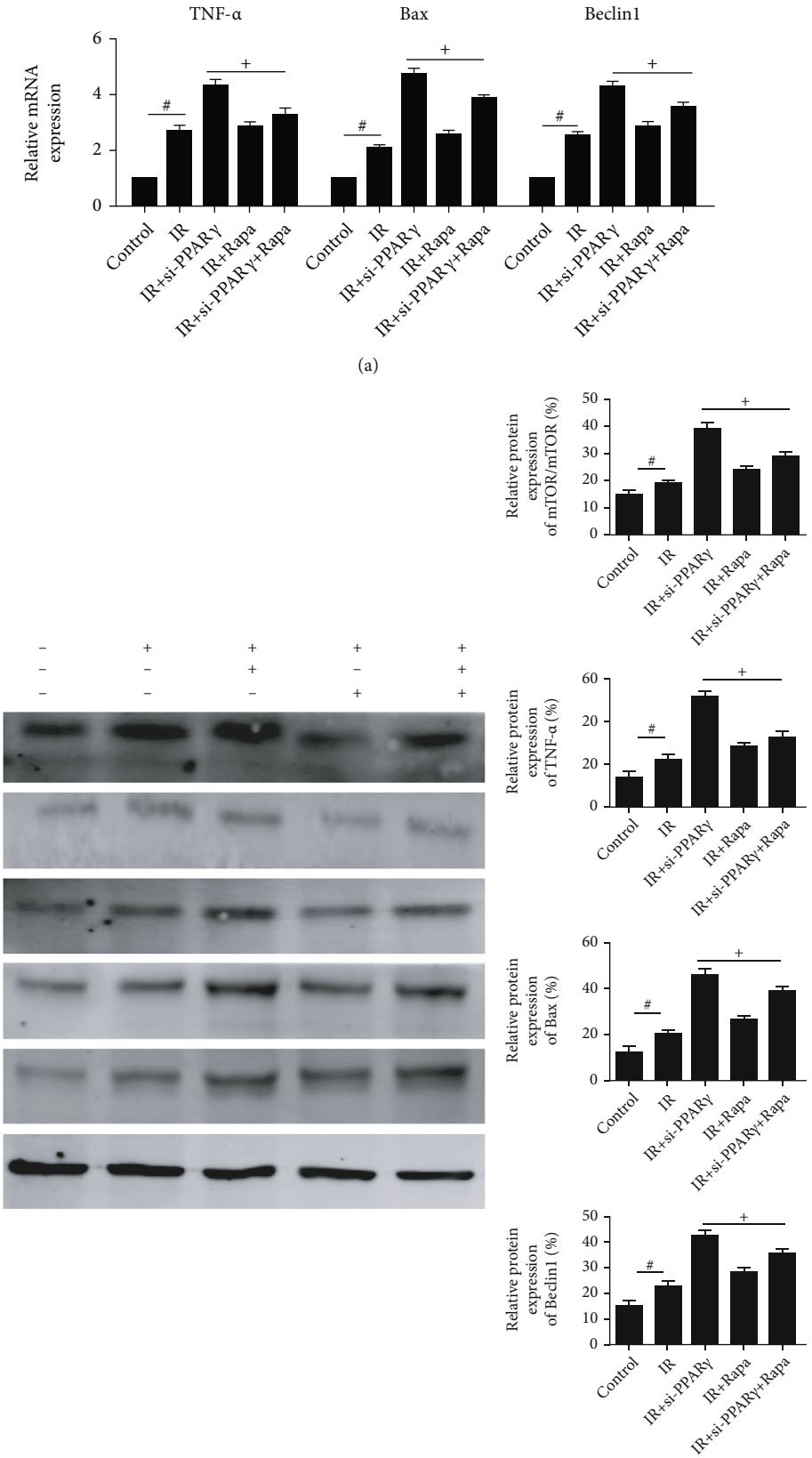

Figure 5: The involvement of AMPK/mTOR in the effects of PPARγ in IR. Notes: (a) relative mRNA expression of TNF-α, Bax, and Beclin1 ($n = 3$, # means $p < 0.05$ for IR versus control, + means $p < 0.05$ for IR ± si-PPARγ±Rapa versus IR); (b) protein expression of mTOR, p-mTOR, TNF-α, Bax, and Beclin1 ($n = 5$, # means $p < 0.05$ for si-PPARγ versus IR, + means $p < 0.05$ for si-PPARγ+Rosi versus si-PPARγ).

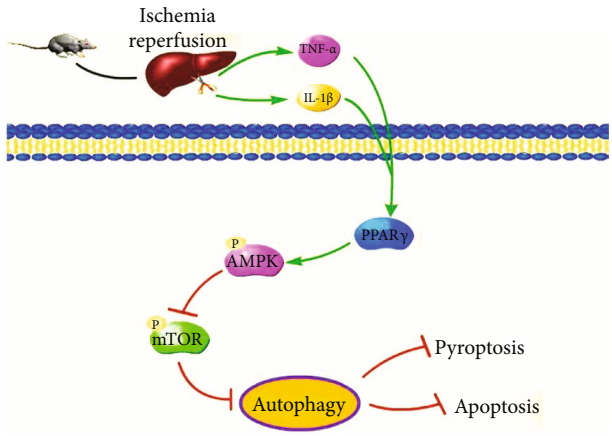

FIGURE 6: The underlying mechanism of PPARγ in IR injury. Notes: activated PPARγ in IR promoted AMPK phosphorylation and inhibited the phosphorylated form of mTOR, which contributed to the suppression of autophagy in mouse livers. And thus, PPARγ exhibited its protective effects in the hepatic IR injury.

inflammatory response and lipotoxicity in hepatocytes. Besides, the link of PPARγ and AMPK/mTOR/autophagy pathway was explored in other disease models [42–48]. To make sure the mechanism, mice were treated with at least one of the si-PPARγ and Rosi. The diminished expression of PPARγ caused by si-PPARγ leads to obvious inhibition of AMPK phosphorylation and thus promoted the phosphorylation of mTOR, inducing autophagy in mouse livers. The treatment of Rosi leads to opposite effects. Further, we treated mice with both si-PPARγ and rosiglitazone and got the same result as expected. In addition, we used rapamycin to confirm the involvement of mTOR and found that inflammation response and apoptosis caused by rapamycin in the IR injury were changed opposite to si-PPARγ. Therefore, we believed that the activation of PPARγ can not only relieve the inflammatory response and hepatocyte apoptosis but also exert its hepatoprotective effect via the AMPK/mTOR/autophagy pathway (Figure 6).

5. Conclusion

In summary, we found that PPARγ is continuously activated in hepatocytes during hepatic IR injury. Mice with significantly diminished expression of PPARγ got more grievous liver injury after hepatic ischemia-reperfusion injury. Conversely, activation of PPARγ caused by rosiglitazone resulted in attenuated liver injury. Through the use of si-PPARγ and rosiglitazone, we confirmed that one possible mechanism by which PPARγ activation results in protection against IR-related liver injury is through AMPK/mTOR-mediated autophagy. These results suggested that PPARγ may be a vital regulator and potential therapeutic target in the liver ischemic injury. And our results provided confidence for the follow-up development of PPARγ-related drugs for IR injury.

Abbreviations

AST: Aspartate aminotransferase
ALT: Alanine aminotransferase
IHC: Histology, immunohistochemical staining
TUNEL: Terminal deoxynucleotidyl transferase dUTP nick end labeling assay
qRT-PCR: Quantitative real-time PCR analysis
IR: Ischemia-reperfusion
PPARγ: Peroxisome proliferator-activated receptor-γ
AMPK: Adenosine monophosphate-activated protein kinase
mTOR: Mammalian target of rapamycin
Rosi: Rosiglitazone.

Data Availability

The datasets generated during and/or analyzed during the current study are available from the corresponding author on reasonable request.

Conflicts of Interest

The authors declare that there is no conflict of interest regarding the publication of this article.

Acknowledgments

This work was supported by the National Natural Science Foundation of China (grant number: 81670472), WBN Hepatology Research Fund of China Hepatitis Prevention and Treatment Foundation (grant number: CFHPC2019031), the Natural Science Foundation of Shanghai (grant number: 19ZR1447700), the Yangfan Plan of Shanghai Science and Technology Commission (grant number: 20YF1443300), the Health System Innovation Project of Shanghai Putuo Science and Technology Commission (grant numbers: PTKWWS201801 and PTKWWS201903), and the Foundation of Hospital in Minhang District (grant number: 2018MHJC08).

Supplementary Materials

Supplementary Materials 1: comparison of control groups. We compared natural group, sham group, vehicle group, drug group, and siRNA-control groups to exclude their influence on the results. We detected serum ALT and AST levels of those groups and observed pathological changes of their liver tissues. Results were exhibited as follows. We found that there is no significant difference among these groups, which meant that they would not cause obvious influence in our study. 2: PPARγ could affect pyroptosis in the IR injury. NOD-like receptor protein 3 (NLRP3) inflammasome plays a big role in the development of pyroptosis and can lead to the activation of caspase1. In the supplementary experiments, we measured the circulating level of IL-18 (a) and the mRNA and protein expression of caspase1 and NLRP3 among different groups of mice (b and c) and detected that relationship among IR, PPARγ, and pyroptosis. We found that pyroptosis was increased in the IR, and the alleviation of PPARγ aggravated pyroptosis, but the upregulation of PPARγ released it. *(Supplementary Materials)*

References

[1] T. Konishi and A. B. Lentsch, "Hepatic ischemia/reperfusion: mechanisms of tissue injury, repair, and regeneration," *Gene Expression*, vol. 17, no. 4, pp. 277–287, 2017.

[2] C. Huguet, A. Gavelli, and S. Bona, "Hepatic resection with ischemia of the liver exceeding one hour," *Journal of the American College of Surgeons*, vol. 178, no. 5, pp. 454–458, 1994.

[3] Y. I. Kim, "Ischemia-reperfusion injury of the human liver during hepatic resection," *Journal of Hepato-Biliary-Pancreatic Surgery*, vol. 10, no. 3, pp. 195–199, 2003.

[4] J. J. Lemasters and and R. G. Thurman, "Reperfusion injury after liver preservation for transplantation," *Annual Review of Pharmacology and Toxicology*, vol. 37, no. 1, pp. 327–338, 1997.

[5] J. Li, C. Guo, and J. Wu, "15-Deoxy-Δ-12,14-Prostaglandin J2 (15d-PGJ2), an Endogenous Ligand of PPAR-: Function and Mechanism," *PPAR Research*, vol. 2019, Article ID 7242030, 10 pages, 2019.

[6] J. Vamecq, J. M. Colet, J. J. Vanden Eynde, G. Briand, N. Porchet, and S. Rocchi, "PPARs: Interference with Warburg' Effect and Clinical Anticancer Trials," *PPAR Research*, vol. 2012, Article ID 304760, 23 pages, 2012.

[7] T. Akahori, M. Sho, K. Hamada et al., "Importance of peroxisome proliferator-activated receptor-γ in hepatic ischemia/reperfusion injury in mice," *Journal of Hepatology*, vol. 47, no. 6, pp. 784–792, 2007.

[8] M. Elias-Miro, M. B. Jimenez-Castro, M. Mendes-Braz, A. Casillas-Ramirez, and C. Peralta, "The current knowledge of the role of PPAR in hepatic ischemia-reperfusion injury," *PPAR Research*, vol. 2012, Article ID 802384, 14 pages, 2012.

[9] W. H. Fong, H. D. Tsai, Y. C. Chen, J. S. Wu, and T. N. Lin, "Anti-apoptotic actions of PPAR-gamma against ischemic stroke," *Molecular Neurobiology*, vol. 41, no. 2-3, pp. 180–186, 2010.

[10] S. Q. Rodríguez-Lara, W. A. Trujillo-Rangel, A. Castillo-Romero et al., "Effect of telmisartan in the oxidative stress components induced by ischemia reperfusion in rats," *Oxidative Medicine and Cellular Longevity*, vol. 2019, Article ID 1302985, 13 pages, 2019.

[11] G. D. Ren, Y. YC, W. L. Li, F. F. Li, and X. Y. Han, "Research on cardioprotective effect of irbesartan in rats with myocardial ischemia-reperfusion injury through MAPK-ERK signaling pathway," *European Review for Medical and Pharmacological Sciences*, vol. 23, no. 12, pp. 5487–5494, 2019.

[12] R. Kumari, L. B. Willing, S. D. Patel et al., "The PPAR-gamma agonist, darglitazone, restores acute inflammatory responses to cerebral hypoxia-ischemia in the diabetic Ob/Ob mouse," *Journal of Cerebral Blood Flow and Metabolism*, vol. 30, no. 2, pp. 352–360, 2010.

[13] H. Kilter, M. Werner, C. Roggia et al., "The PPAR-γ agonist rosiglitazone facilitates Akt rephosphorylation and inhibits apoptosis in cardiomyocytes during hypoxia/reoxygenation," *Diabetes, Obesity & Metabolism*, vol. 11, no. 11, pp. 1060–1067, 2009.

[14] S. Elshazly and E. Soliman, "PPAR gamma agonist, pioglitazone, rescues liver damage induced by renal ischemia/reperfusion injury," *Toxicology and Applied Pharmacology*, vol. 362, pp. 86–94, 2019.

[15] M. Abdelrahman, A. Sivarajah, and C. Thiemermann, "Beneficial effects of PPAR-gamma ligands in ischemia-reperfusion injury, inflammation and shock," *Cardiovascular Research*, vol. 65, no. 4, pp. 772–781, 2005.

[16] K. Inoki, J. Kim, and K. L. Guan, "AMPK and mTOR in cellular energy homeostasis and drug targets," *Annual Review of Pharmacology and Toxicology*, vol. 52, no. 1, pp. 381–400, 2012.

[17] J. Xu, J. Ji, and X. H. Yan, "Cross-talk between AMPK and mTOR in regulating energy balance," *Critical Reviews in Food Science and Nutrition*, vol. 52, no. 5, pp. 373–381, 2012.

[18] T. Ando, J. Ichikawa, T. Fujimaki, N. Taniguchi, Y. Takayama, and H. Haro, "Gemcitabine and rapamycin exhibit additive effect against osteosarcoma by targeting autophagy and apoptosis," *Cancers (Basel)*, vol. 12, no. 11, p. 3097, 2020.

[19] E. A. Dunlop and A. R. Tee, "mTOR and autophagy: a dynamic relationship governed by nutrients and energy," *Seminars in Cell & Developmental Biology*, vol. 36, pp. 121–129, 2014.

[20] L. Wu, Q. Zhang, W. Dai et al., "Quercetin Pretreatment Attenuates Hepatic Ischemia Reperfusion-Induced Apoptosis and Autophagy by Inhibiting ERK/NF-κB Pathway," *Gastroenterology Research and Practice*, vol. 2017, Article ID 9724217, 15 pages, 2017.

[21] K. M. Quesnelle, P. V. Bystrom, and L. H. Toledo-Pereyra, "Molecular responses to ischemia and reperfusion in the liver," *Archives of Toxicology*, vol. 89, no. 5, pp. 651–657, 2015.

[22] V. Trumper, I. Wittig, J. Heidler, F. Richter, B. Brune, and A. von Knethen, "Redox Regulation of PPARγ in Polarized Macrophages," *PPAR Research*, vol. 2020, Article ID 8253831, 16 pages, 2020.

[23] L. J. Holm, M. O. Monsted, M. Haupt-Jorgensen, and K. Buschard, "PPARs and the development of type 1 diabetes," *PPAR Research*, vol. 2020, Article ID 6198628, 11 pages, 2020.

[24] O. Y. Kytikova, J. M. Perelman, T. P. Novgorodtseva et al., "Peroxisome proliferator-activated receptors as a therapeutic target in asthma," *PPAR Research*, vol. 2020, Article ID 8906968, 18 pages, 2020.

[25] A. Kaupang and T. V. Hansen, "The PPAR Ω Pocket: Renewed Opportunities for Drug Development," *PPAR Research*, vol. 2020, Article ID 9657380, 21 pages, 2020.

[26] L. Wu, C. Guo, and J. Wu, "Therapeutic potential of PPARγ natural agonists in liver diseases," *Journal of Cellular and Molecular Medicine*, vol. 24, no. 5, pp. 2736–2748, 2020.

[27] R. M. Evans, "The steroid and thyroid hormone receptor superfamily," *Science*, vol. 240, no. 4854, pp. 889–895, 1988.

[28] S. Kuboki, T. Shin, N. Huber et al., "Peroxisome proliferator-activated receptor-gamma protects against hepatic ischemia/reperfusion injury in mice," *Hepatology*, vol. 47, no. 1, pp. 215–224, 2008.

[29] A. Nakajima, K. Wada, H. Miki et al., "Endogenous PPARγ mediates anti-inflammatory activity in murine ischemia-reperfusion injury," *Gastroenterology*, vol. 120, no. 2, pp. 460–469, 2001.

[30] F. Al Rouq and E. El Eter, "PPAR-γ activator induces neuroprotection in hypercholesterolemic rats subjected to global cerebral ischemia/reperfusion injury: in vivo and in vitro inhibition of oxidative stress," *Experimental Gerontology*, vol. 51, pp. 1–7, 2014.

[31] D. G. Hardie, "AMPK–sensing energy while talking to other signaling pathways," *Cell Metabolism*, vol. 20, no. 6, pp. 939–952, 2014.

[32] D. G. Hardie, B. E. Schaffer, and A. Brunet, "AMPK: an energy-sensing pathway with multiple inputs and outputs," *Trends in Cell Biology*, vol. 26, no. 3, pp. 190–201, 2016.

[33] D. G. Hardie, "AMP-activated/SNF1 protein kinases: conserved guardians of cellular energy," *Nature Reviews. Molecular Cell Biology*, vol. 8, no. 10, pp. 774–785, 2007.

[34] M. Allaire, P. E. Rautou, P. Codogno, and S. Lotersztajn, "Autophagy in liver diseases: time for translation?," *Journal of Hepatology*, vol. 70, no. 5, pp. 985–998, 2019.

[35] R. Cursio, P. Colosetti, P. Codogno, A. M. Cuervo, and H. M. Shen, "The role of autophagy in liver diseases: mechanisms and potential therapeutic targets," *BioMed Research International*, vol. 2015, Article ID 480508, 2 pages, 2015.

[36] J. Gracia-Sancho, S. Guixe-Muntet, D. Hide, and J. Bosch, "Modulation of autophagy for the treatment of liver diseases," *Expert Opinion on Investigational Drugs*, vol. 23, no. 7, pp. 965–977, 2014.

[37] P. E. Rautou, A. Mansouri, D. Lebrec, F. Durand, D. Valla, and R. Moreau, "Autophagy in liver diseases," *Journal of Hepatology*, vol. 53, no. 6, pp. 1123–1134, 2010.

[38] A. Sukumaran, K. Choi, and B. Dasgupta, "Insight on transcriptional regulation of the energy sensing AMPK and biosynthetic mTOR pathway genes," *Frontiers in Cell and Development Biology*, vol. 8, p. 671, 2020.

[39] L. M. Jimenez-Flores, S. Lopez-Briones, M. H. Macias-Cervantes, J. Ramirez-Emiliano, and V. Perez-Vazquez, "A PPARγ, NF-κB and AMPK-dependent mechanism may be involved in the beneficial effects of curcumin in the diabetic db/db mice liver," *Molecules*, vol. 19, no. 6, pp. 8289–8302, 2014.

[40] J. Zhong, W. Gong, L. Lu et al., "Irbesartan ameliorates hyperlipidemia and liver steatosis in type 2 diabetic db/db mice via stimulating PPAR-γ, AMPK/Akt/mTOR signaling and autophagy," *International Immunopharmacology*, vol. 42, pp. 176–184, 2017.

[41] J. Zhong, W. Gong, J. Chen et al., "Micheliolide alleviates hepatic steatosis in db/db mice by inhibiting inflammation and promoting autophagy via PPAR-γ-mediated NF-κB and AMPK/mTOR signaling," *International Immunopharmacology*, vol. 59, pp. 197–208, 2018.

[42] Z. Tu, T. Moss-Pierce, P. Ford, and T. A. Jiang, "Rosemary (Rosmarinus officinalis L.) extract regulates glucose and lipid metabolism by activating AMPK and PPAR pathways in HepG2 cells," *Journal of Agricultural and Food Chemistry*, vol. 61, no. 11, pp. 2803–2810, 2013.

[43] A. Morrison and J. Li, "PPAR-γ and AMPK - Advantageous targets for myocardial ischemia/reperfusion therapy," *Biochemical Pharmacology*, vol. 82, no. 3, pp. 195–200, 2011.

[44] F. Vasheghani, Y. Zhang, Y. H. Li et al., "PPARγ deficiency results in severe, accelerated osteoarthritis associated with aberrant mTOR signalling in the articular cartilage," *Annals of the Rheumatic Diseases*, vol. 74, no. 3, pp. 569–578, 2015.

[45] K. V. Guntur, A. Guilherme, L. Xue, A. Chawla, and M. P. Czech, "*Map4k4* negatively regulates peroxisome proliferator-activated receptor (PPAR) γ protein translation by suppressing the mammalian target of rapamycin (mTOR) signaling pathway in cultured adipocytes," *The Journal of Biological Chemistry*, vol. 285, no. 9, pp. 6595–6603, 2010.

[46] J. Hwang, M. Lee, H. Kim et al., "Antiobesity effect of ginsenoside Rg3 involves the AMPK and PPAR-γsignal pathways," *Phytotherapy Research*, vol. 23, no. 2, pp. 262–266, 2009.

[47] K. H. Yap, G. S. Yee, M. Candasamy et al., "Catalpol ameliorates insulin sensitivity and mitochondrial respiration in skeletal muscle of type-2 diabetic mice through insulin signaling pathway and AMPK/SIRT1/PGC-1α/PPAR-γ activation," *Biomolecules*, vol. 10, no. 10, p. 1360, 2020.

[48] Y. Lu, J. Yao, C. Gong et al., "Gentiopicroside ameliorates diabetic peripheral neuropathy by modulating PPAR-Γ/AMPK/ACC signaling pathway," *Cellular Physiology and Biochemistry*, vol. 50, no. 2, pp. 585–596, 2018.

Hindawi
PPAR Research
Volume 2021, Article ID 6629455, 9 pages
https://doi.org/10.1155/2021/6629455

Research Article

PPAR-Alpha Agonist Fenofibrate Combined with Octreotide Acetate in the Treatment of Acute Hyperlipidemia Pancreatitis

Wen Bao, Rui Kong, Nan Wang, Wei Han, and Jie Lu

Department of Gastroenterology, Shanghai Tenth People's Hospital, Tongji University School of Medicine, Shanghai 200072, China

Correspondence should be addressed to Jie Lu; kennisren@hotmail.com

Received 3 December 2020; Revised 25 February 2021; Accepted 13 April 2021; Published 21 April 2021

Academic Editor: Antonio Brunetti

At present, there are more and more patients with acute hypertriglyceridemia pancreatitis in clinical practice. Common treatment measures include fasting and water withdrawal, fluid resuscitation, and somatostatin. In recent years, studies have pointed out that the PPARa agonist fenofibrate may help improve the condition of such patients. Therefore, through clinical research and analysis, we reported for the first time that fenofibrate combined with octreotide acetate has a more excellent effect in the treatment of patients with acute hypertriglyceridemia pancreatitis, and from the perspective of signal pathways, we revealed that the combination of the two drugs has an effect on NF-κB P65. The synergistic inhibitory effect proves that the combined treatment is beneficial to control inflammation, protect liver function, and improve the prognosis of patients. It is worthy of clinical promotion.

1. Introduction

According to statistics, the incidence of hypertriglyceridemia in the social population is increasing year by year, and the diseased population is showing a younger trend. The disorder of primary or secondary lipoprotein metabolism structure further leads to the occurrence of acute pancreatitis, which becomes an important pathogenic factor after stones and alcohol consumption [1]. It is reported that the incidence of pancreatitis in patients with hypertriglyceridemia accounts for about 15% to 20% [2]. The possible pathogenesis is that lipid globule microembolism affects pancreatic microcirculation and pancreatin breaks down triglycerides to cause toxic fatty acids to directly damage acinar cells. These can activate important pivotal molecules such as NF-κB [3], activator protein 1 (AP-1) [4], and signal transducers and activators of transcription (STATs), thereby increasing the expression of inflammatory mediators downstream of the signaling pathway, such as TNF-α, IL-6, IL-1, and reactive oxygen radicals [5]. The cascading effect of inflammation is also an important cause of clinical complications such as infection or pancreatic cysts in this type of pancreatitis [6]. Therefore, the focus of the treatment of acute hyperlipidemia pancreatitis is to quickly reduce the patient's serum TG level and control the inflammatory response. Peroxisome proliferator-activated receptor (PPARa) is a type of transcription factor activated by ligands, which belongs to the nuclear hormone receptor superfamily. The activation of PPAR can regulate the inflammatory response, proliferation, differentiation, and apoptosis of cells [7], which is closely related to tumors, metabolism [8], or autoimmune diseases [9]. The PPARa agonist fenofibrate is currently the most commonly used clinically for lowering triglycerides. It can significantly reduce the level of apolipoprotein C-III, thereby reducing the synthesis of very-low-density lipoprotein and low-density lipoprotein, and accelerating the metabolism of TG [10]. A large number of studies have shown that the nuclear factor kappa B (NF-κB) pathway is the most widely studied way for PPAR to exert its anti-inflammatory activity. Fenofibrate inhibits the release of interleukin 1β (pro-IL-1β) and pro-IL-18 from pancreatic acinar cells, thereby reducing the expression of chemokines and proinflammatory cytokines, such as IL-1β, IL-6, and tumor necrosis factor-alpha (TNF-α), and may initiate the programmed cell death pathway, prompting local and systemic anti-inflammatory responses [11]. Simultaneously, basic studies have shown that

octreotide, as a somatostatin analog, is currently the first-line drug for the treatment of acute pancreatitis, and it also exerts anti-inflammatory activity by inhibiting the NF-κB signaling pathway [12]. Therefore, this article speculates that there is a synergistic anti-inflammatory therapeutic effect between fenofibrate and octreotide acetate. Therefore, to explore the clinical efficacy of fenofibrate combined with octreotide acetate in the treatment of hyperlipidemia pancreatitis, it is reported as follows.

2. Patients and Methods

2.1. General Information. Sixty patients with hyperlipidemia pancreatitis admitted to the Gastroenterology Ward of Shanghai Tenth People's Hospital from September 2019 to September 2020 were selected as the research objects and were divided into the observation group and the control group by random number table method, with 30 cases each. In the observation group, there were 23 males and 7 females, with an average age of 44.57 ± 15.12 years old. According to the Ranson scale of acute pancreatitis, 25 cases were mild and 5 cases were not mild; in the control group, there were 18 males and 12 females, with an average age of 42.67 ± 9.8 years, and 26 mild cases and 4 nonmild cases. There was no statistically significant difference in baseline data between the two groups ($p > 0.05$), and they were comparable.

2.2. Inclusion Criteria and Exclusion Criteria. Inclusion criteria were as follows: (1) The time from onset to hospital admission is less than 48 h, and the medical history, clinical manifestations, serological indicators, and CT examination of the upper abdomen all meet the relevant diagnostic criteria of the Chinese Guidelines for the Diagnosis and Treatment of Acute Pancreatitis (2014 Edition). (2) The patient is diagnosed with hyperlipidemia: TG > 11.3 mmol/l or TG of 5.65~11.3 mmol/l, and the serum is chylous. (3) The patient has not taken any drugs that may interfere with the results of this study in the past one month and has no allergic reactions to the study drugs. (4) The project was approved by the hospital ethics committee, and the patient and family members signed the relevant informed consent.

Exclusion criteria were as follows: (1) Exclude patients with stones in the biliary system or dilated bile ducts. (2) Exclude patients with dysfunction of the heart, liver, kidney, and other important organs or patients with malignant tumors. (3) Exclude patients with neurological or psychiatric diseases or poor compliance. (4) Exclude patients during pregnancy or lactation.

2.3. Treatment Methods. Both groups of patients underwent rigorous condition assessment at the time of admission and 48 hours after admission. The control group adopts comprehensive treatment measures [13], including fasting and not drinking, ECG monitoring, fluid resuscitation, application of octreotide acetate (Sandostatin, Novartis Pharma Schweiz AG, Switzerland, 0.3 mg/q12h, diluted in 0.9% NaCl 250 ml, intravenously) to inhibit pancreatin secretion, auxiliary oral administration of raw rhubarb, enoxaparin sodium anticoagulation, oxygen inhalation, anti-infection, and other symptomatic support. For treatment, abdominal drainage can be performed depending on the severity of the disease. In the observation group, based on the treatment of the control group, fenofibrate (Fenofibrate Capsules, Recipharm Fontaine, 160 mg/qn, after meal) was added on the second day of admission. Both groups were treated continuously for a course of treatment (7 days), and the clinical efficacy was observed and analyzed.

2.4. Observation Index and Evaluation Standard

(1) According to the requirements of the Ranson standard [14], select and record the serum inflammatory indexes (neutrophil ratio, CRP) of the two groups of patients before and after treatment, the diagnosis and prognosis evaluation indexes (amylase, lipase, AST, LDH, blood calcium, and urea nitrogen) of acute pancreatitis-related diseases, and the changes in the serum TG levels of the patients

(2) Evaluation criteria for treatment effectiveness: markedly effective means that the patient's clinical symptoms disappear, the serological indicators return to normal, and the pancreatic CT severity index (CTSI) returns to Grade I, 0 points; improvement means that the patient's clinical symptoms are reduced, the serological indicators are improved, and the pancreatic CT severity index (CTSI) is improved to Grade I, 1 to 2 points; ineffective means that the patient's clinical symptoms still exist, the serological indicators have not changed, and the pancreatic CT severity index (CTSI) has not changed or even worsened. Total effective rate = apparent efficiency + improvement rate

(3) Statistics and analysis of the metabolic underlying diseases (diabetes, hypertension, hepatic adipose infiltration, etc.) that occurred before the patients suffered from hyperlipidemia pancreatitis and the occurrence of local or systemic complications (pancreatic pseudocyst, hypoproteinemia, infection, etc.) during the treatment

2.5. Sample Collection. To test and confirm that fenofibrate and octreotide acetate can synergistically inhibit the activation of the NF-κB P65 signaling pathway, alleviate inflammatory cell infiltration and reduce the protein expression levels of downstream inflammatory factors TNF-α and IL-6, thereby exerting anti-inflammatory activity [15]. We collected the whole blood samples of two groups of patients before and after treatment and placed them in anticoagulation tubes. After centrifugation at 3000 r/min, the supernatant was collected and collected in the corresponding EP tubes. Whole blood and serum samples were kept separate in a -80°C.

2.6. Enzyme-Linked Immunosorbent Assay (ELISA). TNF-α and IL-6 protein levels in the serum were measured using ELISA kits (Elabscience, Wuhan, China) according to the manufacturer's instructions. Microplate reader model is

Table 1: Statistical analysis of the treatment effect of the two groups of patients (n, %).

Group	Number (n)	Effectivity	Improvement	Nullity	Total effectiveness
Observation group	30	3 (10.00)	25 (83.33)	2 (6.67)	28 (93.33)
Control group	30	1 (3.33)	21 (70.00)	8 (26.67)	22 (73.33)
χ^2 value					4.32
p value					0.037*

*$p < 0.05$: the difference between the groups was statistically significant.

Table 2

(a) Analysis of serum-related indicators in the two groups

Time	Group	Neutrophil ratio	CRP	Amylase	Lipase	AST
Before	Control group	0.79 ± 0.09	124.88 ± 68.81	272.85 ± 298.68	1071.97 ± 1945.65	52.61 ± 51.33
	Observation group	0.8 ± 0.05	128.39 ± 62.7	202.27 ± 154.18	712.7 ± 869.95	33.53 ± 23.98
	T	-0.707	-0.207	1.15	0.923	1.844
	p	0.483	0.837	0.256	0.36	0.072
After	Control group	0.62 ± 0.09	40.06 ± 41.64	72.92 ± 32.71	128.94 ± 142.5	32.74 ± 20.49
	Observation group	0.59 ± 0.08	20.97 ± 18.06	71.57 ± 35.09	69.4 ± 63.57	23.19 ± 14.7
	T	1.488	2.304	0.154	2.09	2.074
	p	0.142	0.027*	0.878	0.041*	0.043*

(b) Analysis of serum-related indicators in the two groups

Time	Group	LDH	Blood calcium	Urea nitrogen	TG
Before	Control group	521.1 ± 242.9	2.15 ± 0.17	4.8 ± 1.95	5.66 ± 4.79
	Observation group	451.03 ± 169.48	2.16 ± 0.22	4.36 ± 1.77	9.45 ± 12.2
	T	1.296	-0.224	0.929	-1.583
	p	0.2	0.823	0.357	0.119
After	Control group	197.83 ± 62.28	2.23 ± 0.18	3.85 ± 1.22	4.93 ± 2.83
	Observation group	163.63 ± 51.4	2.34 ± 0.19	3.32 ± 1.17	3.57 ± 1.39
	T	2.32	-2.485	1.708	2.376
	p	0.024*	0.016*	0.093	0.022*

*$p < 0.05$: the difference between the groups was statistically significant.

Denley Dragon Wellscan MK3, and the analysis software is Ascent software for Multiskan.

2.7. Statistical Analysis. Statistical analyses were performed using SPSS software version 26.0 (SPSS Inc., Chicago, IL, USA). The data were expressed as the mean ± standard deviation and evaluated for normality and homogeneity using the Shapiro-Wilk test and Levene's test. The comparison between groups was performed by t-test, the count data were expressed as a percentage and number of cases, the comparison between groups was performed by χ^2 test, and the correlation analysis was performed by Pearson correlation analysis. Differences were considered significant at $p < 0.05$. All p values were two-tailed.

3. Results

3.1. Clinical Effect. Comparing the treatment effect of the two groups within a course of treatment, the total effective rate of the observation group reached 93.33%, while the control group was only 73.33%. The treatment effect of the observation group was significantly better than the control group, and the difference between the groups was statistically significant ($p = 0.037$, $^*p < 0.05$; Table 1).

3.2. Serological Index Analysis of the Two Groups before and after Treatment. Before treatment, there was no statistically significant difference in neutrophil ratio, CRP, amylase, lipase, AST, LDH, blood calcium, urea nitrogen, and TG

Table 3: Statistical analysis of complications during treatment of two groups of patients (n, %).

Group	Number (n)	Adverse complications	No adverse complications	Adverse complications rate
Observation group	30	4	26	13.33
Control group	30	6	24	20.00
χ^2 value				0.48
p value				0.488

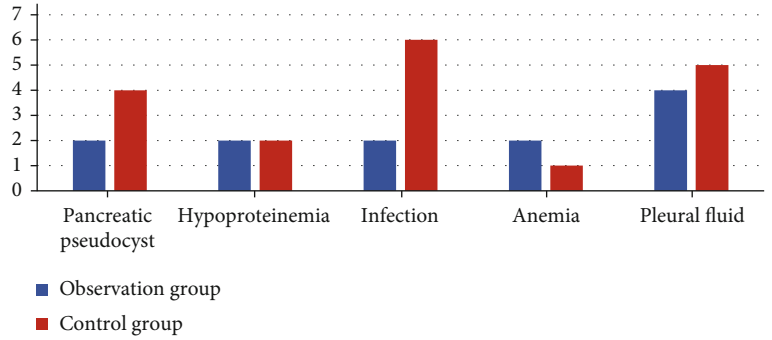

Figure 1: Treatment-related local or systemic complications.

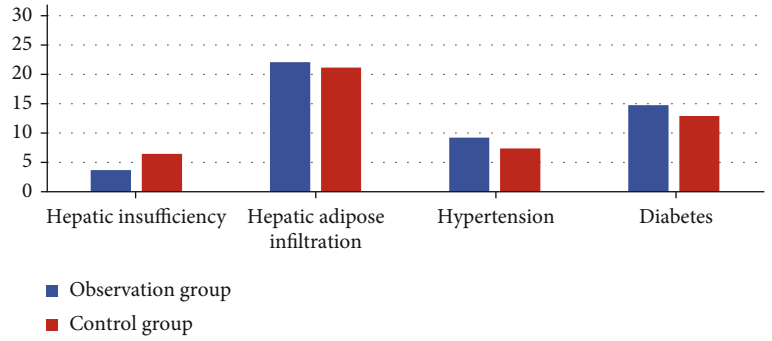

Figure 2: The basic metabolic diseases of the two groups of patients.

Table 4: Pearson analysis between amylase, high-low-density lipoprotein, and TG in HTGP patients.

		HDL	LDL	TG
Amylase	Pearson correlation	0.111	0.435**	0.052
	Sig. (two-tailed)	0.4	0.001	0.694
	N	60	60	60

Note: **At the level of 0.01 (two-tailed), the correlation is significant.

Table 5: Pearson analysis between lipase, high-low-density lipoprotein, and TG in HTGP patients.

		HDL	LDL	TG
Lipase	Pearson correlation	0.158	-0.032	-0.096
	Sig. (two-tailed)	0.227	0.811	0.466
	N	60	60	60

levels between the two groups ($p > 0.05$), which was comparable. After treatment, the inflammatory indexes and TG levels of the two groups of patients were significantly decreased, and the blood calcium level was higher than before. However, in contrast, the observation group increased and decreased more than the control group. The differences in CRP, lipase, AST, LDH, blood calcium, and TG levels were statistically significant ($^*p < 0.05$, Tables 2(a) and 2(b)).

3.3. Comparison of Clinical Complications between the Two Groups. Statistics of the adverse complications of the two groups of patients during hospital treatment found that the incidence of the observation group was 13.33%, and the control group was 20.00%, although the incidence of complications in the observation group was slightly lower. But the difference between the two groups was not statistically significant ($p = 0.488$, $p > 0.05$; Table 3). Among them, the control group had the most infections, followed by pleural effusion. In the observation group, the number of cases of pleural and ascites effusion was the most, and the other four complications had the same number (Figure 1).

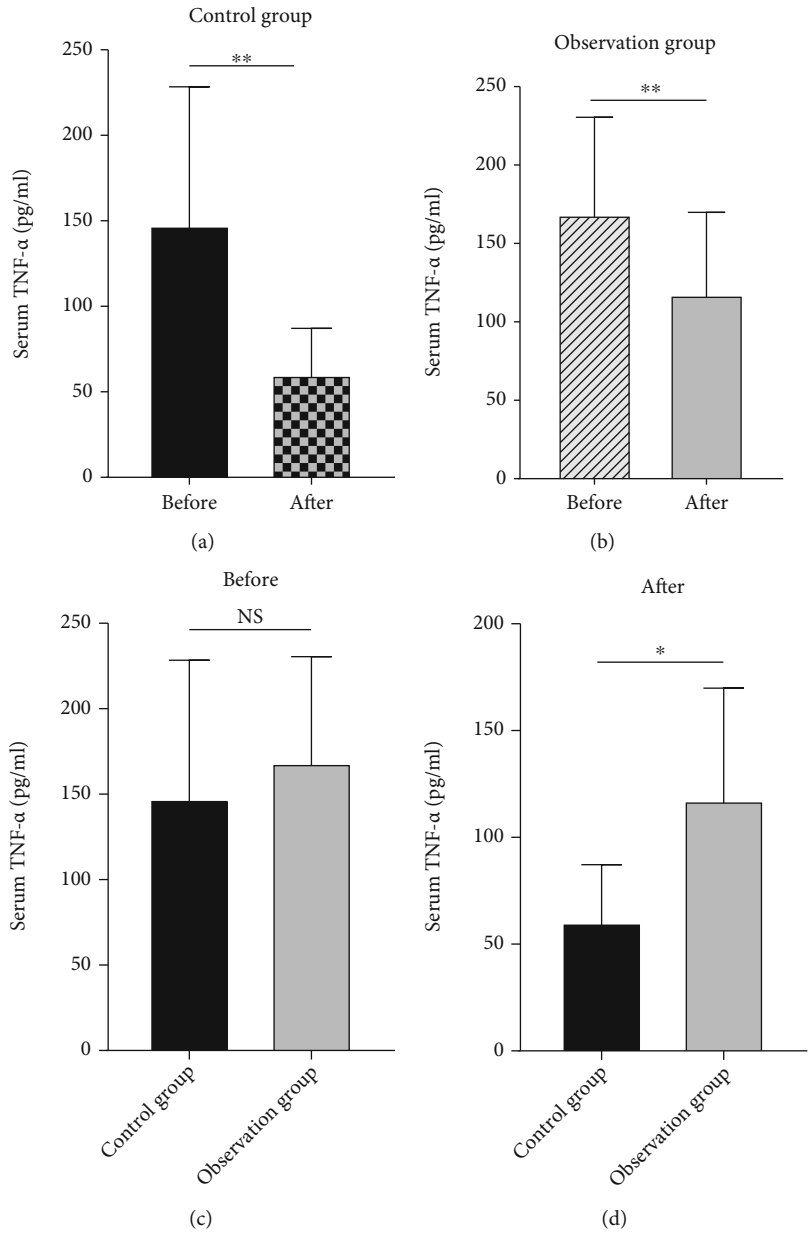

Figure 3: Analyze the changes of TNF-α protein expression before and after treatment in the two groups, observation group (a) and control group (b). Reanalysis of the protein expression level of TNF-α before treatment between the two groups of patients was not statistically significant, proving that the two are comparable (c). Comparing the TNF-α levels of the two groups of patients after treatment, it was found that the protein expression level of the observation group was lower than that of the control group, and the difference was statistically significant (d) ($n = 30$, $**p < 0.01$,$*p < 0.05$, NS: no significance).

3.4. The Status of the Two Groups of Patients with Their Metabolic Underlying Diseases before the Onset. Statistics found that 80% of the patients in the observation group had fatty liver, 53.3% of the patients had diabetes, and 33.3% had hypertension; the control group also showed a similar trend (Figure 2). It can be considered that fatty liver and diabetes are risk factors for hyperlipidemia pancreatitis.

3.5. Pearson Analysis. The results showed that amylase was not related to high-density lipoprotein and TG levels ($p > 0.05$) but was related to low-density lipoprotein levels ($p < 0.05$) and was positively correlated (Table 4). Lipase did not correlate with high-density lipoprotein, low-density lipoprotein, and TG levels (Table 5).

3.6. Comparison of TNF-α and IL-6 Protein Levels. We measure the systemic inflammation index at the protein level. ELISA results are shown in Figures 3 and 4.

4. Discussion

Nowadays, with the continuous improvement of people's living standards, the dietary structure has also undergone tremendous changes. The incidence of hyperlipidemia is also

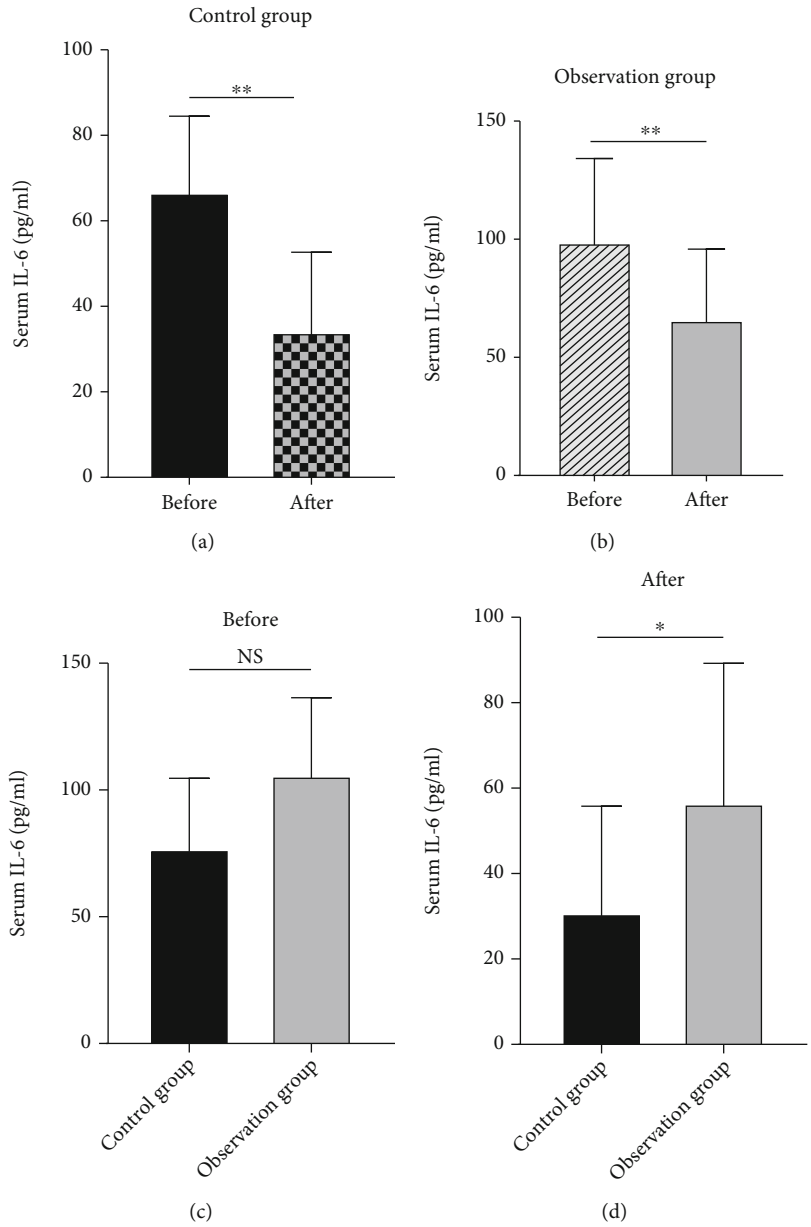

Figure 4: Analyze the changes of IL-6 protein expression before and after treatment in the two groups, observation group (a) and control group (b). Reanalysis of the protein expression level of IL-6 before treatment between the two groups was not statistically significant, proving that the two are comparable (c). Comparing the IL-6 levels of the two groups of patients after treatment, it was found that the protein expression level of the observation group was lower than that of the control group, and the difference was statistically significant (d) ($n = 30$, $**p < 0.01$,$*p < 0.05$, NS: no significance).

getting higher and higher, among which type I and type V hyperlipidemia are the most common, and their main feature is a significant increase in triglyceride levels [16]. Studies have shown that the occurrence of hyperlipidemia pancreatitis is significantly positively correlated with the severity of the disease and TG levels [17]. Acute pancreatitis can be induced by TG levels exceeding 1000 mg/dl (11.4 mmol/l) [18]. Previous studies have pointed out that a large amount of high-concentration free fatty acids can accelerate the activation of trypsinogen and affect the microenvironment around pancreatic tissues [19], resulting in damage to pancreatic capillary endothelial cells, promoting self-digestion of acinar cells and increasing blood vessels. Permeability, at the same time, stimulates the mass production of vasoconstrictors and aggravates pancreatic edema and bleeding [20]. Therefore, in this clinical study, we conducted an in-depth discussion on the treatment strategy of patients with hyperlipidemia pancreatitis and found that in the case of both groups of patients using octreotide acetate, the observation group added with the PPARa agonist fenofibrate showed a more significant anti-inflammatory effect [21]. In the observation group, the abnormal neutrophil ratio and CRP levels in the serum of patients in the observation group decreased faster, and the indexes of lactate dehydrogenase

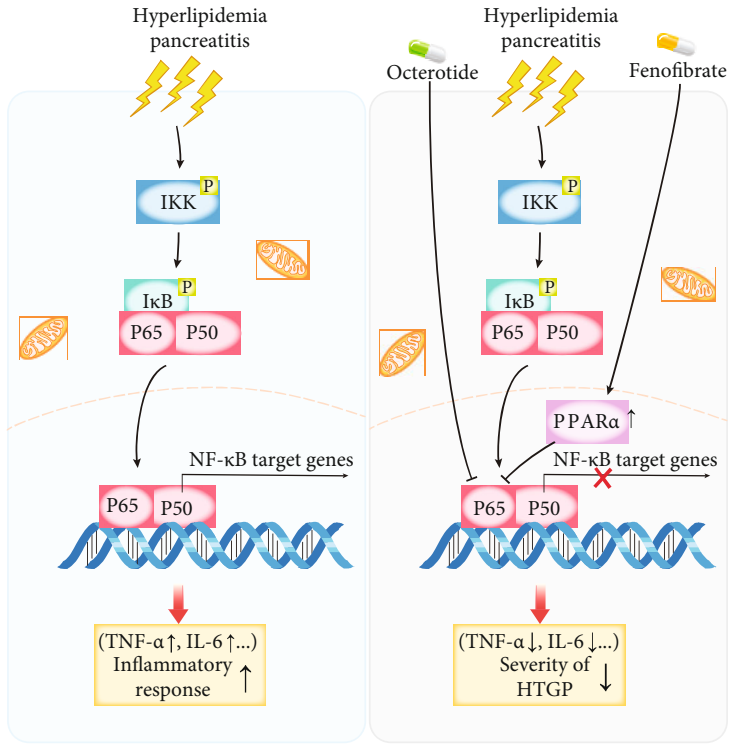

Figure 5: The role of PPARa and octreotide as tightly interacting transcription factors in hyperlipidemia pancreatitis. IKK: IκB kinase; HTGP: hyperlipidemia pancreatitis.

and liver enzymes approached the normal range faster ($p < 0.05$), and the clinical effective rate was higher. More importantly, fenofibrate can significantly reduce blood lipid levels in a short period, fundamentally remove risk factors for disease, increase blood calcium concentration, and improve the prognosis of patients with pancreatitis. This research conclusion suggests that PPARa plays an important role in lipid transport and metabolic regulation [22]. Studies have shown that PPARa can effectively regulate the transcription of constituent gene encoding fatty acid metabolism enzymes and mitochondrial FA oxidation (FAO) activity. This directly inhibits NF-κB P65-induced inflammation genes and reduces the expression of C-reactive protein in human adipocytes induced by the downstream factor (IL-1) of the signaling pathway [23]. Fenofibrate, as a commonly used agonist of PPARa, often inhibits the expression of CD40 induced by TNF-α [24] and IL-6 through SIRT1-dependent signaling pathways and exerts a significant anti-inflammatory effect [25]. This shows that NF-κB P65 is a key part of the anti-inflammatory pathway. Therefore, we tried to search for octreotide-related research [26] and found that animal experiments have confirmed that OCT may protect the pancreas from injury due to PQ by reducing serum pancreatic injury biomarker levels and mitigating leukocyte infiltration in the pancreatic tissue [12]. The signal pathway involved in this article is shown in Figure 5. Therefore, after clinically grouping the collected patient serum samples, ELISA was used to determine the protein levels of TNF-α and IL-6 downstream of NF-κB P65. The final results showed that before treatment, there was no significant difference in the expression levels of TNF-α and IL-6 between the observation group and the control group ($p > 0.05$).

After treatment, the levels of these two inflammatory factors in the patients' serum were lower than before, and the differences between them were statistically significant ($p < 0.05$), which shows that whether it is octreotide acetate alone or fenofibrate combined with octreotide acetate, there is a certain effect on controlling the inflammatory infiltration of patients with hyperlipidemia pancreatitis. The results of this study indicate that the combination of fenofibrate and octreotide acetate has a better therapeutic effect and has a certain synergy in controlling inflammation. This result was in full compliance with previous literature reports and our research assumptions [27]. Using limited patient data, this study also performed a Pearson correlation analysis between patients' serum amylase, lipase, high-density lipoprotein, low-density lipoprotein, and TG. The results showed that amylase had nothing to do with high-density lipoprotein and TG levels ($p > 0.05$) but was related to low-density lipoprotein levels ($p < 0.05$), and there was a positive correlation. There is no obvious correlation between lipase and the above three. This result was similar to that of Ni et al. in 2014 [28]. The results of this study further indicate that pancreatic cells under the action of low-density lipoprotein are more prone to damage and dysfunction [29], which induces a systemic acute inflammatory response and increases the level of amylase in the patient's serum [30]. From this, we have reached the conclusions listed below. However, since we were unable to obtain the lysate of the patient's pancreatic tissue to quantitatively detect the NF-κB P65 itself, we could not

directly confirm this conclusion, which is a shortcoming of this study.

5. Conclusion

(1) Both fenofibrate and octreotide acetate exert their antihyperlipidemic pancreatitis activity by inhibiting the NF-κB signaling pathway, and their therapeutic effects are synergistic

(2) Compared with octreotide acetate alone, fenofibrate combined with octreotide acetate has a better therapeutic effect and is worthy of clinical promotion

(3) Diabetes, fatty liver, and low-density lipoprotein may be related to risk factors leading to the onset of acute hyperlipidemic pancreatitis

(4) For patients with hypertriglyceridemia pancreatitis who suffer from diabetes and fatty liver at the same time, we recommend combined therapy

Data Availability

The data used to support the findings of this study are available from the corresponding author upon request.

Conflicts of Interest

The authors declare that they have no conflicts of interest.

Acknowledgments

The authors would like to sincerely thank Dr. Jie and the staff of the Central Laboratory of Shanghai Tenth People's Hospital for their assistance.

References

[1] A. Kandemir, A. Coşkun, İ. Yavaşoğlu et al., "Therapeutic plasma exchange for hypertriglyceridemia induced acut pancreatitis: the 33 cases experience from a tertiary reference center in Turkey," *The Turkish Journal of Gastroenterology*, vol. 29, no. 6, pp. 676–683, 2018.

[2] A. Adiamah, E. Psaltis, M. Crook, and D. N. Lobo, "A systematic review of the epidemiology, pathophysiology and current management of hyperlipidaemic pancreatitis," *Clinical nutrition*, vol. 37, no. 6, pp. 1810–1822, 2018.

[3] I. Gukovsky and A. Gukovskaya, "Nuclear factor-κB in pancreatitis: jack-of-all-trades, but which one is more important," *Gastroenterology*, vol. 144, no. 1, pp. 26–29, 2013.

[4] A. Gulcubuk, D. Haktanir, A. Cakiris et al., "Effects of curcumin on proinflammatory cytokines and tissue injury in the early and late phases of experimental acute pancreatitis," *Pancreatology*, vol. 13, no. 4, pp. 347–354, 2013.

[5] M. Bhatia, M. Brady, S. Shokuhi, S. Christmas, J. P. Neoptolemos, and J. Slavin, "Inflammatory mediators in acute pancreatitis," *The Journal of Pathology*, vol. 190, no. 2, pp. 117–125, 2000.

[6] H. Gu, J. Werner, F. Bergmann, D. C. Whitcomb, M. W. Büchler, and F. Fortunato, "Necro-inflammatory response of pancreatic acinar cells in the pathogenesis of acute alcoholic pancreatitis," *Cell Death & Disease*, vol. 4, no. 10, article e816, 2013.

[7] S. Du, N. Wagner, and K. D. Wagner, "The emerging role of PPAR beta/delta in tumor angiogenesis," *PPAR research*, vol. 2020, Article ID 3608315, 16 pages, 2020.

[8] M. Botta, M. Audano, A. Sahebkar, C. R. Sirtori, N. Mitro, and M. Ruscica, "PPAR agonists and metabolic syndrome: an established role," *International journal of molecular sciences*, vol. 19, no. 4, p. 1197, 2018.

[9] D. Fanale, V. Amodeo, and S. Caruso, "The interplay between metabolism, PPAR signaling pathway, and cancer," *PPAR Research*, vol. 2017, Article ID 1830626, 2 pages, 2017.

[10] A. Sahebkar, L. E. Simental-Mendía, N. Katsiki et al., "Effect of fenofibrate on plasma apolipoprotein C-III levels: a systematic review and meta-analysis of randomised placebo-controlled trials," *BMJ Open*, vol. 8, no. 11, article e021508, 2019.

[11] R. Hoque, A. F. Malik, F. Gorelick, and W. Z. Mehal, "Sterile inflammatory response in acute pancreatitis," *Pancreas*, vol. 41, no. 3, pp. 353–357, 2012.

[12] Y. Gao, L. Hou, Y. Wang et al., "Octreotide alleviates pancreatic damage caused by paraquat in rats by reducing inflammatory responses and oxidative stress," *Environmental Toxicology and Pharmacology*, vol. 80, article 103456, 2020.

[13] M. Eriksson and B. Angelin, "How to handle hypertriglyceridaemia in acute pancreatitis - still a vote for conservatives," *Journal of Internal Medicine*, vol. 286, no. 6, pp. 723–725, 2019.

[14] L. Yang, J. Liu, Y. Xing et al., "Comparison of BISAP, Ranson, MCTSI, and APACHE II in predicting severity and prognoses of hyperlipidemic acute pancreatitis in Chinese patients," *Gastroenterology research and practice*, vol. 2016, Article ID 1834256, 7 pages, 2016.

[15] J. Zheng, J. Wu, J. Chen et al., "Therapeutic effects of quercetin on early inflammation in hypertriglyceridemia-related acute pancreatitis and its mechanism," *Pancreatology*, vol. 16, no. 2, pp. 200–210, 2016.

[16] D. Yadav and C. S. Pitchumoni, "Issues in hyperlipidemic pancreatitis," *Journal of Clinical Gastroenterology*, vol. 36, no. 1, pp. 54–62, 2003.

[17] S. Sandhu, A. Al-Sarraf, C. Taraboanta, J. Frohlich, and G. A. Francis, "Incidence of pancreatitis, secondary causes, and treatment of patients referred to a specialty lipid clinic with severe hypertriglyceridemia: a retrospective cohort study," *Lipids in Health and Disease*, vol. 10, no. 1, p. 157, 2011.

[18] K. G. Parhofer and U. Laufs, "The diagnosis and treatment of hypertriglyceridemia," *Deutsches Ärzteblatt International*, vol. 116, no. 49, pp. 825–832, 2019.

[19] T. Montalcini, T. Lamprinoudi, A. Morrone et al., "Nutrients utilization in obese individuals with and without hypertriglyceridemia," *Nutrients*, vol. 6, no. 2, pp. 790–798, 2014.

[20] T. Hackert, D. Pfeil, W. Hartwig, M. M. Gebhard, M. W. Büchler, and J. Werner, "Platelet function in acute experimental pancreatitis induced by ischaemia-reperfusion," *The British Journal of Surgery*, vol. 92, no. 6, pp. 724–728, 2005.

[21] R. Stienstra, S. Mandard, D. Patsouris, C. Maass, S. Kersten, and M. Müller, "Peroxisome proliferator-activated receptor alpha protects against obesity-induced hepatic inflammation," *Endocrinology*, vol. 148, no. 6, pp. 2753–2763, 2007.

[22] S. Kersten, "Integrated physiology and systems biology of PPARα," *Molecular metabolism*, vol. 3, no. 4, pp. 354–371, 2014.

[23] R. Kleemann, P. P. Gervois, L. Verschuren, B. Staels, H. M. Princen, and T. Kooistra, "Fibrates down-regulate IL-1-

stimulated C-reactive protein gene expression in hepatocytes by reducing nuclear p50-NFκB–C/EBP-β complex formation," *Blood*, vol. 101, no. 2, pp. 545–551, 2003.

[24] W. Wang, Q. Lin, R. Lin et al., "PPARα agonist fenofibrate attenuates TNF-α-induced CD40 expression in 3T3-L1 adipocytes via the SIRT1-dependent signaling pathway," *Experimental Cell Research*, vol. 319, no. 10, pp. 1523–1533, 2013.

[25] P. Gervois, R. Kleemann, A. Pilon et al., "Global suppression of IL-6-induced acute phase response gene expression after chronic in vivo treatment with the peroxisome proliferator-activated receptor-α activator fenofibrate," *The Journal of Biological Chemistry*, vol. 279, no. 16, pp. 16154–16160, 2004.

[26] J. Li, R. Wang, and C. Tang, "Somatostatin and octreotide on the treatment of acute pancreatitis - basic and clinical studies for three decades," *Current Pharmaceutical Design*, vol. 17, no. 16, pp. 1594–1601, 2011.

[27] R. Wang, F. Yang, H. Wu et al., "High-dose versus low-dose octreotide in the treatment of acute pancreatitis: a randomized controlled trial," *Peptides*, vol. 40, pp. 57–64, 2013.

[28] Q. Ni, L. Yun, R. Xu, and D. Shang, "Correlation between blood lipid levels and chronic pancreatitis: a retrospective case-control study of 48 cases," *Medicine (Baltimore)*, vol. 93, no. 28, article e331, 2014.

[29] M. M. Hartge, T. Unger, and U. Kintscher, "The endothelium and vascular inflammation in diabetes," *Diabetes & Vascular Disease Research*, vol. 4, no. 2, pp. 84–88, 2007.

[30] A. Kontush and M. J. Chapman, "Functionally defective high-density lipoprotein: a new therapeutic target at the crossroads of dyslipidemia, inflammation, and atherosclerosis," *Pharmacological Reviews*, vol. 58, no. 3, pp. 342–374, 2006.

Hindawi
PPAR Research
Volume 2021, Article ID 6663782, 20 pages
https://doi.org/10.1155/2021/6663782

Research Article

Fenofibrate Exerts Antitumor Effects in Colon Cancer via Regulation of DNMT1 and CDKN2A

Rui Kong, Nan Wang, Wei Han, Wen Bao, and Jie Lu

Department of Gastroenterology, Shanghai Tenth People's Hospital Affiliated to Tongji University, Tongji University, School of Medicine, Shanghai 200072, China

Correspondence should be addressed to Jie Lu; kennisren@hotmail.com

Received 17 October 2020; Revised 25 February 2021; Accepted 5 April 2021; Published 19 April 2021

Academic Editor: Stéphane Mandard

Peroxisome proliferator-activated receptor alpha (PPARA) is the molecular target of fibrates commonly used to treat dyslipidemia and diabetes. Recently, the potential role of PPARA in other pathological conditions, such as cancers, has been recognized. Here, using bioinformatics analysis, we found that PPARA was expressed at relatively low levels in pancancers, and Kaplan-Meier analyses revealed that high PPARA protein expression was correlated with better survival of patients with colon cancer. *In vitro* experiments showed that fenofibrate regulated cell cycle distribution, promoted apoptosis, and suppressed cell proliferation and epithelial mesenchymal transition by activating PPARA. PPARA activation inhibited DNMT1 activity and abolished methylation-mediated CDKN2A repression. Downregulation of cyclin-CDK complexes led to the restoration of CDKN2A, which caused cell cycle arrest in the G1 phase via regulation of the CDKN2A/RB/E2F pathway. Finally, we demonstrated that fenofibrate administration inhibited tumor growth and DNMT1 activity *in vivo*. The PPARA agonist, fenofibrate, might serve as an applicable agent for epigenetic therapy of colon cancer patients.

1. Introduction

Colorectal cancer (CRC) ranks third in terms of morbidity and fourth in terms of mortality. CRC is also the most common type of cancer worldwide, with almost 900,000 deaths each year [1, 2]. Although new treatment options, including immunotherapy and neoadjuvant chemotherapy, have significantly improved patient prognosis, the 5-year survival rate of CRC remains below 15% [3]. Thus, investigations of the molecular mechanisms involved in cancer initiation are necessary to develop new therapeutic strategies.

In addition to genetic alterations (i.e., deletion, amplification, and translocation), epigenetic modifications play an important role in malignant progression of tumors. CpG islands (CGI) are contiguous groups of dinucleotides mainly located at the 5′ end of a gene and are characterized by high GC content [4]. Most CGIs in gene promoters are unmethylated, allowing active transcription [5]. CGI methylation changes are hallmarks of many human cancers and lead to concomitant gene inactivation [6–8]. DNA methyltransferase 1 (DNMT1) is a major DNA methyltransferase responsible for methylation maintenance during DNA replication, and inactivation of DNMT1 in mice results in early embryonic lethality [9]. DNMT3a and DNMT3b mainly act as de novo methyltransferases [10].

CRCs are characterized by lower levels of absolute genomic methylation compared with normal tissues, a characteristic that contributes to high genomic instability and results in cancer development [11]. In addition, promoter hypermethylation of specific genes has been identified in CRCs, as well as methylated CGIs that are associated with gene silencing. Hypermethylation in several tumor suppressor genes such as RASSF1, PTEN, and CDKN2A is associated with abnormal cellular activities, including aberrant cell aging, proliferation, and death [12–14].

Peroxisome proliferator-activated receptor alpha (PPARA) is a ligand-activated transcription factor that belongs to the nuclear hormone receptor superfamily [15, 16]. Studies have demonstrated that PPARA plays a critical role in lipid metabolism and the inflammatory response [17, 18]. Fenofibrate is a selective PPARA agonist that regulates lipid transport and metabolism, and is widely used in the treatment of

hyperlipidemia [19]. In addition to the metabolic efficacy, recent studies have revealed the antitumor function of PPARs [20–24]. Studies have also confirmed the oncosuppressive effect of fenofibrate in various human cancer cell lines through different signaling pathways [25–27]. Reports also revealed the inhibitory role of PPARA on DNMT1 activity in mouse models [28]. In the present study, we demonstrated that the PPARA agonist, fenofibrate, inhibited DNMT1-mediated methylation of CDKN2A and exerted anticancer effects by promoting cell apoptosis, inhibiting cell migration, and suppressing cell proliferation via the CDKN2A/RB/E2F pathway.

2. Materials and Methods

2.1. Cell Culture. The colorectal cancer cell line HCT116, the colon cancer cell lines SW480 and Caco-2, and the two normal intestine epithelial cell lines NCM460 and HIEC were obtained from Chinese Academy of Sciences Committee Type Culture Collection Cell Bank (Beijing, China). HCT116 was cultured in complete DMEM (Thermo Fisher Scientific, Waltham, MA), and the other cell lines were maintained in RPMI 1640 (Thermo Fisher Scientific, Waltham, MA) supplemented with 10% fetal bovine serum (FBS, Thermo Fisher Scientific, Waltham, MA) and 1% penicillin-streptomycin.

Inhibition of DNMT1 activity was conducted using 5 μM 5-azacytidine (MedChemExpress, Shanghai, China), and the treatment time was 24 h. The pcDNA DNMT1 was transfected into HCT116 and SW480 cells for upregulation of DNMT1 expression. The pcDNA DNMT1 were synthesized by GenePharma Co. Ltd. (Shanghai, China).

Cells were exposed to different concentrations of fenofibrate (Topscience Co., Ltd., Shanghai, China) for 48 hours, and morphology changes were observed using a phase-contrast microscope and imaged (200x).

2.2. Cell Viability Assay. Colon cancer cell lines SW480 and the colorectal cancer cell line HCT116 were plated at a density of 5000 cells/mL in 96-well plates (100 μL medium per well) with three replicates. Cells were treated with fenofibrate in the pharmacologic concentration range 0–260 μM for 24 h and 48 h. Cell viability was detected using the cell counting kit (YEASEN, Shanghai, China) according to the instructions.

2.3. Colony Formation Assay. Cells were trypsinized, counted, and seeded in a 6-well plate at 700 cells per well, treated with different concentrations of fenofibrate. After 14 days, the visible colonies were counted and photographed.

2.4. Wound Healing Assay. HCT116 and SW480 cells were grown on 6-well plates. Scratch was made using a 200 μL pipette tip when the cell confluence reached 80%-90%. After scratching, cells were washed with phosphate-buffered saline and then cultured in serum-free medium. The healing rate was quantified with measurements of the gap size after the culture using ImageJ software.

2.5. Cell Immunofluorescence. HCT116 and SW480 cells were seeded in 6-well culture plates plated with cell climbing slices. After being treated with fenofibrate for 24 h, cells were fixed with 4% paraformaldehyde and permeabilized with 0.1% Triton X-100. Then, cells were incubated with primary antibodies (E-cadherin, vimentin, PCNA). The chromosomes were counter-stained with DAPI (Beyotime, Shanghai, China). Images were viewed with a fluorescent microscope.

Apoptosis was analyzed by means of TUNEL assay using the EdUTP TUNEL cell detection kit (Beyotime, Shanghai, China) according to the manufacturer's instructions. Photomicrographs were taken under confocal microscopy.

2.6. EDU Staining. 5-Ethynyl-2′-deoxyuridine (EdU) staining assay was carried out on fenofibrate-treated cells utilizing an EdU immunofluorescence staining kit (Ribobio, China) according to the manufacturer's instructions [29]. The results were observed using an inverted fluorescence microscope (200x).

2.7. Flow Cytometry Analysis. HCT116 and SW480 cell lines were treated with various doses of fenofibrate for 24 h, then stained with annexin V FITC and propidium iodide (PI) (BD Biosciences, San Jose, CA). Cell apoptosis was analyzed by flow cytometry (Cytomics FC500; Beckman Coulter, Fullerton, CA).

The distribution of cell cycle phases was analyzed by the cell cycle detection kit (Beyotime, China). Samples were fixed with 75% ethanol at −20°C for 24 h. The fixed cells were treated with RNaseA and stained with propidium iodide following the manufacturer's instruction [30]. The cell cycle analysis was studied by flow cytometry.

2.8. Animal Experiments. Animal experiments were performed according to the National Institutes of Health Guidelines for the Care and Use of Laboratory Animals and were approved by the Animal Care and Use Committee of Shanghai Tongji University, China. The nude mice were randomly divided into 2 groups ($n = 6$), and each mouse was subcutaneously injected with 2×10^7 HCT116 cells in the right axilla. Fenofibrate was suspended in saline and intragastrically administered at 200 mg/kg per mouse once a day. Mice were anesthetized and sacrificed three weeks after fenofibrate administration. Tumor size and mouse weight were recorded during the experiment. Tissues were harvested for further analysis.

Xenografted tissues were fixed with 4% paraformaldehyde and embedded in paraffin, sectioned, and stained with hematoxylin and eosin. Histopathological changes were observed by microscopy (200x).

2.9. DNMT1 Content. The measurement of DNMT1 content in fenofibrate-treated cells or tumor tissues was conducted using Human or Mouse DNMT1 ELISA kit (HZBIO, Shanghai, China). Samples were added to each well in enzyme-labeled coated plates and incubated at 37°C for 30 minutes. After washing, coloration was developed using chromogen reagents A and B; then, the reaction was terminated by stop solution. The absorbance value was measured at 450 nm wavelength using a microplate reader (BioTek microplate reader).

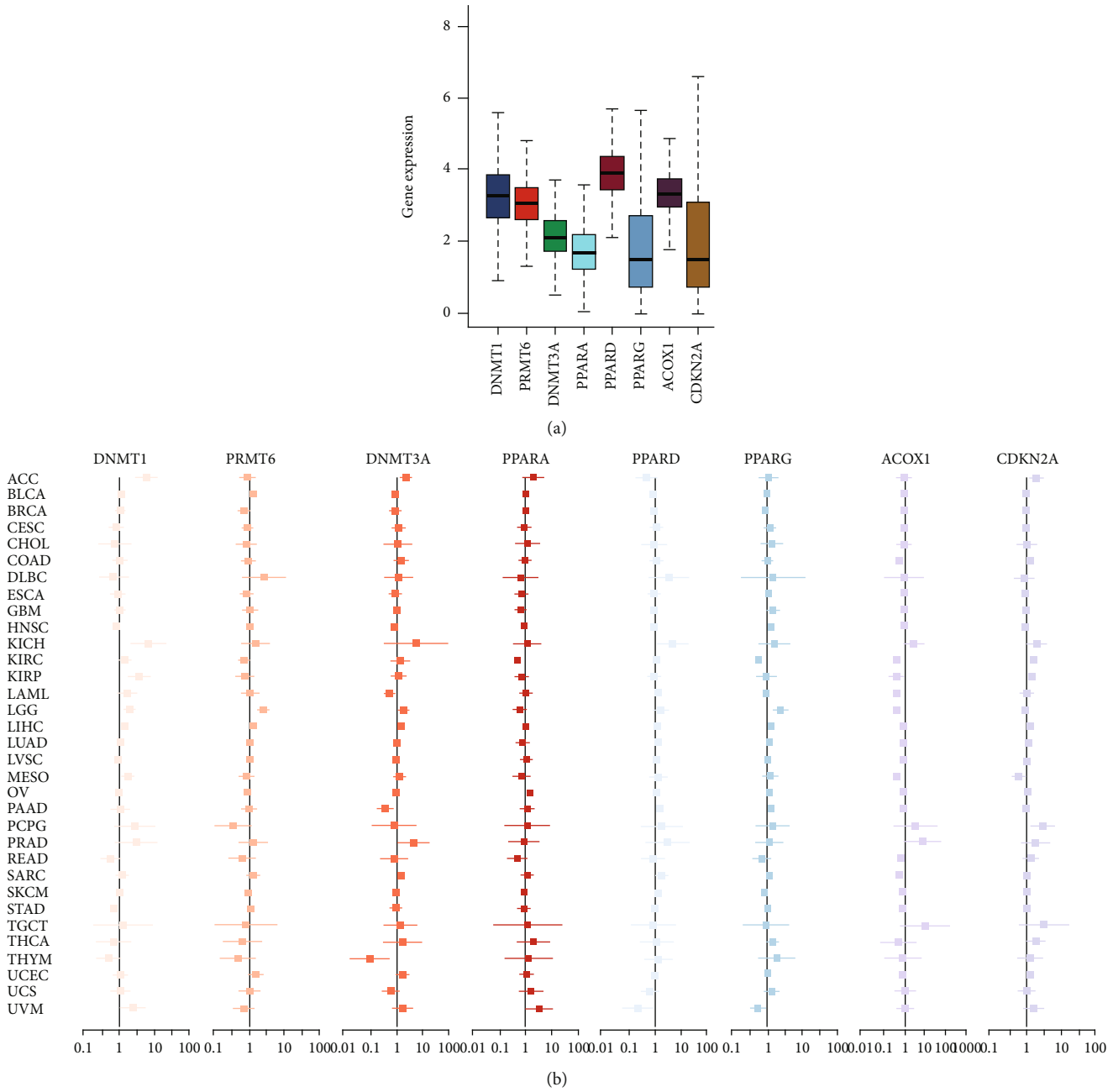

Figure 1: Continued.

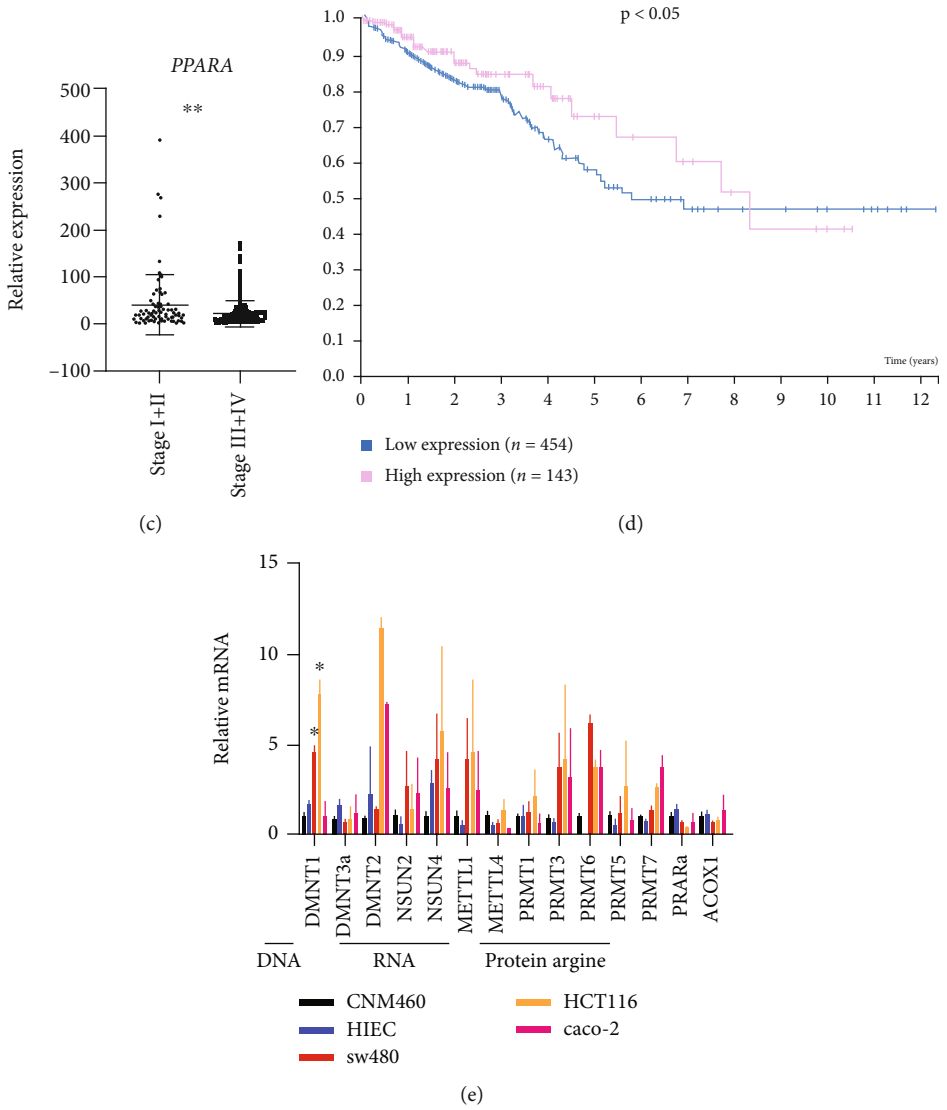

Figure 1: Bioinformatics analysis of PPARA in pancancer: (a) the box plot showing the expression levels of PPARs, DNMT1, PRMT6, ACOX1, and CDKN2A in tumorous tissues; (b) the forest graph showing the hazard ratio of PPARs, ACOX1, CDKN2A, methylation transferase DNMT1, DNMT3a, and PRMT6 in various cancers; (c) box plots of PPARA expression detected in RNA-seq in colon cancer specimens grouped into stage I + II and stage III + IV; (d) survival curve of patients with different PPARA protein expression levels in colon cancer ($P < 0.05$); (e) the relative mRNA expression of PPARA, ACOX1, and methylation transferases was measured using qRT-PCR in SW480, HCT116, Caco-2, HIEC, and NCM460 cell lines. The data is expressed as mean ± SD ($^*P < 0.05$, $^{**}P < 0.01$, $^{***}P < 0.001$).

2.10. Methylation-Specific PCR. Genomic DNA was extracted using a genomic DNA extraction kit (TIANGEN). Eluted DNA (20 μL) was subjected to bisulfite modification using the EpiTect Fast Bisulfite Conversion Kit (Qiagen). Methylation status of CDKN2A promoter was analyzed using the methylation-specific primers (M) and nonmethylation-specific primers (U). The amplification products were separated by agarose gel electrophoresis and visualized by SYBR Green staining under UV light. Primers (Table S1) used in methylation-specific PCR (MSP) were the same as the sequences described by Herman et al. [31].

2.11. Bioinformatics Analysis of Human Tumor Samples from TCGA Dataset. RNA sequencing profiles and relevant clinical information of pancancer samples were retrieved from The Cancer Genome Atlas (TCGA) data portal in October, 2020. RNA-seq data was normalized by fragments per kilobase per million (FPKM) using log2 scale. Transcription levels of DNMT1, DNMT3a, DNMT3b, PPARs, ACOX1, and CDKN2A were analyzed. Survival probabilities were computed by the Kaplan-Meier method. In addition, Cox regression analysis was conducted to calculate the hazard ratios of genes of interest in multiple cancer types. Moreover, the correlation between clinical stage and gene expression was evaluated via "ggpubr" package in R.

2.12. Western Blot Analysis. Total protein from cells or tissues was extracted using RIPA lysate (Invitrogen, USA). Equal amount of protein samples (40 μg for cell samples per lane and 80 μg for tissue samples per lane) was run on

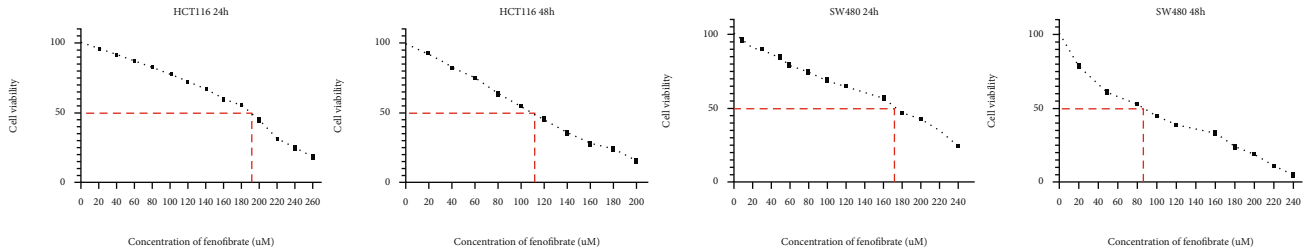

(a)

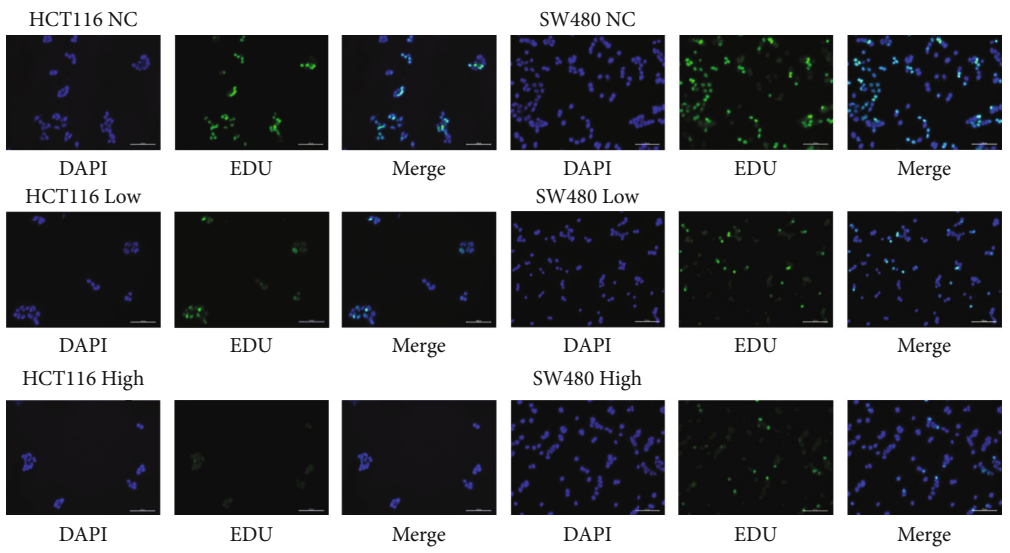

(b)

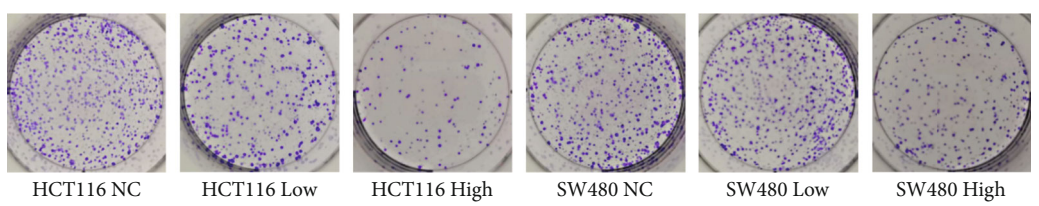

(c)

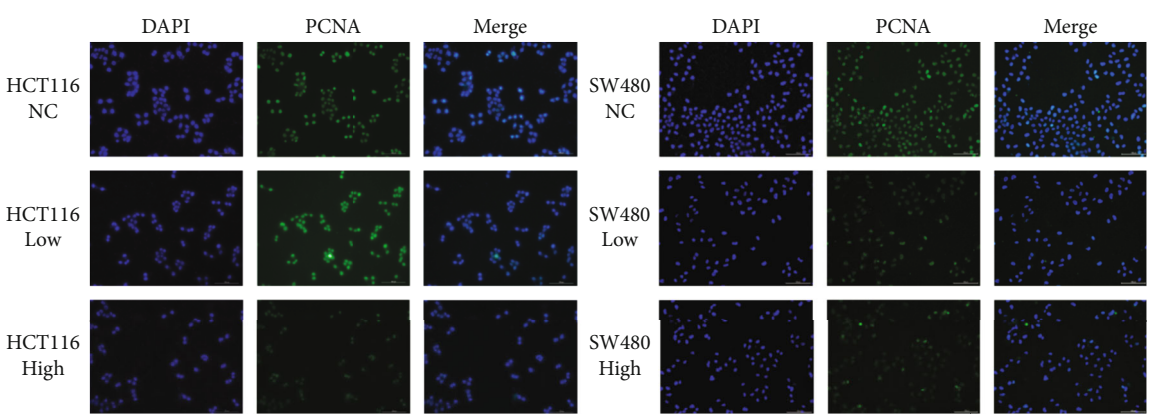

(d)

Figure 2: Continued.

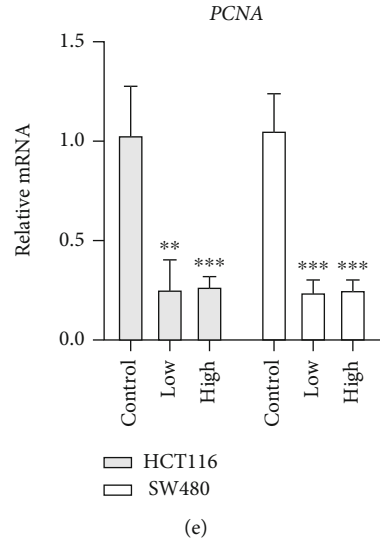

Figure 2: Fenofibrate administration inhibited colon cancer cell proliferation. (a) HCT116 and SW480 cells were treated with a range of concentrations of fenofibrate for 24 h. Cell viability was detected using CCK8. (b) EDU staining of cells was observed after incubation with fenofibrate for 24 h (magnification 200x). Box plot showing the statistics of fluorescence intensity. (c) Colony formation of cancer cells with or without fenofibrate treatment. (d) The PCNA immunofluorescence staining results of cells (magnification 200x). (e) The mRNA expression level of PCNA was measured following fenofibrate treatment. Data was presented as mean ± SD. The experiment was repeated three times with three replicates per experiment ($^{*}P < 0.05$, $^{**}P < 0.01$, $^{***}P < 0.001$).

sodium dodecylsulfate-polyacrylamide (SDS) gel and then transferred to polyvinylidene difluoride (PVDF) membranes. Membranes were blocked with 5% nonfat milk for 1 h and then incubated overnight at 4°C with primary antibodies. Anti-DNMT1 (1 : 500, Abcam, Cambridge, UK), anti-PPARA (1 : 1000, Abcam, Cambridge, UK), anti-E2F1 (1 : 500, Cell Signaling Technology, Danvers, MA), anti-pRb (1 : 500, Cell Signaling Technology, Danvers, MA), anti-CDKN2A (1 : 500, Cell Signaling Technology, Danvers, MA), anti-CyclinD1 (1 : 1000, Cell Signaling Technology, Danvers, MA), anti-CDK4 (1 : 1000, Cell Signaling Technology, Danvers, MA), anti-CDK6 (1 : 1000, Cell Signaling Technology, Danvers, MA), and anti-RB (1 : 200, Santa Cruz Biotechnology, CA) antibodies were used in this experiment. Then, the PVDF membranes were incubated with corresponding secondary antibodies at room temperature for 1 h. Primary and secondary antibody diluent for WB was used in this experiment (YEASEN, Shanghai, China). Signals were detected using the Odyssey Two-color Infrared Laser Imaging System (Li-Cor, Lincoln, NE).

2.13. Quantitative Real-Time PCR Analysis. Total RNA from cells or tissues was extracted using the TRIzol reagent according to the manufacturer's instructions. Approximately 500 ng of extracted RNA was used to synthesize cDNA using the reverse transcription kit (TaKaRa Biotechnology, Dalian, China). Quantitative PCR was carried out in the Applied Biosystems 7500 Real-Time PCR System using 50 ng of cDNA and a SYBR Green PCR master mix (YEASEN, Shanghai, China). Relative gene expression was calculated based on $2^{\triangle\triangle CT}$ algorithm. All the primers were designed using the principle of span exons to avoid genomic DNA contamination. Primer sequences utilized in this study are provided in Table S2.

2.14. Statistical Analyses. Two-group comparisons were analyzed by Student's *t*-test; multigroup comparisons were analyzed via one-way ANOVA. Spearman's correlation analysis was performed to evaluate expression correlation. Kaplan-Meier analysis was carried out to analyze overall survival. Multivariate analysis was performed using the Cox multivariate regression analysis model. P values < 0.05 were considered statistically significant. Statistical analysis was performed with SPSS 17.0 software (IBM).

3. Results

3.1. Analysis of Gene Expression Patterns of PPARA and DNA Methyltransferase in Human Colon Cancer. First, we performed pancancer analyses to identify the mean expression levels of PPARs in different types of tumors. The results indicated that PPARA was lowly expressed in tumorous tissues, as shown in Figure 1(a). Subsequently, the Cox proportional hazards regression analysis was used to evaluate PPARs as prognostic markers in various tumors. Genes with a hazard ratio (HR) > 1 were significantly correlated with patient outcome. The forest plot in Figure 1(b) shows that in most cancer types, PPARs, including PPARA, may serve as a prognostic indicator of digestive tract cancers. Subsequently, we focused on the clinical significance of PPARA expression. PPARA was downregulated in colon cancer and correlated with TNM stage in the TCGA COAD dataset (Figure 1(c)). Furthermore, following the evaluation of PPARA protein levels, the prognosis of patients with high PPARA or low PPARA expression revealed that higher expression exhibited a better prognosis (Figure 1(d)).

Recent reports have demonstrated that DNA hypermethylation of tumor suppressor genes contributes to cancer progression. In the current study, the mean expression levels

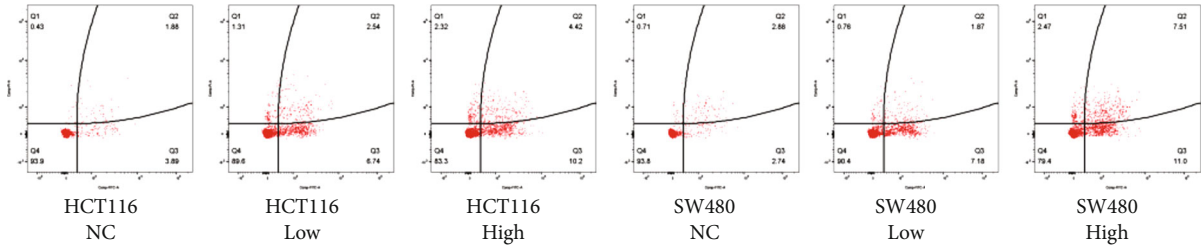

(a)

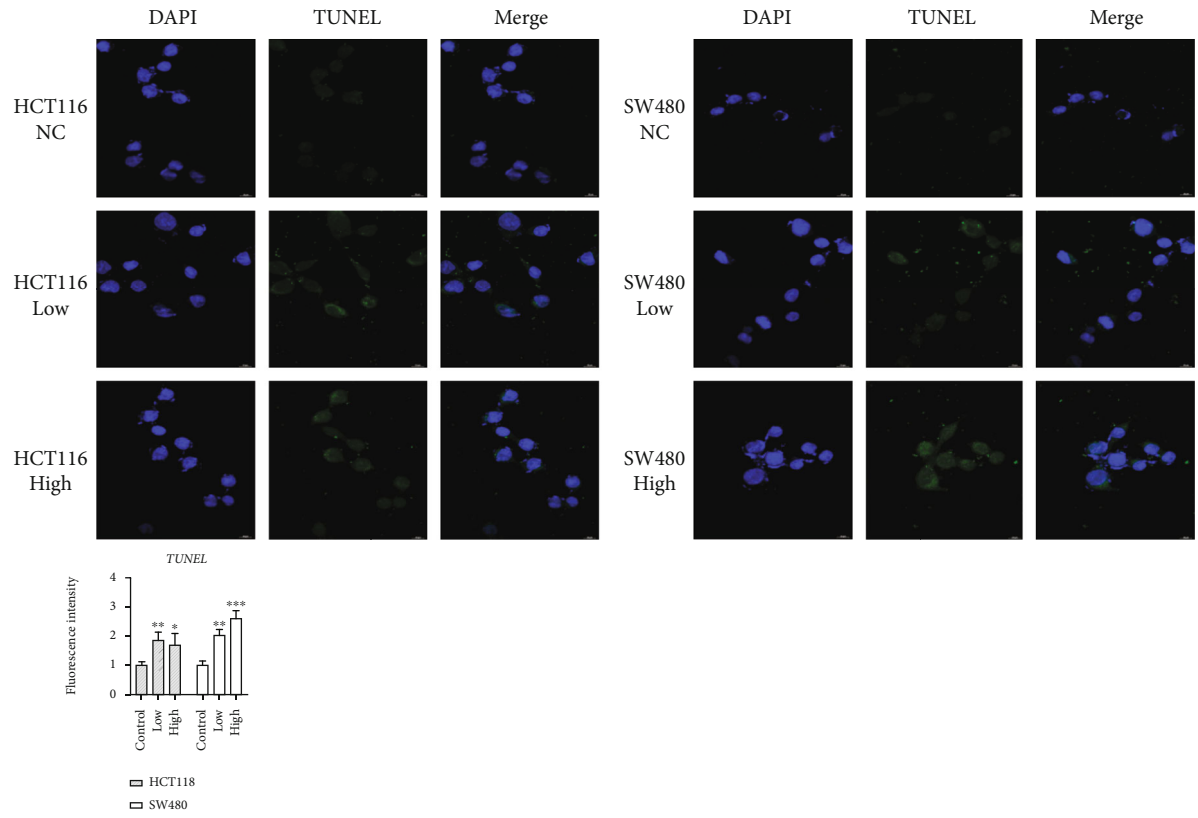

(b)

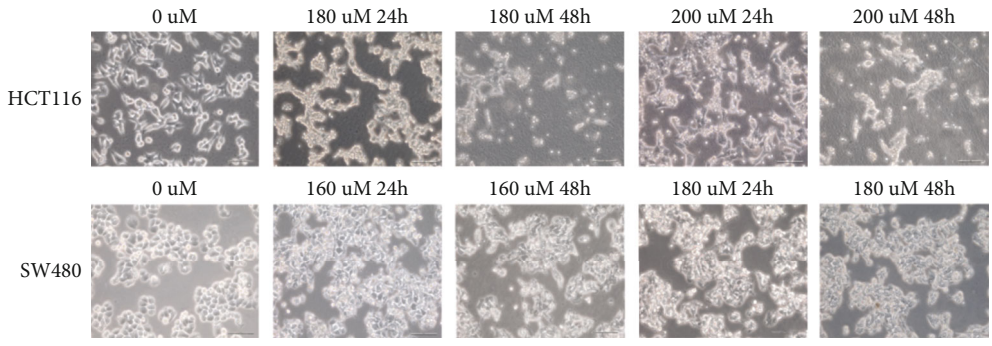

(c)

Figure 3: Continued.

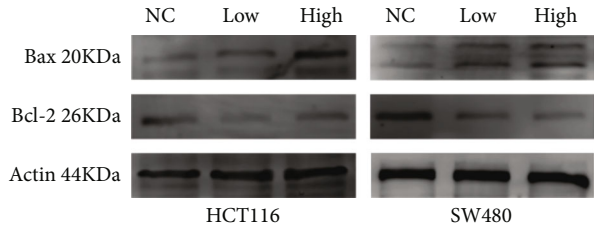

(d)

Figure 3: Fenofibrate treatment promoted colon cancer cell apoptosis. (a) Cell apoptosis was analyzed using flow cytometry. (b) TUNEL staining of colon cancer cells was observed after treatment of fenofibrate for 24 h. TUNEL-stained (green) cells indicate apoptosis-positive cells, DAPI (blue) indicates nucleated cells, and the merge column shows cells stained with TUNEL and DAPI. (c) Morphological changes were observed of HCT116 and SW480 cells after treatment of fenofibrate for 24 h. (d) The protein expression of Bax and Bcl-2 in SW480 and HCT116 cells was measured using western blot.

of the DNA methyltransferases DNMT1 and DNMT3a and the protein arginine methyltransferase, PRMT6, were evaluated in pancancers using bioinformatics analyses. High levels of several methyltransferases were observed in various tumor tissues (Figure 1(a)). The forest graph indicated the prognostic value of DNMT1 in most cancers, with an HR > 1 (Figure 1(b)). In addition, colon cancer cell lines with high endogenous expression of methyltransferases and low endogenous expression of PPARA relative to normal NCM460 and HIEC cells were selected for further *in vitro* assays (Figure 1(e)).

3.2. The PPARA Agonist, Fenofibrate, Attenuated Cell Viability and Proliferation. The effect of the PPAR agonist on colon cancer cell proliferation was assessed by treating 5000 cells with various concentrations of fenofibrate (0–300 μmol/L) for 24 and 48 h. Cell survival was determined using the CCK8 kit. As shown in Figure 2(a), fenofibrate exerted an inhibitory effect on cell proliferation in HCT116 cells with an IC50 range of 180–200 μmol/L (24 h) and 100–120 μmol/L (48 h); fenofibrate also exerted an inhibitory effect on cell proliferation in SW480 cells, with an IC50 range of 160–180 μmol/L (24 h) and 80–100 μmol/L (48 h).

We selected suitable concentrations of fenofibrate (180 and 200 μmol/L for HCT116 cells and 160 and 180 μmol/L for SW480 cells) for subsequent treatments. After incubation with fenofibrate for 24 h, cells were stained with EDU (green) and DAPI (blue). Treatment of fenofibrate decreased the proportion of cells with green fluorescence in a dose-dependent manner ($P < 0.05$) (Figure 2(b)). To further demonstrate the inhibitory effect of fenofibrate on cell growth, the colony formation assay was employed. Treatment of HCT116 and SW480 cells with different doses of fenofibrate reduced clone numbers, especially in the high-dose group (Figure 2(c)). The expression level of PCNA, an endogenous marker of mitogenesis, was detected between the low-dose, high-dose, and vehicle-treated groups using qRT-PCR and immunofluorescence staining. Reduced PCNA mRNA level and protein level upon fenofibrate treatment suggested the suppressive regulation of cell proliferation by fenofibrate (Figures 2(d) and 2(e)).

3.3. The PPAR Agonist, Fenofibrate, Promoted Cell Apoptosis In Vitro. To investigate whether PPARA activation promoted cell apoptosis *in vitro*, colon cancer cells with or without fenofibrate treatment were assessed by flow cytometry. The data suggested that fenofibrate increased cell apoptosis and, in particular, late apoptosis rates (Figure 3(a)). Subsequently, we confirmed the proapoptotic effects of fenofibrate using TUNEL staining, which detects the DNA breaks in apoptotic cells. Figure 3(b) shows that fenofibrate administration increased the number of positively stained cells (green fluorescence). Moreover, the changes in cell shape after incubation with fenofibrate was examined using light microscopy. The number of shedding cells was increased, accompanied with morphological deformation and crumpled appearances. Such morphological changes were observed in a time- and dose-dependent manner (Figure 3(c)). The expression level of Bax, a typical apoptosis-related protein which promotes apoptosis was increased by treatment with fenofibrate, while prosurvival protein Bcl-2 was decreased as shown by western blotting (Figure 3(d)).

3.4. The PPAR Agonist, Fenofibrate, Inhibited Cell Migration and Epithelial Mesenchymal Transition. Cell migration was measured using the wound healing assay in fenofibrate-treated cells. Data from the scratch healing assay are shown in Figure 4(a). Fenofibrate significantly reduced the migratory capacity of CRC cells, which exhibited delays in the closure of scratches. Next, we examined whether there was a repressive effect of PPARA activation on epithelial mesenchymal transition (EMT). The expression of several EMT biomarkers of EMT was tested using qRT-PCR (Figure 4(b)). The mRNA levels of vimentin and MMP9 in the fenofibrate-treated group were reduced, while E-cadherin levels were upregulated. To further confirm the findings, expression changes in the EMT-associated markers induced by fenofibrate were examined using immunofluorescence, and similar results were observed (Figure 4(c)). Taken together, PPARA activation could exert an antitumor effect by restraining cell migration and EMT.

3.5. The PPAR Agonist, Fenofibrate, Enhanced Tumor Suppressor Gene Expression and Repressed DNMT1 Content. The research of Luo et al. [28] substantiated that the loss of PPARA resulted in abnormal expression of several methyltransferases and promoted CRC progression in a mouse model. Therefore, we hypothesized that the PPARA agonist,

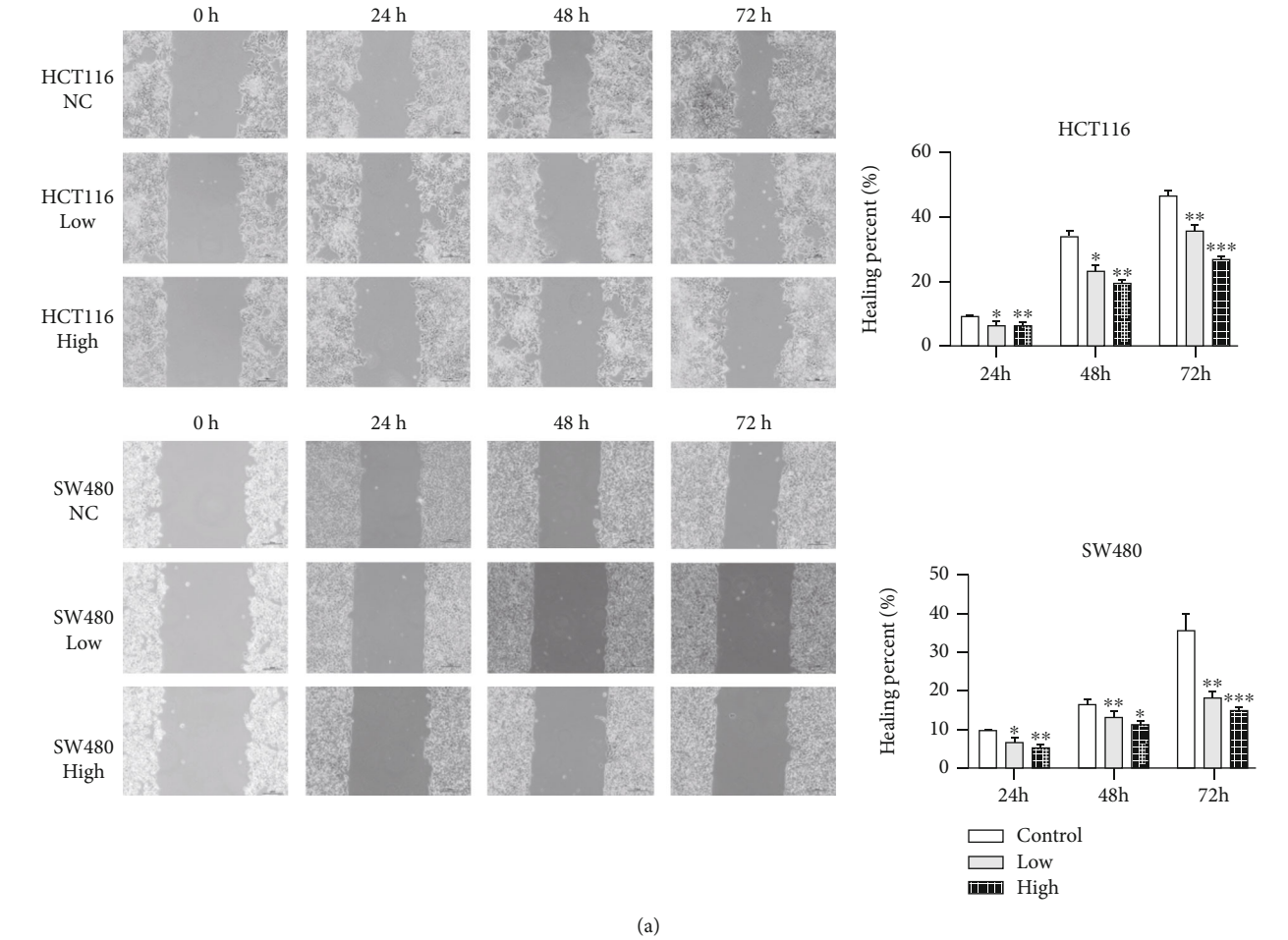

(a)

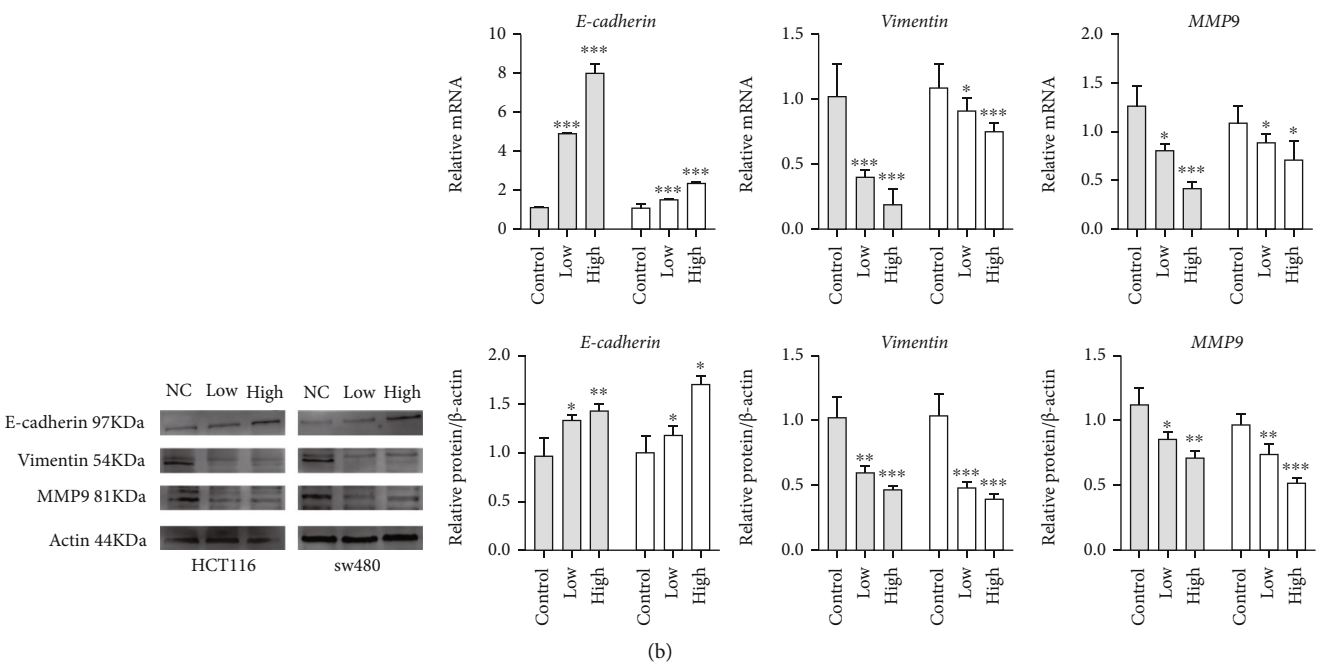

(b)

Figure 4: Continued.

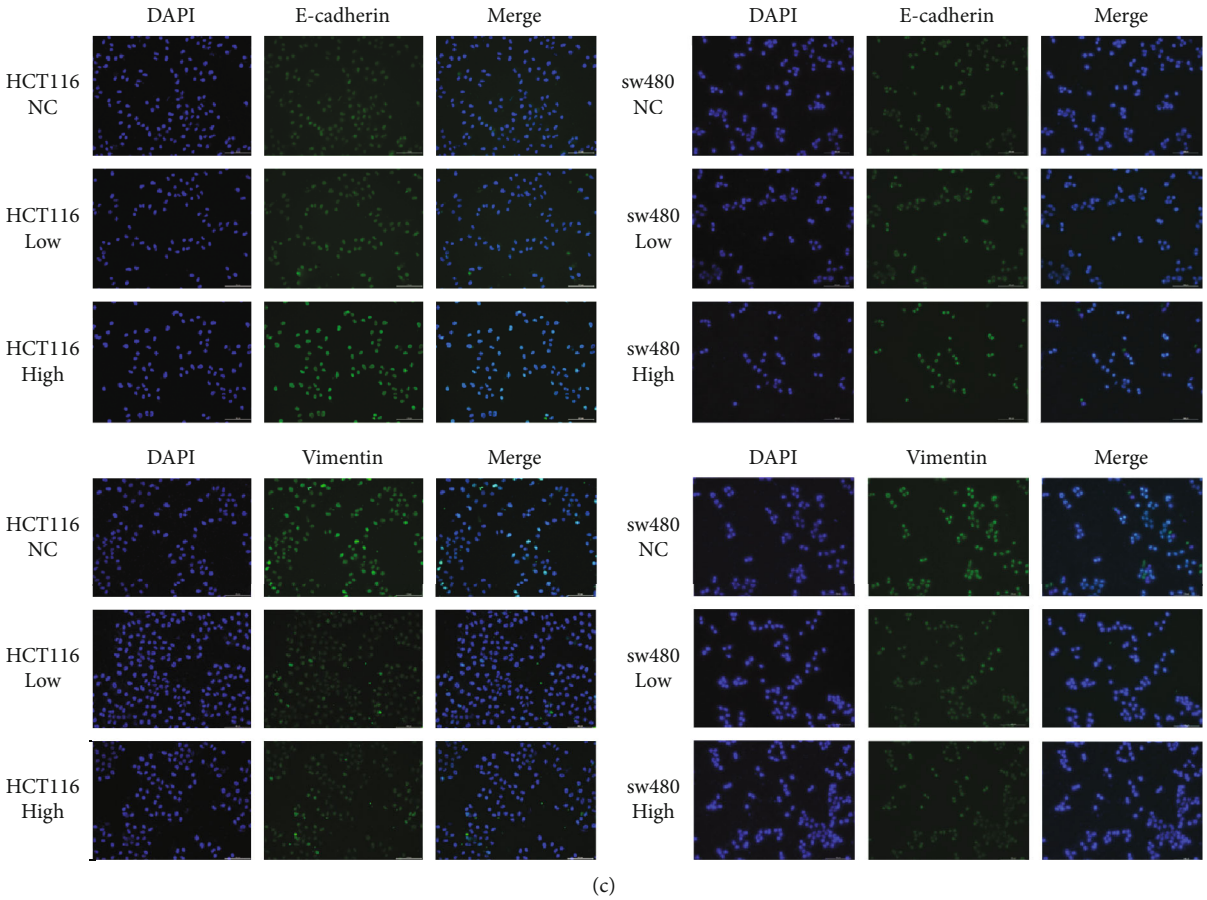

Figure 4: Fenofibrate inhibited cell migration and EMT. (a) Wound healing assay for demonstrating the inhibitory effect of fenofibrate on the migration of colon cancer cells at 0, 24, 48, and 72 h following wounding. (b) The mRNA and protein expression levels of E-cadherin, vimentin, and MMP9 were measured following fenofibrate treatment. Data was presented as mean ± SD ($^{*}P < 0.05$, $^{**}P < 0.01$, $^{***}P < 0.001$). (c) The expression of E-cadherin and vimentin in colon cancer cells was examined using immunofluorescence staining (magnification 200x).

fenofibrate, could reduce the content of DNMT1 and rescue the expression of methylation-silenced tumor suppressor genes. First, we found using qRT-PCR that the DNMT1 mRNA level decreased when PPARA was activated following fenofibrate treatment (Figure 5(a)).

Next, the expression of several tumor suppressor genes was determined (Figure 5(b)). It has been documented that the expression of silenced genes is correlated with promoter hypermethylation. Studies showed that p21, p27, CDKN2A, MLH1, and RASSF1A were reactivated in two cancer cell lines after fenofibrate treatment. We further discovered that the expression of the upstream regulators of DNMT1, Oct4, Nanog, and Sox9 was decreased in fenofibrate-treated cells and were correlated with stemness. In addition, we measured the DNMT1 enzyme content in colon cancer cells and found a significant reduction in enzyme concentration upon high-dose treatment of fenofibrate (Figure 5(c)).

3.6. Fenofibrate Recovered the Expression of CDKN2A via Downregulation of DNMT1. To determine the mechanisms of fenofibrate treatment on the demethylation of the CDKN2A promoter, MSP was carried out to evaluate the methylation status of the CDKN2A promoter. In the Figure 6(a), M and U referred to the PCR products of methylated and unmethylated alleles, respectively. Analyses showed that in the fenofibrate-free group, a methylation product was observed, while no band was observed in the fenofibrate-treated group. Thus, we inferred that the methylation status of the promoter was abolished by fenofibrate treatment (Figure 6(a)).

5-Azacytidine is an effective inhibitor of DNMT1. To investigate the effects of the overexpression or downexpression of DNMT1 on CDKN2A, colon cancer cells were treated with 5-azacytidine, DNMT1 overexpression plasmid, and fenofibrate. The results showed that DNMT1 downexpression resulted in increased CDKN2A mRNA and protein levels, while DNMT1 overexpression caused a decreased level of CDKN2A (Figures 6(b) and 6(c)). The expression changes of CDKN2A induced by 5-azacytidine could be enhanced by fenofibrate treatment. In addition, fenofibrate could reverse the low expression of CDKN2A caused by DNMT1 overexpression plasmid. Taken together, these findings indicated that the PPARA agonist, fenofibrate, could upregulate the expression of CDKN2A by inhibiting gene hypermethylation mediated by DNMT1.

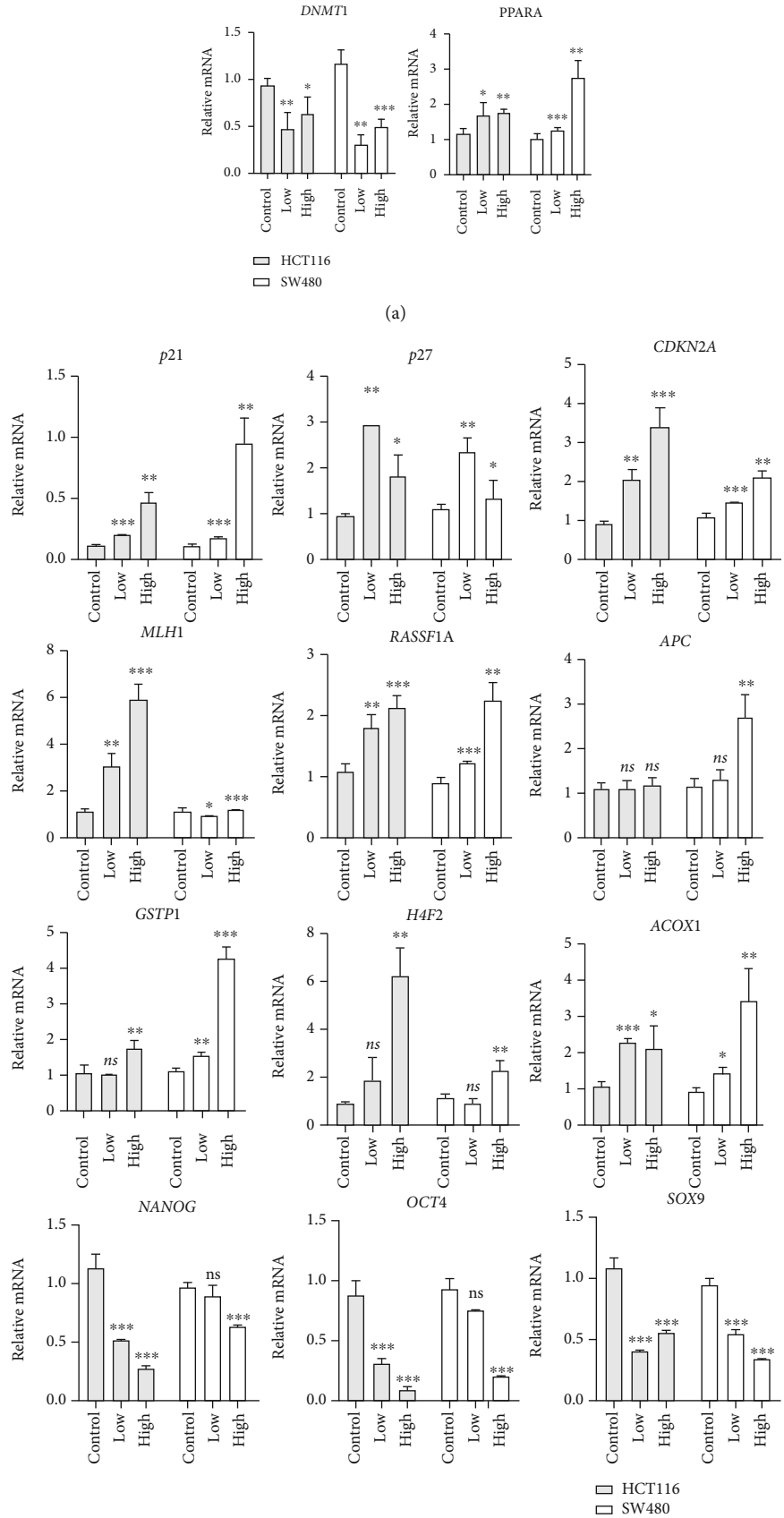

Figure 5: Continued.

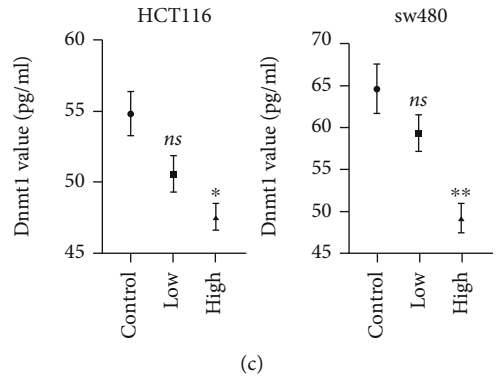

Figure 5: Fenofibrate decreased the content of DNMT1 and increased the expression of tumor suppressor genes. (a) qRT-PCR analysis of DNMT1 and PPARA mRNA expression in HCT116 and SW480 cells following fenofibrate treatment. Data was presented as mean ± SD ($^{*}P < 0.05$, $^{**}P < 0.01$, $^{***}P < 0.001$). (b) The mRNA expression of p21, p27, CDKN2A, MLH1, RASSF1A, APC, GSTP1, H4F2, ACOX1, Oct4, Nanog, and Sox9 was measured. Data was presented as mean ± SD ($^{*}P < 0.05$, $^{**}P < 0.01$, $^{***}P < 0.001$). (c) DMNT1 value was measured using ELISA kit. Data was presented as mean ± SD ($^{*}P < 0.05$, $^{**}P < 0.01$, $^{***}P < 0.001$).

3.7. Fenofibrate Regulates the Cell Cycle via the CDKN2A/RB1/E2F1 Pathway. DNMT1 is responsible for maintaining DNA methylation after each round of the cell cycle. CDKN2A, a CDK inhibitor, acts as a negative regulator of cell cycle process. In the current study, fenofibrate administration suppressed the expression of DNMT1 and relieved the DNMT1-mediated silencing of CDKN2A. Therefore, we investigated the molecular mechanism by which fenofibrate regulated cell cycle distribution. PI staining was conducted on control and drug-treated cells, and the results of cell cycle analysis are shown in Figure 7(a). Fenofibrate treatment suppressed the G1→S transition, induced G0/G1 phase cell arrest, and blocked S phase entry. Since the activity of the cyclin D/CDK4/CDK6 complex is essential to the G1/S transition and can be inhibited by CDK inhibitors, we detected the changes in expression of cyclinD1, CDK4, and CDK6 in cells following fenofibrate treatment. The results from western blot and qRT-PCR analyses suggested that fenofibrate induced the activation of CDKN2A, resulting in low expression levels of CDKs (Figures 7(b) and 7(c)). During the G1 phase, the level of E2F1 was upregulated by the activated cyclin-CDK complex and was released from the RB/E2F contigs in response to abnormal growth stimulation.

To further validate our findings, the expression of key factors involved in the RB/E2F signaling pathway was examined. The expression of total RB was upregulated, while the levels of phosphorylated RB and E2F1 were reduced following fenofibrate treatment. These results demonstrated that fenofibrate treatment decreased the protein and transcript levels of pRB and E2F through the downregulation of cyclin-CDKs by activated CDKN2A.

3.8. The PPAR Agonist, Fenofibrate, Inhibited Tumor Growth in an Animal Model. We established an animal model of HCT116 cell-bearing nude mice. When tumor tissues reached an average volume of 1 mm^3, mice were randomized into two groups. Mice in the treatment group received 200 mg/kg fenofibrate suspended in 200 μL saline by gavage every day. The control group was gavaged with an equal volume of saline. All mice bearing tumors survived during the experiment. Tumor size was significantly smaller in the drug-treated group compared to the cancer group.

The weight of each mouse was recorded twice weekly, and the data are shown in Figure 8(a). Tumor xenografts were sectioned and stained with H&E to observe the pathological changes. Slides from fenofibrate-treated tissues revealed necrotic lesions (Figure 8(b)). DMNT1 content in tissue homogenates was measured by an ELISA assay. Following fenofibrate treatment, DNMT1 enzyme level in tissues from the treatment group was lower than that from the vehicle group (Figure 8(c)). Additionally, fenofibrate significantly downregulated the mRNA and protein levels of DNMT1 and CDK4 and increased the expression levels of PPARA and CDKN2A (Figures 8(d) and 8(e)). Taken together, PPARA activation suppressed tumors *in vivo* by upregulating the expression of CDKN2A.

4. Discussion

The role of PPARA in tumor initiation and development remains controversial. Several studies have elucidated the antitumor effect of PPARA in various cancers, including breast cancer, prostate cancer, and ovarian cancer [32–34]. Some studies have drawn contradictory conclusions, suggesting that prolonged administration of PPARA agonists might cause hepatocarcinogenesis; however, the detailed mechanism remains unclear [35]. In the present study, we analyzed the expression levels of PPARs in pancancers and noted that PPARA was expressed at low levels in several types of tumors, including colon cancer. Colon cancer samples with high PPARA protein expression were observed to have a better prognosis than those with low PPARA levels. These results suggested that PPARA might serve as a tumor suppressor gene in colon cancer. Most recently, PPARA-specific agonists were reported to exhibit anticancer effects in a variety of tumors. Fenofibrate is a PPARA activator that belongs to the fibrate class of drugs. An increasing number of studies have revealed its potential role as an antitumor agent that affects multiple biological pathways [36–39].

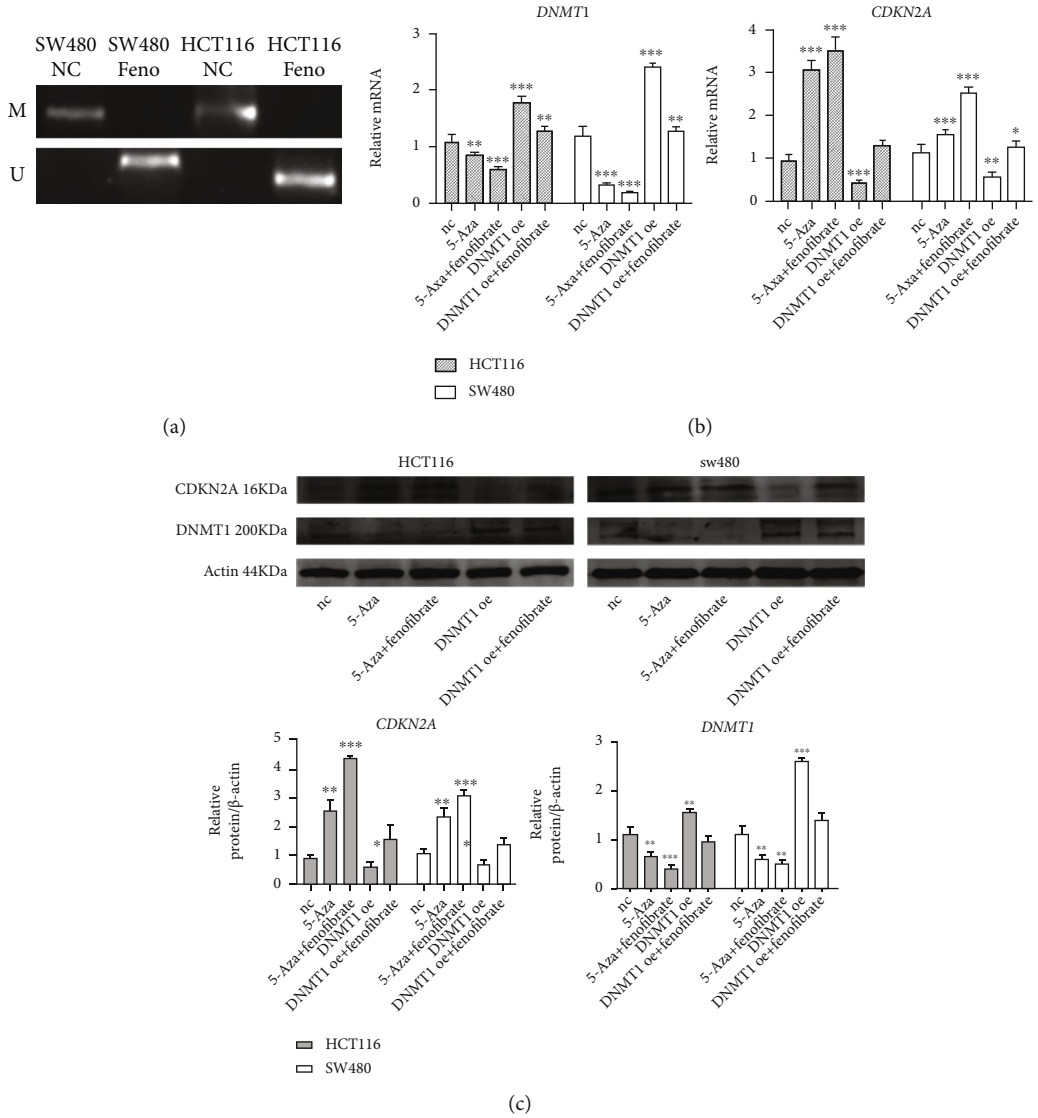

Figure 6: DNMT1 repressed CDKN2A expression by promoter hypermethylation. (a) MSP results showed the methylation status of CDKN2A following fenofibrate treatment. (M: reactions using CDKN2A primers specific for methylated CpG sites; U: reactions using CDKN2A primers specific for unmethylated CpG sites). (b) The mRNA expression of DNMT1 and CDKN2A in cells was measured using qRT-PCR. Data was presented as mean ± SD (NC: untreated cell; 5-Aza: 5-azacytidine treated cell; DNMT1 oe: DNMT1 overexpression cell; $^{*}P < 0.05$, $^{**}P < 0.01$, $^{***}P < 0.001$). (c) The protein expression of CDKN2A and DNMT1 in SW480 and HCT116 cells was measured using western blot.

DNMT1 is responsible for maintaining global methylation and aberrant CGI methylation in human cancer cells, whereas DNMT3a and DNMT3b are believed to act as maintenance and de novo methyltransferases. The elevated expression of DNMT1 has been reported in colon adenocarcinomas, hepatocarcinomas, and lung cancer [40–42].

Hypermethylation of gene promoter regions leads to transcriptional repression. Tse et al. [4] showed that promoter methylation of tumor suppressor genes promoted carcinogenesis of colon cancer. In this study, we observed that fenofibrate treatment increased PPARA expression and decreased DNMT1 activity, accompanied with the elevated expression of a series of established tumor suppressor genes, including RASSF1A, MLH1, p21, and p27. CDKN2A mRNA and protein levels were upregulated in both HCT116 and SW480 fenofibrate-treated cells compared to controls. To confirm the hypothesis that fenofibrate abrogated the hypermethylation of CDKN2A, we detected the methylation status of its promoter using methylation-specific PCR. In reactions using methylation-specific primers, no band for methylated CDKN2A was observed in the fenofibrate-treated group. Furthermore, the expression levels of DNMT1 and CDKN2A were measured in colon cancer cells following treatment with the DNMT1 inhibitor, 5-azacytidine, and DNMT1 overexpression plasmid. The results indicated that fenofibrate functions as a repressor, similar to a methyltransferase inhibitor.

There are several reports suggesting that PPARA activation inhibits cell proliferation by targeting the cyclin-dependent kinase inhibitor, CDKN2A [43, 44]. In the present study, we found that cells treated with fenofibrate were

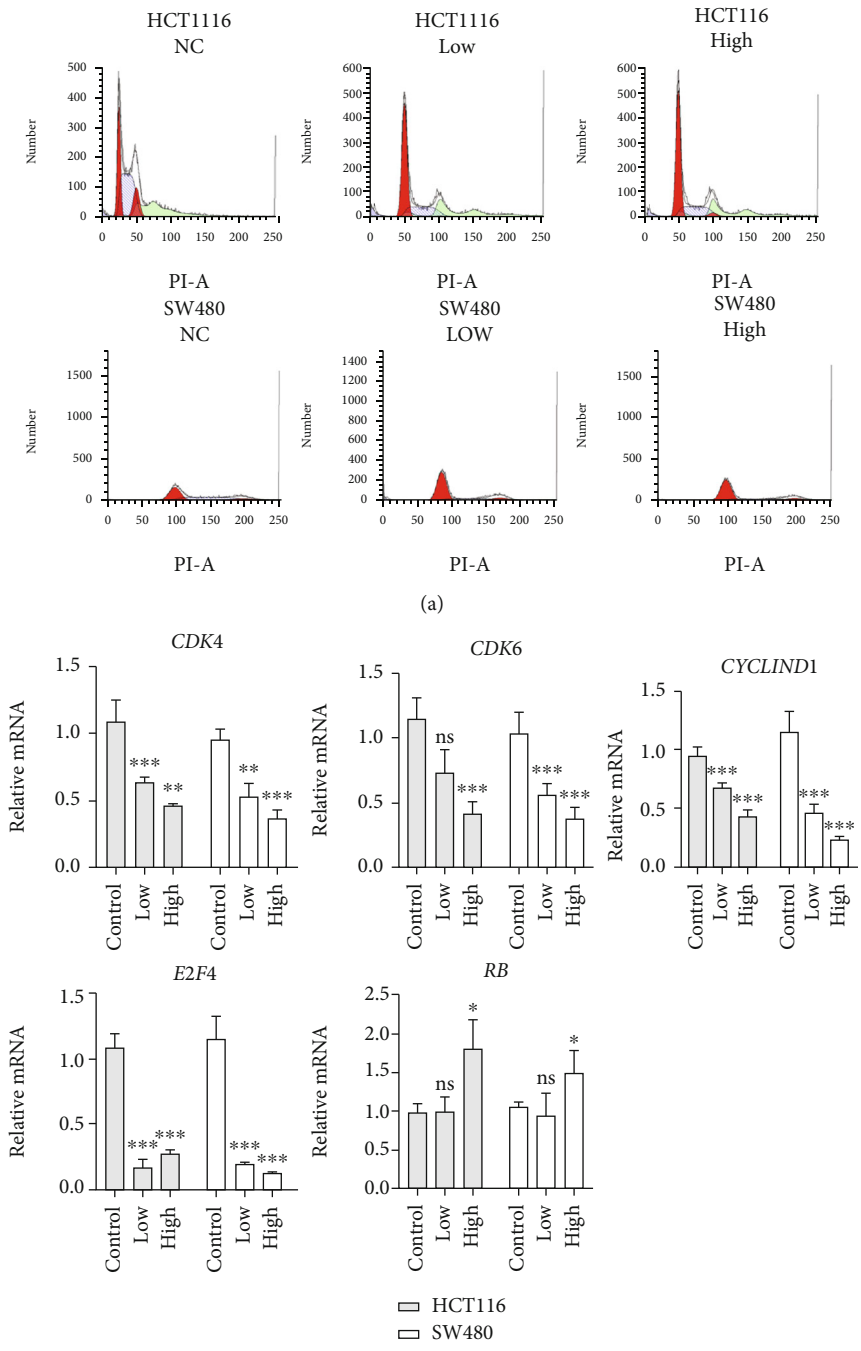

Figure 7: Continued.

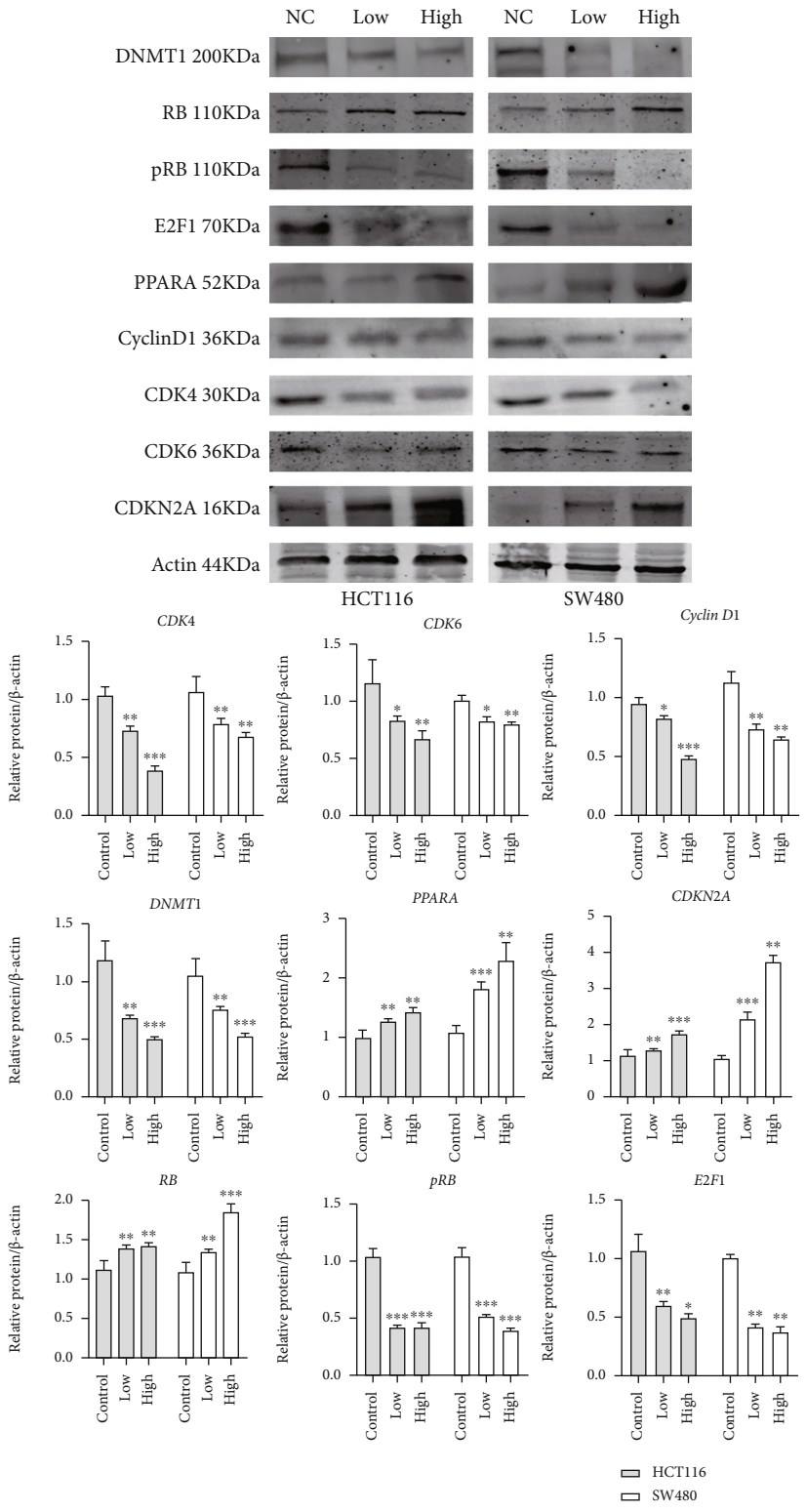

(c)

Figure 7: Fenofibrate modulated cell cycle via CDKN2A/RB/E2F transcript cascade. (a) Cell cycle distribution was examined using flow cytometry. (b) The mRNA expression of RB, E2F1, CDK4, CDK6, and Cyclin D1 was measured using qRT-PCR. Data was presented as mean ± SD ($^{*}P < 0.05$, $^{**}P < 0.01$, $^{***}P < 0.001$). (c) Western blot analysis of DNMT1, RB, pRB, E2F1, PPARA, Cyclin D1, CDK4, CDK6, and CDKN2A expression in colon cancer cells.

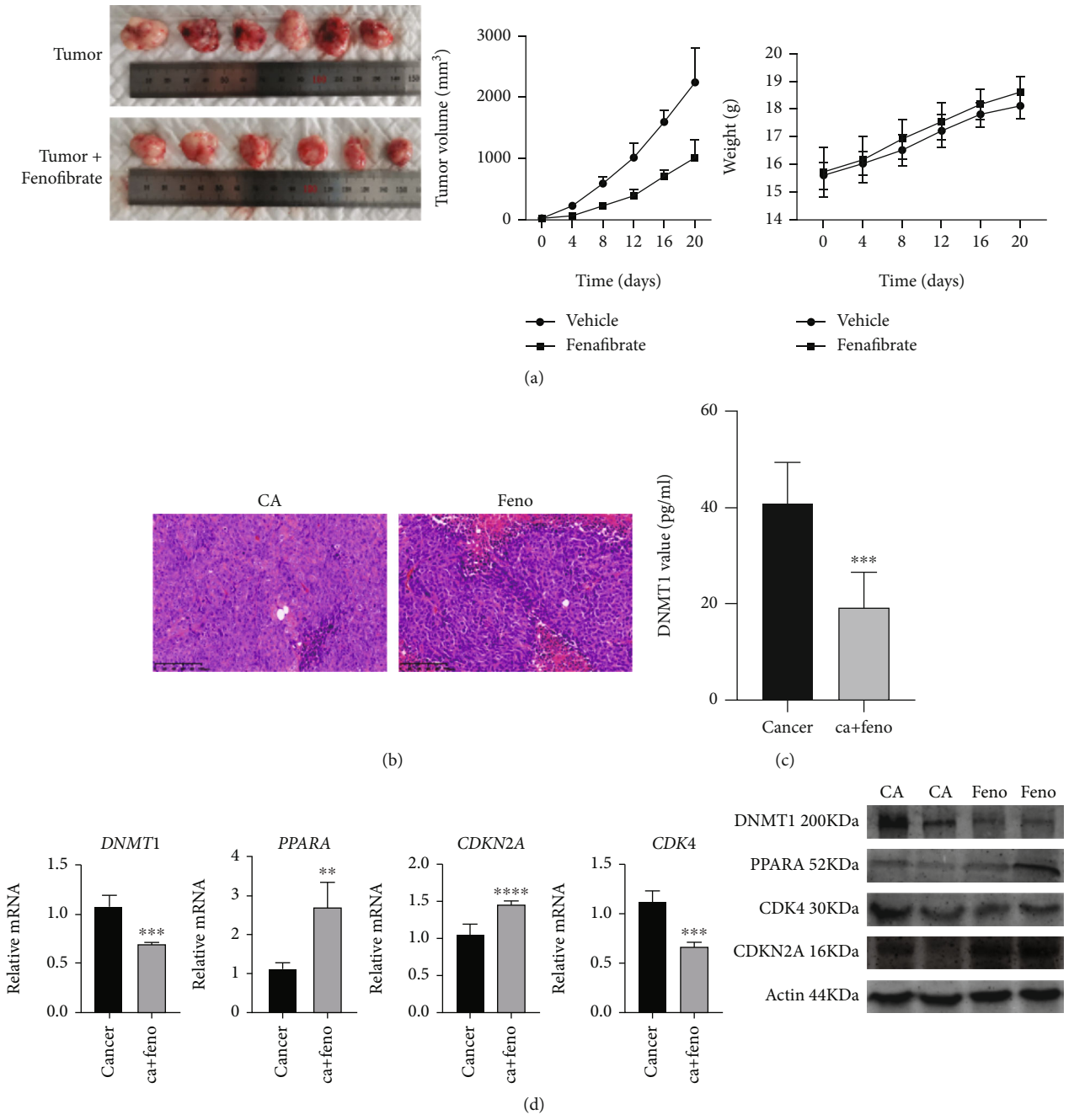

Figure 8: Continued.

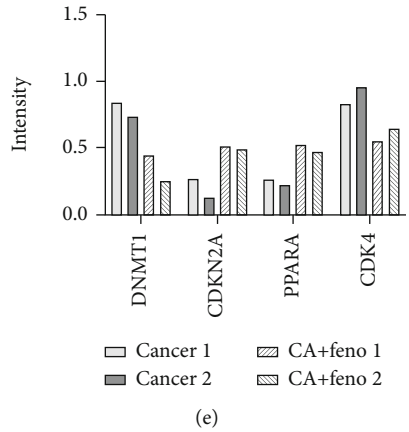

(e)

Figure 8: Fenofibrate suppressed tumor growth and DNMT1 content *in vivo*. (a) Representative images of subcutaneous xenografts from the treatment and vehicle groups ($n = 6$ mice per group). Subcutaneous xenograft growth curves of nude mice of the two groups. Body weight of each mouse was recorded every three days. Data was presented as mean ± SD. (b) H&E staining of subcutaneous xenografts from the treatment group and vehicle group (magnification 200x). (c) The DNMT1 value of tissues was examined using ELISA assay. Data was presented as mean ± SD ($^*P < 0.05$, $^{**}P < 0.01$, $^{***}P < 0.001$). (d) DNMT1, PPARA, CDK4, and CDKN2A mRNA expressions of xenografts from two groups were detected using qRT-PCR. Data was shown as mean ± SD ($^*P < 0.05$, $^{**}P < 0.01$, $^{***}P < 0.001$). (e) DNMT1, PPARA, CDK4, and CDKN2A protein levels in different groups were measured by western blot.

arrested in the G1 phase, and the number of G2/M cells was reduced. Moreover, fenofibrate elevated the level of CDKN2A by suppressing DNMT1 expression, reduced the activation of cyclin D1/CDK complexes, and phosphorylated RB. Cyclin D1/CDK complexes are cell cycle-related molecules that facilitate the G1/S transition [45]. In quiescent cells, hypophosphorylated RB protein interacts with E2F and inhibits its transcription activity. Under growth stimulation or cancerous states, cyclin-CDK complexes are activated to induce RB phosphorylation. Phosphorylated RB then releases the E2F transcription factor, which triggers the transition of the cell cycle from the G1 phase to the S phase, thereby, enabling uncontrolled cell proliferation [46]. In summary, the RB/E2F pathway was involved in fenofibrate-mediated epigenetic changes on CDKN2A, which resulted in the alterations in cell cycle distribution.

Some studies have shown that DNMT1 cooperated directly with E2F1 and HDAC to accelerate aberrant methylation in tumors [47]. The free E2F1 is released by phosphorylated RB and binds to its cognate sites on the DNMT1 promoter region, which played a positive role on DNMT1 expression in cell cycle process [48]. Elevated expression of DNMT1 induced DNA hypermethylation of several tumor suppressor genes, including CDKN2A. However, conflicting results have emerged regarding the relationship between DNMT1 and E2F1. In mesenchymal stem cells, the expression of E2F1 was not correlated with that of DNMT1. Complete cell cycle arrest by serum starvation did not affect the expression of DNMT1, while E2F1 expression was decreased [49]. The above findings revealed that DNMT1 may not be a responsive target of E2F1 during cell cycle arrest.

In the present study, we found that fenofibrate may act in a similar manner as a methylation transferase inhibitor. It reduced DNMT1 activity and E2F1 expression. The mechanistic details behind PPAR agonist on DNMT1 inhibition have not been determined. Whether DNMT1 downregulation caused decreases in free E2F1 requires further investigation.

In addition, we demonstrated that fenofibrate inhibited tumor progression by regulating cell apoptosis and migration. The results from flow cytometry analysis and TUNEL assays showed that fenofibrate caused an increase in late apoptosis in a dose-dependent manner. However, the underlying mechanism for such findings was not determined in our study.

Cellular plasticity mediated by EMT regulatory circuits enhances the invasive properties of cancer cells [50]. Transcriptional repression of E-cadherin is frequently observed in malignant tumor cells. Some studies have verified that DNMT1 caused the suppression of E-cadherin through hypermethylation of its promoter region [51]. We found that E-cadherin expression was increased following fenofibrate treatment *in vitro*; however, whether the upregulation was correlated with reduced DNMT1 activity and promoter demethylation requires further investigation.

Finally, we carried out tumor xenograft experiments using HCT116 cells to investigate the antitumor efficacy of fenofibrate *in vivo*. Fenofibrate decreased the tumor volume significantly compared to the vehicle-treated mice. The necrotic area was identified in H&E-stained samples from fenofibrate-treated mice. The expression of DNMT1, CDK4, and CDKN2A was effectively reduced by fenofibrate treatment compared with control cells. These results demonstrated that fenofibrate could ablate tumors and retard tumor growth.

These findings, coupled with the reversibility of DNA methylation, support the possibility of fenofibrate as a potential epigenetic treatment in colon cancer patients.

5. Conclusions

In conclusion, the present work illustrated that activation of PPARA by fenofibrate administration protected against colon cancer progression through epigenetic modifications.

Fenofibrate weakened DNMT1 activity and restored the expression of the tumor suppressor gene, CDKN2A, which suppressed cell proliferation by blocking the G1 to S transition through the RB/E2F pathway. In addition, fenofibrate inhibited cancer cell invasion by regulating EMT. Therefore, we conclude that fenofibrate could act as an adjuvant agent in colon cancer treatment.

Abbreviations

ACC: Adrenocortical carcinoma
BLCA: Bladder urothelial carcinoma
BRCA: Breast invasive carcinoma
CESC: Cervical squamous cell carcinoma and endocervical adenocarcinoma
CHOL: Cholangiocarcinoma
COAD: Colon adenocarcinoma
DLBC: Lymphoid neoplasm diffuse large B-cell lymphoma
ESCA: Esophageal carcinoma
GBM: Glioblastoma multiforme
HNSC: Head and neck squamous cell carcinoma
KICH: Kidney chromophobe
KIRC: Kidney renal clear cell carcinoma
KIRP: Kidney renal papillary cell carcinoma
AML: Acute myeloid leukemia
LGG: Brain lower grade glioma
LIHC: Liver hepatocellular carcinoma
LUAD: Lung adenocarcinoma
LUSC: Lung squamous cell carcinoma
MESO: Mesothelioma
OV: Ovarian serous cystadenocarcinoma
PAAD: Pancreatic adenocarcinoma
PCPG: Pheochromocytoma and paraganglioma
PRAD: Prostate adenocarcinoma
READ: Rectum adenocarcinoma
SARC: Sarcoma
SKCM: Skin cutaneous melanoma
STAD: Stomach adenocarcinoma
TGCT: Testicular germ cell tumors
THCA: Thyroid carcinoma
THYM: Thymoma
UCEC: Uterine corpus endometrial carcinoma
UCS: Uterine carcinosarcoma
UVM: Uveal melanoma
FPKM: Fragments per kilobase per million
TCGA: The Cancer Genome Atlas
CGI: CpG islands
CRC: Colorectal cancer
PPARA: Peroxisome proliferator-activated receptor alpha
DNMT1: DNA methyltransferase 1
RB: Retinoblastoma
EMT: Epithelial mesenchymal transition
HR: Hazard ratio
qRT-PCR: Quantitative reverse transcription PCR
MSP: Methylation-specific PCR
EdU: 5-Ethynyl-2′-deoxyuridine
PI: Propidium iodide
SDS: Sodium dodecylsulfate-polyacrylamide.

Data Availability

TCGA gene expression data and clinical data were obtained from TCGA data portal (https://portal.gdc.cancer.gov).

Conflicts of Interest

The authors declare that they have no conflicts of interest.

Authors' Contributions

Rui Kong provided the main contribution to this work.

Acknowledgments

This study received support from National Natural Science Foundation of China (81300340, 81471537).

Supplementary Materials

Table S1: list of primers used in the qRT-PCR assay. Table S2: list of primers used in the methylation-specific PCR assay. *(Supplementary Materials)*

References

[1] F. Bray, J. Ferlay, I. Soerjomataram, R. L. Siegel, L. A. Torre, and A. Jemal, "Global cancer statistics 2018: GLOBOCAN estimates of incidence and mortality worldwide for 36 cancers in 185 countries," *CA: A Cancer Journal for Clinicians*, vol. 68, no. 6, pp. 394–424, 2018.

[2] M. Arnold, M. S. Sierra, M. Laversanne, I. Soerjomataram, A. Jemal, and F. Bray, "Global patterns and trends in colorectal cancer incidence and mortality," *Gut*, vol. 66, no. 4, pp. 683–691, 2017.

[3] E. Dekker, P. J. Tanis, J. L. A. Vleugels, P. M. Kasi, and M. B. Wallace, "Colorectal cancer," *Lancet*, vol. 394, no. 10207, pp. 1467–1480, 2019.

[4] J. W. T. Tse, L. J. Jenkins, F. Chionh, and J. M. Mariadason, "Aberrant DNA methylation in colorectal cancer: what should we target?," *Trends in Cancer*, vol. 3, no. 10, pp. 698–712, 2017.

[5] V. V. Lao and W. M. Grady, "Epigenetics and colorectal cancer," *Nature Reviews Gastroenterology & Hepatology*, vol. 8, no. 12, pp. 686–700, 2011.

[6] C. Ili, K. Buchegger, H. Demond et al., "Landscape of genome-wide DNA methylation of colorectal cancer metastasis," *Cancers*, vol. 12, no. 9, p. 2710, 2020.

[7] P. Liu, L. Wu, H. Chand, C. Li, X. Hu, and Y. Li, "Silencing of miR-152 contributes to DNMT1-mediated CpG methylation of the PTEN promoter in bladder cancer," *Life Sciences*, vol. 261, p. 118311, 2020.

[8] M. Mamo, I. C. Ye, J. W. DiGiacomo, J. Y. Park, B. Downs, and D. M. Gilkes, "Hypoxia alters the response to anti-EGFR therapy by regulating EGFR expression and downstream signaling in a DNA methylation-specific and HIF-dependent manner," *Cancer Research*, vol. 80, no. 22, pp. 4998–5010, 2020.

[9] M. Kulis and M. Esteller, "DNA methylation and cancer," *Advances in Genetics*, vol. 70, pp. 27–56, 2010.

[10] M. Laisné, N. Gupta, O. Kirsh, S. Pradhan, and P.-A. Defossez, "Mechanisms of DNA methyltransferase recruitment in mammals," *Genes*, vol. 9, no. 12, p. 617, 2018.

[11] L. Gao, M. Emperle, Y. Guo et al., "Comprehensive structure-function characterization of DNMT3B and DNMT3A reveals distinctive de novo DNA methylation mechanisms," *Nature Communications*, vol. 11, no. 1, article 3355, 2020.

[12] T. Hinoue, D. J. Weisenberger, C. P. E. Lange et al., "Genome-scale analysis of aberrant DNA methylation in colorectal cancer," *Genome Research*, vol. 22, no. 2, pp. 271–282, 2012.

[13] M. S. Fernandes, F. Carneiro, C. Oliveira, and R. Seruca, "Colorectal cancer and RASSF family–a special emphasis on RASSF1A," *International Journal of Cancer*, vol. 132, no. 2, pp. 251–258, 2013.

[14] D. S. Byun, N. Ahmed, S. Nasser et al., "Intestinal epithelial-specific PTEN inactivation results in tumor formation," *American Journal of Physiology-Gastrointestinal and Liver Physiology*, vol. 301, no. 5, pp. G856–G864, 2011.

[15] K. Huang, M. Du, X. Tan et al., "PARP1-mediated PPARα poly(ADP-ribosyl)ation suppresses fatty acid oxidation in non-alcoholic fatty liver disease," *Journal of Hepatology*, vol. 66, no. 5, pp. 962–977, 2017.

[16] L. J. Holm, M. Ø. Monsted, M. Haupt-Jorgensen, and K. Buschard, "PPARs and the development of type 1 diabetes," *PPAR Research*, vol. 2020, Article ID 6198628, 11 pages, 2020.

[17] M. Pawlak, P. Lefebvre, and B. Staels, "Molecular mechanism of PPARα action and its impact on lipid metabolism, inflammation and fibrosis in non-alcoholic fatty liver disease," *Journal of Hepatology*, vol. 62, no. 3, pp. 720–733, 2015.

[18] N. Bougarne, B. Weyers, S. J. Desmet et al., "Molecular actions of PPARα in lipid metabolism and inflammation," *Endocrine Reviews*, vol. 39, no. 5, pp. 760–802, 2018.

[19] L. Wu, J. Li, J. Feng et al., "Crosstalk between PPARs and gut microbiota in NAFLD," *Biomedicine & Pharmacotherapy*, vol. 136, article 111255, 2021.

[20] T. Shigeto, Y. Yokoyama, B. Xin, and H. Mizunuma, "Peroxisome proliferator-activated receptor alpha and gamma ligands inhibit the growth of human ovarian cancer," *Oncology Reports*, vol. 18, no. 4, pp. 833–840, 2007.

[21] Y. Gao, X. Chen, Q. He et al., "Adipocytes promote breast tumorigenesis through TAZ-dependent secretion of resistin," *Proceedings of the National Academy of Sciences of the United States of America*, vol. 117, no. 52, pp. 33295–33304, 2020.

[22] S. Shi, G. Yu, B. Huang, Y. Mi, Y. Kang, and J. P. Simon, "PPARG could work as a valid therapeutic strategy for the treatment of lung squamous cell carcinoma," *PPAR Research*, vol. 2020, Article ID 2510951, 9 pages, 2020.

[23] Y. Xu, X. Li, Y. Han et al., "A new prognostic risk model based on PPAR pathway-related genes in kidney renal clear cell carcinoma," *PPAR Research*, vol. 2020, Article ID 6937475, 13 pages, 2020.

[24] S. Du, N. Wagner, and K.-D. Wagner, "The emerging role of PPAR beta/delta in tumor angiogenesis," *PPAR Research*, vol. 2020, Article ID 3608315, 16 pages, 2020.

[25] T. Li, Q. Zhang, J. Zhang et al., "Fenofibrate induces apoptosis of triple-negative breast cancer cells via activation of NF-κB pathway," *BMC Cancer*, vol. 14, no. 1, p. 96, 2014.

[26] N. W. Chang, M. H. Tsai, C. Lin et al., "Fenofibrate exhibits a high potential to suppress the formation of squamous cell carcinoma in an oral-specific 4-nitroquinoline 1-oxide/arecoline mouse model," *Biochimica et Biophysica Acta*, vol. 1812, no. 4, pp. 558–564, 2011.

[27] G. Augimeri, L. Gelsomino, P. Plastina et al., "Natural and synthetic PPARγ ligands in tumor microenvironment: a new potential strategy against breast cancer," *International Journal of Molecular Sciences*, vol. 21, no. 24, article 9721, 2020.

[28] Y. Luo, C. Xie, C. N. Brocker et al., "Intestinal PPARα Protects Against Colon Carcinogenesis via Regulation of Methyltransferases DNMT1 and PRMT6," *Gastroenterology*, vol. 157, no. 3, pp. 744–759.e4, 2019.

[29] Q. Xu, Y. Xiang, Q. Wang et al., "SETD2 regulates the maternal epigenome, genomic imprinting and embryonic development," *Nature Genetics*, vol. 51, no. 5, pp. 844–856, 2019.

[30] H. R. Liu, L. Y. Meng, Z. Y. Lin, Y. Shen, Y. Q. Yu, and Y. Z. Zhu, "Cochinchina momordica seed extract induces apoptosis and cell cycle arrest in human gastric cancer cells via PARP and p53 signal pathways," *Nutrition and Cancer*, vol. 64, no. 7, pp. 1070–1077, 2012.

[31] J. G. Herman, J. R. Graff, S. Myohanen, B. D. Nelkin, and S. B. Baylin, "Methylation-specific PCR: a novel PCR assay for methylation status of CpG islands," *Proceedings of the National Academy of Sciences of the United States of America*, vol. 93, no. 18, pp. 9821–9826, 1996.

[32] Y. Segawa, R. Yoshimura, T. Hase et al., "Expression of peroxisome proliferator-activated receptor (PPAR) in human prostate cancer," *Prostate*, vol. 51, no. 2, pp. 108–116, 2002.

[33] S. C. Kwong, A. H. A. Jamil, A. Rhodes, N. A. Taib, and I. Chung, "Metabolic role of fatty acid binding protein 7 in mediating triple-negative breast cancer cell death via PPAR-α signaling," *Journal of Lipid Research*, vol. 60, no. 11, pp. 1807–1817, 2019.

[34] Y. Yokoyama, B. Xin, T. Shigeto et al., "Clofibric acid, a peroxisome proliferator-activated receptor α ligand, inhibits growth of human ovarian cancer," *Molecular Cancer Therapeutics*, vol. 6, no. 4, pp. 1379–1386, 2007.

[35] S. Feng, H. Wang, Y. Wang et al., "Apatinib induces 3-hydroxybutyric acid production in the liver of mice by peroxisome proliferator-activated receptor α activation to aid its antitumor effect," *Cancer Science*, vol. 110, no. 10, pp. 3328–3339, 2019.

[36] D. Panigrahy, A. Kaipainen, S. Huang et al., "PPARalpha agonist fenofibrate suppresses tumor growth through direct and indirect angiogenesis inhibition," *Proceedings of the National Academy of Sciences of the United States of America*, vol. 105, no. 3, pp. 985–990, 2008.

[37] D. Yamasaki, N. Kawabe, H. Nakamura et al., "Fenofibrate suppresses growth of the human hepatocellular carcinoma cell via PPARα-independent mechanisms," *European Journal of Cell Biology*, vol. 90, no. 8, pp. 657–664, 2011.

[38] E. Binello, E. Mormone, L. Emdad, H. Kothari, and I. M. Germano, "Characterization of fenofibrate-mediated anti-proliferative pro-apoptotic effects on high-grade gliomas and anti-invasive effects on glioma stem cells," *Journal of Neuro-Oncology*, vol. 117, no. 2, pp. 225–234, 2014.

[39] T. Morinishi, Y. Tokuhara, H. Ohsaki, E. Ibuki, K. Kadota, and E. Hirakawa, "Activation and expression of peroxisome proliferator-activated receptor alpha are associated with tumorigenesis in colorectal carcinoma," *PPAR Research*, vol. 2019, Article ID 7486727, 9 pages, 2019.

[40] L. Chen, J. Peng, Y. Wang et al., "Fenofibrate-induced mitochondrial dysfunction and metabolic reprogramming reversal: the anti-tumor effects in gastric carcinoma cells mediated by the PPAR pathway," *American Journal of Translational Research*, vol. 12, no. 2, pp. 428–446, 2020.

[41] Y. Bai, L. Lang, W. Zhao, and R. Niu, "Long non-coding RNA HOXA11-AS promotes non-small cell lung cancer tumorigenesis through microRNA-148a-3p/DNMT1 regulatory axis," *Oncotargets and Therapy*, vol. 12, pp. 11195–11206, 2019.

[42] J. M. Serrano-Morales, M. D. Vázquez-Carretero, M. J. Peral, A. A. Ilundáin, and P. García-Miranda, "Reelin-Dab1 signaling system in human colorectal cancer," *Molecular Carcinogenesis*, vol. 56, no. 2, pp. 712–721, 2017.

[43] T. L. Kruer, S. M. Dougherty, L. Reynolds et al., "Expression of the lncRNA maternally expressed gene 3 (MEG3) contributes to the control of lung cancer cell proliferation by the Rb pathway," *PLoS One*, vol. 11, no. 11, article e0166363, 2016.

[44] F. Gizard, T. Nomiyama, Y. Zhao et al., "The PPARalpha/-p16INK4a pathway inhibits vascular smooth muscle cell proliferation by repressing cell cycle-dependent telomerase activation," *Circulation Research*, vol. 103, no. 10, pp. 1155–1163, 2008.

[45] Y. Majeed, R. Upadhyay, S. Alhousseiny et al., "Potent and PPARα-independent anti-proliferative action of the hypolipidemic drug fenofibrate in VEGF-dependent angiosarcomas in vitro," *Scientific Reports*, vol. 9, no. 1, article 6316, 2019.

[46] A. N. Srinivas, D. Suresh, F. Mirshahi, P. K. Santhekadur, A. J. Sanyal, and D. P. Kumar, "Emerging roles of AATF: checkpoint signaling and beyond," *Journal of Cellular Physiology*, vol. 236, no. 5, pp. 3383–3395, 2021.

[47] K. D. Robertson, S. Ait-Si-Ali, T. Yokochi, P. A. Wade, P. L. Jones, and A. P. Wolffe, "DNMT1 forms a complex with Rb, E2F1 and HDAC1 and represses transcription from E2F-responsive promoters," *Nature Genetics*, vol. 25, no. 3, pp. 338–342, 2000.

[48] F. Leng, J. Yu, C. Zhang et al., "Methylated DNMT1 and E2F1 are targeted for proteolysis by L3MBTL3 and CRL4DCAF5 ubiquitin ligase," *Nature Communications*, vol. 9, no. 1, article 1641, 2018.

[49] C. C. Tsai, P. F. Su, Y. F. Huang, T. L. Yew, and S. C. Hung, "Oct4 and Nanog directly regulate Dnmt1 to maintain self-renewal and undifferentiated state in mesenchymal stem cells," *Molecular Cell*, vol. 47, no. 2, pp. 169–182, 2012.

[50] M. Saitoh, "Involvement of partial EMT in cancer progression," *Journal of Biochemistry*, vol. 164, no. 4, pp. 257–264, 2018.

[51] A. Fukagawa, H. Ishii, K. Miyazawa, and M. Saitoh, "δEF1 associates with DNMT1 and maintains DNA methylation of the E-cadherin promoter in breast cancer cells," *Cancer Medicine*, vol. 4, no. 1, pp. 125–135, 2015.

Hindawi
PPAR Research
Volume 2021, Article ID 6661828, 15 pages
https://doi.org/10.1155/2021/6661828

Research Article

miR-22-3p/PGC1β Suppresses Breast Cancer Cell Tumorigenesis via PPARγ

Xuehui Wang,[1,2] Zhilu Yao,[1,2] and Lin Fang[1,2]

[1]*Department of Thyroid and Breast Surgery, Shanghai Tenth People's Hospital, School of Medicine, Tongji University, Shanghai 200072, China*
[2]*Nanjing Medical University, Nanjing 211166, China*

Correspondence should be addressed to Lin Fang; fanglin2017@126.com

Received 30 October 2020; Revised 16 December 2020; Accepted 24 February 2021; Published 13 March 2021

Academic Editor: Sainan Li

In this study, we found that miR-22-3p expression was decreased in breast cancer (BC) cell lines and tissues. Overexpression of miR-22-3p inhibited the proliferation and migration of BC cells in vitro and in vivo, while depletion of miR-22-3p exhibited the opposite effect. Importantly, miR-22-3p could directly target PGC1β and finally regulate the PPARγ pathway in BC. In conclusion, miR-22-3p/PGC1β suppresses BC cell tumorigenesis via PPARγ, which may become a potential biomarker and therapeutic target.

1. Introduction

Breast cancer (BC) is the one of the most commonly diagnosed malignancies and the leading cause of cancer-related death in women [1]. Despite the fact that significant advances in surgical and medical management of BC have been exhibited, the incidence and mortality still increased by 18% since 2008 [2]. Higher rates of metastasis, recurrence, and drug resistance are the mainly reasons of poor prognosis and low survival among BC patients. Therefore, further investigating the molecular mechanism and discovery of the new biomarkers remains urgently needed for the diagnosis and treatment of BC.

MicroRNAs (miRNAs) are a class of single-stranded and highly conserved small noncoding RNAs, participating in numerous biological processes [3, 4]. miRNAs typically suppress gene expression at posttranscriptional levels by directly recognizing complementary sequences in the 3′untranslated region (3′-UTR) of target mRNAs. Various miRNAs have been identified to play significant roles in the etiology of BC. For example, miR-135-5p could inhibit TGF-β-induced epithelial-mesenchymal transition and metastasis by targeting SMAD3 in BC [5]. miR-27a facilitates BC progression via GSK-3β [6]. Specifically, low expression of serum miR-22 was found significantly associated with short survival and poor prognosis [7]. However, the role of miR-22 was demonstrated both as a tumor suppressor and a promoter in previous studies [8, 9].

As members of nuclear receptor superfamily, peroxisome proliferator-activated receptors (PPARs) are ligand-activated transcriptional factors (TFs). There are mainly three isotypes of PPARs, including PPARα, PPARβ, and PPARγ [10]. They are involved in cellular differentiation, cell proliferation, and tumorigenesis. Among them, increasing evidence suggests that PPARγ protects against tumors by inhibiting cell proliferation. For example, PPARγ could inhibit the development of lung adenocarcinoma through the regulation of tumor cell proliferation and transmission-related molecules [11, 12]. PPARγ is prone to exert an antiangiogenic effect, which has been known as a hallmark of cancer [13]. Downregulation of PPARγ is associated with decreased terminal differentiation and cell cycle arrest, which induces cell proliferation and leads to tumorigenesis [14].

Peroxisome proliferator-activated receptor gamma coactivators 1 alpha and beta (PPAGC1A/PGC1α and PPARGC1B/PGC1β, respectively) are major regulators of

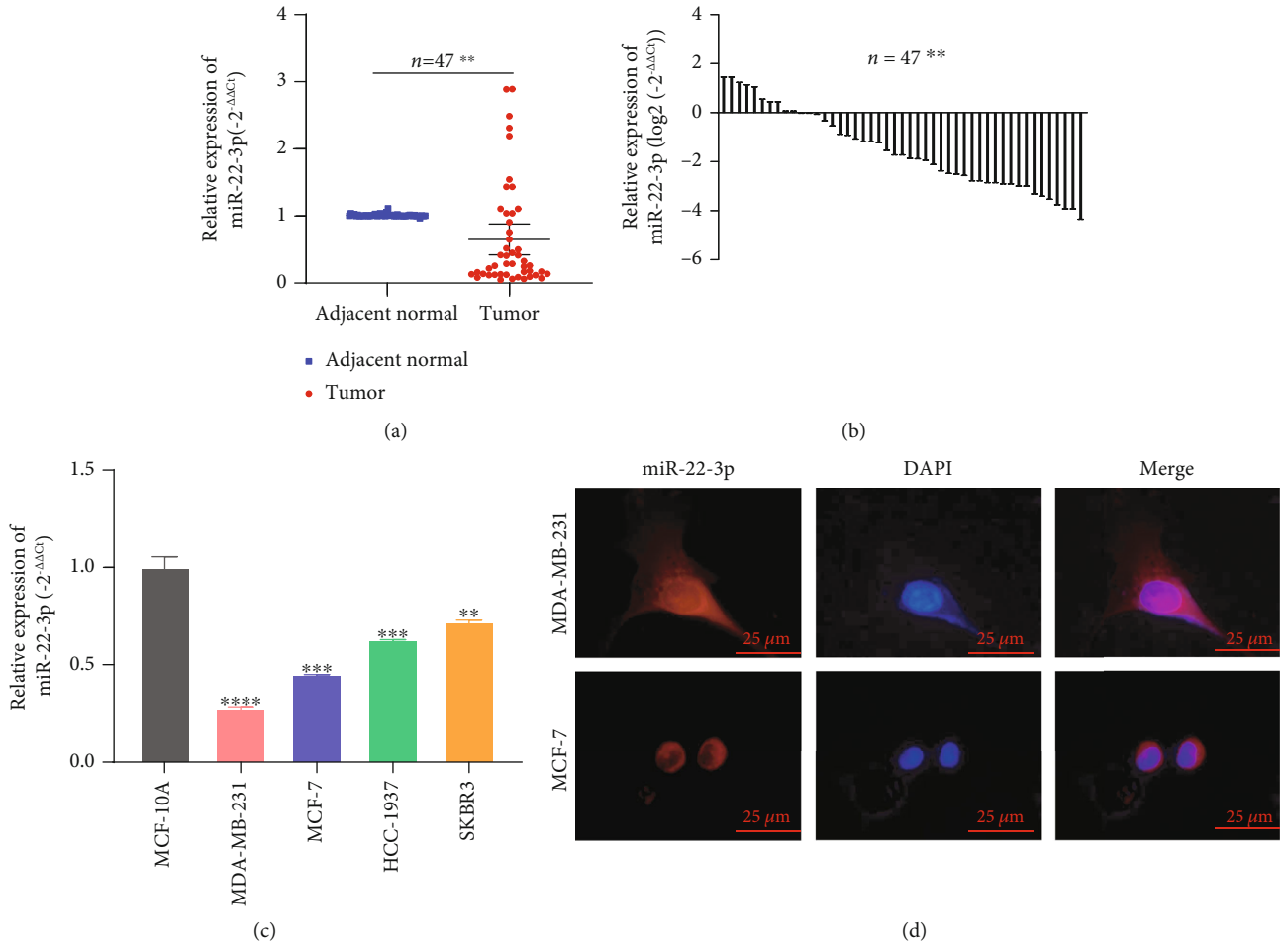

FIGURE 1: miR-22-3p was decreased in BC cell lines and tissues. (a, b) miR-22-3p had low expression in BC tissues compared with adjacent normal tissues. (c) miR-22-3p had low expression in BC cell lines. (d) Detection of colocalization of miR-22-3p in cytoplasm by RNA FISH assay (magnification, ×400). Red, miR-200a-3p; blue, DAPI. $^{**}p < 0.1$; $^{***}p < 0.001$; $^{****}p < 0.0001$.

mitochondrial biogenesis and cellular metabolism [15, 16], playing important roles in the PPAR signaling network [17]. PGC1β has been proved to be associated with several cancers. For example, hepatic PGC1β acts as a transcriptional gatekeeper of mitochondrial function to contribute to hepatocellular carcinoma progression [18]. FOXO3/PGC1β signaling axis was proved essential to sustain the pancreatic ductal adenocarcinoma cancer stem cell properties [19]. Specifically, PGC1β was proved significantly overexpressed in BC and could inhibit the apoptosis of BC cells via the mTOR signaling pathway [20, 21]. PGC1β regulates HER2-overexpressing BC cell proliferation by metabolic and redox pathways [22]. PGC1β regulates BC tumor growth and metastasis by SREBP1-mediated HKDC1 expression [23]. In addition, PGC1β could cooperate with PPARγ, allowing the subsequent interaction between PPARγ and other transcription factors [24]. PGC1β mediates PPARγ activation of osteoclastogenesis [25]. Therefore, we postulated that the PPAR signaling network plays an important role in the development and progression of BC.

In the present study, we found that miR-22-3p was downregulated in BC and suppressed BC cell tumorigenesis. Then, we demonstrated that PGC1β was regulated by miR-22-3p. Moreover, we found that the effects of miR-22-3p/PGC1β on BC were, at least in part, mediated by the PPARγ signaling pathway.

2. Materials and Methods

2.1. Clinical Cancer Tissue Samples. Tumor tissues and their adjacent normal tissues of 47 BC patients were collected from the Department of Breast and Thyroid Surgery of Shanghai Tenth People's Hospital of Tongji University (Shanghai, China). None of the patients received any local or systemic treatment before surgery, and all tissue specimens were immediately snap-frozen in liquid nitrogen until further use. All studies in this manuscript were approved by Institutional Ethics Committees of Shanghai Tenth People's Hospital. We have obtained informed consent from all patients.

Table 1: The relationship between the expression of miR-22-3p and various clinicopathological variables.

Patients characteristics	Total	miR-22-3p expression High ($N = 12$)	Low ($N = 35$)	p value*
Age				0.7065
<60	20	5	15	
≥60	27	7	20	
TNM stage				0.0200*
I and II	30	11	19	
III and IV	17	1	16	
Tumor size (cm)				0.0237*
≤2	26	10	16	
>2	21	2	19	
Lymph node metastasis				0.0423*
Negative	32	11	21	
Positive	15	1	14	
Distant metastasis				0.0931
No	40	12	28	
Yes	7	0	7	

p value from a chi-square test (*$p < 0.05$).

2.2. Cell Culture. The human HEK293T and human BC cell lines (MDA-MB-231, MCF-7, HCC-1937, and SKBR3) and normal breast epithelial cell line (MCF-10A) were obtained from Chinese Academy of Sciences (Shanghai, China). The HEK293T, MDA-MB-231, MCF-7, HCC-1937, and SKBR3 cells were cultured in Dulbecco's Modified Eagle's Medium (DMEM) (Gibco, USA) with 10% Fetal Bovine Serum (FBS) (Gibco, USA), penicillin (100 units/ml), and streptomycin (100 μg/ml) (Enpromise, China). The MCF-10A cells were cultured in Mammary Epithelial Basal Medium (MEBM) (Cambrex, USA). All cells were cultured at 37°C with 5% CO_2.

2.3. Transfection Assay. We purchased miR-22-3p mimics, miR-22-3p inhibitor, and nonspecific miR-negative control (miR-NC) oligo from RiboBio (Guangzhou, China). When the density of MDA-MB-231 or MCF-7 cells reached 80%, cells were transfected with 100 nmol/l miR-22-3p mimics, miR-22-3p inhibitor, or miR-NC using Hieff Trans™ Liposomal Transfection Reagent (Yeasen, China) according to the manufacturer's instructions. After 24-48 h of incubation, cells were harvested for further analysis.

2.4. Quantitative Real-Time Polymerase Chain Reaction (RT-qPCR). Total RNA was extracted from frozen tissues and cultured cells by Trizol reagent (Invitrogen, Carlsbad, CA, USA), and the concentration and purity of RNA samples was assessed with a Nanodrop 2000 spectrophotometer (Thermo Fisher Scientific, USA). CDNA was synthesized by a commercial cDNA synthesis kit (Yeasen, China). We conducted RT-qPCR by using the SYBR Green PCR Kit (Yeasen, China), and primer sequences were designed and synthesized by RiboBio (Guangzhou, China). Expression of miRNAs was assessed by threshold cycle (CT) values and analyzed using the $2^{-\Delta\Delta Ct}$ method. The sequences of primers can be provided upon request.

2.5. MTT Assay. 3-(4,5-Dimethylthiazol-2-yl)-2,5-diphenyltetrazolium bromide (MTT) assay was performed to detect cell proliferation ability. After 24 h transfection, a density of 2000 cells per well was placed into 96-well plates. The cells were detected in accordance with the manufacturer's instructions using 3-(4,5-Dimethylthiazol-2-yl)-2,5-diphenyltetrazolium bromide (MTT) assay kit (Sigma, Santa Clara, CA, USA). The 490 nm optical density was detected by a microplate reader (BioTek, USA).

2.6. Colony Formation Assay. A density of 800-1000 cells per well was transferred into 6-well plates. Cell colonies were washed twice by using cold phosphate-buffered saline (PBS), fixed with 75% ethanol, and stained with 0.1% crystalline purple until the colonies were visible. Then, colonies were photographed and counted.

2.7. Wound Healing Assay. MDA-MB-231 and MCF-7 cells were transfected with a range of constructs as indicated in 6-well plates. When the treated cells reached about 90% confluency, a scratch was produced in the cell monolayer by drawing a 200 μl pipette tip over the surface of each well, holding the tip perpendicular to the plate. The monolayers were cultured in DMEM with 2% FBS. Pictures of wound healing were taken at 0 h and 24 h at the same position to observe cell movement.

2.8. Migration Assays. We used transwell chambers (Corning, Inc., Lowell, MA, USA) to measure the migration ability of the cells. Transfected cells were added into the upper chamber with 200 μl serum-free medium, and medium with 10% FBS was added into the lower chamber. 12-24 h later, cells were removed in the upper chamber by cotton swab. Then, the cells on the opposite side of the filter were fixed with 75% ethanol for 10 min, then stained with 0.1% crystal violet for 10 min. Representative pictures were taken with a microscope (Leica Microsystems, Mannheim, Germany).

2.9. Dual-Luciferase Reporter Assay. According to our previous studies [26, 27], to confirm that miR-22-3p directly targets PGC1β 3′-UTR, wild and mutant reporter plasmids of PGC1β were individually designed and synthesized by IBSBio (Shanghai, China). HEK293T cells were cotransfected with the constructed reporter plasmids, together with miR-22-3p mimics or miR-22-3p-NC using Lipofectamine® 2000 (Invitrogen; Thermo Fisher Scientific, USA). 48 h later, the luciferase activities were measured with the Dual-Luciferase® Reporter Assay kit (Yeasen, China). Firefly to Renilla luciferase ratio was calculated.

2.10. Western Blotting Analysis. Proteins were extracted using RIPA lysis buffer (Beyotime, Jiangsu, China), and the concentrations were detected by using the protein

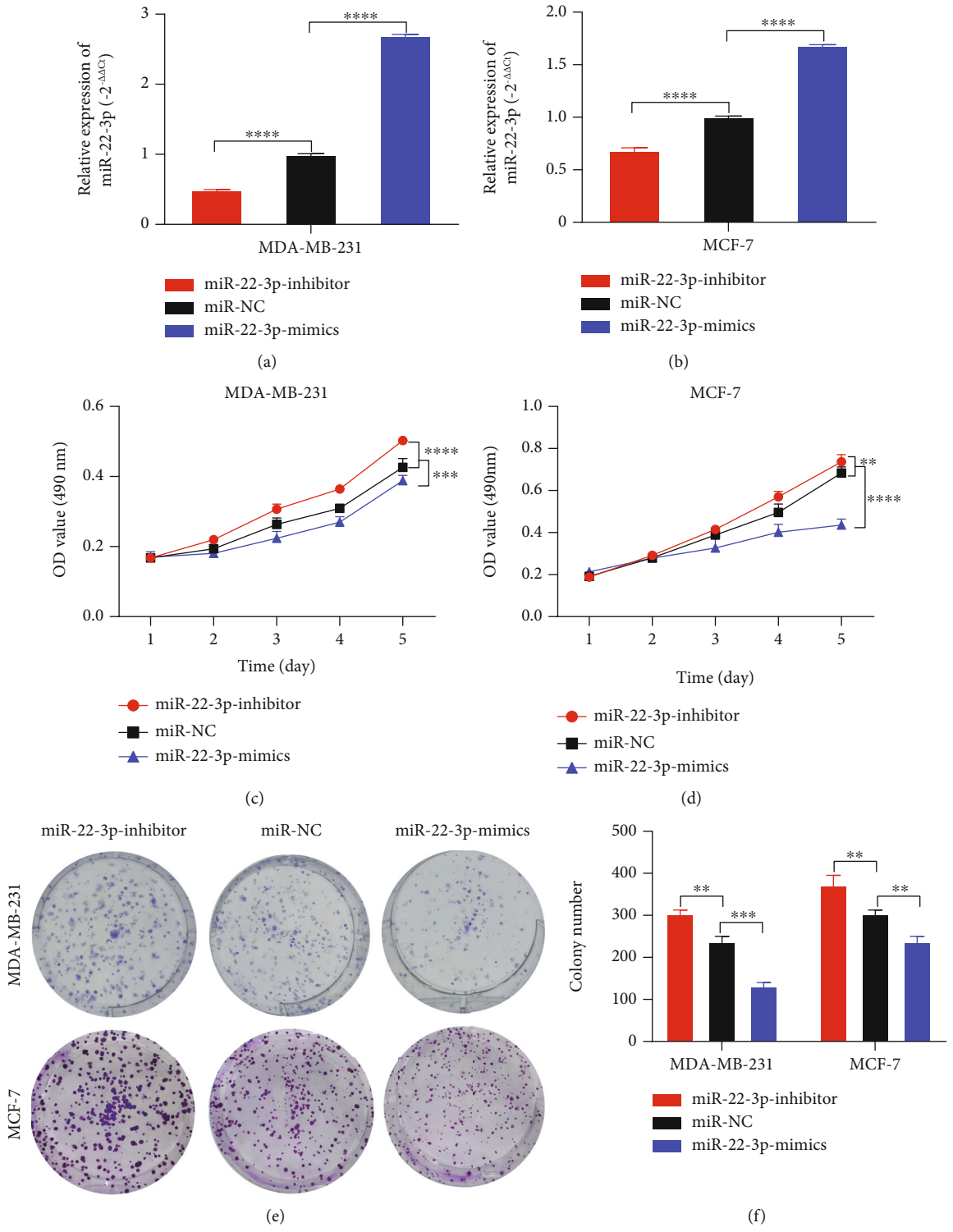

Figure 2: Continued.

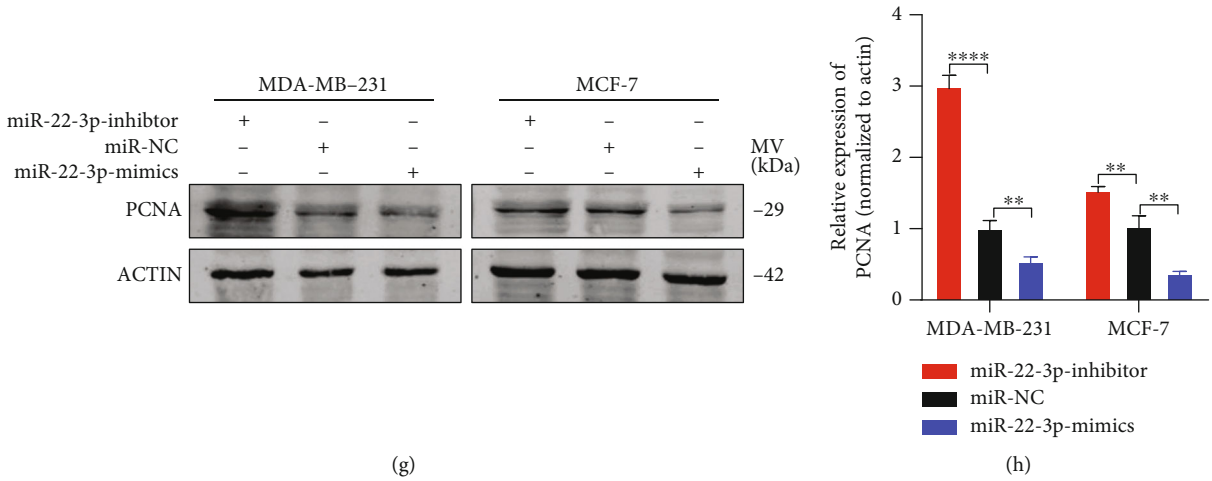

Figure 2: miR-22-3p suppressed cell proliferation of BC cells. (a, b) Expression of miR-22-3p was confirmed by RT-qPCR in MDA-MB-231 and MCF-7 cells. (c, d) Effect of miR-22-3p on proliferation in MDA-MB-231 and MCF-7 cells by MTT assay. (e, f) Effect of miR-22-3p on proliferation in MDA-MB-231 and MCF-7 cells by colony formation assay. (g, h) Effect of miR-22-3p on proliferation in MDA-MB-231 and MCF-7 cells by western blotting. $^{**}p < 0.01$; $^{***}p < 0.001$; $^{****}p < 0.0001$.

assay kit (Beyotime, Jiangsu, China). Protein lysates were separated by 10% sodium dodecyl sulfate-polyacrylamide gels and then transferred to nitrocellulose membrane (Beyotime, Jiangsu, China), which was incubated 1 h with 5% nonfat milk and immunoblotted overnight at 4°C with primary antibodies: anti-PCNA (Proteintech, USA), anti-PGC1β (Abclonal, China), anti-PPARγ (Abclonal, China), anti-NK-κB (CST, USA), anti-C-myc (CST, USA), anti-MMP2 (CST, USA), anti-MMP9 (CST, USA), anti-cyclin D1 (Abcam, USA), and anti-cyclin E (Abcam, USA). The next day, the membranes were incubated in secondary antibodies for 1 h at room temperature. Dilutions of all antibodies used in this study were 1 : 1000. Signals of protein bands were scanned by Odyssey Infrared scanning system (Li-Cor, Lincoln, NE, USA).

2.11. FISH Assay. Ribo™ Fluorescent In Situ Hybridization Kit (Ribo, China) was used in FISH assay. Specific probes for the miR-22-3p were designed and synthesized by IBSBio (Shanghai, China). 4,6-Diamidino-2-Phenylindole (DAPI) was used to stain cell nuclei. A fluorescence microscope (Olympus BX53 Biological Microscope) was used to capture the images of cells.

2.12. Statistical Analysis. The significance of differences between groups was assessed by GraphPad Prism V8.3.0 (GraphPad, CA, USA). All experiments were repeated for three times. Data were obtained from three independent experiments which are presented as the means ± standard deviation (SD). Student's *t*-test (double-tailed) was used to draw a comparison between groups, and p value < 0.05 was considered significant.

3. Results

3.1. miR-22-3p Was Decreased in BC Cell Lines and Tissues. Results obtained from TGCA databases showed that expression of miR-22-3p was decreased in BC (Figure S1A). The expression of miR-22-3p was assessed by RT-qPCR in 47 pairs of BC tissues and adjacent normal tissues. Results of RT-qPCR showed that the expression of miR-22-3p was significantly decreased in BC tissues (35/47, 74.5%) (Figures 1(a) and 1(b)). In addition, we examined the expression of miR-22-3p in BC cell lines (MDA-MB-231, MCF-7, HCC-1937, and SKBR3) and normal breast epithelial cell line (MCF-10A). Consistent with the findings in BC specimens, the miR-22-3p expression was downregulated in BC cell lines (Figure 1(c)). To better explore the function and mechanism of miR-22-3p, RNA fluorescence in situ hybridization (FISH) analysis was performed to detect the localization of miR-22-3p. The FISH analysis revealed that miR-22-3p was mostly stained in the cytoplasm of BC cell lines (Figure 1(d)). After analyzing the relationship between the expression of miR-22-3p and the clinical pathological variables in 47 BC patients, we found that high expression of miR-22-3p was negatively associated with TNM stage, lymph node metastasis, and tumor size but had no correlation with age and distant metastasis (Table 1). The $-2^{\Delta\Delta ct}$ value of miR-22-3p expression in BC tissues greater than that in adjacent normal tissues was considered high expression.

3.2. miR-22-3p Suppressed Cell Proliferation of BC Cells. MDA-MB-231 and MCF-7 cells were transfected with miR-22-3p mimics or inhibitor. RT-qPCR was used to verify the transfection efficiency (Figures 2(a) and 2(b)). The proliferation ability of BC cells transfected was measured by MTT assays and colony formation assays. Overexpression of miR-22-3p could suppress the proliferation of MDA-MB-231 and MCF-7 cells while miR-22-3p depletion showed opposite ability (Figures 2(c)–2(f)). Consistent with the results above, western blotting analysis demonstrated that expression of proliferation marker PCNA was inhibited by

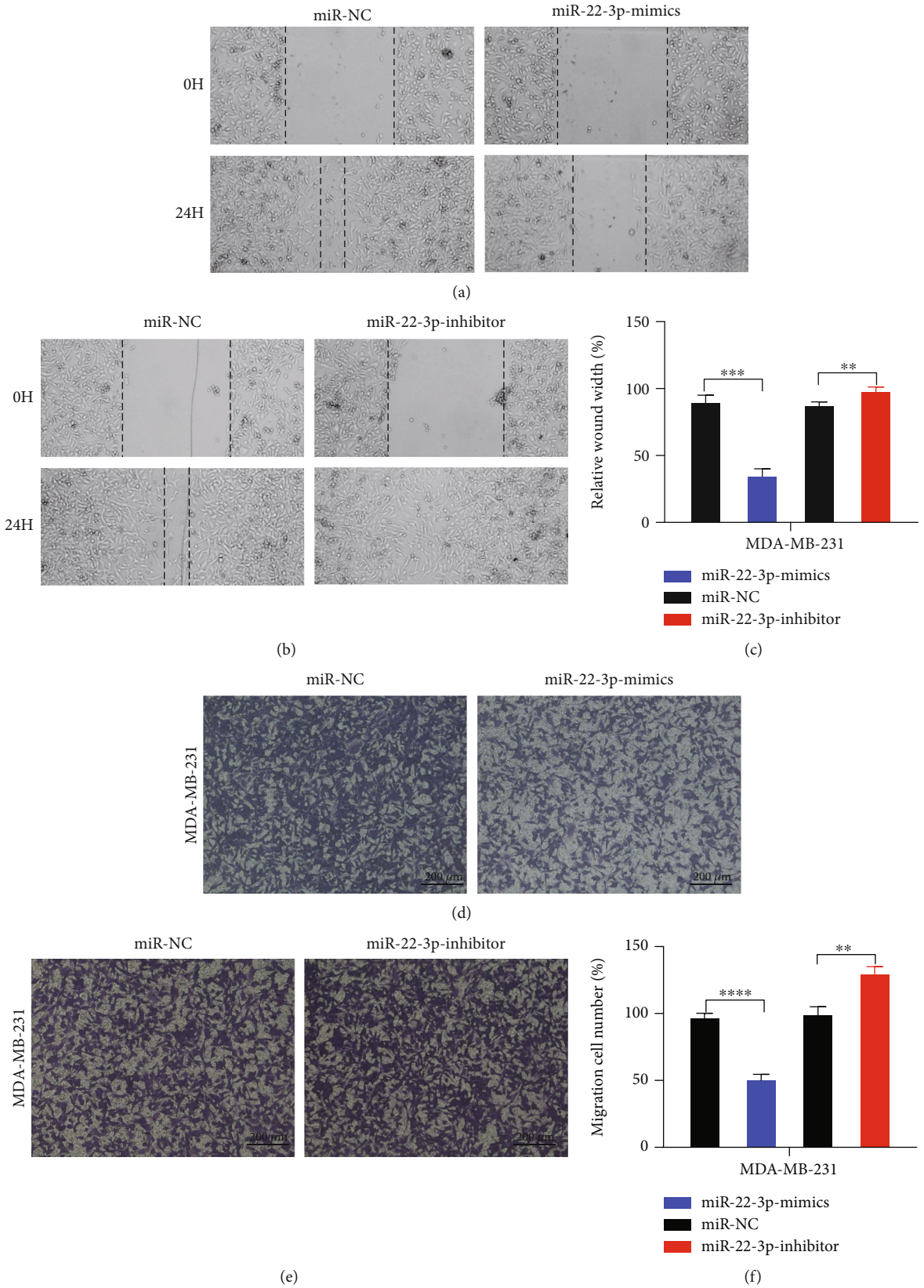

Figure 3: miR-22-3p suppressed cell migration of BC cells. (a–c) Wound healing assays were performed in MDA-MB-231 cell line treated with miR-22-3p mimics or miR-22-3p inhibitor (miR-NC as negative control). (d–f) Cell migration assays were performed in MDA-MB-231 cell line treated with miR-22-3p mimics or miR-22-3p inhibitor (miR-NC as negative control). $^{**}p < 0.01$; $^{***}p < 0.001$; $^{****}p < 0.0001$.

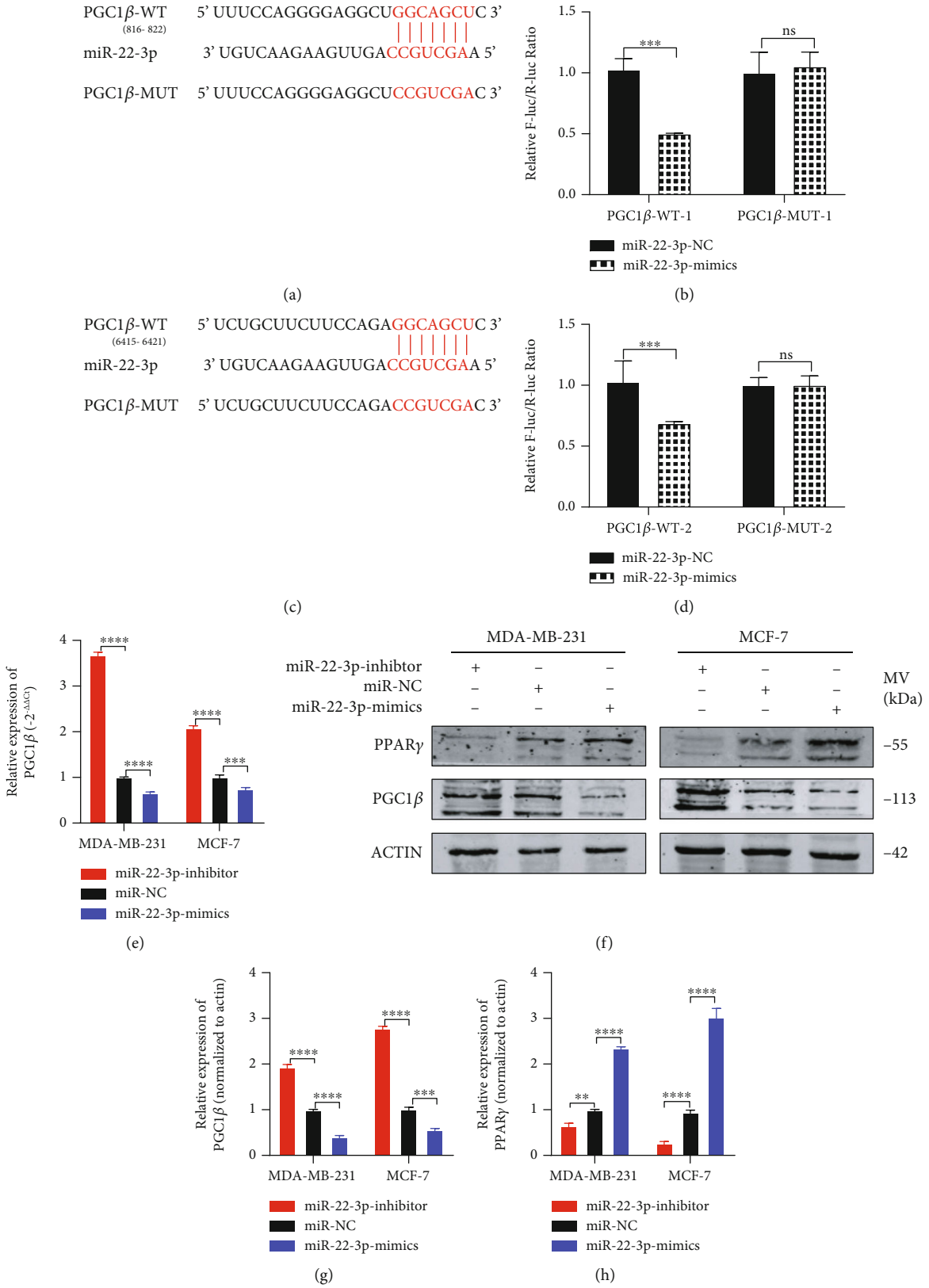

Figure 4: PGC1β is a direct target of miR-22-3p. (a, c) Putative complementary sites within miR-22-3p and PGC1β predicted by bioinformatics analysis (TargetScan). (b, d) Dual-luciferase reporter assays demonstrated that PGC1β is a direct target of miR-22-3p. (e) PGC1β mRNA level was determined by RT-PCR in MDA-MB-231 and MCF-7 cells with different treatment. (f–h) Representative western blots and quantification of PGC1β and PPARγ in MDA-MB-231 and MCF-7 cells with different treatment. β-Actin was used as an internal control. $^{**}p < 0.01$; $^{***}p < 0.001$; $^{****}p < 0.0001$.

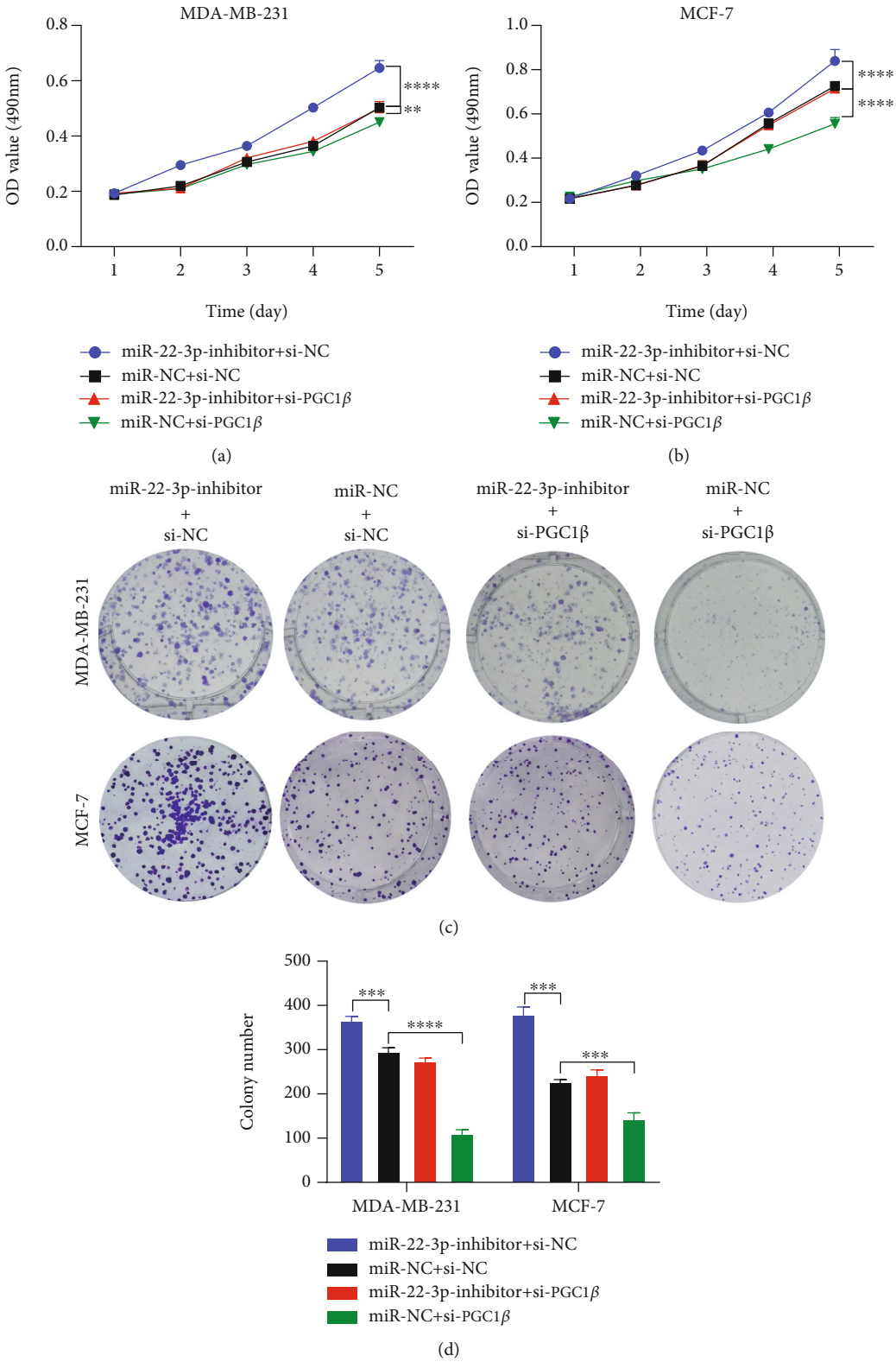

Figure 5: Continued.

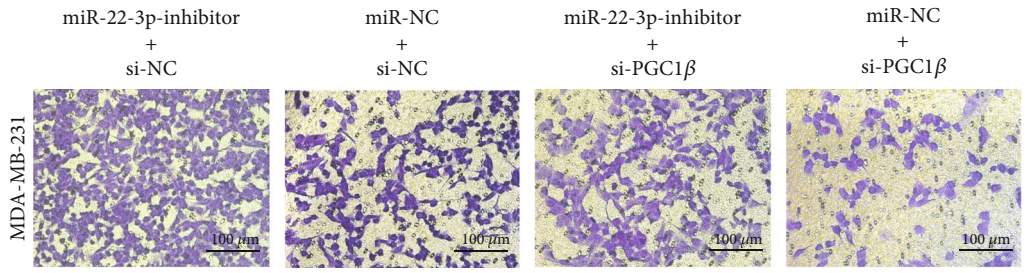

(e)

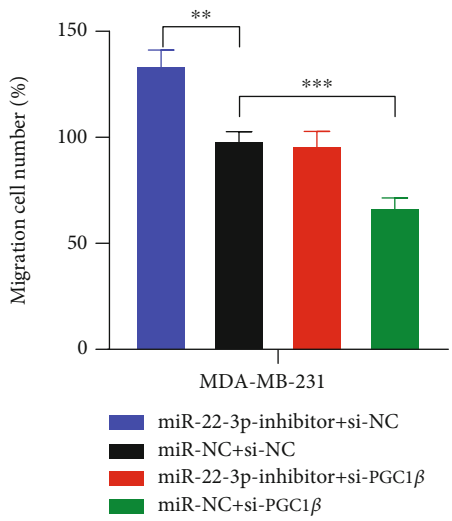

(f)

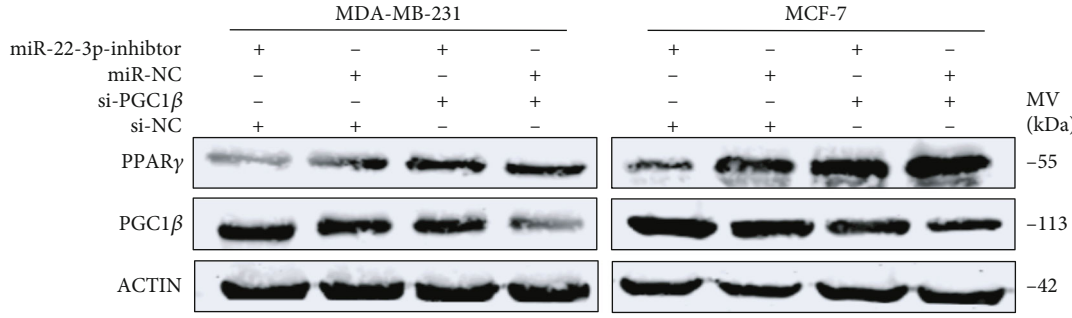

(g)

Figure 5: Continued.

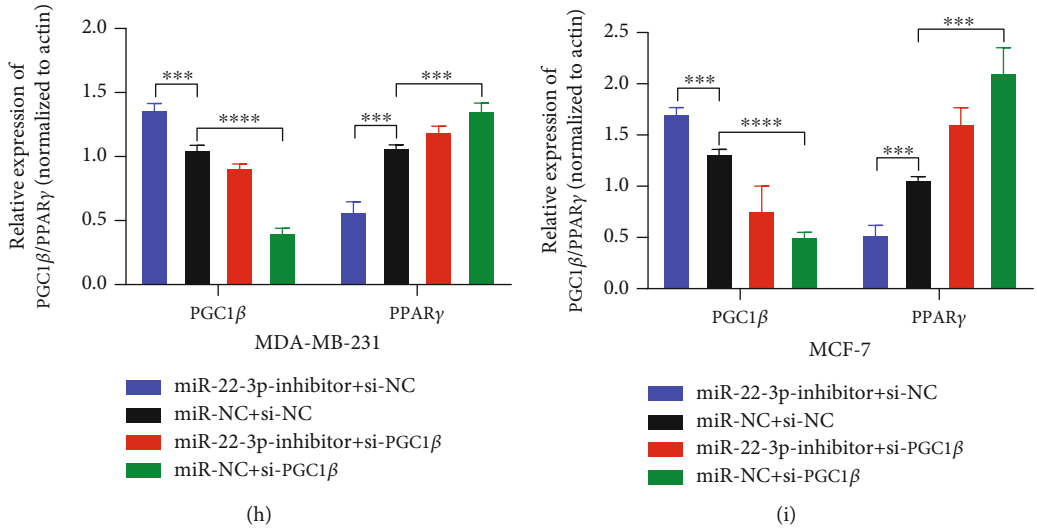

FIGURE 5: miR-22-3p suppressed the proliferation and migration of BC cells via PGC1β. (a–d) Knockdown of PGC1β partially reversed miR-22-3p inhibitor-induced promotion of proliferation in MDA-MB-231 and MCF-7 cells determined by MTT assay and colony assay. (e, f) Knockdown of PGC1β partially reversed miR-22-3p inhibitor-induced promotion of migration in MDA-MB-231 and MCF-7 cells determined by transwell assay. (g–i) Western blotting analysis for PGC1β/PPARγ protein level in MDA-MB-231 and MCF-7 cells. $^{*}p < 0.05$; $^{**}p < 0.01$; $^{***}p < 0.001$; $^{****}p < 0.0001$.

miR-22-3p mimics, (Figures 2(g) and 2(h)). All results above suggested miR-22-3p could suppress proliferation in BC cells.

3.3. miR-22-3p Suppressed Cell Migration of BC Cells. We further explore the biological functions of miR-22-3p in BC migration. Through wound healing assay, limited migration was seen in the miR-22-3p high-expression group compared to the controls undergoing wound healing after 48 hours. Opposite results were observed in the miR-22-3p depletion group (Figures 3(a)–3(c)). Consistently, results of transwell migration assays showed that elevated miR-22-3p decreases cell migration in MDA-MB-231 (Figures 3(d)–3(f)).

3.4. PGC1β Is a Direct Target of miR-22-3p. In accordance with the prediction of TargetScan, PGC1β was found to be the potential target of miR-22-3p (Figures 4(a) and 4(c)). There are two possible binding sites between miR-22-3p and PGC1β. By constructing plasmid and mutant vectors containing 3′-UTRs with wild-type and mutant sequences, dual-fluorescein reporter assay confirmed that PGC1β was the direct target of miR-22-3p (Figures 4(b) and 4(d)). To verify the interaction between miR-22-3p and PGC1β, we detect the expression of PGC1β in MDA-MB-231 and MCF-7 cells transfected with miR-22-3p mimics or miR-22-3p inhibitor. The results indicated that the mRNA level of PGC1β was negatively regulated by miR-22-3p (Figure 4(e)). Consistently, western blotting results indicated that the protein level of PGC1β was significantly downregulated after transfection of miR-22-3p mimics and upregulated after transfection of miR-22-3p inhibitor (Figures 4(f)–4(h)). These results indicated that PGC1β is a direct target of miR-22-3p. Interestingly, when the protein level of PGC1β changed, PPARγ showed the opposite trend. The above results prompted us to explore whether miR-22-3p/PGC1β suppresses BC cell tumorigenesis via PPARγ.

3.5. miR-22-3p Suppressed the Proliferation and Migration of BC Cells via PGC1β. We designed rescue assays in MDA-MB-231 and MCF-7 cells to further verify whether miR-22-3p affects the biological function of BC cells through PGC1β. After being transfected with specific siRNA of PGC1β (si-PGC1β), cell proliferation and migration ability of MDA-MB-231 and MCF-7 cells was suppressed. Meanwhile, si-PGC1β partially reversed the prohibitive effect of miR-22-3p inhibitor on cell proliferation and migration (Figures 5(a)–5(f)). Furthermore, the upregulation effect of the miR-22-3p inhibitor on the PGC1β protein level was partially inverted by si-PGC1β (Figures 5(g)–5(i)). Thus, we confirmed that miR-22-3p suppresses cell proliferation and migration of BC cells via directly targeting PGC1β.

3.6. Inhibition of PPARγ Attenuates Suppression of miR-22-3p on BC Cells. Given the fact that PPARγ has been reported to act as a tumor suppressor in several cancers and PPARγ silencing increased the expression of C-myc, NF-κB, CyclinD1, cyclin E, MMP2, and MMP9 in BC cells [28, 29]. We further explored the changes of the above factors after being transfected with miR-22-3p mimics. As expected, the protein level of PGC1β, C-myc, NF-κB, CyclinD1, cyclin E, MMP2, and MMP9 decreased while the protein level of PPARγ increased with miR-22-3p silencing (Figure 6(a)). To further prove the necessity of the PPARγ signaling pathway in miR-22-3p-mediated regulations, we followed the changes of miR-22-3p

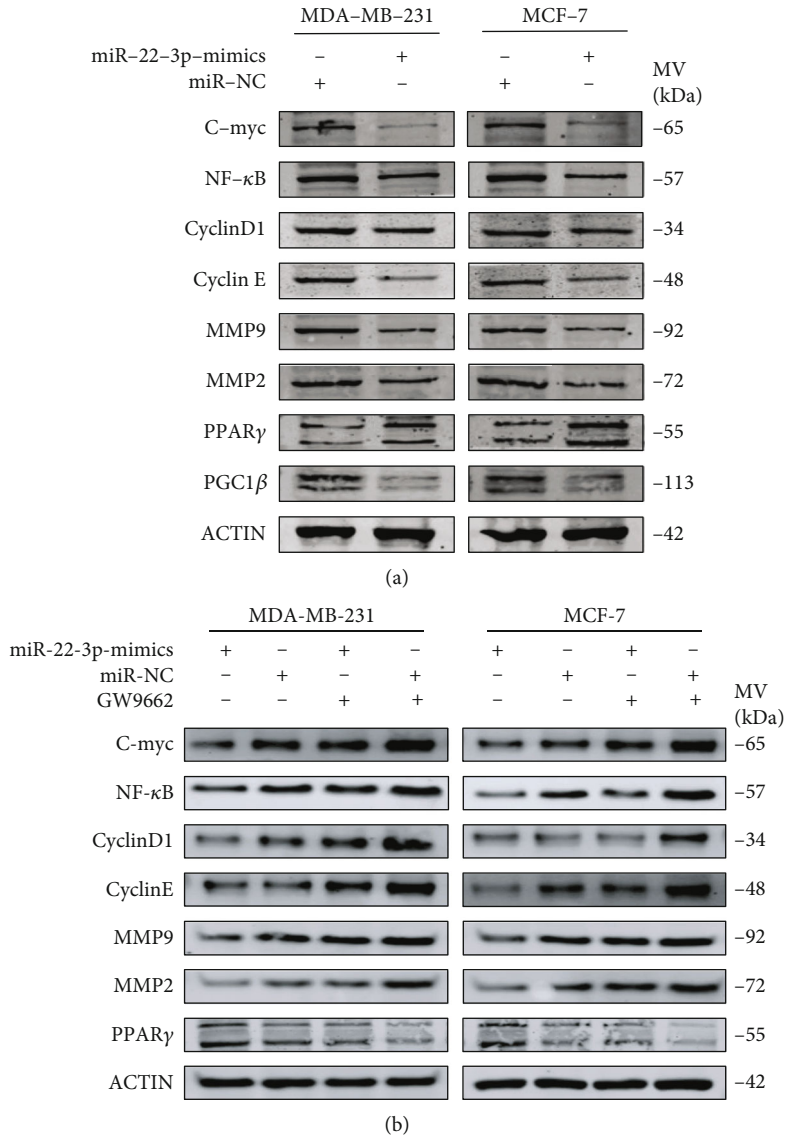

Figure 6: Inhibition of PPARγ attenuates suppression of miR-22-3p on BC cells. (a) Upregulated miR-22-3p increased the expression of PPARγ and decreased the expression of PGC1β, C-myc, NF-κB, CyclinD1, cyclin E, MMP2, and MMP9. (b) Downregulation of C-myc, NF-κB, CyclinD1, cyclin E, MMP2, and MMP9 induced by miR-22-3p was inverted by PPARγ inhibition (GW9662).

overexpressing BC cells in the presence or absence of a potent specific PPARγ inhibitor (GW9662). Western blot analysis showed that the downregulation of C-myc, NF-κB, CyclinD1, cyclin E, MMP2, and MMP9 induced by miR-22-3p was inverted by PPARγ inhibition with GW9662 (Figure 6(b)). Considering the results above, we think that the effects of miR-22-3p/PGC1β on BC were, at least in part, mediated by the PPARγ signaling pathway.

3.7. miR-22-3p Suppressed BC Tumor Growth In Vivo. We established a xenograft tumor model by hypodermic injection of MDA-MB-231 cells stably infected by lentivirus (lv-miR-22-3p or lv-vector) (Figure 7(a)). The tumors were collected and measured, showing that miR-22-3p could markedly decrease the tumor volume compared with the negative control (Figures 7(b) and 7(c)). Western blotting and IHC results indicated that the expression of PGC1β decreased while the expression of PPARγ increased in the higher miR-22-3p expression group. Taking all results *in vivo* and *in vitro* together, we confirmed that miR-22-3p/PGC1β suppresses BC cell tumorigenesis via PPARγ. The mechanism is generated in Figure 7(g).

4. Discussion

miRNAs have been demonstrated to be involved in various physiological and pathological processes. Here, we firstly find that the expression of miR-22-3p was lower in BC tissues than in adjacent normal tissues in TCGA dataset. Then, we found that miR-22-3p was significantly downregulated in human 47 BC samples and associated with tumor size, TNM stage, and lymph node metastasis.

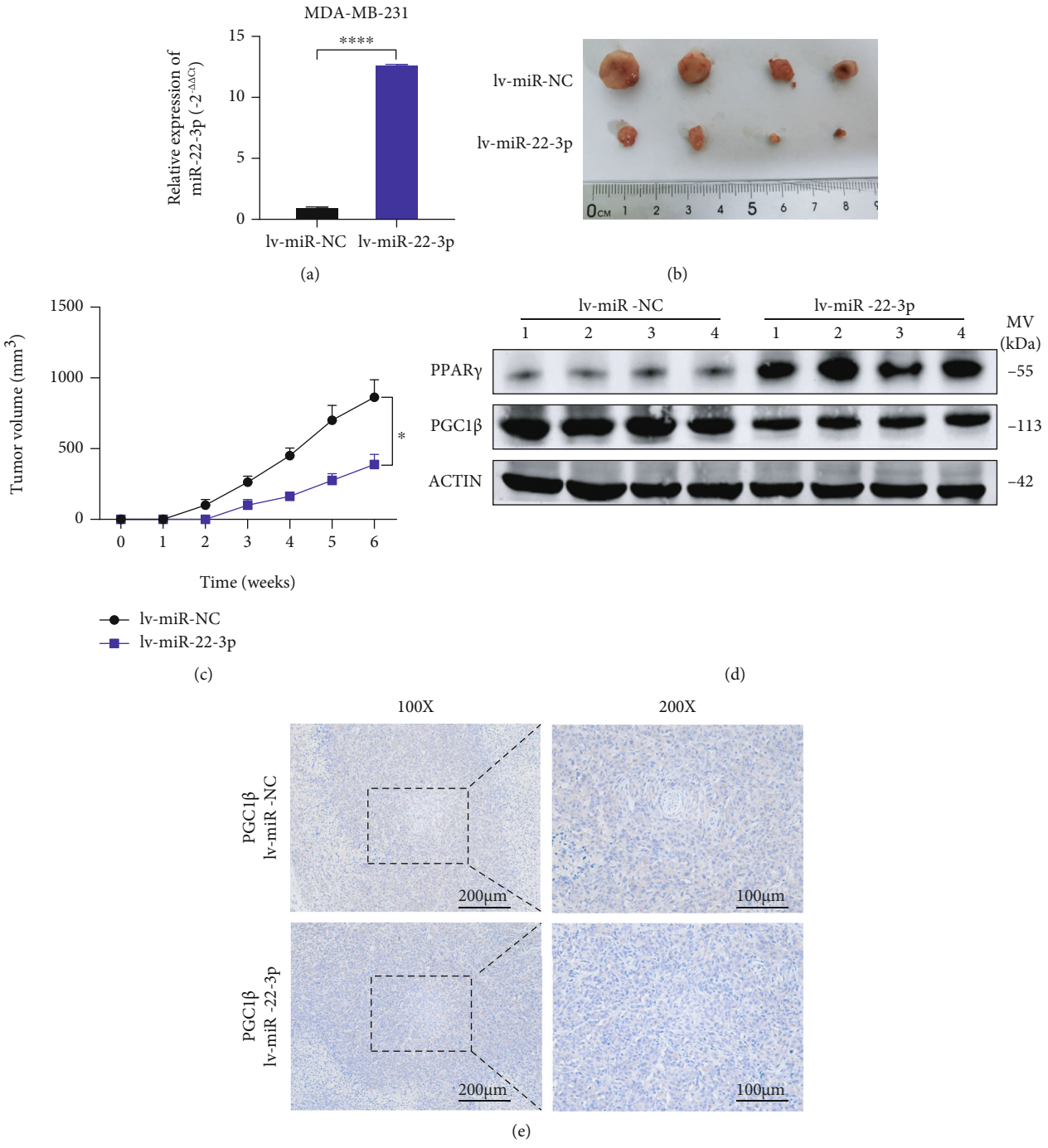

Figure 7: Continued.

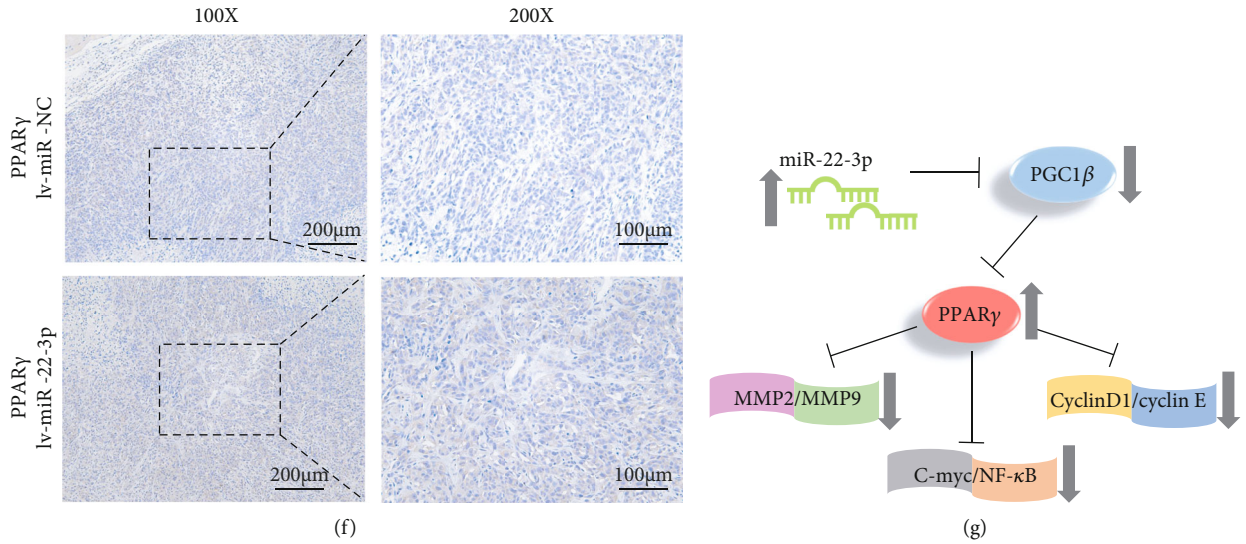

Figure 7: miR-22-3p suppressed BC tumor growth in vivo. (a) Overexpression of miR-22-3p in MDA-MB-231 cells was verified by RT-qPCR. (b) Representative images of xenograft tumors in nude mice. (c) The growth curves of xenografts. (d) Extract protein from tumors and measuring the expression of PGC1β/PPARγ by western blotting. (e, f) Immunohistochemistry (IHC) staining of PGC1β/PPARγ in xenografts. (g) The mechanism diagram was generated to illustrate the mechanism of miR-22-3p-PGC1β-PPARγ in BC. $^{*}p < 0.05$; $^{****}p < 0.0001$.

Overexpression of miR-22-3p markedly suppressed cell proliferation and migration of MDA-MB-231 and MCF-7 cells, indicating that miR-22-3p functions as a tumor suppressor BC. To further investigate the biological roles of miR-22-3p in BC, we demonstrated that miR-22-3p directly targets PGC1β by the results of the dual-luciferase reporter assays.

PGC1β, which has been reported to exert an important role in cancer metabolism and progression, is encoded by the gene PPARGC1β. Previous experimental results have confirmed that PGC1β was significantly overexpressed in BC. Moreover, PGC1β could promote proliferation and migration while inhibiting the apoptosis of BC cells, suggesting it to have a tumor-promoter role in BC [20–23]. Several studies have shown that PPARγ is involved in inflammation, lipid metabolism, glucose homeostasis, and tumorigenesis [30, 31]. Specifically, recent studies showed that PPARγ could inhibit cell proliferation and induces apoptosis of BC in vitro and in vivo [32–34].

To our best knowledge, this is the first study to demonstrate that the miR-22-3p/PGC1β/PPARγ axis regulates the proliferation and migration of BC cells. Our findings suggested that PGC1β was directly regulated by miR-22-3p. More interesting, the protein level of PPARγ increased while the protein level of C-myc, NF-κB, CyclinD1, cyclin E, MMP2, and MMP9 decreased after being transfected with miR-22-3p mimics. To further prove the necessity of the PPARγ signaling pathway in miR-22-3p-mediated regulations, we used a potent specific PPARγ inhibitor (GW9662) in rescue assays. As expected, downregulation of C-myc, NF-κB, CyclinD1, cyclin E, MMP2, and MMP9 induced by miR-22-3p was inverted by PPARγ inhibition with GW9662.

Taken together, our findings suggested that the effects of miR-22-3p/PGC1β on BC were, at least in part, mediated by the PPARγ signaling pathway. These results provided a potential novel biomarker and a therapeutic target for BC.

Abbreviations

BC: Breast cancer
ncRNA: Noncoding RNA
miRNA: MicroRNA
PGC1β: Peroxisome proliferator-activated receptor γ coactivator 1β
PPARγ: Peroxisome proliferators-activated receptor γ
RT-qPCR: Quantitative real-time polymerase chain reaction.

Data Availability

The datasets used and analyzed during the current study are available from the corresponding author on reasonable request.

Consent

We have obtained consents to publish this paper from all the participants of this study.

Disclosure

Xuehui Wang and Zhilu Yao are the co-first authors.

Conflicts of Interest

The authors declare that they have no competing interests.

Authors' Contributions

XW and LF designed the research. XW and ZY performed the research and analyzed the results. XW wrote the paper. All authors read and approved the final manuscript.

Acknowledgments

This work was supported by the National Natural Science Foundation of China (No. 82073204).

Supplementary Materials

Figure S1: expression of miR-22-3p in TCGA database. *(Supplementary Materials)*

References

[1] R. L. Siegel, K. D. Miller, and A. Jemal, "Cancer statistics, 2017," *CA: a Cancer Journal for Clinicians*, vol. 67, no. 1, pp. 7–30, 2017.

[2] Y. F. Zeng and J. Sang, "Five zinc finger protein 350 single nucleotide polymorphisms and the risks of breast cancer: a meta-analysis," *Oncotarget*, vol. 8, no. 63, pp. 107273–107282, 2017.

[3] G. Stefani and F. J. Slack, "Small non-coding RNAs in animal development," *Nature Reviews. Molecular Cell Biology*, vol. 9, no. 3, pp. 219–230, 2008.

[4] R. Garzon, G. A. Calin, and C. M. Croce, "MicroRNAs in cancer," *Annual Review of Medicine*, vol. 60, no. 1, pp. 167–179, 2009.

[5] W. Yang, W. Feng, F. Wu et al., "MiR-135-5p inhibits TGF-β-induced epithelial-mesenchymal transition and metastasis by targeting SMAD3 in breast cancer," *Journal of Cancer*, vol. 11, no. 21, pp. 6402–6412, 2020.

[6] H. Chen, Y. Zhang, X. Cao, and P. Mou, "MiR-27a facilitates breast cancer progression via GSK-3β," *Technology in Cancer Research & Treatment*, vol. 19, p. 153303382096557, 2020.

[7] Y. Shao, Y. Yao, P. Xiao, X. Yang, and D. Zhang, "Serum miR-22 could be a potential biomarker for the prognosis of breast cancer," *Clinical Laboratory*, vol. 65, no. 4/2019, 2019.

[8] F. Yang, Y. Hu, H. X. Liu, and Y. J. Wan, "MiR-22-silenced Cyclin A Expression in Colon and Liver Cancer Cells Is Regulated by Bile Acid Receptor∗," *The Journal of Biological Chemistry*, vol. 290, no. 10, pp. 6507–6515, 2015.

[9] J. H. Lee, S. J. Park, S. Y. Jeong et al., "MicroRNA-22 suppresses DNA repair and promotes genomic instability through targeting of MDC1," *Cancer Research*, vol. 75, no. 7, pp. 1298–1310, 2015.

[10] R. Huang, J. Zhang, M. Li et al., "The role of peroxisome proliferator-activated receptors (PPARs) in pan-cancer," *PPAR Research*, vol. 2020, 2020.

[11] M. Zhao, X. Li, Y. Zhang, H. Zhu, Z. Han, and Y. Kang, "PPARG drives molecular networks as an inhibitor for the pathologic development and progression of lung adenocarcinoma," *PPAR Research*, vol. 2020, Article ID 6287468, 7 pages, 2020.

[12] P. L. Yang, J. S. Wang, X. M. Cheng et al., "PPAR-γ ligand inhibits nasopharyngeal carcinoma cell proliferation and metastasis by regulating E2F2," *PPAR Research*, vol. 2019, Article ID 8679271, 9 pages, 2019.

[13] S. Du, N. Wagner, and K. D. Wagner, "The emerging role of PPAR Beta/Delta in tumor angiogenesis," *PPAR Research*, vol. 2020, Article ID 3608315, 16 pages, 2020.

[14] J. M. Peters, Y. M. Shah, and F. J. Gonzalez, "The role of peroxisome proliferator-activated receptors in carcinogenesis and chemoprevention," *Nature Reviews. Cancer*, vol. 12, no. 3, pp. 181–195, 2012.

[15] J. Lin, C. Handschin, and B. M. Spiegelman, "Metabolic control through the PGC-1 family of transcription coactivators," *Cell Metabolism*, vol. 1, no. 6, pp. 361–370, 2005.

[16] C. Liu and J. D. Lin, "PGC-1 coactivators in the control of energy metabolism," *Acta Biochimica et Biophysica Sinica*, vol. 43, no. 4, pp. 248–257, 2011.

[17] E. Sahin, S. Colla, M. Liesa et al., "Telomere dysfunction induces metabolic and mitochondrial compromise," *Nature*, vol. 470, no. 7334, pp. 359–365, 2011.

[18] E. Piccinin, C. Peres, E. Bellafante et al., "Hepatic peroxisome proliferator-activated receptor γ coactivator 1β drives mitochondrial and anabolic signatures that contribute to hepatocellular carcinoma progression in mice," *Hepatology*, vol. 67, no. 3, pp. 884–898, 2018.

[19] M. Kumazoe, M. Takai, S. Hiroi et al., "The FOXO3/PGC-1β signaling axis is essential for cancer stem cell properties of pancreatic ductal adenocarcinoma," *The Journal of Biological Chemistry*, vol. 292, no. 26, pp. 10813–10823, 2017.

[20] L. Wang, Q. Liu, F. Li et al., "Apoptosis induced by PGC-1β in breast cancer cells is mediated by the mTOR pathway," *Oncology Reports*, vol. 30, no. 4, pp. 1631–1638, 2013.

[21] J. Cao, X. Wang, D. Wang et al., "PGC-1β cooperating with FOXA2 inhibits proliferation and migration of breast cancer cells," *Cancer Cell International*, vol. 19, no. 1, p. 93, 2019.

[22] V. J. Victorino, W. A. Barroso, A. K. Assunção et al., "PGC-1β regulates HER2-overexpressing breast cancer cells proliferation by metabolic and redox pathways," *Tumor Biology*, vol. 37, no. 5, pp. 6035–6044, 2016.

[23] X. Chen, Y. Lv, Y. Sun et al., "PGC1β regulates breast tumor growth and metastasis by SREBP1-mediated HKDC1 expression," *Frontiers in Oncology*, vol. 9, p. 290, 2019.

[24] M. Petr, P. Stastny, A. Zajac, J. J. Tufano, and A. Maciejewska-Skrendo, "The role of peroxisome proliferator-activated receptors and their transcriptional coactivators gene variations in human trainability: a systematic review," *International journal of molecular sciences*, vol. 19, no. 5, p. 1472, 2018.

[25] W. Wei, X. Wang, M. Yang et al., "PGC1beta mediates PPARgamma activation of osteoclastogenesis and rosiglitazone-induced bone loss," *Cell Metabolism*, vol. 11, no. 6, pp. 503–516, 2010.

[26] X. Wang, C. Ji, J. Hu et al., "Hsa_circ_0005273 facilitates breast cancer tumorigenesis by regulating YAP1-hippo signaling pathway," *Journal of experimental & clinical cancer research: CR*, vol. 40, no. 1, p. 29, 2021.

[27] L. Chen, X. Wang, C. Ji, J. Hu, and L. Fang, "MiR-506-3p suppresses papillary thyroid cancer cells tumorigenesis by targeting YAP1," *Pathology, research and practice*, vol. 216, no. 12, p. 153231, 2020.

[28] Y. Xu, X. Lin, J. Xu, H. Jing, Y. Qin, and Y. Li, "SULT1E1 inhibits cell proliferation and invasion by activating PPARγ in breast cancer," *Journal of Cancer*, vol. 9, no. 6, pp. 1078–1087, 2018.

[29] Y. Zhang, X. Huang, J. Zhou, Y. Yin, T. Zhang, and D. Chen, "PPARγ provides anti-inflammatory and protective effects in

intrahepatic cholestasis of pregnancy through NF-κB pathway," *Biochemical and Biophysical Research Communications*, vol. 504, no. 4, pp. 834–842, 2018.

[30] T. Akune, S. Ohba, S. Kamekura et al., "PPAR γ insufficiency enhances osteogenesis through osteoblast formation from bone marrow progenitors," *The Journal of Clinical Investigation*, vol. 113, no. 6, pp. 846–855, 2004.

[31] G. Wang, R. Cao, Y. Wang et al., "Simvastatin induces cell cycle arrest and inhibits proliferation of bladder cancer cells via PPARγ signalling pathway," *Scientific Reports*, vol. 6, no. 1, p. 35783, 2016.

[32] C. Grommes, G. E. Landreth, and M. T. Heneka, "Antineoplastic effects of peroxisome proliferator-activated receptor gamma agonists," *The Lancet. Oncology*, vol. 5, no. 7, pp. 419–429, 2004.

[33] D. Bonofiglio, S. Gabriele, S. Aquila et al., "Peroxisome proliferator-activated receptor gamma activates fas ligand gene promoter inducing apoptosis in human breast cancer cells," *Breast Cancer Research and Treatment*, vol. 113, no. 3, pp. 423–434, 2009.

[34] S. Catalano, L. Mauro, D. Bonofiglio et al., "In vivo and in vitro evidence that PPARγ ligands are antagonists of leptin signaling in breast cancer," *The American Journal of Pathology*, vol. 179, no. 2, pp. 1030–1040, 2011.

Hindawi
PPAR Research
Volume 2021, Article ID 6642939, 10 pages
https://doi.org/10.1155/2021/6642939

Research Article

Identification of a Potential PPAR-Related Multigene Signature Predicting Prognosis of Patients with Hepatocellular Carcinoma

Wenfang Xu,[1] Zhen Chen,[2] Gang Liu,[1] Yuping Dai,[2] Xuanfu Xu,[3] Duan Ma ,[1] and Lei Liu [1]

[1]*Department of Biochemistry and Molecular Biology, School of Basic Medical Sciences and Institutes of Biomedical Sciences, Fudan University, Shanghai, China*
[2]*Department of Pathology, Shidong Hospital, Yangpu District, Shanghai, China*
[3]*Department of Gastroenterology, Shidong Hospital, Yangpu District, Shanghai, China*

Correspondence should be addressed to Duan Ma; duanma@fudan.edu.cn and Lei Liu; liulei_sibs@163.com

Received 15 October 2020; Revised 8 January 2021; Accepted 1 March 2021; Published 13 March 2021

Academic Editor: John Patrick Vanden Heuvel

Peroxisome proliferator-activated receptors (PPARs) and part of their target genes have been reported to be related to the progression of hepatocellular carcinoma (HCC). The prognosis of HCC is not optimistic, and more accurate prognostic markers are needed. This study focused on discovering potential prognostic markers from the PPAR-related gene set. The mRNA data and clinical information of HCC were collected from TCGA and GEO platforms. Univariate Cox and lasso Cox regression analyses were used to screen prognostic genes of HCC. Three genes (*MMP1*, *HMGCS2*, and *SLC27A5*) involved in the PPAR signaling pathway were selected as the prognostic signature of HCC. A formula was established based on the expression values and multivariate Cox regression coefficients of selected genes, that was, risk score = 0.1488 ∗ expression value of *MMP* 1 + (−0.0393) ∗ expression value of *HMGCS*2 + (−0.0479) ∗ expression value of *SLC*27*A*5. The prognostic ability of the three-gene signature was assessed in the TCGA HCC dataset and verified in three GEO sets (GSE14520, GSE36376, and GSE76427). The results showed that the risk score based on our signature was a risk factor with a HR (hazard ratio) of 2.72 (95%CI (Confidence Interval) = 1.87 ~ 3.95, $p < 0.001$) for HCC survival. The signature could significantly ($p < 0.0001$) distinguish high-risk and low-risk patients with poor prognosis for HCC. In addition, we further explored the independence and applicability of the signature with other clinical indicators through multivariate Cox analysis ($p < 0.001$) and nomogram analysis (C-index = 0.709). The above results indicate that the combination of *MMP1*, *HMGCS*2, and *SLC*27*A*5 selected from the PPAR signaling pathway could effectively, independently, and applicatively predict the prognosis of HCC. Our research provided new insights to the prognosis of HCC.

1. Introduction

Liver cancer is a common malignancy and its mortality rate ranks fourth among cancer-related deaths [1]. About 80% of patients with primary liver cancer belong to the hepatocellular carcinoma (HCC) category. HCC is a rapidly developing disease with poor prognosis. Currently, less than 18% of HCC patients have an overall survival (OS) time of more than 5 years [2]. In addition, due to the heterogeneity and the lack of effective prognostic markers for HCC, it is difficult to accurately predict the prognosis of patients with HCC [3, 4]. It is urgent to study the prognostic markers of HCC to ensure that patients could receive more appropriate and effective treatment.

For many cancer types, the identification of specific molecular markers can solve the problem of prognosis differentiation caused by tumor heterogeneity and provide patients with more suitable and effective treatment. For example, the *KRAS* gene mutation shows a high prediction accuracy for the prognosis of patients with metastatic colorectal cancer [5], and accumulated studies have established that the methylation level of the promoter of *MGMT* can be used to predict the efficacy of temozolomide in patients with glioma [6]. However, there are currently no available molecular markers for HCC in clinical applications.

Peroxisome proliferator-activated receptors (PPARs) are nuclear receptors as transcription factors that regulate

physiological activities such as invasion, immune tolerance, metabolism, and inflammation [7, 8]. Numerous studies have revealed that tumorigenesis and cancer progression are usually accompanied by abnormal regulation of the PPAR signaling pathway [9–12]. In addition, in recent studies on HCC prognostic markers, it has been repeatedly reported that the PPAR signaling pathway is dysregulated in high-risk HCC patients with poor prognosis [13–15]. Although the PPAR signaling pathway has been reported as one of the prognostic characteristic pathways of HCC, no one has screened the prognostic markers for HCC from the genes involved in this pathway.

In the context of the above research, this study was dedicated to select a prognostic multigene biomarker in HCC from PPAR-related genes. Based on 365 HCC samples included in TCGA, we analyzed the correlation between the mRNA levels of 69 PPAR-related genes and the overall survival of patients. A combination of three genes (*MMP1*, *HMGCS2*, and *SLC27A5*) was selected as a prognostic marker. Next, the performance of the prognostic marker was evaluated and validated in three validation sets from the GEO database. At the same time, the effects of this marker and other clinical indicators on the OS of HCC were analyzed and compared. Finally, a nomogram was developed to provide the possibility of clinical application of the prognostic multigene biomarker.

2. Materials and Methods

2.1. Sample Acquisition and Data Preprocessing. The 365 primary HCC samples with survival information in the TCGA cohort were selected as the training set. The level 3 values of mRNA and corresponding clinical data of HCC were collected from Xena, University of California, Santa Cruz (UCSC) database. The values of gene expression were the counts obtained by the RSEM algorithm. Used UCSC Xena HUGO probeMap to map genes to reference genomes. For details of the processing method, please refer to the website of the TCGA Genome Characterization Center of the University of North Carolina. In addition, removed low-expressed genes that were not expressed in more than 75% of patients and whose average values of expression were less than 1.

The validation sets were three HCC datasets in the GEO database: GSE14520 ($n = 221$), GSE36376 ($n = 223$), and GSE76427 ($n = 115$) (n represents the number of samples). We chose the normalized mRNA data. For details, please refer to the "_series_matrix.txt" files of the three datasets in GEO. Gene annotation was completed according to the annotation files provided by the microarray sequencing platforms (that is, GSE14520 corresponds to GPL3921, and GSE36376 and GSE76427 both correspond to GPL10558). When a gene matched multiple probes, the average expression value of multiple probes was selected as the expression value of the gene.

In addition, 69 PPAR signaling pathway-related genes were obtained from the Kyoto Encyclopedia of Genes and Genomes (KEGG) database (KEGG pathway ko03320).

2.2. Screening and Evaluating Prognostic Genes. To find an efficient prognostic gene combination for HCC from 69 genes related to the PPAR signaling pathway, firstly, based on the expression values of these 69 genes, we used the univariate Cox regression algorithm to analyze the OS of HCC patients. The genes with $p < 0.05$ were considered as genes related to the OS of HCC. Subsequently, based on the candidate genes selected in the previous step, using the lasso Cox regression algorithm, and applying tenfold cross-validation to select the best penalty coefficient, the best combination of HCC prognostic genes could be obtained [16].

To evaluate the effectiveness of the prognostic gene combination we selected, we used Equation (1) to establish a prognostic model:

$$\text{Risk score} = \sum_{i}^{n} x_i * \beta_i, \tag{1}$$

where x_i indicates the expression value of gene i; meanwhile β_i means the coefficient of gene i generated from the multivariate Cox regression analysis. The risk score of each HCC sample was calculated according to Equation (1), and the samples were divided into high- and low-risk groups according to the median value of the risk score. To assess the survival difference between the two groups to show the efficiency of our prognostic genes, a log-rank test analysis was performed. In addition, we evaluated the specificity and sensitivity of the multigene marker in predicting the 1-, 3-, and 5-year survival rates of HCC and compared them with other clinical indicators such as age, gender, AFP, and TNM staging, and the method used was a time-dependent receiver operating characteristic (ROC) curve. The predictive effect of the multigene marker eventually was verified in the GSE14520, GSE36376, and GSE76427 datasets.

2.3. Detecting the Independence of the Multigene Signature. To find out whether this multigene marker could be independent of other clinically commonly used prognostic indicators of HCC, we applied univariate and multivariate Cox regression analysis methods to analyze the survival of HCC patients. As for the clinical factors that might affect the prognosis of HCC, we selected six indicators: age, gender, AFP, TNM staging, histological grade, and vascular tumor invasion. Risk score and age were treated as continuous variables, while the remaining variables were categorical variables. Clinical indicators associated with survival were initially identified; then, the association between risk scores and other survival-associated clinical indicators was assessed with a log-rank test. A nomogram was constructed using those variables that were identified as independent predictors, which the predictions of 1-, 3-, and 5-year survival rates were corrected by correcting for the consistency between true and predicted values.

2.4. Statistical Methods. The R software (version 3.6.1) was used for all analyses in the present study. Microarray data were analyzed with the "GEOquery" package, while the "edgeR" package was employed for differential gene screening. The "survival::coxph" function was used to conduct

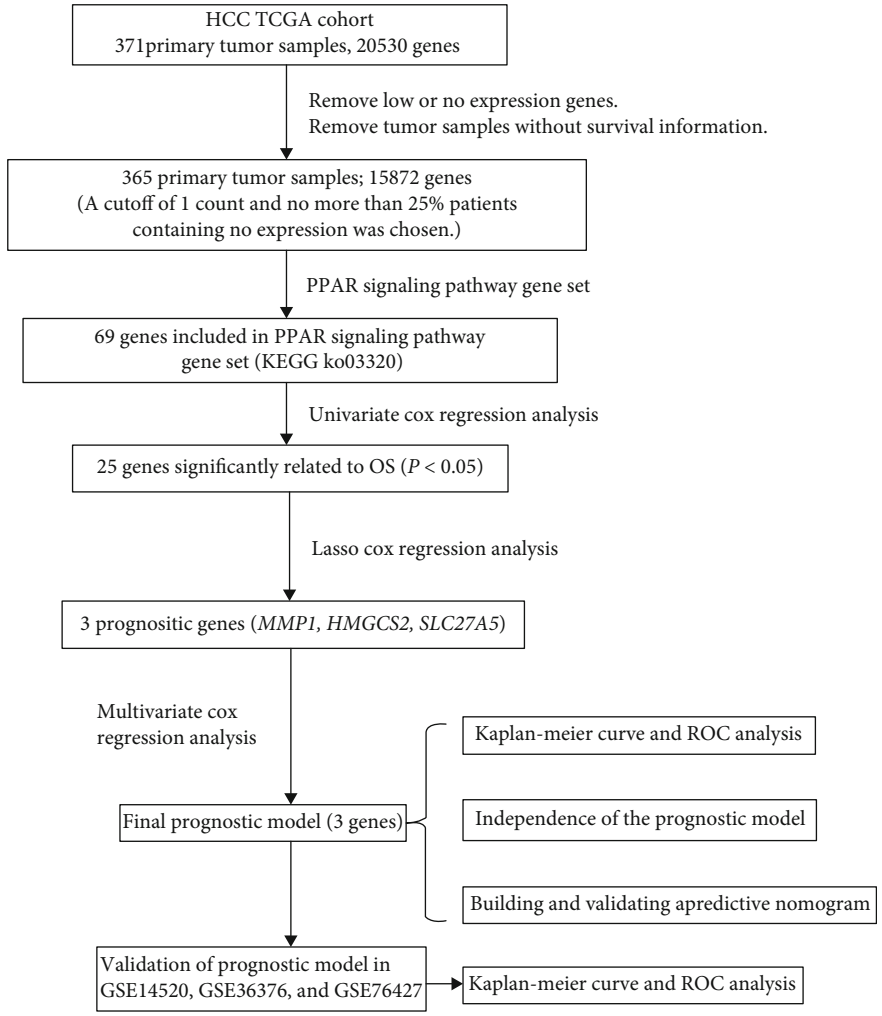

Figure 1: The flow chart about the study of PPAR-related gene signature in predicting survival of HCC.

univariate and multivariate Cox analyses, while lasso Cox regression analyses were performed with the web-based tool (ESurv) [17]. The "survdiff" function from the "survival" package was utilized for log-rank testing, and time-dependent ROC analyses were similarly conducted with the "timeROC" package. Heatmaps were prepared with the "ggplot::heatmap" function, while the "forestplot" package was used to generate forest plots, and the nomogram was established and implemented with the "rms" package.

3. Results

3.1. PPAR-Related Prognostic Genes for HCC. Our study was carried out through the procedure which is shown in Figure 1. To determine genes related to the OS of HCC from the PPAR signaling pathway, we analyzed the transcriptome data of 365 primary HCC samples in TCGA and used univariate cox regression analysis. Twenty-five PPAR-related genes were identified as being related to the OS of HCC ($p < 0.05$). Finally, three prognostic genes (including *MMP1*, *HMGCS2*, and *SLC27A5*) were obtained by lasso Cox regression analysis from candidate prognostic genes (Figure 2).

3.2. Prognostic Model Establishment and Evaluation. A prognostic model was next established to evaluate the relevance of *MMP1*, *HMGCS2*, and *SLC27A5* as predictors of HCC patient outcomes based upon the expression of these three genes. Regression coefficients for each gene were obtained through a multivariate Cox regression analysis, yielding the following model: risk score = 0.1488 ∗ expression value of *MMP1* + (−0.0393) ∗ expression value of *HMGCS2* + (−0.0479) ∗ expression value of *SLC27A5*. The predictive efficacy of this model was then assessed by assigning risk scores to 365 HCC patient samples in the TCGA database (Supplemental file 1). In this analysis, patients in the high-risk group exhibited as significantly poorer prognosis relative to patients in the low-risk group ($p < 0.0001$; Figure 3(a)). Specifically, high-risk patients had a median OS of 17.8 months, whereas low-risk patients had a median OS of 22.0 months. Time-dependent ROC analyses were additionally performed to assess 1-, 3-, and 5-year OS, yielding corresponding area under the curve (AUC) values of 0.702, 0.694, and 0.652, consistent with satisfactory model performance (AUC > 0.5; Figure 3(b)). Additionally, high-risk scores were associated with the earlier happened death incident of the patient, coinciding with higher *MMP1* expression and lower *HMGCS2*

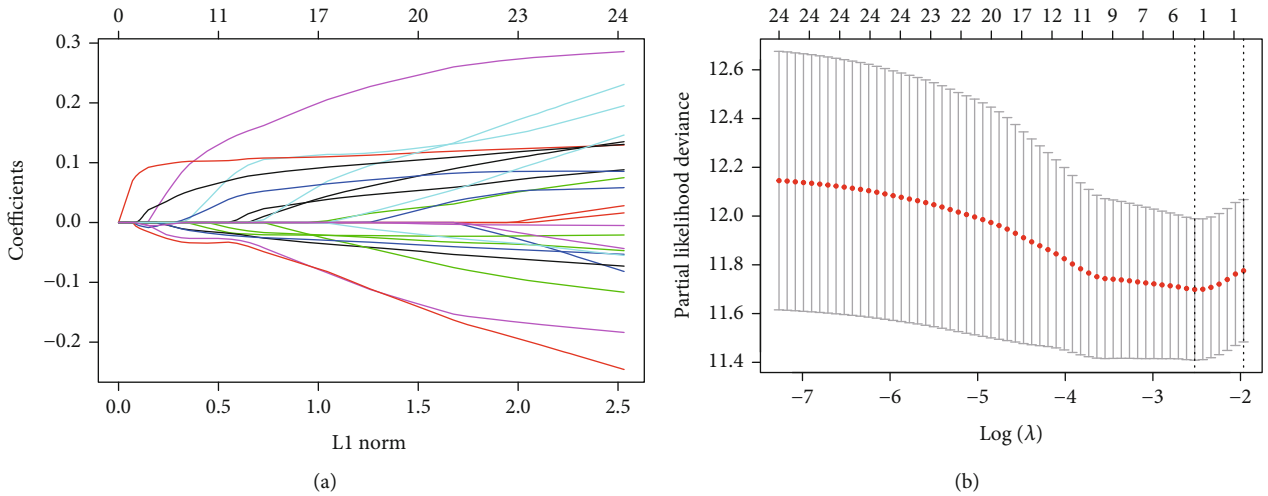

Figure 2: Prognostic gene screening was conducted through lasso Cox regression analyses. Positive and negative regression coefficients, respectively, correspond to positive and negative correlations between numbers (a). The best parameter (λ) in the lasso analysis was then selected (b).

and *SLC27A5* expression (Figure 3(c)). These data suggested that *MMP1* was not advantageous for the prognosis of HCC, whereas *HMGCS2* and *SLC27A5* were. To compare the prognostic efficacy of our risk scores to other clinical factors, time-dependent ROC analyses were additionally performed based upon patient 1-year OS. Of the analyzed risk factors, risk scores exhibited the best prognostic efficacy, yielding an AUC value of 0.702 (Figure 3(d)). As such, these data indicate that we were able to successfully establish a PPAR-related HCC prognostic model in which *MMP1*, *HMGCS2*, and *SLC27A5* serve as effective predictors of HCC patient outcomes.

3.3. Verification of the Prognostic Efficacy of the Multigene Signature. To ensure that this multigene signature was not prognostic as a consequence of data overfitting, we validated this signature using three independent datasets GSE14520, GSE36376, and GSE76427. The median OS of patients in the high-risk group (32.8 months in GSE14520 (Figure 4(a)), 63.7 months in GSE36376 (Figure 4(d)), and 11.8 months in GSE76427 (Figure 4(g))) was significantly decreased ($p = 0.00014$, $p = 0.0087$, and $p = 0.045$) relative to that of patients in the low-risk group (53.7 months in GSE14520, 82.7 months in GSE36376, and 16.6 months in GSE76427), consistent with the results from our training dataset. In the three datasets, the AUC values for 1-, 3-, and 5-year OS were 0.693, 0.696, and 0.640 (Figure 4(b)); 0.784, 0.693, and 0.652 (Figure 4(e)); and 0.566, 0.632, and 0.784, respectively (Figure 4(h)). Furthermore, in line with the results from the TCGA cohort, higher risk scores were consistent with the earlier happened patient's death incident and with higher *MMP1* and lower *HMGCS2* and *SLC27A5* expression (Figures 4(c), 4(f), and 4(i)). These results suggest that this PPAR-related risk model was robust across platforms.

3.4. The Independence of the Prognostic Multigene Signature. To confirm the independent predictive value of this multigene signature, we next explored the relationship between HCC patient clinical characteristics, risk score, and outcomes in the TCGA cohort. In univariate Cox regression analyses, TNM stage and risk score were both significantly associated with patient OS ($p < 0.001$). Correlations between vascular tumor invasion and OS approached but did not reach significance ($p = 0.056$). These three factors were then incorporated as covariates in a multivariate Cox regression analysis which revealed both risk score (HR = 2.29, 95%CI = 1.45-3.61, $p < 0.001$) and TNM stage (HR = 2.14, 95%CI = 1.41-3.25, $p < 0.001$) to be independent prognostic factors for HCC patient OS (Figure 5(a)). Additionally, we found that whether a patient exhibited early (stage I+II, Figure 5(b)) or advanced (stage III+IV, Figure 5(c)) stage disease and whether or not they exhibited vascular invasion (Figures 5(d) and 5(e)) were predictive of patient survival, underscoring the independent prognostic value of our multigene signature.

3.5. Nomogram Establishment and Evaluation. To assess the ability of our model to reliably predict the clinical prognosis of HCC, we next established a nomogram incorporating TNM stage and risk scores as two independent prognostic factors associated with HCC patient 1-, 3-, and 5-year OS (Figure 6(a)). This nomogram yielded a C-index value of 0.709. Calibration plots for all three of these survival time points additionally indicated that the nomogram exhibited good predictive ability (Figure 6(b)). As such, we were able to successfully confirm the reliability and potential clinical value of our multigene signature.

4. Discussion

The role of PPARs in the development of cancers including HCC has been revealed by a growing body of research literature [18]. In HCC, current studies on the sensitivity to chemotherapy of PPARs [19] and the correlation between PPARs' target genes and the survival of patients with HCC [20] suggest that finding prognostic markers from PPAR-related genes is more clinically meaningful. Therefore, in this

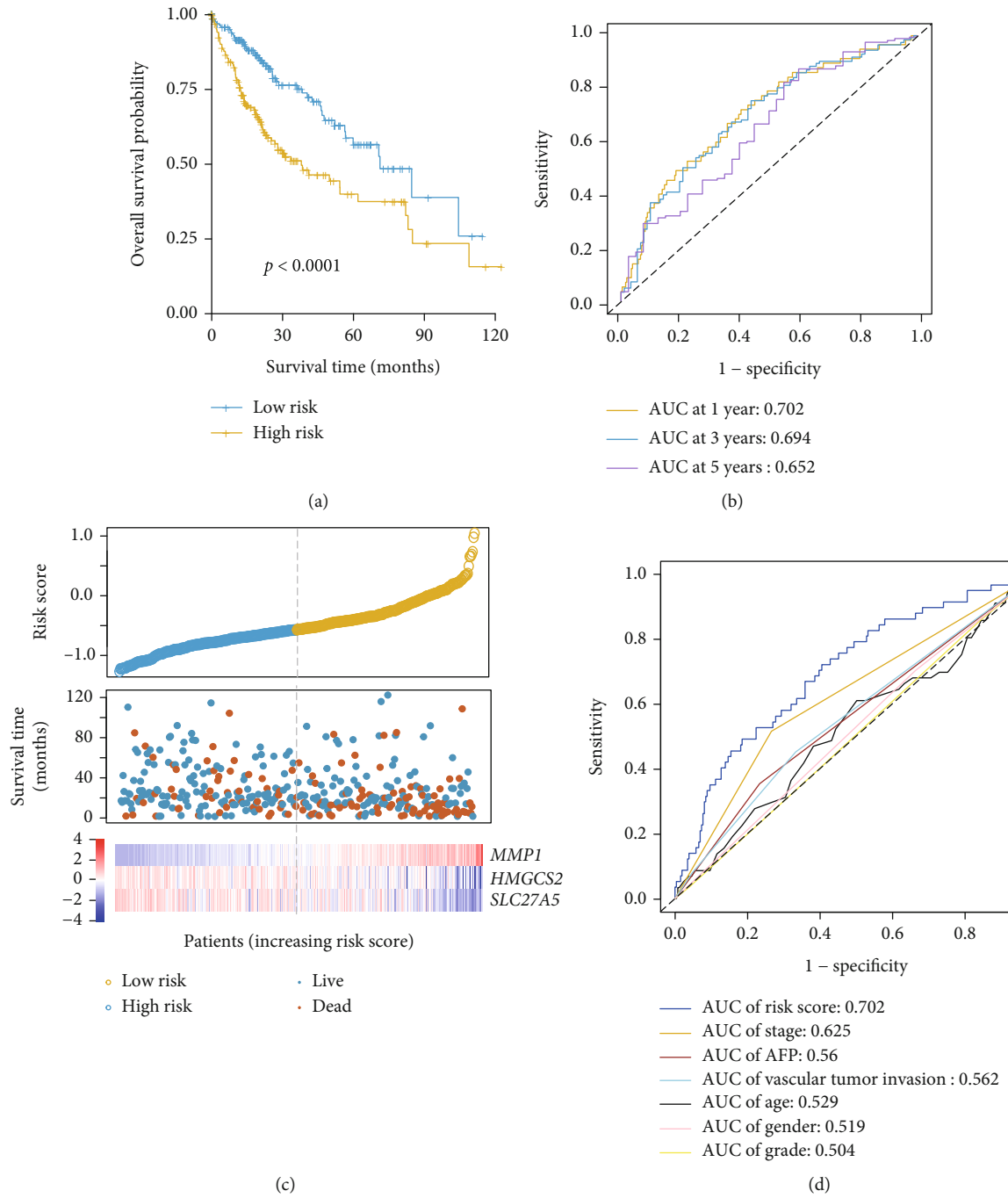

Figure 3: PPAR-associated prognostic genes were significantly associated with HCC patient overall survival. A Kaplan-Meier analysis of low- and high-risk patients in the TCGA HCC patient cohort, revealing a poorer prognosis for those with high-risk scores (a). A ROC analysis of risk scores was performed to assess their sensitivity and specificity (b). The relationship between risk scores, mortality, and characteristic gene expression (c). Risk score AUC values and clinical indicators at the one-year OS are shown (d).

study, to find out the PPAR-related prognostic markers of HCC, we used the HCC patient data collected in TCGA to analyze the 69 genes involved in the PPAR signaling pathway. Finally, the combination of *MMP1*, *HMGCS2*, and *SLC27A5* was screened out as a multigene marker for the prognosis of HCC. The prognostic performance of the marker we selected was good, and the verification in the GEO validation sets shows that there was no sample bias.

In this study, among the three PPAR-related prognostic genes screened, *MMP1* is unfavorable for the prognosis of HCC, while *HMGCS2* and *SLC27A* are favorable (Figure 3(c)). These results were verified by using the Pathology Atlas of the Human Protein Atlas (HPA) database (https://www.proteinatlas.org/). *MMP1* is a member of the matrix metalloproteinase family which has been reported as a risk factor for cancer development [21–23]. In addition,

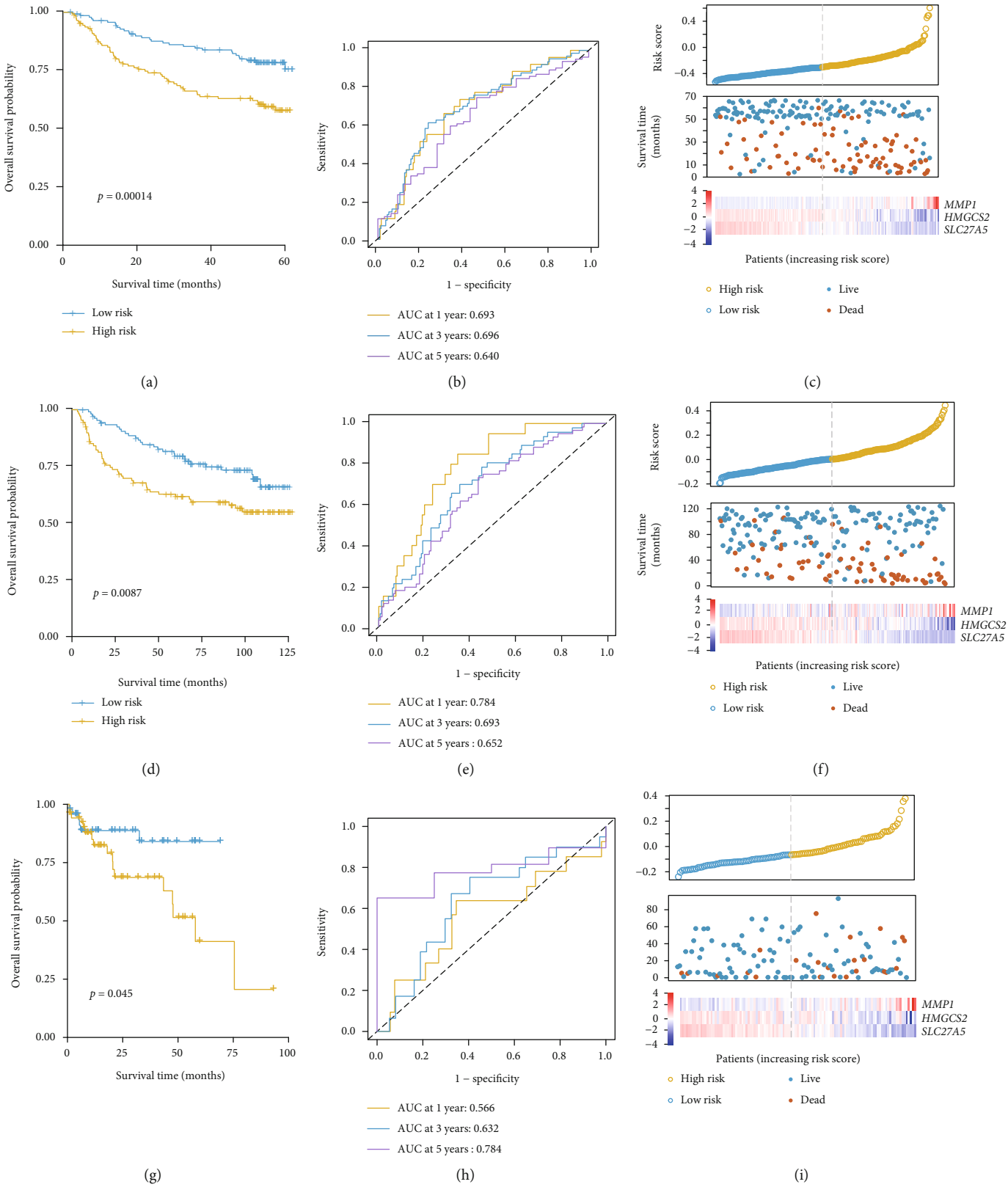

Figure 4: Prognostic model validation. The prognostic efficacy of this model was assessed with the GSE14520 (a–c), GSE36376 (d–f), and GSE76427 (g–i) verification datasets.

Characteristics	HR (95% CI)	P value
Univariate analysis		
Risk score (−1.40~1.07)	2.72 (1.87–3.95)	<0.001
Age (16~90 years)	1.01 (1.00–1.03)	0.079
Gender (male/female)	0.82 (0.57–1.16)	0.263
AFP (≥ = 400/<400 ng/ml)	1.05 (0.65–1.73)	0.831
TNM stage (III+IV/I+II)	2.48 (1.76–3.50)	<0.001
Histologic grade (4/3/2/1)	1.12 (0.89–1.42)	0.339
Vascular tumor invasion (macro/micro/none)	1.37 (0.99–1.90)	0.056
Multivariate analysis		
Risk score (−1.40~1.07)	2.29 (1.45–3.61)	<0.001
TNM stage (III+IV/I+II)	2.14 (1.41–3.25)	<0.001
Vascular tumor invasion (macro/micro/none)	1.08 (0.77–1.50)	0.655

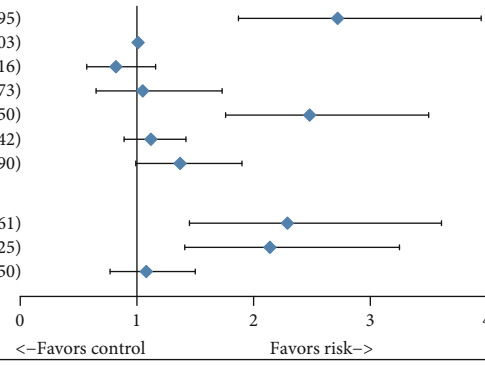

(a)

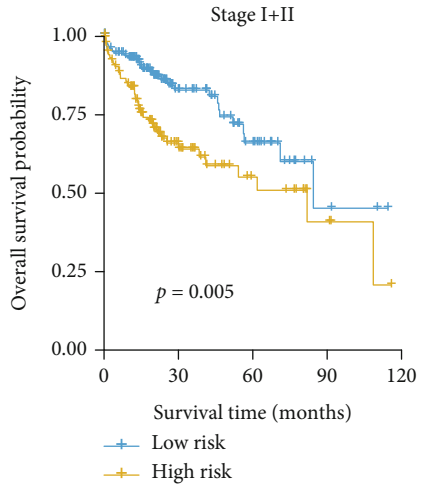

(b)

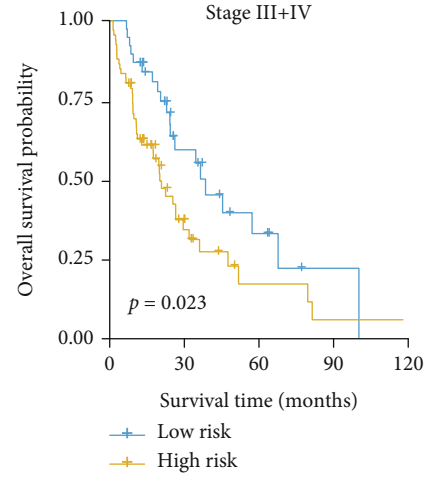

(c)

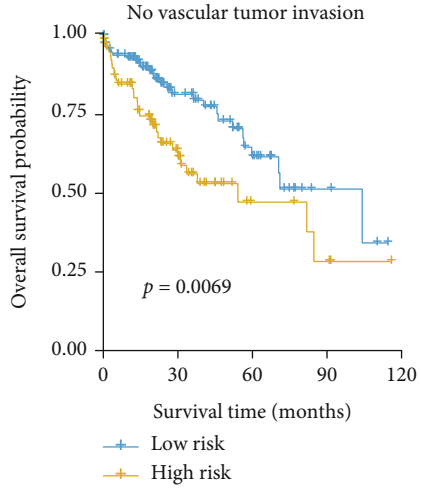

(d)

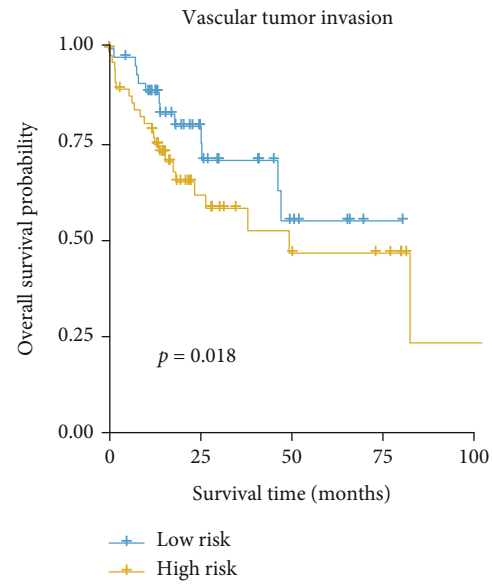

(e)

Figure 5: Risk scores are an independent predictor of patient outcomes. Forest plots corresponding to univariate and multivariate Cox regression analyses of the relationship between HCC patient OS and various clinical indicators and risk scores (a). Patients were classified based upon whether they exhibited vascular invasion and based upon their TNM stage. Risk score performance in each patient subcategory was then assessed (b–e).

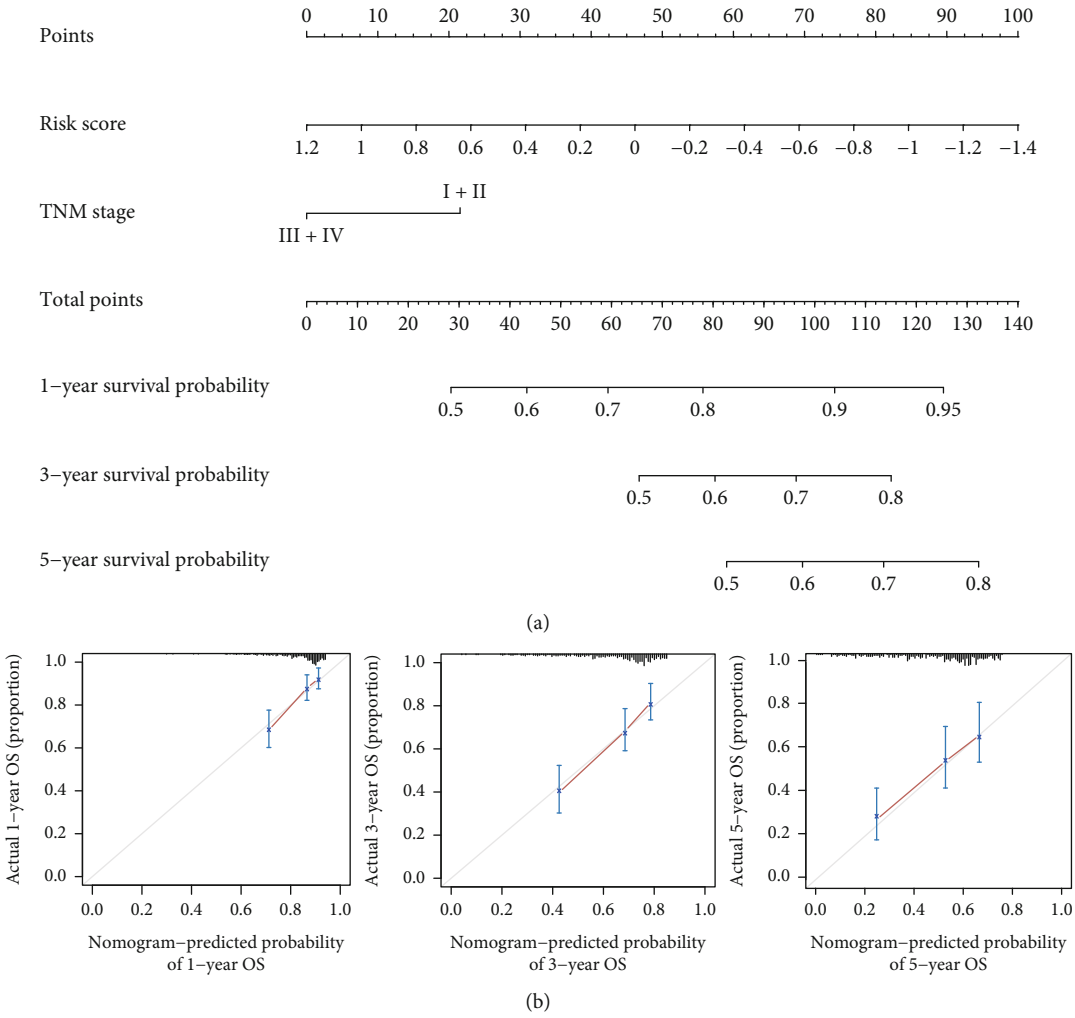

Figure 6: The established nomogram exhibited good predictive ability. This nomogram was generated using a combination of risk scores and TNM stage to predict HCC patient OS (a). Calibration charts corresponding to the prediction of 1-, 3-, and 5-year survival in the training cohort. Horizontal and vertical axes, respectively, correspond to the predicted and actual survival probability (b).

Liao et al. explored the prognostic value of *MMP1* in HCC [24], and the results were consistent with this article. Regarding *HMGCS2*, it is confirmed by researchers as a cancer suppressor [25]. In HCC, the reduction of *HMGCS2* is accompanied by a poor prognosis and promotes cancer cell migration [26]. *SLC27A* is an isozyme of very long-chain acyl-CoA synthetase (VLCS) expressed in the liver. In the current study, the effect of *SLC27A* in HCC or any other cancer has not been reported. In summary, regarding the *MMP1* and *HMGCS2* selected in this article, studies have reported their possible role in the prognosis of HCC. Judging from the current reports, the prognostic genes we selected are relatively reliable. As for *SLC27A*, which has not yet reported its role in HCC or any other cancer, our research presents new possibilities.

5. Conclusions

In summary, we found that the PPAR-associated multigene signature selected in this study was able to reliably serve as an independent predictor of HCC prognosis. This signature is robust owing to the cross-platform and cross-batch predictions conducted herein. Overall, our study highlights new potential directions for preclinical research and for the implementation of personalized medicine-based approaches to evaluating HCC patient prognosis and treatment.

Data Availability

The mRNA and corresponding phenotype data were obtained from UCSC Xena (https://tcga.xenahubs.net/download/TCGA.LIHC.sampleMap/HiSeqV2.gz; https://tcga.xenahubs.net/download/TCGA.LIHC.sampleMap/LIHC_clinicalMatrix) and GEO (GSE14520_GPL3921, GSE36376_GPL10558, and GSE76427_GPL10558).

Conflicts of Interest

The authors have declared that no competing interest exists.

Authors' Contributions

Wenfang Xu and Zhen Chen contributed equally to this work and are considered to be co-first authors.

Acknowledgments

This study was supported by the National Key Research and Development Program of China (No. 2018YFC0910700), Shanghai Science and Technology Committee (No. 17ZR1427000), and National Natural Science Fund of China (No. 81772591).

Supplementary Materials

Supplemental File 1: the risk scores and groupings of 365 HCC samples in TCGA. *(Supplementary Materials)*

References

[1] A. J. Craig, J. von Felden, T. Garcia-Lezana, S. Sarcognato, and A. Villanueva, "Tumour evolution in hepatocellular carcinoma," *Nature Reviews. Gastroenterology & Hepatology*, vol. 17, no. 3, pp. 139–152, 2020.

[2] R. L. Siegel, K. D. Miller, and A. Jemal, "Cancer statistics, 2020," *CA: a Cancer Journal for Clinicians*, vol. 70, no. 1, pp. 7–30, 2020.

[3] S. Colagrande, A. L. Inghilesi, S. Aburas, G. G. Taliani, C. Nardi, and F. Marra, "Challenges of advanced hepatocellular carcinoma," *World Journal of Gastroenterology*, vol. 22, no. 34, pp. 7645–7659, 2016.

[4] J. A. Marrero, M. Kudo, and J. P. Bronowicki, "The challenge of prognosis and staging for hepatocellular carcinoma," *The Oncologist*, vol. 15, Supplement 4, pp. 23–33, 2010.

[5] C. J. Allegra, J. M. Jessup, M. R. Somerfield et al., "American Society of Clinical Oncology provisional clinical opinion: testing for KRAS gene mutations in patients with metastatic colorectal carcinoma to predict response to anti-epidermal growth factor receptor monoclonal antibody therapy," *Journal of Clinical Oncology*, vol. 27, no. 12, pp. 2091–2096, 2009.

[6] J. T. Jordan, E. R. Gerstner, T. T. Batchelor, D. P. Cahill, and S. R. Plotkin, "Glioblastoma care in the elderly," *Cancer*, vol. 122, no. 2, pp. 189–197, 2016.

[7] C. H. Lee, P. Olson, and R. M. Evans, "Minireview: lipid metabolism, metabolic diseases, and peroxisome proliferator-activated receptors," *Endocrinology*, vol. 144, no. 6, pp. 2201–2207, 2003.

[8] A. Oyefiade, L. Erdman, A. Goldenberg et al., "PPAR and GST polymorphisms may predict changes in intellectual functioning in medulloblastoma survivors," *Journal of Neuro-Oncology*, vol. 142, no. 1, pp. 39–48, 2019.

[9] S. D. Lv, W. Wang, H. Y. Wang, Y. T. Zhu, and C. Y. Lei, "PPARγ activation serves as therapeutic strategy against bladder cancer via inhibiting PI3K-Akt signaling pathway," *BMC Cancer*, vol. 19, no. 1, p. 204, 2019.

[10] Y. K. Zou, A. Watters, N. Cheng et al., "Polyunsaturated fatty acids from astrocytes activate PPARγ signaling in cancer cells to promote brain metastasis," *Cancer Discovery*, vol. 9, no. 12, pp. 1720–1735, 2019.

[11] W. H. Chang and A. G. Lai, "The pan-cancer mutational landscape of the PPAR pathway reveals universal patterns of dysregulated metabolism and interactions with tumor immunity and hypoxia," *Ann Ny Acad Sci.*, vol. 1448, no. 1, pp. 65–82, 2019.

[12] X. X. Zhang, J. N. Yao, H. L. Shi, B. Gao, and L. F. Zhang, "LncRNA TINCR/microRNA-107/CD36 regulates cell proliferation and apoptosis in colorectal cancer via PPAR signaling pathway based on bioinformatics analysis," *Biological Chemistry*, vol. 400, no. 5, pp. 663–675, 2019.

[13] G. Ning, Y.-L. Huang, L.-M. Zhen et al., "Prognostic value of complement component 2 and its correlation with immune infiltrates in hepatocellular carcinoma," *BioMed Research International*, vol. 2020, Article ID 3765937, 12 pages, 2020.

[14] Z. Zeng, Z. Cao, and Y. Tang, "Identification of diagnostic and prognostic biomarkers, and candidate targeted agents for hepatitis B virus-associated early stage hepatocellular carcinoma based on RNA-sequencing data," *Oncology Letters*, vol. 20, no. 5, p. 1, 2020.

[15] Z. Zhao, L. Yang, S. Fang et al., "The effect of m6A methylation regulatory factors on the malignant progression and clinical prognosis of hepatocellular carcinoma," *Frontiers in Oncology*, vol. 10, p. 1435, 2020.

[16] R. Tibshirani, "The lasso method for variable selection in the Cox model," *Statistics in Medicine*, vol. 16, no. 4, pp. 385–395, 1997.

[17] K. Pak, S. O. Oh, T. S. Goh et al., "A user-friendly, web-based integrative tool (ESurv) for survival analysis: development and validation study," *Journal of Medical Internet Research*, vol. 22, no. 5, article e16084, 2020.

[18] J. Youssef and M. Badr, "Peroxisome proliferator-activated receptors and cancer: challenges and opportunities," *British Journal of Pharmacology*, vol. 164, no. 1, pp. 68–82, 2011.

[19] M. J. Kim, Y. K. Choi, S. Y. Park et al., "PPARδ reprograms glutamine metabolism in sorafenib-resistant HCC," *Molecular Cancer Research*, vol. 15, no. 9, pp. 1230–1242, 2017.

[20] H. Nojima, S. Kuboki, K. Shinoda et al., "Activation of peroxisome proliferator-activated receptor-gamma inhibits tumor growth by negatively regulating nuclear factor-κB activation in patients with hepatocellular carcinoma," *Journal of Hepato-Biliary-Pancreatic Sciences*, vol. 23, no. 9, pp. 574–584, 2016.

[21] S. S. Zhao and M. X. Yu, "Identification ofMMP1as a potential prognostic biomarker and correlating with immune infiltrates in cervical squamous cell carcinoma," *DNA and Cell Biology*, vol. 39, no. 2, pp. 255–272, 2020.

[22] F. R. de Matos, E. de Moura Santos, H. B. de Pontes Santos et al., "Association of polymorphisms in _IL-8_ , _MMP-1_ and _MMP-13_ with the risk and prognosis of oral and oropharyngeal squamous cell carcinoma," *Archives of Oral Biology*, vol. 108, p. 104547, 2019.

[23] Y. Ma, X. Yang, Y. P. Xie, C. Yi, F. Zhao, and Y. Huang, "Association of matrix metalloproteinase1-1607 1G>2G polymorphism and lung cancer risk: an update by meta-analysis," *Asian Pacific Journal of Cancer Prevention*, vol. 20, no. 6, pp. 1841–1847, 2019.

[24] M. Liao, P. Tong, J. Zhao et al., "Prognostic value of matrix metalloproteinase-1/ proteinase-activated receptor-1 signaling axis in hepatocellular carcinoma," *Pathology Oncology Research*, vol. 18, no. 2, pp. 397–403, 2012.

[25] S. Wan, M. Xi, H. B. Zhao et al., "HMGCS2 functions as a tumor suppressor and has a prognostic impact in prostate cancer," *Pathology, Research and Practice*, vol. 215, no. 8, p. 152464, 2019.

[26] S.-G. Su, M. Yang, M.-F. Zhang et al., "miR-107-mediated decrease of HMGCS2 indicates poor outcomes and promotes cell migration in hepatocellular carcinoma," *The International Journal of Biochemistry & Cell Biology*, vol. 91, no. Part A, pp. 53–59, 2017.

Hindawi
PPAR Research
Volume 2021, Article ID 6632137, 15 pages
https://doi.org/10.1155/2021/6632137

Research Article

Pemafibrate Pretreatment Attenuates Apoptosis and Autophagy during Hepatic Ischemia-Reperfusion Injury by Modulating JAK2/STAT3β/PPARα Pathway

Ziqi Cheng and Chuanyong Guo

Department of Gastroenterology, Shanghai Tenth People's Hospital, Tongji University School of Medicine, Shanghai 200072, China

Correspondence should be addressed to Chuanyong Guo; guochuanyong@hotmail.com

Received 6 November 2020; Accepted 1 March 2021; Published 11 March 2021

Academic Editor: Christopher Lau

Hepatic ischemia-reperfusion injury (HIRI) is a common phenomenon in liver transplantation and liver surgery. This article is aimed at clarifying the role of pemafibrate in HIRI through JAK2/STAT3β/PPARα. In the experiment, we divided Balb/c into seven groups, namely, normal control (NC), Sham, PEM (1.0 mg/kg), IRI, IRI + PEM (0.1 mg/kg), IRI + PEM (0.5 mg/kg), and IRI + PEM (1.0 mg/kg). We used biochemical assay, histopathological evaluation, immunohistochemistry, RT-PCR and qRT-PCR, ELISA analysis, and other methods to determine the level of serum AST, ALT, IL-1β, and TNF-α in the liver at three time points (2 h, 8 h, and 24 h) after reperfusion of apoptosis factor, autophagy factor, and the JAK2/STAT3/PPARα content in tissues. Our experiment results showed that the pemafibrate can effectively reduce the level of hepatic IR injury. In addition, pemafibrate has anti-inflammatory, antiapoptotic, and antiautophagy effects, which are mediated by the JAK2/STAT3β/PPARα pathway.

1. Introduction

Hepatic ischemia-reperfusion injury (HIRI) is the injury caused by reperfusion after liver ischemia [1, 2]. After the blood supply to liver tissue was interrupted due to liver ischemia, the subsequent blood reperfusion brings in a large number of inflammatory cells, which leads to serious damages to the structure and function of the liver [3–5]. Ischemia-reperfusion injury is a complicated pathophysiological process. A large number of studies have shown that HIRI, involving amounts of cells and multiple molecular mechanisms, is characterized by oxidative stress and the release of reactive oxygen species (ROS) [3, 6–8]. ROS is the starting point that causes a cascade of reactions dominated by inflammatory cells, cytokine release, apoptosis, and autophagy [9, 10]. This damage not only affects the liver but also has serious negative effects on the brain, heart, kidneys, and gastrointestinal tract, which is a complex systemic process.

When senescent macromolecular substances appear in and damage the cells, the cells will initiate programmed cell death. Autophagy, a kind of programmed cell death, is a complex process that ensures the normal function of cells and recirculates the digested materials to efficiently maintain the normal activities of cells [11]. Although autophagy is considered to be a self-protection mechanism, excessive upregulation can also cause cell death [12]. Apoptosis, another kind of programmed cell death, has very obvious morphological characteristics, including cell volume reduction, nuclear chromatin shrinkage, and the formation of apoptotic bodies. There are two core molecular families of the apoptosis pathway: the BCL-2 family and the Caspase family [13].

Janus kinase (JAK)/signal transducer and activator of transcription (STAT) participate in signal transduction induced by a number of cytokines and interferons in vivo. After receiving the signal from JAK2, STAT3 forms the dimer after phosphorylation and enters the nucleus to reg-

ulate the transcription of related genes. STAT3 is mainly involved in regulating cell proliferation, differentiation, apoptosis, and inflammation [14–16]. There are two subtypes of STAT3: STAT3α and STAT3β. Interestingly, studies have shown that STAT3α and STAT3β have opposite effects on cancer, but the role of STAT3β in cells is still controversial [17].

Peroxisome proliferator-activated receptor (PPAR) is a member of the nuclear receptor superfamily [18]. As a transcription factor, PPAR establishes a link between transcription and signal molecules, including PPARα, PPARβ, and PPARγ. PPARα is highly expressed in the liver, intestinal epithelial cells, and cardiac muscle cells and plays an important role in fatty acid oxidation. It will combine with retinoid X receptor (RXR) to form a heterodimer, activate the PPAR Response Element (PPRE) located in the upstream of the target gene, and participate in the regulation of nuclear factor κB (NF-κB) and activator protein 1 (AP-1) [18, 19]. Pemafibrate, a new type of selective PPARα modulator (SPPARM α), enhances PPARα's activity and has high selectivity by introducing side chains into fibric acid. These side chains later form a Y-shaped structure and fill in the ligand binding site of PPARα, thereby promoting massive activation of PPARα. Compared with other fibrates, pemafibrate has a feature of basic EC50 value and higher selectivity. Pemafibrate could better aim at specific targets and reduce the risk of binding multiple sites.

Although there are many studies on HIRI, neither the molecular mechanism nor effective drugs to this injury was still not identified. Therefore, to find out the specific drugs that can alleviate HIRI and to clarify the drug action mechanism are urgent problems to be solved at present. We hypothesized that pemafibrate can alleviate HIRI by inhibiting inflammation, apoptosis, and autophagy and conducted the following experiments.

2. Materials and Methods

2.1. Reagents. The pemafibrate was purchased from MedChemExpress (Monmouth Junction, NJ, USA) and used by adding 10% DMSO and 90% corn oil in our experiments. The microplate test kits used for measuring the levels of alanine aminotransferase (ALT) and aspartate aminotransferase (AST) were bought from the Jiancheng Bioengineering Institute (Jiancheng Biotech, Nanjing, China). Enzyme-linked immunosorbent assay (ELISA) kits were acquired from Anogen (Ontario, Canada). The PrimeScript RT Reagent Kit and SYBR Premix Ex Taq were purchased from TaKaRa Biotechnology (Dalian, China).

During the whole experimental process, we used many antibodies, including anti-Bax, anti-caspase 3, anti-caspase 9, anti-Beclin-1, PPARα (Proteintech, Chicago, IL, USA), anti-TNF-α, anti-Bcl-2, anti-microtubule associated protein 1 light chain 3 (LC3), anti-JAK2, anti-STAT3, anti-p-STAT3 (Cell Signaling Technology, Danvers, MA, USA), anti-IL-6, and anti-IL-1β (Antibody Revolution, San Diego, CA, USA).

2.2. Animal Preparation. The protocol of this study was approved by the Animal Care and Use Committee of Shanghai Tongji University. We handled and took care of the animals under the guidance of the National Institutes of Health Guidelines and tried our best to minimize the pain and suffering of mice throughout the whole experiment. We raised the male Balb/c mice (6–8 weeks old, 23 ± 2 g) purchased from the Shanghai SLAC Laboratory Animal Co., Ltd. (Shanghai, China) in a clean and temperature-controlled environment at 24°C ± 2°C under a 12 h : 12 h/light : dark cycle. In the environment, standard laboratory food and water were available freely for mice.

2.3. Experimental Design. We divided the one hundred and two mice randomly into seven groups as follows:

(1) *Normal Control (NC)*. Six mice were only injected with vehicle (10% DMSO and 90% corn oil)

(2) *Sham*. Eighteen mice took laparotomy after anesthesia, and their abdominal cavity was stitched without IRI

(3) *PEM (1.0 mg/kg)*. Six mice were only injected with 1.0 mg/kg PEM

(4) *IRI*. Eighteen mice suffered ischemia and reperfusion

(5) *IRI + PEM (0.1 mg/kg)*. Before IRI, eighteen mice were injected with 0.1 mg/kg PEM for 5 days

(6) *IRI + PEM (0.5 mg/kg)*. Before IRI, eighteen mice were injected with 0.5 mg/kg PEM for 5 days

(7) *IRI + PEM (1.0 mg/kg)*. Before IRI, eighteen mice were injected with 1.0 mg/kg PEM for 5 days [20–22]

Given the pharmacokinetics and initial experiment of PEM for 5 days before IRI, a certain dose of PEM determined by a previous study and initial experiments was injected into mice's abdomens. At 2 h, 8 h, or 24 h after IRI, we randomly killed six mice in each group and then collected blood and liver tissues for further experiments.

2.4. Establishment of a Hepatic IRI Mouse Model. In this experiment, we established a warm hepatic IRI animal model. Before surgery, we kept mice not taking food for twelve hours but allowed them to drink water freely, then used sodium pentobarbital (40 mg/kg, 1.25%) (Nembutal, St Louis, MO, USA) to anesthetize the mice by intraperitoneal injection. When the algesia of these mice disappears completely, we started to perform laparotomy. After disinfecting the skin with alcohol, we made an incision along the linea alba and entered into the abdominal cavity through the incision. After spotting the liver, we turned the hepatic lobes over to expose the first porta hepatis. Following that, we clipped the portal vein, hepatic artery, and common bile duct with microarterial clamps to block the hepatic blood flow. Once hepatic ischemia occurred, the color of liver lobes turned immediately from dark red to pale red. Then, we placed the mice on an electric blanket to maintain their body temperature with a humid saline gauze covered on their incisions. We

removed the clamps after blocking the blood flow for 45 min and then let the blood flow back to the liver, by which the liver completed a reperfusion process. In the final step, we stitched the abdominal cavity and placed these mice on electric blankets [23, 24].

2.5. Biochemical Assays. We collected the orbital blood samples of the mice who had suffered hepatic ischemia and reperfusion processes, then extracted serum from the samples by centrifuging at 2,000 × g at 4°C for 10 min and stored it at −80°C. Following the instructions of the manufacturer protocols, we used the microplate test kits (Olympus AU1000, Olympus, Tokyo, Japan) to detect serum levels of ALT and AST and used the ELISA kits to measure serum levels of IL-1β and TNF-α.

2.6. Histopathological Evaluation. We removed the liver from the abdomen cavity of mice, then put the liver tissue in 4% paraformaldehyde for twenty-four hours for renovation. On the next day, we dehydrated it with ethanol of different concentrations. After that, we embedded paraffin into the tissues and cut them into slices about 3 μm thick. Finally, we stained the slices with hematoxylin and eosin (H&E) to observe the degree of damage.

2.7. Immunohistochemistry. We put these liver slices in a baking oven at 60°C for 20 min to remove the residual wax on them and then rehydrated the slices with xylene and ethanol. After that, we retrieved the antigen by heating the slices at 95°C for 10 min and then cooled them to 25°C. Blocking endogenous peroxidase activity was achieved by immersing the slices in hydrogen peroxide (H_2O_2) solution (3%) for 20 min at 37°C. In order to avoid generating high backgrounds, we used 5% bovine serum albumin to block nonspecific binding sites for 1 h. Then, the liver slices were incubated overnight with primary antibodies against Bcl-2 (1 : 500), Bax (1 : 500), Beclin-1 (1 : 500), and LC3 (1 : 500) at 4°C. In the next morning, we added the slices into a secondary antibody which can bond the primary antibodies specifically and incubated them for 1 h at 37°C. The efficacy of antibody binding can be detected by a diaminobenzidine kit. Lastly, we observed slices under an optical microscope.

2.8. Reverse Transcription Polymerase Chain Reaction (RT-PCR) and Quantitative Real-Time PCR (qRT-PCR). All RNAs of liver tissues were extracted by TRIzol reagent (Thermo Fisher Scientific, Waltham, MA, USA) and then reversely transcribed into cDNA. We performed qRT-PCR by SYBR Premix EX Taq under the guidance of the manufacturer instructions to detect the level of mRNA with a 7900HT Fast PCR System (Applied Biosystems, Foster City, CA, USA). The primers were β-actin, forward GGCTGTATT CCCCTCCATCG, reverse CCAGTTGGTAACAATGCCA TGT; IL-1β, forward GAATGCCACCTTTTGACAGTG, reverse TGGATGCTCTCATCAGGACAG; IL-6, forward CTGCAAGAGACTTCCATCCAG, reverse AGTGGTATA GACAGGTCTGTTGG; TNF-α, forward CAGGCGGTGCC TATGTCTC, reverse CGATCACCCCGAAGTTCAGTAG; Bcl-2, forward GCTACCGTCGTCGTGACTTCGC, reverse CCCCACCGAACTCAAAGAAGG; Bax, forward AGAC AGGGGCCTTTTTGCTAC, reverse AATTCGCCGGA GACACTCG; Caspase 3, forward CTCGCTCTGGTACG GATGTG, reverse TCCCATAAATGACCCCTTCATCA; Caspase 9, forward GGCTGTTAAACCCCTAGACCA, reverse TGACGGGTCCAGCTTCACTA; Beclin-1, forward ATGGAGGGGTCTAAGGCGTC, reverse TGGGCTGTG GTAAGTAATGGA; LC, forward GACCGCTGTAAGGA GGTGC, reverse AGAAGCCGAAGGTTTCTTGGG; and P62, forward GAGGCACCCCGAAACATGG, reverse ACTTATAGCGAGTTCCCACCA.

2.9. Western Blot Analysis. We extracted the protein from liver tissue by homogenizing with radioimmunoprecipitation assay lysis buffer (Kaiji Biology, Nanjing, China), phenylmethane-sulfonyl fluoride, and protease inhibitors. The protein concentration was measured by a bicinchoninic acid assay (Kaiji Biology). Before performing electrophoresis, we boiled the protein samples at 100°C for 5 min, then used 10% or 12.5% SDS-PAGE to separate proteins from protein samples during electrophoresis at 120 V. Next, we chose the wet transfer method to transfer proteins onto polyvinylidene fluoride membranes (Hybond™; Escondido, CA, USA). One hour later, we used 5% nonfat milk to block the nonspecific binding sites for at least 1 hour, then incubated the membranes overnight at 4°C with the following primary antibodies: anti-β-actin (1 : 1,000), anti-IL-6 (1 : 500), anti-TNF-α (1 : 500), anti-Bcl-2 (1 : 1,000), anti-Bax (1 : 1,000), anti-caspase 3 (1 : 500), anti-caspase 9 (1 : 500), anti-Beclin-1 (1 : 1,000), anti-LC3 (1 : 1,000), anti-JAK2 (1 : 1000), anti-STAT3 (1 : 1000), and anti-p-STAT3 (1 : 1000). In the next morning, we used the 0.1% Tween-contained PBST to wash the membranes for three times, then incubated the membranes with the secondary antibody for 1 h at 37°C, and washed the membranes with PBST for another three times. The aforementioned secondary antibody could be anti-mouse or anti-rabbit antibodies (1 : 2000). Finally, we used an Odyssey two-color infrared laser imaging system (Licor, Lincoln, NE, USA) to observe the chromogenic results.

2.10. Statistical Analysis. In order to ensure the veracity of our study, we performed all experiments at least three times and presented the data as mean ± SD. We analyzed the data and results of the serum levels of ALT, AST, Western blot, ELISA, and qRT-PCR were analyzed by Student's t-test or two-way analysis of variance (followed by post hoc Dunnett's test). When the P values are less than 0.05, we consider the results as statistically significant. All statistical graphs were drawn by GraphPad Prism 8 (GraphPad Software, Inc., San Diego, CA, USA).

3. Results

3.1. Pemafibrate and Surgery Will Not Produce Side Effects on the Structure and Function of the Liver. In order to determine whether liver damage is only caused by the model and whether pemafibrate is hepatotoxic, we detected ALT and AST in the blood samples of the NC group, Sham group, and pemafibrate (1.0 mg/kg) group of mice. The results showed that there was no significant statistical difference in

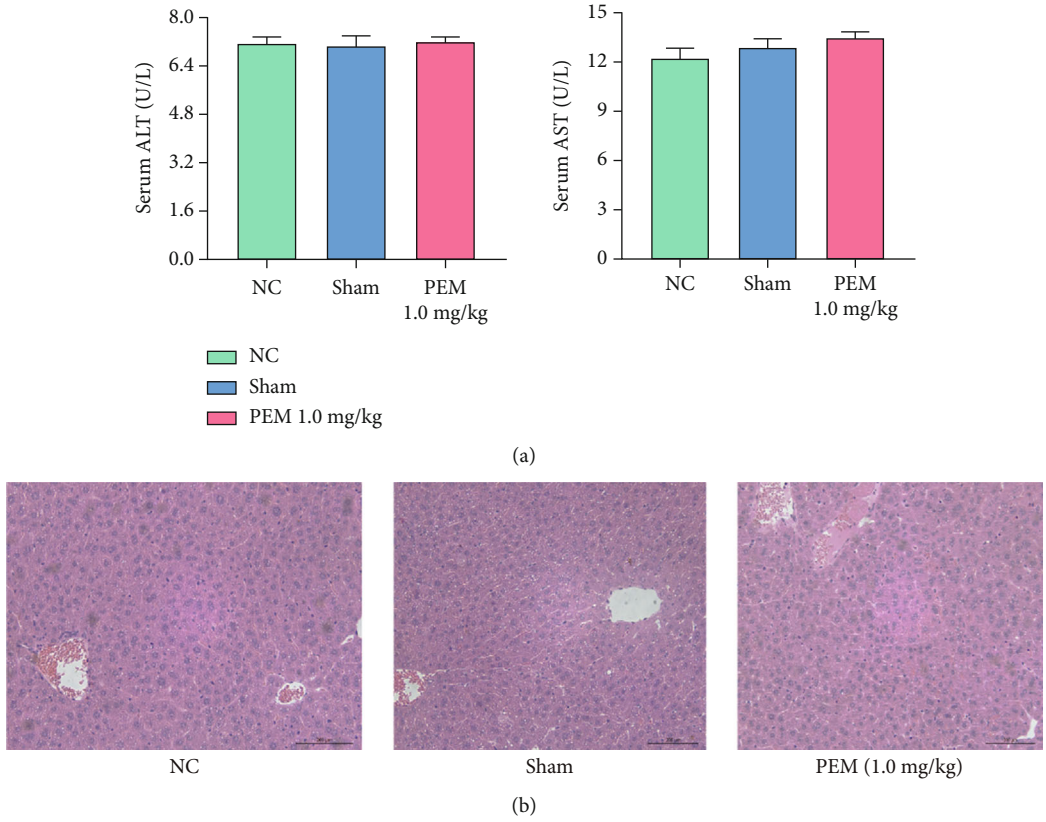

Figure 1: Pemafibrate has no toxic and side effects on liver structure and function. (a) The levels of ALT and AST were shown as mean ± SD by GraphPad Prism 8 ($n = 6$; $P < 0.01$). In these three groups, there was no significant difference in transaminase expression between two groups. (b) After H&E staining, the liver was observed under the light microscope (original magnetization, ×200).

the levels of AST and ALT (Figure 1(a)). Observation on the mouse liver tissues with H&E staining found that the structure and function of the liver tissues were not remarkably changed in H&E-stained sections (Figure 1(b)). Therefore, we believe that the concentration of pemafibrate and surgery do not affect liver function.

3.2. Pemafibrate Pretreatment Can Relieve Liver IRI. By comparing H&E-stained sections, ALT and AST levels in Sham, IR, low-dose, medium-dose, and high-dose groups, we found that in the three time points, the liver tissues of the IRI group were significantly damaged. However, the level of transaminase of the pemafibrate pretreated group decreased, and the effect of high concentration of pemafibrate in alleviating damage was better than that of low concentration, which was dose-dependent (Figure 2(a)). Observation by optical microscope found that there was no obvious damage in the Sham group, but the liver tissue in the IRI group showed structural changes, such as ballooning, necrosis, and inflammatory cell infiltration. Especially at the time point of 8 h, the liver injury in the IRI group was more severe. However, these changes were relieved in the PEM-treated group. In short, these experimental results once again corroborate the aforementioned conclusion: liver damage is mainly caused by the vascular ligation instead of the surgical operation. In addition, H&E results indicate that pemafibrate can alleviate the inflammatory damage and necrosis of IRI (Figure 2(b)).

3.3. Pemafibrate Inhibits Inflammation. Based on the above H&E staining results, the expression levels of common inflammatory factors—IL-1β, IL-6, and TNF-α—were detected. We tested the expression levels in liver tissues by ELISA (Figure 3(a)) and found that in the three time periods, the expression level of IRI group was significantly higher than that of the Sham group. However, under the intervention of pemafibrate, the level of inflammatory factors decreased in a dose-dependent manner. The qRT-PCR (Figure 3(b)) and Western blot analysis (Figures 3(c) and 3(d)) results also showed that IL-1β and TNF-α were significantly increased. And IHC showed that the levels of IL-1β and TNF-α were lower than those of the IR group, showing a downward trend (Figure 3(e)). These results indicated that pemafibrate can inhibit the release of inflammatory factors such as IL-1β, IL-6, and TNF-α.

3.4. Pemafibrate Inhibits Programmed Cell Death in HIRI, including Apoptosis and Autophagy. There are extensive programmed cell deaths in HIRI, including in ways of apoptosis and autophagy. The experimental results of extracting mRNA for qRT-PCR and observing the distribution of molecules in the sliced liver tissue were found to be consistent with that of WB (Figure 4(a)). We selected BCL-2, Bax, Caspase 3, and Caspase 9 to detect the degree of apoptosis in HIRI. Western blot result showed that, compared with the level of IR group, the degree of Bcl-2 had a rising trend,

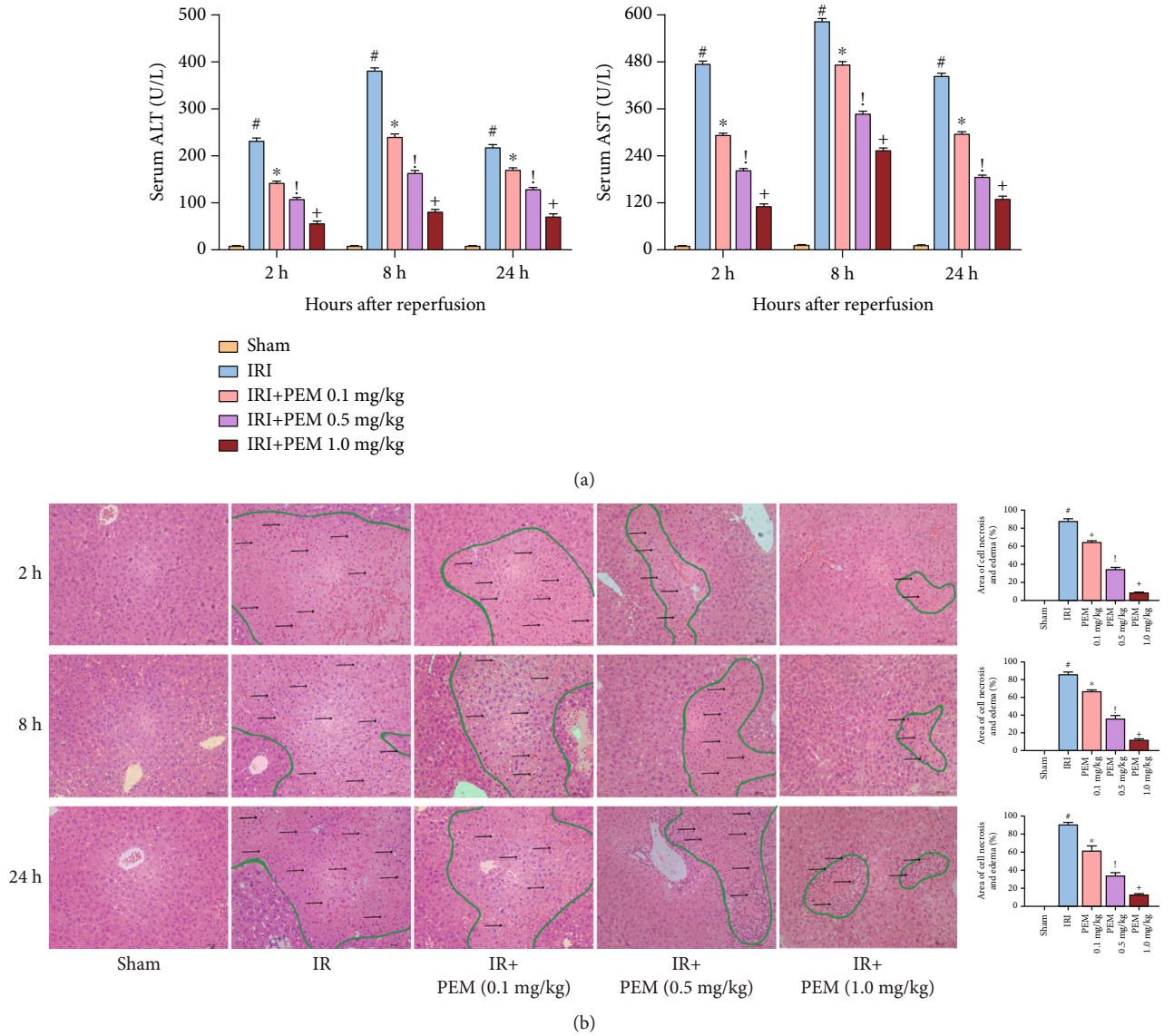

Figure 2: Pemafibrate can significantly alleviate the changes of liver structure and function after ischemia-reperfusion. (a) In three time points, the transaminase level of IRI mice increased significantly and improved after treatment, showing a dose-dependent. ALT and AST levels were expressed by mean ± SD. (b) H&E-stained hepatic sections were examined under light microscopy and imaged at a ×20 magnification. In the IRI group, there were a lot of eosinophilic and unorganized necrotic areas (circled by green lines) and increased inflammatory reactions (indicated by black arrows). However, this phenomenon was alleviated by PEM. Data was given as mean ± SD ($n = 6$, $^{\#}P < 0.05$ for Sham versus IRI, $^{*}P < 0.05$ for IRI + PEM 0.1 mg/kg versus IRI, $^{!}P < 0.05$ for IRI + PEM 0.1 mg/kg versus IRI + PEM 0.5 mg/kg, and $^{+}P < 0.05$ for IRI + PEM 0.5 mg/kg versus IRI + PEM 1.0 mg/kg; (a) two-way ANOVA; (b) Student's t-test).

and degrees of Bax, Caspase 3, and Caspase 9 decreased significantly (Figures 4(b) and 4(c)). Another form of cell death in HIRI is autophagy. With the use of common detection molecules for autophagy including Beclin-1, LC3 and P62, and Western blot to observe the expression trend of each molecule under different intervention conditions, we found that the expression of P62 at 1.0 mg/kg was higher than 0.01 mg/kg, and Beclin-1 and LC3 showed a downward trend. The IHC results are the same as the previous two (Figure 4(d)). In conclusion, pemafibrate can relieve apoptosis and autophagy in liver ischemia-reperfusion injury.

3.5. Pemafibrate Protects the Liver by Regulating the JAK2/STAT3β/PPARα Signaling Pathway. We tested JAK2, Stat3, and p-Stat3 and found that the expression level of JAK2 in the PEM-treated group was lower than that in the IRI group, and the levels of Stat3α and Stat3β did not change significantly. The expression saw a different trend of p-Stat3α and p-Stat3β, increasing considerably at level of p-Stat3α but falling markedly at level of p-Stat3β, compared with the IRI group. When pemafibrate acts as a PPARα agonist, Western blot results indicate that under the action of different concentrations of pemafibrate, the expression of PPARα in liver

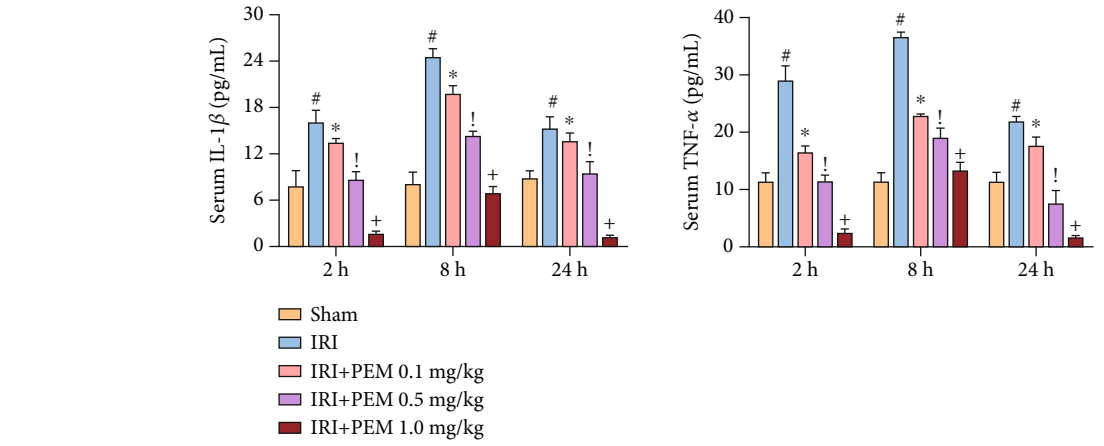

(a)

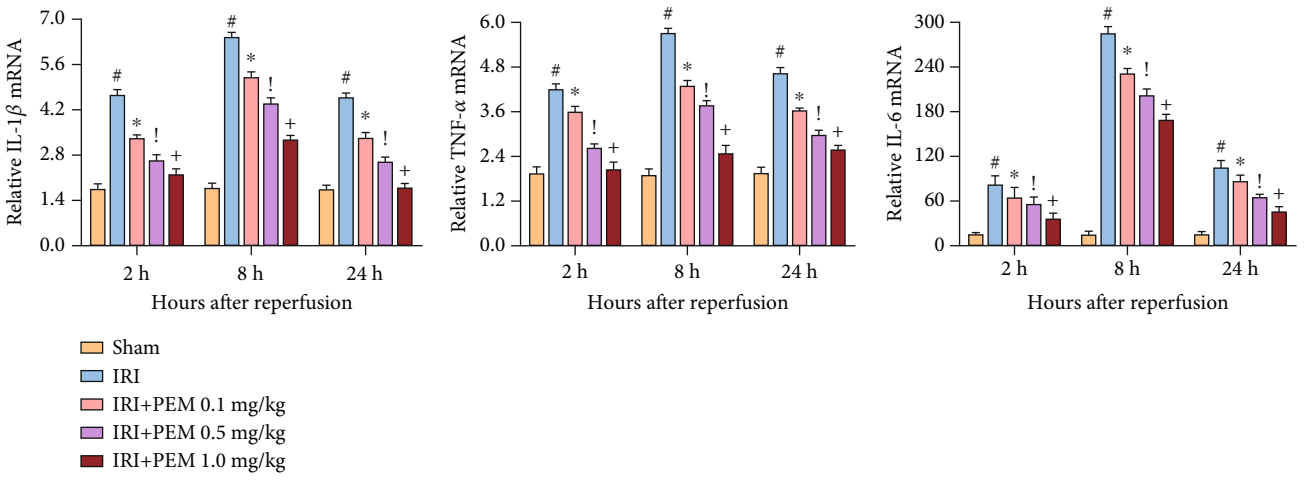

(b)

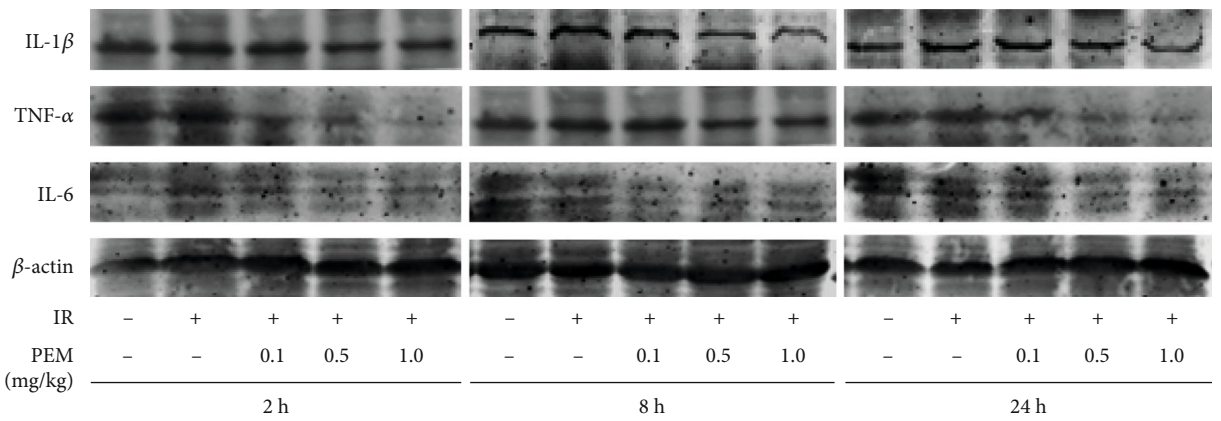

(c)

Figure 3: Continued.

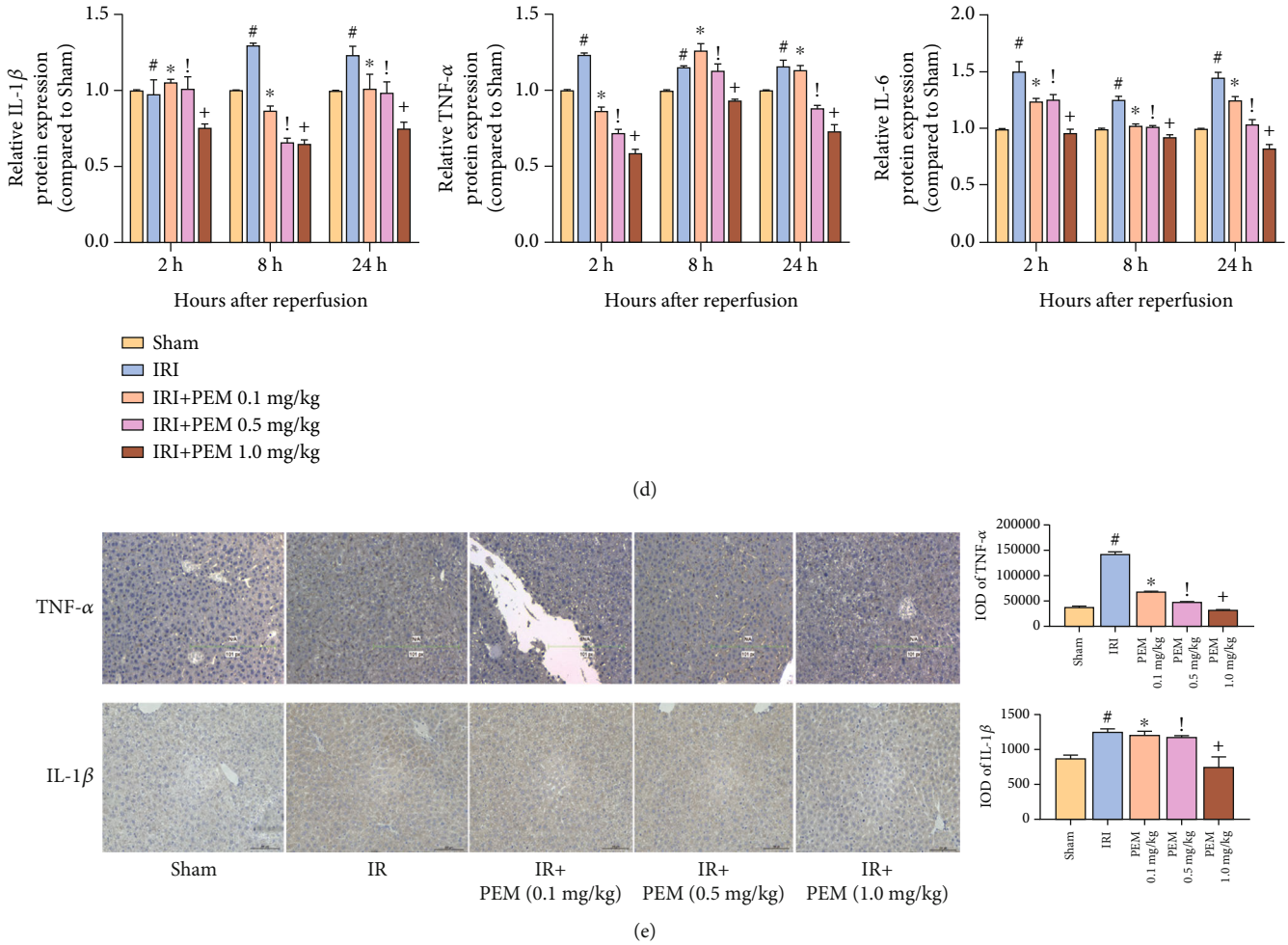

Figure 3: PEM pretreatment inhibits the production of IL-1β, IL-6, and TNF-α in hepatic IRI. (a) The serum IL-1β and TNF-α levels were measured by ELISA and given as mean ± SD at 2, 8, and 24 hours after reperfusion in mice. (b) The relative mRNA levels of IL-1β, IL-6, and TNF-α were evaluated in each group, as shown by qRT-PCR. (c, d) Protein expression of IL-1β, IL-6, and TNF-α was detected by Western blot. (e) Immunohistochemistry was used to detect TNF-α and IL-1β expression in liver tissues (original magnification, ×200). The IOD sum was analyzed with the Image-Pro Plus software 6.0. Data was presented as the mean ± SD ($n = 6$, $^{\#}P < 0.05$ for Sham versus IRI, $^{*}P < 0.05$ for IRI + PEM 0.1 mg/kg versus IRI, $^{!}P < 0.05$ for IRI + PEM 0.1 mg/kg versus IRI + PEM 0.5 mg/kg, and $^{+}P < 0.05$ for IRI + PEM 0.5 mg/kg versus IRI + PEM 1.0 mg/kg; (a, b, d) two-way ANOVA; (e) Student's t-test). Expression levels of IL-1β, TNF-α, and IL-6 were significantly increased in IRI mice. PEM pretreatment dramatically reduced the levels, particularly at 1.0 mg/kg.

tissues increased sequentially (Figures 5(a) and 5(b)). These results, further verified in immunohistochemistry experiments (Figure 5(c)), indicate that pemafibrate can inhibit the JAK2/STAT3β/PPARα signaling pathway.

4. Discussion

We measured the serum levels of ALT and AST in 1.0 mg/kg PEM group, normal control group, and Sham group and compared the changes of liver tissue structure after H&E staining, in order to ensure that the drug dose did not damage the liver. We showed that 1.0 mg/kg PEM had no obvious toxic effect on liver. After verifying that the drug has no toxic effect on the liver, we established the hepatic IRI mouse model. The results showed that the levels of both in the IRI group were significantly increased, but pemafibrate could inhibit this change. At the same time, liver necrosis induced by HIRI was observed under light microscope, and the accumulation of inflammatory cells was improved after PEM treatment.

There are many mechanisms for the occurrence and development of HIRI, such as ATP depletion, endothelin (ET)/nitric oxide ratio imbalance, Ca_2^+ overload, and macrophage activation [25]. In this process, a large amount of ROS is released, which stimulates the cascade of immune cells. Immune cells are composed of Kupffer cells, natural killer cells, and dendritic cells. Activated macrophages secrete a large number of inflammatory factors, such as IL-1β, IL-6, and TNFα [4, 26, 27]. Based on previous studies, we detected the levels of IL-1β, IL-6, and TNF-α in liver tissues and observed the liver tissues under a microscope. A number of inflammatory cells infiltrated, and inflammatory factors significantly increased, which means it proved that the liver tissues after IRI did have structural changes. But pemafibrate

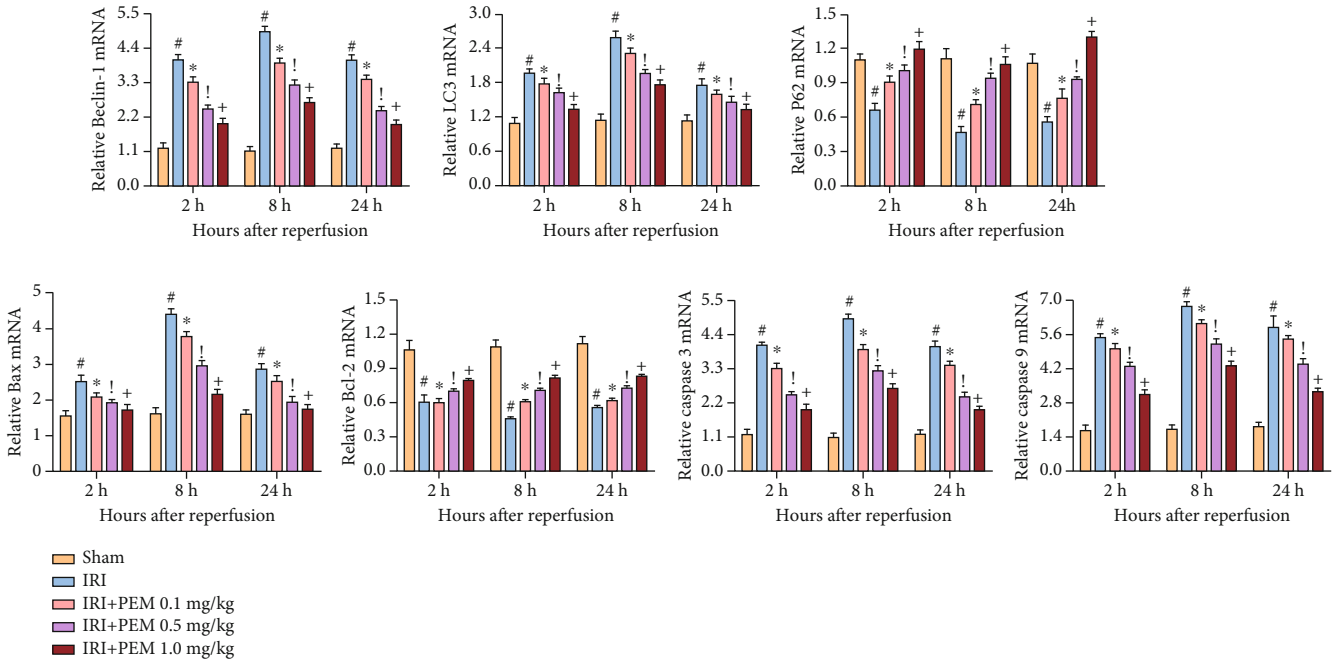

(a)

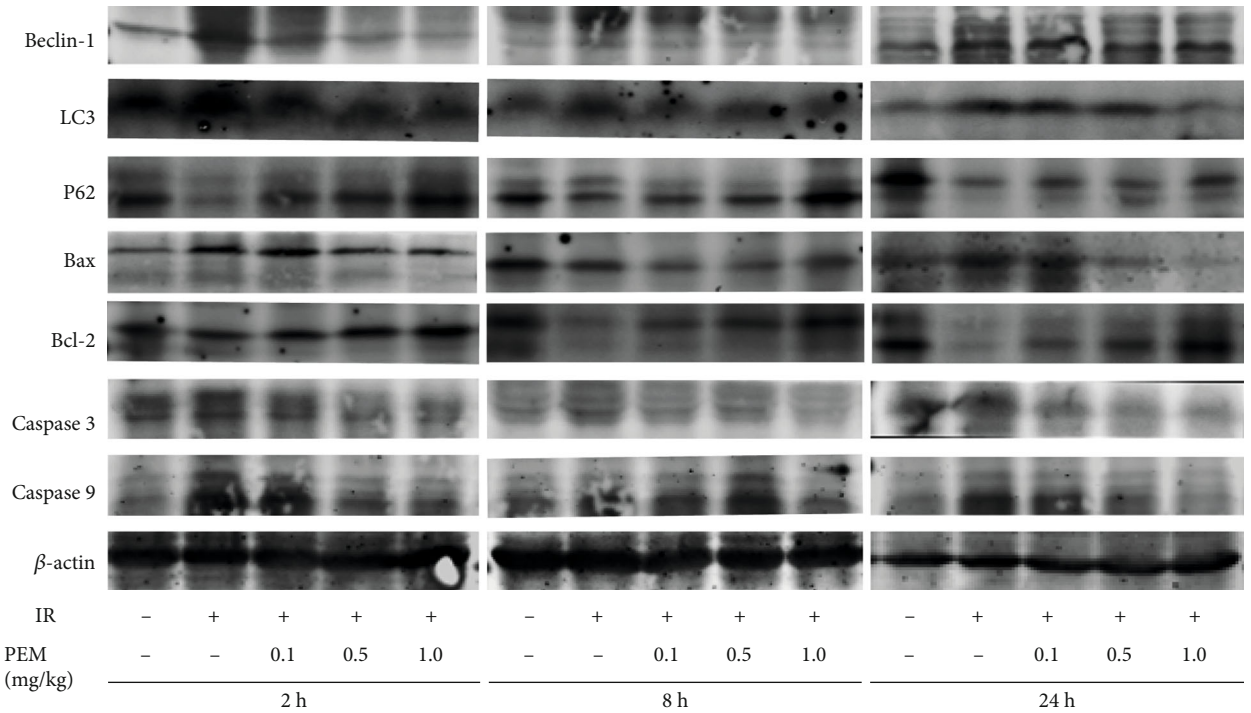

(b)

Figure 4: Continued.

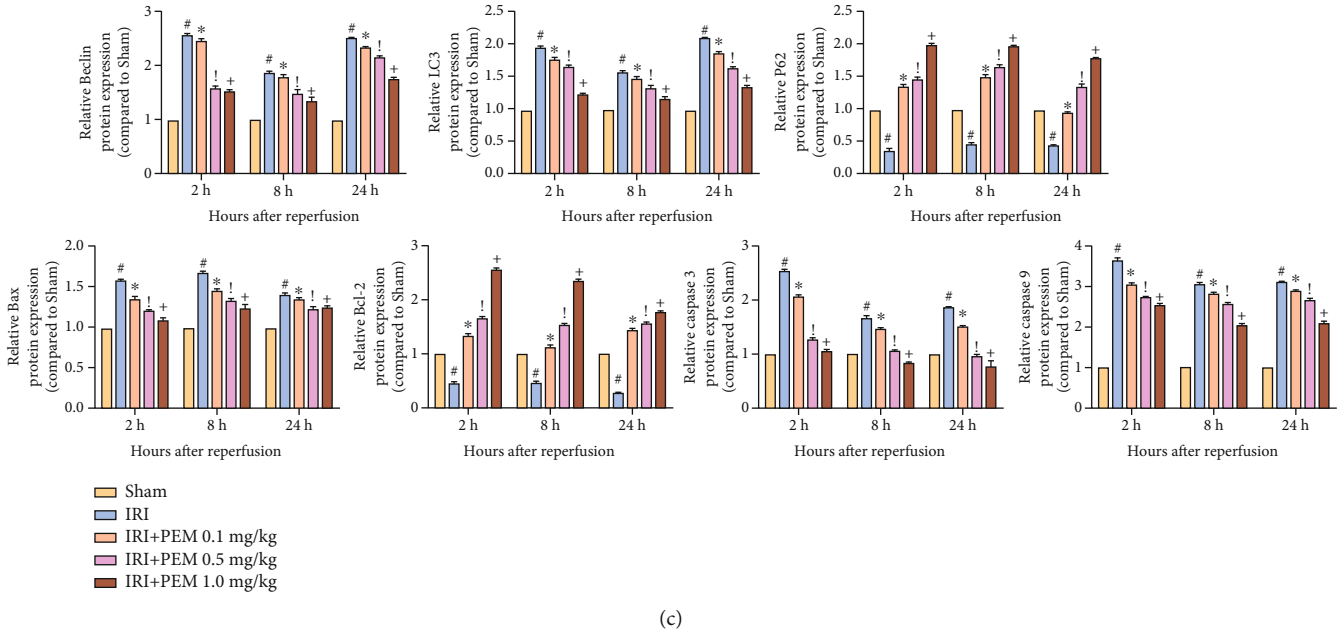

(c)

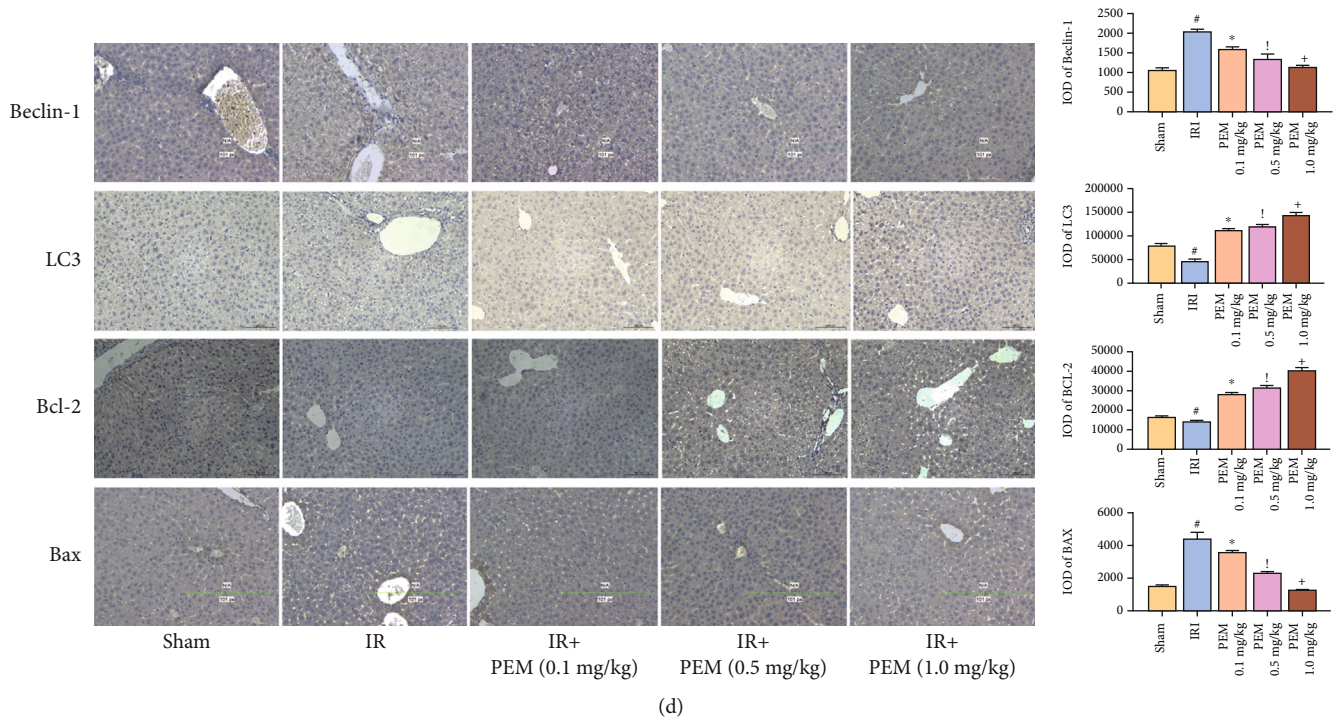

(d)

FIGURE 4: PEM pretreatment ameliorates apoptosis and autophagy in hepatic IRI. (a) The relative mRNA levels of Bcl-2, Bax, Caspase 3, Caspase 9, Beclin-1, LC3, and P62. (b, c) Protein expression of apoptosis- and autophagy-related proteins. (d) Immunohistochemistry was used to detect Bcl-2, Bax, Beclin-1, and LC3 expression in liver tissues (original magnification, ×200). The IOD sum of brown area to total area was analyzed with the Image-Pro Plus software 6.0. Data was presented as the mean ± SD ($n = 6$, $^{\#}P < 0.05$ for Sham versus IRI, $^{*}P < 0.05$ for IRI + PEM 0.1 mg/kg versus IRI, $^{!}P < 0.05$ for IRI + PEM 0.1 mg/kg versus IRI + PEM 0.5 mg/kg, and $^{+}P < 0.05$ for IRI + PEM 0.5 mg/kg versus IRI + PEM 1.0 mg/kg; (a, c) two-way ANOVA; (d) Student's t-test). In the IRI group, the expression of P62 and Bcl-2 was significantly lower than that in the NC group, while the others were significantly higher. PEM could reverse this change.

can alleviate inflammation and protect the liver to a certain extent.

The release of ROS could stimulate autophagy and apoptosis in the liver [9, 10]. We determined Beclin-1 and LC3 as well as P62 (autophagy markers) and Bcl-2 family as well as Caspase family (apoptosis markers) by qRT PCR, WB, and immunohistochemistry [13, 28]. We found that PEM injection enabled the injured liver to produce more P62 and Bcl-2 and reduce Beclin-1, LC3, Bax, Caspase 9, and Caspase 3. These results indicated that PEM could alleviate the programmed cell death. Autophagy is a continuous cytological behavior. In the study of the molecular mechanism of

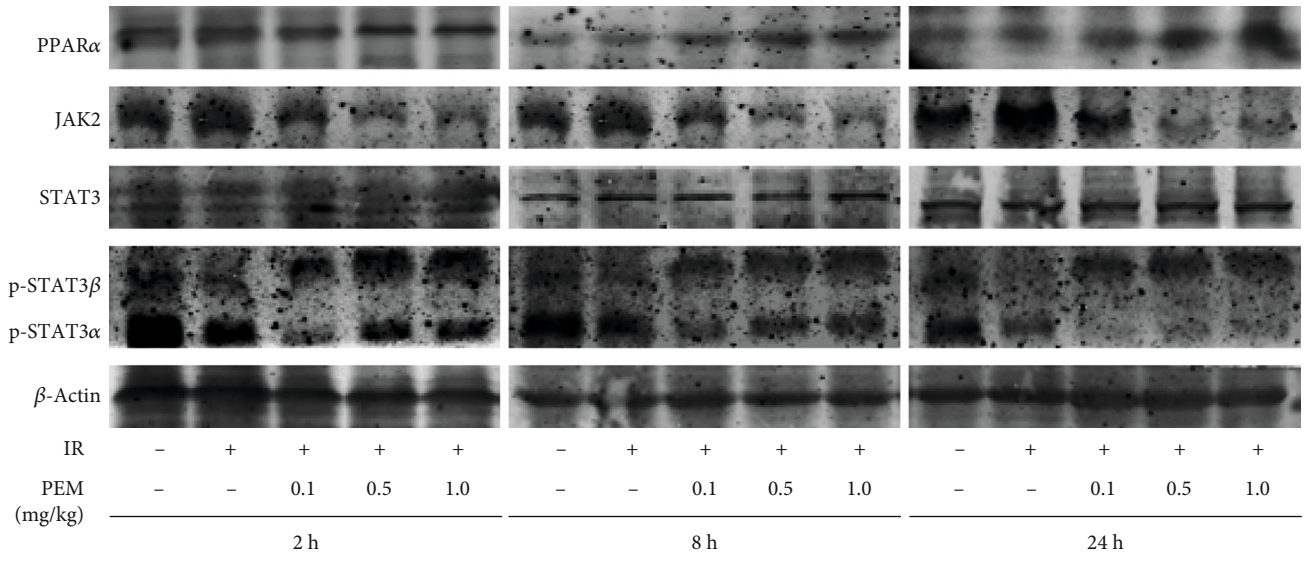

(a)

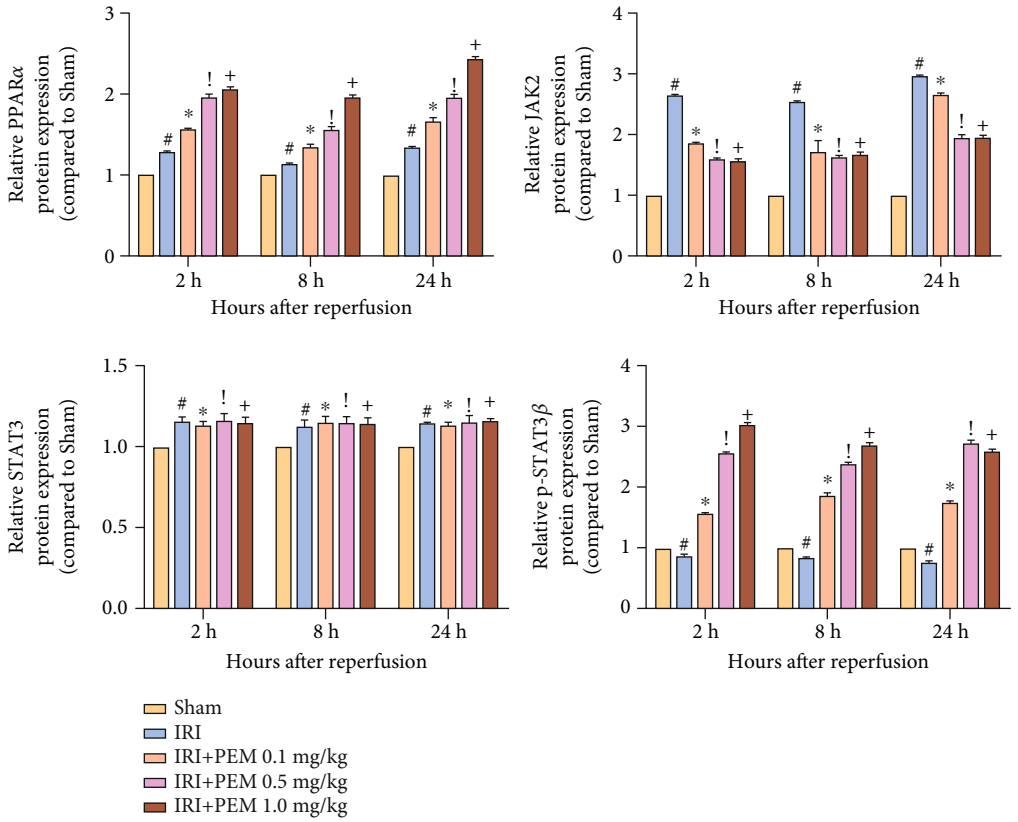

(b)

Figure 5: Continued.

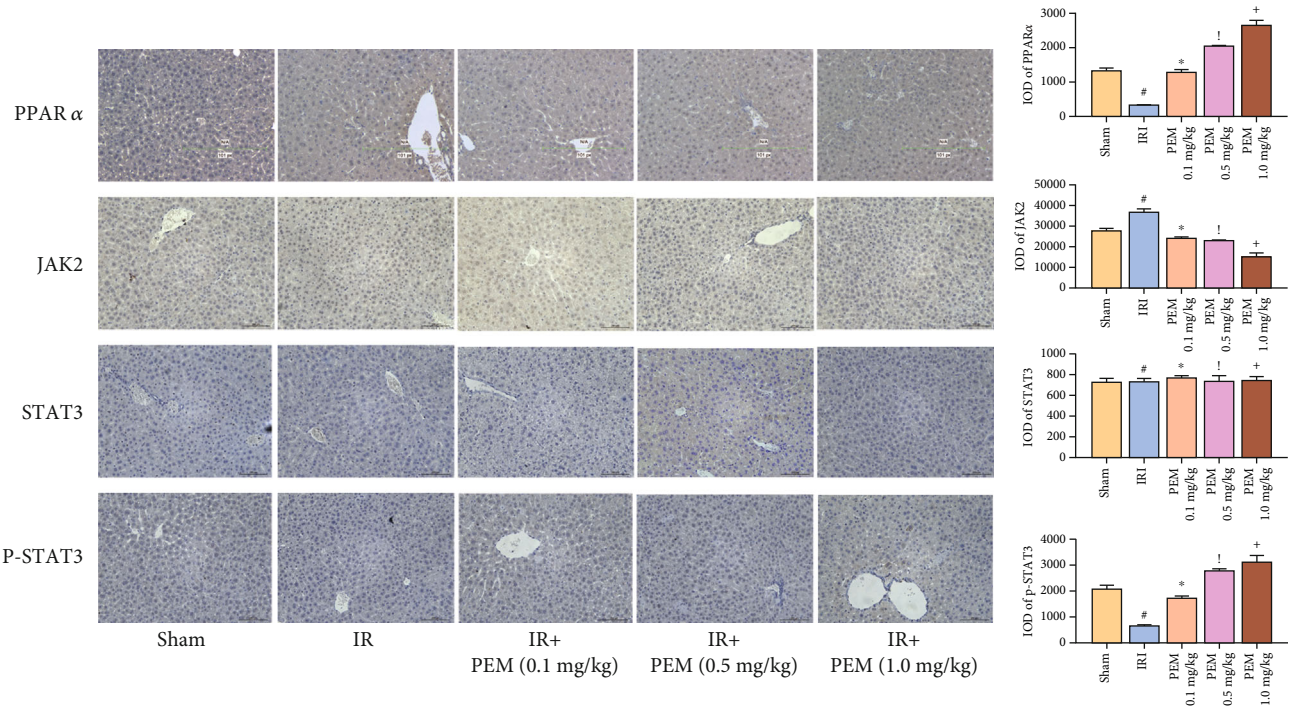

(c)

Figure 5: PEM modulates the phosphorylation of JAK2/STAT3β in hepatic IRI. (a, b) Protein expression of PPARα, JAK2, STAT3, and p-STAT3. (c) The quantitative analysis of Western blot results of JAK2/STAT3β/PPARα. Data was presented as the mean ± SD ($n = 6$, $^{\#}P < 0.05$ for Sham versus IRI, $^{*}P < 0.05$ for IRI + PEM 0.1 mg/kg versus IRI, $^{!}P < 0.05$ for IRI + PEM 0.1 mg/kg versus IRI + PEM 0.5 mg/kg, and $^{+}P < 0.05$ for IRI + PEM 0.5 mg/kg versus IRI + PEM 1.0 mg/kg; (b) two-way ANOVA; (c) Student's t-test). The expression of PPARα and p-STAT3β was notably increased, but JAK2 saw a steep drop.

autophagy, a large number of autophagy-related proteins have gradually been discovered and given the same name. These ATG proteins play an important role in both the initiation of autophagy and the production of autophagosomes [29, 30]. P62 and LC3 are also key proteins for autophagy. P62 is considered to be an autophagy-specific substrate that can interact with LC3 to enter the autophagosome and is degraded by the lysosome in the autophagosome. Beclin-1 combines with BCL-2 to form a Beclin-1/BCL-2 complex [31, 32]. It can be seen that autophagy and apoptosis are closely related. In the process of apoptosis, mitochondria are considered to be at the center of apoptosis regulation. Bcl-2 and Bax, as important members, participate in regulating, releasing Cyto C, and recruiting Caspase 9 [33, 34]. Caspase 9 belongs to the apoptosis-initiating subclass, but Caspase 3 belongs to the apoptotic effect subclass [35, 36]. In other words, Caspase 9 is located at the upstream of Caspase 3 and can regulate its protein level.

Since the expression level of STAT3α : STAT4 β is 4 : 1, most studies ignore the role of STAT3β and regard STAT3α as STAT3 study [33, 34]. The two subtypes were determined to further understand the expression of the two subtypes. In our experiment, compared with the IRI group, the levels of JAK2 and p-STAT3α decreased, while the p-STAT3β remarkably increased, and STAT3 had no change. The significant difference between the two isoforms of p-STAT3 indicated that the two have opposite effects, and p-STAT3β has a positive effect on liver damage, which meant that the upstream stimulator acts on JAK2 and then stimulates p-STAT3β, not STAT3β and STAT3α. This might be related to p-STAT3β:p-STAT3α heterodimer and p-STAT3α:p-STAT3α homodimer [34]. The decrease of JAK2 resulted in the decrease of p-STAT3α and the increase of monomerized p-STAT3β. According to previous researches, JAK2/STAT3β plays an important role in the immune response. The activation of macrophages caused by IRI injury produces a substantial number of inflammatory mediators, such as IL-1β, IL-6, and TNF-α [37–39]. These inflammatory factors can act on receptors on the surface of liver cells, activate JAK2 after entering the cells, and phosphorylate STAT3β [40] (Figure 6). Multiple previous studies have shown that the activation of PPARα by IL-6 is mediated by the JAK2/STAT3 pathway [41–43].

Pemafibrate is also important in autophagy and apoptosis [44, 45]. The mechanism of pemafibrate is still unclear, but the inhibitory effect on autophagy is not mediated by SIRT [46]. As a PPARα agonist, PEM might activate ATG and TEFEB, both essential parts of the autophagy process, and inhibit autophagy [46–49]. TEFEB is also involved in immune response and inflammatory response [50]. When PPARα is knocked out, the agonist is not able to reverse the inhibition of autophagy or to induce lipid degradation and lipid phagocytosis [51]. PPARα binds to RXR to form a dimer to regulate of the target genes. The inhibited expression of PPARα would lead to the weakened antiapoptotic effect of the drug and the lost of protection of

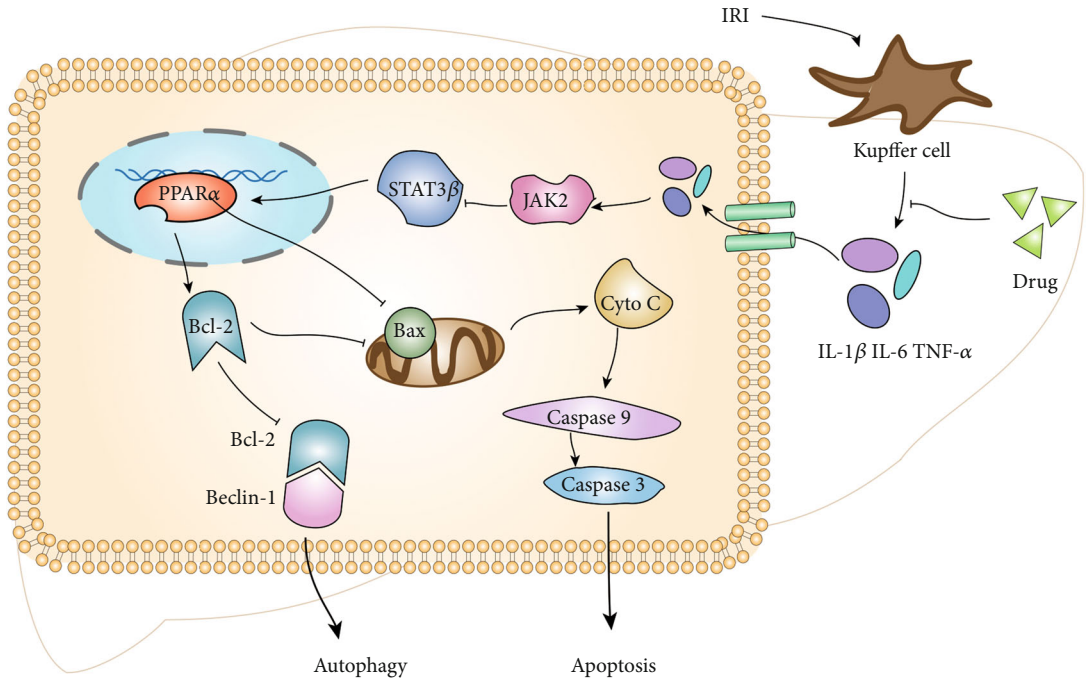

Figure 6: Kupffer cells produce a number of inflammatory mediators, which can bind to cell membrane receptors, promote JAK2, and inhibit p-STAT3β and PPAR alpha. Once PPARα was inhibited, Bcl-2 decreased, and Bax increased, which could stimulate apoptosis and autophagy. Pemafibrate can inhibit the release of inflammatory factors and reduce the subsequent reactions. It could protect the liver from excessive programmed cell death by increasing the levels of p-STAT3β and PPARα in the hepatic IRI.

mitochondria [52]. DOX-DNA complex and DOX-TOP2β complex can inhibit the expression of PPARα, cause cell apoptosis, and promote the release of ROS. PEM is also closely related to inflammation [53–59]. The myocardial IRI will lower the level of PPARα and increase the secretion of ROS by myocardium [60, 61]. After the expression of PPARα was inhibited, mice are more susceptible to oxidative stress. Our experimental results also showed that PEM can alleviate autophagy and apoptosis, and the key molecules such as Bcl-2, Bax, Caspase 3, Caspase 9, LC3, P62, and Beclin-1 all had corresponding changes. Besides, the level of IL-1β, IL-6, and TNF-α rose with the increase of PPARα. These results suggested that the effect of PEM was dose-dependent, which indicated that the anti-inflammatory, antiapoptotic, and antiautophagic effects of three doses (0.1 m/kg, 0.5 mg/kg, and 1.0 mg/kg) increase in turn.

In summary, our study found that HIRI stimulates liver Kupffer cells to release amount of inflammatory factors, which enter liver cells by binding to cell membrane receptors. These inflammatory mediators promote the secretion of JAK2 and the phosphorylation of STAT3α and inhibit the phosphorylation of STAT3β. When pemafibrate intervened, the above reaction was reversed. Increased levels of p-STAT3β activate PPARα, thereby inhibiting cell apoptosis and autophagy. There are some limitations in our research. For example, the relationship between pemafibrate and JAK2/STAT3 β still needs further study. Whether pemafibrate is safe in clinical treatment is unknown. Its therapeutic effect needs to be compared with the commonly used drugs in clinic.

5. Conclusions

Our study found that pemafibrate can effectively inhibit IR damage to the liver of Balb/c mice. In our experiments, pemafibrate significantly reduces serum ALT and AST levels and relieves liver pathophysiological changes. In addition, pemafibrate inhibits the release of inflammatory factors, including IL-1β, IL-6, and TNF-α, as well as cell deaths such as apoptosis and autophagy by regulating JAK2/STAT3β/PPARα. In conclusion, our research suggests that pemafibrate could be a potential therapeutic agent for HIRI.

Data Availability

The data used to support the findings of this study are available from the corresponding author upon request.

Conflicts of Interest

The authors declare that they have no conflicts of interest.

Authors' Contributions

Ziqi Cheng makes the main contribution to this work.

Acknowledgments

This work was supported by the National Natural Science Foundation of China (Grant nos. 82002539).

References

[1] M. Jiménez-Castro, M. Cornide-Petronio, J. Gracia-Sancho, and C. Peralta, "Inflammasome-mediated inflammation in liver ischemia-reperfusion injury," *Cells*, vol. 8, no. 10, p. 1131, 2019.

[2] T. Taner and J. Heimbach, "Something wicked this way comes," *Hepatology*, vol. 71, no. 3, pp. 1119–1121, 2020.

[3] C. Kan, L. Ungelenk, A. Lupp, O. Dirsch, and U. Dahmen, "Ischemia-reperfusion injury in aged livers-the energy metabolism, inflammatory response, and autophagy," *Transplantation*, vol. 102, no. 3, pp. 368–377, 2018.

[4] L. Lu, H. Zhou, M. Ni et al., "Innate immune regulations and liver ischemia-reperfusion injury," *Transplantation*, vol. 100, no. 12, pp. 2601–2610, 2016.

[5] M. Donadon, A. Molinari, F. Corazzi et al., "Pharmacological modulation of ischemic-reperfusion injury during Pringle maneuver in hepatic surgery. A prospective randomized pilot study," *World Journal of Surgery*, vol. 40, no. 9, pp. 2202–2212, 2016.

[6] K. Go, S. Lee, I. Zendejas, K. Behrns, and J. Kim, "Mitochondrial dysfunction and autophagy in hepatic ischemia/reperfusion injury," *BioMed Research International*, vol. 2015, Article ID 183469, 14 pages, 2015.

[7] J. Li, R. Li, G. Lv, and H. Liu, "The mechanisms and strategies to protect from hepatic ischemia-reperfusion injury," *European Review for Medical and Pharmacological Sciences*, vol. 19, no. 11, pp. 2036–2047, 2015.

[8] P. Olthof, R. van Golen, B. Meijer et al., "Warm ischemia time-dependent variation in liver damage, inflammation, and function in hepatic ischemia/reperfusion injury," *Molecular Basis of Disease*, vol. 1863, no. 2, pp. 375–385, 2017.

[9] H. Li, J. Sun, G. Chen et al., "Carnosic acid nanoparticles suppress liver ischemia/reperfusion injury by inhibition of ROS, Caspases and NF-κB signaling pathway in mice," *Biomedicine & Pharmacotherapy = Biomedecine & Pharmacotherapie*, vol. 82, pp. 237–246, 2016.

[10] M. Abu-Amara, S. Yang, N. Tapuria, B. Fuller, B. Davidson, and A. Seifalian, "Liver ischemia/reperfusion injury: processes in inflammatory networks–a review," *Liver Transplantation : official publication of the American Association for the Study of Liver Diseases and the International Liver Transplantation Society*, vol. 16, no. 9, pp. 1016–1032, 2010.

[11] A. C. Racanelli, S. A. Kikkers, A. M. K. Choi, and S. M. Cloonan, "Autophagy and inflammation in chronic respiratory disease," *Autophagy*, vol. 14, no. 2, pp. 221–232, 2018.

[12] N. Ktistakis and S. Tooze, "Digesting the expanding mechanisms of autophagy," *Trends in Cell Biology*, vol. 26, no. 8, pp. 624–635, 2016.

[13] A. Chinnaiyan, "The apoptosome: heart and soul of the cell death machine," *Neoplasia*, vol. 1, no. 1, pp. 5–15, 1999.

[14] E. Chai, M. Shanmugam, F. Arfuso et al., "Targeting transcription factor STAT3 for cancer prevention and therapy," *Pharmacology & Therapeutics*, vol. 162, pp. 86–97, 2016.

[15] D. Johnson, R. O'Keefe, and J. Grandis, "Targeting the IL-6/JAK/STAT3 signalling axis in cancer," *Clinical Oncology*, vol. 15, no. 4, pp. 234–248, 2018.

[16] T. Wang, J. Fahrmann, H. Lee et al., "JAK/STAT3-regulated fatty acid β-oxidation is critical for breast cancer stem cell self-renewal and chemoresistance," *Cell Metabolism*, vol. 27, no. 1, pp. 136–150.e5, 2018.

[17] L. Avalle, S. Pensa, G. Regis, F. Novelli, and V. Poli, "STAT1 and STAT3 in tumorigenesis: a matter of balance," *Jak-Stat*, vol. 1, no. 2, pp. 65–72, 2014.

[18] V. Zoete, A. Grosdidier, and O. Michielin, "Peroxisome proliferator-activated receptor structures: ligand specificity, molecular switch and interactions with regulators," *Biochimica et Biophysica Acta*, vol. 1771, no. 8, pp. 915–925, 2007.

[19] V. Chandra, P. Huang, Y. Hamuro et al., "Structure of the intact PPAR-γ-RXR-α nuclear receptor complex on DNA," *Nature*, vol. 456, no. 7220, pp. 350–356, 2008.

[20] T. Dong, J. Lyu, H. Imachi et al., "Selective peroxisome proliferator-activated receptor-α modulator K-877 regulates the expression of ATP-binding cassette transporter A1 in pancreatic beta cells," *European Journal of Pharmacology*, vol. 838, pp. 78–84, 2018.

[21] K. Ogawa, T. Yagi, T. Guo et al., "Pemafibrate, a selective PPARα modulator, and fenofibrate suppress microglial activation through distinct PPARα and SIRT1-dependent pathways," *Biochemical and Biophysical Research Communications*, vol. 524, no. 2, pp. 385–391, 2020.

[22] S. Ogawa, S. Uehara, Y. Tsunenari, H. Kawai, H. Suemizu, and H. Yamazaki, "Prediction of circulating human metabolites of pemafibrate, a novel antidyslipidemic drug, using chimeric mice with humanized liver," *Xenobiotica; the fate of foreign compounds in biological systems*, vol. 50, no. 7, pp. 769–775, 2020.

[23] J. Feng, Q. Zhang, W. Mo et al., "Salidroside pretreatment attenuates apoptosis and autophagy during hepatic ischemia-reperfusion injury by inhibiting the mitogen-activated protein kinase pathway in mice," *Drug Design, Development and Therapy*, vol. Volume 11, pp. 1989–2006, 2017.

[24] J. Ji, L. Wu, J. Feng et al., "Cafestol preconditioning attenuates apoptosis and autophagy during hepatic ischemia-reperfusion injury by inhibiting ERK/PPARγ pathway," *International Immunopharmacology*, vol. 84, article 106529, 2020.

[25] Y. Q. Zhang, N. Ding, Y. F. Zeng et al., "New progress in roles of nitric oxide during hepatic ischemia reperfusion injury," *World Journal of Gastroenterology*, vol. 23, no. 14, pp. 2505–2510, 2017.

[26] B. Dong, Y. Zhou, W. Wang et al., "Vitamin D receptor activation in liver macrophages ameliorates hepatic inflammation, steatosis, and insulin resistance in mice," *Hepatology*, vol. 71, no. 5, pp. 1559–1574, 2020.

[27] X. Du, M. Wu, D. Tian, J. Zhou, L. Wang, and L. Zhan, "MicroRNA-21 Contributes to Acute Liver Injury in LPS-Induced Sepsis Mice by Inhibiting PPARα Expression," *PPAR Research*, vol. 2020, Article ID 6633022, 7 pages, 2020.

[28] Q. Xia, M. Xu, P. Zhang, L. Liu, X. Meng, and L. Dong, "Therapeutic potential of autophagy in glioblastoma treatment with phosphoinositide 3-kinase/protein kinase B/mammalian target of rapamycin signaling pathway inhibitors," *Frontiers in Oncology*, vol. 10, article 572904, 2020.

[29] H. Nakatogawa, K. Suzuki, Y. Kamada, and Y. Ohsumi, "Dynamics and diversity in autophagy mechanisms: lessons from yeast," *Nature Reviews Molecular Cell Biology*, vol. 10, no. 7, pp. 458–467, 2009.

[30] H. Suzuki, T. Osawa, Y. Fujioka, and N. Noda, "Structural biology of the core autophagy machinery," *Current Opinion in Structural Biology*, vol. 43, pp. 10–17, 2017.

[31] J. Chipuk, L. Bouchier-Hayes, and D. Green, "Mitochondrial outer membrane permeabilization during apoptosis: the innocent bystander scenario," *Differentiation*, vol. 13, no. 8, pp. 1396–1402, 2006.

[32] D. Acehan, X. Jiang, D. Morgan, J. Heuser, X. Wang, and C. Akey, "Three-dimensional structure of the apoptosome: implications for assembly, procaspase-9 binding, and activation," *Molecular Cell*, vol. 9, no. 2, pp. 423–432, 2002.

[33] I. Marzo, C. Brenner, N. Zamzami et al., "The permeability transition pore complex: a target for apoptosis regulation by caspases and bcl-2-related proteins," *The Journal of Experimental Medicine*, vol. 187, no. 8, pp. 1261–1271, 1998.

[34] B. Gajkowska, U. Wojewódzka, and J. Gajda, "Translocation of Bax and Bid to mitochondria, endoplasmic reticulum and nuclear envelope: possible control points in apoptosis," *Journal of Molecular Histology*, vol. 35, no. 1, pp. 11–19, 2004.

[35] J. Adams, "Ways of dying: multiple pathways to apoptosis," *Genes & Development*, vol. 17, no. 20, pp. 2481–2495, 2003.

[36] Y. Shi, "Mechanical aspects of apoptosome assembly," *Current Opinion in Cell Biology*, vol. 18, no. 6, pp. 677–684, 2006.

[37] S. Pullamsetti, W. Seeger, and R. Savai, "Classical IL-6 signaling: a promising therapeutic target for pulmonary arterial *hypertension*," *Journal of Clinical Investigation*, vol. 128, no. 5, pp. 1720–1723, 2018.

[38] Y. Tamura, C. Phan, L. Tu et al., "Ectopic upregulation of membrane-bound IL6R drives vascular remodeling in pulmonary arterial *hypertension*," *Journal of Clinical Investigation*, vol. 128, no. 5, pp. 1956–1970, 2018.

[39] R. Paulin, J. Meloche, and S. Bonnet, "STAT3 signaling in pulmonary arterial hypertension," *Jak-Stat*, vol. 1, no. 4, pp. 223–233, 2014.

[40] J. O'Shea, D. Schwartz, A. Villarino, M. Gadina, I. McInnes, and A. Laurence, "The JAK-STAT pathway: impact on human disease and therapeutic intervention," *Annual Review of Medicine*, vol. 66, no. 1, pp. 311–328, 2015.

[41] G. Chew, S. Myers, A. Shu-Chien, and T. Muhammad, "Interleukin-6 inhibition of peroxisome proliferator-activated receptor alpha expression is mediated by JAK2- and PI3K-induced STAT1/3 in HepG2 hepatocyte cells," *Molecular and Cellular Biochemistry*, vol. 388, no. 1-2, pp. 25–37, 2014.

[42] Q. Guo, G. Wang, and S. Namura, "Fenofibrate improves cerebral blood flow after middle cerebral artery occlusion in mice," *Journal of Cerebral Blood Flow and Metabolism : official journal of the International Society of Cerebral Blood Flow and Metabolism*, vol. 30, no. 1, pp. 70–78, 2010.

[43] G. Sugga, R. Khanam, and M. U. Khan, "Protective role of fibrates in cardiac ischemia/reperfusion," *Journal of Advanced Pharmaceutical Technology & Research*, vol. 3, no. 3, pp. 188–192, 2012.

[44] N. Fujita, K. Sase, C. Tsukahara, I. Arizono, H. Takagi, and Y. Kitaoka, "Pemafibrate prevents retinal neuronal cell death in NMDA-induced excitotoxicity via inhibition of p-c-Jun expression," *Molecular Biology Reports*, vol. 48, no. 1, pp. 195–202, 2021.

[45] J. Boeckmans, A. Natale, M. Rombaut et al., "Human hepatic in vitro models reveal distinct anti-NASH potencies of PPAR agonists," *Cell Biology and Toxicology*, 2020.

[46] C. Settembre, R. de Cegli, G. Mansueto et al., "TFEB controls cellular lipid metabolism through a starvation-induced autoregulatory loop," *Nature Cell Biology*, vol. 15, no. 6, pp. 647–658, 2013.

[47] X. Luo, L. Zhong, L. Yu et al., "TRIB3 destabilizes tumor suppressor PPARα expression through ubiquitin-mediated proteasome degradation in acute myeloid leukemia," *Life Sciences*, vol. 257, article 118021, 2020.

[48] Y. Kim, H. Lee, J. Kim et al., "PPAR-α activation mediates innate host defense through induction of TFEB and lipid catabolism," *Journal of Immunology*, vol. 198, no. 8, pp. 3283–3295, 2017.

[49] A. Ghosh, M. Jana, K. Modi et al., "Activation of Peroxisome Proliferator-activated Receptor α Induces Lysosomal Biogenesis in Brain Cells:," *The Journal of Biological Chemistry*, vol. 290, no. 16, pp. 10309–10324, 2015.

[50] O. Visvikis, N. Ihuegbu, S. Labed et al., "Innate host defense requires TFEB-mediated transcription of cytoprotective and antimicrobial genes," *Immunity*, vol. 40, no. 6, pp. 896–909, 2014.

[51] J. M. Lee, M. Wagner, R. Xiao et al., "Nutrient-sensing nuclear receptors coordinate autophagy," *Nature*, vol. 516, no. 7529, pp. 112–115, 2014.

[52] W. Wang, Q. Fang, Z. Zhang, D. Wang, L. Wu, and Y. Wang, "PPARα ameliorates doxorubicin-induced cardiotoxicity by reducing mitochondria-dependent apoptosis via regulating MEOX1," *Frontiers in Pharmacology*, vol. 11, article 528267, 2020.

[53] N. Hennuyer, I. Duplan, C. Paquet et al., "The novel selective PPARα modulator (SPPARMα) pemafibrate improves dyslipidemia, enhances reverse cholesterol transport and decreases inflammation and atherosclerosis," *Atherosclerosis*, vol. 249, pp. 200–208, 2016.

[54] H. Konishi, K. Miyauchi, A. Onishi et al., "Effect of pemafibrate (K-877), a novel selective peroxisome proliferator-activated receptor α modular (SPPARMα), in atherosclerosis model using low density lipoprotein receptor knock-out swine with balloon injury," *PloS One*, vol. 15, no. 11, article e0241195, 2020.

[55] Y. Sasaki, M. Asahiyama, T. Tanaka et al., "Pemafibrate, a selective PPARα modulator, prevents non-alcoholic steatohepatitis development without reducing the hepatic triglyceride content," *Scientific Reports*, vol. 10, no. 1, p. 7818, 2020.

[56] R. Mansouri, E. Baugé, B. Staels, and P. Gervois, "Systemic and distal repercussions of liver-specific peroxisome proliferator-activated Receptor-α control of the acute-phase response," *Endocrinology*, vol. 149, no. 6, pp. 3215–3223, 2008.

[57] S. Standage, C. Caldwell, B. Zingarelli, and H. Wong, "Reduced peroxisome proliferator-activated receptor α expression is associated with decreased survival and increased tissue bacterial load in sepsis," *Shock*, vol. 37, no. 2, pp. 164–169, 2012.

[58] K. Drosatos, Z. Drosatos-Tampakaki, R. Khan et al., "Inhibition of c-Jun-N-terminal Kinase Increases Cardiac Peroxisome Proliferator-activated Receptor α Expression and Fatty Acid Oxidation and Prevents Lipopolysaccharide-induced Heart Dysfunction∗„" *The Journal of Biological Chemistry*, vol. 286, no. 42, pp. 36331–36339, 2011.

[59] F. Penas, G. Mirkin, M. Vera et al., "Treatment _in vitro_ with PPAR α and PPARγ ligands drives M1-to-M2 polarization of macrophages from _T. cruzi_ -infected mice," *Biochimica et Biophysica Acta*, vol. 1852, no. 5, pp. 893–904, 2015.

[60] H. Vosper, G. Khoudoli, T. Graham, and C. Palmer, "Peroxisome proliferator-activated receptor agonists, hyperlipidaemia, and atherosclerosis," *Pharmacology & Therapeutics*, vol. 95, no. 1, pp. 47–62, 2002.

[61] E. Robinson and D. Grieve, "Significance of peroxisome proliferator-activated receptors in the cardiovascular system in health and disease," *Pharmacology & Therapeutics*, vol. 122, no. 3, pp. 246–263, 2009.

Hindawi
PPAR Research
Volume 2021, Article ID 6629842, 12 pages
https://doi.org/10.1155/2021/6629842

Research Article

DOCK4 Is a Platinum-Chemosensitive and Prognostic-Related Biomarker in Ovarian Cancer

Qianqian Zhao,[1] **Jie Zhong**,[2] **Ping Lu**,[1] **Xiao Feng**,[3] **Ying Han**,[2] **Chenqi Ling**,[2] **Wenke Guo**,[1] **Weijin Zhou**,[1] **and Fudong Yu**[1,2]

[1]*NHC Key Laboratory of Reproduction Regulation (Shanghai Institute of Planned Parenthood Research), Public Health School, Fudan University, Shanghai, China*
[2]*Department of Gynecology, Shidong Hospital, Yangpu District, Shanghai, China*
[3]*Department of Gynecology, Shanghai First Maternity and Infant Hospital, Tongji University School of Medicine, Shanghai, China*

Correspondence should be addressed to Weijin Zhou; zw0822@sina.com and Fudong Yu; fdyu@fudan.edu.cn

Received 15 October 2020; Revised 7 January 2021; Accepted 21 January 2021; Published 4 February 2021

Academic Editor: Jingjing Li

Ovarian carcinoma (OV) is a lethal gynecological malignancy. Most OV patients develop resistance to platinum-based chemotherapy and recurrence. Peroxisome proliferator-activated receptors (PPARs) are the ligand activating transcription factor of the nuclear receptor superfamily. PPARs as important transcriptional regulators regulate important physiological processes such as lipid metabolism, inflammation, and wound healing. Several reports point out that PPARs can also have an effect on the sensitivity of tumor cells to platinum-based chemotherapy drugs. However, the role of PPAR-target related genes (PPAR-TRGs) in chemotherapeutic resistance of OV remains unclear. The present study is aimed at optimizing candidate genes by integrating platinum-chemotherapy expression data and PPAR family genes with their targets. The gene expression profiles were obtained from Gene Expression Omnibus (GEO) and The Cancer Genome Atlas (TCGA) database. A total of 4 genes (*AP2A2*, *DOCK4*, *HSDL2*, and *PDK4*) were the candidate differentially expressed genes (DEGs) of PPAR-TRGs with platinum chemosensitivity. After conducting numerous survival analyses using different cohorts, we found that only the upexpression of *DOCK4* has important significance with the poor prognosis of OV patients. Meanwhile, *DOCK4* is detected in plasma and enriched in neutrophil and monocyte cells of the blood. We further found that there were significant correlations between *DOCK4* expression and the levels of CD4+ T cell infiltration, dendritic cell infiltration, and neutrophil infiltration in OV. In addition, we verified the expression level of *DOCK4* in OV cell lines treated with platinum drugs and found that *DOCK4* is potentially responsive to platinum drugs. In conclusion, *DOCK4* is potentially associated with immune cell infiltration and represents a valuable prognostic biomarker in ovarian cancer patients.

1. Introduction

Ovarian cancer (OV) is the fifth-leading cause of mortality among women with gynecological tumors in modern society. There are more than 240 000 women diagnosed with OV each year in the world. OV mainly comprises three large types, namely, epithelial, germ cell, and specialized stromal cell tumors, of which epithelial ovarian cancer is the most common type of ovarian cancer. Epithelial ovarian cancer can be further classified into five histological subtypes including high-grade serous, low-grade serous, endometriosis, clear cell, and mucinous ovarian carcinoma. Since 70% of advanced cancer patients are diagnosed at stage III or IV, they suffer from poor prognosis with tumor metastases, relapses, and even death from the disease [1, 2]. Nowadays, tumor debulking surgery followed by platinum-taxane chemotherapy is the primary treatment. However, the platinum-resistant cancer recurrence rate is close to 25% within six months [3, 4]. The lack of effective adjuvant therapeutics requires a greater understanding of the biology of its progression. Despite intensive research efforts, the overall survival (OS) of patients has been slightly improved over the past years. Reliable biomarkers, as a potential improvement for OV patients involving detection, diagnosis, prognosis, response

to therapy, and outcome, are urgently required. Therefore, this article hopes to find out the prognostic biomarkers related to ovarian cancer chemotherapy sensitivity by studying the relationship between peroxisome proliferator-activated receptors (PPARs) and OV chemotherapy sensitivity.

PPARs are ligand-activated transcription factors which belong to the nuclear receptor superfamily including PPARα, PPARβ/δ, and PPARγ three isoforms [5, 6]. PPARs interact with other transcription regulators to regulate the transcription of its target genes involved in energy metabolism and important cellular biological functions like inflammation, cellular proliferation, and differentiation [7, 8]. In recent years, it has been reported that PPARs can also have an effect on the sensitivity of tumor cells to platinum-based chemotherapy drugs [9]. Increasing evidence shows that PPARs are important regulators of innate immunity and inflammatory response [10]. Given these crucial biological process regulatory roles of PPARs, abnormal expression of PPARs is associated with chronic diseases, such as diabetes, obesity, and cardiovascular disease [11]. Likewise, several previous studies suggested that PPAR involved processes were correlated with tumorigenesis including terminal differentiation, cell cycle arrest, and apoptosis of cancer cells [12]. In addition, the excessive activation of PPARs can lead to the increase of regulatory T cells and immunosuppression. However, the role of PPARs in ovarian cancer was poorly understood. Therefore, it will contribute to the prognosis to evaluate gene expression patterns in various cancers.

To further explore the roles of PPAR-target related genes (PPAR-TRGs) in OV prognosis, we collected GEO database (GSE51373, GSE63885) from primary patients that underwent chemotherapy to analyze the differences in chemotherapeutic sensitivity of platinum, then screened the candidate genes from the PPAR gene database, and finally used TCGA database for prognostic survival analysis; we found that *DOCK4* is the regulatory gene of PPARs which is associated with chemotherapy sensitivity and OV prognosis. This article will further analyze and study *DOCK4*, Rho GTPases, a receptor for calcium adhesions, which can drive the cytoskeleton reorganization, which is widely studied in cell adhesion and migration [13]. The *DOCK* family is a nonclassical type of cancer-associated Rho GTPase exchange factor. *DOCK4*, as a key guanine nucleotide exchange factor, is involved in regulation of the small GTPase Rac1 and a Ras-like small GTPase Rap1. It is increasingly recognized that *DOCK4* induced Rac activation and *Wnt*/β-catenin pathway to stimulate cell polarization, migration, and invasion, which are associated with cancer progression and metastasis. For instance, *DOCK4* forms a complex with *ELMO* and *SH3YL1* to induce Rac-dependent cell migration [14].

To investigate the deregulation of PPAR target gene *DOCK4* and involved mechanism in ovarian cancer, we use public data to analyze the characteristics of chemotherapy sensitivity and prognostic survival analysis and then found that there were significant correlations between *DOCK4* expression and the levels of CD4+ T cell infiltration, dendritic cell infiltration, and neutrophil infiltration in ovarian cancer. Meanwhile, *DOCK4* is detected in plasma and enriched in neutrophil and monocyte cells of the blood. The results identify that *DOCK4* is promising to become a prognostic biomarker related to OV chemotherapy.

2. Materials and Methods

2.1. Patient Information

2.1.1. TCGA Cohort. The data used for our analysis based on datasets of The Cancer Genome Atlas Research Network (TCGA) is retrieved from UCSC (http://xena.ucsc.edu/public). In whole, we include a total of $N = 304$ ovarian cancer samples of RNA-Seq data (Illumina HiSeq pancan normalized data) with nonzero OS time from the latest TCGA sequencing sample. The clinical information of OV samples was revised by the TCGA Pan-Cancer Clinical Data Resource (TCGA-CDR) [15].

2.1.2. Validation Cohort. Two independent cohorts (AOCS, MSKCC) are enrolled in this project as validation cohort datasets. The AOCS (Australian Ovarian Cancer Study) cohort ($n = 278$) samples (1992–2006) have more than 5 years of follow-up clinical information. The MSKCC cohort ($n = 195$) samples (1990–2003) have more than 5 years of follow-up. The mRNA expression data are as follows: AOCS cohort (GSE9891) and MSKCC cohort (GSE26172) using the Affymetrix human U133A microarray downloaded from GEO datasets.

2.1.3. Platinum-Treated Patients. Information of patients receiving platinum chemotherapy is downloaded from GEO datasets (GSE51373 ($n = 28$) and GSE63885 ($n = 75$)). We divide the patients in each dataset into two groups: chemotherapy-sensitive (GSE51373—18 samples, GSE63885—41 samples) and chemotherapy-resistant (GSE51373—10 samples, GSE63885—34 samples) groups on the basis of their Platinum-Free Interval (PFI), defined as the time between the last dose of first-line carboplatin-based chemotherapy and the date of tumor progression; patients were defined as "resistant" (PFI < 6 months), "partially sensitive" (PFI 6-12 months), and "sensitive" (PFI > 12 months). "Partially sensitive" is included in the sensitive group [16].

2.2. Data of PPAR Family Genes and Their Targets. The candidate genes about the PPAR family transcription factors and their target genes are downloaded from the PPAR gene database [17]. The PPAR target genes used in this study are selected by those experimentally verified targets. After removing redundant genes, there were 130 genes involved in this study with the candidate genes PPAR-TRGs of the PPAR family transcription factors and target genes.

2.3. Platinum-Treated Cell Lines. To investigate the cellular responses of ovarian cancer cells to cisplatin, we performed transcriptome analysis in 46 ovarian cancer cell lines treated with GI50 doses of cisplatin (data from GSE47856). (GI50 is the cisplatin dosage required to cause a 50% reduction in the increase in viable cell number over 48 h as compared with untreated control cells).

2.4. Immune Cell Infiltration Analysis. TIMER (https://cistrome.shinyapps.io/timer/) is a database designed for

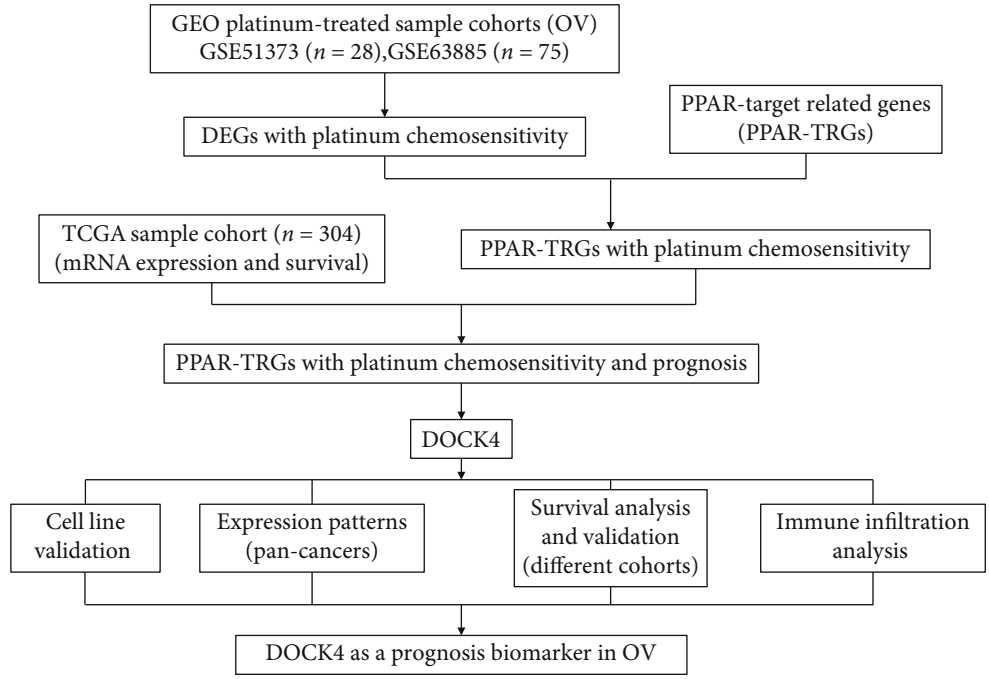

Figure 1: The flow chart shows the scheme of our study on mRNA prognostic signatures for OV (ovarian cancer).

analyzing immune cell infiltration in multiple cancers [18]. This database employs pathological examination-validated statistical methodology in order to estimate tumor immune infiltration by neutrophils, macrophages, dendritic cells, B cells, and CD4/CD8 T cells. We further executed Kaplan-Meier curve analyses to explore the survival of PPAR-TRG candidates and immune cells. In addition, this webserver could analyze the correlation relationship between gene expression and immune cells.

2.5. DOCK4 Prognosis Analysis. The Kaplan-Meier plotter offers a means of readily exploring the impact of a wide array of genes on patient survival in 21 different types of cancer, with large sample sizes for the ovarian ($n = 2190$) cancer cohorts [19]. We therefore used this database to explore the association between *DOCK4* expression and outcome in patients with ovarian cancer. The candidate gene survival analysis used R packages "survival," "survminer," "glmnet," and "dplyr." The cutoff of p value was 0.05 by using log-rank p value.

2.6. Statistical Analysis. Kaplan-Meier plotter and TIMER databases were used for generating survival plots in respective analysis, with data including either HR and p values or p values derived from a log-rank test. Statistical analyses were performed using R software v3.5.0 and GraphPad Prism v5.00. We used the multivariable Cox proportional hazard model to analyze prognosis-related multivariate of ovarian cancer. We used a limma package to analyze the mRNA gene expression for different expression genes. The selection of cutoff was 0.05 in this study. In addition, we used R packages "survival," "survminer," "glmnet," and "dplyr" to produce survival plots.

3. Results

3.1. Optimization of Candidate Genes of PPAR Family Genes with Their Targets by Integrating Platinum-Chemotherapy Expression Data and Survival Signature. For the sake of obtaining candidate genes related to PPARs and platinum chemosensitivity, we collected platinum-chemotherapy expression data of OV in GEO database (GSE51373 ($n = 28$) and GSE63885 ($n = 75$)) and divided each dataset into the chemotherapy-sensitive (GSE51373—18 samples, GSE63885—41 samples) and chemotherapy-resistant (GSE51373—10 samples, GSE63885—34 samples) groups. Compared with the sensitive group, 269 DEGs were platinum sensitive in OV. It is increasingly recognized that PPARs as transcription regulators play critical roles in a great amount of cellular function. Based on previous studies, we collected 143 candidate gene PPAR-TRGs from the PPAR gene database (http://www.ppargene.org/.). There were only 4 PPAR-TRGs (*AP2A2*, *DOCK4*, *HSDL2*, and *PDK4*) out of 269 DEGs, which are associated with platinum chemosensitivity in ovarian cancer. Subsequently, we analyzed the survival analysis of these 4 genes by using the clinical information of RNA-Seq ovarian cancer patients from TCGA database. Finally, we found that only the upexpression of *DOCK4* has significant clinical outcome with the poor prognosis of OV patients. We conducted our study as described in the flow chart (Figure 1). Therefore, we have reason to believe that *DOCK4* might be the potential prognosis biomarker for ovarian cancer.

3.2. Overexpression of DOCK4 Predicts Poor Prognosis for Ovarian Cancer. In order to decipher the prognostic value of *DOCK4* in patients with OV, we explored the link between the expression of *DOCK4* and clinical outcome from TCGA

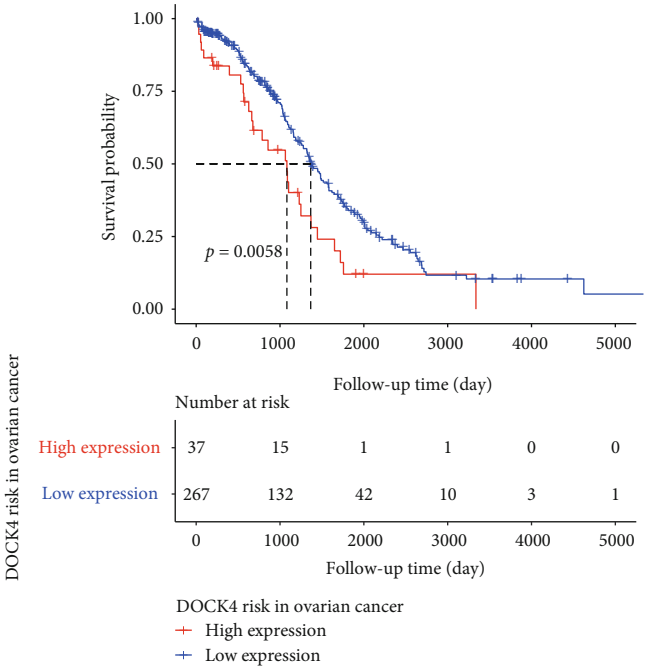

(a)

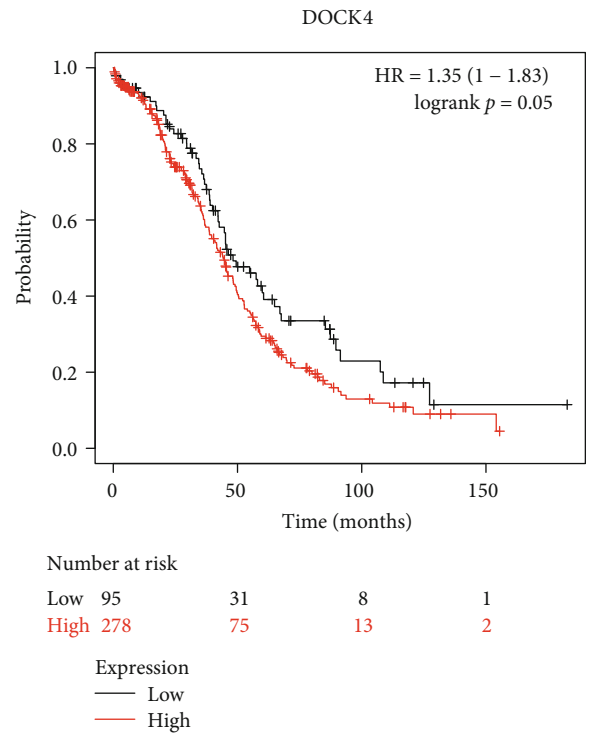

(b)

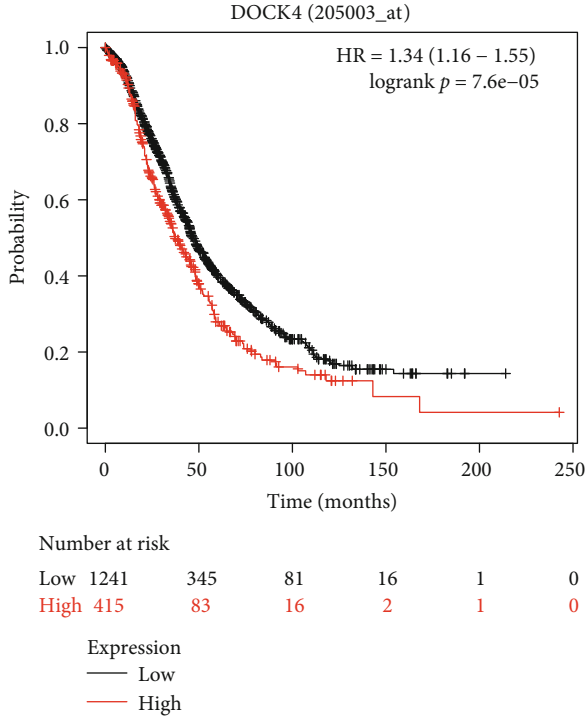

(c)

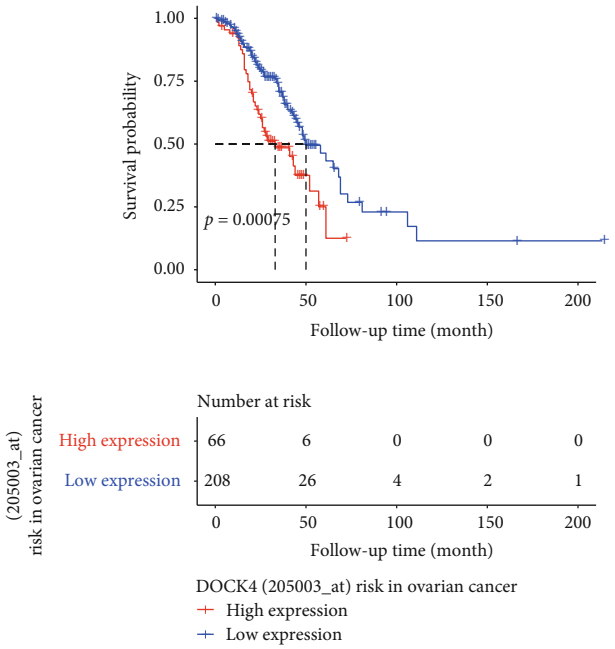

(d)

Figure 2: Continued.

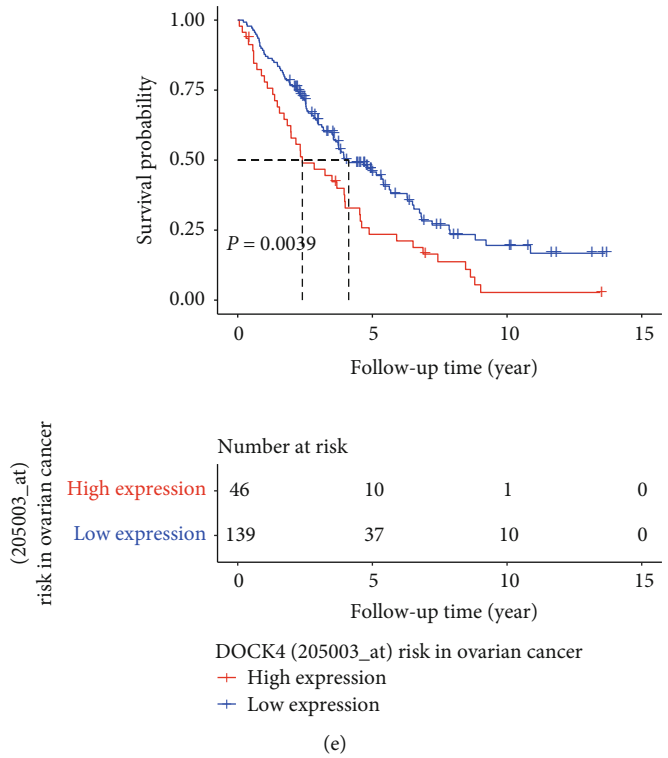

(e)

Figure 2: The prognostic value of DOCK4 in OV. Kaplan-Meier curves show the association between DOCK4 expression and overall survival, using data from (a) TCGA, (b, c) Kaplan-Meier plotter, and (d, e) GEO in ovarian cancer.

patient dataset with only RNA-Seq expression data ($n = 304$) (Figure 2(a)). We found that *DOCK4* upexpression was associated with a worse prognosis in ovarian cancer. To verify DOCK4 clinical significance in ovarian cancer, we used other datasets such as array expression data ($n = 1656$) and RNA-Seq expression data ($n = 374$) by using the webserver of Kaplan-Meier plotter (https://kmplot.com/analysis/). The overall survival analysis results of array data (Figure 2(b)) and RNA-Seq data (Figure 2(c)) from Kaplan-Meier plotter indicated that DOCK4 gene upexpression was a poor prognosis of ovarian cancer patients. The analysis results from different data indicate that downexpression of *DOCK4* correlates with better clinical outcome. For further validation, we employed other two independent cohorts (AOCS (1992–2006), MSKCC (1990–2003)) from the GEO database to assess how *DOCK4* expression relates to prognosis in OV, revealing its elevation to be significantly linked with a poorer prognosis in OV (Figures 2(d) and 2(e)). In general, the upexpression of *DOCK4* is correlated with OS in OV patients. These results thus clearly demonstrate that *DOCK4* expression significantly correlated with poorer outcome in ovarian cancer and might be a potential prognostic biomarker for OV.

3.3. Assessment of DOCK4 Expression Pattern in Pan-Cancers. To evaluate the possibility of *DOCK4* as a prognostic marker in different tumors, we applied different cancer tissue RNA-Seq datasets from TCGA datasets. The webserver of Kaplan-Meier plotter (https://kmplot.com/analysis/) was applied to do overall survival analysis by using RNA-Seq expression data of 33 tumors. The survival analysis result suggested high-expression DOCK4 gene as a potential poor prognosis biomarker among sarcoma (SARC), stomach adenocarcinoma (STAD), and uterine corpus endometrial carcinoma (UCEC) (Figures 3(a)–3(c)), while low-expression DOCK4 gene as a potential poor prognosis biomarker among kidney renal clear cell carcinoma (KIRC) and head and neck squamous cell carcinoma (HNSC) (Figures 3(d) and 3(e)). In order to detect DOCK4 expression pattern among different tumors, the webserver of UALCAN (http://ualcan.path.uab.edu/analysis.html) was employed to present DOCK4 gene expression pattern among 33 tumors with TCGA RNA-Seq expression data (Figure 3(f)), which indicated that DOCK4 gene does not have low expression in ovarian cancer. Furthermore, compared with normal tissues, *DOCK4* was relatively upexpressed in many cancer types including ESCA, HNSC, KIRC, KIRP, LIHC, PPAD, PCPG, SKCM, and STAD, while it is downexpressed in BLCA, BRCA, CESC, CHOL, COAD, GBM, KICH, LUAD, LUSC, PRAD, READ, SARC, THCA, THYM, and UCEC (Figure 3(g)). In summary, *DOCK4* has the potential to become a general biomarker in many tumors.

3.4. DOCK4 Expression in Plasma. To further explore the future application of *DOCK4* as a prognostic indicator to the clinic, in view of the previously known fact that *DOCK4* is highly expressed in OV tissues, we further tested the expression level of *DOCK4* in the blood and found that *DOCK4* can be detected as a secreted protein in peripheral blood in different datasets. In addition, *DOCK4* is specifically enriched in neutrophils (Figure 4), which indicated that DOCK4 could be a secreted protein detected in peripheral blood.

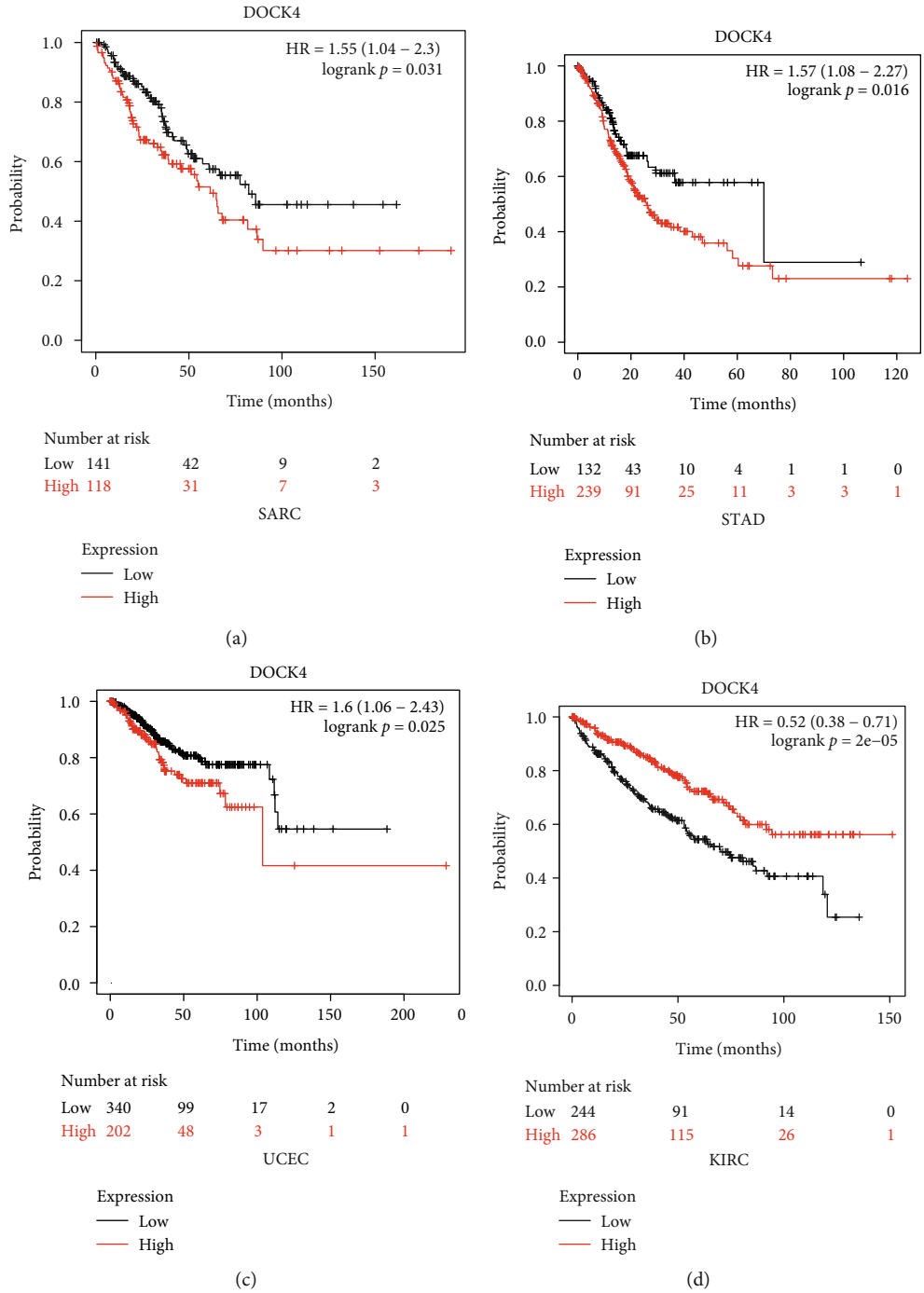

Figure 3: Continued.

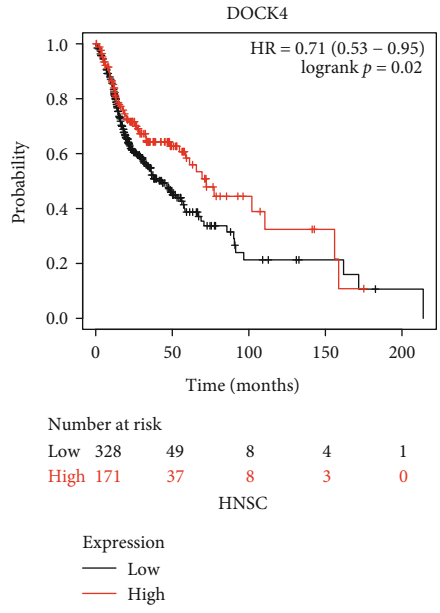

(e)

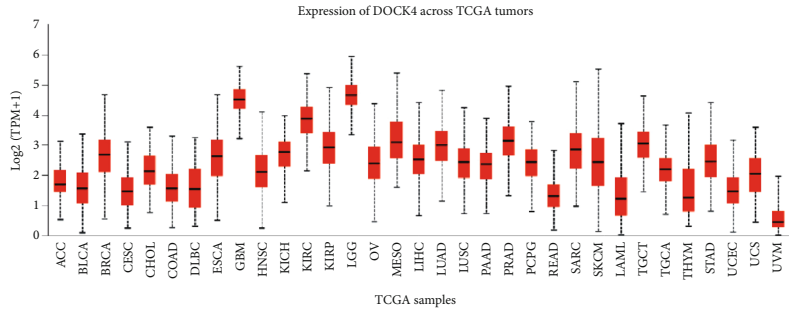

(f)

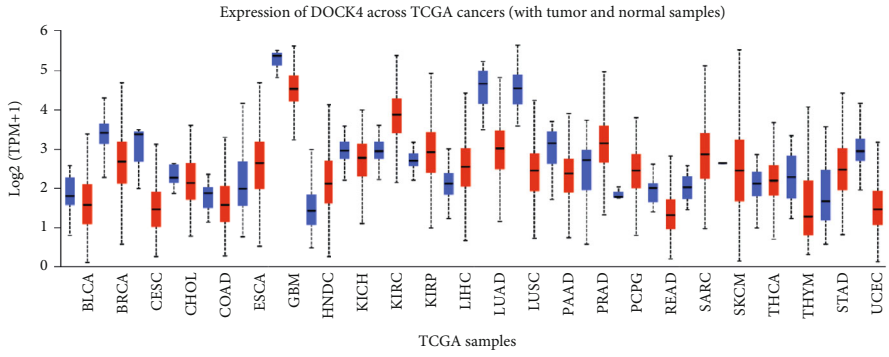

(g)

Figure 3: The survival analysis of DOCK4 in various cancers and expression patterns of DOCK4 across TCGA cancer types. (a–e) Kaplan-Meier curves show the correlation between DOCK4 expression and overall survival of SARC, STAD, UCEC, KIRC, and HNSC patients, respectively. (f) The summary of the expression pattern of DOCK4 across 33 tumors. ACC: adrenocortical carcinoma; BLCA: bladder urothelial carcinoma; BRCA: breast invasive carcinoma; CESC: cervical squamous cell carcinoma and endocervical adenocarcinoma; CHOL: cholangiocarcinoma; COAD: colon adenocarcinoma; DLBC: lymphoid neoplasm diffuse large B cell lymphoma; ESCA: esophageal carcinoma; GBM: glioblastoma multiforme; HNSC: head and neck squamous cell carcinoma; KICH: kidney chromophobe; KIRC: kidney renal clear cell carcinoma; KIRP: kidney renal papillary cell carcinoma; LGG: brain lower grade glioma; OV: ovarian cancer; MESO: mesothelioma; LIHC: liver hepatocellular carcinoma; LUAD: lung adenocarcinoma; LUSC: lung squamous cell carcinoma; PAAD: pancreatic adenocarcinoma; PCPG: pheochromocytoma and paraganglioma; PRAD: prostate adenocarcinoma; READ: rectum adenocarcinoma; SARC: sarcoma; SKCM: skin cutaneous melanoma; LAML: acute myeloid leukemia; TGCT: testicular germ cell tumors; THCA: thyroid carcinoma; THYM: thymoma; STAD: stomach adenocarcinoma; UCEC: uterine corpus endometrial carcinoma; UCS: uterine carcinosarcoma; UVM: uveal melanoma. (g) The changed expression of DOCK4 in 24 cancer cohorts compared to normal tissues.

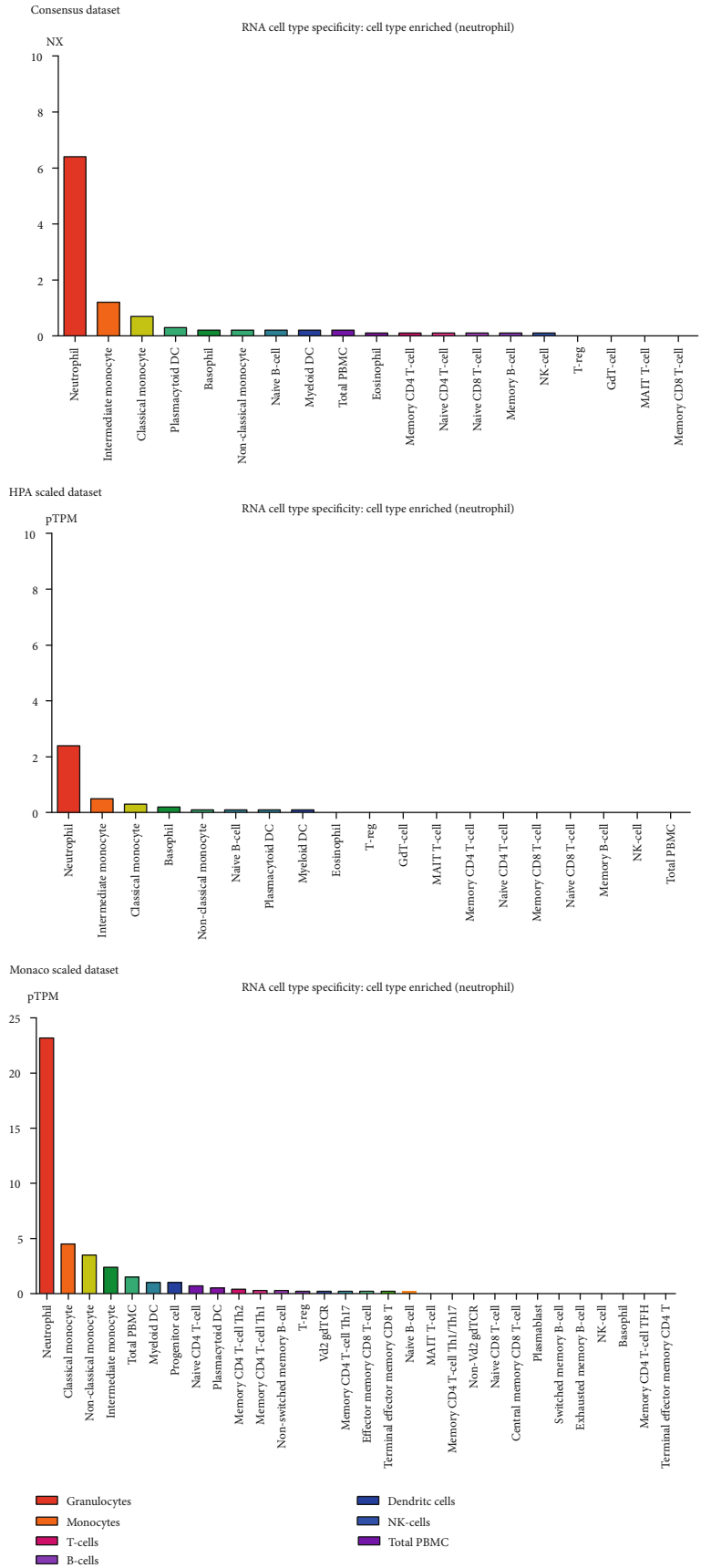

Figure 4: The relative expression of DOCK4 in various cells in peripheral blood.

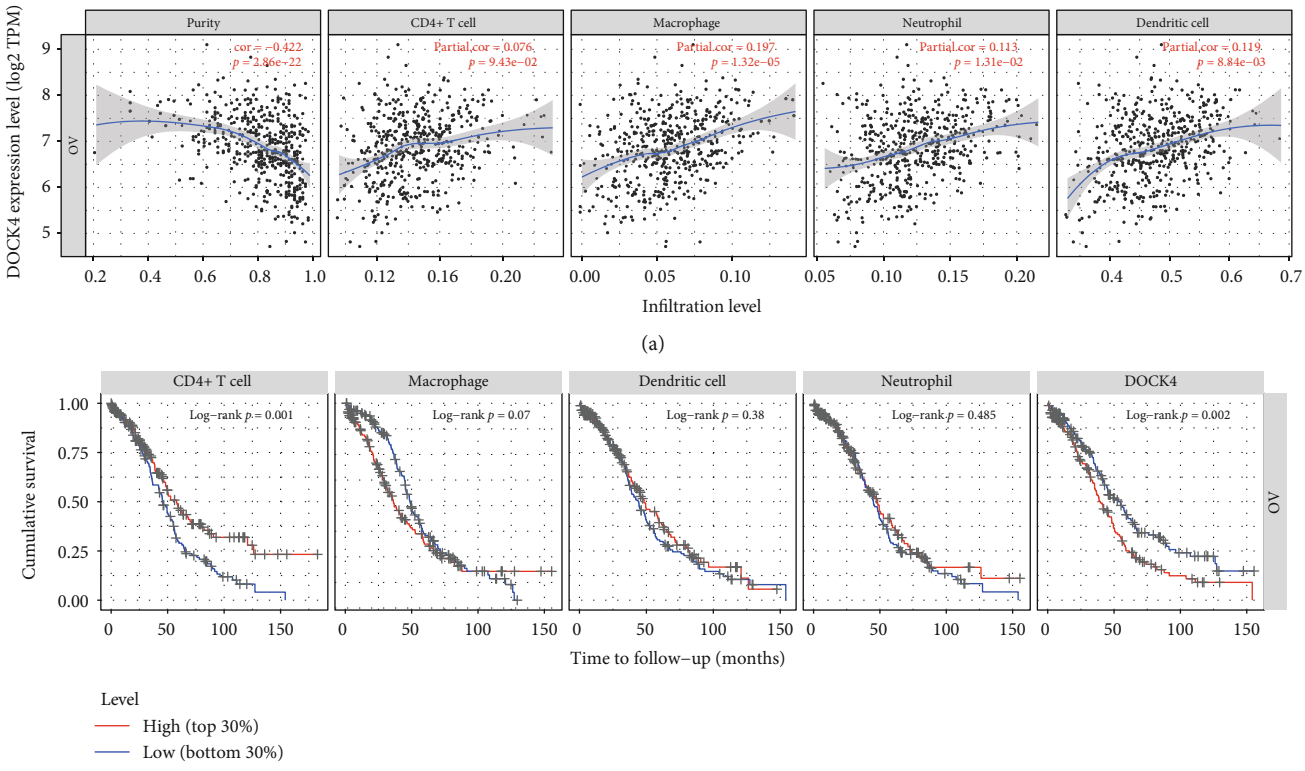

Figure 5: Assessment of the correlation between DOCK4 expression and immune cell infiltration. (a) DOCK4 expression is correlated with the level of immune infiltration in ovarian cancer. (b) Kaplan-Meier plots of immune infiltration and DOCK4 expression levels in ovarian cancer.

Table 1: Multivariate analysis associated with overall survival in ovarian cancer patients ($n = 547$).

Parameters	Coefficient	HR (95% CI)	p
Age	0.022	1.022 (1.012-1.033)	0.000
CD4+ T cell	-11.633	0.000 (0.000-0.004)	0.000
Macrophage	5.307	201.833 (0.897-45431.169)	0.055
Dendritic cell	-3.703	0.025 (0.001-0.947)	0.047
Neutrophil	9.762	17362.900 (4.858-62051075.704)	0.019
DOCK4	0.248	1.281 (1.092-1.503)	0.002

3.5. DOCK4 Expression Correlates with Immune Cell Infiltration. Since *DOCK4* is mainly enriched in neutrophils, it is necessary for us to study its relationship with other immune cells. Therefore, we analyzed the relationship between *DOCK4* expression and the degree of immune cell infiltration OV in the TIMER database. In 6 types of immune cells including B cells, CD4+ T cells, CD8+ T cells, neutrophils, macrophages, and dendritic cells, we found that *DOCK4* expression weakly positively correlated with the levels of CD4+ T cell infiltration, dendritic cell infiltration, and neutrophil infiltration in OV (Figure 5(a)). We further found CD4+ T cell infiltration to be significantly associated with OV prognosis (Figure 5(b)).

We explored the OV prognosis relevance of tumor immune subsets, with multiple covariates including age, ethnicity, *DOCK4* expression, and tumor stages in a multivariable Cox proportional hazard model. We found that only variables including age, CD4+ T cell, dendritic cell, neutrophils, macrophage, and *DOCK4* can be included in the model (Table 1).

This suggests that *DOCK4* plays a moderate role in interacting with immune cell infiltration in ovarian cancer. Certainly, further work will be necessary to identify the role of *DOCK4* in immune activity regulation in ovarian cancer.

3.6. DOCK4 Expression in Ovarian Cell Lines with Platinum Treatment. We further want to verify the reactivity of *DOCK4* to platinum treatment in vitro. 46 ovarian cancer cell lines were treated with cisplatin (data from GSE47856), and we observed the changes in *DOCK4* expression levels. We found that *DOCK4* expression in OVCA420 and FU-OV-1 cell lines was significantly inhibited in the cisplatin-treated group compared with the control group (Figure 6). *DOCK4* expression in other cell lines was not significantly different which might be due to the dissimilarity between cell lines in vitro and tumor in vivo (S1). Therefore, to some extent,

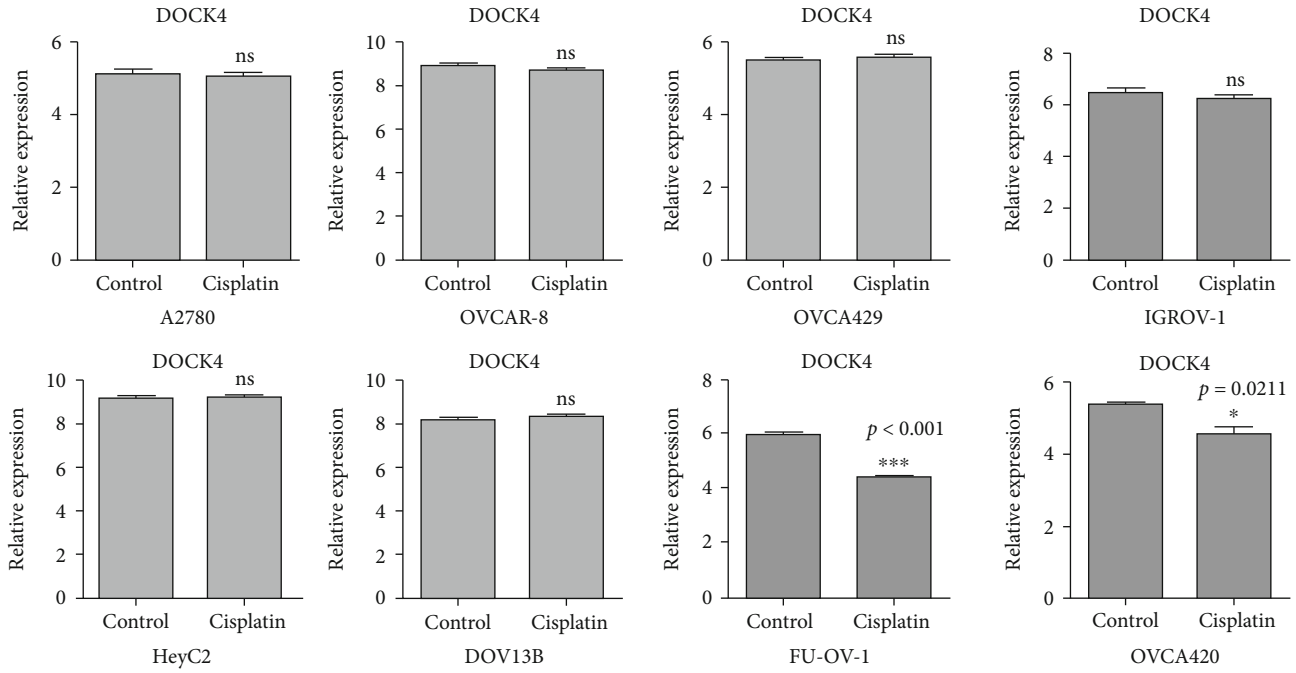

Figure 6: Changes in DOCK4 expression levels in some ovarian cancer cells treated with cisplatin.

we believe that *DOCK4* might be sensitive to the treatment of platinum drugs and can be used as a prognostic indicator for certain types of OV selection of platinum chemotherapy drugs.

4. Discussion

PPARs as ligand-activated transcriptional factors play dominative biological functions such as glucose and lipid metabolism. However, PPAR-TRGs involved in platinum chemosensitivity and prognosis remain to be interpreted further. Ovarian cancer is the fifth common cancer accompanied with poor prognosis of which the 5-year relative survival is less than 45% [20]. Consequently, constructing molecular signatures of prognosis shows high priority to improve the treatment of these patients. This study mainly focused on illuminating the role of PPAR-TRGs in platinum chemosensitivity and prognosis of ovarian cancer to establish the molecular signature for clinical application. In this study, 4 DEGs were identified as the candidate genes of PPAR-TRGs with platinum chemosensitivity by analyzing chemotherapy-sensitive and chemotherapy-resistant samples. Meanwhile, our results suggest that *DOCK4*, a Rho GTPase exchange factor for Rac, is negatively correlated with the survival of ovarian cancer patients, supporting previous reports that the abnormal expression of *DOCK4* has been associated with tumor migration and metastasis in breast cancer and lung adenocarcinoma [21, 22]. Since *DOCK4* as a member of the *DOCK* family is targeted by PPARs which shows close association with numerous cancer types, we characterized the expression of *DOCK4* in 24 cancers. The result shows that *DOCK4* is upexpressed in 9 cancer species and downexpressed in 15 cancer species which may be due to the distribution and function of *DOCK* family 11 members which are variant in different tissues and cells. These results indicate that *DOCK4* might be a general biomarker for many cancer types. Further survival analysis demonstrated that *DOCK4* indeed correlates with prognosis of some cancer types. Therefore, much more efforts are required to clarify the relationship between the *DOCK* family and the cancer process.

Given that *DOCK4*, the promising biomarker for prognosis of ovarian cancer patients, could be detected in blood contributing to clinical treatment, we then investigated the expression pattern of *DOCK4* in blood samples consistent with *DOCK4* encoding a secreted protein. Our results showed that *DOCK4* could be detected in the peripheral blood of ovarian cancer patients. It is widely recognized that the infiltration of tumor-infiltrating lymphocytes (TILs) has been positively associated with prognosis and platinum chemosensitivity in a great deal of cancers, including ovarian cancer [23–25]. In parallel with the importance of immune response in cancers, our results further confirmed that *DOCK4* was mainly enriched in neutrophils. Several reports have confirmed that neutrophils participate in the regulation of inflammation and the induction of angiogenesis within the tumor. On the other hand, numerous studies have indicated that PPARs play important roles in innate immunity and inflammatory response which are involved in tumor progression and cancer cell metabolism. In particular, PPARβ/δ also has an effect on proangiogenic effects in several researches [26]. Therefore, the role of *DOCK4* in neutrophils remains to be explored in ovarian cancer progression. We further found that the expression of *DOCK4* is correlated with the levels of CD4+ T cell infiltration, dendritic cell infiltration, and neutrophil infiltration in these ovarian cancer patients. Combined with previous studies, our results demonstrated that *DOCK4* targeted by PPARδ has a hand in immunological construction. Therefore, much more efforts are demanded to reveal the mechanism of *DOCK4* targeted by PPARδ in ovarian cancer patients' immune cells, especially neutrophils.

Since ovarian cancer is a heterogeneous disease encompassing a group of neoplasms with distinct clinicopathological and genetic features [27], the cancer sample size should be enlarged and classified into different groups for extended research. Furthermore, other experimental methods in vivo and in vitro would be considered to characterize the regulation mechanism of *DOCK4* in ovarian cancer. Other members of the *DOCK* family might be further explored to contribute to the related research of ovarian cancer.

5. Conclusion

In this study, we firstly identified a potential function suggesting the chemotherapy-sensitive role of *DOCK4* in ovarian cancer, which might be correlated with immune cell infiltration. Altogether, *DOCK4* might be a candidate prognosis biomarker for ovarian cancer patients. The function and mechanism of *DOCK4* in ovarian cancer need further research.

Data Availability

The data in our study are available from the corresponding author upon reasonable request.

Conflicts of Interest

The authors declare that there is no conflict of interest regarding the publication of this paper.

Authors' Contributions

Qianqian Zhao and Jie Zhong contributed equally to this work.

Acknowledgments

This research was funded by a grant from the Shanghai Talent Development Funding for the project (No. 2018124), Science and Technology Climbing Fund of SIPPR (No. PD2017-9), and hospital level project of Shanghai Shidong Hospital (No. 20170036).

Supplementary Materials

File 1: changes in DOCK4 expression levels in all cell lines treated with cisplatin. *(Supplementary Materials)*

References

[1] A. McPherson, A. Roth, E. Laks et al., "Divergent modes of clonal spread and intraperitoneal mixing in high-grade serous ovarian cancer," *Nature Genetics*, vol. 48, no. 7, pp. 758–767, 2016.

[2] J. Ferlay, E. Steliarova-Foucher, J. Lortet-Tieulent et al., "Cancer incidence and mortality patterns in Europe: estimates for 40 countries in 2012," *European Journal of Cancer*, vol. 49, no. 6, pp. 1374–1403, 2013.

[3] L. A. Torre, B. Trabert, C. E. DeSantis et al., "Ovarian cancer statistics, 2018," *CA: a Cancer Journal for Clinicians*, vol. 68, no. 4, pp. 284–296, 2018.

[4] T. J. Herzog and B. Pothuri, "Ovarian cancer: a focus on management of recurrent disease," *Nature Clinical Practice. Oncology*, vol. 3, no. 11, pp. 604–611, 2006.

[5] L. A. Moraes, L. Piqueras, and D. Bishop-Bailey, "Peroxisome proliferator-activated receptors and inflammation," *Pharmacology & Therapeutics*, vol. 110, no. 3, pp. 371–385, 2006.

[6] S. Shi, G. Yu, B. Huang, Y. Mi, Y. Kang, and J. P. Simon, "PPARG could work as a valid therapeutic strategy for the treatment of lung squamous cell carcinoma," *PPAR Research*, vol. 2020, Article ID 2510951, 9 pages, 2020.

[7] K. D. Wagner and N. Wagner, "Peroxisome proliferator-activated receptor beta/delta (PPARbeta/delta) acts as regulator of metabolism linked to multiple cellular functions," *Pharmacology & Therapeutics*, vol. 125, no. 3, pp. 423–435, 2010.

[8] P. L. Yang, J. S. Wang, X. M. Cheng et al., "PPAR-γ ligand inhibits nasopharyngeal carcinoma cell proliferation and metastasis by regulating E2F2," *PPAR Research*, vol. 2019, Article ID 8679271, 9 pages, 2019.

[9] G. D. Girnun, E. Naseri, S. B. Vafai et al., "Synergy between PPARgamma ligands and platinum-based drugs in cancer," *Cancer Cell*, vol. 11, no. 5, pp. 395–406, 2007.

[10] W. H. Chang and A. G. Lai, "The pan-cancer mutational landscape of the PPAR pathway reveals universal patterns of dysregulated metabolism and interactions with tumor immunity and hypoxia," *Annals of the New York Academy of Sciences*, vol. 1448, no. 1, pp. 65–82, 2019.

[11] A. Z. Mirza, I. I. Althagafi, and H. Shamshad, "Role of PPAR receptor in different diseases and their ligands: physiological importance and clinical implications," *European Journal of Medicinal Chemistry*, vol. 166, pp. 502–513, 2019.

[12] S. Nomura, A. Nakajima, S. Ishimine, N. Matsuhashi, T. Kadowaki, and M. Kaminishi, "Differential expression of peroxisome proliferator-activated receptor in histologically different human gastric cancer tissues," *Journal of Experimental & Clinical Cancer Research*, vol. 25, no. 3, pp. 443–448, 2006.

[13] K. Hiramoto, M. Negishi, and H. Katoh, "Dock4 is regulated by RhoG and promotes Rac-dependent cell migration," *Experimental Cell Research*, vol. 312, no. 20, pp. 4205–4216, 2006.

[14] M. Kobayashi, K. Harada, M. Negishi, and H. Katoh, "Dock4 forms a complex with SH3YL1 and regulates cancer cell migration," *Cellular Signalling*, vol. 26, no. 5, pp. 1082–1088, 2014.

[15] J. Liu, T. Lichtenberg, K. A. Hoadley et al., "An integrated TCGA pan-cancer clinical data resource to drive high-quality survival outcome analytics," *Cell*, vol. 173, no. 2, pp. 400–416.e11, 2018.

[16] I. Romero and R. C. Bast Jr., "Minireview: human ovarian cancer: biology, current management, and paths to personalizing therapy," *Endocrinology*, vol. 153, no. 4, pp. 1593–1602, 2012.

[17] L. Fang, M. Zhang, Y. Li, Y. Liu, Q. Cui, and N. Wang, "PPARgene: a database of experimentally verified and computationally predicted PPAR target genes," *PPAR Research*, vol. 2016, Article ID 6042162, 6 pages, 2016.

[18] T. Li, J. Fan, B. Wang et al., "TIMER: a web server for comprehensive analysis of tumor-infiltrating immune cells," *Cancer Research*, vol. 77, no. 21, pp. e108–e110, 2017.

[19] A. Lánczky, Á. Nagy, G. Bottai et al., "miRpower: a web-tool to validate survival-associated miRNAs utilizing expression data from 2178 breast cancer patients," *Breast Cancer Research and Treatment*, vol. 160, no. 3, pp. 439–446, 2016.

[20] C. Stewart, C. Ralyea, and S. Lockwood, "Ovarian cancer: an integrated review," *Seminars in Oncology Nursing*, vol. 35, no. 2, pp. 151–156, 2019.

[21] J. A. Westbrook, S. L. Wood, D. A. Cairns et al., "Identification and validation of DOCK4 as a potential biomarker for risk of bone metastasis development in patients with early breast cancer," *The Journal of Pathology*, vol. 247, no. 3, pp. 381–391, 2019.

[22] J. R. Yu, Y. Tai, Y. Jin et al., "TGF-β/Smad signaling through DOCK4 facilitates lung adenocarcinoma metastasis," *Genes & Development*, vol. 29, no. 3, pp. 250–261, 2015.

[23] W. T. Hwang, S. F. Adams, E. Tahirovic, I. S. Hagemann, and G. Coukos, "Prognostic significance of tumor-infiltrating T cells in ovarian cancer: a meta-analysis," *Gynecologic Oncology*, vol. 124, no. 2, pp. 192–198, 2012.

[24] E. Sato, S. H. Olson, J. Ahn et al., "Intraepithelial CD8+ tumor-infiltrating lymphocytes and a high CD8+/regulatory T cell ratio are associated with favorable prognosis in ovarian cancer," *Proceedings of the National Academy of Sciences of the United States of America*, vol. 102, no. 51, pp. 18538–18543, 2005.

[25] L. Zhang, J. R. Conejo-Garcia, D. Katsaros et al., "Intratumoral T cells, recurrence, and survival in epithelial ovarian cancer," *The New England Journal of Medicine*, vol. 348, no. 3, pp. 203–213, 2003.

[26] S. Du, N. Wagner, and K. D. Wagner, "The emerging role of PPAR beta/delta in tumor angiogenesis," *PPAR Research*, vol. 2020, Article ID 3608315, 16 pages, 2020.

[27] M. Kossaï, A. Leary, J. Y. Scoazec, and C. Genestie, "Ovarian cancer: a heterogeneous disease," *Pathobiology*, vol. 85, no. 1-2, pp. 41–49, 2018.

Hindawi
PPAR Research
Volume 2021, Article ID 6658944, 16 pages
https://doi.org/10.1155/2021/6658944

Research Article

Fenofibrate Ameliorates Hepatic Ischemia/Reperfusion Injury in Mice: Involvements of Apoptosis, Autophagy, and PPAR-α Activation

Jie Zhang,[1,2] **Ping Cheng**,[3] **Weiqi Dai**,[1,4] **Jie Ji**,[1] **Liwei Wu**,[1] **Jiao Feng**,[1] **Jianye Wu**,[4] **Qiang Yu**,[1] **Jingjing Li**,[1,4] **and Chuanyong Guo**[1]

[1]*Department of Gastroenterology, Shanghai Tenth People's Hospital, Tongji University School of Medicine, Shanghai 200072, China*
[2]*Shanghai Tenth Hospital, School of Clinical Medicine of Nanjing Medical University, Shanghai 200072, China*
[3]*Department of Gerontology, Shanghai Minhang District Central Hospital, Shanghai 201100, China*
[4]*Department of Gastroenterology, Putuo People's Hospital, Tongji University School of Medicine, Shanghai 200060, China*

Correspondence should be addressed to Jingjing Li; sealjj@126.com

Received 8 October 2020; Revised 22 December 2020; Accepted 16 January 2021; Published 1 February 2021

Academic Editor: John P. Vanden Heuvel

Hepatic ischemia and reperfusion injury is characterized by hepatocyte apoptosis, impaired autophagy, and oxidative stress. Fenofibrate, a commonly used antilipidemic drug, has been verified to exert hepatic protective effects in other cells and animal models. The purpose of this study was to identify the function of fenofibrate on mouse hepatic IR injury and discuss the possible mechanisms. A segmental (70%) hepatic warm ischemia model was established in Balb/c mice. Serum and liver tissue samples were collected for detecting pathological changes at 2, 8, and 24 h after reperfusion, while fenofibrate (50 mg/kg, 100 mg/kg) was injected intraperitoneally 1 hour prior to surgery. Compared to the IR group, pretreatment of FF could reduce the inflammatory response and inhibit apoptosis and autophagy. Furthermore, fenofibrate can activate PPAR-α, which is associated with the phosphorylation of AMPK.

1. Introduction

Ischemia/reperfusion (I/R) injury is a major concern during surgical procedures such as liver resection, trauma, and transplantation, which can lead to liver injury or even failure for its inevitable interruption and subsequent restoration of circulation [1, 2]. Hepatic IR is a complex phenomenon, and its various mechanisms have been investigated extensively. As the main target, hepatocytes are attacked by hypoxia, nutrient deprivation, and oxidative stress in ischemia/reperfusion injury [3]. IR-resulted hepatocytes then produce damage-associated molecular patterns (DAMPs), which trigger immune responses and inflammation [4]. Proinflammatory cytokine-mediated apoptosis and reactive oxygen species-(ROS-) induced necrosis is the leading cause of hepatocyte death in IRI [5]. Autophagy is an intracellular self-digestive lysosomal recycling pathway, and its role in hepatic IR injury has been widely studied [4, 6].

Fenofibrate belongs to the group of fibrate drugs, which are generally used in the treatment of dyslipidemia and combined hyperlipidemia patients [7]. Also, fenofibrate is known as peroxisome proliferator-activated receptor-α (PPARα) agonist, the nuclear receptor superfamily member, which was discovered in 1990 [8]. As an activator of nuclear receptor, fenofibrate regulates gene/protein interactions that are involved in various pathophysiological processes, such as regulation of β-oxidation of fatty acids, inflammation, oxidative stress, and even tumorigenesis and cancer progression [9, 10]. Several studies have shown anti-inflammatory, antioxidant, and antiapoptotic effects of fenofibrate to attenuate I/R injury in the brain, heart, kidney, and intestine [11–14]. But to date, no literatures have been reported for the liver

protection of fenofibrate in hepatic I/R injury of mice. Moreover, the specific mechanisms of fenofibrate in IR remain unclear.

AMPK, adenosine monophosphate–activated protein kinase, a key sensor of cellular nutrient supply and energy status, plays crucial roles in regulating cellular growth and metabolism and is related to processes such as autophagy in eukaryotes [15]. It was observed that the activation of the AMPK pathway inhibited macrophage activation to prevent inflammation response [16]. Fenofibrate has a therapeutic effect on HFD-induced kidney injury, through the activation of AMPK and induction of subsequent downstream effectors: autophagy and antioxidants [17]. Experiment demonstrated that fenofibrate activates AMPK in endothelial cells, leading to reduce inflammation, as well as inhibition of apoptosis [18]. The activation of AMPK is a trigger to downstream mediators, including PPAR-α, and they together participate in mechanisms like inflammation, apoptosis, autophagy, and oxidative stress that are involved in IR. There are reasons to believe fenofibrate may function through activating the AMPK/PPAR-α pathway.

Herein, we evaluated the value of fenofibrate in hepatocellular protection during hepatic ischemia/reperfusion injury. The present study investigated whether and how fenofibrate administration would affect liver functions and its underlying mechanisms in a well-established murine IR model based on our previous research [19]. We hypothesized that FF could function by inhibiting inflammation response, apoptosis, and autophagy in a PPAR-α- and AMPK-dependent manner.

2. Materials and Methods

2.1. Reagents. Fenofibrate was purchased from Kingmorn Life Science (Shanghai, China) and suspended with 10% DMSO. ALT and AST regent kits were obtained from Jiancheng Bioengineering Institute (Nanjing, China). The enzyme-linked immunosorbent assay (ELISA) kits were acquired from eBioscience (San Diego, CA, USA). The RNA polymerase chain reaction (PCR) kit was from Takara Biotechnology (Dalian, China). The antibodies for PPAR-α, IL-6, Bax, Bcl-2, Beclin-1, P62, LC3, Casepase-9, Caspase-3, and Nrf-2 were provided by Proteintech (Chicago, IL, USA). The TNF-α and IL-1β antibodies were from Abcam (Cambridge, MA, USA). The AMPK and p-AMPK antibodies were from CST (Danvers, MA, USA). The TdT-mediated dUTP nick end labeling (TUNEL) apoptosis assay kit was from Roche (Roche Ltd., Basel, Switzerland).

2.2. Animals. Male Balb/c mice weighing 23 ± 2 g and aged 6–8 weeks old were obtained from Shanghai SLAC Laboratory Animal Co. Ltd. (Shanghai, China). The mice were group-housed in standard plastic cages at ambient temperature (23 ± 1°C) and 55% humidity with a 12 h light-dark cycle, having access to food and water ad libitum. All animal experiments were carried out in accordance with the National Institutes of Health Guidelines and with approval of the Animal Care and Use Committee of Shanghai Tongji University.

2.3. Treatment Protocol. 78 mice were randomly assigned to one of five groups as follows: (a) normal control group ($n = 6$); (b) sham group ($n = 18$); (c) I/R without any pretreatment ($n = 18$); (d) I/R with pretreatment of FF (50 mg/kg); and (e) I/R with pretreatment of FF (100 mg/kg). Fenofibrate was administered by intravenous route 1 h before surgery. A total of six mice were selected to sacrifice from each group (except normal control group) at 2, 8, and 24 hours after reperfusion to obtain blood and tissue samples.

Blood samples were collected and then placed at 4°C for 5 hours. Serum was separated by centrifugation of the blood at 4600 × g (4°C) for 10 minutes. Serum was collected, aliquoted, and stored at −80°C until the biochemical analysis. A portion of the median and left liver lobes was quickly isolated and preserved in 4% paraformaldehyde solution for at least 24 hours at 4°C for histopathological assessment while the remaining liver tissue was collected, snap frozen with liquid nitrogen, and stored at −80°C for the subsequent experiments.

2.4. I/R Model Establishment. A model of segmental (70%) hepatic warm IR was used, as previously described [6]. Food was withheld for a period of 12 h before surgery, but mice had free access to water. Mice were anesthetized with 1.25% sodium pentobarbital (Nembutal, St. Louis, MO, USA) by injection intraperitoneally, and then a midline laparotomy was performed.

The hepatoduodenal ligament was dissected, and a microvascular atraumatic clamp was placed on the portal pedicle to the median and left lobe of the liver for partial hepatic ischemia. After 45 minutes, the clamp was removed to initiate liver reperfusion and the wound was sewn with 4–0 silk. Sham groups were subjected to the same procedure but without vascular occlusion. A constant warm body temperature was needed to be maintained during the procedure.

2.5. Determination of Serum Parameters. Serum alanine aminotransferase (ALT) and aspartate aminotransferase (AST) were measured with commercially available colorimetric assay kits as described by the manufacturers of Jiancheng Bioengineering Institute. The amount of IL-1β and TNF-α was determined using ELISA kits, following the manufacturer's instructions.

2.6. Histopathological Evaluation. The prepared liver specimens were dehydrated with ethanol and embedded in paraffin. Samples were sliced into 5 μm thick sections and stained with hematoxylin and eosin (H&E). Inflammation and tissue damage were confirmed with a light microscope.

2.7. Western Blot Analysis. Total protein of liver tissue was extracted from liver tissues stored in liquid nitrogen with radioimmunoprecipitation assay (RIPA) lysis buffer mixed with protease inhibitors (PI) and phenylmethyl-sulfonyl fluoride (PMSF). Protein concentration was quantified using the bicinchoninic acid protein assay kit (Kaiji, China). Equal amounts of total protein were separated on 7.5–12.5% SDS-polyacrylamide gels and then transferred onto 0.22 μm polyvinylidene fluoride membranes. Nonspecific binding sites were blocked with PBS containing 5% nonfat milk for at least

1 h at room temperature, and the membranes were incubated overnight at 4°C with the following primary antibodies and dilutions: β-actin (1 : 1,000), TNF-α (1 : 1,000), IL-1β (1 : 1,000), IL-6 (1 : 1,000), LC3 (1 : 500), Beclin-1 (1 : 500), Bcl-2 (1 : 1,000), Bax (1 : 1,000), caspase3 (1 : 1,000), caspase9 (1 : 1,000), P62 (1 : 1,000), PPAR-α (1 : 500), AMPK (1 : 1,000), p-AMPK (1 : 1,000), and Nrf-2 (1 : 1,000). The next day, membranes were washed three times for 10 min each using PBST (PBS containing 0.1% Tween 20) and then incubated with secondary antibodies at 1 : 2000 for 1 h at room temperature protected from light. Membranes were then washed 3 times with PBST and scanned with the Odyssey two-color infrared laser imaging system (LI-COR, Lincoln, NE, USA). The gray values were quantified using ImageJ analysis software.

2.8. Immunohistochemistry. Paraffin-embedded liver sections were dewaxed in xylene and dehydrated with gradient alcohol. Antigen retrieval was performed by citrate buffer and incubated in a 95°C water bath for 20 min. To block endogenous peroxidases, the sections were incubated with 3% hydrogen peroxide for 10 min at room temperature. Sections were washed with PBS three times and then treated with 5% bovine serum albumin (BSA) for 20 min to block nonspecific proteins. Next, the liver specimens were incubated overnight at 4°C with the following primary antibodies and dilutions: anti-TNF-α, anti-IL-1β, anti-Bcl-2, anti-Bax, anti-Beclin-1, anti-PPAR-α, and anti-Nrf-2 (all 1 : 200), anti-LC3, and p-AMPK (1 : 100), followed by incubation in secondary antibody (1: 50) for 1 h at 37°C. A diaminobenzidine (DAB) kit was used to analyze antibody binding under a light microscope. The stained area was measured by using Image-Pro Plus software (version 6.0).

2.9. RNA Isolation and Quantitative Real-Time PCR (RT-qPCR). Total RNA was extracted from stored frozen liver specimens using TRIzol reagent (Tiangen Biotech, China). RNA was reverse-transcribed into cDNA with a Reverse-Transcription Kit (TaKaRa Biotechnology, China). Gene expression was measured using SYBR Premix Ex Taq (TaKaRa Biotechnology, China), and cDNA was quantified with the 7900HT Fast Real-Time PCR System (Applied Biosystems, CA, USA). Oligonucleotide primer sequences are listed in Table 1. The relative expression levels were analyzed using the $2-\triangle\triangle Ct$ method and normalized relation to β-actin.

2.10. TUNEL Staining. The hepatocyte apoptosis was determined by TUNEL assay. Followed by dewaxing and rehydrating, the prepared 5 μm sections were then digested with 20 μg/ml proteinase K for 30 min. After washing 4 times with PBS, the sections were added with TUNEL reaction mixture. Finally, the positive areas were observed by the light microscope.

2.11. Statistical Analysis. Experimental data were presented as the mean ± standard deviation (SD), and experiments were repeated at least three times. Statistical differences between groups were analyzed by Student's t-test and one-way analysis of variance (ANOVA) followed by Tukey's post hoc test. $P < 0.05$ was considered statistically significant. Statistical analyses were performed, and the graphic charts were plotted by GraphPad Prism 6 software.

Table 1: Oligonucleotide sequences of primers used for qRT-PCR.

Gene	DNA strand	Primer sequence (5′-3′)
β-Actin	Forward	GGCTGTATTCCCCTCCATCG
	Reverse	CCAGTTGGTAACAATGCCATGT
TNF-α	Forward	CAGGCGGTGCCTATGTCTC
	Reverse	CGATCACCCCGAAGTTCAGTAG
IL-1β	Forward	GAAATGCCACCTTTTGACAGTG
	Reverse	TGGATGCTCTCATCAGGACAG
Bax	Forward	AGACAGGGGCCTTTTTGCTAC
	Reverse	AATTCGCCGGAGACACTCG
Bcl-2	Forward	GCTACCGTCGTCGTGACTTCGC
	Reverse	CCCCACCGAACTCAAAGAAGG
Casepase-9	Forward	GGCTGTTAAACCCCTAGACCA
	Reverse	TGACGGGTCCAGCTTCACTA
Casepase-3	Forward	CTCGCTCTGGTACGGATGTG
	Reverse	TCCCATAAATGACCCCTTCATCA
Beclin-1	Forward	ATGGAGGGGTCTAAGGCGTC
	Reverse	TGGGCTGTGGTAAGTAATGGA
LC3	Forward	GACCGCTGTAAGGAGGTGC
	Reverse	AGAAGCCGAAGGTTTCTTGGG
P62	Forward	GAGGCACCCCGAAACATGG
	Reverse	ACTTATAGCGAGTTCCCACCA
PPAR-α	Forward	AACATCGAGTGTCGAATATGTGG
	Reverse	CCGAATAGTTCGCCGAAAGAA
p-AMPK	Forward	ATTGGATTTCCGAAGTATTGATG
	Reverse	CCTGGTCTTGGAGCTACGTCA

3. Results

3.1. FF Improved Hepatic Structure and Function of Mice Subjected to IR Injury. The levels of biomarkers of hepatic function, ALT and AST, in serum were significantly elevated in the IR group at 3 time points (Figure 1(a)). This indicated the successful establishment of a segmental hepatic IR model. In parallel, we observed the aminotransferase was at its highest level at 8 h. ALT and AST at the same time points were markedly lower in the fenofibrate-treated groups. The variation, which was more pronounced in the high-dose compared with the low-dose group. To further determine the drug effect on HIRI, we performed H&E staining. The pathological changes showed that in the sham group, liver tissue structure remained intact, whereas marked congestion, edema, necrosis, massive neutrophil infiltration, and accumulation appeared in the IR group at the three time points (especially in the 24 h group) (Figure 1(b)). Pretreatment with FF at 50 and 100 mg/kg alleviated the liver histopathological alterations in IR groups. From the above results, it could be concluded that fenofibrate exerted a protective effect on liver injury, and the higher the dose, the better the effect.

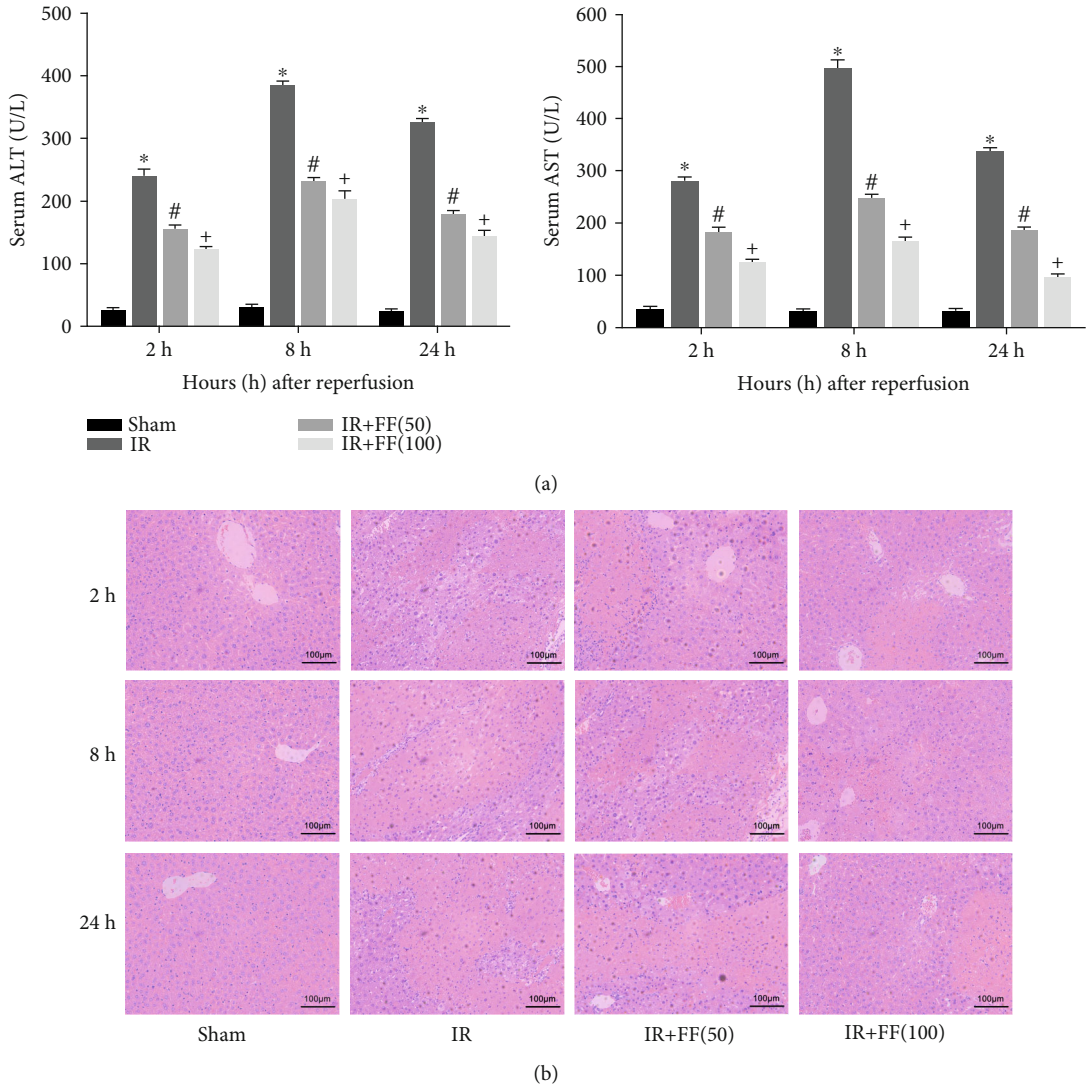

Figure 1: Fenofibrate pretreatment ameliorated hepatic function in IR-induced liver injury. (a) The levels of serum ALT and AST are presented as mean ± SD ($n = 6$; $^{*}P < 0.05$ for IR vs. sham; $^{\#}P < 0.05$ for IR+FF (50) vs. IR; $^{+}P < 0.05$ for IR+FF (100) vs. IR; $\wedge P < 0.05$ for IR+FF (50) vs. IR+FF (100)). (b) Liver sections were stained with H&E and examined under light microscopy (magnification, 200x).

3.2. FF Prevented Hepatic and Systemic Inflammation Induced by Hepatic IR. It has been suggested that the release of inflammatory factors strongly promotes HIR injury. So, TNF-α, IL-6, and IL-1β, the proinflammatory cytokines, were detected to explore the effect of FF on inflammation in terms of serology, protein levels, and gene transcription. As shown by ELISA results, the expression of TNF-α and IL-1β in serum was significantly higher than that in the sham group and peaked at 8 hours after reperfusion (Figure 2(a)). The protein levels also increased in the IR group as shown by western blotting (Figure 2(c)). In addition, the results of immunohistochemistry (IHC) staining and the mRNA expression of PCR were consistent with the results mentioned above (Figures 2(b) and 2(d)). Pretreatment of mice with fenofibrate significantly diminished the expression of inflammatory factors subjected to IR at all time points, and this effect was evident at 100 mg/kg dose. Besides, in H&E staining, the IR group exhibited more inflammatory cell infiltration than the other groups (Figure 1(b)). In summary, inflammatory cascades induced by hepatic ischemia/reperfusion injury in mice could be inhibited by fenofibrate.

3.3. FF Improved Apoptosis Induced by HIR. Large area of hepatocyte apoptosis is one of the serious consequences of hepatic IR. Therefore, alleviated apoptosis becomes an essential part of IRI treatment. First of all, TUNEL staining assay was used to evaluate the degree of apoptotic death from samples at 8 hours after reperfusion. The results indicated that apoptotic hepatocytes were largely observed in tissues of the IR group, while TUNEL-positive cells were significantly decreased in the fenofibrate pretreatment group (Figure 3(a)). Performing qRT-PCR, western blotting, and IHC to detect the expression of apoptosis-related markers, we found that the mRNA and protein expressions of Bax, Caspase-3, and Caspase-9 were elevated in the IR group

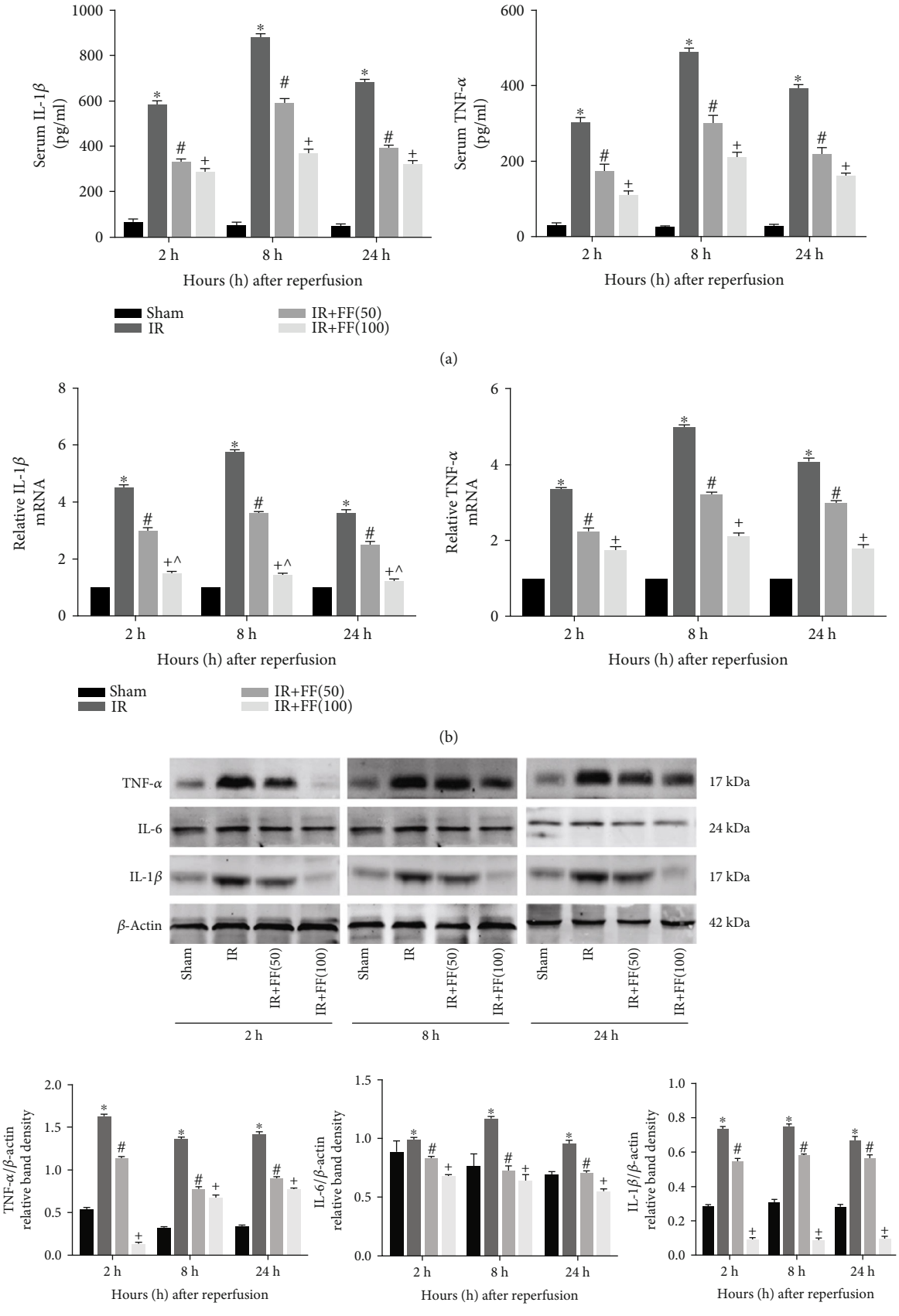

Figure 2: Continued.

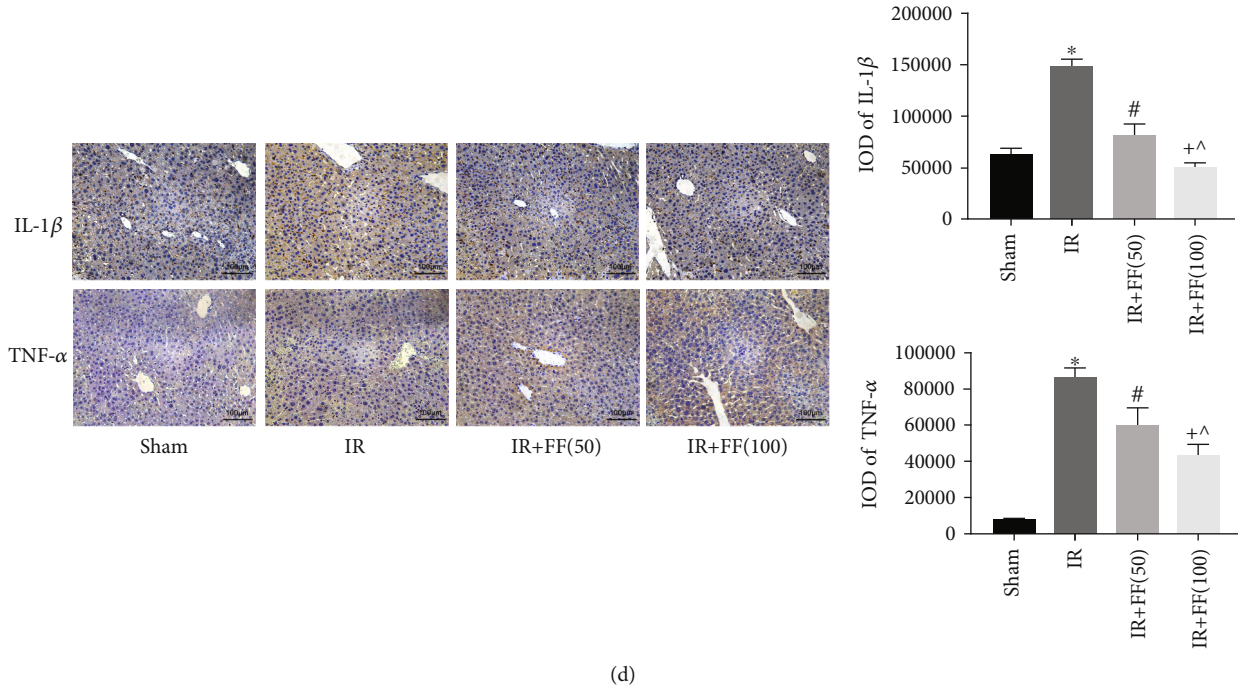

(d)

Figure 2: Fenofibrate reduced the expression of inflammatory cytokines. (a) Serum IL-1β and TNF-α were detected by ELISA. (b) Relative IL-1β and TNF-α mRNA levels were determined by qRT-PCR. (c) Western blot analysis of TNF-α, IL-6, and IL-1β protein levels. The western blot results were quantified with ImageJ 8.0 software. (d) Immunohistochemical staining (200x) showed expression of IL-1β and TNF-α protein in liver tissues at 8 hours after reperfusion. Final evaluations were made using Image-Pro Plus 6.0 software to calculate the IOD of the positive staining area. Data are presented as mean ± SD ($n = 6$; $^{*}P < 0.05$ for IR vs. sham; $^{\#}P < 0.05$ for IR+FF (50) vs. IR; $^{+}P < 0.05$ for IR+FF (100) vs. IR; $^{\wedge}P < 0.05$ for IR+FF (50) vs. IR+FF (100)).

and downregulated in IR+FF (50 mg/kg and 100 mg/kg) groups at each time points after reperfusion. Meanwhile, Bcl-2, an antiapoptotic protein, showed a marked drop in the IR group but was obviously upregulated in fenofibrate preconditioning groups (Figures 3(b) and 3(c)). The expression of Bax and Bcl-2 on IHC staining, distinctly shown in Figure 3(d), presented a similar trend as on PCR and western blotting. In conclusion, fenofibrate can also reduce apoptosis in IR-induced liver injury.

3.4. FF Inhibited Hepatocyte Autophagy. It is well known that autophagy plays a vital role in hepatic IR injury. Autophagy-associated markers including LC3, Beclin-1, and P62 were evaluated to further assess the potential role of FF in IR injury. The expression of Beclin-1 and LC3 in hepatic tissues was detected by real-time PCR. The results revealed that hepatic IR obviously activated the transcription of Beclin-1 and LC3 compared to the sham group. The expression of antiautophagy protein P62 presented an opposite trend to LC3 and Beclin-1. When FF was taken to the mice, Beclin-1 and LC3 expressions were downregulated and P62 expressions were upregulated. (Figure 4(a)). Western blotting results were in accordance with this trend (Figure 4(b)). Analyses of IHC further confirmed the antiautophagy effect of FF (Figure 4(c)). Thus, we deduced from our results that FF could inhibit autophagy in a dose-dependent manner during hepatic IR injury in mice.

3.5. FF Attenuated the Downregulation of the PPAR-α during HIR. Fenofibrate, as a PPARα agonist, showed potential hepatoprotective effects on IR from the above results. To explore the underlying mechanism of fenofibrate, we measured PPAR-α levels in the liver. The results suggested that PPAR-α levels were downregulated in IR groups, and fenofibrate preconditioning could markedly increase the PPAR-α expression, consistent with the expression of Bcl-2 and P62. And the high-dose group (100 mg/kg) performed obviously (Figures 5(a)–5(c)).

3.6. FF Activated the Phosphorylation of AMPK and the Expression of Nrf-2. To verify our hypothesis, we further assessed the AMPK expression conditions. We could see that fenofibrate did not affect the total expression of AMPK between the four groups. However, phosphorylated AMPK (p-AMPK) showed a clear difference between the IR group and IR+FF (50 mg/kg, 100 mg/kg) groups, which may indicate that fenofibrate could activate the phosphorylation of AMPK. These conclusions could be confirmed by PCR, western blotting, and IHC (Figures 5(a)–5(c)). As it is known that the oxidative stress damage is also one of the major drivers of IR injury, we detected the protein Nrf-2, a nuclear transcription factor associated with antioxidant effect, and found that fenofibrate preconditioning increased the expression and accumulation of Nrf-2 (Figures 5(b) and 5(c)). In conclusion, fenofibrate could take effect by activating the phosphorylation of AMPK and increasing Nrf-2 expression.

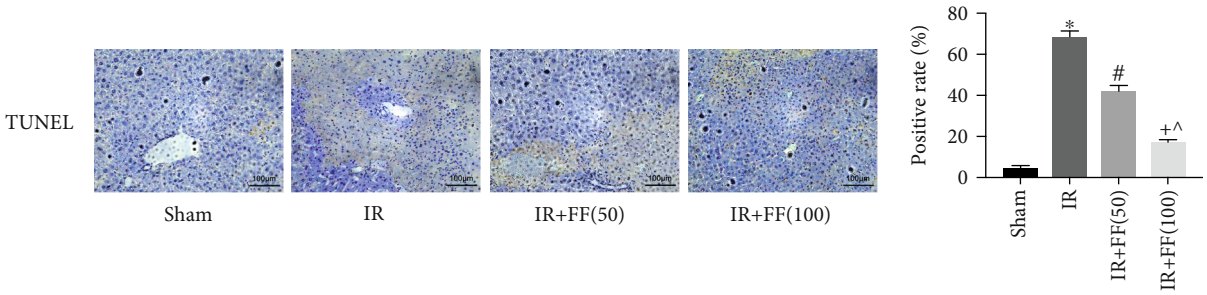

(a)

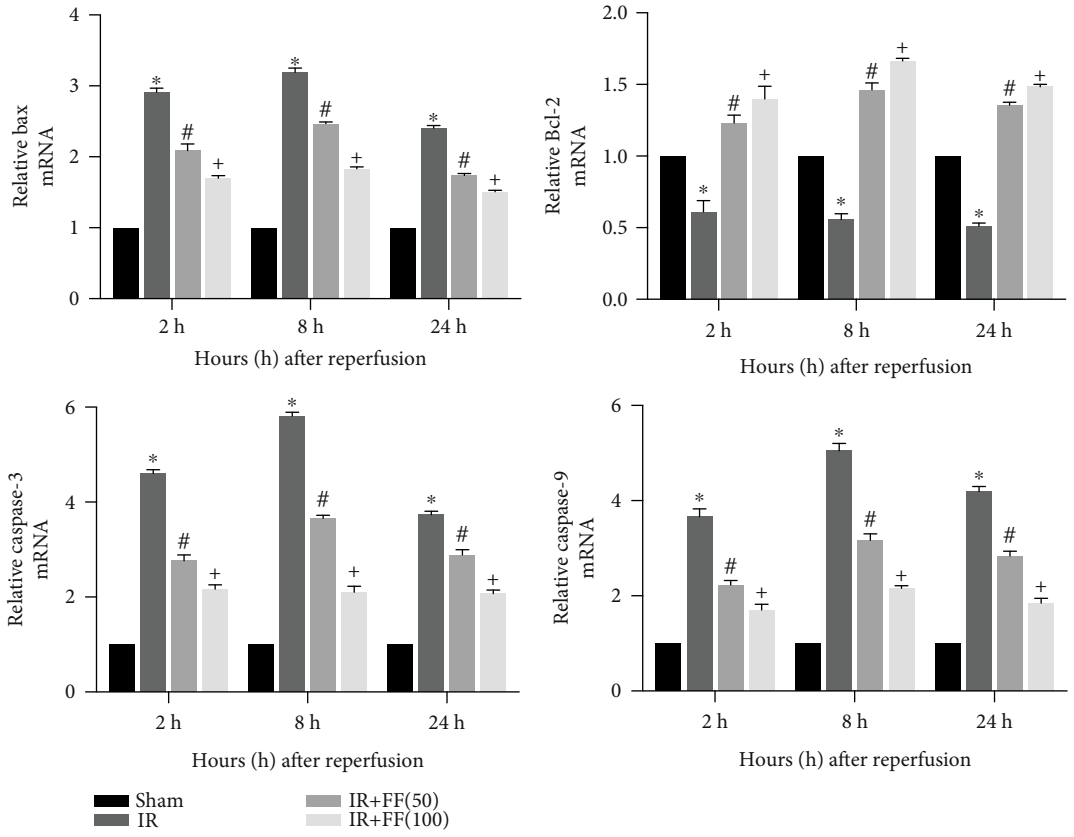

(b)

Figure 3: Continued.

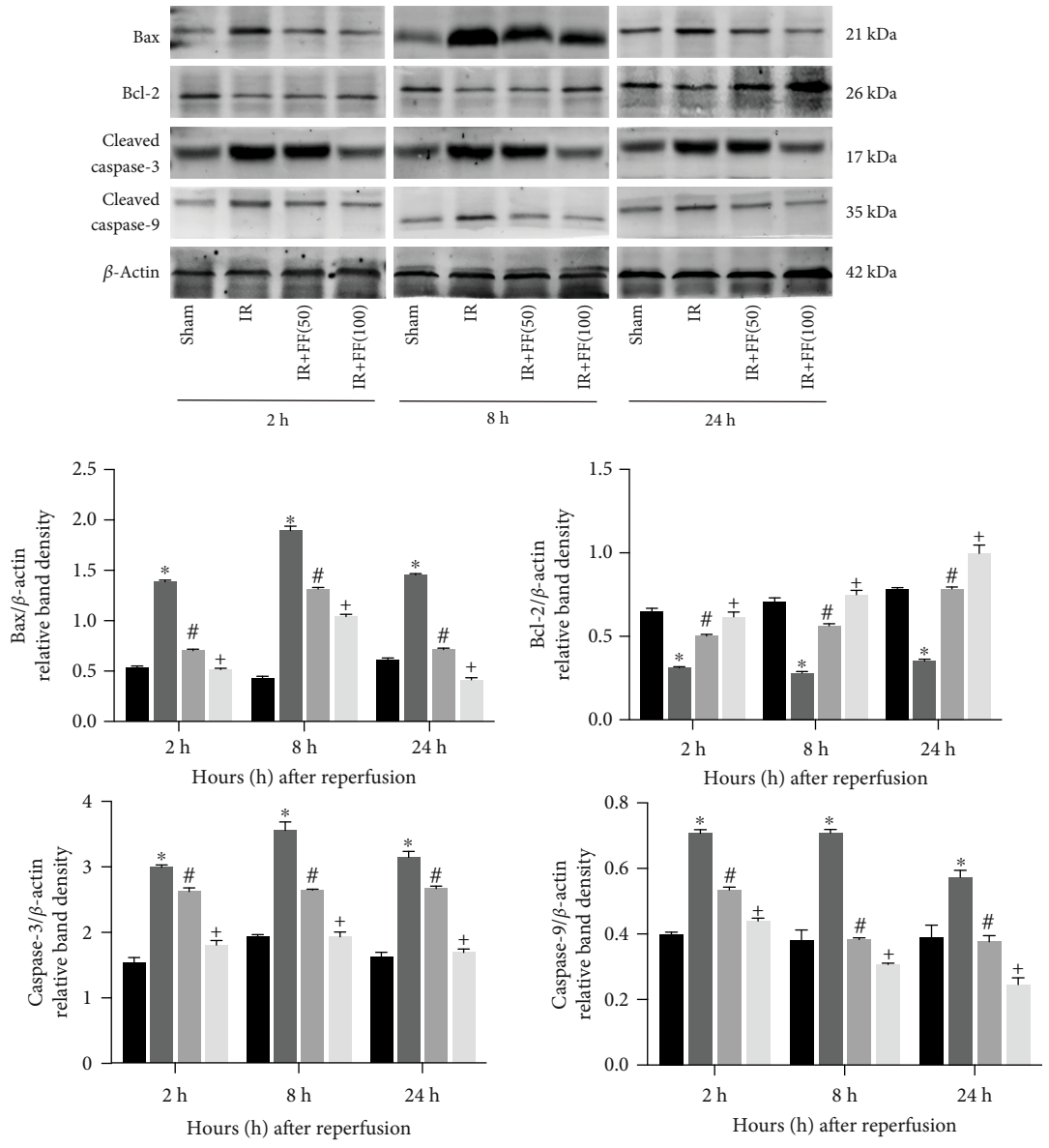

(c)

Figure 3: Continued.

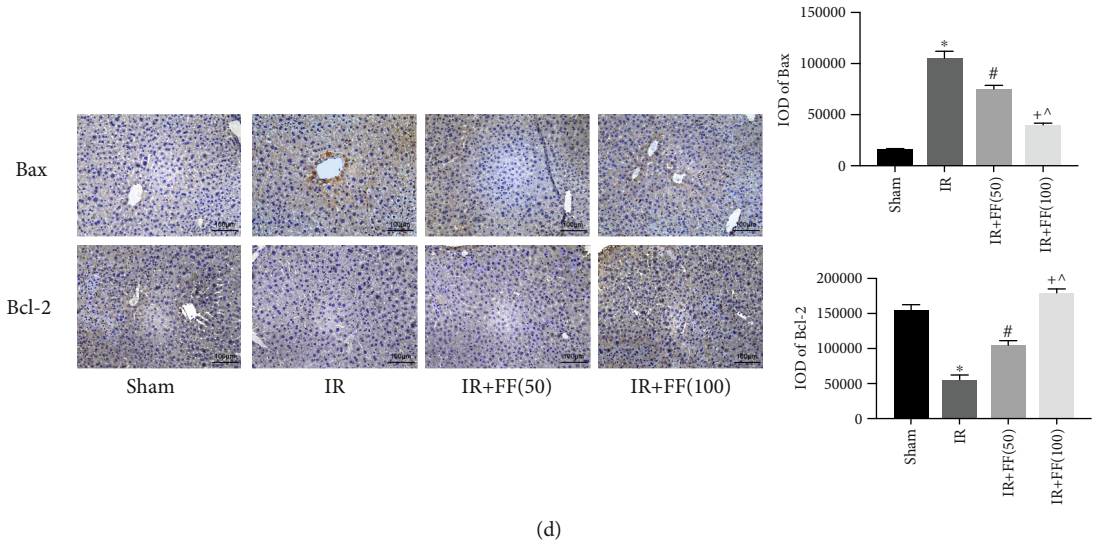

(d)

Figure 3: Fenofibrate attenuated IR-induced apoptosis. (a) After 8 h reperfusion, liver tissues were stained by TUNEL and observed under microscopy (magnification, 200x). Final evaluations were made using Image-Pro Plus 6.0 software to calculate the percentage of positive cells. (b) Relative Bax, Bcl-2, Caspase-3, and Caspase-9 mRNA levels were determined by qRT-PCR. (c) Western blot analysis of Bax, Bcl-2, cleaved Caspase-3, and cleaved Caspase-9 levels. The western blot results were quantified with ImageJ 8.0 software. (d) Bax and Bcl-2 protein expressions in liver tissues at 8 hours after reperfusion are shown by immunohistochemical staining (200x). Final evaluations were made using Image-Pro Plus 6.0 software to calculate the IOD of the positive staining area. Data are presented as mean ± SD ($n = 6$; $^{*}P < 0.05$ for IR vs. sham; $^{\#}P < 0.05$ for IR+FF (50) vs. IR; $^{+}P < 0.05$ for IR+FF (100) vs. IR; $\wedge P < 0.05$ for IR+FF (50) vs. IR+FF (100)) (reproduced from Ji et al. [19]).

4. Discussion

Hepatic IR injury is a clinically relevant processes that occurs in liver resection, trauma, and transplantation, which is the paradoxical damage increasing upon reperfusion of ischemic organs [20]. Hence, the underlying mechanisms need to be explored and potential strategies offered for the liver I/R prophylaxis and treatment should be suggested. Fenofibrate, as a known agonist of PPAR alpha, has been commonly used as a clinical drug to modify blood lipids for treatment of hypertriglyceridemia, hyperlipidemia, and cholestatic liver disease like primary biliary cirrhosis [21]. Fenofibrate is verified to ameliorate liver injury such as sunitinib-induced liver damage and concanavalin- or diet-induced hepatitis [22, 23]. It exhibits potential anti-inflammatory, antioxidant, and antiapoptotic properties. In the current study, we would like to confirm the role of fenofibrate on hepatic I/R in mice and explore the mechanisms behind.

For the above purpose, we used a well-established Balb/c mice model of hepatic IR injury. Ischemia-reperfusion process resulted in elevated serum ALT and AST levels, both of which are indicators of early acute hepatic damage, while fenofibrate pretreatment decreased liver enzyme activities, and this protective effect was dose-related. These results were further validated by the findings of pathological changes. The necrotic area and massive inflammatory cell infiltration indicated that FF could reduce the severity of liver injury caused by hepatic IR.

The physiological and pathophysiological processes involved in hepatic IR injury are complicated. During the initial phase, the oxidative phosphorylation levels of hepatocytes decrease due to oxygen deficiency, thus affecting the generation of adenosine triphosphate (ATP). The levels of mitochondrial reactive oxygen species (ROS) production in hepatocytes are out of control under abnormal circumstances such as ATP depletion [2]. Kupffer cells in the liver are activated by ROS, to further induce the release of proinflammatory cytokines, such as IL-6, IL-1β, and TNF-α [24]. Neutrophils and T cells accumulate and are activated by the Kupffer cells, then stimulate more inflammatory factors, which exacerbate ischemic injury [25]. Besides, proinflammatory cytokines in turn drive the generation of ROS, forming a vicious cycle [4]. In the present study, we first analyzed the expression of inflammatory cytokines in serum and liver tissues by ELISA, western blotting, qRT-PCR, and IHC. Our findings clearly showed that fenofibrate administration attenuated hepatic IR-induced release of TNF-α, IL-6, and IL-1β. And the favorable anti-inflammatory profiles are potentiated in the high-dose group (100 mg/kg).

The proinflammatory cytokine TNF-α plays a pivotal role in various signaling pathways according to previous studies, which could result in extrinsic hepatocyte apoptosis in HIR injury [26]. Moreover, ROS resulting in mitochondrial permeability transition (MPT) can lead to the intrinsic apoptosis pathway. Apoptosis is involved in hepatic IRI [27]. The proapoptotic protein Bax is mostly present in the cytoplasm but migrates to the outer mitochondrial membrane under stimulation, which can lead to the release of intermembrane proteins cytochrome C (Cyto C) to initiate apoptosis. Then, Cyto C subsequently promotes caspase activation and elicits cell death via the intrinsic mitochondrial apoptotic pathway [28]. Bcl-2, the antiapoptosis protein, localized to intracellular mitochondria membranes can restrain the release of cytochrome C during apoptosis to play

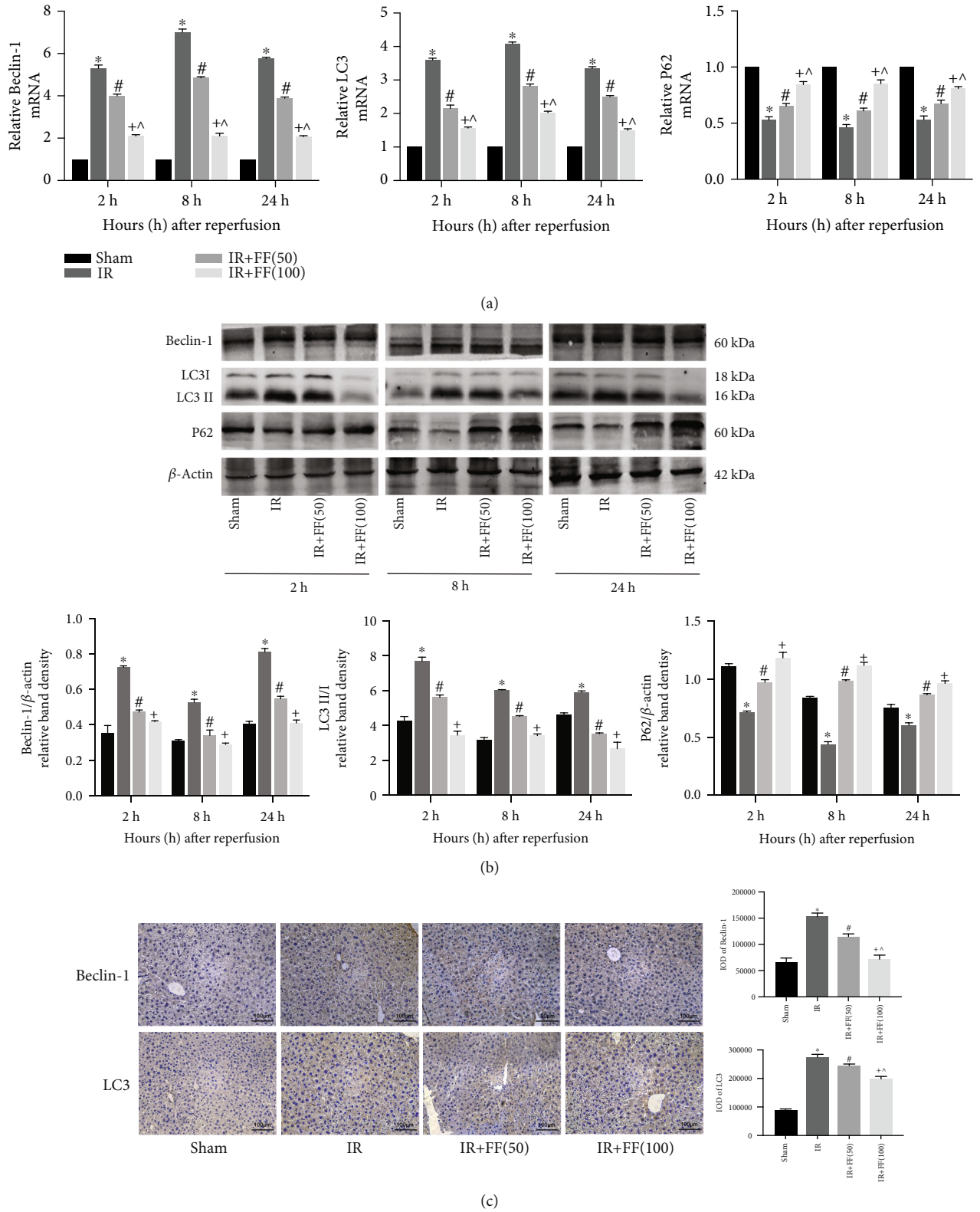

Figure 4: Fenofibrate inhibited autophagy activity during IR injury. (a) Relative Beclin-1, LC3, and P62 mRNA levels were determined by qRT-PCR. (b) Western blot analysis of Beclin-1, LC3, and P62 protein levels. The western blot results were quantified with ImageJ 8.0 software. (c) Beclin-1 and LC3 protein expression in liver tissues at 8 hours after reperfusion was shown by immunohistochemical staining (200x). Final evaluations were made using Image-Pro Plus 6.0 software to calculate the IOD of the positive staining area. Data are presented as mean ± SD ($n = 6$; $^{*}P < 0.05$ for IR vs. sham; $^{\#}P < 0.05$ for IR+FF (50) vs. IR; $^{+}P < 0.05$ for IR+FF (100) vs. IR; $^{\wedge}P < 0.05$ for IR+FF (50) vs. IR+FF (100)) (reproduced from Ji et al. [19]).

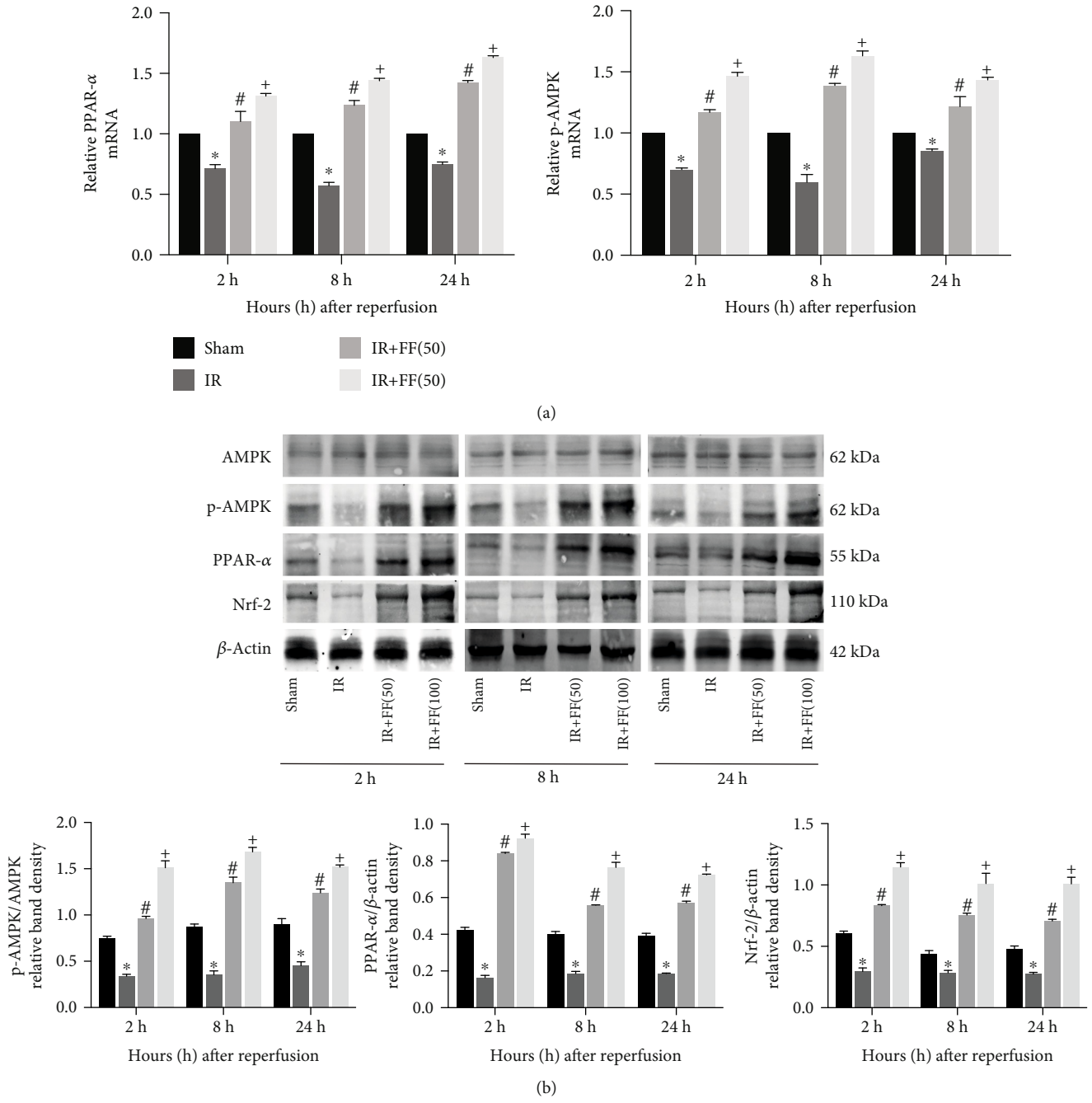

Figure 5: Continued.

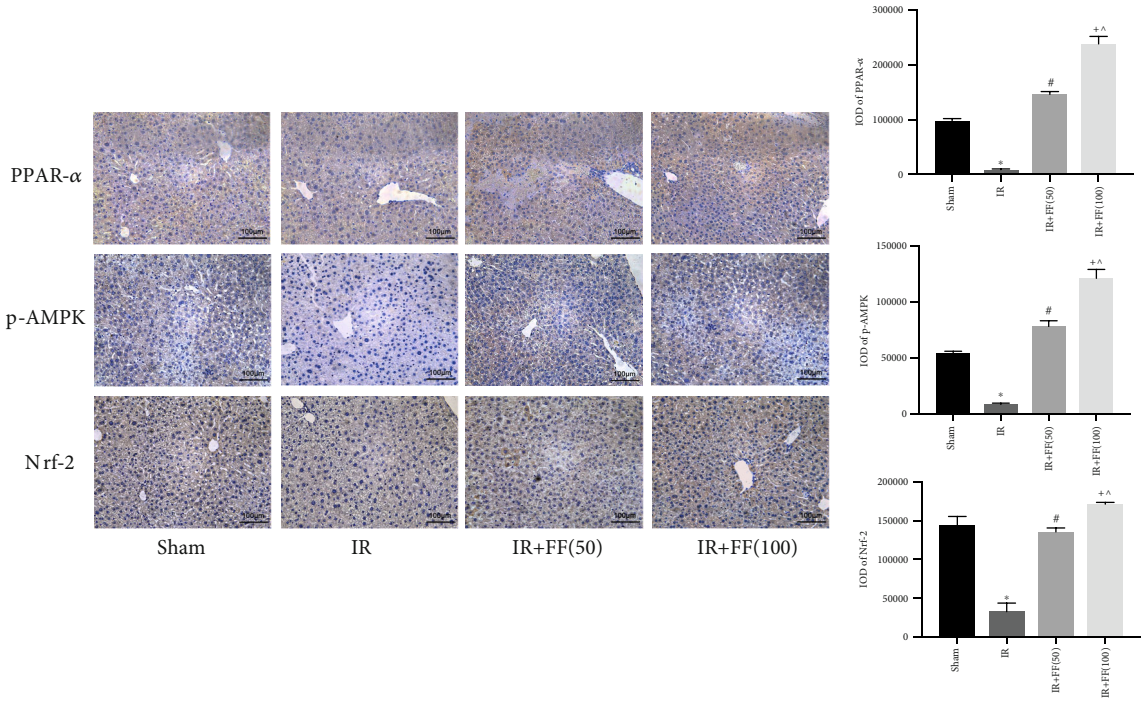

(c)

Figure 5: The protective effect of fenofibrate during hepatic IR injury is closely related with the activation of PPAR-α. (a) Relative PPAR-α and p-AMPK mRNA levels were determined by qRT-PCR. (b) Western blot analysis of AMPK, p-AMPK, PPAR-α, and Nrf-2 levels. The western blot results were quantified with ImageJ 8.0 software. (c) Levels of p-AMPK, PPAR-α, and Nrf-2 in liver tissues at 8 hours after reperfusion are shown by immunohistochemical staining (200x). Final evaluations were made using Image-Pro Plus 6.0 software to calculate the IOD of the positive staining area. Data are presented as mean ± SD ($n = 6$; $^{*}P < 0.05$ for IR vs. sham; $^{\#}P < 0.05$ for IR+FF (50) vs. IR; $^{+}P < 0.05$ for IR+FF (100) vs. IR; $^{\wedge}P < 0.05$ for IR+FF (50) vs. IR+FF (100).

a protective role [29]. In our experiments, fenofibrate attenuating apoptosis was verified by the results of TUNEL. Next, we detected the expression of protein in connection with apoptosis, including Bcl-2, Bax, Caspase-3, and Caspase-9, to ensure how fenofibrate functioned to reduce the damage of HIRI. As expected, we further found the decreased levels of Bax while increased Bcl-2 in FF-administration groups. Caspase-9 and Caspase-3 had similar trends to those observed for Bax. The above results indicated FF could alleviate hepatocyte apoptosis induced by hepatic IR injury.

There are profound interactions between autophagy and apoptosis: they can mutually reinforce and inhibit in many physical activities [4, 30]. Bcl-2 is the intermediary between apoptosis and autophagy, which is participated in the formation of Beclin-1/Bcl-2 complex. Bcl-2 protein binds to Beclin-1 through its BH3 domain [31]. Under the circumstance of apoptosis, Bcl-2 is inactivated and the complex is divided [32]. Subsequently, the free Beclin-1 promotes the induction of autophagy. Increased Bcl-2 could combine with free Beclin-1 and decrease the conversion of LC3 I to LC3 II, which further blocked autophagosome formation [33, 34]. P62 is another autophagy-related protein, which is selectively incorporated into autophagosomes through direct binding to LC3-II and is efficiently degraded in the autophagy [35]. We measured the signature proteins involved in autophagy, such as Beclin-1, LC3, and P62. The results of qRT-PCR, western blotting, and IHC showed that the upregulation of Beclin-1 and LC3 could be reversed by fenofibrate pretreatment. This was also the case for P62. So, we concluded that fenofibrate could attenuate autophagy during IR.

Next, we need to explore the mechanisms of fenofibrate on how to attenuate the injury of IR. PPAR-α is a key transcription factor that mediates the nucleus–mitochondrial interactions to regulate inflammation, lipid metabolism, and mitochondrial functions in various tissues and cells, and it has become a main target in NFALD [36, 37]. PPAR-α activation increases the expression of sirtuin-1 (SIRT1), which inhibits NF-κB, depending on the AMPK pathway and thus reducing inflammation [38, 39]. Dealing with hyperlipidemia, fenofibrate decreased TNFα and IFN-γ, but the levels had increased in PPARα knockout mice [40]. It was reported that PPAR-α activation could decrease IR-induced liver, heart, and brain injury by suppressing inflammation, apoptosis, and lipid peroxidation [41, 42]. Furthermore, PPAR-α can promote the expression of Bcl-2 and subsequently inactivate apoptosis [43]. An experimental study suggested that fenofibrate could inhibit apoptosis through SIRT1-mediated deacetylation of FoxO1 [44]. PPAR-α can also regulate hepatocyte autophagy. Evidence showed that PPAR-α activation attenuated the immune response and protect liver from acute failure through autophagic activation [45]. A study reported that SIRT3, as the upstream of PPAR-α, can regulate the expression of PPARα to affect autophagy [46]. However, the role of FF in mouse

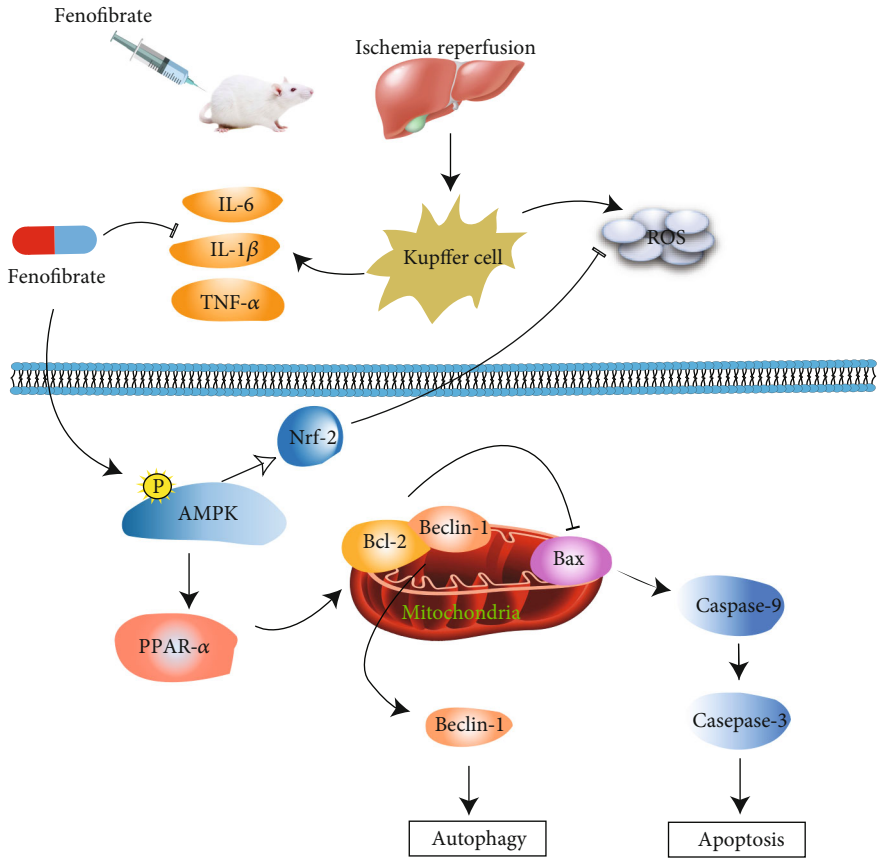

Figure 6: Possible mechanisms of fenofibrate during hepatic IR injury. In our IR-induced liver injury model, activated Kupffer cells promoted the release of proinflammatory cytokines such as TNF-α, IL-1β, and IL-6 and production of ROS. Fenofibrate can activate PPAR-α via phosphorylating AMPK, collaboratively regulating inflammation response, apoptosis, and autophagy downstream. Furthermore, AMPK activation increased accumulation of Nrf-2 to reduce ROS generation. FF shows hepatoprotective effects against IR injury by inhibiting inflammation and attenuating apoptosis and autophagy through the AMPK/PPAR-α pathway.

IR injury was largely unknown. Therefore, we need to determine the expression of PPAR-α to assess whether it also took part in IR injury and found that PPAR-α expression was upregulated in fenofibrate preconditioning groups.

AMPK is a serine/threonine kinase that can be activated by ATP depletion, antioxidant interference, and ROS production [47]. In hepatocytes, AMPK activation is necessary for response to diverse metabolic stresses like inflammation, hypoxia, and oxidative stress [48]. Moreover, activating the AMPK pathway could attenuate oxidative stress and exhibit further protective effects through preventing ROS production [49]. There are plenty of evidence showing that via the AMPK signaling pathway, acute liver injury, nonalcoholic fatty liver diseases, and even hepatocellular carcinoma can be attenuated [50–53]. Also, Padrissa-Altes et al. found that the upregulation of AMPK activity acted in hepatic cold ischemia and reperfusion [54]. AMPK is known to suppress inflammation, through reducing proinflammatory marker and NF-κB levels [55]. In addition, AMPK activation can ultimately contribute to the inhibition of apoptosis via inhibiting proinflammatory cytokines or ROS production. AMPK signaling activation promoted autophagy in hepatocyte, which related to the mTOR signal transduction pathway to control autophagic proteolysis [32]. As mentioned above, AMPK is associated with ROS and can also stimulate nuclear accumulation of Nrf2 [56]. Nrf2, which is an essential transcription factor for modulating the intracellular adaptive antioxidant response to oxidative stress. It was regarded to be vital for defending against oxidative stress and inflammation through antioxidant cascades [57]. Accumulating evidence from studies indicates that the Nrf2/HO-1 pathway is closely involved in alleviating hepatic I/R injury [58, 59]. We indeed observed that Nrf2 expression and accumulation were enhanced in the fenofibrate treatment groups, in which AMPK was phosphorylated. Nevertheless, the detailed mechanism of Nrf-2 remains to be determined by searching for downstream or upstream gene proteins. In our study, we just elucidate its relevance to HIR in brief.

It has been reported that AMPK, the activation of which is a trigger to downstream mediators such as SIRT-1, PGC-1α, and PPAR-α, helps modulate hepatic lipid metabolism for the improvement of liver injury [60]. It is well-documented that phosphorylated AMPK (p-AMPK) can activate PPARα [61]. AdipoRon, a drug for restoration of DKD, performed protective role against lipotoxicity and oxidative stress by enhancing the AMPK/PPARα pathway [62]. Liu et al. clarified that autophagy induction in a D-GalN/LPS model appeared to form a hepatoprotective mechanism that

may involve AMPK and PPARα [52]. Furthermore, AICAR, an activator of AMPK, enhanced PPAR-α expression by promoting PPAR-α transcriptional activity, while treating with compound C, an AMPK inhibitor, could reverse the expression of PPAR-α, which illustrated that PPAR-α activation was in an AMPK-dependent way [52, 61, 63]. Results showed that compared with the IR group, total AMPK stayed unchanged while p-AMPK was significantly upregulated in the FF group, in which the expression of PPAR-α was increased. In the meantime, the expression of apoptosis- and autophagy-related proteins was consistent with our idea. We concluded that fenofibrate protected the liver from damage by activating the AMPK/PPAR-α pathway and accordingly inhibited apoptosis and autophagy.

Thus, our study showed that fenofibrate can activate PPAR-α via the phosphorylation of AMPK, which could alleviate apoptosis and autophagy in hepatic IR injury 6). However, there are several limitations to our study. Fenofibrate and its exact targets and pathway in HIR still require further investigation. Lots of trials need be conducted to verify whether fenofibrate can effectively protect the liver from IR injury clinically.

5. Conclusion

Taken together, fenofibrate alleviated hepatic ischemia/reperfusion injury in mice effectively. Fenofibrate reduced the release of inflammatory cytokines and inhibited hepatocyte apoptosis, autophagy, and ROS. And this protective effect is partly based on the activation of the AMPK/PPAR-α pathway.

Data Availability

The data used to support the findings of this study are available within the article.

Conflicts of Interest

The authors declare no conflicts of interest in this work.

Authors' Contributions

Jie Zhang and Ping Cheng contributed equally to this work and share the same first authorship. Jie Zhang, Ping Cheng, Weiqi Dai, Jie Ji, Liwei Wu, Jiao Feng, Jianye Wu, and Qiang Yu conducted the experiments and analyzed the data. Jingjing Li and Chuanyong Guo provided the reagents and materials. Jie Zhang and Ping Cheng wrote the manuscript.

Acknowledgments

This research was supported by the Yangfan Project of Shanghai Science and Technology Commission (No. 20YF1443300), Natural Science Foundation of Shanghai (No. 19ZR1447700), the Health System Innovation Plan of Shanghai Putuo District Science and Technology Committee (No. PTKWWS201801; PTKWWS201903), the WBN Liver Disease Research Fund of China Hepatitis Prevention Foundation (No. CFHPC2019031), the Minhang District Central Hospital Foundation of Shanghai (No. 2018MHJC08), and the National Natural Science Foundation of China (No. 81670472).

References

[1] C. Peralta, M. B. Jimenez-Castro, and J. Gracia-Sancho, "Hepatic ischemia and reperfusion injury: effects on the liver sinusoidal milieu," *Journal of Hepatology*, vol. 59, no. 5, pp. 1094–1106, 2013.

[2] J. Bi, J. Zhang, Y. Ren et al., "Irisin alleviates liver ischemia-reperfusion injury by inhibiting excessive mitochondrial fission, promoting mitochondrial biogenesis and decreasing oxidative stress," *Redox Biology*, vol. 20, pp. 296–306, 2019.

[3] M. E. Guicciardi, H. Malhi, J. L. Mott, and G. J. Gores, "Apoptosis and necrosis in the liver," *Comprehensive Physiology*, vol. 3, no. 2, pp. 977–1010, 2013.

[4] W. A. Dar, E. Sullivan, J. S. Bynon, H. Eltzschig, and C. Ju, "Ischaemia reperfusion injury in liver transplantation: Cellular and molecular mechanisms," *Liver International*, vol. 39, no. 5, pp. 788–801, 2019.

[5] K. Chen, J. J. Li, S. N. Li et al., "15-Deoxy-$\Delta^{12,14}$-prostaglandin J_2 alleviates hepatic ischemia-reperfusion injury in mice via inducing antioxidant response and inhibiting apoptosis and autophagy," *Acta Pharmacologica Sinica*, vol. 38, no. 5, pp. 672–687, 2017.

[6] W. Wang, L. Wu, J. Li et al., "Alleviation of hepatic ischemia reperfusion injury by oleanolic acid pretreating via reducing HMGB1 release and inhibiting apoptosis and autophagy," *Mediators of Inflammation*, vol. 2019, Article ID 3240713, 10 pages, 2019.

[7] K. McKeage and G. M. Keating, "Fenofibrate," *Drugs*, vol. 71, no. 14, pp. 1917–1946, 2011.

[8] I. Issemann and S. Green, "Activation of a member of the steroid hormone receptor superfamily by peroxisome proliferators," *Nature*, vol. 347, no. 6294, pp. 645–650, 1990.

[9] T. Morinishi, Y. Tokuhara, H. Ohsaki, E. Ibuki, K. Kadota, and E. Hirakawa, "Activation and expression of peroxisome proliferator-activated receptor alpha are associated with tumorigenesis in colorectal carcinoma," *PPAR Research*, vol. 2019, Article ID 7486727, 9 pages, 2019.

[10] C. Zhang, Y.-W. Liu, Z. Chi, and B. Chen, "Ligand-activated peroxisome proliferator-activated receptor β/δ facilitates cell proliferation in human cholesteatoma keratinocytes," *PPAR Research*, vol. 2020, Article ID 8864813, 9 pages, 2020.

[11] I. A. Bukhari, A. A. Almotrefi, O. Y. Mohamed, A. A. Al-Masri, and S. A. Sheikh, "Protective effect of fenofibrate against ischemia-/reperfusion-induced cardiac arrhythmias in isolated rat hearts," *Fundamental & Clinical Pharmacology*, vol. 32, no. 2, pp. 141–146, 2018.

[12] N. S. Patel, R. di Paola, E. Mazzon, D. Britti, C. Thiemermann, and S. Cuzzocrea, "Peroxisome proliferator-activated Receptor-α contributes to the resolution of inflammation after renal ischemia/reperfusion injury," *Journal of Pharmacology and Experimental Therapeutics*, vol. 328, no. 2, pp. 635–643, 2009.

[13] P. Losey, E. Ladds, M. Laprais et al., "The role of PPAR activation during the systemic response to brain injury," *Journal of Neuroinflammation*, vol. 12, no. 1, 2015.

[14] Q. Zhao, Z. Cui, Y. Zheng et al., "Fenofibrate protects against acute myocardial I/R injury in rat by suppressing mitochondrial apoptosis as decreasing cleaved caspase-9

activation," *Cancer Biomarkers*, vol. 19, no. 4, pp. 455–463, 2017.

[15] D. Qi and L. H. Young, "AMPK: energy sensor and survival mechanism in the ischemic heart," *Trends in Endocrinology and Metabolism*, vol. 26, no. 8, pp. 422–429, 2015.

[16] C. O. Souza, A. A. S. Teixeira, L. A. Biondo et al., "Palmitoleic acid reduces high fat diet-induced liver inflammation by promoting PPAR-γ-independent M2a polarization of myeloid cells," *Biochimica et Biophysica Acta Molecular and Cell Biology of Lipids*, vol. 1865, no. 10, article 158776, 2020.

[17] M. Sohn, K. Kim, M. J. Uddin et al., "Delayed treatment with fenofibrate protects against high-fat diet-induced kidney injury in mice: the possible role of AMPK autophagy," *American Journal of Physiology Renal Physiology*, vol. 312, no. 2, pp. F323–F334, 2017.

[18] A. Tomizawa, Y. Hattori, T. Inoue, S. Hattori, and K. Kasai, "Fenofibrate suppresses microvascular inflammation and apoptosis through adenosine monophosphate-activated protein kinase activation," *Metabolism*, vol. 60, no. 4, pp. 513–522, 2011.

[19] J. Ji, L. Wu, J. Feng et al., "Cafestol preconditioning attenuates apoptosis and autophagy during hepatic ischemia-reperfusion injury by inhibiting ERK/PPARγ pathway," *International Immunopharmacology*, vol. 84, article 106529, 2020.

[20] S. K. Chun, S. Lee, J. Flores-Toro et al., "Loss of sirtuin 1 and mitofusin 2 contributes to enhanced ischemia/reperfusion injury in aged livers," *Aging Cell*, vol. 17, no. 4, article e12761, 2018.

[21] N. Bougarne, B. Weyers, S. J. Desmet et al., "Molecular actions of PPARα in lipid metabolism and inflammation," *Endocrine Reviews*, vol. 39, no. 5, pp. 760–802, 2018.

[22] D. I. Mohamed, A. A. M. Elmelegy, L. F. A. El-Aziz, H. S. Abdel Kawy, A. A. A. El-Samad, and O. A. El-Kharashi, "Fenofibrate A peroxisome proliferator activated receptor-α agonist treatment ameliorates Concanavalin A-induced hepatitis in rats," *European Journal of Pharmacology*, vol. 721, no. 1-3, pp. 35–42, 2013.

[23] A. Rajamoorthi, N. Arias, J. Basta, R. G. Lee, and Á. Baldán, "Amelioration of diet-induced steatohepatitis in mice following combined therapy with ASO-Fsp27 and fenofibrate," *Journal of Lipid Research*, vol. 58, no. 11, pp. 2127–2138, 2017.

[24] M. Ni, H. Fu, F. Huang et al., "Vagus nerve attenuates hepatocyte apoptosis upon ischemia-reperfusion via α7 nicotinic acetylcholine receptor on Kupffer cells in mice," *Anesthesiology*, vol. 125, no. 5, pp. 1005–1016, 2016.

[25] S. Xiang, K. Chen, L. Xu, T. Wang, and C. Guo, "Bergenin Exerts Hepatoprotective effects by inhibiting the release of inflammatory factors, apoptosis and autophagy via the PPAR-γ pathway," *Drug Design Development and Therapy*, vol. Volume 14, pp. 129–143, 2020.

[26] W. A. Siddiqui, A. Ahad, and H. Ahsan, "The mystery of BCL2 family: Bcl-2 proteins and apoptosis: an update," *Archives of Toxicology*, vol. 89, no. 3, pp. 289–317, 2015.

[27] A. M. Zaki, D. M. El-Tanbouly, R. M. Abdelsalam, and H. F. Zaki, "Plumbagin ameliorates hepatic ischemia-reperfusion injury in rats: role of high mobility group box 1 in inflammation, oxidative stress and apoptosis," *Biomedicine & Pharmacotherapy*, vol. 106, pp. 785–793, 2018.

[28] A. Peña-Blanco and A. J. García-Sáez, "Bax, Bak and beyond — mitochondrial performance in apoptosis," *FEBS Journal*, vol. 285, no. 3, pp. 416–431, 2017.

[29] H. Flores-Romero and A. J. García-Sáez, "The incomplete puzzle of the BCL2 proteins," *Cells*, vol. 8, no. 10, article 1176, 2019.

[30] K. Wang, "Autophagy and apoptosis in liver injury," *Cell Cycle*, vol. 14, no. 11, pp. 1631–1642, 2015.

[31] N. Tilija Pun and P.-H. Park, "Adiponectin inhibits inflammatory cytokines production by Beclin-1 phosphorylation and B-cell lymphoma 2 mRNA destabilization: role for autophagy induction," *British Journal of Pharmacology*, vol. 175, no. 7, pp. 1066–1084, 2018.

[32] M. Antonioli, M. Di Rienzo, M. Piacentini, and G. M. Fimia, "Emerging mechanisms in initiating and terminating autophagy," *Trends in Biochemical Sciences*, vol. 42, no. 1, pp. 28–41, 2017.

[33] S. M. Hill, L. Wrobel, and D. C. Rubinsztein, "Post-translational modifications of Beclin 1 provide multiple strategies for autophagy regulation," *Cell Death & Differentiation*, vol. 26, no. 4, pp. 617–629, 2019.

[34] Y. Xia, J. Li, K. Chen, J. Feng, and C. Guo, "Bergenin attenuates hepatic fibrosis by regulating autophagy mediated by the PPAR-γ/TGF-β pathway," *PPAR Research*, vol. 2020, Article ID 6694214, 13 pages, 2020.

[35] A. Caccamo, E. Ferreira, C. Branca, and S. Oddo, "Retracted article: p62 improves AD-like pathology by increasing autophagy," *Molecular Psychiatry*, vol. 22, no. 6, pp. 865–873, 2017.

[36] S. Kersten, "Integrated physiology and systems biology of PPARα," *Molecular Metabolism*, vol. 3, no. 4, pp. 354–371, 2014.

[37] J. Li, C. Guo, and J. Wu, "Astaxanthin in liver health and disease: a potential therapeutic agent," *Drug Design, Development and Therapy*, vol. Volume 14, pp. 2275–2285, 2020.

[38] M. Pawlak, P. Lefebvre, and B. Staels, "Molecular mechanism of PPARα action and its impact on lipid metabolism, inflammation and fibrosis in non-alcoholic fatty liver disease," *Journal of Hepatology*, vol. 62, no. 3, pp. 720–733, 2015.

[39] O. Y. Kytikova, J. M. Perelman, T. P. Novgorodtseva et al., "Peroxisome proliferator-activated receptors as a therapeutic target in asthma," *PPAR Research*, vol. 2020, Article ID 8906968, 2020.

[40] L. J. Holm, M. Ø. Mønsted, M. Haupt-Jorgensen, and K. Buschard, "PPARs and the development of type 1 diabetes," *PPAR Research*, vol. 2020, Article ID 6198628, 11 pages, 2020.

[41] J. Zúñiga, M. Cancino, F. Medina et al., "N-3 PUFA supplementation triggers PPAR-α activation and PPAR-α/NF-κB interaction: anti-inflammatory implications in liver ischemia-reperfusion injury," *PLoS One*, vol. 6, no. 12, article e28502, 2011.

[42] Y. Li, Z. Xiong, W. Yan et al., "Branched chain amino acids exacerbate myocardial ischemia/reperfusion vulnerability via enhancing GCN2/ATF6/PPAR-α pathway-dependent fatty acid oxidation," *Theranostics*, vol. 10, no. 12, pp. 5623–5640, 2020.

[43] Z. Zeng, Q. Huang, Z. Shu et al., "Effects of short-chain acyl-CoA dehydrogenase on cardiomyocyte apoptosis," *Journal of Cellular and Molecular Medicine*, vol. 20, no. 7, pp. 1381–1391, 2016.

[44] W. R. Wang, E. Q. Liu, J. Y. Zhang et al., "Activation of PPAR alpha by fenofibrate inhibits apoptosis in vascular adventitial fibroblasts partly through SIRT1-mediated deacetylation of FoxO1," *Experimental Cell Research*, vol. 338, no. 1, pp. 54–63, 2015.

[45] M. Jiao, F. Ren, L. Zhou et al., "Peroxisome proliferator-activated receptor α activation attenuates the inflammatory response to protect the liver from acute failure by promoting the autophagy pathway," *Cell Death & Disease*, vol. 5, no. 8, article e1397, 2014.

[46] T. S. Kim, Y. B. Jin, Y. S. Kim et al., "SIRT3 promotes antimycobacterial defenses by coordinating mitochondrial and autophagic functions," *Autophagy*, vol. 15, no. 8, pp. 1356–1375, 2019.

[47] R. C. Rabinovitch, B. Samborska, B. Faubert et al., "AMPK maintains cellular metabolic homeostasis through regulation of mitochondrial reactive oxygen species," *Cell Reports*, vol. 21, no. 1, pp. 1–9, 2017.

[48] B. Viollet, B. Guigas, J. Leclerc et al., "AMP-activated protein kinase in the regulation of hepatic energy metabolism: from physiology to therapeutic perspectives," *Acta Physiologica*, vol. 196, no. 1, pp. 81–98, 2009.

[49] K. Dong, M. Wu, X. Liu et al., "Glutaredoxins concomitant with optimal ROS activate AMPK through S-glutathionylation to improve glucose metabolism in type 2 diabetes," *Free Radical Biology & Medicine*, vol. 101, pp. 334–347, 2016.

[50] R. Mo, R. Lai, J. Lu et al., "Enhanced autophagy contributes to protective effects of IL-22 against acetaminophen-induced liver injury," *Theranostics*, vol. 8, no. 15, pp. 4170–4180, 2018.

[51] T. Zhou, L. Chang, Y. Luo, Y. Zhou, and J. Zhang, "Mst1 inhibition attenuates non-alcoholic fatty liver disease via reversing Parkin-related mitophagy," *Redox Biology*, vol. 21, article 101120, 2019.

[52] Y. M. Liu, J. H. Ma, Q. L. Zeng et al., "MiR-19a affects hepatocyte autophagy via regulating lncRNA NBR2 and AMPK/PPARα in D-GalN/lipopolysaccharide-stimulated hepatocytes," *Journal of Celularl Biochemistry*, vol. 119, no. 1, pp. 358–365, 2018.

[53] X. Yang, Y. Liu, M. Li et al., "Predictive and preventive significance of AMPK activation on hepatocarcinogenesis in patients with liver cirrhosis," *Cell Death & Disease*, vol. 9, no. 3, article 264, 2018.

[54] S. Padrissa-Altes, M. A. Zaouali, R. Bartrons, and J. Rosello-Catafau, "Ubiquitin-proteasome system inhibitors and AMPK regulation in hepatic cold ischaemia and reperfusion injury: possible mechanisms," *Clinical Science*, vol. 123, no. 2, pp. 93–98, 2012.

[55] B.-P. Huang, C.-H. Lin, H.-M. Chen, J.-T. Lin, Y.-F. Cheng, and S.-H. Kao, "AMPK activation inhibits expression of proinflammatory mediators through downregulation of PI3K/p 38 MAPK and NF-κB signaling in murine macrophages," *DNA and Cell Biology*, vol. 34, no. 2, pp. 133–141, 2015.

[56] M. S. Joo, W. D. Kim, K. Y. Lee, J. H. Kim, J. H. Koo, and S. G. Kim, "AMPK facilitates nuclear accumulation of Nrf2 by phosphorylating at serine 550," *Molecular and Cellular Biology*, vol. 36, no. 14, pp. 1931–1942, 2016.

[57] Z. Yi, M. Deng, M. J. Scott et al., "Immune-Responsive Gene 1/Itaconate Activates Nuclear Factor Erythroid 2–Related Factor 2 in Hepatocytes to Protect Against Liver Ischemia–Reperfusion Injury," *Hepatology*, vol. 72, no. 4, pp. 1394–1411, 2020.

[58] Q. Zhang, Y. Lai, J. Deng et al., "Vagus nerve stimulation attenuates hepatic ischemia/reperfusion injury via the Nrf2/HO-1 pathway," *Oxidative Medicine and Cellular Longevity*, vol. 2019, Article ID 9549506, 10 pages, 2019.

[59] M. Ge, W. Yao, D. Yuan et al., "Brg1-mediated Nrf2/HO-1 pathway activation alleviates hepatic ischemia- reperfusion injury," *Cell Death & Disease*, vol. 8, no. 6, article e2841, 2017.

[60] J. Zhang, S. D. Zhang, P. Wang et al., "Pinolenic acid ameliorates oleic acid-induced lipogenesis and oxidative stress _via_ AMPK/SIRT1 signaling pathway in HepG2 cells," *European Journal of Pharmacology*, vol. 861, article 172618, 10 pages, 2019.

[61] F. Wen, C. An, X. Wu et al., "MiR-34a regulates mitochondrial content and fat ectopic deposition induced by resistin through the AMPK/PPARα pathway in HepG2 cells," *International Journal of Biochemistry & Cell Biology*, vol. 94, pp. 133–145, 2018.

[62] Y. Kim and C. W. Park, "Mechanisms of adiponectin action: implication of adiponectin receptor agonism in diabetic kidney disease," *International Journal of Molecular Sciences*, vol. 20, no. 7, article 1782, 2019.

[63] Y. Zhao, Y. Liu, Z. Jing et al., "N-oleoylethanolamide suppresses intimal hyperplasia after balloon injury in rats through AMPK/PPARα pathway," *Biochemical and Biophysical Researh Communications*, vol. 496, no. 2, pp. 415–421, 2018.

Hindawi
PPAR Research
Volume 2021, Article ID 6651839, 15 pages
https://doi.org/10.1155/2021/6651839

Research Article

Apigenin Alleviates Liver Fibrosis by Inhibiting Hepatic Stellate Cell Activation and Autophagy via TGF-β1/Smad3 and p38/PPARα Pathways

Jie Ji, Qiang Yu, Weiqi Dai, Liwei Wu, Jiao Feng, Yuanyuan Zheng, Yan Li, and Chuanyong Guo

Department of Gastroenterology, Shanghai Tenth People's Hospital, Tongji University School of Medicine, Shanghai 200072, China

Correspondence should be addressed to Chuanyong Guo; guochuanyong@hotmail.com

Received 31 October 2020; Revised 10 January 2021; Accepted 15 January 2021; Published 28 January 2021

Academic Editor: Sainan Li

Objective. The aim of this study is to confirm the hepatocellular protective functions of apigenin and the molecular mechanism on liver fibrosis in mice. *Methods*. Carbon tetrachloride (CCl_4) and bile duct ligature (BDL) mouse fibrosis models were used to investigate the effects of apigenin on liver fibrosis. Sixty-six male C57 mice were randomly divided into eight groups, including the vehicle group, CCl_4 group, CCl_4+L-apigenin (20 mg/kg) group, CCl_4+H-apigenin (40 mg/kg) group, sham group, BDL group, BDL+L-apigenin(20 mg/kg) group, and BDL+H-apigenin(40 mg/kg) group. Serum liver enzymes (ALT and AST), proteins associated with autophagy, and indicators linked with the TGF-β1/Smad3 and p38/PPARα pathways were detected using qRT-PCR, immunohistochemical staining, and western blotting. *Results*. Our findings confirmed that apigenin could decrease the levels of ALT and AST, suppress the generation of ECM, inhibit the activation of HSCs, regulate the balance of MMP2 and TIMP1, reduce the expression of autophagy-linked protein, and restrain the TGF-β1/Smad3 and p38/PPARα pathways. *Conclusion*. Apigenin could alleviate liver fibrosis by inhibiting hepatic stellate cell activation and autophagy via TGF-β1/Smad3 and p38/PPARα pathways.

1. Introduction

Liver fibrosis is a chronic pathological change caused by a variety of reasons, such as chronic infection by hepatotropic viruses, excess alcohol consumption, nonalcoholic fatty liver disease, autoimmune liver diseases, and hereditary disease, and is a necessary stage for the development of many liver diseases to liver cirrhosis and even liver cancer [1, 2]. Liver fibrosis is a wound healing response characterized by excessive deposition of extracellular matrix (ECM). The possible treatments for liver fibrosis including curing the primary disease, reducing inflammation and immune response, inhibiting stellate cell activation, and increasing the degradation of scar matrix had been generally accepted [3, 4]. Although liver transplantation is the most efficient therapy, there are great limitations because of huge cost of treatment and shortage of liver donor available for transplantation [1, 5, 6]. Therefore, revealing the molecular mechanism of liver fibrosis and finding key drug targets are an important issue that needs to be solved urgently.

The progression of fibrosis is a complex process which involves nonparenchymal hepatocytes, parenchymal hepatocytes, and infiltrating immune cells. The activation of inflammation mediators and profibrotic genes caused by cell death in both nonparenchymal and infiltrating immune cells thereby trigger the fibrosis process. Hepatic stellate cells (HSCs) are the most powerful fibrogenic effector cells and are also considered as the initial process during liver fibrosis [4, 7–10]. The activation of HSCs by several cellular events including immune/inflammatory injury as well as molecular regulation especially transforming growth factor-β1 (TGF-β1) will contribute to the excessive accumulation of ECM which promotes liver fibrosis [11]. It had been reported that suppressing the activation HSCs and expression of TGF-β1 could reduce the levels of myofibroblast markers, increase the ratio of MMPs/TIMPs, and decrease Smad2/Smad3

associated collagen production which further attenuated liver fibrosis [11–15].

Autophagy is a self-selective mode of cell death, which can remove necrotic cells to maintain organ homeostasis [12]. Results have shown that autophagy could provide energy for the activation of HSCs by stimulating the metabolism of lipid droplets [16]. At the same time, many literatures have confirmed that inhibiting the autophagy of HSCs can play a positive role in liver protection [17–20]. So, inhibition of autophagy which could significantly reduce activation of HSCs can attenuate liver fibrosis [21, 22].

Apigenin is a kind of dietary flavonoid extracted mainly from celery, parsley, thyme, chamomile, and onions [23]. Recently, apigenin has reported many pharmacological effects including anticancer [24–28], anti-inflammation [29–32], antifibrosis [33–36], and so on. Zhang et al. confirmed apigenin could downregulate the miR34a expression to suppress mouse peritoneal fibrosis [35]. Jiao et al. demonstrated that apigenin could inhibit fibroblast proliferation and reduce epidural fibrosis by suppressing the Wnt3a/β-catenin signaling pathway [34]. However, whether apigenin has the antihepatic fibrosis effect and the specific molecular mechanism of this effect are still unclear and need to be explored.

Carbon tetrachloride (CCl_4) and bile duct ligature (BDL) mouse models are extremely practical models to investigate the underlying molecular mechanisms of liver fibrosis, which have been widely applied to the establishment of liver fibrosis [15, 37]. Therefore, this study is aimed at exploring the antihepatic fibrosis effect and the specific molecular mechanism of apigenin using the CCl_4 and BDL models. We hypothesized that apigenin could alleviate liver fibrosis by inhibiting hepatic stellate cell activation and autophagy via TGF-β1/Smad3 and p38 MAPK/PPARα pathways.

2. Materials and Methods

2.1. Drugs and Reagents. Apigenin (HPLC ≥ 98% CAS:520-36-5) was purchased from Shanghai Yuanye Bio-Technology Co., Ltd. (Shanghai, China). When used, it is dissolved into dimethyl sulfoxide (DMSO) at 2 mg/ml and 4 mg/ml concentrations. Carbon tetrachloride (CCl_4) was purchased from China Sinopharm International Corporation (Shanghai, China). Alanine aminotransferase (ALT) and aspartate aminotransferase (AST) were tested by microplate test kits purchased from Nanjing Jiancheng Bioengineering Institute (Nanjing, China). Quantitative real-time (qRT) PCR kits were purchased from TaKaRa (Dalian, China). The primers were obtained from Generay (Shanghai, China). Detailed information of the primary antibodies used in this study are listed in Table 1. Dulbecco's Modified Eagle Medium (DMEM) and foetal bovine serum (FBS) were purchased from HyClone (GE Healthcare). Apigenin was dissolved in DMSO (<0.1% [*v*/*v*]) for in vitro treatment.

2.2. Cell Culture and CCK8 Assay. The human immortal LX2 cell line was cultured in high glucose DMEM with 10% FBS, 100 U/mL of penicillin, and 100 g/mL of streptomycin. The apparent logarithmic phase cells were seeded in 96-well plates for 48 hours, then apigenin was added at concentrations of 10, 20, 30, 40, 50, 60, 70, or 80 μM for 24 hours, and the cytotoxicity analysis was performed. Cell viability was then measured with the CCK8 assay according to the manufacturer's protocol. All the experiments were performed in triplicate.

Table 1: The primary antibodies used for western blotting and immunohistochemistry in the study.

Antibody	Species	Targeted species	Supplier	Catalogue number
β-Actin	M	H, M, R	CST	3700
IL-1β	Rbt	M	CST	12507
α-SMA	M	H, M, R	Abcam	ab7817
Collagen 1	Rbt	H, M, R	Abcam	ab34710
MMP2	Rbt	H, M, R	PT	10373-2-AP
TIMP1	Rbt	H, M, R	PT	10753-1-AP
p62	Rbt	H, M, R	PT	55274-1-AP
LC3	Rbt	H, M, R	PT	14600-1-AP
Beclin-1	Rbt	H, M, R	PT	11306-1-AP
TGF-β1	Rbt	H, M, R	PT	21898-1-AP
Smad3	Rbt	H, M, R	Abcam	ab40854
p-Smad3	Rbt	H, M	Abcam	ab52903
p38 MAPK	Rbt	H, M, R	Zenbio	200782
p-p38 MAPK	Rbt	H, M, R	CST	4511
PPARα	Rbt	H, M, R	PT	15540-1-AP

Abbreviations: H: human; M: mouse; Rbt: rabbit; R: rat; CST: Cell Signaling Technology (Danvers, MA, USA); PT: Proteintech (Chicago, IL, USA).

2.3. BrdU Assay. Proliferation of the cells was evaluated using the BrdU Cell Proliferation ELISA Kit (ab126556, Abcam, Cambridge, MA) according to the manufacturer's instruction. Briefly, cells were cultured in 96-well plates and exposed to apigenin (20, 40, and 60 μM) for 24 hours. Subsequently, 10 μM BrdU was added to each well, and samples were incubated for 12 h at 37°C. BrdU signaling was determined by measuring the absorbance at 450 nm.

2.4. Animals. 66 six-week-old male C57 mice (22-26 g) were obtained from Shanghai SLAC Laboratory Animal (Shanghai, China) and housed in a standard animal laboratory with free access to food and water. All experimental procedures involving mice were approved by the Animal Care and Use Committee of Shanghai Tongji University. Handling and care of mice conformed to the National Institutes of Health Guidelines.

2.5. Establishment of Mouse Liver Fibrosis Models. We established two different mouse liver fibrosis models. To create the CCl_4-induced liver fibrosis model, mice were injected with 10% CCl4 (1.0 mL/kg, diluted in peanut oil) intraperitoneally three times a week for 8 weeks. In the bile duct ligation-(BDL-) induced liver fibrosis model, all mice were fasted for 12 h and anesthetized intraperitoneally by 1.25% pentobarbital sodium salt (40 mg/kg). After opening the abdomen via

Table 2: Oligonucleotide sequences of primers used for qRT-PCR.

Gene name	Forward (5′-3′)	Reverse (5′-3′)
β-Actin	GTGACGTTGACATCCGTAAAGA	GCCGGACTCATCGTACTCC
IL-1β	GAAATGCCACCTTTTGACAGTG	TGGATGCTCTCATCAGGACAG
Collagen 1	CAATGGCACGGCTGTGTGCG	AGCACTCGCCCTCCCGTCTT
α-SMA	CCCAGACATCAGGGAGTAATGG	TCTATCGGATACTTCAGCGTCA
MMP2	GGACAAGTGGTCCGCGTAAA	CCGACCGTTGAACAGGAAGG
TIMP1	CGAGACCACCTTATACCAGCG	ATGACTGGGGTGTAGGCGTA
p62	GAGGCACCCCGAAACATGG	ACTTATAGCGAGTTCCCACCA
LC3	TTATAGAGCGATACAAGGGGGAG	CGCCGTCTGATTATCTTGATGAG
Beclin-1	ATGGAGGGGTCTAAGGCGTC	TGGGCTGTGGTAAGTAATGGA
TGF-β1	CCACCTGCAAGACCATCGAC	CTGGCGAGCCTTAGTTTGGAC
PPARα	AACATCGAGTGTCGAATATGTGG	CCGAATAGTTCGCCGAAAGAA

Abbreviation: qRT-PCR: quantitative real-time PCR.

the linea alba, the bile duct was exposed and isolated over a certain length. Two surgical knots were tied in the isolated bile duct, which was then cut between the knots. The abdomen was then closed.

2.6. Experimental Design

2.6.1. Preliminary Study. In order to verify whether the apigenin dose (20 mg/kg and 40 mg/kg) could cause damage to the structure and function of the liver and other internal organs, we designed a preliminary experiment. The eighteen mice were randomly divided into the following 3 groups.

(1) Normal control (NC) ($n = 6$): no treatment

(2) Vehicle group ($n = 6$): mice were injected intraperitoneally with DMSO three times a week

(3) API (40 mg/kg) group ($n = 6$): apigenin (40 mg/kg) was given to mice by intragastric administration three times a week.

2.6.2. Formal Experiment. In the CCl_4-induced liver fibrosis model, 24 mice were randomly divided into the following 4 groups.

(1) Vehicle group ($n = 6$): mice were injected intraperitoneally with DMSO three times a week for 8 weeks

(2) CCl_4 group ($n = 6$): mice were injected with CCl_4 intraperitoneally three times a week for 8 weeks

(3) CCl_4+L-API group ($n = 6$): mice were injected with CCl_4 intraperitoneally and gavaged with 20 mg/kg apigenin three times a week for 8 weeks

(4) CCl_4+H-API group ($n = 6$): mice were injected with CCl_4 intraperitoneally and gavaged with 40 mg/kg apigenin three times a week for 8 weeks

In the BDL-induced liver fibrosis model, 24 mice were randomly divided into the following 4 groups.

(1) Sham group ($n = 6$): all mice underwent laparotomy without BDL

(2) BDL group ($n = 6$): all mice underwent BDL surgery

(3) BDL+L-API group ($n = 6$): all mice were gavaged with 20 mg/kg apigenin once a day for 14 days after BDL

(4) BDL+H-API group ($n = 6$): all mice were gavaged with 40 mg/kg apigenin once a day for 14 days after BDL

Vehicle and sham groups were used as controls in both models. At the end of the experiment, blood samples and liver tissues were collected with diethyl ether anesthesia. Serum was acquired by centrifugation (4,500 rpm, 4°C, 10 min) and kept at −80°C. Liver tissues were stored at −80°C.

2.7. Serum Biochemical Analysis. The blood sample collected from the mouse orbit was placed at 4°C for 5 hours. And then, the serum sample was separated from the blood by centrifuging at 4,600 × g at 4°C for 10 minutes. Serum levels of ALT and AST were detected by microplate test kits.

2.8. Histopathology. A part of the fresh left liver lobe was excised and then fixed in 4% paraformaldehyde for 24 h. The tissues were dehydrated with ethanol and embedded in paraffin. Next, the liver tissues were cut into 3 μm thick sections and stained with hematoxylin and eosin (H&E) to determine the severity of injury.

2.9. Reverse Transcription PCR (RT-PCR) and Quantitative Real-Time PCR (qRT-PCR). The total RNA was extracted from 100 mg liver tissue by TRIzol (Thermo Fisher Scientific, Waltham, MA, USA). Then, the purified RNA was reverse-transcribed into cDNA. The levels of mRNA were determined by SYBR Premix EX Taq through a 7900HT fast PCR system (Applied Biosystems, Foster City, CA, USA). The primers used for qRT-PCR are listed in Table 2.

2.10. Immunohistochemistry (IHC). Paraffin sections were baked in a 60°C oven for 1 hour and then dewaxed and

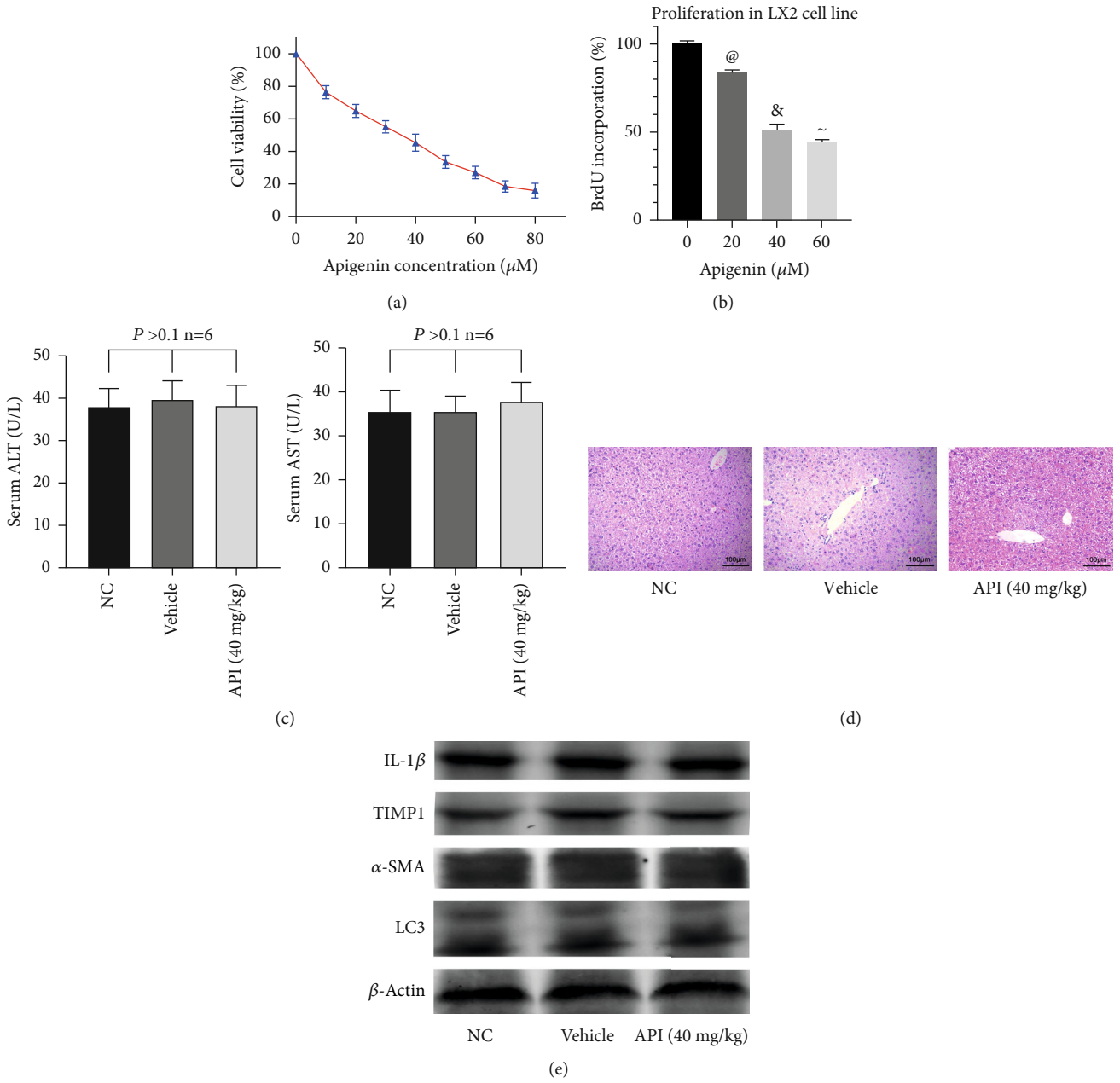

Figure 1: Effects of apigenin on liver and LX2 cells. Notes: (a) the CCK8 assay was used to determine the effects of apigenin on the viability of LX2 cells. (b) Cells were treated with the indicated concentrations of apigenin for 24 hours, and the degree of apigenin to inhibit cell proliferation was measured using BrdU Cell Proliferation ELISA Kit ($^{@}P < 0.05$ for 20 μM apigenin vs. 0 μM apigenin; $^{\&}P < 0.05$ for 40 μM apigenin vs. 20 μM apigenin; $^{\sim}P < 0.05$ for 60 μM apigenin vs. 40 μM apigenin). (c) The levels of serum ALT and AST are presented as mean ± SD. One-way ANOVA indicated that there was no significant difference among the three groups ($n = 6$; $P > 0.1$). (d) Representative H&E-stained hepatic sections were examined under light microscopy and imaged at a 200x magnification. (e) Western blot analysis of IL-1β, TIMP1, α-SMA, and LC3 protein levels.

rehydrated. Antigen was placed into a citrate buffer, which was then heated to 95°C for 10 minutes and cooled to room temperature. Next, the sections were covered in 3% hydrogen peroxide for 20 minutes to block endogenous peroxidase activity, and then 5% BSA was added to block nonspecific binding for 15 minutes (both at room temperature). Slices were then incubated overnight at 4°C with the following antibodies: anti-IL-1β, anti-α-SMA, anti-Col, anti-LC3, anti-Beclin-1, anti-p62-, anti-TGF-β1-, anti-p-Smad3-, anti-p-38-, and anti-PPARα (all 1 : 200). Then, the primary antibodies in the liver sections were incubated with secondary antibodies using a diaminobenzidine (DAB) kit. Final evaluations were performed with Image-Pro Plus software 6.0 to calculate the mean of integrated optical densities (MIOD = sum IOD/sum area) of the positive staining area.

2.11. Western Blotting. Firstly, liver tissues were ground (100 mg) into powder in liquid nitrogen, and then the

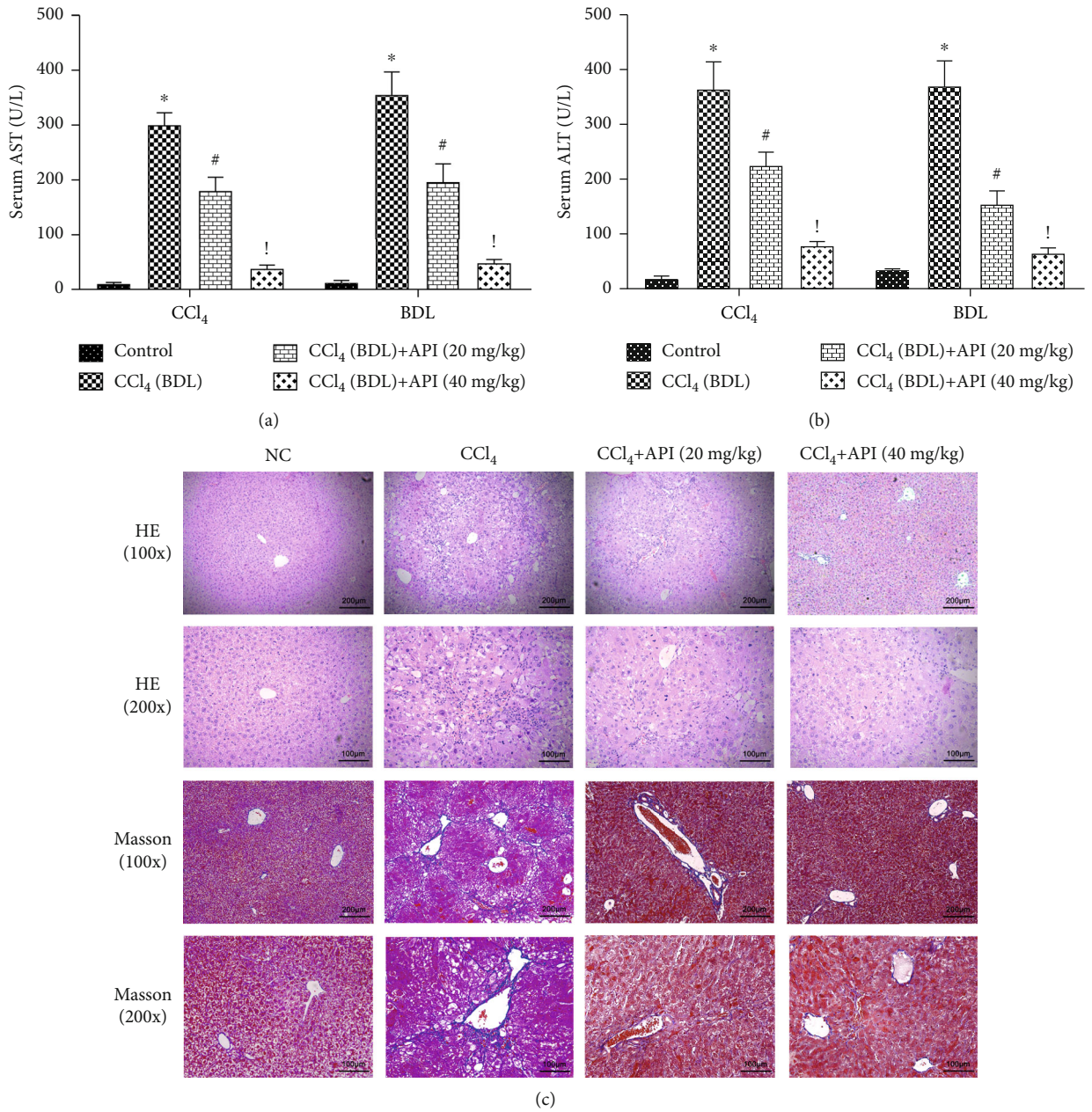

Figure 2: Continued.

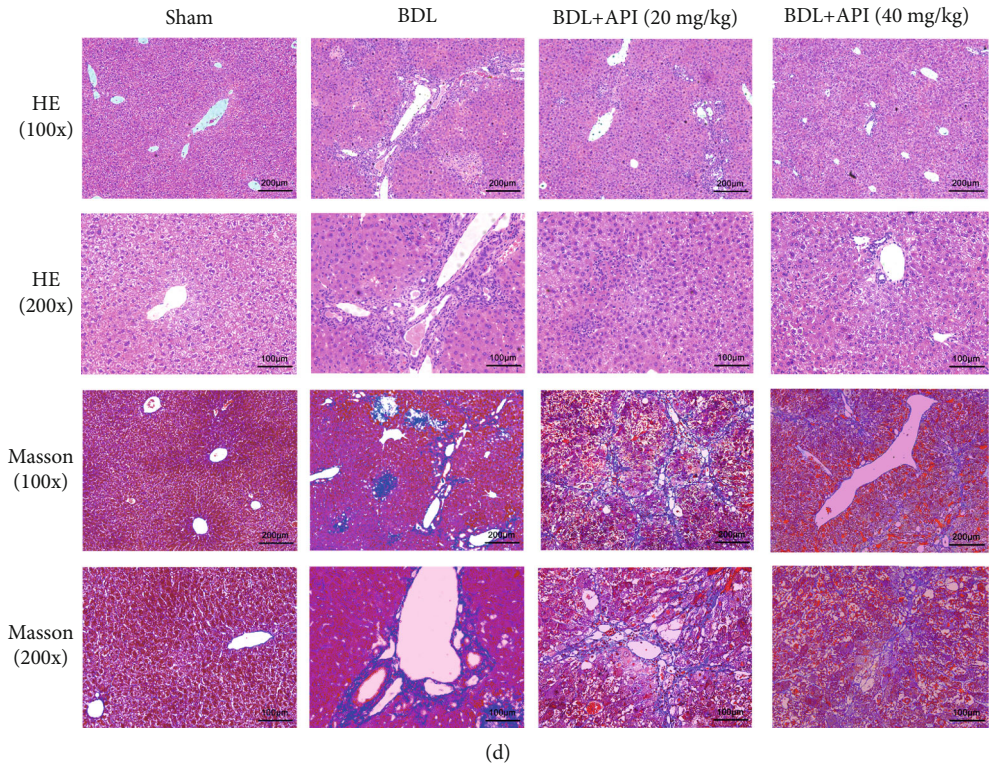

(d)

Figure 2: Apigenin protects the liver against fibrosis induced by CCl_4 and BDL in mice. Notes: (a, b) the levels of serum ALT and AST are presented as mean ± SD ($n = 6$; $^*P < 0.05$ for CCl_4 (BDL) group vs. control group; $^{\#}P < 0.05$ for CCl_4 (BDL)+apigenin (20 mg/kg) group vs. CCl_4 (BDL) group; $^{!}P < 0.05$ for CCl_4 (BDL)+apigenin (40 mg/kg) group vs. CCl_4 (BDL)+apigenin (20 mg/kg) group). (c, d) Representative H&E- and Masson-stained hepatic sections were examined under light microscopy and imaged at 200x and 100x magnifications.

powder was homogenized in RIPA lysis containing phenylmethanesulfonyl fluoride (PMSF) and protease inhibitors (PI). The protein concentrations were detected using the bicinchoninic acid method before being mixed with a 6x loading buffer and boiled at 100°C for 10 minutes. Secondly, protein samples were electrophoresed by 10% or 12.5% SDS-PAGE and transferred onto polyvinylidene fluoride or nitrocellulose membranes. Next, membranes were blocked with 5% skimmed milk for at least 1 hour and subsequently incubated overnight at 4°C with the primary antibodies (Table 1). Thirdly, the membranes were incubated with anti-rabbit or anti-mouse secondary antibodies after washing thrice with PBST (1% Tween diluted in PBS). Finally, the expression of protein was measured by an Odyssey two-color infrared laser imaging system (LI-COR Biosciences, Lincoln, NE, USA).

2.12. Statistical Analysis. Experimental data which was repeated at least three times was presented as mean ± SD ($n = 6$; $^*P < 0.05$ for CCl_4 (BDL) vs. control; $^{\#}P < 0.05$ for CCl_4 (BDL)+API (20 mg/kg) vs. CCl_4 (BDL); $^{+}P < 0.05$ for CCl_4 (BDL)+API (40 mg/kg) vs. CCl_4 (BDL); $^{!}P < 0.05$ for CCl_4 (BDL)+API (40 mg/kg) vs. CCl_4 (BDL)+API(20 mg/kg)). One-way ANOVA using the Student–Newman–Keuls method was used to compare statistical differences among three or four groups using SPSS version 20.0 software (IBM, Armonk, NY, USA). $P < 0.05$ was regarded as statistically significant.

3. Result

3.1. Effects of Apigenin on Liver and LX2 Cells. The human immortal HSC cell line (LX2 cells) was used in this study to investigate the effect of apigenin on HSCs. The CCK8 assay was used to measure the toxicity of apigenin in LX2 cells (Figure 1(a)). Apigenin decreased the viability of LX2 cells in a dose-dependent manner, and the half-maximal inhibitory concentration (IC50) was 28.80 μM. At the same time, the BrdU incorporation assay was performed to explore the effect of apigenin on cell proliferation. As shown in Figure 1(b), apigenin could reduce the proportion of proliferating cells in a dose-dependent manner. Besides, in the preliminary experiment, 12 mice were injected with vehicle (DMSO) or gavaged with 40 mg/kg apigenin to explore security of drug and solvent used in this study. As shown in Figure 1(c), there was no hepatocellular injury or structural damage compared with the NC group. The results of ALT, AST, and western blotting shown in Figures 1(b) and 1(d) could also verify no statistically significant differences between the vehicle, apigenin, and NC groups. So, we got the conclusion that the apigenin could inhibit proliferation and decrease the viability of LX2 cells, but has no harmful effects on the liver tissues.

3.2. Apigenin Protects the Liver against Fibrosis Induced by CCl_4 and BDL in Mice. The levels of serum ALT and AST are important indicators of liver parenchymal damage. So,

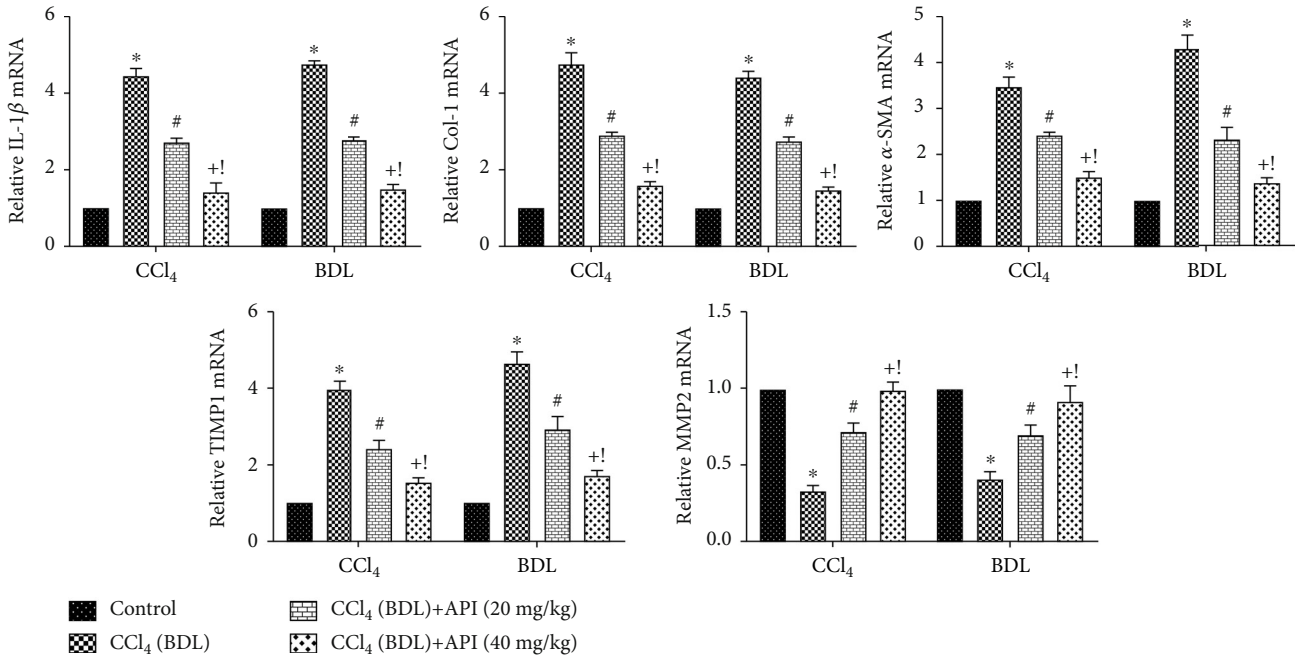

(a)

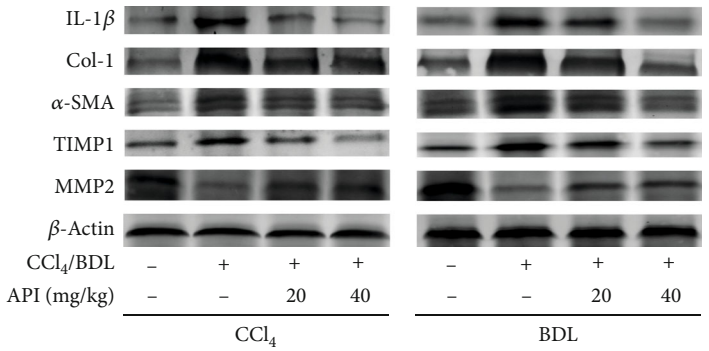

(b)

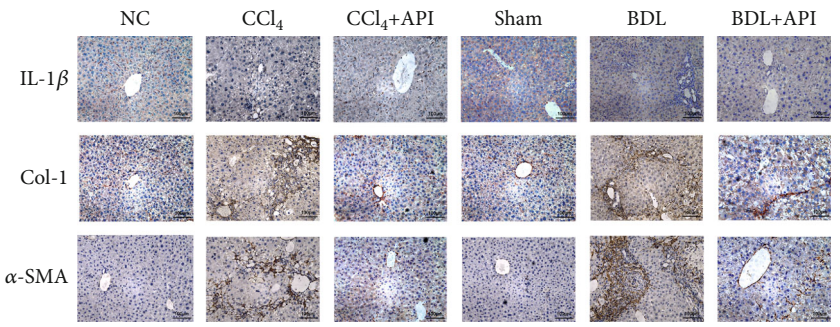

(c)

Figure 3: Continued.

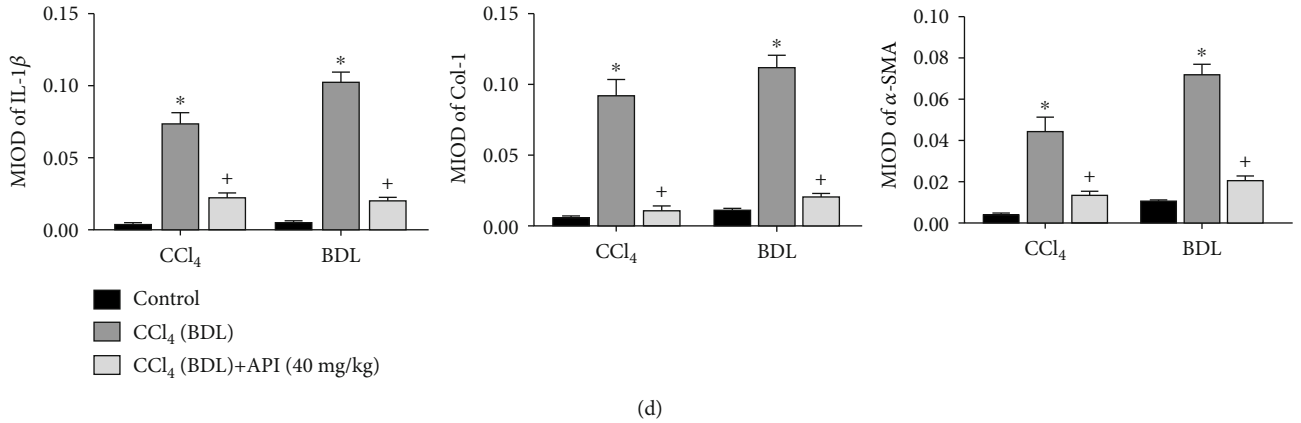

(d)

Figure 3: Apigenin restrained the activation of HSC and regulated the balance of TIMP1 and MMP2. Notes: (a) relative IL-1β, Col-1, α-SMA, TIMP1, and MMP2 mRNA levels were determined by qRT-PCR. (b) Western blot analysis of IL-1β, Col-1, α-SMA, TIMP1, and MMP2 protein levels. (c) IL-1β, Col-1, and α-SMA protein expressions in liver tissues are shown by immunohistochemical staining (200x). (d) Final evaluations were made using Image-Pro Plus 6.0 software to calculate the MIOD of the positive staining area. Data are presented as mean ± SD ($n = 6$; $^{*}P < 0.05$ for CCl_4 (BDL) group vs. control group; $^{\#}P < 0.05$ for CCl_4 (BDL)+apigenin (20 mg/kg) group vs. CCl_4 (BDL) group; $^{+}P < 0.05$ for CCl_4 (BDL)+apigenin (40 mg/kg) group vs. CCl_4 (BDL) group; $^{!}P < 0.05$ for CCl_4 (BDL)+apigenin (40 mg/kg) group vs. CCl_4 (BDL)+apigenin (20 mg/kg) group). Abbreviation: MIOD: mean of integrate optical density.

we detected the levels of ALT and AST in the serum to explore the extent of liver parenchymal damage in both fibrosis models. We could see it clearly from the Figures 2(a) and 2(b) that ALT and AST elevated dramatically in model groups compared with vehicle and sham groups. However, we also noticed apigenin groups could reverse the increase induced by CCl_4 and BDL surgery in a dose-dependent manner. Next, HE and Masson staining were used to evaluate the pathological changes of liver tissues. HE staining showed that the morphology and structure of mouse liver cells in the control groups were normal, with normal arrangement, normal hepatic lobules and portal area, and no inflammatory cell exudation. Compared with the control groups, the disordered arrangement of liver cells, the damaged normal structure, the exudation of many inflammatory cells, and the proliferation of collagen fibers were significantly observed in the CCl_4 and BDL groups. When apigenin was given at the same time, the disordered arrangement of liver cells was significantly reduced, the structure of portal area was almost normalized, fibrous tissue hyperplasia and inflammatory cell infiltration were significantly decreased, and the morphological structure was close to normal liver tissue (Figures 2(c) and 2(d)). The results of Masson staining could further confirm the protective effect on liver fibrosis of apigenin. The above results showed that apigenin had an obviously protective effect on CCl_4- and BDL-induced liver fibrosis in mice.

3.3. Apigenin Restrained the Activation of HSC and Regulated the Balance of TIMP1 and MMP2. α-SMA was an important indicator of HSC activation, and collagen 1 was the main component of ECM, which were often used as important indicators to test the degree of liver fibrosis. In order to further prove the effect of apigenin on mouse liver fibrosis, mRNA and protein expression of collagen 1, α-SMA, and IL-1β in the mouse liver tissues were measured by real-time PCR, western blotting, and IHC. The results showed that compared with the vehicle or sham control groups, mRNA and protein expression of collagen 1, α-SMA, and IL-1β in the model group were significantly increased, but their expressions were decreased after apigenin treatment (Figures 3(a)–3(c)). The synthesis and degradation of hepatic ECM are regulated by matrix metalloproteinases (MMPs) and matrix metalloproteinase inhibitors (TIMPs). Injury factors can lead to the activation of HSC, resulting in the imbalance of MMPS/TIMPs; therefore, we measured the levels of TIMP1 and MMP2 in liver tissues. The results indicated that the expression of TIMP1 increased obviously in the CCl_4 and BDL groups, and this trend could be inhibited by apigenin treatment. On the contrary, MMP2 decreased in the fibrosis model groups but increased in the apigenin groups. In general, the above experimental results showed that apigenin could restrain the activation of HSC and regulated the balance of TIMP1 and MMP2 to relieve liver fibrosis in mice.

3.4. Apigenin Alleviated Autophagy during Liver Fibrosis. Beclin-1, LC3, and p62, which are autophagy signature proteins, were analyzed by qRT-PCR, IHC, and western blotting to explore the protective effect of apigenin. As demonstrated in Figures 4(a)–4(d) and S1, the expressions of Beclin-1 and LC3II/LC3I augmented obviously, while p62 decreased drastically, in the CCl_4 and BDL groups. However, apigenin groups could ameliorate these changes in a dose-dependent manner. The above results suggested that apigenin could alleviate autophagy during liver fibrosis.

3.5. Apigenin Could Relieve Hepatic Fibrosis Induced by CCl_4 and BDL via Downregulating TGF-β1/Smad3 and p38/PPARα Pathways. TGF-β1 is a pluripotent cytokine that is involved in inflammatory infiltration, cell growth, apoptosis, differentiation, and other processes in fibrosis. The Smad protein family is the downstream molecule of TGF-β1. Therefore, we evaluated the expressions of the TGF-

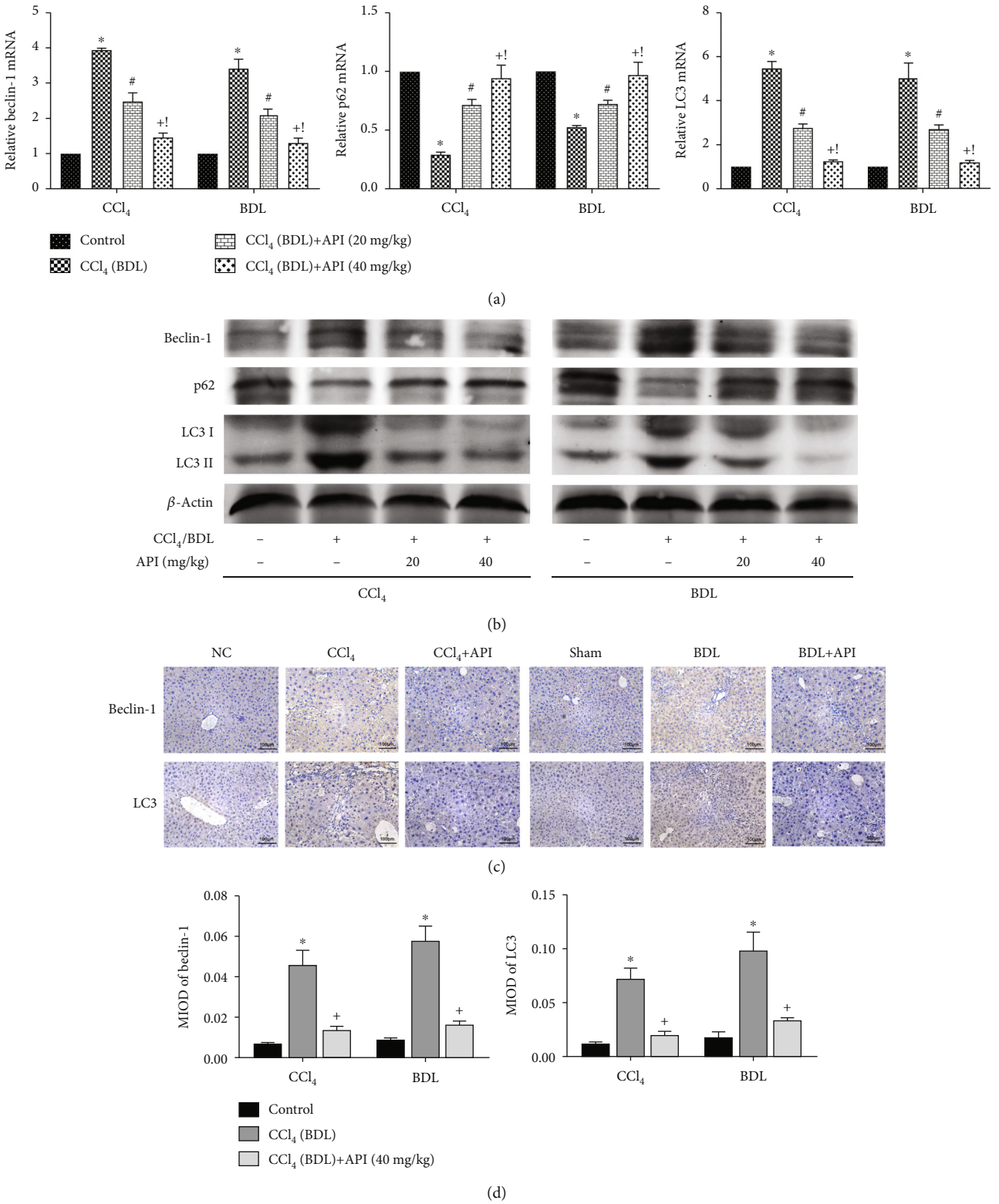

Figure 4: Apigenin alleviated autophagy during liver fibrosis. Notes: (a) relative Beclin-1, p62, and LC3 mRNA levels were determined by qRT-PCR. (b) Western blot analysis of Beclin-1, p62, and LC3. (c) Beclin-1 and LC3 protein expressions in liver tissues are shown by immunohistochemical staining (200x). (d) Final evaluations were made using Image-Pro Plus 6.0 software to calculate the MIOD of the positive staining area. Data are presented as mean ± SD ($n = 6$; $^{*}P < 0.05$ for CCl_4 (BDL) group vs. control group; $^{\#}P < 0.05$ for CCl_4 (BDL)+apigenin (20 mg/kg) group vs. CCl_4 (BDL) group; $^{+}P < 0.05$ for CCl_4 (BDL)+apigenin (40 mg/kg) group vs. CCl_4 (BDL) group; $^{!}P < 0.05$ for CCl_4 (BDL)+apigenin (40 mg/kg) group vs. CCl_4 (BDL)+apigenin (20 mg/kg) group). Abbreviation: MIOD: mean of integrate optical density.

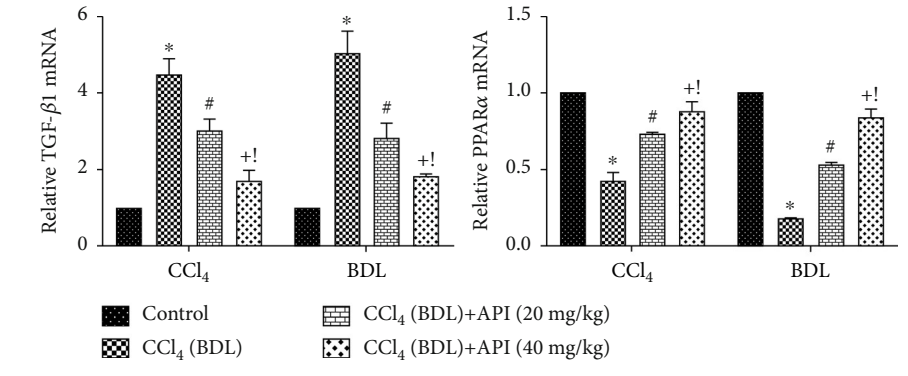

(a)

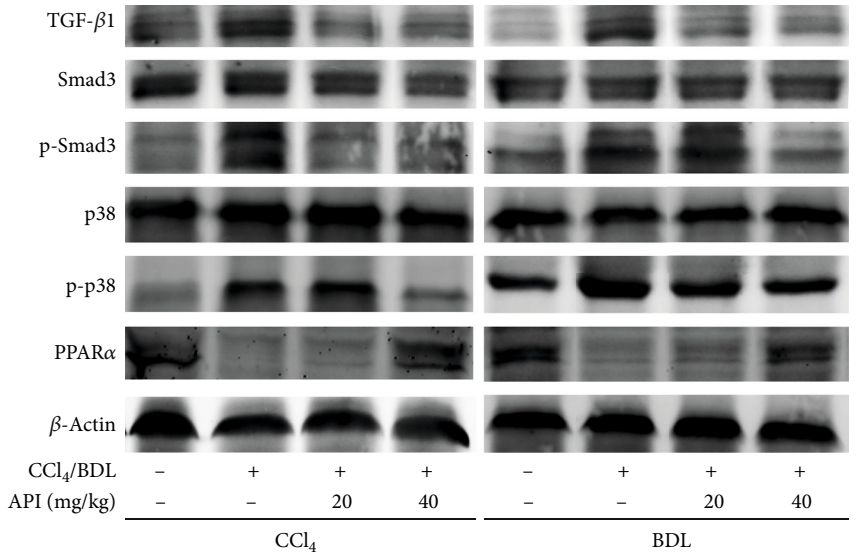

(b)

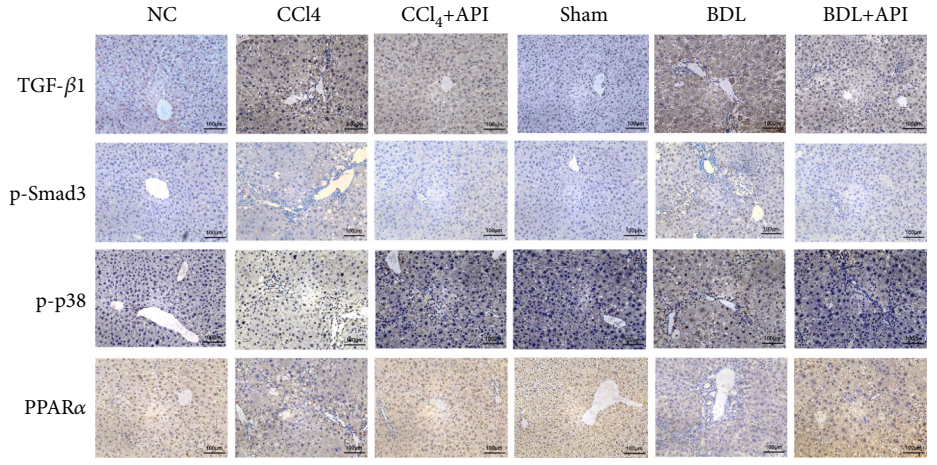

(c)

Figure 5: Continued.

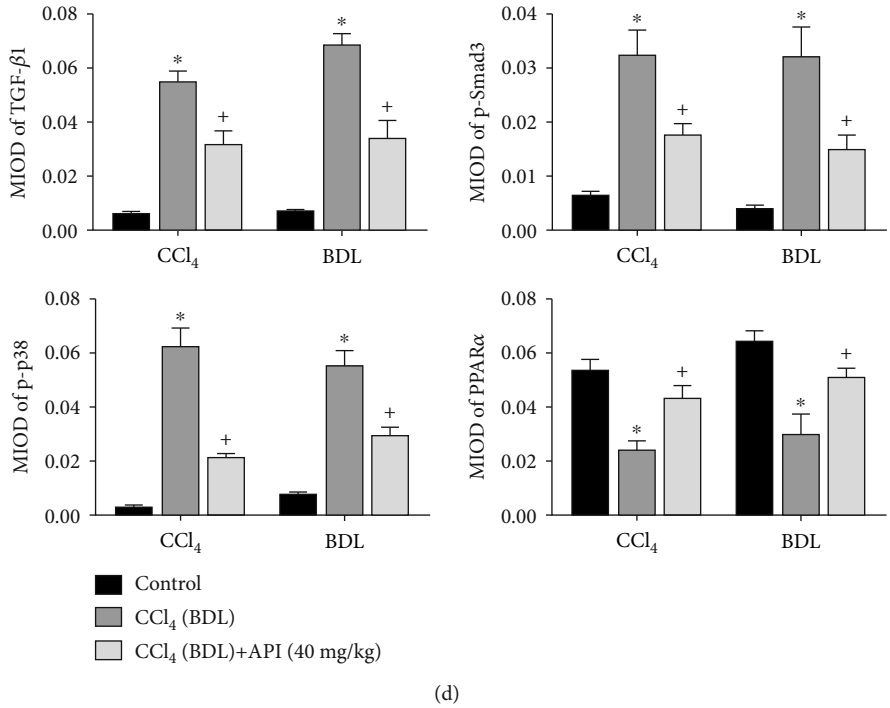

(d)

Figure 5: Apigenin could relieve hepatic fibrosis induced by CCl_4 and BDL via downregulating TGF-β1/Smad3 and p38/PPARα pathways. Notes: (a) relative TGF-β1 and PPARα mRNA levels were determined by qRT-PCR. (b) Western blot analysis of TGF-β1, Smad3, p-Smad3, p38, p-p38, and PPARα. (c) TGF-β1, p-Smad3, p-p38, and PPARα protein expressions in liver tissues are shown by immunohistochemical staining (200x). (d) Final evaluations were made using Image-Pro Plus 6.0 software to calculate the MIOD of the positive staining area. Data are presented as mean ± SD ($n = 6$; $^{*}P < 0.05$ for CCl_4 (BDL) group vs. control group; $^{\#}P < 0.05$ for CCl_4 (BDL)+apigenin (20 mg/kg) group vs. CCl_4 (BDL) group; $^{+}P < 0.05$ for CCl_4 (BDL)+apigenin (40 mg/kg) group vs. CCl_4 (BDL) group; $^{!}P < 0.05$ for CCl_4 (BDL)+apigenin (40 mg/kg) group vs. CCl_4 (BDL)+apigenin (20 mg/kg) group). Abbreviation: MIOD: mean of integrate optical density.

β1/Smad3 pathway. The results of qRT-PCR, IHC, and western blotting in Figures 5(a)–5(d) illustrated that CCl_4 and BDL surgery could significantly active the TGF-β1/Smad3 pathway, but apigenin treatment could reverse this activation. It means that the protective effects of apigenin were associated with restraining the TGF-β1/Smad3 pathway. Next, we measured the levels of p38 and PPARα which was also a downstream molecule of TGF-β1. In our results, we found that liver fibrosis induced by CCl_4 and BDL surgery could lead to phosphorylation of p38, which further inhibited PPARα. In apigenin treatment groups, p-p38 was dramatically downregulated and PPARα increased obviously. Therefore, we can draw the conclusion that apigenin could relieve hepatic fibrosis induced by CCl4 and BDL via downregulating the TGF-β1/Smad3 and p38/PPARα pathways.

4. Discussion

Liver fibrosis is a chronic wounding-healing response with a long-time liver injury [4, 38]. Although there are little symptoms at the beginning of liver fibrosis, the risk of mortality increases significantly once liver fibrosis progresses to cirrhosis and even hepatocellular carcinoma [2]. More than 30,000 deaths per year caused by cirrhosis and 1,000 deaths per year occurred related to liver cancer in the United States are enough to warn us that halting and reversing the progression of fibrosis is currently an effective way to reduce mortality rather than only relying on highly limited liver transplants [39].

Apigenin is a kind of dietary flavonoid extracted mainly from celery, parsley, thyme, chamomile, and onions [23]. It had been reported that apigenin is of great effect in antifibrosis [33–36] and liver protection [26, 40–42]. Mirzoeva et al. demonstrated that apigenin could reduce TGF-β-induced VEGF production and suppress prostate carcinogenesis by regulating the Smad2/3 and Src/Fak/Akt pathways. Apigenin is also reported to inhibit metastasis and angiogenesis by the p38 MAPK pathway [43].These indicate that apigenin may become an efficient drug to prevent liver fibrosis, and the molecular mechanism might be closely related to the TGF-β and p38 MAPK pathway. Therefore, in our study, CCl_4- and BDL-induced liver fibrosis models are used to explore the effects of apigenin and the specific molecular mechanism. Our results of HE and Masson staining confirmed that apigenin could improve liver fibrosis in a dose-dependent manner.

The first step to try to stop and reverse liver fibrosis is to explore the molecular mechanisms of this disease. The formation of liver fibrosis is a complex pathophysiological process involving many cells, molecules, and signaling pathways. The accumulation of ECM is regarded as the important character, and the activation of HSCs is considered as the initial process of liver fibrosis [2, 7, 10]. HSCs are one of the mesenchymal cells which account for one-third of the

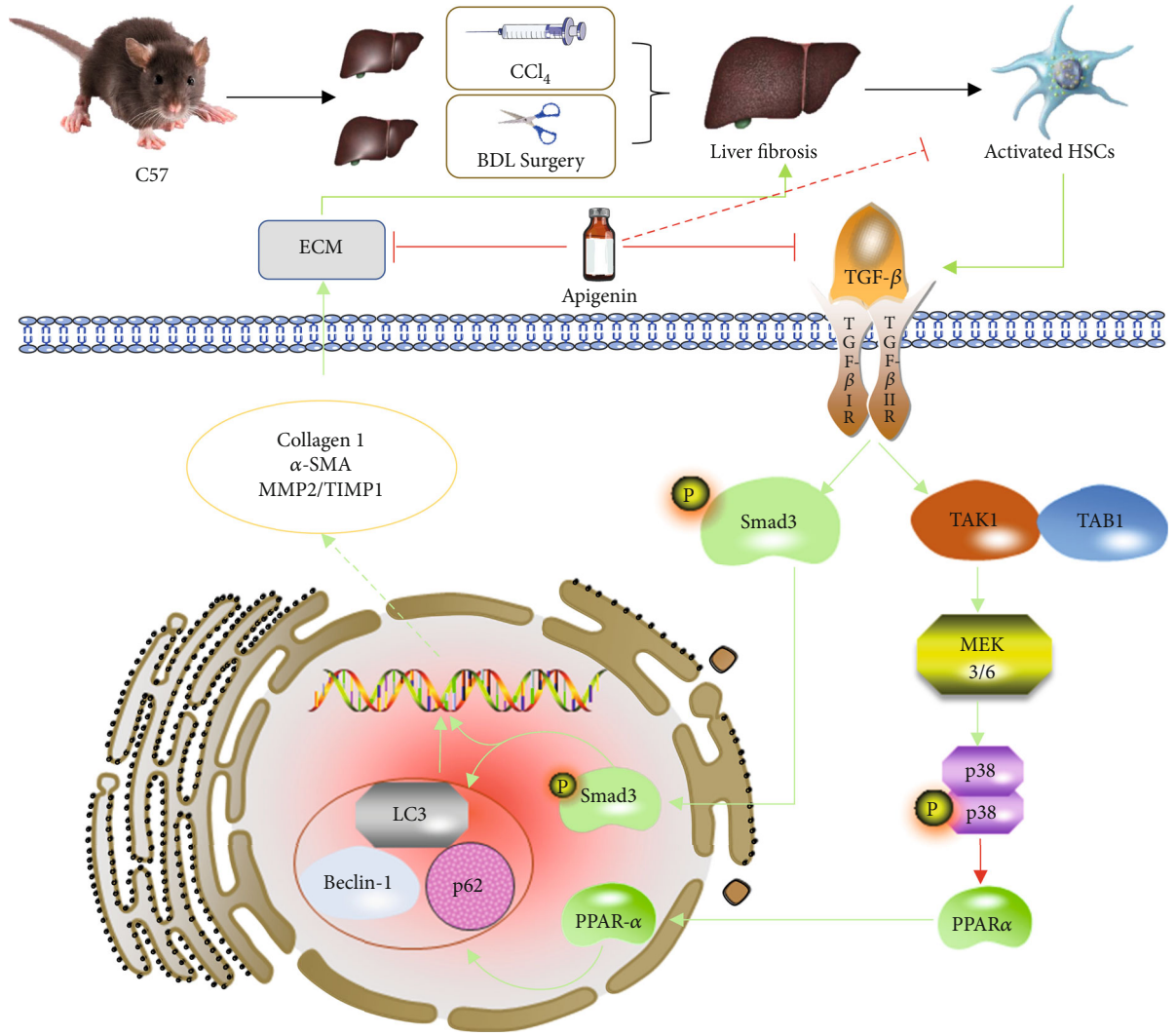

FIGURE 6: Probable mechanisms of apigenin against liver fibrosis. Notes: apigenin inhibits the production of TGF-β1 in HSCs. The decrease of TGF-β1 results in the reduced activation of HSCs and downregulation of the TGF-β1/Smad3 and p38/PPARα signaling pathway, including decreased ECM production and inhibition of autophagy. Abbreviations: BDL: bile duct ligation; CCl_4: carbon tetrachloride; ECM: extracellular matrix; HSCs: hepatic stellate cells.

nonparenchymal cells in the liver and 15% of the total number of liver cells [11]. In normal conditions, HSC is at a quiescent condition and could store vitamin A and triglycerides in the cytoplasm [44]. However, when the liver suffers from acute or chronic injury, HSCs are activated and differentiated into myofibroblasts, which have a strong ability of proliferation, migration, and secretion. Activated HSCs are the main cells to produce ECM, and a large amount of ECM is continuously deposited in the Disse space. In addition, the main components of ECM also change from type IV collagen to type I collagen [45], resulting in the increase of density and hardness of ECM, and accumulated ECM also becomes the liver fibrosis tissue microenvironment containing α-SMA, TGF-β1, chemokines such as PDGF, hepatocyte growth factor (HGF), fibroblast growth factor (FGF), epidermal growth factor (EGF), and VEGF [46]. The synthesis and degradation of liver ECM is regulated by the combination of matrix metalloproteinases (MMPs) and tissue matrix metalloproteinase inhibitors (TIMPs). Under normal conditions, MMPs and TIMPs can be synthesized by hepatocytes and various mesenchymal cells and play a key role in maintaining the dynamic balance between ECM synthesis and degradation in normal liver tissues through complex regulatory mechanisms [12, 13, 47]. In our study, we explored the function of apigenin in the activation of HSCs and the levels of ECM. Our results illustrated that apigenin could suppress the activation of HSCs and decrease ECM by increasing the ratio of MMP2/TIMP1.

TGF-β is generally considered to be the strongest fibrogenic factor. The activation of the TGF-β1/Smad3 signaling pathway plays an important role in liver fibrosis [48]. Smad3 is phosphorylated into p-Smad3 which could promote the transcription of type 1 and type 3 collagen after the activation of TGF-β1 [49]. In addition, TGF-β can also activate the p38 MAPK signaling pathway to promote the transcription of collagen which is the main ingredient of ECM [50]. Besides,

large amounts of literature have confirmed that inhibiting the TGF-β1/Smad pathway could efficiently reduce the injury of liver fibrosis [4, 15, 47, 51–53]. In our study, we proved that TGF-β1 and Smad3 expressed much more in fibrosis model groups than in control groups, and at the same time, apigenin groups obviously reduced the expression of TGF-β1, Smad3, and the other related proteins. Thus, we concluded that the protective effect of apigenin was closely related to the inhibition of the TGF-β1/Smad3 pathway.

p38 MAPK belongs to the family of MAPKs that affects a variety of intracellular responses including cell-cycle regulation, inflammation, cell death, and tumorigenesis [54]. p38 MAPK could be phosphorylated by many extracellular stimulants through a classic MAPK pathway, and phosphorylated p38 (p-p38) could further regulate many substrates that include transcription factors, peroxisome proliferator-activated receptors (PPARs), and so on [54, 55]. The study of Liu et al. demonstrated that p38 MAPK activated by TGF-β1 could exert a positive effect on liver fibrosis [12]. In addition, Lu et al. illustrated that the inhibition of p-p38 MAPK could increase the expression of PPARα to protect liver from concanavalin A-induced injury [55]. PPARs which belong to the subfamily of the nuclear receptor superfamily containing PPARα, PPAR β/δ, and PPARγ have many biological functions such as liver protection, antitumor, antiasthma, antidiabetes, and antineuropathic pain [56–62]. It was reported that PPARα could reverse fibrosis by reducing lipid peroxides and inhibiting the activation of HSCs and Kupffer cells (KCs) [63, 64]. So, in our study, we detected the expressions of p-p38 and PPARα and proved that apigenin could inhibit the phosphorylation of p38 which further increased PPARα to protect the liver from fibrosis.

Autophagy is a self-selective mode of cell death which contributes a lot to the basic liver functions [65]. Hernandez-Gea and Friedman demonstrated that autophagy could provide energy for the activation of HSCs by stimulating metabolism of lipid droplets [16]. However, inappropriate autophagy activity may aggravate damage in hepatic injury such as liver fibrosis [66]. The conclusion of Li et al. proved that suppressing autophagy could alleviate liver fibrosis [52]. Autophagy is closely related to the TGF-β1/Smad3 pathway, which could increase the expression of Bechin1 and LC3 and decrease the generation of p62 [67]. In addition, the inhibition of autophagy via the p38/PPARα pathway could exert positive effects in liver injury [55]. Our current results confirmed that apigenin could ameliorate liver fibrosis by inhibiting autophagy via the TGF-β1/Smad3 and p38/PPARα pathways.

In general, our study illustrated the liver-protective effect of apigenin in CCl_4- and BDL-induced liver fibrosis models. Apigenin could inhibit the activation of HSCs which promote the accumulation of ECM and the secretion of many fibrogenic factors such as α-SMA and collagen 1. In addition, the TGF-β1/Smad3 and p38/PPARα pathways are proven to be the main signaling pathways through which apigenin exerts its function (Figure 6). Therefore, apigenin may be a new clinical option for the treatment of fibrosis; however, more drug safety and clinical trials need to be accomplished before clinical applications.

5. Conclusion

Our study illustrated the liver-protective effect of apigenin in CCl_4- and BDL-induced liver fibrosis models. Inhibiting the TGF-β1/Smad3 and p38/PPARα pathways, reducing autophagy, and decreasing ECM formation are the major mechanism of the antifibrotic effects of apigenin.

Data Availability

The data used to support the findings of this study are available from the corresponding author upon request.

Conflicts of Interest

The authors declare that they have no conflicts of interest.

Authors' Contributions

Jie Ji, Qiang Yu, Weiqi Dai, Liwei Wu, and Jiao Feng conducted the experiments. Jie Ji, Yuanyuan Zheng, and Yan Li analyzed the data. Jie Ji wrote the manuscript. Chuanyong Guo provided the reagents and materials.

Acknowledgments

This research was funded by the National Natural Science Foundation of China (grant number: 81670472), the Yangfan Plan of the Shanghai Science and Technology Commission (grant number: 20YF1443300), the National Natural Science Foundation of Shanghai (grant number: 19ZR1447700), the Health System Innovation Plan of Shanghai Putuo District Science and Technology Committee (grant numbers: PTKWWS2018001 and PTKWWS201903), and the WBN Liver Disease Research Fund of China Hepatitis Prevention Foundation (grant number: CFHPC2019031).

Supplementary Materials

supplementary Figure S1: the quantitative data of western blotting of relative LC3II/LC3I ratio. *(Supplementary Materials)*

References

[1] M. Parola and M. Pinzani, "Liver fibrosis: pathophysiology, pathogenetic targets and clinical issues," *Molecular Aspects of Medicine*, vol. 65, pp. 37–55, 2019.

[2] V. Hernandez-Gea and S. L. Friedman, "Pathogenesis of liver fibrosis," *Annual Review of Pathology*, vol. 6, no. 1, pp. 425–456, 2011.

[3] S. L. Friedman, "Liver fibrosis - from bench to bedside," *Journal of Hepatology*, vol. 38, pp. 38–53, 2003.

[4] J. Feng, K. Chen, Y. Xia et al., "Salidroside ameliorates autophagy and activation of hepatic stellate cells in mice via NF-κB and TGF-β1/Smad3 pathways," *Drug Design, Development and Therapy*, vol. Volume 12, pp. 1837–1853, 2018.

[5] Y. W. Eom, K. Y. Shim, and S. K. Baik, "Mesenchymal stem cell therapy for liver fibrosis," *The Korean Journal of Internal Medicine*, vol. 30, no. 5, pp. 580–589, 2015.

[6] A. J. Czaja, "Hepatic inflammation and progressive liver fibrosis in chronic liver disease," *World Journal of Gastroenterology*, vol. 20, no. 10, pp. 2515–2532, 2014.

[7] C. Trautwein, S. L. Friedman, D. Schuppan, and M. Pinzani, "Hepatic fibrosis: concept to treatment," *Journal of Hepatology*, vol. 62, no. 1, pp. S15–S24, 2015.

[8] Y. A. Lee, M. C. Wallace, and S. L. Friedman, "Pathobiology of liver fibrosis: a translational success story," *Gut*, vol. 64, no. 5, pp. 830–841, 2015.

[9] M. Pinzani and J. Macias-Barragan, "Update on the pathophysiology of liver fibrosis," *Expert Review of Gastroenterology & Hepatology*, vol. 4, no. 4, pp. 459–472, 2014.

[10] R. Bataller and D. A. Brenner, "Liver fibrosis," *Journal of Clinical Investigation*, vol. 115, no. 2, pp. 209–218, 2005.

[11] T. Higashi, S. L. Friedman, and Y. Hoshida, "Hepatic stellate cells as key target in liver fibrosis," *Advanced Drug Delivery Reviews*, vol. 121, pp. 27–42, 2017.

[12] N. Liu, J. Feng, X. Lu et al., "Isorhamnetin inhibits liver fibrosis by reducing autophagy and inhibiting extracellular matrix formation via the Tgf-Beta1/Smad3 and Tgf-Beta1/P38 Mapk pathways," *Mediators of Inflammation*, vol. 2019, Article ID 6175091, 2019.

[13] S. Hemmann, J. Graf, M. Roderfeld, and E. Roeb, "Expression of Mmps and Timps in liver fibrosis - a systematic review with special emphasis on anti-fibrotic strategies," *Journal of Hepatology*, vol. 46, no. 5, pp. 955–975, 2007.

[14] M. Shen, K. Chen, J. Lu et al., "Protective Effect of Astaxanthin on Liver Fibrosis through Modulation of TGF-β1 Expression and Autophagy," *Mediators of Inflammation*, vol. 2014, Article ID 954502, 2014.

[15] L. Wu, Q. Zhang, W. Mo et al., "Quercetin prevents hepatic fibrosis by inhibiting hepatic stellate cell activation and reducing autophagy via the TGF-β1/Smads and PI3K/Akt pathways," *Scientific Reports*, vol. 7, no. 1, p. 9289, 2017.

[16] V. Hernandez-Gea and S. L. Friedman, "Autophagy fuels tissue fibrogenesis," *Autophagy*, vol. 8, no. 5, pp. 849-850, 2014.

[17] J. Ji, L. Wu, J. Feng et al., "Cafestol preconditioning attenuates apoptosis and autophagy during hepatic ischemia-reperfusion injury by inhibiting Erk/Pparγ pathway," *International Immunopharmacology*, vol. 84, 2020.

[18] Q. Yu, L. Wu, T. Liu et al., "Protective effects of levotetrahydropalmatine on hepatic ischemia/reperfusion injury are mediated by inhibition of the ERK/NF-κB pathway," *International Immunopharmacology*, vol. 70, pp. 435–445, 2019.

[19] J. Deng, J. Feng, T. Liu et al., "Beraprost sodium preconditioning prevents inflammation, apoptosis, and autophagy during hepatic ischemia-reperfusion injury in mice via the P38 and Jnk pathways," *Drug Design, Development and Therapy*, vol. - Volume 12, pp. 4067–4082, 2018.

[20] L. Wu, Q. Zhang, W. Dai et al., "Quercetin Pretreatment Attenuates Hepatic Ischemia Reperfusion-Induced Apoptosis and Autophagy by Inhibiting ERK/NF-κB Pathway," *Gastroenterology Research and Practice*, vol. 2017, Article ID 9724217, 2017.

[21] V. Hernández-Gea, Z. Ghiassi-Nejad, R. Rozenfeld et al., "Autophagy releases lipid that promotes fibrogenesis by activated hepatic stellate cells in mice and in human tissues," *Gastroenterology*, vol. 142, no. 4, pp. 938–946, 2012.

[22] L. F. R. Thoen, E. L. M. Guimarães, L. Dollé et al., "A role for autophagy during hepatic stellate cell activation," *Journal of Hepatology*, vol. 55, no. 6, pp. 1353–1360, 2011.

[23] J. Madunic, I. V. Madunic, G. Gajski, J. Popic, and V. Garaj-Vrhovac, "Apigenin: a dietary flavonoid with diverse anticancer properties," *Cancer Letters*, vol. 413, pp. 11–22, 2018.

[24] D. Bauer, E. Mazzio, and K. F. A. Soliman, "Whole transcriptomic analysis of apigenin on Tnfα immuno-activated Mda-Mb-231 breast cancer cells," *Cancer Genomics Proteomics*, vol. 16, no. 6, pp. 421–431, 2019.

[25] J. Yang, C. Pi, and G. Wang, "Inhibition of Pi3k/Akt/Mtor pathway by apigenin induces apoptosis and autophagy in hepatocellular carcinoma cells," *Biomedicine & Pharmacotherapy*, vol. 103, pp. 699–707, 2018.

[26] S. Bhattacharya, L. Mondal, B. Mukherjee et al., "Apigenin loaded nanoparticle delayed development of hepatocellular carcinoma in rats," *Nanomedicine*, vol. 14, no. 6, pp. 1905–1917, 2018.

[27] H. Shao, K. Jing, E. Mahmoud, H. Huang, X. Fang, and C. Yu, "Apigenin sensitizes colon cancer cells to antitumor activity of Abt-263," *Molecular Cancer Therapeutics*, vol. 12, no. 12, pp. 2640–2650, 2013.

[28] É. C. Lefort and J. Blay, "Apigenin and its impact on gastrointestinal cancers," *Molecular Nutrition & Food Research*, vol. 57, no. 1, pp. 126–144, 2013.

[29] P. Chen, X. Huo, W. Liu, K. Li, Z. Sun, and J. Tian, "Apigenin exhibits anti-inflammatory effects in Lps-stimulated Bv2 microglia through activating Gsk3β/Nrf2 signaling pathway," *Immunopharmacology and Immunotoxicology*, vol. 42, no. 1, pp. 9–16, 2020.

[30] Q. Zhou, K. W. Cheng, J. Gong, E. T. S. Li, and M. Wang, "Apigenin and its methylglyoxal-adduct inhibit advanced glycation end products- induced oxidative stress and inflammation in endothelial cells," *Biochemical Pharmacology*, vol. 166, pp. 231–241, 2019.

[31] S. Mirzoeva, X. Tong, B. B. Bridgeman, M. P. Plebanek, and O. V. Volpert, "Apigenin inhibits Uvb-induced skin carcinogenesis: the role of thrombospondin-1 as an anti-inflammatory factor," *Neoplasia*, vol. 20, no. 9, pp. 930–942, 2018.

[32] F. Li, F. Lang, H. Zhang et al., "Apigenin alleviates endotoxin-induced myocardial toxicity by modulating inflammation, oxidative stress, and autophagy," *Oxidative Medicine and Cellular Longevity*, vol. 2017, Article ID 2302896, 10 pages, 2017.

[33] H. Wang, B. Guo, S. Lin, P. Chang, and K. Tao, "Apigenin inhibits growth and migration of fibroblasts by suppressing Fak signaling," *Aging (Albany NY)*, vol. 11, no. 11, pp. 3668–3678, 2019.

[34] R. Jiao, H. Chen, Q. Wan et al., "Apigenin inhibits fibroblast proliferation and reduces epidural fibrosis by regulating Wnt3a/*B*-catenin signaling pathway," *Journal of Orthopaedic Surgery and Research*, vol. 14, no. 1, p. 258, 2019.

[35] Y. Zhang, Q. Sun, X. Li et al., "Apigenin suppresses mouse peritoneal fibrosis by down-regulating Mir34a expression," *Biomedicine & Pharmacotherapy*, vol. 106, pp. 373–380, 2018.

[36] X. Wei, P. Gao, Y. Pu et al., "Activation of Trpv4 by dietary apigenin antagonizes renal fibrosis in deoxycorticosterone acetate (Doca)-salt-induced hypertension," *Clinical Science (London, England)*, vol. 131, no. 7, pp. 567–581, 2017.

[37] S. C. Yanguas, B. Cogliati, J. Willebrords et al., "Experimental models of liver fibrosis," *Archives of Toxicology*, vol. 90, no. 5, pp. 1025–1048, 2016.

[38] K. Bottcher and M. Pinzani, "Pathophysiology of liver fibrosis and the methodological barriers to the development of anti-

fibrogenic agents," *Advanced Drug Delivery Reviews*, vol. 121, pp. 3–8, 2017.

[39] H. B. El-Serag and K. L. Rudolph, "Hepatocellular carcinoma: epidemiology and molecular carcinogenesis," *Gastroenterology*, vol. 132, no. 7, pp. 2557–2576, 2007.

[40] S. Yue, N. Xue, H. Li, B. Huang, Z. Chen, and X. Wang, "Hepatoprotective effect of apigenin against liver injury via the non-canonical Nf-*K*b pathway in vivo and in vitro," *Inflammation*, vol. 43, no. 5, pp. 1634–1648, 2020.

[41] F. Wang, J. C. Liu, R. J. Zhou et al., "Apigenin protects against alcohol-induced liver injury in mice by regulating hepatic Cyp2e1-mediated oxidative stress and Ppar*α*-mediated lipogenic gene expression," *Chemico-Biological Interactions*, vol. 275, pp. 171–177, 2017.

[42] X. Feng, W. Yu, X. Li et al., "Apigenin, a modulator of Ppar*γ*, attenuates Hfd-induced Nafld by regulating hepatocyte lipid metabolism and oxidative stress via Nrf2 activation," *Biochemical Pharmacology*, vol. 136, pp. 136–149, 2017.

[43] Q. Peng, Z. Deng, H. Pan, L. Gu, O. Liu, and Z. Tang, "Mitogen-activated protein kinase signaling pathway in oral cancer," *Oncology Letters*, vol. 15, no. 2, pp. 1379–1388, 2018.

[44] Y. Shirakami, S. A. Lee, R. D. Clugston, and W. S. Blaner, "Hepatic metabolism of retinoids and disease associations," *Biochimica et Biophysica Acta*, vol. 1821, no. 1, pp. 124–136, 2012.

[45] T. Tsuchida and S. L. Friedman, "Mechanisms of hepatic stellate cell activation," *Nature Reviews. Gastroenterology & Hepatology*, vol. 14, no. 7, pp. 397–411, 2017.

[46] S. L. Friedman, D. Sheppard, J. S. Duffield, and S. Violette, "Therapy for fibrotic diseases: nearing the starting line," *Science Translational Medicine*, vol. 5, no. 167, p. 167sr1, 2013.

[47] T. Liu, L. Xu, C. Wang et al., "Alleviation of hepatic fibrosis and autophagy via inhibition of transforming growth factor-*β*1/Smads pathway through Shikonin," *Journal of Gastroenterology and Hepatology*, vol. 34, no. 1, pp. 263–276, 2019.

[48] X. M. Meng, D. J. Nikolic-Paterson, and H. Y. Lan, "TGF-*β*: the master regulator of fibrosis," *Nature Reviews. Nephrology*, vol. 12, no. 6, pp. 325–338, 2016.

[49] M. J. Macias, P. Martin-Malpartida, and J. Massague, "Structural determinants of Smad function in TGF-*β* signaling," *Trends in Biochemical Sciences*, vol. 40, no. 6, pp. 296–308, 2015.

[50] S. Tsukada, J. K. Westwick, K. Ikejima, N. Sato, and R. A. Rippe, "Smad and P38 Mapk signaling pathways independently regulate *α*1(I) collagen gene expression in unstimulated and transforming growth factor-*β*-stimulated hepatic stellate cells," *The Journal of Biological Chemistry*, vol. 280, no. 11, pp. 10055–10064, 2005.

[51] S. Xu, Y. Mao, J. Wu et al., "TGF-*β*/Smad and Jak/Stat pathways are involved in the anti-fibrotic effects of propylene glycol alginate sodium sulphate on hepatic fibrosis," *Journal of Cellular and Molecular Medicine*, vol. 24, no. 9, pp. 5224–5237, 2020.

[52] J. Li, K. Chen, S. Li et al., "Protective effect of fucoidan from Fucus vesiculosus on liver fibrosis via the Tgf-beta1/Smad pathway-mediated inhibition of extracellular matrix and autophagy," *Drug Design, Development and Therapy*, vol. 10, pp. 619–630, 2016.

[53] Y. Xia, J. Li, K. Chen, J. Feng, and C. Guo, "Bergenin attenuates hepatic fibrosis by regulating autophagy mediated by the Ppar-*Γ*/Tgf-*B* pathway," *PPAR Research*, vol. 2020, 13 pages, 2020.

[54] L. R. Coulthard, D. E. White, D. L. Jones, M. F. McDermott, and S. A. Burchill, "$p38^{MAPK}$: stress responses from molecular mechanisms to therapeutics," *Trends in Molecular Medicine*, vol. 15, no. 8, pp. 369–379, 2009.

[55] X. Lu, T. Liu, K. Chen et al., "Isorhamnetin: a hepatoprotective flavonoid inhibits apoptosis and autophagy via P38/Ppar-a pathway in mice," *Biomedicine & Pharmacotherapy*, vol. 103, pp. 800–811, 2018.

[56] X. Du, M. Wu, D. Tian et al., "Microrna-21 contributes to acute liver injury in Lps-induced sepsis mice by inhibiting Ppar*α* expression," *PPAR Research*, vol. 2020, 7 pages, 2020.

[57] O. Y. Kytikova, J. M. Perelman, T. P. Novgorodtseva et al., "Peroxisome proliferator-activated receptors as a therapeutic target in asthma," *PPAR Research*, vol. 2020, Article ID 8906968, 18 pages, 2020.

[58] P. L. Yang, J. S. Wang, X. M. Cheng et al., "Ppar-*Γ* ligand inhibits nasopharyngeal carcinoma cell proliferation and metastasis by regulating E2f2," *PPAR Research*, vol. 2019, Article ID 8679271, 9 pages, 2019.

[59] L. J. Holm, M. O. Monsted, M. Haupt-Jorgensen, and K. Buschard, "Ppars and the development of type 1 diabetes," *PPAR Research*, vol. 2020, Article ID 6198628, 2020.

[60] A. Blitek and M. Szymanska, "Expression and role of peroxisome proliferator-activated receptors in the porcine early placenta trophoblast," *Domestic animal endocrinology*, vol. 67, pp. 42–53, 2019.

[61] T. Morinishi, Y. Tokuhara, H. Ohsaki, E. Ibuki, K. Kadota, and E. Hirakawa, "Activation and expression of peroxisome proliferator-activated receptor alpha are associated with tumorigenesis in colorectal carcinoma," *PPAR Research*, vol. 2019, Article ID 7486727, 2019.

[62] M. Alsalem, M. Haddad, S. A. Aldossary et al., "Effects of dual peroxisome proliferator-activated receptors alpha and gamma activation in two rat models of neuropathic pain," *PPAR Research*, vol. 2019, Article ID 2630232, 2019.

[63] E. Ip, G. Farrell, P. Hall, G. Robertson, and I. Leclercq, "Administration of the potent Pparalpha agonist, Wy-14,643, reverses nutritional fibrosis and steatohepatitis in mice," *Hepatology*, vol. 39, no. 5, pp. 1286–1296, 2004.

[64] M. Pawlak, P. Lefebvre, and B. Staels, "Molecular mechanism of PPAR*α* action and its impact on lipid metabolism, inflammation and fibrosis in non-alcoholic fatty liver disease," *Journal of Hepatology*, vol. 62, no. 3, pp. 720–733, 2015.

[65] T. Ueno and M. Komatsu, "Autophagy in the liver: functions in health and disease," *Nature reviews. Gastroenterology & hepatology*, vol. 14, no. 3, pp. 170–184, 2017.

[66] A. Mallat, J. Lodder, F. Teixeira-Clerc, R. Moreau, P. Codogno, and S. Lotersztajn, "Autophagy: a multifaceted partner in liver fibrosis," *BioMed Research International*, vol. 2014, Article ID 869390, 7 pages, 2014.

[67] K. Kiyono, H. I. Suzuki, H. Matsuyama et al., "Autophagy is activated by Tgf-Beta and potentiates Tgf-Beta-mediated growth inhibition in human hepatocellular carcinoma cells," *Cancer Research*, vol. 69, no. 23, pp. 8844–8852, 2009.

Hindawi
PPAR Research
Volume 2021, Article ID 8894752, 6 pages
https://doi.org/10.1155/2021/8894752

Research Article

Amorfrutins Relieve Neuropathic Pain through the PPARγ/CCL2 Axis in CCI Rats

Pengfei Gao, Jiayu Wang, Zhen Su, Fayin Li, and Xianlong Zhang

Department of Anesthesiology, The Affiliated Huaian No. 1 People's Hospital of Nanjing Medical University, Huaian, China

Correspondence should be addressed to Xianlong Zhang; hayyzxl@njmu.edu.cn

Received 25 September 2020; Revised 29 December 2020; Accepted 4 January 2021; Published 22 January 2021

Academic Editor: Xiao-Jie Lu

Neuropathic pain is a public health problem. Although many pharmaceuticals are used to treat neuropathic pain, effective and safe drugs do not yet exist. In this study, we tested nociceptive responses in CCI rats, and ELISA assay was performed to examine the expression of proinflammatory cytokines. We found that amorfrutins significantly reduce the pain behaviors in CCI rats and suppress the expression of proinflammatory cytokines (TNFα, IL-6, and IL-1β) and chemokines (CCL2/CCR2) in the spinal cord. However, concurrent administration of a PPARγ antagonist, GW9662, reversed the antihyperalgesic effect induced by amorfrutins. The results indicate that amorfrutins inhibit the inflammation and chemokine expression by activating PPARγ, thus relieving neuropathic pain in CCI rats. Therefore, PPARγ-CCL2/CCR2 pathway might represent a new treatment option for neuropathic pain.

1. Introduction

Neuropathic pain is maladaptive pain caused by a lesion or disease affecting the somatosensory system [1]; its clinical symptoms are spontaneous ongoing or shooting pain and stimulus-evoked pain [2]. Pharmacological treatment is the first-line options for neuropathic pain; however, the currently used drugs such as tricyclic antidepressants and serotonin-noradrenalin reuptake inhibitors have limited efficacy and serious side effects [3]. Therefore, the mechanisms of neuropathic pain should be further explored to develop novel therapeutic strategies. Current studies have shown that proinflammatory cytokines contribute to the generation and maintenance of neuropathic pain [4]. Based on this concept, it provides possibilities concerning other treatment strategies.

Peroxisome proliferator-activated receptors (PPARs) are ligand-activated transcription factor belonging to a nuclear hormone receptor superfamily, containing three isoforms PPARα, PPARβ/δ, and PPARγ [5]. PPARγ is ubiquitously expressed throughout the body; it is the regulator of adipocyte differentiation and plays a role in lipid metabolism and glucose homeostasis. In addition, increasing researches have illustrated the pivotal roles of PPARγ in inflammatory gene repression [6]. PPARγ agonists could suppress the production of proinflammatory cytokines in cultured monocytes [7]. As the natural agonists of PPARγ, amorfrutins are found in *Glycyrrhiza foetida* and *Amorpha fruticosa* [8]. Amorfrutins bind to and activate PPARγ without these side effects caused by synthetic PPARγ agonists [9].

Chemokines and their receptors are key mediators of inflammation [10]. Chemokines are induced by proinflammatory cytokines and modulate immune cell recruitment into inflamed tissues. However, elevated expression of chemokines contributes to chronic inflammation, which plays a role in neuropathic pain [11]. Experimental evidence has shown that several chemokines are linked to neuropathic pain in animal models [12], and CCL2/CCR2 signaling has garnered great attention. CCL2 belongs to CC chemokine subfamily and preferentially binds the CCR2 chemokine receptor [13, 14]. In neuropathic pain models, the development of mechanical allodynia was totally abrogated in CCR2−/− mice [15]. In other models, CCL2 and CCR2 remain upregulated for a long period after injury [16]. These researches represent a promising therapeutic target.

Neuropathic inflammation contributes to the maintenance of neuropathic pain, but PPARγ can inhibit the inflammation gene expression. Chemokines play a role in neuropathic pain as key inflammatory mediators [17]. Accordingly, the aim of this study was to assess whether amorfrutins can alleviate pain through PPARγ/CCL2 signaling in neuropathic pain models.

2. Materials and Methods

2.1. Cell Culture. HMC3 cell line was obtained from Procell (Wuhan, China) and cultured in Modified Eagle's Medium (MEM) supplemented with 10% fetal bovine serum (FBS) and 1% P/S under 5% CO_2 at 37°C.

2.2. Animal Models. Chronic constriction injury (CCI) model was established according to procedures described by Bennett and Xie [18]. Rats were anesthetized with pentobarbital. An incision was made just below the hip bone, parallel to the sciatic nerve. The nerve was exposed, and four 4-0 hromic gut sutures were used to loosely ligate the nerve with 1 mm intervals. The same surgery was performed in the sham operation group except ligating the sciatic nerve. There is no autophilia in CCI rats. The behavioral performance of the sham operation group is the same as before the operation.

All male Sprague-Dawley rats (200-300 g) were obtained from Huai'an First People's Hospital. The rats were randomly divided into four groups: (a) the sham group treated with vehicle, (b) chronic constriction injury (CCI) rats treated with vehicle, (c) chronic constriction injury (CCI) rats treated with amorfrutins (60 mg/kg), and (d) chronic constriction injury (CCI) rats treated with amorfrutins and GW9662 (30 mg/kg).

2.3. Behavioral Testing

2.3.1. PWMT. Paw withdrawal mechanical threshold (PWMT) was tested using the electric von Frey filament (IITC, USA). Put the rats into separate plexiglas boxes with a metal mesh floor. Before the test, the rats were adapted for 30 minutes to eliminate tension. The von Frey filament was pointed at the plantar surface of rats. When the rats show paw withdrawal reaction, the value of electric von Frey filament was considered as the paw withdrawal threshold. Each measurement should be repeated 3 times at 5 minutes interval.

2.3.2. PWTL. Paw withdrawal thermal latency (PWTL) was performed using the Plantar Analgesia Meter for thermal paw (IITC, USA). The rats were adapted to the environment for more than 30 minutes. Then, slide the test head and align the heat source with the bottom of the rats' hind paw. Set the stimulation time within 30 s, and automatically record the time of rats show paw withdrawal reaction. The interval between each measurement is more than 5 minutes. Repeat the measurement 3 times and take the average.

2.4. ELISA. The expression of TNF-α, IL-1β, and IL-6 in the spinal cord was examined using the LEGEND MAX™ Rat TNF-α ELISA Kit (Biolegend, China), Rat IL-1β ELISA Kit (Dakewe, China), and LEGEND MAX™ Rat IL-6 ELISA Kit (Biolegend, China).

2.5. Western Blot. The rats in each group were immediately decapitated after completing the pain behavior test on the 14th treatment day. Take out the L4~6 spinal cord, quickly put it in liquid nitrogen, and then transfer to the -80°C refrigerator.

The frozen samples were lysed using lysis buffer containing protease inhibitors. Protein (30 μg) was separated by sodium dodecyl sulphate-polyacrylamide gel electrophoresis. After the protein was transferred to polyvinylidene fluoride membranes, the membranes were incubated with primary antibodies (anti-CCL2, anti-CCR2, and anti-β actin; 1 : 2000; Abcam, UK) and HRP-conjugated secondary antibodies (1 : 10000; Amyjet, China). The protein bands were visualized using the Clarity Western ECL Substrate (Bio-Rad, USA).

2.6. Statistical Analysis. The significance between groups was analyzed by Student's t-test and one-way ANOVA. All statistical analysis was performed using SPSS 22.0 (IBM, Chicago, USA) and GraphPad Prism 8.0.0 (San Diego, California, USA).

3. Results

3.1. Amorfrutins Suppress CCL2/CCR2 Expression through PPARγ Activation. To explore the connection between PPAR and chemokines in neuropathic pain, we detected the CCL2/CCR2 expression in LPS-induced HMC3 cells. As shown in Figure 1, amorfrutins remarkably decreased the CCL2/CCR2 protein expression, whereas coadministration of amorfrutins and GW9662 (PPARγ antagonist) restored the expression of CCL2/CCR2. The results indicated that amorfrutins could suppressed the expression of CCL2/CCR2 protein through PPARγ activation.

3.2. Amorfrutins Relieve the Neuropathic Pain Responses in CCI Rats. Based on the results of the cell experiments, the CCI rat model was used to examine the function of amorfrutins in neuropathic pain. At 3 days after CCI surgery, all groups were treated with the corresponding drugs once a day for two weeks. At 1 h after injection, PWMT was measured by the same researcher (Figure 2(a)). In CCI rats, the mechanical thresholds were significantly reduced. However, after the administration of amorfrutins, the mechanical thresholds were increased from day 3 and reached its maximum after a week. To verify whether amorfrutins relieve neuropathic pain by activating PPAR$\boldsymbol{\gamma}$, GW9662 was coadministrated with amorfrutins. As shown in Figure 2(a), there were no significant changes in PWMT of CCI rats treated with amorfrutins+GW9662. PTWL was performed after PWMT (Figure 2(b)). Consistent with the above results, amorfrutins remarkably alleviated the thermal allodynia of CCI rats, but GW9662 reversed this effect. The results showed that amorfrutins relieved neuropathic pain in CCI rats by activating PPAR$\boldsymbol{\gamma}$.

3.3. Amorfrutins Reduce the Inflammation in CCI Rats. Inflammation has been proven to contribute to the

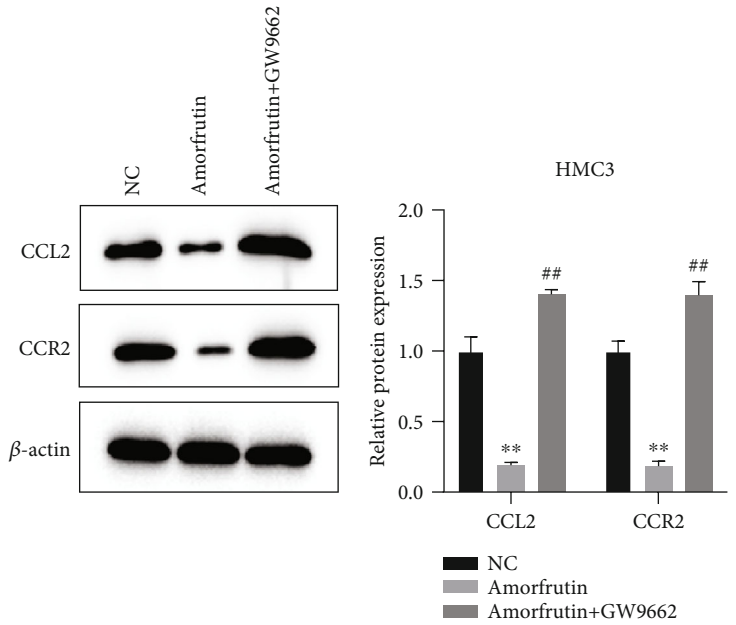

Figure 1: Amorfrutins suppressed the CCL2/CCR2 expression by activating PPARγ. The CCL2 and CCR2 protein expressions were significantly decreased in the amorfrutin group, whereas the GW9662 reversed the effects induced by amorfrutins.

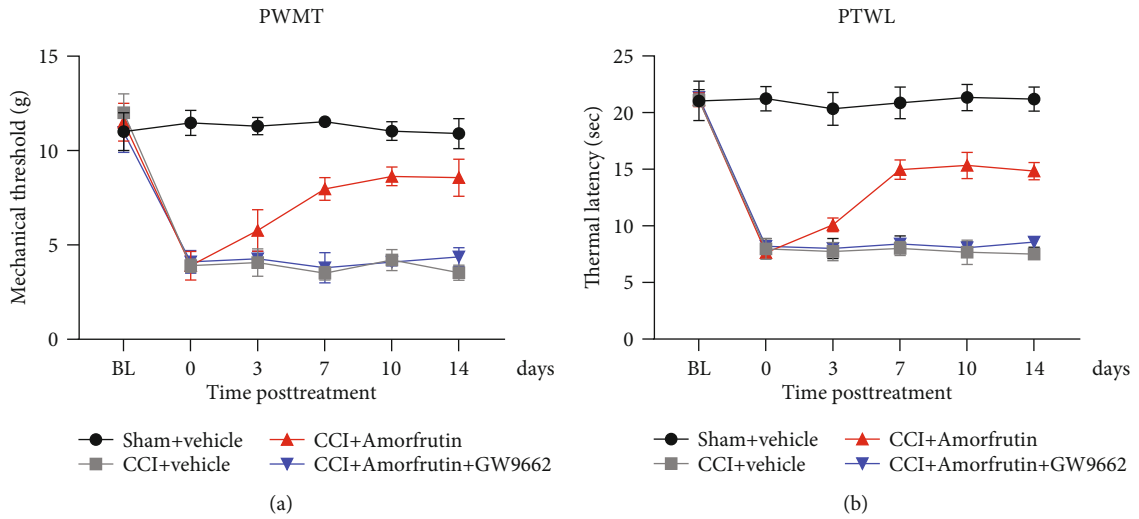

Figure 2: Amorfrutins relieved the neuropathic pain responses in CCI rats. (a) The PWMT of different groups were measured using the electric von Frey filament. (b) The PTWL of different groups were measured using the Plantar Analgesia Meter for thermal paw. Amorfrutins increased the PWMT and PTWL of CCI rats by activating PPARγ.

maintenance of neuropathic pain. To verify whether amorfrutins reduce neuropathic pain is related to inflammation, the proinflammatory cytokines in the spinal cord including TNF-α, IL-1β, and IL-6 were detected using ELISA (Figures 3(a)–3(c)). The results showed that the levels of TNF-α, IL-1β, and IL-6 were higher in the CCI groups than in the sham group. And amorfrutin administration markedly inhibited the upregulation of these proinflammatory cytokines. However, GW9662 reverses the effects induced by amorfrutins, indicating that amorfrutins decrease the inflammation by activating PPARγ. These findings revealed that amorfrutins might alleviate neuropathic pain by reducing inflammation.

3.4. PPARγ Activation Suppresses Chemokines CCL2/CCR2 Expression in CCI Rats. To further explore the connection between PPARγ and chemokines in neuropathic pain, we detected the CCL2 and CCR2 expression in the spinal cord (Figure 4). Compared with the sham group, the CCL2/CCR2 expression in the CCI group was increased. In those drug-treated rats, amorfrutins significantly reduced the expression of CCL2/CCR2; however, GW9662 blocked this effect and

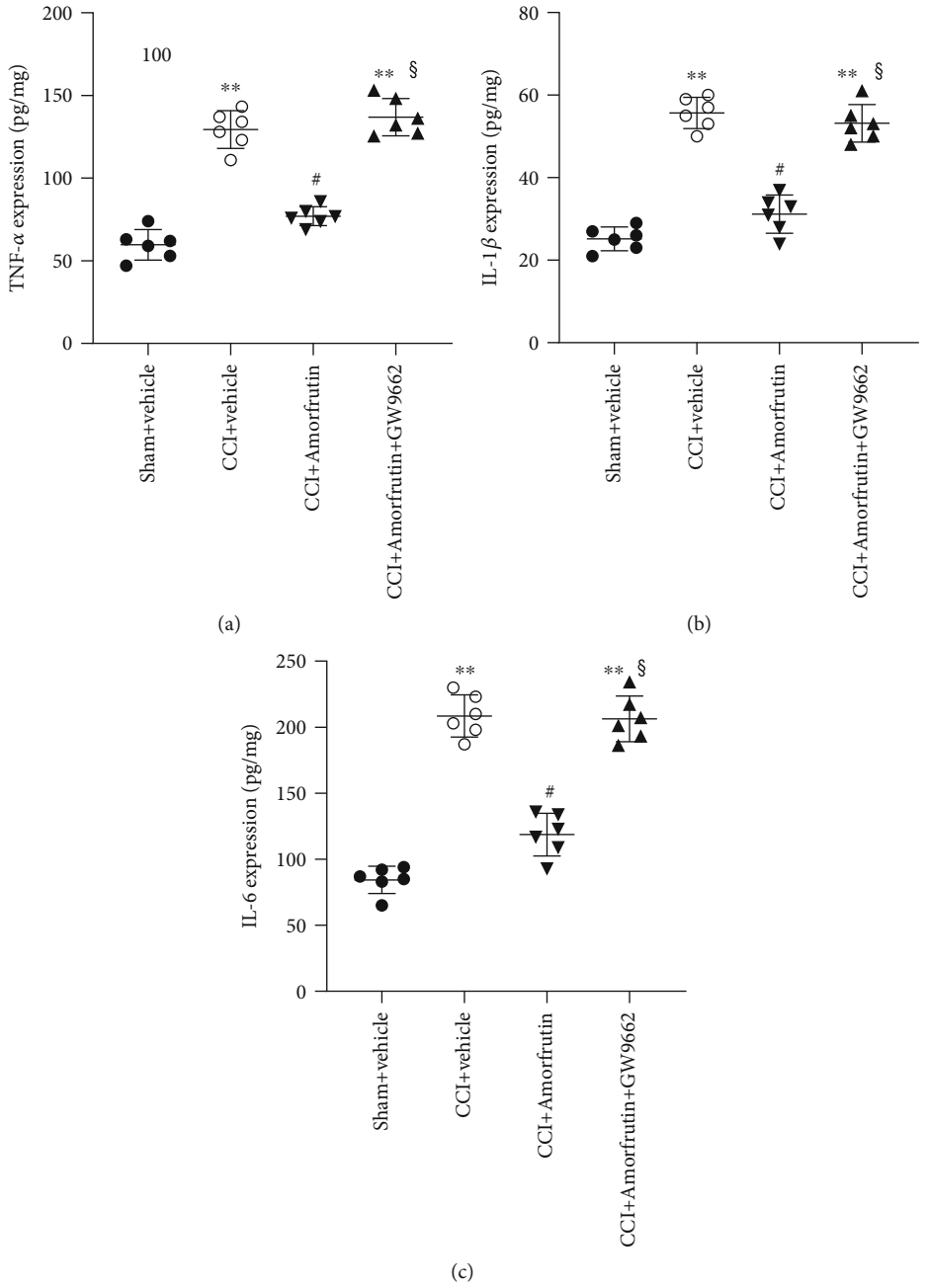

Figure 3: Amorfrutins reduced the inflammation in CCI rats. (a) The TNF-α expression in the spinal cord of different groups were detected using ELISA. (b) The IL-1β expression in spinal cord of different groups were detected using ELISA. (c) The IL-6 expression in spinal cord of different groups was detected using ELISA. Amorfrutins reduced the levels of TNF-α, IL-1β, and IL-6 through PPARγ activation.

restored the CCL2/CCR2 expression. The results indicated that amorfrutins (PPARγ agonist) inhibited chemokine CCL2/CCR2 expression through PPARγ activation. In summary, these data established the link between PPARγ and CCL2 in neuropathic pain, which may represent a novel therapy for neuropathic pain.

4. Discussion

In this report, we showed that amorfrutins significantly reduce neuropathic pain in CCI rats. And the levels of inflammation cytokines and chemokines CCL2/CCR2 were decreased. In addition, PPARγ antagonist GW9662 reversed the changes produced by amorfrutins.

Increasing evidence has shown that PPAR activation plays a role in alleviating neuropathic pain. In animal models, PPAR agonists pioglitazone, rosiglitazone, and palmitoylethanolamide (PEA) and fenofibrate have been proven to reduce pain [19]. In humans, the endogenous PPARα agonist PEA shows great efficacy in the treatment of various human pain conditions, including diabetic neuropathy, sciatic pain, and postoperative pain [20, 21]. Little information

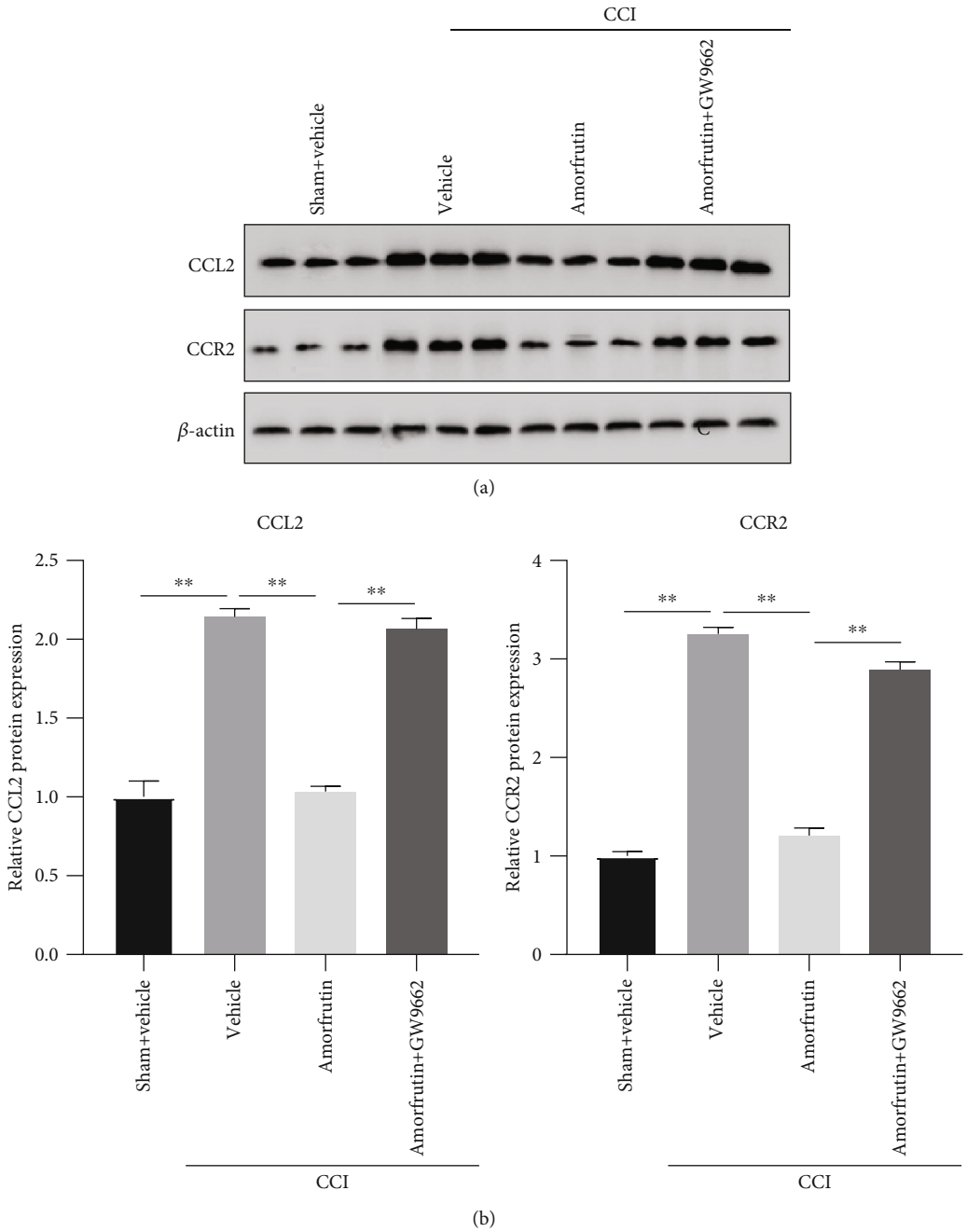

Figure 4: PPARγ activation suppressed chemokines CCL2/CCR2 expression in CCI rats. The expression of CCL2/CCR2 protein was examined by western blot. Amorfrutins decreased the CCL2/CCR2 expression through the PPARγ activation.

is available on the use of PPARγ agonists for neuropathic pain treatment in humans, partly because the undesirable side effects of the key agonists, thiazolidinediones (TZDs). However, amorfrutins are natural PPARγ agonists, showing the anti-inflammatory effect in HFD mice without unwanted side effects [9]. In this study, our findings represent that PPARγ agonist amorfrutins attenuate mechanical hyperalgesia and thermal hyperalgesia in CCI rats. PPARγ antagonist GW9662 coadministration with amorfrutins blocked the role of Amor, indicating that amorfrutins alleviate neuropathic pain by activating PPARγ. These data suggest that amorfrutins may be a new drug therapy for neuropathic pain.

Chemokine expression is stimulated by inflammatory cytokines like TNFα and IL-1β. Researches have revelated the connection between chemokines and pain; the chemokine expression was upregulated in animal models and maintained for weeks [22]. In addition, the connection between PPAR and chemokines was also revealed in some studies. For example, in traumatic brain injury model, the CCL2 expression was significantly suppressed by TZDs [23]. 15d-PGJ2 and rosiglitazone also inhibited the CCL2 production in LPS-stimulated microglia [24]. Here, we found that cytokine (TNFα, IL-6, and IL-1β) and chemokine (CCL2/CCR2) expressions increased in the spinal cord of CCI rats.

Amorfrutins inhibited the production of these procytokines and chemokines, but GW9662 reversed the inhibitory effect of amorfrutins. The results illustrate that the PPARγ activation can reduce the inflammation and suppress the chemokine CCL2/CCR2 expression.

5. Conclusions

Collectively, our results demonstrate that the PPARγ agonist amorfruitins alleviate neuropathic pain in CCI rats, at least in part, via downregulating proinflammatory cytokines and chemokines CCL2/CCR2. This study may suggest a potential treatment option for neuropathic pain.

Data Availability

The data that support the findings of this study are available from the corresponding author upon reasonable request.

Conflicts of Interest

The authors confirm that there are no conflicts of interest.

Acknowledgments

We sincerely appreciate all lab members.

References

[1] R. D. Treede, T. S. Jensen, J. N. Campbell et al., "Neuropathic pain: redefinition and a grading system for clinical and research purposes," *Neurology*, vol. 70, no. 18, pp. 1630–1635, 2008.

[2] J. Gierthmuhlen and R. Baron, "Neuropathic pain," *Seminars in Neurology*, vol. 36, no. 5, pp. 462–468, 2016.

[3] L. Xu, Y. Zhang, and Y. Huang, "Advances in the treatment of neuropathic pain," *Advances in Experimental Medicine and Biology*, vol. 904, pp. 117–129, 2016.

[4] G. Moalem and D. J. Tracey, "Immune and inflammatory mechanisms in neuropathic pain," *Brain Research Reviews*, vol. 51, no. 2, pp. 240–264, 2006.

[5] J. Korbecki, R. Bobiński, and M. Dutka, "Self-regulation of the inflammatory response by peroxisome proliferator-activated receptors," *Inflammation research*, vol. 68, pp. 443–458, 2019.

[6] M. Ricote, A. C. Li, T. M. Willson, C. J. Kelly, and C. K. Glass, "The peroxisome proliferator-activated receptor-gamma is a negative regulator of macrophage activation," *Nature*, vol. 391, no. 6662, pp. 79–82, 1998.

[7] C. Jiang, A. T. Ting, and B. Seed, "PPAR-γ agonists inhibit production of monocyte inflammatory cytokines," *Nature*, vol. 391, no. 6662, pp. 82–86, 1998.

[8] L. Wang, B. Waltenberger, E. M. Pferschy-Wenzig et al., "Natural product agonists of peroxisome proliferator-activated receptor gamma (PPARγ): a review," *Biochemical Pharmacology*, vol. 92, no. 1, pp. 73–89, 2014.

[9] C. Weidner, J. C. de Groot, A. Prasad et al., "Amorfrutins are potent antidiabetic dietary natural products," *Proceedings of the National Academy of Sciences of the United States of America*, vol. 109, no. 19, pp. 7257–7262, 2012.

[10] I. F. Charo and R. M. Ransohoff, "The many roles of chemokines and chemokine receptors in inflammation," *The New England Journal of Medicine*, vol. 354, no. 6, pp. 610–621, 2006.

[11] F. A. White, S. K. Bhangoo, and R. J. Miller, "Chemokines: integrators of pain and inflammation," *Nature Reviews. Drug Discovery*, vol. 4, no. 10, pp. 834–844, 2005.

[12] S. B. Oh, P. B. Tran, S. E. Gillard, R. W. Hurley, D. L. Hammond, and R. J. Miller, "Chemokines and glycoprotein120 produce pain hypersensitivity by directly exciting primary nociceptive neurons," *The Journal of neuroscience : the official journal of the Society for Neuroscience*, vol. 21, no. 14, pp. 5027–5035, 2001.

[13] E. J. Leonard, A. Skeel, and T. Yoshimura, "Biological aspects of monocyte chemoattractant protein-1 (MCP-1)," *Advances in Experimental Medicine and Biology*, vol. 305, pp. 57–64, 1991.

[14] G. Banisadr, F. Quéraud-Lesaux, M. C. Boutterin et al., "Distribution, cellular localization and functional role of CCR2 chemokine receptors in adult rat brain," *Journal of Neurochemistry*, vol. 81, no. 2, pp. 257–269, 2002.

[15] C. Abbadie, J. A. Lindia, A. M. Cumiskey et al., "Impaired neuropathic pain responses in mice lacking the chemokine receptor CCR2," *Proceedings of the National Academy of Sciences of the United States of America*, vol. 100, no. 13, pp. 7947–7952, 2003.

[16] A. Flügel, G. Hager, A. Horvat et al., "Neuronal MCP-1 expression in response to remote nerve injury," *Journal of Cerebral Blood Flow & Metabolism*, vol. 21, no. 1, pp. 69–76, 2001.

[17] Y. Chen, S. R. Green, J. Ho, A. Li, F. Almazan, and O. Quehenberger, "The mouse CCR2 gene is regulated by two promoters that are responsive to plasma cholesterol and peroxisome proliferator-activated receptor gamma ligands," *Biochemical and Biophysical Research Communications*, vol. 332, no. 1, pp. 188–193, 2005.

[18] G. J. Bennett and Y. K. Xie, "A peripheral mononeuropathy in rat that produces disorders of pain sensation like those seen in man," *Pain*, vol. 33, no. 1, pp. 87–107, 1988.

[19] C. M. Freitag and R. J. Miller, "Peroxisome proliferator-activated receptor agonists modulate neuropathic pain: a link to chemokines?," *Frontiers in Cellular Neuroscience*, vol. 8, p. 238, 2014.

[20] C. Schifilliti, L. Cucinotta, V. Fedele, C. Ingegnosi, S. Luca, and C. Leotta, "Micronized palmitoylethanolamide reduces the symptoms of neuropathic pain in diabetic patients," *Pain Research and Treatment*, vol. 2014, Article ID 849623, 5 pages, 2014.

[21] D. J. Kopsky and J. M. Keppel Hesselink, "Multimodal stepped care approach with acupuncture and PPAR-α agonist palmitoylethanolamide in the treatment of a patient with multiple sclerosis and central neuropathic pain," *Acupuncture in Medicine*, vol. 30, no. 1, pp. 53–55, 2012.

[22] Z. J. Zhang, B. C. Jiang, and Y. J. Gao, "Chemokines in neuron-glial cell interaction and pathogenesis of neuropathic pain," *Cellular and Molecular Life Sciences*, vol. 74, no. 18, pp. 3275–3291, 2017.

[23] J. H. Yi, S. W. Park, N. Brooks, B. T. Lang, and R. Vemuganti, "PPARgamma agonist rosiglitazone is neuroprotective after traumatic brain injury via anti-inflammatory and anti-oxidative mechanisms," *Brain Research*, vol. 1244, pp. 164–172, 2008.

[24] P. D. Storer, J. Xu, J. Chavis, and P. D. Drew, "Peroxisome proliferator-activated receptor-gamma agonists inhibit the activation of microglia and astrocytes: implications for multiple sclerosis," *Journal of Neuroimmunology*, vol. 161, no. 1-2, pp. 113–122, 2005.

Hindawi
PPAR Research
Volume 2020, Article ID 6694214, 13 pages
https://doi.org/10.1155/2020/6694214

Research Article

Bergenin Attenuates Hepatic Fibrosis by Regulating Autophagy Mediated by the PPAR-γ/TGF-β Pathway

Yujing Xia, Jingjing Li, Kan Chen, Jiao Feng, and Chuanyong Guo

Department of Gastroenterology, Shanghai Tenth People's Hospital, School of Clinical Medicine of Nanjing Medical University, Shanghai 200072, China

Correspondence should be addressed to Chuanyong Guo; guochuanyong@hotmail.com

Received 14 October 2020; Revised 6 December 2020; Accepted 15 December 2020; Published 31 December 2020

Academic Editor: Ravinder K. Kaundal

Liver fibrosis is a pathological process involving diffuse extracellular matrix (ECM) deposition in the liver. It is typical of many chronic liver diseases, including cirrhosis, and effective drugs are needed. In this study, we explored the protective effect of bergenin on liver fibrosis induced by carbon tetrachloride and bile duct ligation. A variety of molecular biological methods (qRT-PCR, western blotting, and immunohistochemistry) were employed to confirm the increased degree of hepatocyte injury and ECM formation in the disease model, consistent with autophagy and activation of the TGF-β pathway. Bergenin activated PPAR-γ and inhibited TGF-β and autophagy and decreased liver fibrosis by inhibiting hepatocyte necrosis and ECM formation in a dose-dependent manner. The results suggest that bergenin may be a promising drug candidate for the treatment of liver fibrosis.

1. Introduction

Liver fibrosis is a pathophysiological process in which various pathogenic factors continually damage the liver, resulting in extracellular matrix (ECM) deposition and fibrous scar formation [1]. According to statistics, more than one million people worldwide die of end-stage liver disease caused by liver fibrosis every year [2]. Therefore, in recent years, experts in the field have explored treatments for liver diseases, especially liver fibrosis and cirrhosis. The consensus is that new drugs are needed to improve both diagnosis and treatment.

Peroxisome proliferator-activated receptor (PPAR) is a ligand-activated receptor belonging to the type II nuclear hormone receptor superfamily that includes PPAR-α, PPAR-β/δ, and PPAR-γ subtypes [3, 4]. PPAR-γ is a key transcription factor of cell differentiation, which is closely related to fibrosis in important organs [5, 6]. Stavniichuk et al. confirmed that dual soluble epoxide hydrolase inhibitors can reduce renal fibrosis by activating PPAR-γ, and the same effect was observed in heart and lung fibrosis [7–9]. In liver fibrosis, PPAR-γ is involved in hepatic stellate cell (HSC) activation and fibroblast transformation, which can reduce the overexpression of α-smooth muscle actin (α-SMA), type I collagen, and hydroxyproline in HSCs and thereby inhibit liver fibrosis [10–12].

Autophagy, an important form of programmed cell death, is a highly conserved degradation process mediated by lysosomes in eukaryotes. The autophagy-related gene LC3-II was significantly upregulated in a carbon tetrachloride- (CCl_4-) induced liver fibrosis model, and inhibition of autophagy activity could delay its progress. This may be because autophagy-mediated lipid degradation provides energy for HSC activation, thereby promoting ECM formation and the progression of liver fibrosis. However, PPAR-γ activation has been linked to autophagy [13, 14], but whether PPAR-γ plays an important role in the occurrence and development of liver fibrosis requires further investigation.

Existing liver fibrosis drugs acting at a single target are not particularly effective, and they cause unwanted side effects. Some active components of traditional Chinese medicines, such as procyanidin, crocin, astaxanthin, and fucoidan, are reported to exert strong antifibrosis effects [12, 15–17]. Some reportedly regulate adipocytokines, thereby reducing liver inflammation and lowering oxidative stress

[17, 18]. Bergenin is a natural secondary metabolite extracted from the roots, bark, and leaves of many families and genera of plants. Its pharmacological activities are diverse, and antitumour, antiviral, immune enhancement, wound repair, anticoagulant, analgesic, antitussive, antifungal, antiarrhythmic, antimalarial, and anti-inflammatory activities have been reported [19–23]. However, liver fibrosis activity has not been reported.

The etiology and mechanism of liver fibrosis are complex. Traditional Chinese medicines can inhibit the activation of HSCs and exert antifibrosis effects via different mechanisms. The aim of the present study was to explore the antifibrosis effect of bergenin and its action mechanism based on the successful establishment of a liver fibrosis model.

2. Materials and Methods

2.1. Establishment of a Hepatic Fibrosis Model. C57 mice weighing 20-25 g were purchased from Shanghai Experimental Animal Co., Ltd. (Shanghai, China). They were reared at 25°C under a 12 h light/12 h dark cycle. All mice were allowed free access to food and water. The CCl_4-induced liver fibrosis model was established by intraperitoneal injection of 1 mL/kg body weight CCl_4 (1 : 10 *v*/*v*; Sigma-Aldrich, St. Louis, MO, USA) in olive oil twice a week for 8 weeks [15]. In the BDL model, C57 mice were fasted for 12 h, injected intraperitoneally with 1.25% Nembutal (Sigma-Aldrich), anesthetised, and disinfected. Skin and muscle were removed layer by layer from the midline of the abdomen and ~1 cm above the perineum. The transparent bile duct accompanying the portal vein was found in the hilar region, and two 6-0 surgical sutures were embedded, and surgical knots were made. After confirming that there was no visceral injury or bleeding in the abdominal cavity, the abdomen was closed layer by layer and disinfected again. Mice were resuscitated in a dry and warm environment [24]. All animal experiments were carried out according to, and approved by, the Animal Care and Use Committee of Nanjing Medical University.

2.2. Reagents and Experiment Design. Bergenin (CAS: 477-90-7, purity ≥ 98.0%) was purchased from Sigma-Aldrich and dissolved in physiological saline. Primary antibodies α-SMA, CoI-I, TIMP1, LC3-I/II, Beclin-1, and β-actin were acquired from Proteintech Group (Chicago, IL, USA), and PPAR-γ, RXR-α, TGF-β1, Smad2, Smad3, and p-Smad2/3 were from Cell Signaling Technology (Danvers, MA, USA). SYBR Premix Ex Taq was purchased from TaKaRa Biotechnology (Dalian, China).

A total of 64 mice were randomly divided into the CCl_4 model group and the BDL model group, and serum and liver tissue samples were obtained as follows:

Sham operation group (sham, $n = 8$): intragastric administration of normal saline.

Model group (CCl_4 or BDL, $n = 8$): model established as above.

Low dose group (CCl_4/BDL+B20, $n = 8$): daily gavage, bergenin (20 mg/kg).

High dose group (CCl_4/BDL+B40, $n = 8$): daily gavage, bergenin (40 mg/kg).

Table 1: Nucleotide sequences of primers used for qRT-PCR.

Gene		Primer sequence (5′-3′)
LC3-II	Forward	GACCGCTGTAAGGAGGTGC
	Reverse	AGAAGCCGAAGGTTTCTTGGG
Beclin-1	Forward	ATGGAGGGGTCTAAGGCGTC
	Reverse	TGGGCTGTGGTAAGTAATGGA
TIMP-1	Forward	CGAGACCACCTTATACCAGCG
	Reverse	ATGACTGGGGTGTAGGCGTA
α-SMA	Forward	CCCAGACATCAGGGAGTAATGG
	Reverse	TCTATCGGATACTTCAGCGTCA
TGF-β1	Forward	CCCCTGCAAGACCATCGAC
	Reverse	CTGGCGAGCCTTAGTTTGGAC
CoI-1α1	Forward	CAATGGCACGGCTGTGTGCG
	Reverse	AGCACTCGCCCTCCCGTCTT
PPAR-γ	Forward	GGAAGACCACTGCATTCCTT
	Reverse	GTAATCAGCAACCATTGGGTCA
β-Actin	Forward	CTGGAACGGTGAAGGTGACA
	Reverse	AAGGGACTTCCTGTAACAATGCA

2.3. Assessment of Liver Function. Serum alanine aminotransferase (ALT), aspartate aminotransferase (AST), and hydroxyproline were determined using an Olympus AU1000 Automatic Chemical Analyzer (Olympus Corporation, Tokyo, Japan) in the hospital laboratory.

2.4. Pathological Evaluation. Liver tissue was used to prepare paraffin sections that were stained with hematoxylin and eosin (HE) according to the manufacturer's instructions. HE staining solution is alkaline, which stains chromatin and nucleic acid in the nucleus purple/blue, and eosin is an acidic dye, which stains components in the cytoplasm and extracellular matrix red, thereby revealing cell necrosis. In addition, Masson staining was used to probe the degree of fibrosis. Collagen fibers stain blue, and muscle fibers stain red, revealing fibers and inflammatory factors in tissues.

2.5. Quantitative Real-Time PCR. Total RNA was extracted from freeze-dried tissue and analysed for purity and concentration. RNA was reverse-transcribed into cDNA and stored at -20°C. Each 20 μL reaction included a predenaturation step at 93°C for 2 min, followed by 40 cycles of 1 min at 93°C, 1 min at 55°C, and 1 min at 72°C, and a final extension at 72°C for 7 min. Expression levels of target genes were determined relative to β-actin. The sequences of primers used in the experiment are shown in Table 1.

2.6. Western Blotting. Total protein was extracted from tissues, quantified by bicinchoninic acid protein assay (Kaiji, China), mixed with 5x loading buffer, and stored at -20°C. Based on the protein molecular weight, proteins were separated by sodium dodecyl sulphate-polyacrylamide gel electrophoresis (SDS-PAGE) at 80 V using appropriate gels.

When the sample reached the lower layer of the gel, the voltage was changed to 120 V, and electrophoresis was stopped when the bromophenol blue indicator reached the bottom of the separating gel. Proteins were transferred to a polyvinylidene fluoride (PVDF) membrane at 200 mA, then incubated on a decolourising shaker at room temperature for 1 h. The PVDF membrane was incubated overnight at 4°C with primary antibodies diluted in phosphate-buffered saline (PBS) containing Tween (PBST). After washing with fresh PBST, the membrane was incubated in the secondary antibody solution for 1 h, then quickly rinsed. An Odyssey Two-colour Infrared Laser Imaging System (LI-COR Biosciences, Lincoln, NE, USA) was used to scan and image the membranes. The quantitative evaluation was determined by relative band density.

2.7. Immunohistochemical Staining. The prepared paraffin sections were placed in a 60°C incubator and incubated for 120 min. After a series of dewaxing and hydration treatments, they were incubated at room temperature with 3% H_2O_2 for 10 min to eliminate endogenous peroxidase activity. After washing with distilled water to elicit antigen repair, the slices were placed in a container containing PBS and heated in a microwave oven for 15 min to keep the liquid temperature in the container between 92°C and 98°C, then cooled at room temperature for 20 min. After blocking, samples were incubated again at room temperature for 15 min. The working solution of the first antibody was added dropwise overnight at 4°C. After adding the second antibody, samples were washed and stained with DAB. After staining with HE and mixing with hydrochloric acid and alcohol, samples were dehydrated until transparent, sealed with neutral resin and a cover glass, and visualised under a light microscope, revealing the target molecules as yellow particles.

2.8. Electron Microscopy. Fresh liver tissues were fixed with 3% glutaraldehyde, incubated with 0.2 mM calcium carbonate buffer for 4 h, and then fixed with 1% osmium tetroxide for 1 h. Samples were dehydrated using a series of ethanol solutions, soaked with epoxy resin, and sliced. Autophagy was observed using a JEM-1230 electron microscope (JEOL, Tokyo, Japan).

2.9. Statistical Analysis. SPSS 22.0 software (IBM Corporation, Armonk, NY, USA) was used for statistical analysis. Data were compared as means ± standard deviation calculated by Student-Newman-Keuls tests and one-way analysis of variance (ANOVA). A p value < 0.05 was considered statistically significant.

3. Results

3.1. Bergenin Significantly Decreases Liver Fibrosis. Liver enzymes and hydroxyproline are important indicators that reflect the severity of liver fibrosis; hence, serum and pathological examination was carried out to evaluate the effects of the drug. The results showed that levels of ALT and AST in the CCl_4 and BDL groups were increased, while levels of liver enzymes in drug treatment groups were significantly decreased, and the effect was more obvious with an increasing dose (Figure 1(a)). In accordance with the levels of liver enzymes, hydroxyproline was increased in the disease model groups, while bergenin treatment significantly reduced hydroxyproline levels (Figure 1(a)). HE staining revealed degeneration and necrosis of hepatocytes and proliferation of connective tissue in the disease model groups, and inflammatory cell infiltration was observed in some areas. Additionally, numerous blue collagen fibers were observed by Masson staining. Compared with the disease model groups, necrosis was improved in the drug groups, and the quantity of collagen fibers was decreased in a dose-dependent manner (Figure 1(b)). These results suggest that bergenin can effectively decrease levels of liver enzymes and alleviate liver fibrosis.

3.2. Bergenin Inhibits the Formation of Extracellular Matrix. The main components of ECM are hyaluronic acid (HA), fibronectin (FN), laminin (LN), type I collagen (CoI-I), α-SMA, matrix metalloproteinases (MMPs), and tissue inhibitors of metalloproteinases (TIMPs). The results showed that levels of HA and LN in the disease model groups were significantly increased, while those in the bergenin groups were significantly decreased, and the effect was proportional to the drug concentration (Figure 2(a)). Furthermore, we used molecular biological methods to measure levels of α-SMA, CoI-I, and TIMP1. At the transcriptional level, all were significantly increased in the CCl_4 and BDL model groups, while high concentrations of bergenin downregulated the expression of these markers (Figures 2(b) and 2(c)). Similarly, the results of immunohistochemistry were consistent with the observed serum levels (Figure 2(d)). These results suggest that bergenin inhibits ECM depositions and thereby prevents liver fibrosis.

3.3. Bergenin Decreases Autophagy by Downregulating Beclin-1 and LC-3. Autophagy involves the phagocytosis of cytoplasmic proteins and organelles, their inclusion into vesicles, and fusion with lysosomes to form autophagic lysosomes, which provides energy for the activation of HSCs. The main proteins involved are LC-3II, Beclin-1, and p62. The results showed that mRNA levels of autophagy-related genes LC-3II and Beclin-1 in liver fibrosis model groups were significantly increased, while those in bergenin treatment groups were decreased in a dose-dependent manner (Figure 3(a)). In addition, western blotting and immunohistochemistry were used to measure the expression levels of tissue proteins, and the results were consistent with the gene transcription levels (Figure 3(b) and 3(c)). In the model group, more Beclin-1 and LC3-II proteins were stained with brown yellow particles by DAB compared with the sham group, while the positive area of the drug treatment group decreased with the increase of concentration. Electron microscopy was performed to observe autophagy directly, and the results showed that the number of autophagosomes was increased significantly in the disease model groups, but not in the drug groups (Figure 3(d)). In summary, bergenin could effectively reduce the levels of autophagy and block the energy supply needed for HSC activation.

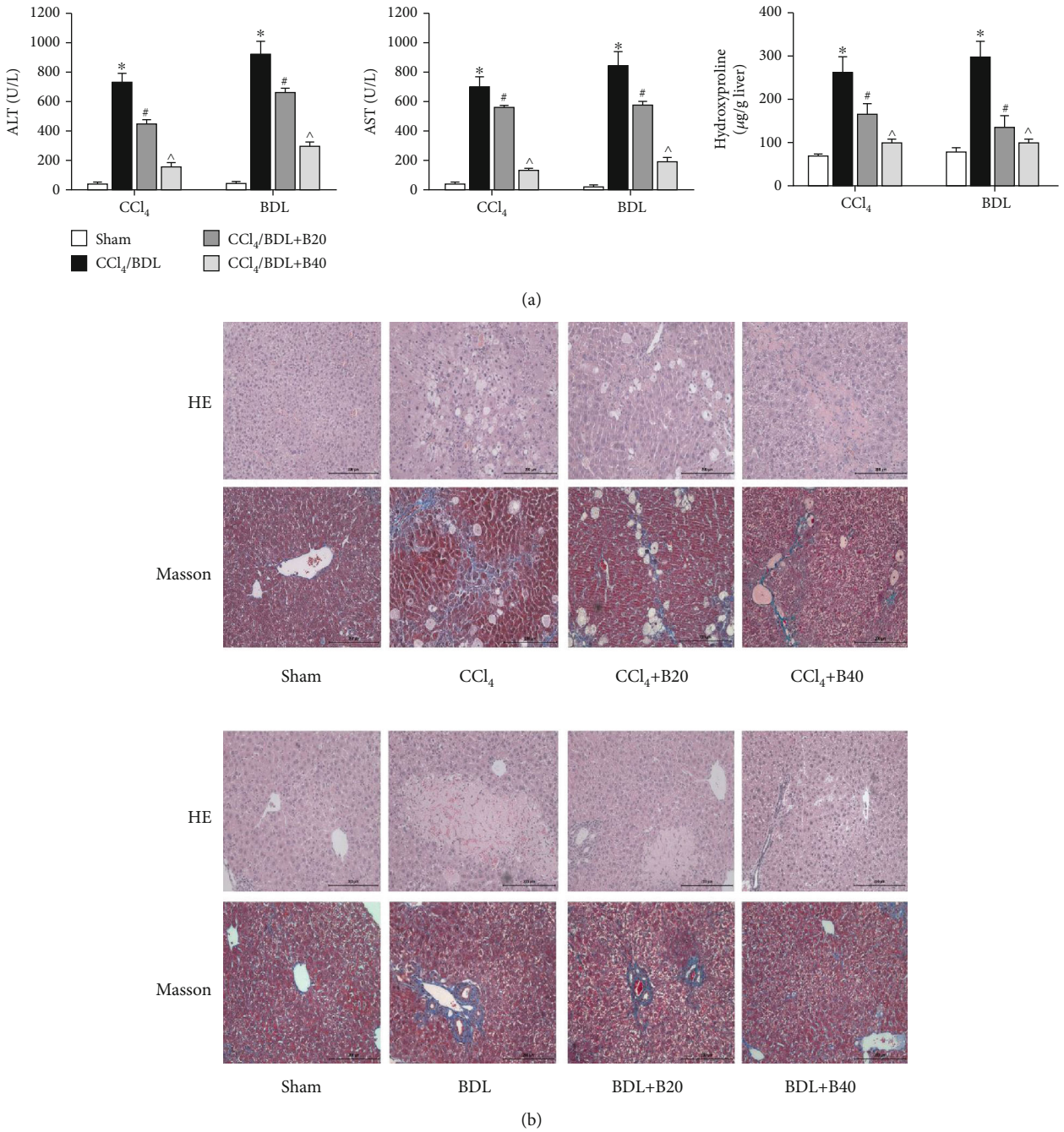

Figure 1: Bergenin significantly decreases liver fibrosis. (a) Levels of serum ALT and AST expressed as the mean ± SD ($n = 8$). (b) HE and Masson staining of liver sections (original magnification = 200x).

3.4. Bergenin Inhibits the TGF-β1/Smads Pathway by Activating PPAR-γ. TGF-β1 mediates necrosis and autophagy by activating phosphorylated Smads in the nuclear region. PPAR-γ is a key molecule regulating TGF-β1, which is known to be inhibited by bergenin. In order to clarify the mechanism of action of the drug, we analysed gene and protein expression levels of related pathways. The results showed that expression of PPAR-γ was decreased in the liver fibrosis model, but the expression was stimulated by the drug. However, TGF-β1, active Smad2, and Smad3 displayed the opposite trend (Figures 4(a) and 4(b)). Based on the consistent expression of total Smad2 and Smad3, levels of TGF-β1 and phosphorylated Smad2 and Smad3 were upregulated in the liver fibrosis model, but decreased in the drug group, and the differences were statistically significant. Immunohistochemical staining was also used to elucidate the changes in the expression of pathway molecules. In the model group, the brown granules in the nucleus of PPAR-γ were significantly decreased but were upregulated in the drug treatment group. On the contrary, more TGF-β1 proteins were stained by DAB into brown granules compared with the sham group, while the yellow area of the drug treatment group showed a

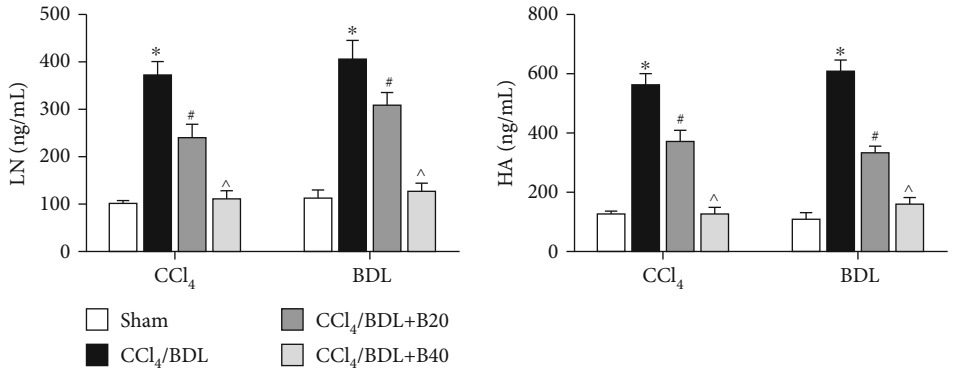

(a)

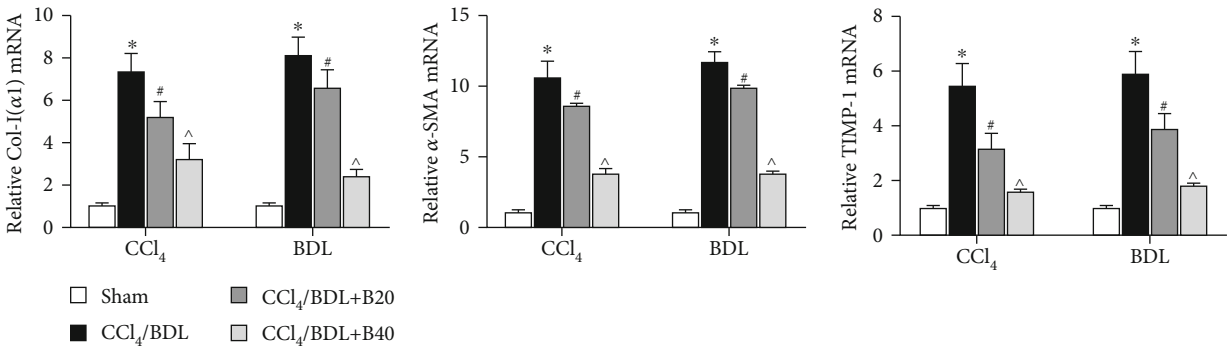

(b)

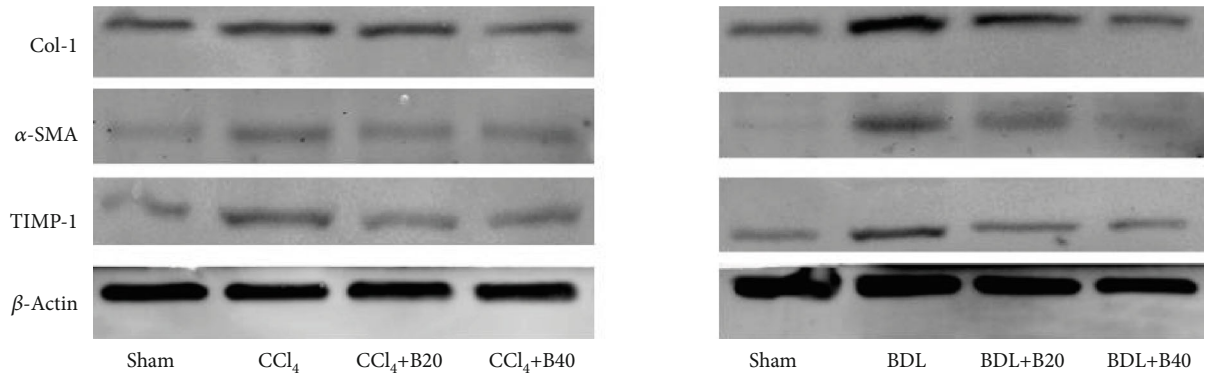

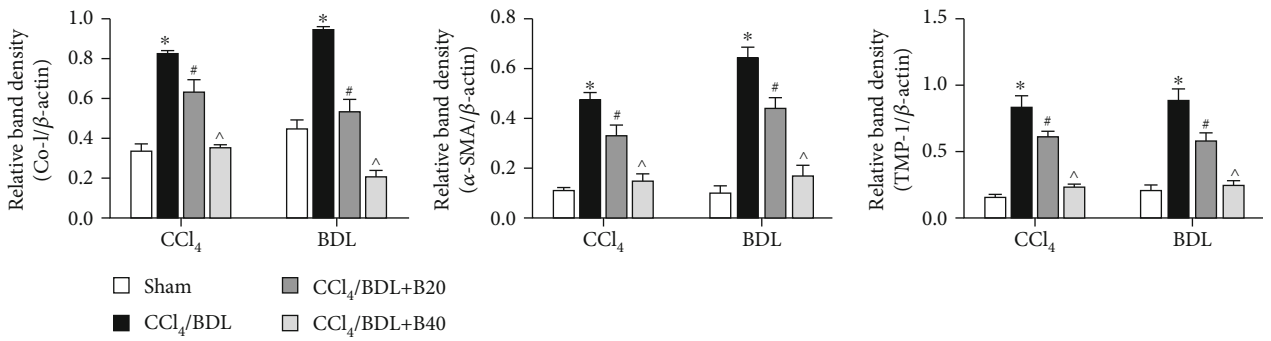

(c)

Figure 2: Continued.

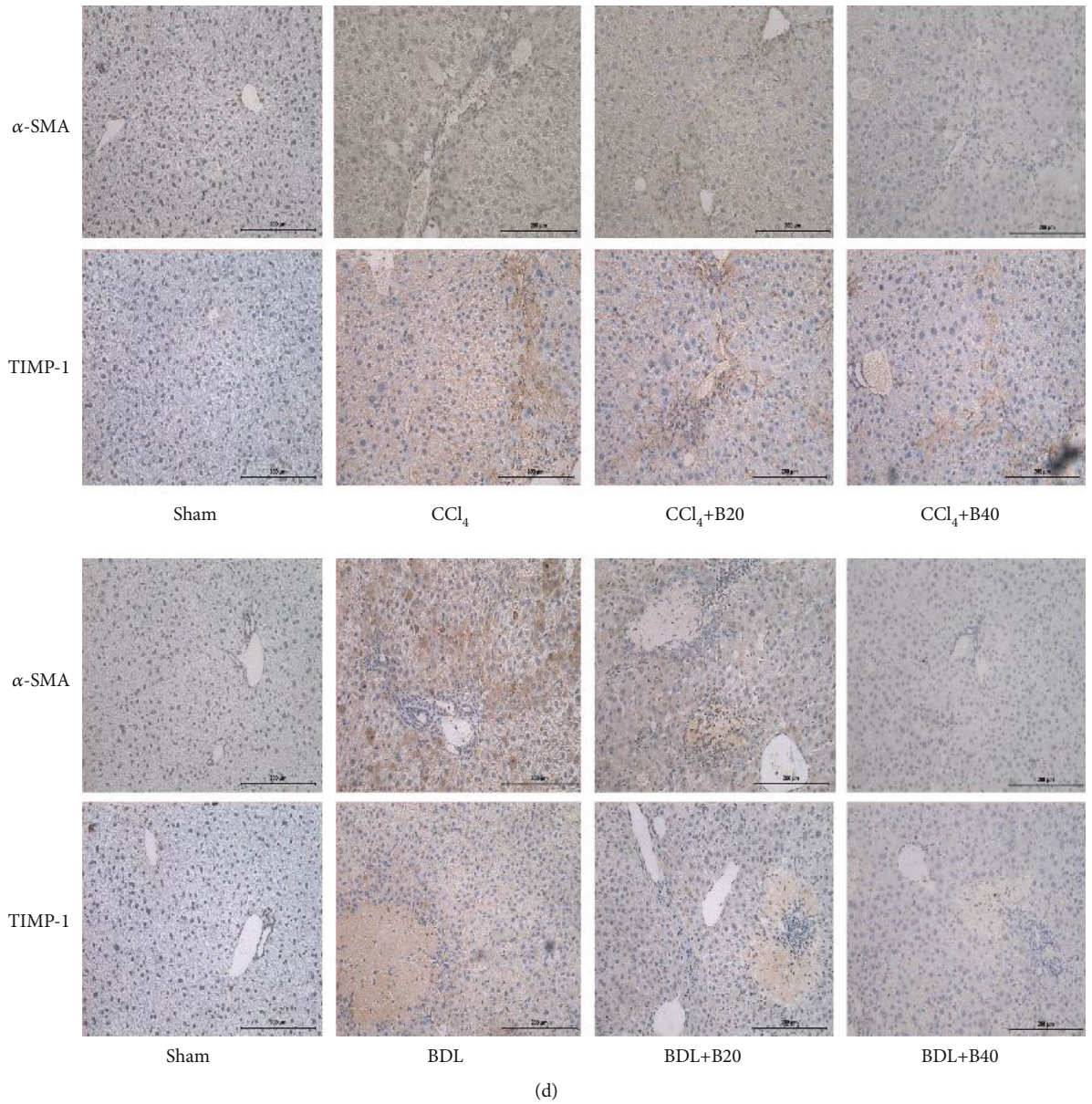

Figure 2: Bergenin inhibits the formation of the extracellular matrix. (a) Levels of serum HA and LN expressed as the mean ± SD ($n = 8$). (b) mRNA expression of collagen I, α-SMA, and TIMP1 assessed by real-time PCR ($n = 8$). (c) Protein expression of collagen I, α-SMA, and TIMP1 assessed by western blotting. The quantitative evaluation was determined by relative band density. (d) Immunohistochemical staining of α-SMA and TIMP1 (original magnification = 200x). $^{*}p < 0.05$ for CCl_4/BDL vs. sham, $^{\#}p < 0.05$ for CCl_4/BDL+B20 vs. CCl_4/BDL, and $^{\wedge}p < 0.05$ for CCl_4/BDL+B40 vs. CCl_4/BDL+B20.

downward trend (Figure 4(c)). These results suggest that bergenin can inhibit the TGF-β1/Smads pathway by activating PPAR-γ, thereby halting the progression of autophagy in liver fibrosis.

4. Discussion

Modern medicine has shown that liver fibrosis is a dynamic process. However, whether this process is progressive or related to the presence of liver injury factors and whether liver injury lesions continue to develop remain unknown. Research on liver fibrosis has recently entered a new era. Great progress has been made in understanding liver fibrosis and drug-targeted therapy [1, 25]. Natural plant extracts have been shown to exert strong biological effects, and bergenin is effective for decreasing fibrosis in various organs. Herein, we explored the protective effects of bergenin on the liver.

CCl_4 is one of the most widely used chemical toxicants to induce liver fibrosis and cirrhosis in experimental animals. In the endoplasmic reticulum of hepatocytes, free radicals produced by CCl_4 can bind covalently to macromolecules in hepatocytes after being activated by cytochrome P450 oxidase in liver microsomes, which leads to the production of reactive oxygen species and lipid peroxidation, resulting in

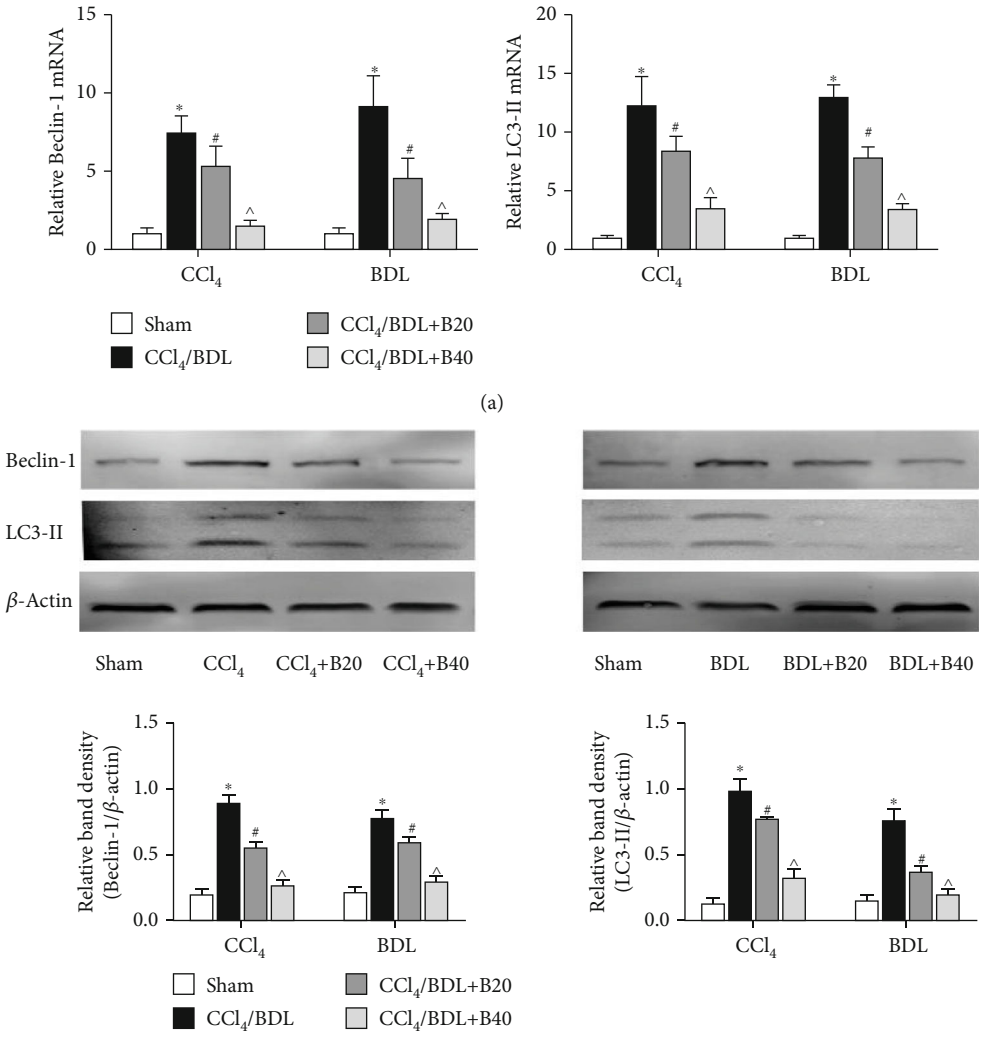

Figure 3: Continued.

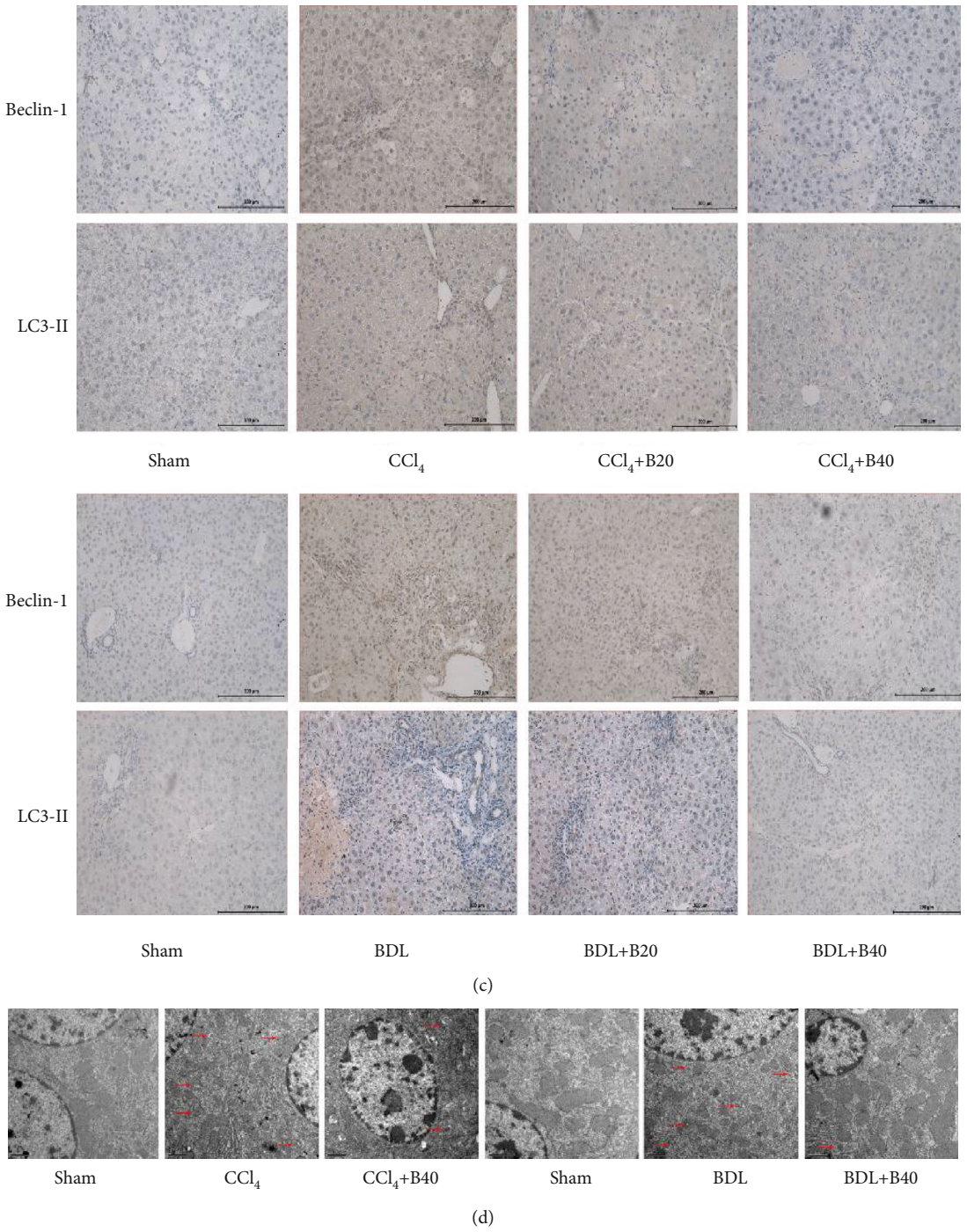

Figure 3: Bergenin decreases autophagy by downregulating Beclin-1 and LC-3. (a) mRNA expression of Beclin-1 and LC3-II assessed by real-time PCR ($n = 8$). (b) Protein expression of Beclin-1 and LC3-II assessed by western blotting. The quantitative evaluation was determined by relative band density. (c) Immunohistochemical staining of Beclin-1 and LC3-II (original magnification = 200x). (d) The amount of autophagosome significantly decreased as showed by TEM (original magnification: ×10000). $^{*}p < 0.05$ for CCl_4/BDL vs. sham, $^{\#}p < 0.05$ for CCl_4/BDL+B20 vs. CCl_4/BDL, and $^{\wedge}p < 0.05$ for CCl_4/BDL+B40 vs. CCl_4/BDL+B20.

liver fibrosis [26]. By contrast, the BDL model is characterised by cholestasis and inflammation due to blockage of the extrahepatic biliary system, leading to a strong fibrosis reaction around the portal vein. The two models complement each other and are used to comprehensively evaluate the effects of drugs.

First, we explored the effects of the drug on liver function and quantitatively evaluated liver function and the degree of liver fibrosis based on ALT, AST, and hydroxyproline. The results showed that liver enzymes and hydroxyproline were increased in the serum of the liver fibrosis model, while the drug effectively reduced the levels of these indicators,

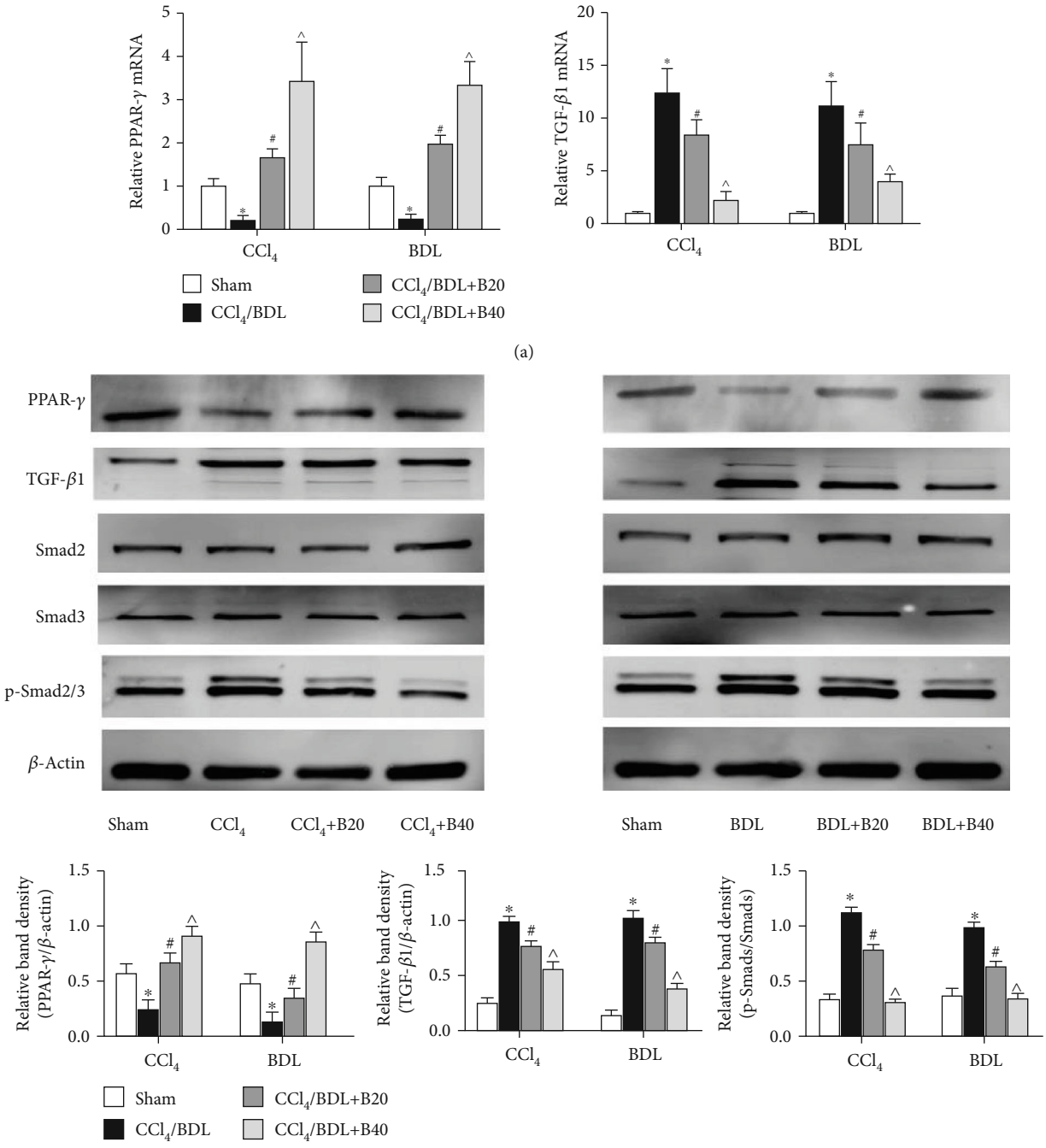

Figure 4: Continued.

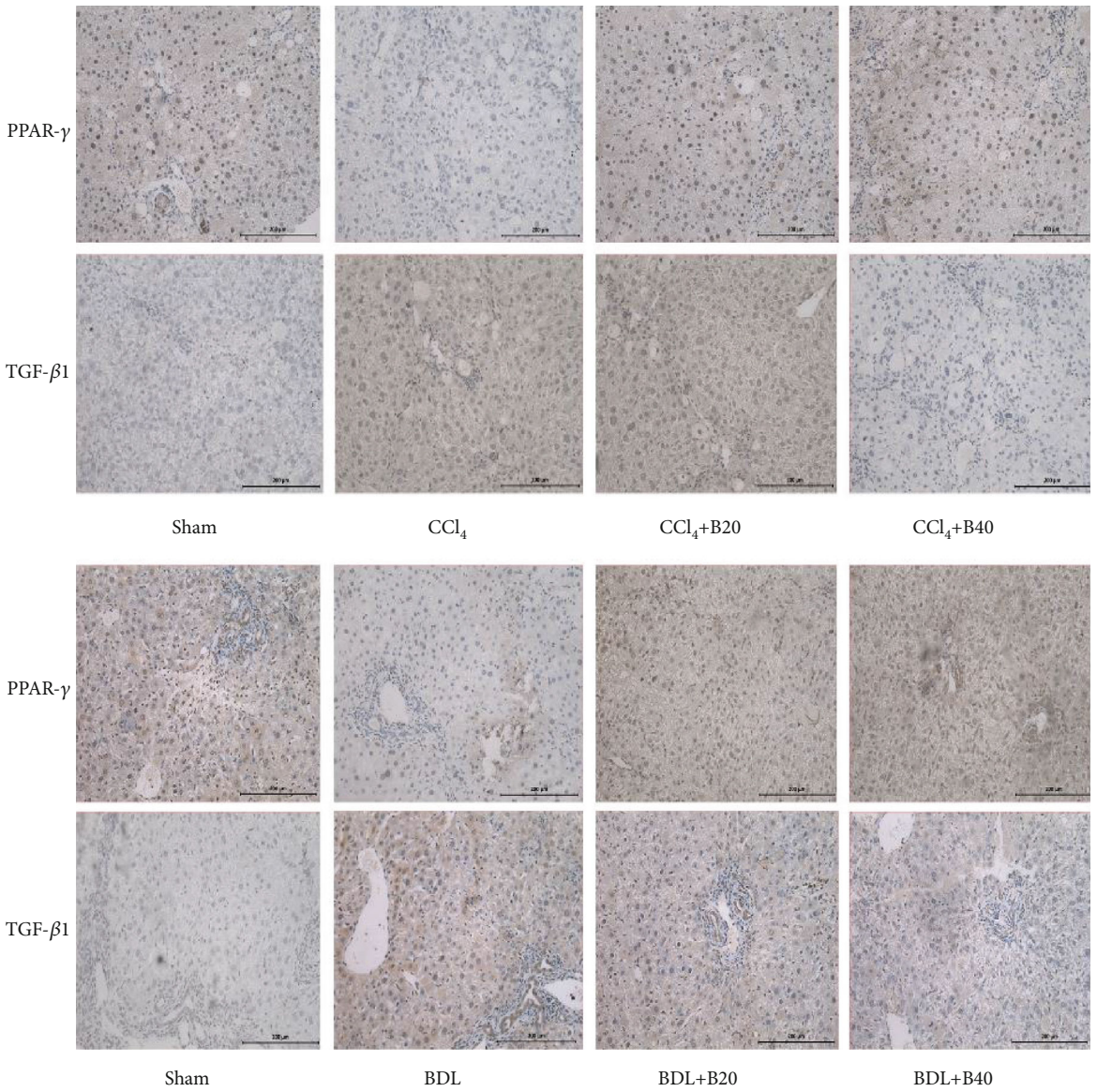

Figure 4: Bergenin inhibits the TGF-β1/Smads pathway by activating PPAR-γ. (a) mRNA expression of PPAR-γ and TGF-β1 assessed by real-time PCR ($n = 8$). (b) Protein expression of PPAR-γ and TGF-β1 assessed by western blotting. The quantitative evaluation was determined by relative band density. (c) Immunohistochemical staining of PPAR-γ and TGF-β1 (original magnification = 200x). $^{*}p < 0.05$ for CCl_4/BDL vs. sham, $^{\#}p < 0.05$ for CCl_4/BDL+B20 vs. CCl_4/BDL, and $^{\wedge}p < 0.05$ for CCl_4/BDL+B40 vs. CCl_4/BDL+B20.

suggesting that bergenin could effectively inhibit the release of ALT and AST and reduce the production of collagen.

Pathological staining of hepatocyte necrosis and Masson staining of collagen formation directly reflected the effectiveness of the drug, consistent with previous studies [13]. Furthermore, activation of HSCs, phenotypic changes, and ECM deposition are the central links in the occurrence of liver fibrosis [1]. Therefore, it is of great significance to study ECM components when evaluating the severity of liver fibrosis. Our results showed that bergenin decreased levels of α-SMA, CoI-I, MMP2, and TIMP1. Therefore, bergenin may protect hepatocytes from hepatic fibrosis and inhibit the formation of key components of ECM in serum and tissues, thereby inhibiting the process of liver fibrosis.

Autophagy involves phagocytosis of cytoplasmic proteins and organelles, their inclusion into vesicles, and fusion with lysosomes to form autophagic lysosomes, which degrade their contents [27, 28]. Studies have shown that when HSCs are activated, autophagy increases to provide energy to promote the secretion of ECM components [29]. One study demonstrated that miR-96-5p inhibits the activation of HSCs by regulating ATG7 to block autophagy [30], and another demonstrated that fucoidan can inhibit ECM deposition and autophagy in liver fibrosis [15]. Therefore, if autophagy can be effectively inhibited, liver fibrosis may be inhibited to some extent. Beclin-1 and LC3-II are markers of autophagy that are increased significantly during liver fibrosis, and bergenin effectively reduced their levels in the present work.

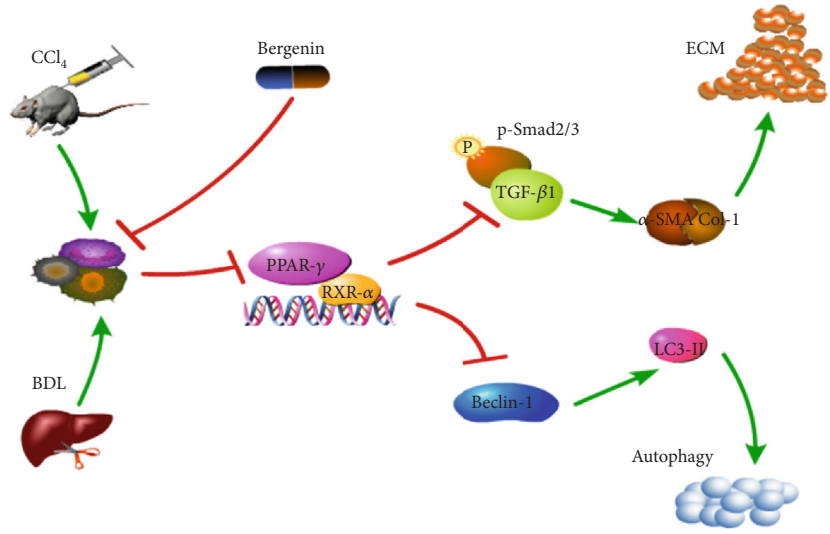

Figure 5: Mechanism of action of bergenin in liver fibrosis. The expression of PPAR-γ and RXR-α was increased, and the TGF-β pathway was inhibited following treatment with bergenin. The Smad2/3 that act downstream were not activated by phosphorylation and transported into the nucleus. Furthermore, Beclin-1 could not be bound to promote transcription, which reduced the likelihood of LC3-I to LC3-II transformation, which decreased fibrosis due to a lack of energy supply for HSC activation.

By contrast, expression of P62 was higher when autophagy was decreased and lower when autophagy was increased. Therefore, bergenin increased the expression level of P62 in tissues. These results are consistent with previous findings showing that inhibition of autophagy can significantly inhibit liver fibrosis.

PPAR-γ is a member of the nuclear transcription factor superfamily and can form a heterodimer with retinol X receptor (RXR) to regulate the expression of related genes [31, 32]. The TGF-β/Smads pathway is important in the process of liver fibrosis and can be regulated by PPAR-γ. Various drugs can inhibit TGF-β production by activating PPAR-γ during fibrosis in different tissues [33, 34]. PPAR-γ binds directly to Smad3 and inhibits the expression of connective tissue growth factor (CTGF) induced by TGF-β in smooth muscle cells [35].

We also measured the expression of PPAR-γ and members of the TGF-β/Smads pathway in both disease model and drug treatment groups. The results showed that expression of PPAR-γ and RXR was increased to varying degrees following treatment with bergenin, which indicates that it might be a potential activator of PPAR-γ, similar to rosiglitazone and 15d-PGJ2 [36–39]. In the drug treatment group, the TGF-β pathway was inhibited, and Smad2/3 that act downstream were not activated by phosphorylation and transported into the nucleus. Furthermore, the specific DNA sequence of Beclin-1 could not be bound to promote transcription, which reduced the likelihood of LC3-I to LC3-II transformation, resulting in P62 accumulation and blockage of autophagy, which decreased fibrosis due to a lack of energy supply for HSC activation (Figure 5).

In conclusion, bergenin inhibits autophagy and blocks the energy supply required for HSC activation, thereby decreasing ECM formation and hepatocyte damage, which may affect the PPAR-γ/TGF-β/Smads axis. These findings establish bergenin as a potentially promising drug for the treatment of liver fibrosis.

Data Availability

All data can be found in the study.

Conflicts of Interest

The authors declare that there is no conflict of interest regarding the publication of this paper.

Acknowledgments

This work was funded by the Chinese Foundation for Hepatitis Prevention and Control WBN liver Disease Research Fund, grant number CFHPC2019031, and Innovation Plan of Health System of Science and Technology Commission of Putuo District, Shanghai, grant number ptkwws201901.

References

[1] S. Mahdinloo, S. H. Kiaie, A. Amiri, S. Hemmati, H. Valizadeh, and P. Zakeri-Milani, "Efficient drug and gene delivery to liver fibrosis: rationale, recent advances, and perspectives," *Acta Pharmaceutica Sinica B*, vol. 10, no. 7, pp. 1279–1293, 2020.

[2] T. H. Schwantes-An, R. Darlay, P. Mathurin et al., "Genome-wide association study and meta-analysis on alcohol-related liver cirrhosis identifies novel genetic risk factors," *Hepatology*, 2020.

[3] V. Trümper, I. Wittig, J. Heidler, F. Richter, B. Brüne, and A. von Knethen, "Redox regulation of PPARgamma in polarized macrophages," *PPAR Research*, vol. 2020, Article ID 8253831, 16 pages, 2020.

[4] J. Cordoba-Chacon, "Loss of hepatocyte-specific PPARgamma expression ameliorates early events of steatohepatitis in mice fed the methionine and choline-deficient diet," *PPAR Research*, vol. 2020, Article ID 9735083, 13 pages, 2020.

[5] Š. Tajnšek, D. Petrovič, M. G. Petrovič, and T. Kunej, "Association of peroxisome proliferator-activated receptors (PPARs)

with diabetic retinopathy in human and animal models: analysis of the literature and genome browsers," *PPAR Research*, vol. 2020, Article ID 1783564, 8 pages, 2020.

[6] Y. O. Yemchenko, V. I. Shynkevych, K. Y. Ishcheikin, and I. P. Kaidashev, "PPAR-gamma agonist pioglitazone reduced CD68+ but not CD163+ macrophage dermal infiltration in obese psoriatic patients," *PPAR Research*, vol. 2020, Article ID 4548012, 6 pages, 2020.

[7] H. Zhang, L. You, and M. Zhao, "Rosiglitazone attenuates paraquat-induced lung fibrosis in rats in a PPAR gamma-dependent manner," *European Journal of Pharmacology*, vol. 851, pp. 133–143, 2019.

[8] C. Liu, S. T. Lim, M. H. Y. Teo et al., "Collaborative regulation of LRG1 by TGF-β1 and PPAR-β/δ modulates chronic pressure overload-induced cardiac fibrosis," *Circulation. Heart Failure*, vol. 12, no. 12, article e005962, 2019.

[9] A. Stavniichuk, M. A. Hye Khan, M. M. Yeboah et al., "Dual soluble epoxide hydrolase inhibitor/PPAR-γ agonist attenuates renal fibrosis," *Prostaglandins & Other Lipid Mediators*, vol. 150, p. 106472, 2020.

[10] C. Panebianco, J. A. Oben, M. Vinciguerra, and V. Pazienza, "Senescence in hepatic stellate cells as a mechanism of liver fibrosis reversal: a putative synergy between retinoic acid and PPAR-gamma signalings," *Clinical and Experimental Medicine*, vol. 17, no. 3, pp. 269–280, 2017.

[11] M. N. Makled, M. H. Sharawy, and M. S. El-Awady, "The dual PPAR-α/γ agonist saroglitazar ameliorates thioacetamide-induced liver fibrosis in rats through regulating leptin," *Naunyn-Schmiedeberg's Archives of Pharmacology*, vol. 392, no. 12, pp. 1569–1576, 2019.

[12] J. Chhimwal, S. Sharma, P. Kulurkar, and V. Patial, "Crocin attenuates CCl4-induced liver fibrosis via PPAR-γ mediated modulation of inflammation and fibrogenesis in rats," *Human & Experimental Toxicology*, vol. 39, no. 12, pp. 1639–1649, 2020.

[13] S. Xiang, K. Chen, L. Xu, T. Wang, and C. Guo, "Bergenin exerts hepatoprotective effects by inhibiting the release of inflammatory factors, apoptosis and autophagy via the PPAR-γ pathway," *Drug Design, Development and Therapy*, vol. 14, pp. 129–143, 2020.

[14] W. Wang, C. Li, Z. Zhang, and Y. Zhang, "Arsenic trioxide in synergy with vitamin D rescues the defective VDR-PPAR-gamma functional module of autophagy in rheumatoid arthritis," *PPAR Research*, vol. 2019, Article ID 6403504, 11 pages, 2019.

[15] C. Guo, J. Li, K. Chen et al., "Protective effect of fucoidan from Fucus vesiculosus on liver fibrosis via the TGF-beta 1/Smad pathway-mediated inhibition of extracellular matrix and autophagy," *Drug Design, Development and Therapy*, vol. 10, pp. 619–630, 2016.

[16] L. Wu, Q. Zhang, W. Mo et al., "Quercetin prevents hepatic fibrosis by inhibiting hepatic stellate cell activation and reducing autophagy via the TGF-β1/Smads and PI3K/Akt pathways," *Scientific Reports*, vol. 7, no. 1, p. 9289, 2017.

[17] J. Feng, C. Wang, T. Liu et al., "Procyanidin B2 inhibits the activation of hepatic stellate cells and angiogenesis via the Hedgehog pathway during liver fibrosis," *Journal of Cellular and Molecular Medicine*, vol. 23, no. 9, pp. 6479–6493, 2019.

[18] T. Liu, L. Xu, C. Wang et al., "Alleviation of hepatic fibrosis and autophagy via inhibition of transforming growth factor-β1/Smads pathway through shikonin," *Journal of Gastroenterology and Hepatology*, vol. 34, no. 1, pp. 263–276, 2019.

[19] C. F. Villarreal, D. S. Santos, P. S. S. Lauria et al., "Bergenin reduces experimental painful diabetic neuropathy by restoring redox and immune homeostasis in the nervous system," *International Journal of Molecular Sciences*, vol. 21, no. 14, 2020.

[20] Y. Ren, M. Shen, Y. Ding et al., "Study on preparation and controlled release in vitro of bergenin-amino polylactic acid polymer," *International Journal of Biological Macromolecules*, vol. 153, pp. 650–660, 2020.

[21] Y. Ji, D. Wang, B. Zhang, and H. Lu, "Bergenin ameliorates MPTP-induced Parkinson's disease by activating PI3K/Akt signaling pathway," *Journal of Alzheimer's Disease*, vol. 72, no. 3, pp. 823–833, 2019.

[22] J. Feng, W. Dai, Y. Mao et al., "Simvastatin re-sensitizes hepatocellular carcinoma cells to sorafenib by inhibiting HIF-1α/PPAR-γ/PKM2-mediated glycolysis," *Journal of experimental & clinical cancer research: CR*, vol. 39, no. 1, p. 24, 2020.

[23] M. Chen, C. Chen, Y. Gao et al., "Bergenin-activated SIRT1 inhibits TNF-α-induced proinflammatory response by blocking the NF-κB signaling pathway," *Pulmonary Pharmacology & Therapeutics*, vol. 62, p. 101921, 2020.

[24] C. G. Tag, S. Sauer-Lehnen, S. Weiskirchen et al., "Bile duct ligation in mice: induction of inflammatory liver injury and fibrosis by obstructive cholestasis," *Journal of Visualized Experiments*, 2015.

[25] K. Grat, M. Grat, and O. Rowinski, "Usefulness of different imaging modalities in evaluation of patients with non-alcoholic fatty liver disease," *Biomedicines*, vol. 8, no. 9, 2020.

[26] G. K. Michalopoulos, "Hepatostat: liver regeneration and normal liver tissue maintenance," *Hepatology*, vol. 65, no. 4, pp. 1384–1392, 2017.

[27] L. Galluzzi, J. M. Bravo-San Pedro, B. Levine, D. R. Green, and G. Kroemer, "Pharmacological modulation of autophagy: therapeutic potential and persisting obstacles," *Nature Reviews. Drug Discovery*, vol. 16, no. 7, pp. 487–511, 2017.

[28] M. Antonioli, M. Di Rienzo, M. Piacentini, and G. M. Fimia, "Emerging mechanisms in initiating and terminating autophagy," *Trends in Biochemical Sciences*, vol. 42, no. 1, pp. 28–41, 2017.

[29] L. F. Thoen, E. L. Guimarães, L. Dollé et al., "A role for autophagy during hepatic stellate cell activation," *Journal of Hepatology*, vol. 55, no. 6, pp. 1353–1360, 2011.

[30] X. Lu, T. Liu, K. Chen et al., "Isorhamnetin: a hepatoprotective flavonoid inhibits apoptosis and autophagy via P 38/PPAR-α pathway in mice," *Biomedicine & pharmacotherapy = Biomedecine & pharmacotherapie*, vol. 103, pp. 800–811, 2018.

[31] O. Y. Kytikova, J. M. Perelman, T. P. Novgorodtseva et al., "Peroxisome proliferator-activated receptors as a therapeutic target in asthma," *PPAR Research*, vol. 2020, Article ID 8906968, 18 pages, 2020.

[32] J. Li, C. Guo, and J. Wu, "15-Deoxy–(12, 14)-prostaglandin J2 (15d-PGJ2), an endogenous ligand of PPAR-gamma: function and mechanism," *PPAR Research*, vol. 2019, Article ID 7242030, 10 pages, 2019.

[33] C. Vaamonde-Garcia, O. Malaise, E. Charlier et al., "15-Deoxy-Δ-12, 14-prostaglandin J2 acts cooperatively with prednisolone to reduce TGF-β-induced pro-fibrotic pathways in human osteoarthritis fibroblasts," *Biochemical Pharmacology*, vol. 165, pp. 66–78, 2019.

[34] A. Saidi, M. Kasabova, L. Vanderlynden et al., "Curcumin inhibits the TGF-β1-dependent differentiation of lung fibroblasts via PPARγ-driven upregulation of cathepsins B and L," *Scientific Reports*, vol. 9, no. 1, p. 491, 2019.

[35] M. Fu, J. Zhang, X. Zhu et al., "Peroxisome proliferator-activated receptor γ inhibits transforming growth factor β-induced connective tissue growth factor expression in human aortic smooth muscle cells by interfering with Smad3," *The Journal of Biological Chemistry*, vol. 276, no. 49, pp. 45888–45894, 2001.

[36] X. Sun, C. Guo, F. Zhao et al., "Vasoactive intestinal peptide stabilizes intestinal immune homeostasis through maintaining interleukin-10 expression in regulatory B cells," *Theranostics*, vol. 9, no. 10, pp. 2800–2811, 2019.

[37] A. Sikora-Wiorkowska, A. Smolen, G. Czechowska, K. Wiorkowski, and A. Korolczuk, "The role of PPAR gamma agonists - rosiglitazone and 15-deoxy-delta (12, 14)-prostaglandin J2 in experimental cyclosporine A hepatotoxicity," *Journal of Physiology and Pharmacology*, vol. 70, no. 6, 2019.

[38] Z. Heidari, I. M. Chrisman, M. D. Nemetchek et al., "Definition of functionally and structurally distinct repressive states in the nuclear receptor PPARγ," *Nature Communications*, vol. 10, no. 1, p. 5825, 2019.

[39] L. Wu, C. Guo, and J. Wu, "Therapeutic potential of PPARγ natural agonists in liver diseases," *Journal of Cellular and Molecular Medicine*, vol. 24, no. 5, pp. 2736–2748, 2020.

Hindawi
PPAR Research
Volume 2020, Article ID 8864813, 9 pages
https://doi.org/10.1155/2020/8864813

Research Article

Ligand-Activated Peroxisome Proliferator-Activated Receptor β/δ Facilitates Cell Proliferation in Human Cholesteatoma Keratinocytes

Chen Zhang[1,2] **Yang-Wenyi Liu**[1,2] **Zhangcai Chi**[1,2] **and Bing Chen**[1,2]

[1]*ENT Institute and Department of Otolaryngology, Eye & ENT Hospital, Fudan University, Shanghai 200031, China*
[2]*NHC Key Laboratory of Hearing Medicine (Fudan University), Shanghai 200031, China*

Correspondence should be addressed to Zhangcai Chi; zhangcai.chi@fdeent.org and Bing Chen; bingchen@fudan.edu.cn

Received 29 August 2020; Revised 11 October 2020; Accepted 11 December 2020; Published 28 December 2020

Academic Editor: Jingjing Li

Cholesteatoma is characterized by both the overgrowth of hyperkeratinized squamous epithelium and bone erosion. However, the exact mechanism underlying the hyperproliferative ability of cholesteatoma remains unknown. In this study, we investigated PPAR β/δ expression in human surgical specimens of cholesteatoma and analyzed its functional role as a regulator of epithelial keratinocyte hyperproliferation. We found that the expression of PPAR β/δ was significantly upregulated in cholesteatoma and ligand-activated PPAR β/δ markedly promoted the proliferation of cholesteatoma keratinocytes. Furthermore, we showed that PPAR β/δ activation increased PDK1 expression and decreased PTEN generation, which led to increased phosphorylation of AKT and GSK3β and increased the expression level of Cyclin D1. Overall, our data suggested that the proliferating effect of PPAR β/δ on the cholesteatoma keratinocytes was mediated by the positive regulation of the PDK1/PTEN/AKT/GSK3β/Cyclin D1 pathway. These findings warranted further investigation of PPAR β/δ as a therapeutic target for recurrent or residual cholesteatoma.

1. Introduction

Cholesteatoma is a benign epidermally derived temporal bone lesion that is locally destructive and frequently recurrent. It is characterized by both the overgrowth of hyperkeratinized squamous epithelium and bone erosion in the middle ear and mastoid cavity. Cholesteatoma causes a myriad of complications including, but not limited to, hearing loss, ossicular erosion, labyrinthine fistula, facial weakness, and intracranial infections. Unfortunately, the molecular events governing cholesteatoma formation are not well established. Nowadays, increasing attention has been paid to the hyperproliferative activity of epithelium, which would play an important role in the pathophysiologic cascade of cholesteatoma [1].

Presently, surgery is the only effective intervention for cholesteatoma. Despite progress in surgical technique, the overall estimated proportion with recurrence 10 years after surgery is more than 70% [2]. It is reported that the high recurrence rate of cholesteatoma is related to cell hyperproliferation [3, 4]. Therefore, we speculate that the hyperproliferative ability of epithelium might play a significant role in the pathogenesis and recurrent pattern of cholesteatoma.

Peroxisome proliferator-activated receptors (PPARs) are members of the nuclear hormone receptor superfamily and include three distinct isoforms, namely, PPAR α, PPAR γ, and PPAR β/δ [5]. After binding with specific ligands, PPARs regulate a wide of cellular processes, such as cell proliferation and differentiation, apoptosis, inflammatory responses, and metabolism. During the past decade, the expression of PPAR γ has been reported to be upregulated in the cholesteatoma epithelium and to be related to cholesteatoma differentiation [6]. Since PPAR β/δ is the predominant subtype in human keratinocytes [7] and keratinocytes are the main component of cholesteatoma matrix, it is logical that PPAR β/δ would also be expressed in cholesteatoma

tissues. However, to our knowledge, the potential expression and distribution of PPAR β/δ in human cholesteatoma has not been investigated.

A number of researches have demonstrated that ligand activation of PPAR β/δ can induce terminal differentiation of keratinocytes and epithelium [8]. Consistent with these findings, many researchers have also shown that PPAR β/δ inhibits cell proliferation in epithelium and other cell types, including colonocytes, keratinocytes, cardiomyocytes, fibroblasts, and cancer cell lines [8]. However, the role of PPAR β/δ in keratinocyte growth remains questioned as there are limited reports demonstrating that ligand-activated PPAR β/δ can potentiate cell proliferation [9–11]. Di-Poï et al. demonstrated this mechanism by elucidating that the proliferative effect of PPAR β/δ was mediated through the direct repression of gene expression of phosphatase and tensin homolog deleted on chromosome ten (PTEN) and increase expression of 3-phosphoinositide-dependent-protein kinase 1 (PDK1), which then activated the phosphorylation of protein kinase B (Akt), leading to cell proliferation of keratinocytes [12]. Thus, these evidences suggest that the role of PPAR β/δ is cell type- and organ-specific.

Previous researches [13] have proved that the PI3K/Akt/PTEN/Cyclin D1 signaling pathway is indeed active in cholesteatoma epithelium and plays a vital role in cholesteatoma keratinocyte hyperproliferation. Since PPAR β/δ promoted cell proliferation of keratinocytes by modulating PTEN/PDK1/ILK/Akt activity [12], consequently, in this study, we hypothesized that the activation of PI3K/Akt/Cyclin D1 signaling mediated by PPAR β/δ may be involved in the abnormal hyperproliferation of keratinocytes in cholesteatoma epithelium. Furthermore, given the therapeutic potential of PPAR β/δ antagonists, further research of its functional role in cholesteatoma is necessary. To test our hypothesis, we investigated the expression and distribution of PPAR β/δ in middle ear cholesteatoma, elevated the effects of ligand-activated PPAR β/δ, and explored the mechanisms by which PPAR β/δ mediated the cell proliferation in the cultured cholesteatoma keratinocytes.

2. Materials and Methods

2.1. Materials. Highly selective PPAR β/δ agonist GW0740 and PPAR β/δ antagonist GSK0660 were purchased from MedChem Express (NJ, United States). All other reagents were obtained from the supplier as indicated and were at least analytical grade. The antibodies used and their sources were also indicated below.

2.2. Tissue Preparation and Immunofluorescence. Specimens were obtained from 10 patients (five patients with acquired primary cholesteatoma and five healthy external canal skins) and used for immunofluorescence. Each specimen was fixed in 4% paraformaldehyde for 24 h and then embedded in paraffin. Then, five 5 mm sections were used for immunofluorescence as previously described [14]. The sections were blocked for 1 h in 10% normal goat serum after deparaffinization and rehydration in graded alcohol. After a brief rinse, the sections were incubated overnight with rabbit polyclonal anti-PPAR β/δ antibody (Genetex, Cambridge, MA, USA) at 250-fold dilution. Subsequently, the sections were incubated with Alexa 555-labeled goat anti-rabbit antibody for 1 hour at room temperature and then stained using blue fluorescent 4′,6-diamidino-2-phenylindole (DAPI). Finally, the sections were examined with an Axioskop microscope (Carl Zeiss, Oberkochen, Germany). This study was approved by the Research Ethics Committee of the Eye and ENT Hospital of Fudan University. Informed consent was obtained from all cholesteatoma patients included in this study.

2.3. Cell Culture and Stimuli. Cholesteatoma keratinocytes were isolated and characterized as previously described [14]. In brief, cholesteatoma tissue was obtained and hand carried to the lab after surgical resection. The tissue was then cut into small pieces with scissors and digested with 200 U/ml collagenase IV (Sigma-Aldrich, St. Louis, MO, USA) at 4°C overnight. The digested cells were washed twice with HBSS and then centrifuged at 1,500 rpm for 5 min. The pellet was removed, added to 10 ml keratinocyte serum-free medium (KSFM; Invitrogen, Carlsbad, CA, USA) with 500 units/ml penicillin/streptomycin (Invitrogen, Carlsbad, CA, USA), and cultured in 5% CO_2 humidified atmosphere at 37°C. The KSFM media and antibiotics were changed every 3 days. Cell cultures between the third and fourth passages were used in this study.

2.4. EdU Staining Proliferation Assay. Cell proliferation in response to different treatments was confirmed using EdU imaging kit (Invitrogen, Carlsbad, CA), and analysis was done according to the manufacturer's instructions. Cholesteatoma keratinocytes ($5 * 10^3$ cells/well) were plated in a Lab-Tech chamber slide (Nalge Nunc International, Cambridge, MA, USA) and grown to 70-80% confluence in KSFM medium, and then treated with control (DMSO), GW0742 (100 nM), or GSK0660 (5 μM) for 24 h. Edu (10 μM) was added 8 h prior to the end of each measurement period. After being fixed for 15 min with 4% paraformaldehyde, the cells were permeabilized with 0.3%Triton X-100 in PBS for 15 min. Then, the cells were incubated with a Click reaction cocktail containing Click reaction buffer, $CuSO_4$, Alexa Fluor® 555 azide, and reaction buffer additive for 30 min while protected from light. Next, the cells were incubated with 5 μg/ml Hoechst 33342 for 10 min for DNA staining. Finally, the cells were imaged with fluorescence microscopy, and the percentage of EdU-positive cells was evaluated.

2.5. Western Blot Analysis. Cholesteatoma keratinocytes were cultured on 35 mm culture dishes. The cells were grown to 70-80% confluence and then placed in KSFM with control (DMSO), GW0742 (100 nM), or GSK0660 (5 μM). After 24 h of treatment, the cells were washed and isolated using cell lysis buffer (Beyotime Institute of Biotechnology, China) containing protease inhibitors. Equal amounts of total protein were separated on 8% SDS-PAGE and transferred to a PVDF membrane (100 V for 60 min). The membrane was incubated with the primary antibodies overnight at 4°C, followed by the secondary peroxidase-conjugated antibody for 1 h. The bands were visualized by enhanced

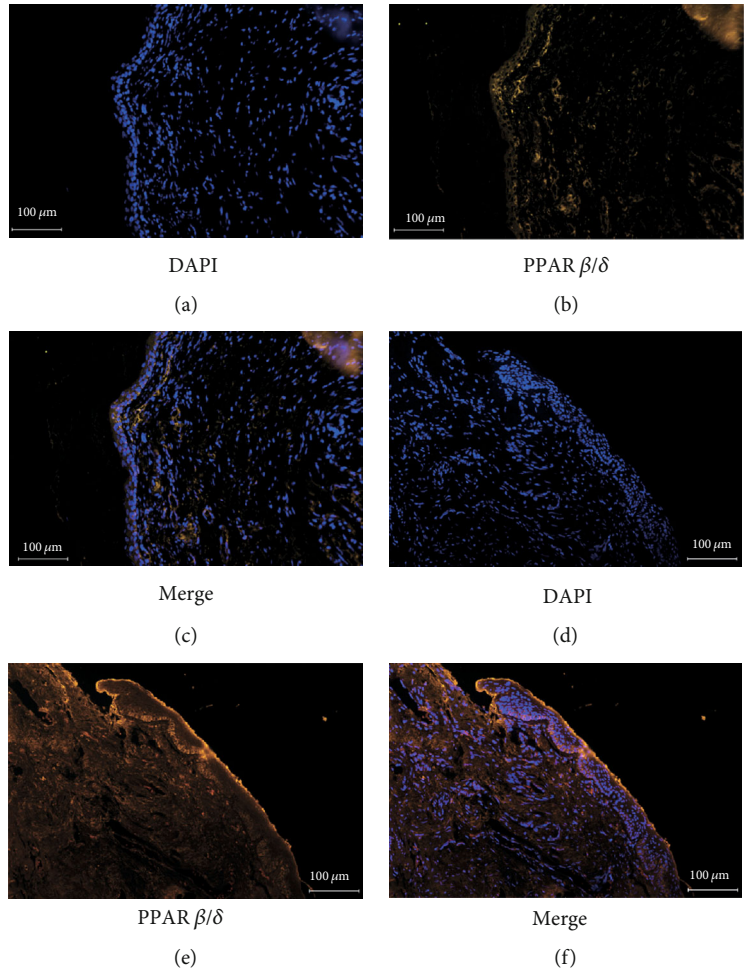

Figure 1: Immunohistochemical staining for proliferator-activated receptor β/δ. PPAR β/δ is scantily expressed in external auditory canal skin (a–c). PPAR β/δ is expressed in the cells mainly in the parabasal and basal layers of cholesteatoma epithelium (d–f). The intensity of its expression is decreased in the granular and prickle cell layers (magnification, ×200).

chemiluminescence and exposure to ECL Hyperfilm (GE Healthcare). The densitometry of bands was quantified with NIH Image 1.63 software. The protein expression was normalized to the amount of beta-actin. The following primary antibodies were used: anti-phospho-PDK1, anti-protein kinase B (AKT), anti-phospho-AKT, anti-phospho-GSK3β, and anti-phospho-PTEN (all from Cell Signaling Technology, Danvers, MA, USA). Antibodies against β-actin, Cyclin D1, and PPAR β/δ were from Genetex, Inc. (Genetex, CA, USA).

2.6. Statistical Analysis. Statistical analysis was performed using the statistical software package SPSS (Version 11.5). All data were presented as the mean ± standard deviation (M ± SD) and analyzed by the t-test. $p < 0.05$ was considered statistically significant.

3. Results

3.1. Immunolocalization of PPAR β/δ. PPAR β/δ was distinctly expressed in the nuclei of cells, mainly in basal and parabasal cell layers (Figures 1(d)–1(f)). However, the intensity of its expression was generally weakened in the granular and prickle cell layers (Figures 1(d)–1(f)). In the control skin, scanty staining of PPAR β/δ was found (Figures 1(a)–1(c)). Immunofluorescent staining for PPAR β/δ in epithelial tissues of cholesteatoma was consistently stronger than that in control skin.

3.2. Cholesteatoma Keratinocyte Proliferation Is Promoted in the Presence of PPAR β/δ-Selective Agonists. To determine the effect of ligand-activated PPAR β/δ in cholesteatoma keratinocyte, we treated the cells for 24 h with either GW0742 (a high affinity PPAR β/δ agonist) or GSK0660 (a high affinity PPAR β/δ antagonist) and quantified the proliferated cell number following treatment. Because EdU is a thymidine analogue and is incorporated into newly synthesized DNA during S phase, EdU-positive cells are usually the newborn and proliferating cells. As showed in Figure 2, significant increases were observed after 24 h of 100 nM GW0742 treatment in the cholesteatoma keratinocyte (Figures 2(a) and 2(b)). Meanwhile, an antiproliferated effect was observed in cholesteatoma keratinocyte treated with GSK0660, where EdU-positive cell rate decreased significantly following

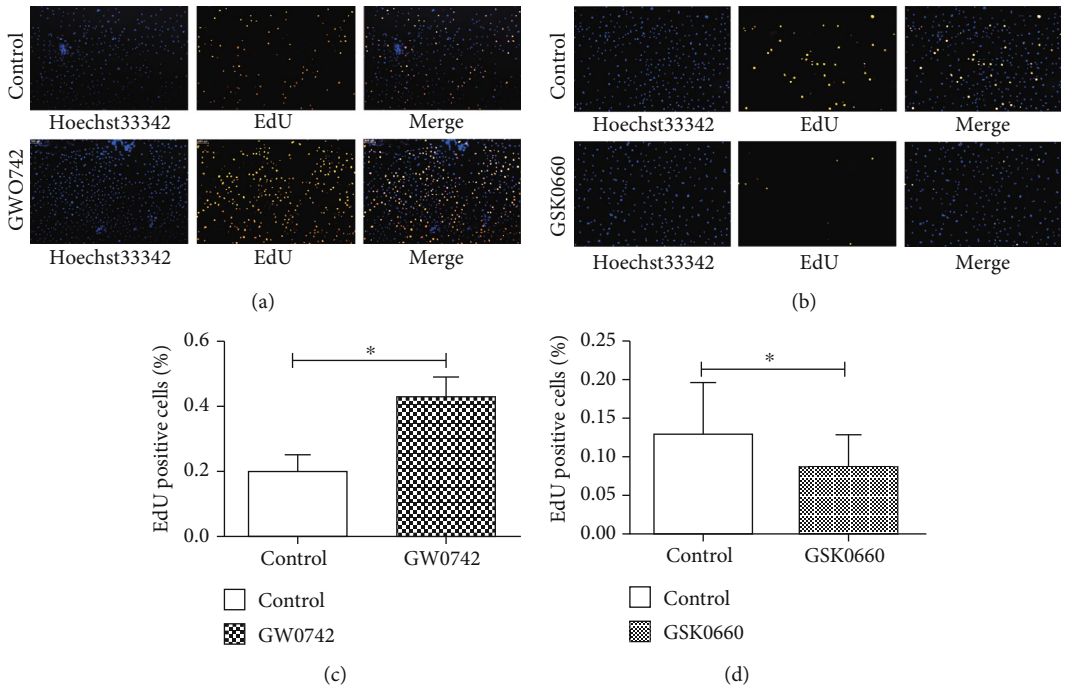

Figure 2: Ligand activation of PPAR β/δ facilitates the proliferation of human cholesteatoma keratinocytes in vitro. (a, c) The effect of GW0742 (a high affinity PPAR β/δ agonist) (a) and GSK0660 (a high affinity PPAR β/δ antagonist) (c) on cell proliferation was detected by EdU assays. (b, d) Data were based on at least three independent experiments and presented as the mean ± SD; $^*p < 0.05$ (vs. control group).

5 μM GSK0660 treatment (Figures 2(c) and 2(d)). These results suggest that ligand-activated PPAR β/δ can promote the proliferation of human cholesteatoma keratinocytes.

3.3. Activation of PPAR β/δ by Specific Ligands Increases Expression of PDK1. Cholesteatoma keratinocyte is a transformed keratinocyte cell type with unique biologic behavior that distinguishes it from healthy keratinocytes [15]. PPAR β/δ is known to be highly expressed in the skin and keratinocytes. To determine whether cholesteatoma keratinocytes express a functional PPAR β/δ, cells were treated with either 100 nM GW0742 or 5 μM GSK0660. Western blot analysis demonstrated that cholesteatoma keratinocytes constitutively expressed PPAR β/δ and that GW0742 or GSK0660 had no effect on PPAR β/δ expression (Figures 3(a)–3(d)). To verify that the proliferation promotion effect of GW0742 is associated with specific ligand activation of PPAR β/δ, the expression of known and putative PPAR β/δ-dependent target genes was examined. The expression of the putative PPAR β/δ target gene PDK1 [13] was significantly induced by GW0742 (Figures 3(e)–3(f)). In addition, treatment with GSK0660, an antagonist of PPAR β/δ, also significantly reversed the effect of GW0742 on the expression of PDK1 (Figures 3(g)–3(h)). These data show that cholesteatoma keratinocytes are responsive to PPAR β/δ ligands, as demonstrated by the induction of a known PPAR β/δ-dependent target genes within 24 h of treatment.

3.4. Activation of PPAR β/δ Promotes the Proliferation of Cholesteatoma Keratinocytes through the PDK1/AKT/GSK-3β/Cyclin D1 Pathway. Previous studies suggested that ligand activation of PPAR β/δ in mouse primary keratinocytes caused antiapoptotic signaling mediated by inhibition of PTEN expression and increased expression of the oncogenes PDK1 and ILK1 leading to increased phosphorylation of Akt [12]. To determine whether this pathway function was similarly in cholesteatoma keratinocytes, we analyzed the expression of PTEN and AKT phosphorylation by means of quantitative western blot analysis. Following treatment with 100 nM GW0742, the cholesteatoma keratinocytes demonstrated increased phosphorylation of AKT and lower expression of PTEN (Figure 4(a)). To fully characterize the signaling pathway, we examined the expression of PTEN, PDK1, AKT, and their downstream targets. The immunoblot (Figure 4(a)) showed that the GW0742 treatment increased the P-AKT (ser473) and its downstream effector Cyclin D1 and inhibited the level of PTEN, with altering phosphorylation activity of GSK3β in the cholesteatoma keratinocytes. To determine whether this is a PPAR β/δ-mediated effect, the specific antagonist of PPAR β/δ, GSK0660, was used. As shown in Figure 4(b), GSK0660 had the reverse effect on the basal phosphorylation of these kinases. These results indicating that ligand-activated PPAR β/δ promotes the proliferation of cholesteatoma keratinocytes via upregulation the PDK1/AKT/PTEN/GSK3β/Cyclin D1 signaling pathway.

4. Discussion

In the present study, we have demonstrated for the first time the localization and elevated expression of the nuclear antigen PPAR β/δ protein in human middle ear cholesteatoma epithelium. PPAR β/δ is known to be mainly present in

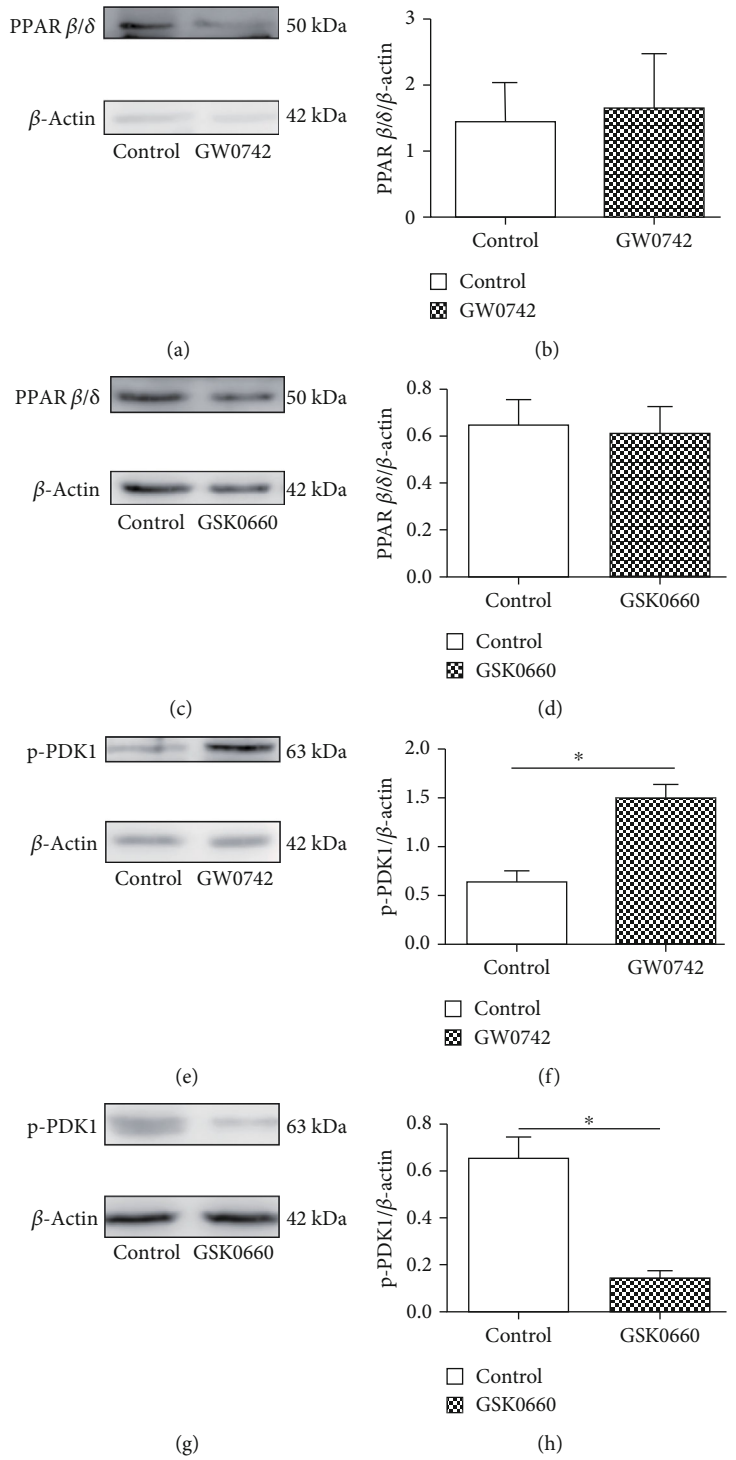

Figure 3: Expression of PPAR β/δ and ligand activation of target gene (PDK1) in cholesteatoma keratinocytes. (a, c) Expression of PPAR β/δ was quantified by immunoblot after treating with 100 nM GW0742 (a) or 5 μM GSK0660 (c) for 24 h. (e, g) The effect of PPAR β/δ agonist (e) or antagonist (g) on expression of the PPAR β/δ-dependent target gene PDK1 was determined by immunoblot following ligand activation of PPAR β/δ with 100 nM GW0742 or 5 μM GSK0660 for 24 h. (b, d, f, and h) Data are expressed as the mean ± SD of the mean for experiments run in triplicate. $^*p < 0.05$ (vs. control group).

keratinocytes [7] and plays an important role in regulating inflammation, immune responses, cell proliferation, cell differentiation, and apoptosis. In addition, cholesteatoma keratinocyte is a transformed keratinocyte cell type with increased proliferation ability. These results indicated a potential role of PPAR β/δ overexpression in the pathogenesis of cholesteatoma.

Previously, the PI3K/Akt/Cyclin D1signaling pathway is known to play a crucial role in cholesteatoma epithelial hyperproliferation [13]. The activated PI3K can produce a

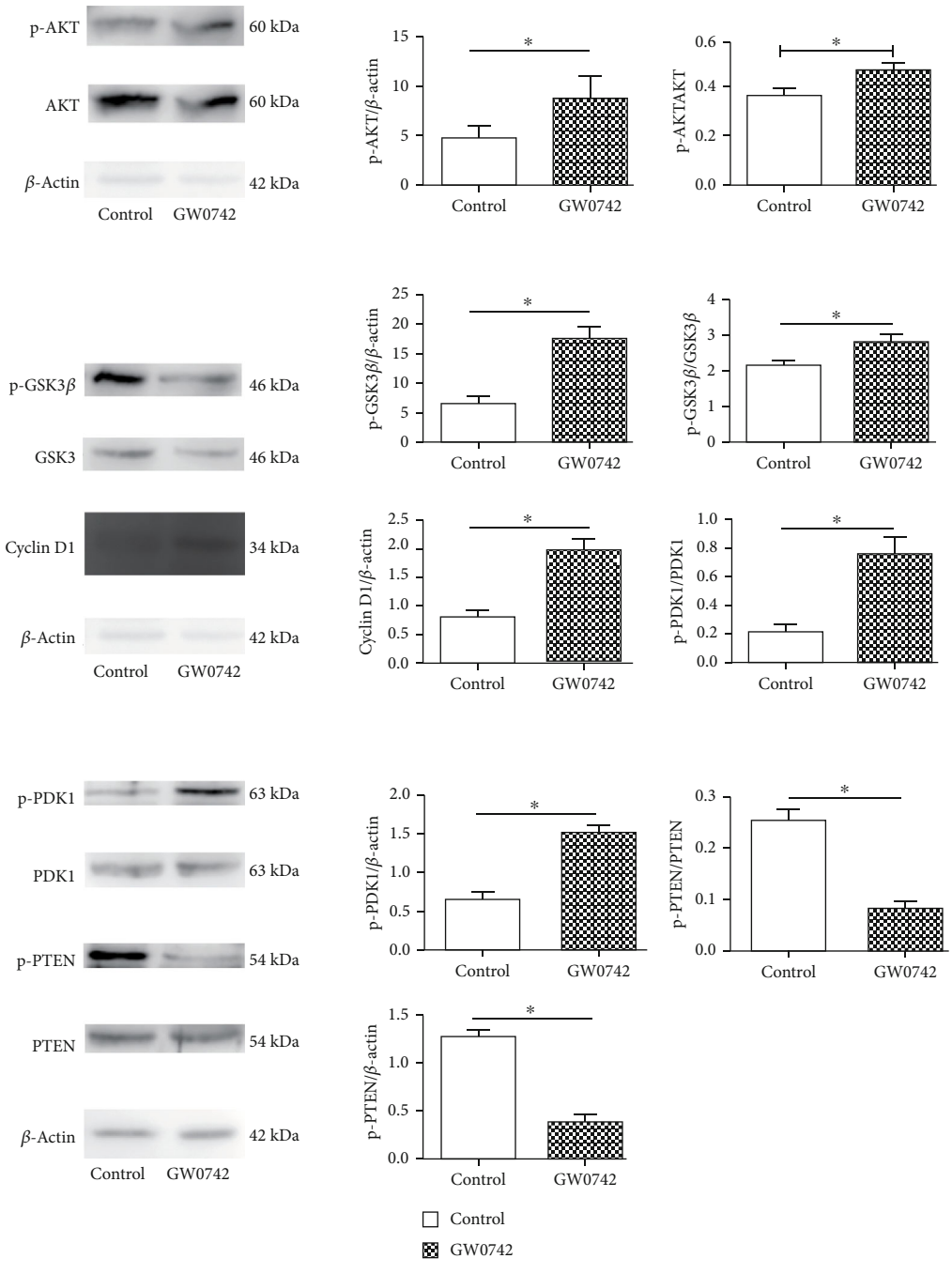

Figure 4: Continued.

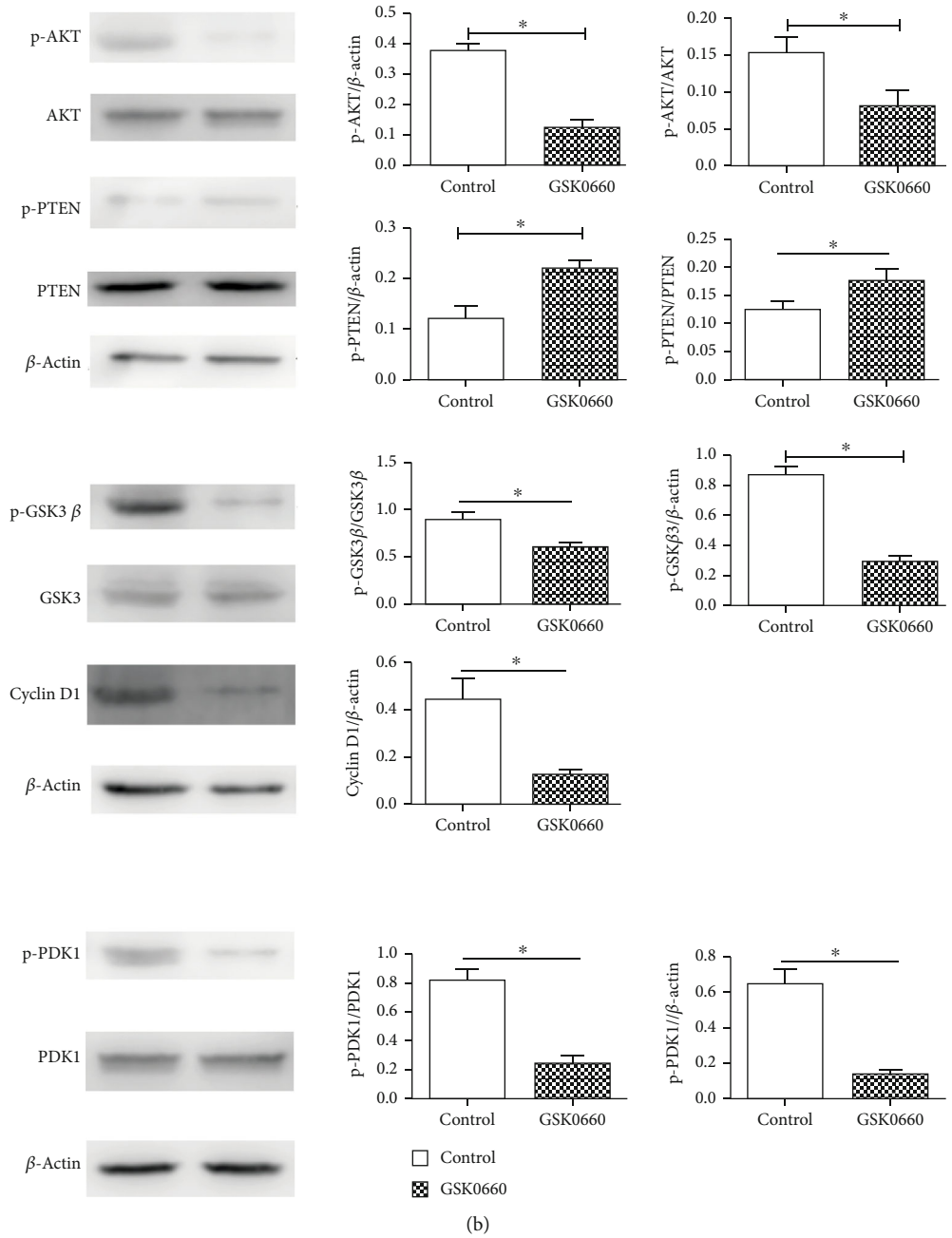

Figure 4: Ligand activation of PPAR β/δ had effect on PDK1/PTEN/AKT/GSK3β/Cyclin D1 signal pathway in cultured cholesteatoma keratinocytes. (a) Western blot showing changes in PDK1/PTEN/AKT/GSK3β/Cyclin D1 pathway after treating with 100 nM GW0742 for 24 h. (b) Immunoblots demonstrating the effect of GSK0660 treatment (5 μM, 24 h) on the PDK1/PTEN/AKT/GSK3β/Cyclin D1 pathway. β-Actin served as loading control. $^*p < 0.05$.

second messenger PIP3, PIP3 recruits PDK1 and PDK2 to the cell membrane, and then PDK1/PDK2 cooperate to activate Akt completely [13]. In our study, we found that PPAR β/δ agonist can induce the expression of PDK1, which is served as a putative PPAR β/δ-dependent target gene [11], significantly affecting the Akt/Cyclin D1 pathway. In addition, PPAR β/δ activated with highly selective synthetic ligands had an obvious proliferating effect on cholesteatoma keratinocytes. As well as treating the cells with PPAR β/δ antagonists could reverse this effect. These results lead us to suppose that the PDK1/PTEN/AKT/GSK3β/Cyclin D1 pathway is involved in the process of ligand-activated PPAR β/δ-induced cell proliferation of cholesteatoma keratinocytes. Our work provides a crucial clue for regarding PPAR β/δ as a potential target to inhibit epidermal keratinocyte proliferation for cholesteatoma therapy.

Another mechanism suggests that PPAR β/δ promotes cell survival and proliferation via regulation of the PTEN-AKT pathway. As a negative regulator of the PI3K/AKT signaling pathway, the tumor suppressor gene PTEN can regulate cell growth, proliferation, and survival [16]. Previous studies demonstrated that PTEN expression was

significantly lower in cholesteatoma epithelium and a significantly inverse correlation between PTEN and p-Akt expressions was found in cholesteatoma [17, 18]. Our study showed decreased PTEN expression in cholesteatoma keratinocytes treated with the PPAR β/δ agonist GW0742. Although we did not directly determine the effects of activated PPAR β/δ on PI3K activity, we did detect an increase of phosphorylated PDK1 and AKT, a known downstream target of PI3K. These results suggest that activated PPAR β/δ decreases PTEN expression and upregulates the AKT signaling pathway to promote proliferation in cholesteatoma keratinocytes.

Glycogen synthase kinase-3β (GSK3β) has been found to be involved in a variety of cellular processes, such as metabolism, differentiation, and apoptosis [19]. As the Akt substrate, GSK3β can be phosphorylated and inactivated by all three isoforms of Akt and is negatively regulated by Akt activity [20, 21]. In our study, GW0742 treatment enhanced the phosphorylation of Akt (Ser473) and GSK3β (Ser9) by activating the PDK1/AKT/GSK3β signaling pathway. Once GSK3β is phosphorylated, the degradation of Cyclin D1 induced by GSK3β would be inhibited. Because of the inhibition of PTEN and the activation of AKT, Cyclin D1 would also be induced and its expression level increased. Together, these results may partly explain the mechanism by which the PPAR β/δ-selective agonists cause proliferation in cholesteatoma keratinocytes.

Based on the findings described above, we propose a model for the role of PPAR β/δ in regulating cell proliferation in cholesteatoma keratinocytes. After activation of PPAR β/δ, increased PDK1 expression and decreased PTEN generation lead to increased phosphorylation of AKT and GSK3β. These changes increase the expression level of Cyclin D1, which, in turn, promotes the cell cycle transition from G1 to S phase. Taken together, our findings indicate that PPAR β/δ activation promotes cell proliferation in cholesteatoma keratinocytes through the regulation of the PDK1/AKT/PTEN/GSK3β/Cyclin D1 pathway.

In summary, we demonstrated that ligand activation of PPAR β/δ regulates cell proliferation in cholesteatoma keratinocytes and that upregulation of PDK1 and modulation of the AKT/PTEN/GSK3β/Cyclin D1 pathway may be involved. These findings have important implications not only for understanding the molecular mechanism of PPAR β/δ in cholesteatoma but also by providing novel insights into the treatment of recurrent or residual cholesteatoma.

Data Availability

The data used or analyzed during the current study are available from the corresponding author on a reasonable request.

Conflicts of Interest

The authors declare that there is no conflict of interest regarding the publication of this paper.

Authors' Contributions

Zhangcai Chi designed the study, collected and organized the data, and wrote the manuscript. Yang-Wenyi Liu and Chen Zhang collected and organized the data. Bing Chen designed the study and wrote and reviewed the manuscript.

Acknowledgments

This work was supported by the Science Project of Shanghai Municipal Health Bureau (No. 20174Y0062).

References

[1] S. Xie, X. Wang, H. Ren, X. Liu, J. Ren, and W. Liu, "HB-EGF expression as a potential biomarker of acquired middle ear cholesteatoma," *Acta Oto-Laryngologica*, vol. 137, no. 8, pp. 797–802, 2017.

[2] Y. Si, Y. B. Chen, S. J. Chen et al., "TLR4 drives the pathogenesis of acquired cholesteatoma by promoting local inflammation and bone destruction," *Scientific Reports*, vol. 5, no. 1, p. ???, 2015.

[3] S. A. Schraff and B. Strasnick, "Pediatric cholesteatoma: a retrospective review," *International Journal of Pediatric Otorhinolaryngology*, vol. 70, no. 3, pp. 385–393, 2006.

[4] E. A. Server, Department of Otorhinolaryngology, I. Training et al., "Predictive role of Ki-67 and proliferative-cell nuclear antigen (PCNA) in recurrent cholesteatoma," *The Journal of International Advanced Otology*, vol. 15, no. 1, pp. 38–42, 2019.

[5] S. Kuenzli and J. H. Saurat, "Peroxisome proliferator-activated receptors in cutaneous biology," *The British Journal of Dermatology*, vol. 149, no. 2, pp. 229–236, 2003.

[6] S. J. Hwang, H. J. Kang, J. J. Song et al., "Up-regulation of peroxidase proliferator-activated receptor gamma in cholesteatoma," *Laryngoscope*, vol. 116, no. 1, pp. 58–61, 2006.

[7] M. Gupta, V. K. Mahajan, K. S. Mehta, P. S. Chauhan, and R. Rawat, "Peroxisome proliferator-activated receptors (PPARs) and PPAR agonists: the "future" in dermatology therapeutics?," *Archives of Dermatological Research*, vol. 307, no. 9, pp. 767–780, 2015.

[8] J. M. Peters, H. E. Hollingshead, and F. J. Gonzalez, "Role of peroxisome-proliferator-activated receptor beta/delta (PPAR-beta/delta) in gastrointestinal tract function and disease," *Clinical Science (London, England)*, vol. 115, no. 4, pp. 107–127, 2008.

[9] R. A. Gupta, D. Wang, S. Katkuri, H. Wang, S. K. Dey, and R. N. DuBois, "Activation of nuclear hormone receptor peroxisome proliferator-activated receptor-δ accelerates intestinal adenoma growth," *Nature Medicine*, vol. 10, no. 3, pp. 245–247, 2004.

[10] D. Wang, H. Wang, Y. Guo et al., "Crosstalk between peroxisome proliferator-activated receptor and VEGF stimulates cancer progression," *Proceedings of the National Academy of Sciences of the United States of America*, vol. 103, no. 50, pp. 19069–19074, 2006.

[11] T. T. Schug, D. C. Berry, N. S. Shaw, S. N. Travis, and N. Noy, "Opposing effects of retinoic acid on cell growth result from alternate activation of two different nuclear receptors," *Cell*, vol. 129, no. 4, pp. 723–733, 2007.

[12] N. di-Poï, N. S. Tan, L. Michalik, W. Wahli, and B. Desvergne, "Antiapoptotic role of PPARβ in keratinocytes via transcriptional control of the Akt1 signaling pathway," *Molecular Cell*, vol. 10, no. 4, pp. 721–733, 2002.

[13] S. Xie, Y. Xiang, X. Wang et al., "Acquired cholesteatoma epithelial hyperproliferation: roles of cell proliferation signal pathways," *Laryngoscope*, vol. 126, no. 8, pp. 1923–1930, 2016.

[14] Z. Chi, Z. Wang, Q. Liang, Y. Zhu, and Q. du, "Induction of cytokine production in cholesteatoma keratinocytes by extracellular high-mobility group box chromosomal protein 1 combined with DNA released by apoptotic cholesteatoma keratinocytes," *Molecular and Cellular Biochemistry*, vol. 400, no. 1-2, pp. 189–200, 2015.

[15] C. W. Hilton, F. G. Ondrey, B. R. Wuertz, and S. C. Levine, "Interleukin-8 production in response to tumor necrosis factor-alpha by cholesteatoma keratinocytes in cell culture," *Laryngoscope*, vol. 121, no. 2, pp. 372–374, 2011.

[16] B. D. Hopkins, C. Hodakoski, D. Barrows, S. M. Mense, and R. E. Parsons, "PTEN function: the long and the short of it," *Trends in Biochemical Sciences*, vol. 39, no. 4, pp. 183–190, 2014.

[17] T. Y. Yune and J. Y. Byun, "Expression of PTEN and phosphorylated Akt in human cholesteatoma epithelium," *Acta Oto-Laryngologica*, vol. 129, no. 5, pp. 501–506, 2009.

[18] M. A. Huisman, E. De Heer, and J. J. Grote, "Survival signaling and terminal differentiation in cholesteatoma epithelium," *Acta Oto-Laryngologica*, vol. 127, no. 4, pp. 424–429, 2009.

[19] P. P. Ruvolo, "GSK-3 as a novel prognostic indicator in leukemia," *Advances in Biological Regulation*, vol. 65, pp. 26–35, 2017.

[20] E. Beurel, S. F. Grieco, and R. S. Jope, "Glycogen synthase kinase-3 (GSK3): regulation, actions, and diseases," *Pharmacology & Therapeutics*, vol. 148, pp. 114–131, 2015.

[21] F. Chang, J. T. Lee, P. M. Navolanic et al., "Involvement of PI3K/Akt pathway in cell cycle progression, apoptosis, and neoplastic transformation: a target for cancer chemotherapy," *Leukemia*, vol. 17, no. 3, pp. 590–603, 2003.

Hindawi
PPAR Research
Volume 2020, Article ID 6633022, 7 pages
https://doi.org/10.1155/2020/6633022

Research Article

MicroRNA-21 Contributes to Acute Liver Injury in LPS-Induced Sepsis Mice by Inhibiting PPARα Expression

Xianjin Du,[1] **Miao Wu**,[2] **Dan Tian**,[2] **Jianlin Zhou**,[3] **Lu Wang**,[1] **and Liying Zhan**[1]

[1]*Department of Critical Care Medicine, Renmin Hospital of Wuhan University, 238 Jiefang Road, Wuchang, Wuhan, Hubei 430060, China*
[2]*Department of Emergency, Renmin Hospital of Wuhan University, 238 Jiefang Road, Wuchang, Wuhan, Hubei 430060, China*
[3]*Department of Orthopedics, Renmin Hospital of Wuhan University, 238 Jiefang Road, Wuchang, Wuhan, Hubei 430060, China*

Correspondence should be addressed to Xianjin Du; duxianjin@whu.edu.cn, Jianlin Zhou; zhoujianlin2005@sina.com, and Liying Zhan; zhanliying@whu.edu.cn

Received 13 October 2020; Accepted 11 December 2020; Published 22 December 2020

Academic Editor: Xiao-Jie Lu

The severity of sepsis may be associated with excessive inflammation, thus leading to acute liver injury. MicroRNA-21 is highly expressed in the liver of a variety of inflammation-related diseases, and PPARα is also proved to participate in regulating inflammation. In the present study, the LPS-induced sepsis model was established. We found that microRNA-21 expression was upregulated in the liver of sepsis mice, and microRNA-21 inhibition significantly reduced the liver injury. The expression of liver injury markers, inflammation cytokines, and PPARα in the septic mice was higher than in antagomir-21 treated septic mice. In addition, we also found that PPARα is the target gene of microRNA-21; PPARα antagonist GW6471 could reverse the effect of antagomir-21. In conclusion, our study illustrated that microRNA-21 exacerbate acute liver injury in sepsis mice by inhibiting PPARα expression.

1. Introduction

Sepsis is a common cause of death in intensive care units [1]. It is a public health problem worldwide, and approximately 19 million people suffer from sepsis yearly [2]. Sepsis was defined as a "life-threatening organ dysfunction caused by a deregulated host response to infection" at the Sepsis-3 conference [3]. The acute liver injury occurs at any stage of sepsis; the dysregulation of hepatocyte function may be related to cytokine storm [4]. Liver injury can not only aggravate the development of the disease but also lead to death [5]. Despite the urgent need for effective therapeutic options, many new therapies have not improved the survival rate [6]. Therefore, understanding the pathogenesis of sepsis is very important for the treatment of sepsis.

Peroxisome proliferator-activated receptors (PPARs) are ligand-activated transcription factors belonging to a nuclear hormone receptor superfamily [7]. PPARα is an isoform of peroxisome proliferator-activated receptors, which regulates adipocyte differentiation, fatty acid oxidation, and glucose metabolism [8]. More recently, emerging evidence revealed that PPARα activation could reduce the inflammatory response by promoting NF-κB inactivation [9]. In addition, the liver PPARα expression was found to be disturbed during sepsis. In a murine model of sepsis, liver PPARα expression was significantly associated with survival [10].

MicroRNA is a class of noncoding RNA, 19-22 nucleotides in length [11], which regulates gene expression at the posttranscriptional level by degrading message RNA or inhibiting its transcription [12]. MicroRNA microarray analysis showed the upregulation of microRNA-21 in sepsis patients [13]. Nevertheless, the role of microRNA-21 in sepsis-induced liver injury has not been fully elucidated.

In this study, we aim to explore the role of miR-21 and PPARα in the pathogenesis of sepsis-induced liver injury. For this purpose, we used antagomir-21 to inhibit miR-21 expression in murine sepsis model and detected the levels of proinflammatory cytokines (TNF-α, IL-1β,

and IL-6), liver injury markers (AST, ALT), and PPARα expression.

2. Materials and Methods

2.1. Animal Models. All male C57BL/6 mice were obtained from Hubei Provincial Center for Disease Control and Prevention. The mice were housed in a pathogen-free facility with standard laboratory diet and water. At the age of 8 weeks, the mice were received three retroorbital intravenous injections of antagomir-21 (5'-UCAACAUCAGUCUGAUAAGCUA-3'; 16 mg/kg; $n = 6$), antagomir control (5'-AAGGCAAGCUGACCCUGAAGUU-3'; 16 mg/kg; $n = 6$), antagomir-21+GW6471 (16 mg/kg; 30 mg/kg; $n = 6$), phosphate saline (PBS; $n = 12$). Six PBS-treated mice were used as controls; the other mice received intraperitoneal injection of 5 mg/kg lipopolysaccharide to induce sepsis. At 24 h after LPS injection, all mice were sacrificed.

All experiments were performed in accordance with the *Guidelines for the Care and Use of Laboratory Animals* published by the National Institutes of Health (2011).

2.2. Cell Culture. Mouse Biliary Duct Epithelial Cells and 293T cells were obtained from Newgainbio (Wuxi, China) and cultured in DM/F12 medium or Dulbecco's Modified Eagle's Medium (DMEM) supplemented with 10% fetal bovine serum (FBS), 100 U/mL penicillin and 100 μg/mL streptomycin under 5% CO2 at 37°C.

2.3. Luciferase Reporter Assay. MiR-21 mimics (5'-UAGCUUAUCAGACUGAUGUUGA-3') and NC-mimics (5'-UUCUCCGAACGUGUCACGUTT-3') were purchased from Ribobio (Guangzhou, China). The pGL3 Luciferase Reporter Vectors (Promega) containing the PPARα-MT (5'-AAAAAAUCUGUUAGAUAAGCUA-3') and PPARα-MuT (5'-AAUUAUAGUCAUACUAUUCGAA-3') sequences were cotransfected with miR-21 mimics or NC-mimics (50 nM) into 293T and MBDEC cells. All transfections were performed using Lipofectamine 3000 (Invitrogen, USA). After 24 hours of incubation, 1×PLB was used to lyse the cells, and the luciferase activities were measured using the Dual-Luciferase Reporter Assay System (Promega).

2.4. RNA Isolation and qRT-PCR. Total RNA was extracted from snap frozen mouse liver samples using TRIzol reagent (Invitrogen, USA). MiR-21 and mRNA levels were quantified by qRT-PCR assay. For miRNA, U6 was applied as endogenous control. For mRNA, GAPDH was used as endogenous control. All reactions were run on the ABI 7500Real-Time PCR System (Life Technologies, USA). The relative expression was calculated using $2^{-\Delta\Delta CT}$ method. All primers used in this study are as follows.

MiR-21 (stem-loop RT primer): 5'-GTCGTATCCAGTGCAGGGTCCGAGGTATTCGCACTGGATACGACTCAACA-3'

MiR-21-F: 5'-GTGCAGGGTCCGAGGT-3'

MiR-21-R: 5'-GCCGCTAGCTTATCAGACTGATGT-3'

U6-F: 5'-AGCCCGCACTCAGAACATC-3'

U6-R: R: 5'-GCCACCAAGACAATCATCC-3'

GAPDH-F: 5'-CGTCCCGTAGACAAA ATGGTGAA-3'

GAPDH-R: 5'-GCCGTGAGTGGAGTCATACTGGAACA-3'

PPARα-F: 5'-AACCTGAGGAAGCCGTTCTGTGACAT-3'

PPARα-R: 5'-GACCAGCTGCCGAAGGTCCACCAT-3'.

2.5. ELISA. The TNF-α, IL-1β, and IL-6 levels in liver or cultured supernatant were quantified using the Mouse TNF-α Precoated Elisa kit, Mouse IL-1β Precoated Elisa kit, and Mouse IL-6 Precoated ELISA kit, respectively.

2.6. Metabolic Analyses. Serum alanine aminotransferase (ALT) and aspartate aminotransferase (AST) levels were determined using the VITROS350 chemistry system (Johnson & Johnson, USA).

2.7. Histological Analysis of Liver. Liver samples from mice were fixed in 4% paraformaldehyde, then stained with hematoxylin and eosin. The liver damage photos were observed and recorded under light microscopy.

2.8. Western Blot. The nuclear protein of liver samples was extracted using NE-PER™ Nuclear Extraction Reagents (Thermo Fisher, USA). Protein was quantified using BCA Protein Assay (Thermo Fisher, USA). Total protein (50 μg) was separated by sodium dodecyl sulphate-polyacrylamide gel electrophoresis (SDS-PAGE) and transferred to polyvinylidene fluoride (PVDF) membranes (Millipore, USA). Membranes were incubated with the primary antibodies (1 : 1000) overnight at 4°C. After HRP-conjugated secondary antibodies (1 : 5000) incubation; the protein bands were visualized using the Clarity Western ECL Substrate (Bio-Rad, USA).

2.9. Statistical Analyses. Student's t test and one-way analysis of variance were used to analyze the significance between groups. $p < 0.05$ was considered statistically significant. Data analysis was performed using SPSS 22.0 (IBM, Chicago, USA), and figures were designed using GraphPad Prism 8.3.0.

3. Results

3.1. Expression of miR-21 Is Increased in the Liver of Sepsis Mice. The animal experiments were performed according to the design (Figure 1(a)). After these mice were sacrificed, we collected the serum of the mice and isolated the livers. Subsequently, the expression of miR-21 in the liver was detected using qRT-PCR (Figure 1(b)). The results showed that miR-21 expression was significantly upregulated in septic mice; nevertheless, the injection of antagomir-21 totally blocked the upregulation of miR-21, suggesting that the sepsis mouse models with miR-21 inhibition were successfully established.

3.2. Antagomir-21 Reduces Liver Injury and Inflammation in Sepsis Mice. To further investigate the function of miR-21 in sepsis-induced liver injury, we next evaluated the pathological damage of livers and the levels of proinflammatory cytokines. As shown in Figures 2(a) and 2(b), the degree of liver damage in septic mice was significantly increased.

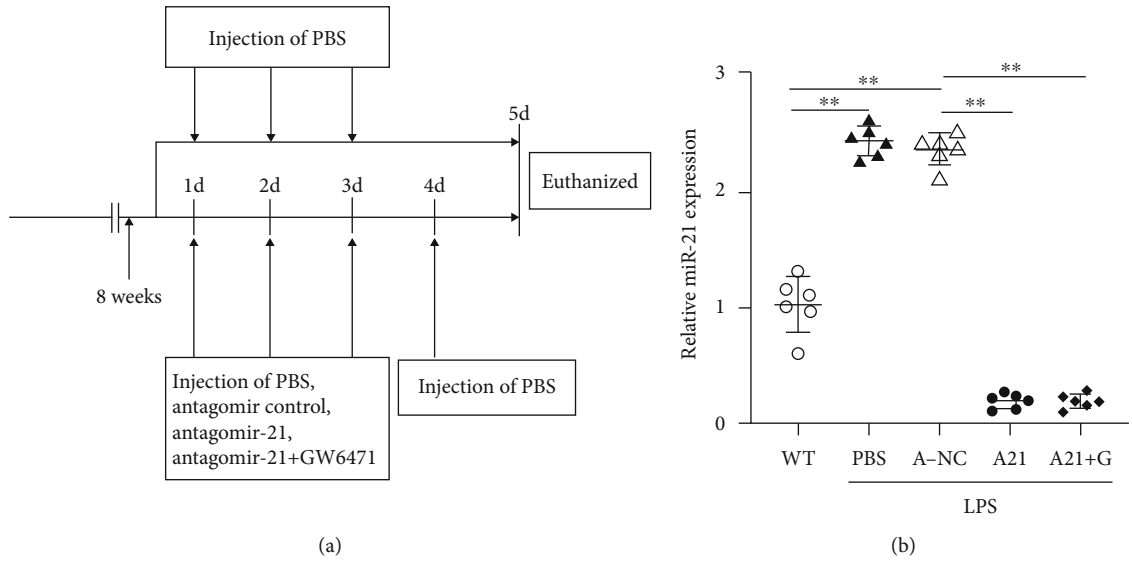

Figure 1: MiR-21 expression was increased in the liver of sepsis mice. (a) Mouse study design. (b) The miR-21 expression in the liver of the wide-type mice treated with PBS (WT) and the LPS-induced mice treated with PBS, antagomir-21 control (NC), antagomir-21 (A21), antagomir-21, and PPARα antagonist GW6471 (A21+G). QRT-PCR assay was used to detect the expression of miR-21. $**p < 0.01$.

Antagomir-21 administration alleviated the liver injury; however, in the antagomir-21 and GW6471 coadministration group, the degree of liver injury showed no changes. As expected in these mice of sepsis, the expression of liver injury markers (serum AST and serum ALT; Figures 2(c) and 2(d)) and proinflammatory cytokines (TNF-α, IL-1β, and IL-6; Figures 2(e)–2(j)) was notably reduced by antagomir-21. Nevertheless, GW6471 restored the levels of these cytokines again. To sum up above results, it demonstrated that miR-21 inhibition strongly decreased the liver injury and inflammation in septic mice. But the effects produced by miR-21 inhibition were reversed by PPARα antagonist GW6471.

3.3. MiR-21 Directly Interacts with PPARα. It is well known that miRNAs participate in a variety of physiological activities by regulating gene expression at the posttranscriptional level. To investigate the molecular mechanisms of miR-21 in sepsis, we used TargetScan to identify the potential genes, and PPARα was found to be one of the most relevant genes to sepsis. Starbase (http://starbase.sysu.edu.cn) was used to predict the putative binding sites between PPARα and miR-21 (Figure 3(a)). Luciferase report assay was performed to test whether miR-21 can directly bind to PPARα. As shown in Figure 3(b), in the 293T and MBDEC cells that cotransfected with PPARα WT and miR-21 mimics, the luciferase activities were significantly reduced, but there were no changes in the PPARα-MuT group. The results indicated that PPARα is a target gene of miR-21.

3.4. Antagomir-21 Reduces Liver Injury and Inflammation by Restoring PPARα Expression. To further verify whether miR-21 regulates the expression of PPARα in the liver. We detected the PPARα expression in the liver of five groups; three liver samples was randomly selected from each groups (Figures 4(a) and 4(b)). The total RNA was extracted from liver tissues, and the protein was extracted from the nucleus. The results showed that PPARα expression in PBS and AC groups was markedly decreased compared with the WT group. In addition, antagomir-21 treatment increased the PPARα expression in the liver, but GW6471 inhibited the level of PPARα nuclear protein. Aggregating all the results, we found that antagomir-21 alleviated liver injury and inflammation by restoring PPARα expression.

4. Discussion

This study illustrated that miR-21 suppression attenuated liver injury in LPS-induced sepsis mice, by potentiating PPARα expression, which suggested a contribution of miR-21 in the pathogenesis of sepsis-induced liver injury. In addition, antagomiR-21 and PPARα represented anti-inflammatory activities in septic mice. These findings demonstrated that the miR-21/PPARα pathway might serve as a potential target in sepsis therapy.

A proinflammatory status is the key feature of sepsis, and the liver plays an important role in inflammation [14]. According to reports, miR-21 is upregulated in various inflammatory diseases, including myocardial injury [15], nonalcoholic steatohepatitis [16], and osteoarthritis [17]. However, the role of miR-21 in sepsis has not been fully elucidated. At first, we confirmed that miR-21 expression was elevated in the liver of LPS-induced sepsis mice. Then, to investigate the molecular mechanism of miR-21 in sepsis, we screened out some genes with miR-21 binding sites. Previous reports have shown that PPARα expression is reduced in the liver of NASH patients, and PPARα activation inhibits liver fibrosis in mice [18, 19]. These researches promoted us to verify the connection between miR-21 and PPARα. Subsequently, we found that in the liver of sepsis mice model, PPARα expression was decreased when miR-21 expression was increased. In addition, antagomir-21 restored PPARα expression and attenuated

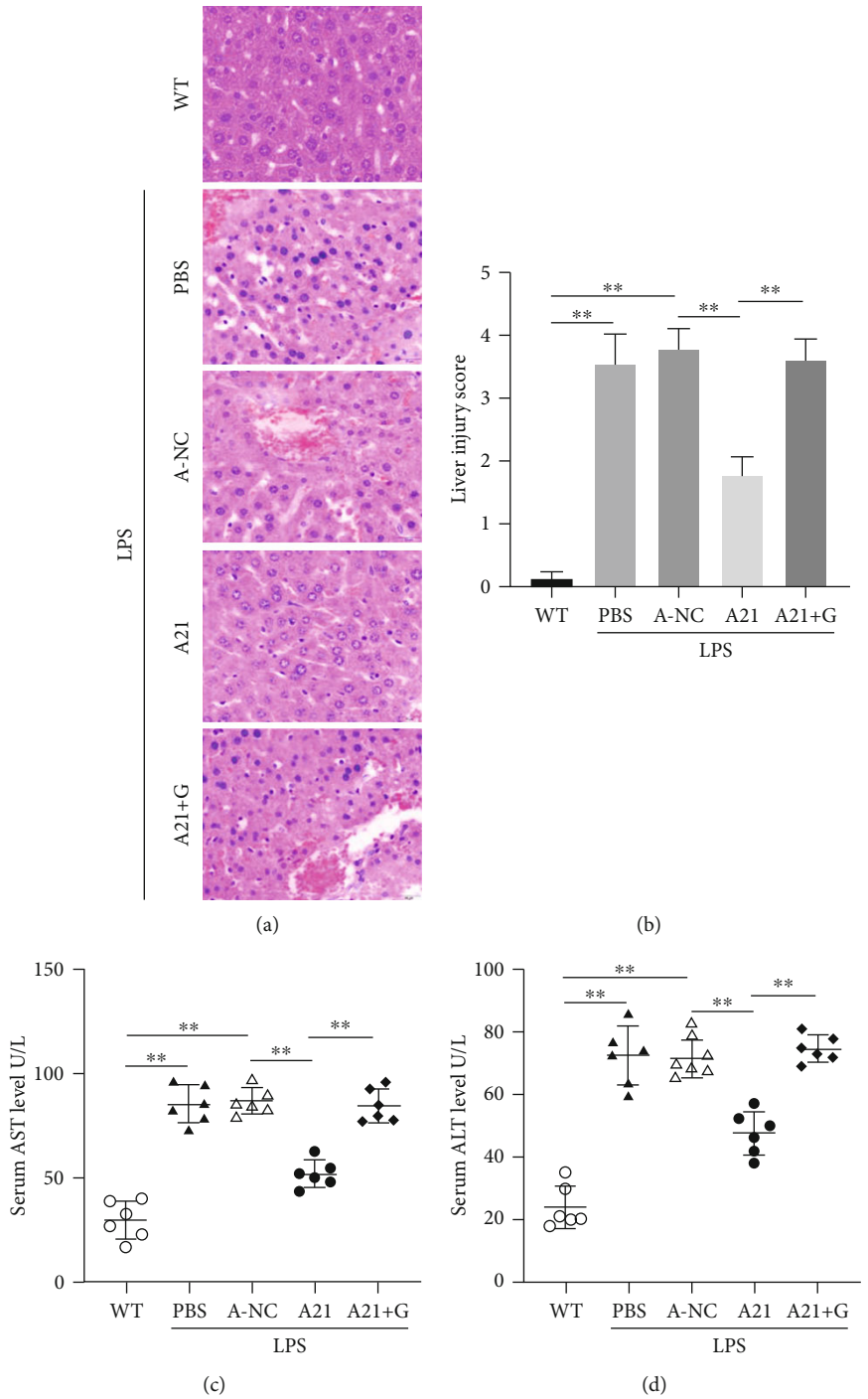

Figure 2: Continued.

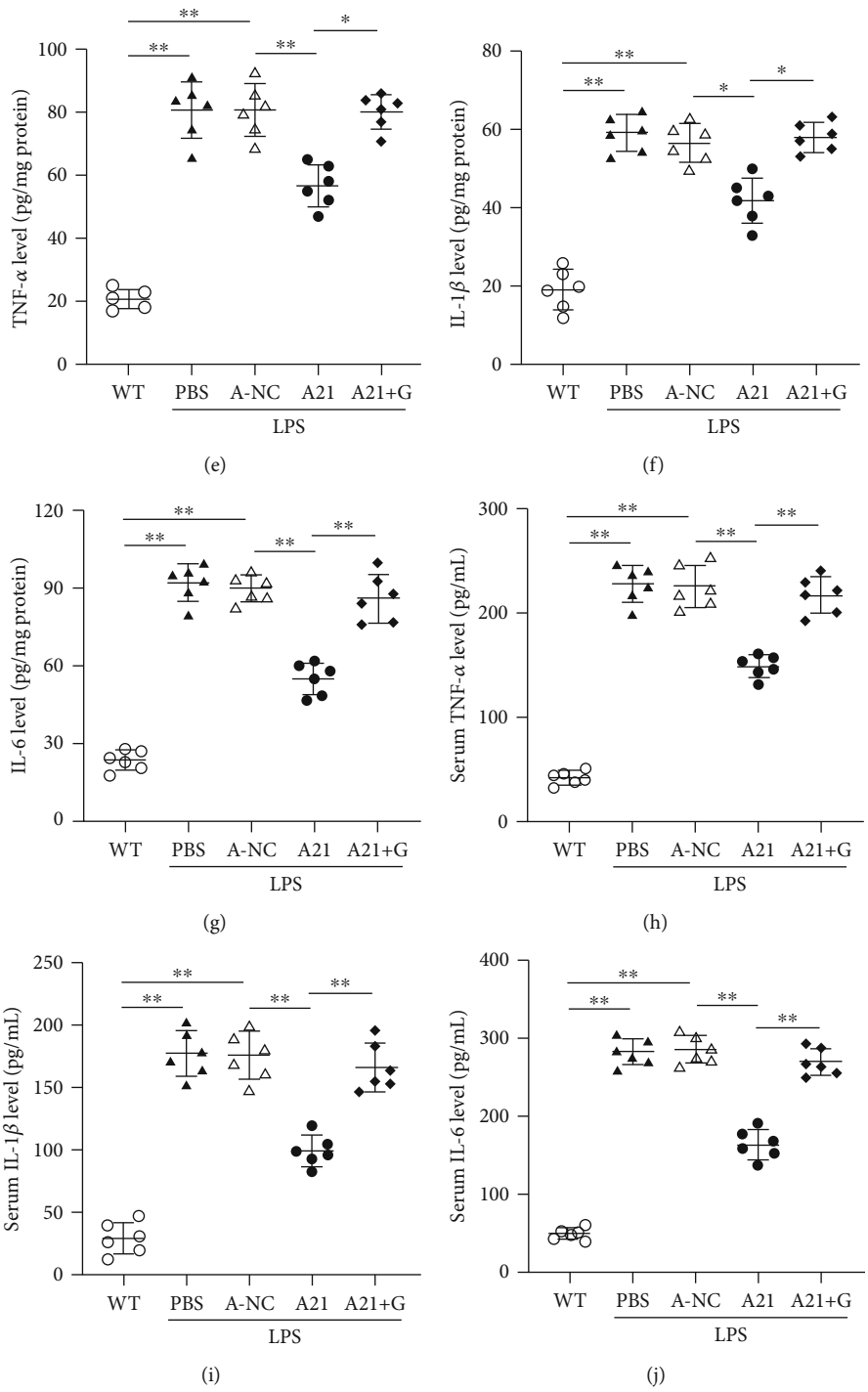

Figure 2: Antagomir-21 reduces liver injury and inflammation. (a, b) Histological analysis of livers. Tissue damages were scored in a scale of 0–4, with 0, 1, 2, 3, and 4 corresponding to 0%, <25%, 26%–50%, 51%–75%, and ≥76% of liver injury, respectively. (c, d) The serum aspartate aminotransferase (AST) and alanine aminotransferase (ALT) levels. (e–g) ELISA assay was used to determine the levels of TNF-α, IL-1β, and IL-6 in livers. (h–i) ELISA assay was used to determine the levels of TNF-α, IL-1β, and IL-6 in serum. $*p < 0.05$, $**p < 0.01$.

sepsis-induced liver injury, whereas PPARα antagonist GW6471 blocked the inhibitory effect of antagomir-21 on liver injury. Altogether, our study indicated that miR-21 regulated liver inflammation through PPARα inhibition.

Nevertheless, there are several limitations in our study. Recent studies reported that miR-21 was primarily expressed in biliary and inflammatory cells in the liver, rather than in hepatocytes. In this study, the cellular source of miR-21 was not elucidated; the function of miR-21/PPARα axis needs to be further explored.

In addition, miR-21 and PPAR agonists are considered druggable targets [20, 21]. This study showed that the mir-

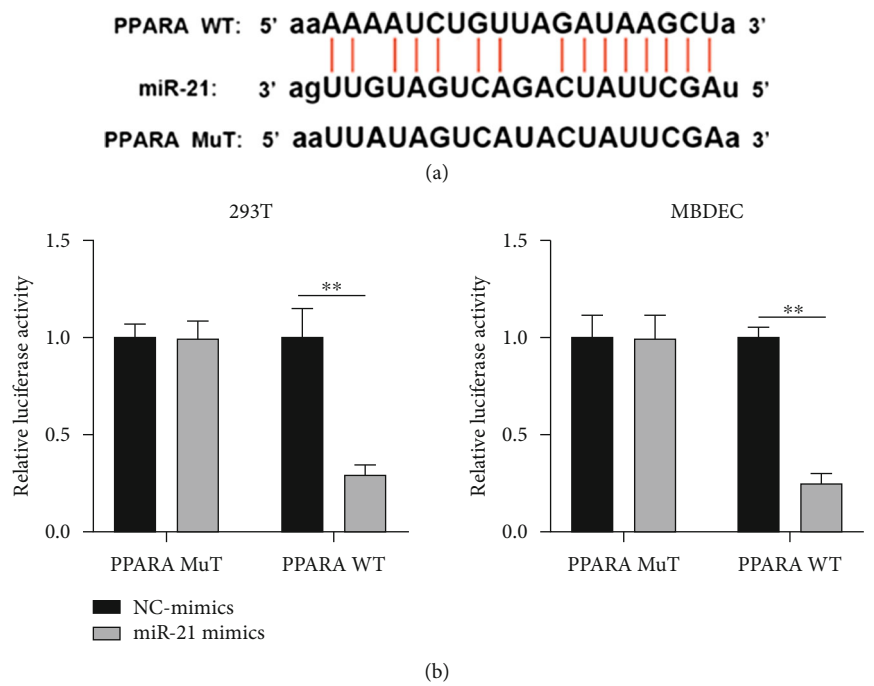

Figure 3: MiR-21 directly interacts with PPARα. (a) The putative binding sites between PPARA WT and miR-21. (b) Luciferase activity was detected in luciferase reporter vectors harboring PPARA WT/MuT sequences and miR-21 mimics cotransfected 293T and MBDEC cells. $**p < 0.01$.

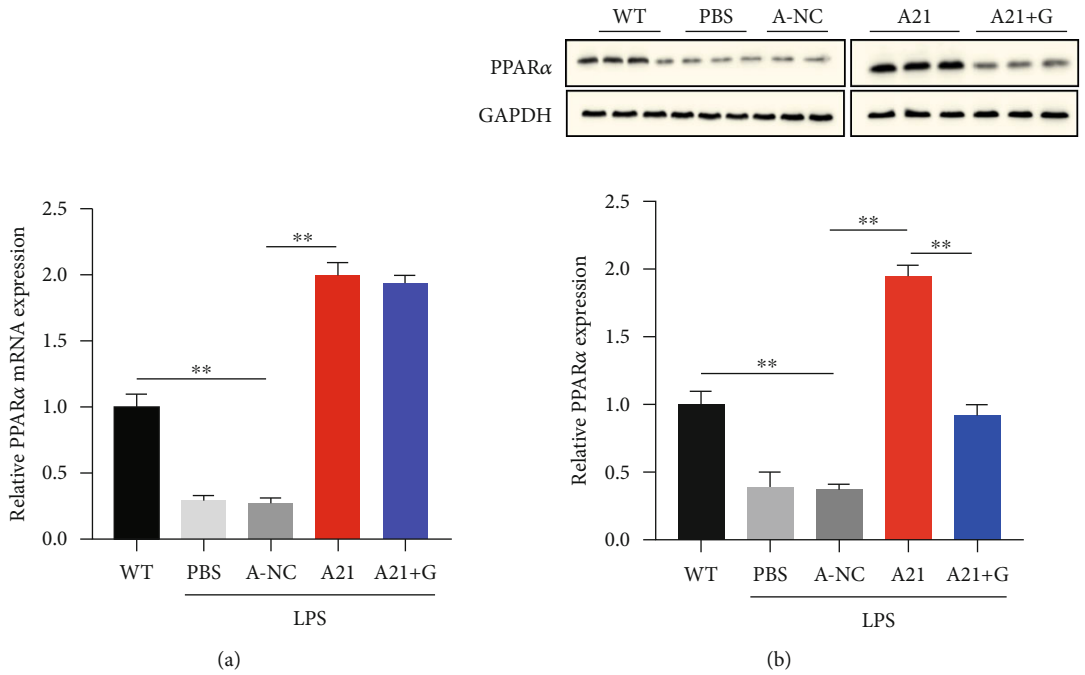

Figure 4: Antagomir-21 reduced liver injury and inflammation by restoring PPARα expression. (a) The expression of PPARα mRNA in livers was detected by qRT-PCR. (b) The expression of PPARα nuclear protein in livers was detected using western blot. $**p < 0.01$.

21/PPARα pathway might be an interesting new strategy for sepsis treatment. Some PPAR agonists, however, show side effects that cause them to be discontinued [22], and mir-21 antagonism treatment may also have side effects. Therefore, rigorous study design and safety monitoring are essential.

In conclusion, in LPS-induced sepsis mice model, we demonstrated that miR-21 contributed sepsis-induced liver injury and inflammation by inhibiting PPARα expression. Therefore, this study may provide an attractive potential target for the treatment of sepsis.

Data Availability

The data that support the findings of this study are available from the corresponding author upon reasonable request.

Conflicts of Interest

The authors confirm that there are no conflicts of interest.

Acknowledgments

This study was supported by the National Natural Science Foundation of China (No. 81601670) and Hubei Province Natural Science Fund (2014CFB302). We sincerely appreciate all lab members.

References

[1] J. Cohen, J.-L. Vincent, N. K. J. Adhikari et al., "Sepsis: a roadmap for future research," *The Lancet. Infectious diseases*, vol. 15, no. 5, pp. 581–614, 2015.

[2] L. Van Wyngene, T. Vanderhaeghen, S. Timmermans et al., "Hepatic PPARα function and lipid metabolic pathways are dysregulated in polymicrobial sepsis," *EMBO Molecular Medicine*, vol. 12, no. 2, article e11319, 2020.

[3] M. Singer, C. S. Deutschman, C. W. Seymour et al., "The third international consensus definitions for sepsis and septic shock (Sepsis-3)," *JAMA*, vol. 315, no. 8, pp. 801–810, 2016.

[4] N. Nesseler, Y. Launey, C. Aninat, F. Morel, Y. Mallédant, and P. Seguin, "Clinical review: the liver in sepsis," *Critical Care*, vol. 16, no. 5, p. 235, 2012.

[5] J. Yan, S. Li, and S. Li, "The role of the liver in sepsis," *International Reviews of Immunology*, vol. 33, no. 6, pp. 498–510, 2014.

[6] T. Evans, "Diagnosis and management of sepsis," *Clinical Medicine*, vol. 18, no. 2, pp. 146–149, 2018.

[7] I. Issemann and S. Green, "Activation of a member of the steroid hormone receptor superfamily by peroxisome proliferators," *Nature*, vol. 347, no. 6294, pp. 645–650, 1990.

[8] B. Tunctan, S. P. Kucukkavruk, M. Temiz-Resitoglu, D. S. Guden, A. N. Sari, and S. Sahan-Firat, "Bexarotene, a selective RXRα agonist, reverses hypotension associated with inflammation and tissue injury in a rat model of septic shock," *Inflammation*, vol. 41, no. 1, pp. 337–355, 2018.

[9] J. Korbecki, R. Bobinski, and M. Dutka, "Self-regulation of the inflammatory response by peroxisome proliferator-activated receptors," *Inflammation research: official journal of the European Histamine Research Society*, vol. 68, pp. 443–458, 2019.

[10] S. W. Standage, C. C. Caldwell, B. Zingarelli, and H. R. Wong, "Reduced peroxisome proliferator-activated receptor alpha expression is associated with decreased survival and increased tissue bacterial load in sepsis," *Shock*, vol. 37, no. 2, pp. 164–169, 2012.

[11] D. Portius, C. Sobolewski, and M. Foti, "MicroRNAs-dependent regulation of PPARs in metabolic diseases and cancers," *PPAR Research*, vol. 2017, Article ID 7058424, 2017.

[12] T. X. Lu, A. Munitz, and M. E. Rothenberg, "MicroRNA-21 is up-regulated in allergic airway inflammation and regulates IL-12p35 expression," *Journal of Immunology*, vol. 182, no. 8, pp. 4994–5002, 2009.

[13] Z. Xue, Q. Xi, H. Liu et al., "miR-21 promotes NLRP3 inflammasome activation to mediate pyroptosis and endotoxic shock," *Cell death & disease*, vol. 10, p. 461, 2019.

[14] P. Strnad, F. Tacke, A. Koch, and C. Trautwein, "Liver - guardian, modifier and target of sepsis," *Nature Reviews. Gastroenterology & Hepatology*, vol. 14, no. 1, pp. 55–66, 2017.

[15] R. Ji, Y. Cheng, J. Yue et al., "MicroRNA expression signature and antisense-mediated depletion reveal an essential role of MicroRNA in vascular neointimal lesion formation," *Circulation Research*, vol. 100, no. 11, pp. 1579–1588, 2007.

[16] X. Loyer, V. Paradis, C. Hénique et al., "Liver microRNA-21 is overexpressed in non-alcoholic steatohepatitis and contributes to the disease in experimental models by inhibiting PPARalpha expression," *Gut*, vol. 65, no. 11, pp. 1882–1894, 2016.

[17] D. Iliopoulos, K. N. Malizos, P. Oikonomou, and A. Tsezou, "Integrative microRNA and proteomic approaches identify novel osteoarthritis genes and their collaborative metabolic and inflammatory networks," *PLoS One*, vol. 3, no. 11, article e3740, 2008.

[18] S. Francque, A. Verrijken, S. Caron et al., "PPARalpha gene expression correlates with severity and histological treatment response in patients with non-alcoholic steatohepatitis," *Journal of Hepatology*, vol. 63, no. 1, pp. 164–173, 2015.

[19] M. Pawlak, E. Baugé, W. Bourguet et al., "The transrepressive activity of peroxisome proliferator-activated receptor alpha is necessary and sufficient to prevent liver fibrosis in mice," *Hepatology*, vol. 60, no. 5, pp. 1593–1606, 2014.

[20] X. W. Wang, N. H. Heegaard, and H. Orum, "MicroRNAs in liver disease," *Gastroenterology*, vol. 142, no. 7, pp. 1431–1443, 2012.

[21] J. M. Hesselink and T. A. Hekker, "Therapeutic utility of palmitoylethanolamide in the treatment of neuropathic pain associated with various pathological conditions: a case series," *Journal of Pain Research*, vol. 5, pp. 437–442, 2012.

[22] J. C. Fruchart, "Selective peroxisome proliferator-activated receptor alpha modulators (SPPARMalpha): the next generation of peroxisome proliferator-activated receptor alpha-agonists," *Cardiovascular diabetology*, vol. 12, p. 82, 2013.

Hindawi
PPAR Research
Volume 2020, Article ID 6661642, 7 pages
https://doi.org/10.1155/2020/6661642

Research Article

PPARα Agonist WY-14643 Relieves Neuropathic Pain through SIRT1-Mediated Deacetylation of NF-κB

Wanshun Wen,[1] Jinlin Wang,[2] Biyu Zhang,[3] and Jun Wang[3]

[1]*Department of Rehabilitation Medicine, Zhejiang Provincial People's Hospital, People's Hospital of Hangzhou Medical College, Hangzhou, Zhejiang Province, China*
[2]*Department of Anesthesiology, Wuhan Children's Hospital (Wuhan Maternal and Child Healthcare Hospital), Tongji Medical College, Huazhong University of Science & Technology, Wuhan, China*
[3]*Department of Anesthesiology, Huai'an Second People's Hospital and the Affiliated Huai'an Hospital of Xuzhou Medical University, Huai'an, Jiangsu, China*

Correspondence should be addressed to Biyu Zhang; zhangbiyu001@sina.com and Jun Wang; wangjuncn@aliyun.com

Received 15 October 2020; Revised 9 November 2020; Accepted 23 November 2020; Published 14 December 2020

Academic Editor: Xiao-Jie Lu

Inflammation caused by neuropathy contributes to the development of neuropathic pain (NP), but the exact mechanism still needs to be understood. Peroxisome proliferator-activated receptor α (PPARα), an important inflammation regulator, might participate in the inflammation in NP. To explore the role of PPARα in NP, the effects of PPARα agonist WY-14643 on chronic constriction injury (CCI) rats were evaluated. The results showed that WY-14643 stimulation could decrease inflammation and relieve neuropathic pain, which was relative with the activation of PPARα. In addition, we also found that the SIRT1/NF-κB pathway was involved in the WY-14643-induced anti-inflammation in NP, and activation of PPARα increased SIRT1 expression, thus reducing the proinflammatory function of NF-κB. These data suggested that WY-14643 might serve as an inflammation mediator, which may be a potential therapy option for NP.

1. Introduction

Neuropathic pain (NP), a complicated disease of the somatosensory nervous system, affects 7%-10% of the general population worldwide [1]. Patients who are diagnosed with NP will be accompanied with shooting and burning pain and tingling sensation so that their life quality decreases [2]. At present, the causative factors of NP is underestimated and the management of NP is on challenge [1]. Many studies show that there exists immune system dysfunction in NP, which leads to the process of allergic inflammation, as a way of the elevated proinflammatory cytokines and decreased anti-inflammatory cytokines [3–7]. However, the molecular mechanism of inflammation in NP still needs to be well established.

Peroxisome proliferator-activated receptor α (PPARα) that belongs to PPAR families is a ligand-activated transcription factor that regulates lipid metabolism, neuronal survival, cardiac pathophysiology, cell cycle, and inflammation [8, 9]. It is reported that PPARα exhibits inflammation-suppressing effects in obesity, atherosclerosis, autosomal dominant polycystic kidney disease, and acute kidney injury [10–13], but the role of PPARα in inflammation in NP still remains unclear. WY-14643, as a PPARα agonist, has been proved to reduce inflammation in several pathological processes [14]. Nevertheless, whether WY-14643 can suppress inflammation in NP is not elaborated.

Sirtuin 1 (SIRT1), a nicotinamide adenosine dinucleotide-dependent class III histone/protein deacetylase, participates in many cellular processes including aging, cell cycle, differentiation, apoptosis, metabolism, and inflammation [15, 16]. It is widely accepted that SIRT1 functioned as an inhibitor of nuclear factor-kappa B (NF-κB) signaling and p65 acetylation was considered a pacemaker of the NF-

κB pathway [17]. Subsequent accumulating evidence shows that SIRT1 has the capacity of inhibiting inflammation by NF-κB inhibition [18, 19].

In this study, we hypothesized that WY-14643 could alleviate the inflammation in NP via SIRT1/NF-κB signaling. To verify the hypothesis, the chronic constriction injury (CCI) rat model was established. Pain tests were performed to examine whether WY-14643 could relieve the NP in CCI rats, and the expression of proinflammatory cytokines was detected to evaluate the inflammation in CCI rats.

2. Materials and Method

2.1. Animals. Adult male Sprague-Dawley rats (200-250 g, 8 weeks) were used in this study and purchased from Zhejiang Provincial People's Hospital. All rats were randomly divided into 10 groups ($n = 6$). The animal experiments were approved by People's Hospital of Hangzhou Medical College and performed in accordance with the *Guidelines for the Care and Use of Laboratory Animals* published by the National Institutes of Health (2011).

2.2. CCI Model. Chronic constriction injury (CCI) surgery was performed according to the procedure described by Bennett and Xie [20]. Rats were anesthetized with sodium pentobarbital (40 mg/kg, i.p.). An incision was made below the hip bone and parallel to the sciatic nerve. In the CCI rat groups, the bilateral sciatic nerves of two legs were exposed and ligated loosely by 4-0 chromic gut sutures with about 1 mm spacing, while nothing was ligated in the sham group. The surgery was performed by the same researcher. After operation, CCI rats gradually showed typical signs of spontaneous hyperalgesia, but the behavioral performance of the sham group is the same as before the operation.

After surgery, the CCI rats were treated with WY-14643 (10 mg/kg) [21]; GW6471 (30 mg/kg) [22]; and si-SIRT1 (250 nm/kg); the drugs were given by intrathecal injection. Two hours after the injection, pain tests were performed.

2.3. Pain Tests

2.3.1. Mechanical Hyperalgesia. Paw withdrawal mechanical threshold (PWMT) [23] was determined applying electronic von Frey filament. Put the rats into plexiglass boxes ($50 \times 30 \times 30$ cm) with metal mesh floor. The filament was pressed on the plantar surface until the rats withdraw their paws. Record the values displayed by the electronic von Frey filament. Repeat each measurement 3 times at a 5-minute interval.

2.3.2. Thermal Hyperalgesia. Paw withdrawal thermal latency (PWTL) [23] was determined using the thermal radiation. Put the rats into plexiglass boxes for more than 30 minutes to adapt to the environment. The heat source was pointed at the plantar surface of the hind paws, and the time when rats show paw withdrawal was recorded. The thermal stimulus was repeated 3 times at 5-minute interval, and the average value was considered PWTL. All behavioral tests were performed by the same person.

2.4. RNA Extraction and qRT-PCR. When all pain tests were finished, the rats were decapitated immediately. Collect the serum and store it in a -80°C refrigerator. The L4-6 spinal cord was frozen by liquid nitrogen. Total RNA of the frozen spinal cord was extracted using Trizol reagent (Invitrogen, USA), and the concentration of RNA was measured using NanoDrop 2000. Then, the reverse transcription PCR was performed using PrimeScript RT Master Mix (Takara, Japan). The qRT-PCR was performed using SYBR Premix Ex Taq (Takara, Japan) and run on the ABI 7500 Real-Time PCR System (Life Technologies, USA). GAPDH was used as internal control. The relative expression was calculated with the $2^{-\Delta\Delta CT}$ algorithm.

2.5. ELISA. The TNF-α, IL-1β, and IL-6 levels of serum and spinal cords were detected using Rat TNF-α, IL-1β, and IL-6 Precoated Kits (Dakewe, China).

2.6. Western Blot. The frozen samples were lysed using T-PER Tissue Protein Extraction Reagent (Thermo Scientific, USA). Protein concentration was measured by BCA Protein Assay Kit (Leagene, China). 30 μg protein was separated by sodium dodecyl sulphate-polyacrylamide gel electrophoresis (SDS-PAGE) and transferred to polyvinylidene fluoride membranes. The membranes were incubated with primary antibodies (anti-SIRT1, 1 : 1000; anti-acetyl-NF-κB p65, 1 : 1000) overnight at 4°C and secondary antibodies (1 : 5000) at room temperature for 1 h. Western ECL Substrate (Bio-Rad, USA) was used to visualize the protein bands. ImageJ was used to analyze the gray value of protein bands.

2.7. Statistical Analysis. Results were presented as the mean ± standard deviation. The significance of the difference between two groups is determined by Student's t-test; differences between more than three groups were analyzed by one-way analysis of variance. The SPSS 23.0 (IBM, USA) and GraphPad Prism 6. Ink (GraphPad, California) were used for major analysis. $P < 0.05$ was regarded statistically significant.

3. Results

3.1. Acute WY-14643 Treatment Temporarily Alleviates NP. WY-14643 is a synthetic PPARα agonist; current researches show that PPARα plays a role in the development of NP. Therefore, to determine the antinociceptive effect of WY-14643 in NP, CCI rats were treated with WY-14643. Mechanical hyperalgesia and thermal allodynia were evaluated by PWMT and PWTL. Compared with the sham group, the PWMT and PWTL of the CCI group were significantly reduced. However, the PWMT was increased between 2 and 3 h after WY-14643 administration (Figure 1(a)). The PMTL was also improved between 2 and 4 h by WY-14643 treatment (Figure 1(b)). These results indicated that acute WY-14643 administration relieved NP temporarily.

3.2. Repeated WY-14643 Administration Alleviates NP in CCI Rats by Activating PPARα. Given the above findings, we next tested whether repeated WY-14643 treatment could promote

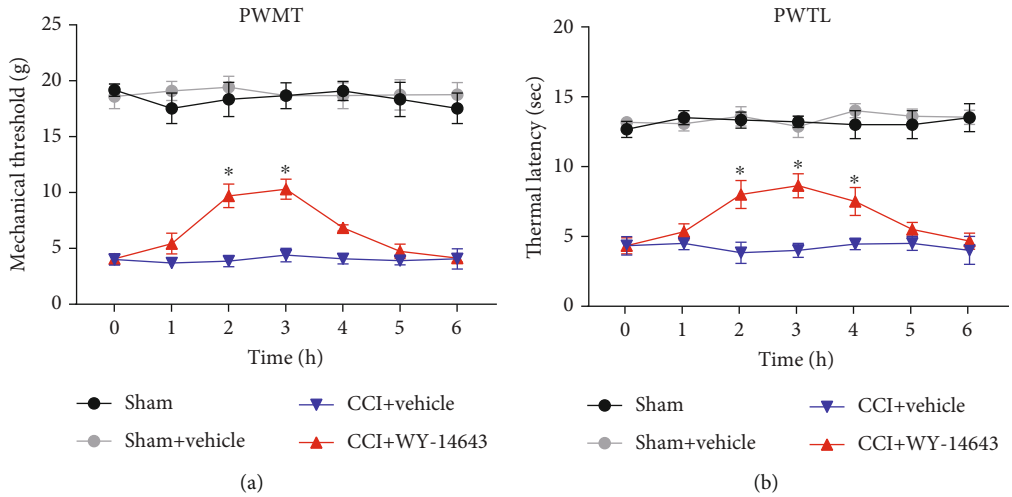

Figure 1: Acute WY-14643 treatment temporarily alleviated NP. (a) WY-14643 improved the paw withdrawal mechanical threshold (PWMT) of CCI rats. (b) WY-14643 improved the paw withdrawal thermal latency (PWTL) of CCI rats.

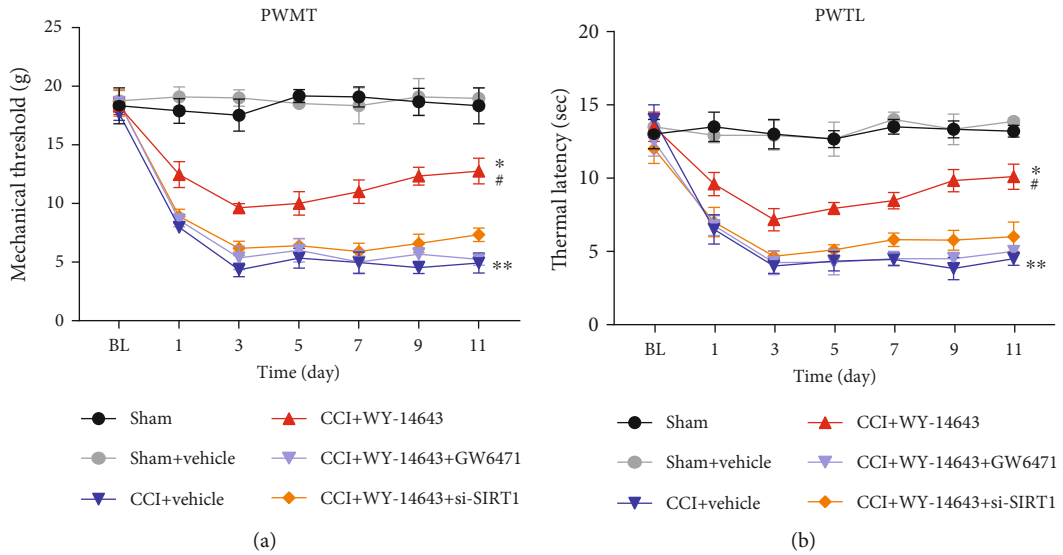

Figure 2: Repeated WY-14643 administration alleviated NP in CCI rats by activating PPARα. (a) WY-14643 increased the PWMT of CCI rats, but GW6471 and si-SIRT1 reversed this effect. (b) WY-14643 increased the PWTL of CCI rats, but GW6471 and si-SIRT1 reversed this effect.

the recovery of NP in CCI rats. Rats were treated with WY-14643 once a day for 11 days after surgery. In addition, it has been reported that SIRT1 is involved in inflammation regulation and interacts with PPAR. Therefore, PPARα antagonist GW6471 (MedChemExpress, USA) and in vivo si-SIRT1 (RiboBio, China) were also used to explore the mechanism of WY-14643 treating NP. Mechanical hyperalgesia was significantly reduced in the WY-14643 group, but GW6471 and si-SIRT1 aggravated the pain again (Figure 2(a)). Thermal hyperalgesia was also reduced by WY-14643 administration; however, GW6471 and si-SIRT1 reversed the antinociceptive effect of WY-14643 (Figure 2(b)). These data illustrated that WY-14643 relieved NP by acting as a PPARα agonist, and SIRT1 inhibition blocked the function of WY-14643 in NP.

3.3. Repeated WY-14643 Administration Reduces Inflammation in CCI Rats by Activating PPARα. Recent studies indicate that activation of PPARα increases the expression and activity of SIRT1, which leads to deacetylation of p65 NF-κB, thus inhibiting the expression of inflammatory cytokines [24, 25]. Since inflammation has been reported to be involved in the pathogenesis of neuropathic pain, the expression of proinflammatory cytokines including IL-1β, IL-6, and TNF-α was determined using ELISA. The serum and spinal cord samples were collected immediately after finishing all behavior tests. In CCI rats, IL-1β, IL-6, and TNF-α levels in serum were significantly increased (Figure 3(a)). Repeated WY-14643 treatment decreases the levels of these proinflammatory cytokines. However, PPARα antagonist (GW6471) and si-SIRT1 increase IL-1β, IL-6, and TNF-α levels in serum

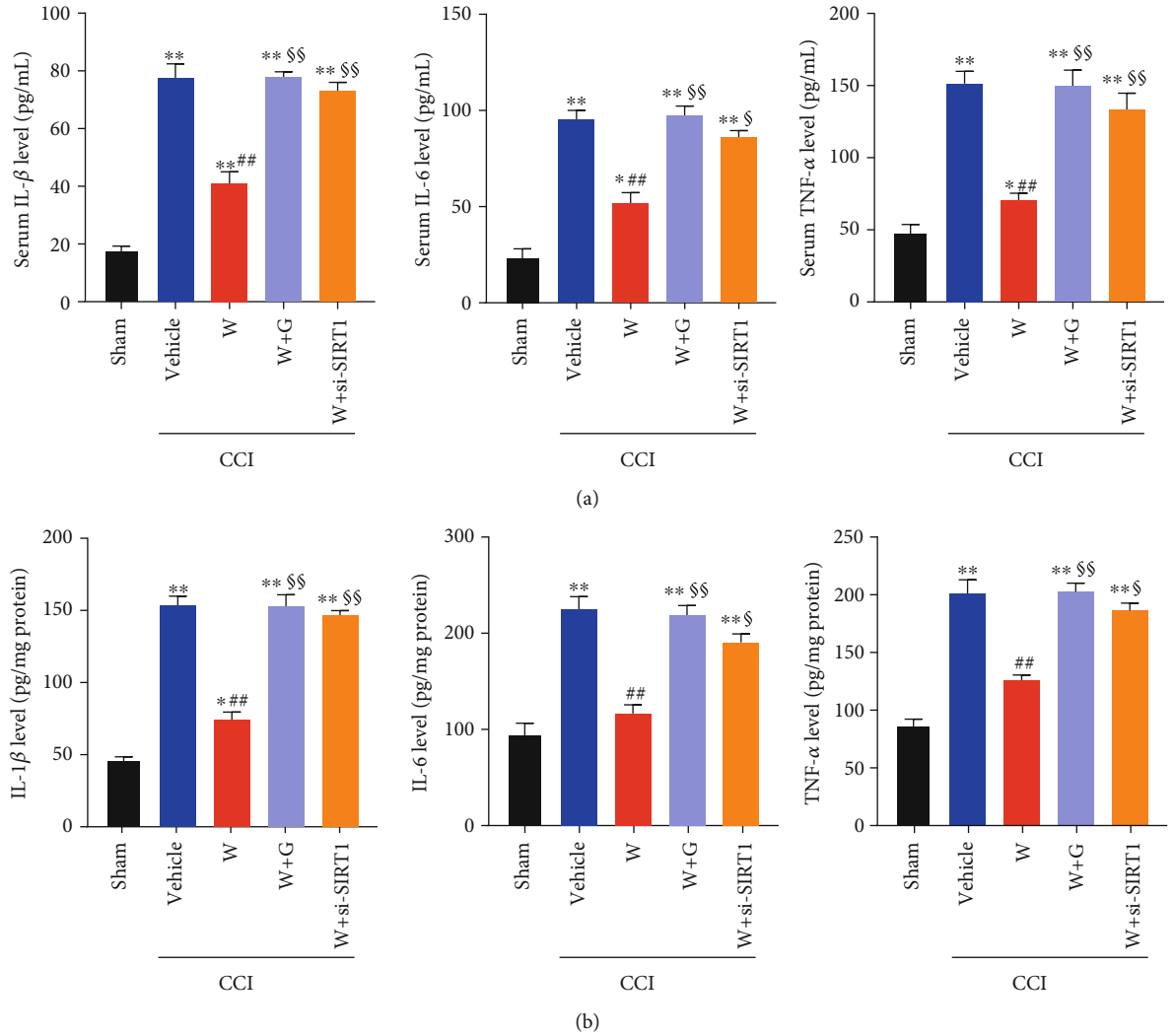

Figure 3: Repeated WY-14643 administration reduced inflammation in CCI rats by activating PPARα. (a) WY-14643 reduced IL-1β, IL-6, and TNF-α levels in serum of CCI rats, whereas GW6471 and si-SIRT1 reversed the anti-inflammatory effect. (b) WY-14643 reduced IL-1β, IL-6, and TNF-α levels in the spinal cord of CCI rats, whereas GW6471 and si-SIRT1 reversed the anti-inflammatory effect.

(Figure 3(a)). We also detected the expression of IL-1β, IL-6, and TNF-α in the spinal cord. WY-14643 markedly suppressed the inflammation in CCI rats, whereas GW6471 and si-SIRT1 reversed the anti-inflammatory effect induced by WY-14643 (Figure 3(b)). Taken together, the results showed that WY-14643 reduced the inflammation in NP through the PPARα/SIRT1 pathway.

3.4. SIRT1/NF-κB Pathway Mediates WY-14643-Induced Inhibition of NP. NF-κB is a key inflammatory mediator, which participates in the regulation of inflammatory response. SIRT1, a nicotinamide adenine dinucleotide-dependent deacetylase, has been shown to inhibit NF-κB signaling by deacetylating the p65 subunit of NF-κB complex [24]. To further explore the molecular mechanism of NP, we detected the expression of SIRT1 and acetylated NF-κB p65 (Ac-NF-κB p65). CCI decreases SIRT1 expression (Figure 4(a)), whereas Ac-NF-κB p65 expression was significantly increased (Figure 4(b)). WY-14643 treatment increased SIRT1 expression, thus deacetylating NF-κB p65. But GW6471 and si-SIRT1 inhibited the expression of SIRT1 and restored the Ac-NF-κB p65 expression (Figures 4(a) and 4(b)). These results demonstrated that WY-14643 alleviated NP through the PPARα-mediated SIRT1/NF-κB pathway in CCI rats.

4. Discussion

The underlying basis of NP is the chronic ectopic electrical activity of nociceptive neurons. The cells located in the injury site release proinflammatory cytokines, leading to a proinflammatory environment [7]. Therefore, a deep understanding of how to reduce inflammation is urgent for NP treatment. PPARα has gained great attention for its anti-inflammatory effects in many disease models. However, the molecular mechanism between PPARα activation and inflammation in CCI model has not been fully elucidated. In this study, we first used PPARα agonist WY-14643 to

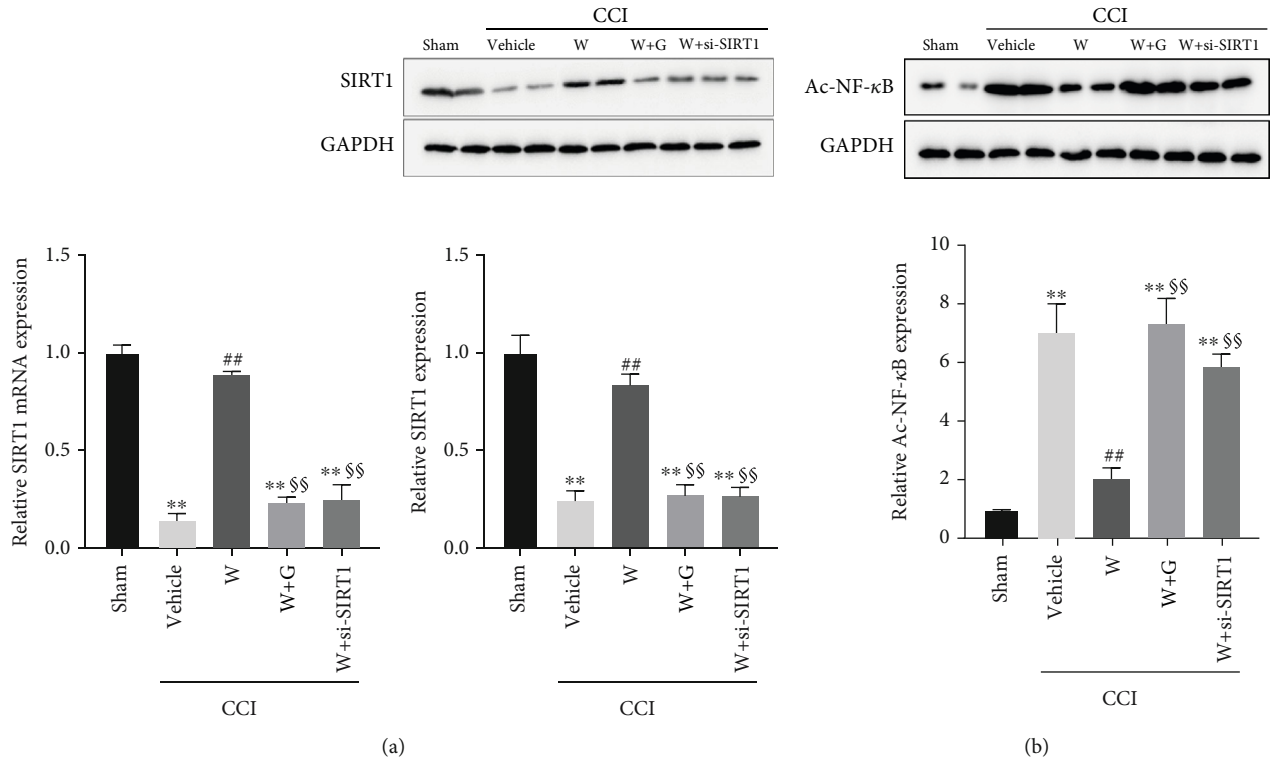

Figure 4: WY-14643 mediated the SIRT1/NF-κB pathway by activating PPARα. (a) The expression of SIRT1 in different groups was detected by qRT-PCR and western blot. WY-14643 administration increased SIRT1 expression. (b) The expression of acetylated NF-κB p65 in different groups was detected by western blot. WY-14643 administration decreased acetylated NF-κB p65 expression, but SIRT1 inhibition increased acetylated NF-κB p65 expression. The relative protein expression was normalized according to the gray value of the band, which was analyzed by ImageJ.

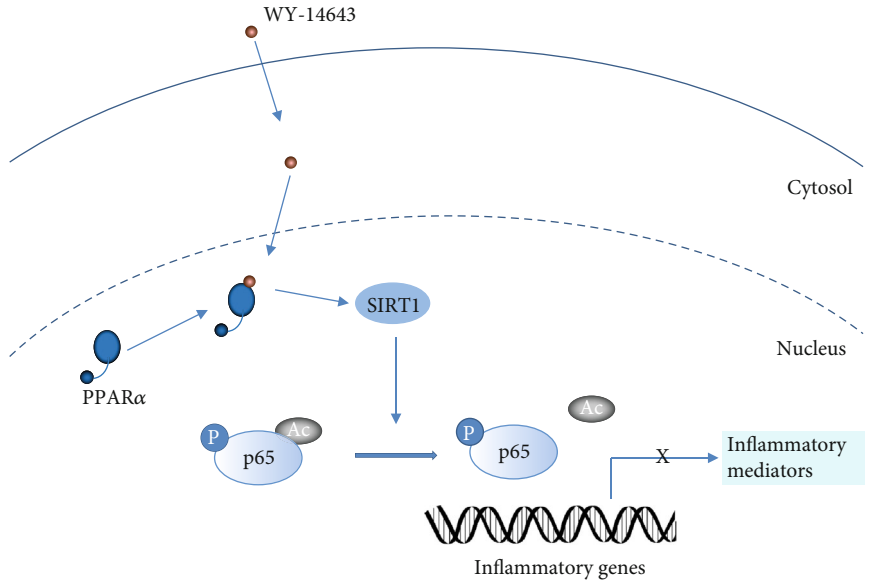

Figure 5: The PPARα/SIRT1/NF-κB pathway in the inflammation in NP.

explore the signaling pathway between the PPARα activation and inflammation in NP.

Firstly, we found that the PWMT and PWTL of CCI rats were significantly lower than those of the sham group, whereas PPARα agonist WY-14643 treatment would increase the PWMT and PWTL. Subsequently, we compared the effects of WY-14643 and PPARα antagonist GW6471 on the CCI rats. The significant reduction of mechanical and thermal hyperalgesia in WY-14643-treated group was observed; however, GW6471 administration blocked these

effects. The above results suggested that WY-14643 owned potential treatment value for NP. And this is the first time that the function of WY-14643 in NP was studied.

Previous evidences demonstrated that PPARα could activate SIRT1 and play a role in many biological processes. Oka et al. reported that the PPARα/SIRT1 pathway took part in the progression of heart failure by promoting mitochondrial dysfunction [26]. Ogawa et al. found that the repression of microglial activation was associated with SIRT1-dependent PPARα signaling [27]. Sandoval-Rodriguez et al. showed that PPARα improved nonalcoholic steatohepatitis via acting on SIRT1 [28]. However, whether the PPARα/SIRT1 pathway was involved in NP development was unclear. In CCI rats, we found that mechanical and thermal hyperalgesia was downregulated in the WY-14643 group, whereas coadministration of si-SIRT1 and WY-14643 would recover the damage again in rats. These findings proved that the PPARα/SIRT1 pathway might participate in the pathogenesis of NP.

To explore the effects of PPARα/SIRT1 signaling on inflammation, we detected the expression of inflammatory cytokines and noticed that the inflammatory cytokines were evidently increased in CCI rats, but WY-14643 treatment restrained the inflammation. Further treatment with si-SIRT1 would reverse the anti-inflammatory effect stimulated by WY-14643. It suggested that PPARα/SIRT1 signaling might be relative to the inflammation progression of NP. The results were consistent with the clues that PPARα had a hand in inflammation by regulating SIRT1 [28]. Moreover, since SIRT1 was capable of bating inflammation by inhibition of NF-κB [15, 17], we also determined the levels of SIRT1 and acetylated NF-κB p65 in CCI rats. WY-14643 could make SIRT1 activated and deacetylate NF-κB p65, but GW6471 and si-SIRT1 would reduce the expression of SIRT1 and upregulate the expression of Ac-NF-κB p65. The regulating pathway is shown in Figure 5.

However, there are still limitations in our study. Currently, sufficient evidence to support the clinical application of WY-14643 for NP is lacking, and the side effects of WY-14643 are uncertain. Consequently, the safety of WY-14643 should be further considered. And we will also further explore the safety of WY-14643 in the future.

In conclusion, our study illustrates that PPARα agonist WY-14643 relieves inflammation in NP via the SIRT1/NF-κB pathway.

Data Availability

All data are available upon request.

Conflicts of Interest

The authors declare that there is no conflict of interest.

Authors' Contributions

Wanshun Wen and Jinlin Wang performed the experiments, analyzed the data, and wrote the manuscript. Biyu Zhang and Jun Wang designed the experiments and revised the manuscript. All authors read and approved the final manuscript. Wanshun Wen and Jinlin Wang are co-first authors.

Acknowledgments

The authors thank the Zhejiang Provincial People's Hospital, Wuhan Children's Hospital, and Huai'an Second People's Hospital for the support.

References

[1] D. Szok, J. Tajti, A. Nyári, L. Vécsei, and L. Trojano, "Therapeutic approaches for peripheral and central neuropathic pain," *Behavioural Neurology*, vol. 2019, Article ID 8685954, 13 pages, 2019.

[2] K. Liu and L. Wang, "Optogenetics: therapeutic spark in neuropathic pain," *Bosnian Journal of Basic Medical Sciences*, vol. 19, no. 4, pp. 321–327, 2019.

[3] D. J. Allison, A. Thomas, K. Beaudry, and D. S. Ditor, "Targeting inflammation as a treatment modality for neuropathic pain in spinal cord injury: a randomized clinical trial," *Journal of Neuroinflammation*, vol. 13, no. 1, 2016.

[4] G. M. Alexander, M. A. van Rijn, J. J. van Hilten, M. J. Perreault, and R. J. Schwartzman, "Changes in cerebrospinal fluid levels of pro-inflammatory cytokines in CRPS," *Pain*, vol. 116, no. 3, pp. 213–219, 2005.

[5] N. Eijkelkamp, C. Steen-Louws, S. A. Hartgring et al., "IL4-10 fusion protein is a novel drug to treat persistent inflammatory pain," *The Journal of Neuroscience*, vol. 36, no. 28, pp. 7353–7363, 2016.

[6] L. J. Zhou, J. Peng, Y. N. Xu et al., "Microglia are indispensable for synaptic plasticity in the spinal dorsal horn and chronic pain," *Cell Reports*, vol. 27, no. 13, pp. 3844–3859.e6, 2019.

[7] D. P. Kuffler, "Mechanisms for reducing neuropathic pain," *Molecular Neurobiology*, vol. 57, no. 1, pp. 67–87, 2020.

[8] E. A. Pearsall, R. Cheng, K. Zhou et al., "PPARα is essential for retinal lipid metabolism and neuronal survival," *BMC Biology*, vol. 15, no. 1, article 113, 2017.

[9] N. Bougarne, B. Weyers, S. J. Desmet et al., "Molecular actions of PPARα in lipid metabolism and inflammation," *Endocrine Reviews*, vol. 39, no. 5, pp. 760–802, 2018.

[10] D. E. Stec, D. M. Gordon, J. A. Hipp et al., "Loss of hepatic PPARα promotes inflammation and serum hyperlipidemia in diet-induced obesity," *American Journal of Physiology-Regulatory, Integrative and Comparative Physiology*, vol. 317, no. 5, pp. R733–R745, 2019.

[11] N. Hennuyer, I. Duplan, C. Paquet et al., "The novel selective PPARα modulator (SPPARMα) pemafibrate improves dyslipidemia, enhances reverse cholesterol transport and decreases inflammation and atherosclerosis," *Atherosclerosis*, vol. 249, pp. 200–208, 2016.

[12] R. Lakhia, M. Yheskel, A. Flaten, E. B. Quittner-Strom, W. L. Holland, and V. Patel, "PPARα agonist fenofibrate enhances fatty acid β-oxidation and attenuates polycystic kidney and liver disease in mice," *American Journal of Physiology-Renal Physiology*, vol. 314, no. 1, pp. F122–F131, 2018.

[13] T. Iwaki, B. G. Bennion, E. K. Stenson et al., "PPARα contributes to protection against metabolic and inflammatory derangements associated with acute kidney injury in experimental sepsis," *Physiological Reports*, vol. 7, no. 10, article e14078, 2019.

[14] R. Yang, P. Wang, Z. Chen et al., "WY-14643, a selective agonist of peroxisome proliferator-activated receptor-α, ameliorates lipopolysaccharide-induced depressive-like behaviors by

preventing neuroinflammation and oxido-nitrosative stress in mice," *Pharmacology Biochemistry and Behavior*, vol. 153, pp. 97–104, 2017.

[15] S. R. Yang, J. Wright, M. Bauter, K. Seweryniak, A. Kode, and I. Rahman, "Sirtuin regulates cigarette smoke-induced proinflammatory mediator release via RelA/p65 NF-κB in macrophages in vitro and in rat lungs in vivo: implications for chronic inflammation and aging," *American Journal of Physiology-Lung Cellular and Molecular Physiology*, vol. 292, no. 2, pp. L567–L576, 2007.

[16] S. Stein and C. M. Matter, "Protective roles of SIRT1 in atherosclerosis," *Cell Cycle*, vol. 10, no. 4, pp. 640–647, 2014.

[17] H. S. Kwon, M. M. Brent, R. Getachew et al., "Human immunodeficiency virus type 1 Tat protein inhibits the SIRT1 deacetylase and induces T cell hyperactivation," *Cell Host & Microbe*, vol. 3, no. 3, pp. 158–167, 2008.

[18] J. Chen, Y. Zhou, S. Mueller-Steiner et al., "SIRT1 protects against microglia-dependent Amyloid-β toxicity through inhibiting NF-κB signaling," *The Journal of Biological Chemistry*, vol. 280, no. 48, pp. 40364–40374, 2005.

[19] W. Wang, L. Bai, H. Qiao et al., "The protective effect of fenofibrate against TNF-α-induced CD40 expression through SIRT1-mediated deacetylation of NF-κB in endothelial cells," *Inflammation*, vol. 37, no. 1, pp. 177–185, 2014.

[20] G. J. Bennett and Y. K. Xie, "A peripheral mononeuropathy in rat that produces disorders of pain sensation like those seen in man," *Pain*, vol. 33, no. 1, pp. 87–107, 1988.

[21] A. A. Santilli, A. C. Scotese, and R. M. Tomarelli, "A potent antihypercholesterolemic agent: (4-chloro-6-(2,3-xylidino)-2-pyrimidinylthio) acetic acid (Wy-14643)," *Experientia*, vol. 30, no. 10, pp. 1110-1111, 1974.

[22] H. E. Xu, T. B. Stanley, V. G. Montana et al., "Structural basis for antagonist-mediated recruitment of nuclear co-repressors by PPARα," *Nature*, vol. 415, no. 6873, pp. 813–817, 2002.

[23] J. Chen and H. S. Chen, "Pivotal role of capsaicin-sensitive primary afferents in development of both heat and mechanical hyperalgesia induced by intraplantar bee venom injection," *Pain*, vol. 91, no. 3, pp. 367–376, 2001.

[24] A. Kauppinen, T. Suuronen, J. Ojala, K. Kaarniranta, and A. Salminen, "Antagonistic crosstalk between NF-κB and SIRT1 in the regulation of inflammation and metabolic disorders," *Cellular Signalling*, vol. 25, no. 10, pp. 1939–1948, 2013.

[25] S. A. Khan, A. Sathyanarayan, M. T. Mashek, K. T. Ong, E. E. Wollaston-Hayden, and D. G. Mashek, "ATGL-catalyzed lipolysis regulates SIRT1 to control PGC-1α/PPAR-α signaling," *Diabetes*, vol. 64, no. 2, pp. 418–426, 2015.

[26] S. Oka, R. Alcendor, P. Zhai et al., "PPARα-Sirt1 complex mediates cardiac hypertrophy and failure through suppression of the ERR transcriptional pathway," *Cell Metabolism*, vol. 14, no. 5, pp. 598–611, 2011.

[27] K. Ogawa, T. Yagi, T. Guo et al., "Pemafibrate, a selective PPARα modulator, and fenofibrate suppress microglial activation through distinct PPARα and SIRT1-dependent pathways," *Biochemical and Biophysical Research Communications*, vol. 524, no. 2, pp. 385–391, 2020.

[28] A. Sandoval-Rodriguez, H. C. Monroy-Ramirez, A. Meza-Rios et al., "Pirfenidone is an agonistic ligand for PPARα and improves NASH by activation of SIRT1/LKB1/pAMPK," *Hepatology Communications*, vol. 4, no. 3, pp. 434–449, 2020.

Hindawi
PPAR Research
Volume 2020, Article ID 8894525, 12 pages
https://doi.org/10.1155/2020/8894525

Research Article

Nonclassical Axis of the Renin-Angiotensin System and Neprilysin: Key Mediators That Underlie the Cardioprotective Effect of PPAR-Alpha Activation during Myocardial Ischemia in a Metabolic Syndrome Model

María Sánchez-Aguilar,[1] **Luz Ibarra-Lara**,[1] **Leonardo del Valle-Mondragón**,[1] **Elizabeth Soria-Castro**,[2] **Juan Carlos Torres-Narváez**,[1] **Elizabeth Carreón-Torres**,[3] **Alicia Sánchez-Mendoza**,[1] **and María Esther Rubio-Ruíz**[4]

[1]*Department of Pharmacology, Instituto Nacional de Cardiología Ignacio Chávez, Juan Badiano 1, Sección XVI, Tlalpan, Mexico City 14080, Mexico*
[2]*Department of Cardiovascular Biomedicine, Instituto Nacional de Cardiología Ignacio Chávez, Juan Badiano 1, Sección XVI, Tlalpan, Mexico City 14080, Mexico*
[3]*Department of Molecular Biology, Instituto Nacional de Cardiología Ignacio Chávez, Juan Badiano 1, Sección XVI, Tlalpan, Mexico City 14080, Mexico*
[4]*Department of Physiology, Instituto Nacional de Cardiología Ignacio Chávez, Juan Badiano 1, Sección XVI, Tlalpan, Mexico City 14080, Mexico*

Correspondence should be addressed to María Esther Rubio-Ruíz; esther_rubio_ruiz@yahoo.com

María Sánchez-Aguilar and Luz Ibarra-Lara contributed equally to this work.

Received 14 September 2020; Revised 10 November 2020; Accepted 11 November 2020; Published 28 November 2020

Academic Editor: Sainan Li

The activation of the renin-angiotensin system (RAS) participates in the development of metabolic syndrome (MetS) and in heart failure. PPAR-alpha activation by fenofibrate reverts some of the effects caused by these pathologies. Recently, nonclassical RAS components have been implicated in the pathogenesis of hypertension and myocardial dysfunction; however, their cardiac functions are still controversial. We evaluated if the nonclassical RAS signaling pathways, directed by angiotensin III and angiotensin-(1-7), are involved in the cardioprotective effect of fenofibrate during ischemia in MetS rats. Control (CT) and MetS rats were divided into the following groups: (a) sham, (b) vehicle-treated myocardial infarction (MI-V), and (c) fenofibrate-treated myocardial infarction (MI-F). Angiotensin III and angiotensin IV levels and insulin increased the aminopeptidase (IRAP) expression and decreased the angiotensin-converting enzyme 2 (ACE2) expression in the hearts from MetS rats. Ischemia activated the angiotensin-converting enzyme (ACE)/angiotensin II/angiotensin receptor 1 (AT1R) and angiotensin III/angiotensin IV/angiotensin receptor 4 (AT4R)-IRAP axes. Fenofibrate treatment prevented the damage due to ischemia in MetS rats by favoring the angiotensin-(1-7)/angiotensin receptor 2 (AT2R) axis and inhibiting the angiotensin III/angiotensin IV/AT4R-IRAP signaling pathway. Additionally, fenofibrate downregulated neprilysin expression and increased bradykinin production. These effects of PPAR-alpha activation were accompanied by a reduction in the size of the myocardial infarct and in the activity of serum creatine kinase. Thus, the regulation of the nonclassical axis of RAS forms part of a novel protective effect of fenofibrate in myocardial ischemia.

1. Introduction

The renin-angiotensin system (RAS) is a complex hormone system that plays a critical role in cardiovascular physiology. Indeed, RAS has a central role in the development of metabolic syndrome (MetS), insulin resistance, and heart failure [1].

The RAS is a system composed of different angiotensin peptides with different biological actions mediated by distinct receptor subtypes. The classical RAS comprises the renin angiotensin-converting enzyme (ACE)/angiotensin II (Ang II)/angiotensin receptor 1 (AT1R) axis and promotes vasoconstriction and increases oxidative stress, fibrosis, cellular growth, and inflammation [1]. In contrast, the nonclassical RAS, composed mainly by the angiotensin-converting enzyme 2 (ACE2)/angiotensin-(1-7) (Ang-(1-7))/Mas receptor (MasR)/angiotensin receptor 2 (AT2R) pathway, improves the cardiac function of hearts subjected to myocardial infarction (MI) and has a beneficial role in insulin resistance, hypertriglyceridemia, fatty liver disease, and obesity [1–4].

Currently, additional metabolites of RAS and some of their biological functions have been described. Ang III, formed from Ang II by aminopeptidase A (APA), is cleaved by aminopeptidase N (APN) forming Ang IV. Ang IV binds to the angiotensin type 4 receptor (AT4), identified as an insulin-regulated aminopeptidase (IRAP), and it plays a potential role in the regulation of glucose homeostasis and inflammatory processes and in the metabolism of various hormones including vasopressin, oxytocin, and somatostatin [5, 6]. Ang III and APA are potential therapeutic targets for the treatment of hypertension; however, the roles of Ang III and Ang IV in cardiac function remain controversial [7–10].

On the other hand, neprilysin (NEP) is a ubiquitous endopeptidase of RAS, essential for the metabolism of the biologically active natriuretic peptides and several other vasoactive compounds, including adrenomedullin, endothelin 1, and bradykinin [11]. Moreover, plasmatic NEP levels have been positively associated with heart failure, obesity, and MetS [12, 13]. This enzyme is a target of multiple clinical trials given its importance in cardiovascular diseases, and a new class of drugs called "ARNI" (angiotensin receptor blocker-neprilysin inhibitor) is currently being used as therapy for hypertension and heart failure [14, 15].

Fenofibrate acts as an agonist of the peroxisome proliferator-activated receptor alpha (PPAR-α) that regulates the expression of target genes, including some components of RAS. Fenofibrate has pleiotropic effects besides lowering lipids, such as improving vascular endothelial function and reducing oxidative stress, inflammation, and fibrosis during cardiac ischemia [1, 16, 17]. However, the exact mechanism underlying the beneficial effect of fenofibrate on cardiovascular diseases remains uncertain.

Our previous work demonstrated that fenofibrate treatment decreased ischemic damages by favoring an antioxidant environment as a consequence of reducing the Ang II/AT1R signaling pathway and reestablishing the cardiac insulin signaling pathway. Although numerous experimental studies have focused on an alternative RAS cascade, to our knowledge, there are no reports on the effect of fenofibrate on these novel important components of RAS in myocardial ischemia. Therefore, the aim of the current study was to evaluate if the nonclassical RAS signaling pathways, directed by Ang III, Ang-(1-7), and NEP expression, are involved in the cardioprotective effect of fenofibrate during ischemia in MetS rats.

2. Methods

2.1. Animals and Surgical Procedures. All the experiments were conducted in accordance with our Institutional Ethical Guidelines (Ministry of Agriculture, SAGARPA, NOM-062-ZOO-1999, Mexico). Male 25-day-old Wistar rats weighing 45 ± 9 g were randomly separated into two groups of 10-12 animals: group 1, control rats that were given tap water for drinking; group 2, MetS rats that received 30% sugar in drinking water during 24 weeks. The animals were maintained under standard conditions of light and temperature with water and food *ad libitum* (LabDiet 5001; Richmond, IN, USA). Systolic arterial blood pressure was determined in conscious animals by a plethysmographic method described previously [1].

Animals from each experimental group were divided to receive one of the subchronic (two weeks) oral gavage treatments: (a) vehicle (NaCl 0.9%) or (b) fenofibrate (100 mg/kg/day). This dose was selected based on previous publications and from a dose-response curve to fenofibrate [1, 16, 17]. At the end of the treatment, the animals were anesthetized (ketamine hydrochloride 80 mg/kg and xylazine hydrochloride 10 mg/kg, I.M.) and they were assigned to either sham-operated (Sh) or myocardial infarction (MI) for 60 min. As previously reported, MI was achieved occluding the left anterior descending coronary artery with 7-0 PROLENE® polypropylene suture (Ethicon, São José dos Campos, Brazil) [1]. Then, the rats were sacrificed, the heart was cut out, and the ischemic area was separated to perform the analysis. Additionally, the abdominal white adipose tissue was removed and weighed.

2.2. Measurement of Serum Biochemical Parameters. The fasting measurements of glucose, HDL-C, non-HDL-C, and triglycerides were performed with commercial enzymatic kits. Serum insulin levels were measured using a rat-specific insulin radioimmunoassay (Linco Research, Inc., Missouri, USA). Insulin resistance was estimated from the homeostasis model (HOMA-IR) [18].

Creatine kinase (CK) activity was spectrophotometrically determined at 340 nm (UV-test, Roche Cobas C-501, Roche Diagnostics, Indianapolis, IN, USA) after the MI procedure. The determination of CK was carried out using the reverse reaction and activation by N-acetylcysteine (NAC) at 37°C. Equimolar quantities of NADPH and ATP are formed at the same rate. The photometrically measured rate of formation of NADPH is directly proportional to the CK activity [19].

2.3. Electrophoretic Determinations. Ang II, Ang III, Ang IV, and Ang-(1-7) concentrations were evaluated in myocardial

ischemic areas from the different experimental groups by capillary zone electrophoresis (CZE, P/ACE MDQ Capillary Electrophoresis System, Beckman Coulter, Inc., Fullerton, CA, USA) according to the methods previously described [1, 18]. Bradykinin was evaluated by capillary electrophoresis with a laser-induced fluorescence detector, as previously reported [20].

2.4. Western Blotting Analysis. The frozen myocardial ischemic area was homogenized with a polytron (model PT-MR2100; Kinematica AG, Lucerne, Switzerland) (25% w/v) in a lysis buffer pH = 7.4 (Tris-HCl 250 mM, NaF 0.2 M, Na_3VO_4 10 mM, and NP40 1%) and a protease inhibitor cocktail (cOmplete® tablets, Roche Applied Science, Mannheim, Germany) at 4°C. A total of 100 μg protein was separated on a SDS-PAGE (12% bis-acrylamide-Laemmli gel) and transferred to a polyvinylidene difluoride (PVDF) membrane. Blots were blocked for 3 h at room temperature using Tris-buffered saline with 0.05% Tween (TBS-T) and 5% nonfat dehydrated milk. Afterwards, membranes were incubated overnight with primary antibodies at 4°C. ACE, ACE2, AT1R, AT2R, MasR, APA, APN, and NEP primary antibodies were acquired from Santa Cruz Biotechnology (Santa Cruz, CA, USA); IRAP antibody was from Cell Signaling Technology (Danvers, MA, USA). Secondary horseradish peroxidase-labeled antibodies were from Jackson ImmunoResearch (Suffolk, UK). All blots were incubated with β-actin antibody as a load control. After incubation, the blots were visualized using the Immobilon chemiluminescent system (Immobilon Western, Millipore, MA, USA) [1]. Images from films were digitally obtained using a GS-800 densitometer with the Quantity One software (Bio-Rad Laboratories, Inc.) and are reported as arbitrary units (AU).

2.5. Determination of the Infarct Size. After 60 min of ischemia, the rats were euthanized, and the hearts were rapidly excised. Later, the hearts were perfused with 1.5 mL of 0.05% Evans blue dye on the Langendorff system; this procedure was performed to outline the ischemic myocardium (and area at risk). The hearts were frozen at -20°C for 1 hour, and then 2 mm thick cross-sections were obtained. The slices were covered completely with 2,3,5-triphenyl tetrazolium hydrochloride (TTC) at 1% in phosphate-buffered saline (PBS) (1 M, pH 7.2) and incubated for 20 min at 37°C to distinguish the viable myocardium from the necrotic tissue. Later, the slices were incubated in 10% formalin for one hour and maintained in PBS until the image was obtained. The slices were photographed to show the ischemic area with a Multiphot Canon camera EOS 6D (Tokyo, Japan) [17].

2.6. Statistical Analysis. Results are expressed as mean ± standard error of the mean (SEM). Experimental data were examined using the one-way ANOVA followed by the Newman-Keuls *post hoc* test. Differences were considered statistically significant when $p < 0.05$. All analyses were performed using the statistical package GraphPad Prism version 5.03 (GraphPad Software, La Jolla, CA).

3. Results

The characterization of the MetS model was done by analyzing the animal's body weight, blood pressure, and intra-abdominal fat and by the serum biochemical analysis. As shown in Table 1, MetS animals developed central obesity, hypertension, dyslipidemia (high levels of triglycerides and non-HDL-C and low levels of HDL-C), hyperinsulinemia, and insulin resistance (HOMA-IR).

As expected, the treatment with fenofibrate significantly reduced the concentration of triglycerides and non-HDL-C levels and restored the insulin resistance index (HOMA-IR) in the MetS group. In the CT group, fenofibrate administration significantly reduced the concentration of non-HDL-C and did not affect the other parameters.

Serum CK activity was determined in all groups. No significant difference was found between the CT and MetS sham-operated groups (533.30 ± 48.14 vs. 626.50 ± 101.40). After MI, CK activity was significantly higher in MetS than in CT rats treated with vehicle (Table 1). Fenofibrate treatment significantly reduced CK activity in serum from the CT and MetS animals (23% and 14%, respectively).

Figure 1 shows the expression of ACE and ACE2 in the homogenate from the left ventricles from each experimental group. ACE expression was slightly higher in the MetS group than in CT. Ischemia promoted an increase in ACE expression in the CT group, while the expression remained essentially unchanged in hearts from MetS rats. Fenofibrate treatment significantly diminished ACE expression in the same proportion in both experimental groups (Figures 1(a) and 1(b)).

Due to the relevance of ACE2 for the production of Ang-(1-7), we studied whether fenofibrate exerts an effect on this enzyme. ACE2 expression was significantly decreased in the MetS group compared to the CT group (Figure 1(c)). When the hearts were subjected to ischemia, ACE2 increased in the MetS group and no change was observed in CT rats. The administration of fenofibrate significantly increased ACE2 expression in the CT group and had no effect on MetS animals.

According to the pathophysiology, the left ventricular Ang II levels increased in MetS rats in comparison to CT rats (Figure 2(a)). When the hearts were under ischemic conditions, Ang II levels increased in CT and there was a further increase in MetS rats; however, fenofibrate administration significantly diminished Ang II concentrations. Importantly, in the MetS group, the Ang-(1-7) levels were significantly higher in basal conditions, but under ischemic conditions, Ang-(1-7) levels decreased (Figure 2(b)). Fenofibrate treatment significantly increased the concentration of this peptide in both groups (Figure 2(b)).

Western blot analyses revealed differences in the expression of AT1R, AT2R, and MasR in hearts from the CT and MetS groups (Figures 3(a)–3(d)). As expected, AT1R expression was higher in MetS rats compared to CT rats. Ischemia promoted an increase in AT1 expression in both the CT and MetS groups. Fenofibrate treatment significantly diminished the AT1R expression in both groups, although this effect was more evident in the MetS rats (Figures 3(a) and

Table 1: The effects of fenofibrate administration on body characteristics and biochemical parameters from the control (CT) and MetS rats.

	CT-V	CT-F	MetS-V	MetS-F
Body weight (g)	503.0 ± 18.3	490.5 ± 19.8	518.7 ± 14.6	502.5 ± 13.5
Blood pressure (mmHg)	98.6 ± 5.8	101.5 ± 1.3	148.1 ± 6.5[a]	141.5 ± 11.3[a]
Intra-abdominal fat (g)	6.4 ± 0.7	5.2 ± 0.5	13.4 ± 0.8[a]	12.9 ± 0.9
Triglycerides (mg/dL)	60.8 ± 11.3	48.8 ± 5.3	135.6 ± 10.9[a]	53.7 ± 10.2[b]
HDL-C (mg/dL)	42.5 ± 4.8	41.7 ± 1.3	21.8 ± 3.9[a]	23.5 ± 5.8
Non-HDL-C (mg/dL)	19.9 ± 2.1	11.7 ± 1.8[b]	34.8 ± 2.8[a]	12.8 ± 2.6[b]
Total cholesterol (mg/dL)	58.6 ± 4.3	52.5 ± 3.8	61.7 ± 1.2	48.8 ± 6.4
Glucose (mg/dL)	101.3 ± 6.7	98.5 ± 3.2	110.6 ± 10.3	100.4 ± 5.8
Insulin (ng/mL)	0.16 ± 0.05	0.11 ± 0.03	0.39 ± 0.06[a]	0.14 ± 0.07[b]
HOMA-IR	1.1 ± 0.2	0.9 ± 0.1	4.1 ± 0.9[a]	1.6 ± 0.7[b]
CK activity (U/L)	1556.0 ± 77.77	1190.33 ± 73.12[c]	1964.0 ± 52.03[a]	1688.6 ± 54.18[a,c]

Values are mean ± SEM. The serum biochemical determinations were performed after the myocardial insult. CT-V: control vehicle-treated; CT-F: control fenofibrate-treated; MetS-V: metabolic syndrome vehicle-treated; MetS-F: metabolic syndrome fenofibrate-treated; HOMA-IR: homeostatic model assessment of insulin resistance; HDL-C: high-density lipoprotein cholesterol; CK: creatine kinase. $n = 6$. [a]$p < 0.01$ MetS vs. CT same treatment; [b]$p < 0.05$ against vehicle corresponding group; [c]$p < 0.01$ against vehicle corresponding group.

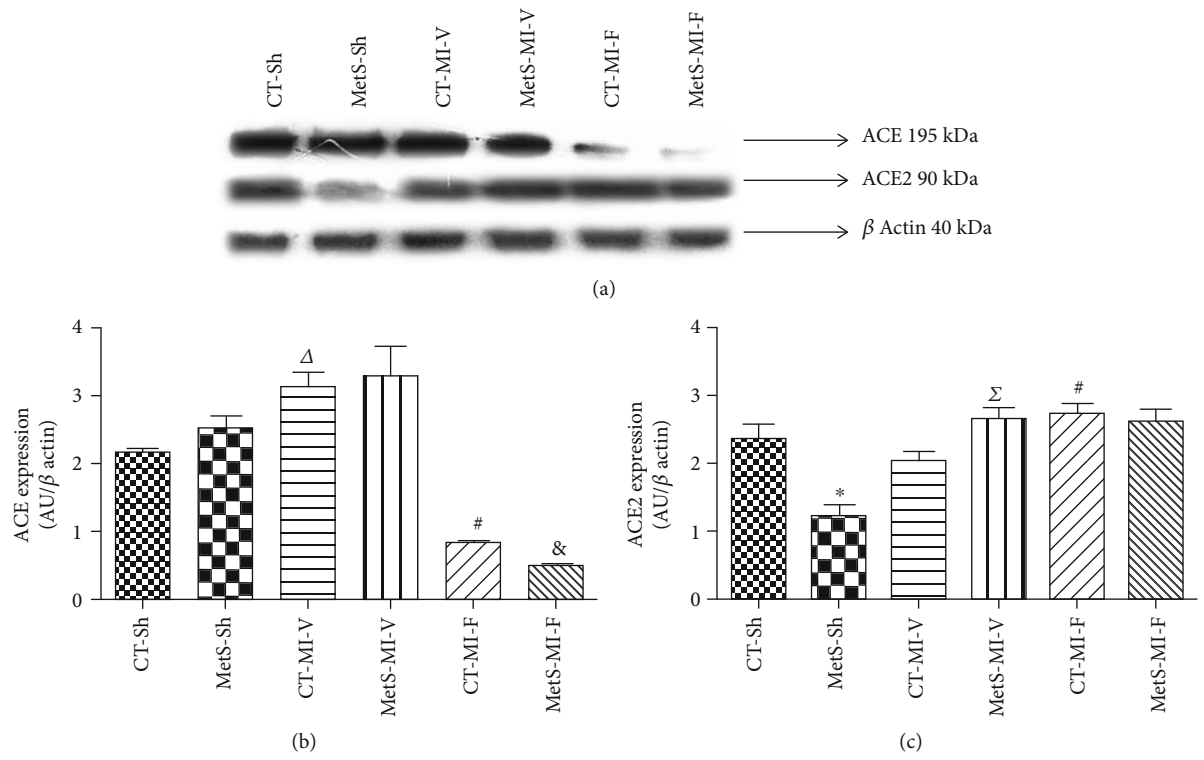

Figure 1: Effect of fenofibrate on the expression of renin-angiotensin-converting enzyme (ACE) and ACE2. The expression was evaluated in the left ventricles from the control (CT) and metabolic syndrome (MetS) rats subjected to sham (Sh) or myocardial infarction (MI) and treated for two weeks with either vehicle (V) or fenofibrate (F). (a) Representative western blot analysis. (b) ACE protein expression. (c) ACE2 protein expression. Data represent mean ± SEM ($n = 5$ per group). $^{*}p < 0.05$ vs. CT-Sh; $^{\Delta}p < 0.05$ vs. CT-Sh; $^{\Sigma}p < 0.05$ vs. MetS-Sh; $^{\#}p < 0.05$ vs. CT-MI-V; $^{\&}p < 0.05$ vs. MetS-MI-V. Analysis of variance-Newman-Keuls.

3(b)). Results show that AT2R expression did not differ between the two sham-operated groups. When the hearts were subjected to ischemia, a significant decrease of AT2R expression in the CT and MetS groups was observed. The administration of fenofibrate significantly increased the expression of this receptor in both groups (Figures 3(a) and 3(c)). MasR expression was significantly higher in MetS-Sh compared to CT-Sh animals; the expression of this receptor under ischemic conditions was comparable to values from sham experimental groups. The treatment with fenofibrate

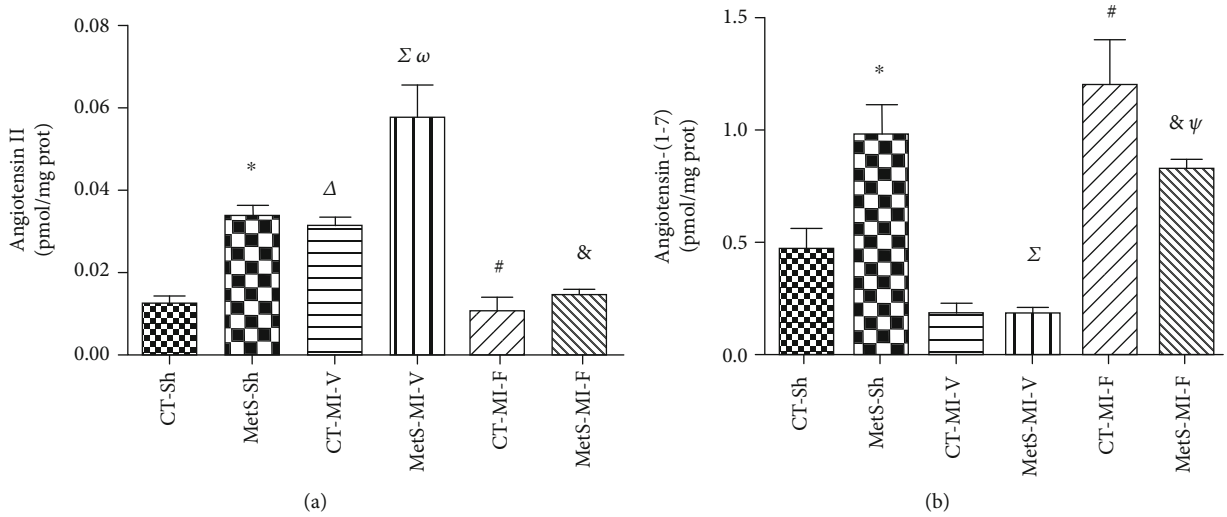

Figure 2: Effect of fenofibrate on angiotensin II and angiotensin-(1-7) levels. (a) Angiotensin II and (b) angiotensin-(1-7) concentrations were determined in the homogenate from myocardial ischemic areas from the sham (Sh), myocardial infarction (MI) vehicle-treated, and MI fenofibrate-treated experimental groups. The values show the mean ± SEM ($n = 5$ per group). $^{*}p < 0.05$ vs. CT-Sh; $^{\Delta}p < 0.05$ vs. CT-Sh; $^{\Sigma}p < 0.05$ vs. MetS-Sh; $^{\#}p < 0.05$ vs. CT-MI-V; $^{\omega}p < 0.05$ vs. CT-MI-V; $^{\&}p < 0.05$ vs. MetS-MI-V; $^{\Psi}p < 0.05$ vs. CT-MI-F. Analysis of variance-Newman-Keuls.

promoted an increase in MasR expression in CT rats, while its expression remained unchanged in hearts from MetS (Figures 3(a) and 3(d)).

Since Ang III and Ang IV have been identified as new biologically active peptides of RAS, we studied the effect of fenofibrate on the production of these metabolites. Figures 4(a)–4(c) show that the expression of APA (the major enzyme metabolizing Ang II to Ang III) and Ang III concentration were significantly increased in the left ventricle of MetS-Sh animals compared to CT-Sh. This effect was also observed under ischemic conditions. Fenofibrate was able to prevent the increase in APA and Ang III levels in MetS animals.

We also investigated if fenofibrate induced variations in Ang III concentrations which might be associated with the Ang IV-IRAP pathway. Our results showed that hearts from MetS-Sh had significantly higher levels of APN, Ang IV, and IRAP when compared to the corresponding CT group (Figures 5(a)–5(d)). Ischemia was accompanied by a decrease in the components analyzed in hearts from MetS rats; however, the levels of APN and Ang IV did not change significantly in the CT group. Fenofibrate treatment was able to prevent the activation of the Ang IV-IRAP axis in the left ventricles from MetS rats (Figures 5(a)–5(d)).

Due to the beneficial effects of the inhibition of NEP and the cardioprotective effects of bradykinin, we evaluated the effect of fenofibrate on NEP expression and bradykinin production. Figures 6(a) and 6(b) show that under basal conditions, MetS hearts expressed more NEP when compared to CT hearts.

In CT-MI vehicle-treated animals, the expression of this enzyme increased under ischemic conditions; nevertheless, in the MetS-MI vehicle-treated group, NEP levels were not modified. The concentrations of bradykinin showed the opposite effect (Figure 6(c)). The administration of fenofibrate was associated with a significant decrease in NEP expression and a consequent increase in bradykinin production in both groups.

The infarct size was evaluated using Evans blue dye plus TTC at 1%. Blue-dyed myocardial tissue represents viable tissue. Left ventricles obtained from the CT-Sh group exhibit an extensive blue area. Tissue from MetS-Sh shows a blue periphery that signals the border of the central zone colored in red. The red area represents the area at risk (Figure 7). In MI groups treated with vehicle, the TCC-stained heart slice confirms infarcted areas (white spots within the viable area); nevertheless, the area at risk (red-colored region) was greater in hearts from MetS rats. The treatment with fenofibrate attenuated the tissue injury in the ischemic area of the MetS and CT rats. The improvement was larger in the CT group where the area at risk and ischemic regions decreased (limited at the central area). However, these areas were widely distributed in the tissue in hearts from MetS rats (Figure 7).

4. Discussion

This work shows that fenofibrate treatment generates cardioprotection in an experimental model of MetS subjected to ischemia, by regulating the nonclassical pathways of RAS. Our study demonstrated that the pharmacological treatment was associated with the activation of Ang-(1-7)/AT2R and inhibition of Ang III/Ang IV/IRAP pathways. Moreover, another novel finding of this study was that the treatment with fenofibrate may decrease the expression of NEP with the consequent increase of bradykinin production.

Extensive research has revealed that the activation of specific molecules of RAS participates in the development of MetS and heart failure. Fenofibrate therapy reverts some of the effects caused by these pathologies by regulating several processes mediated by Ang II/AT1, such as energy metabolism, oxidative stress, inflammation, and cell differentiation

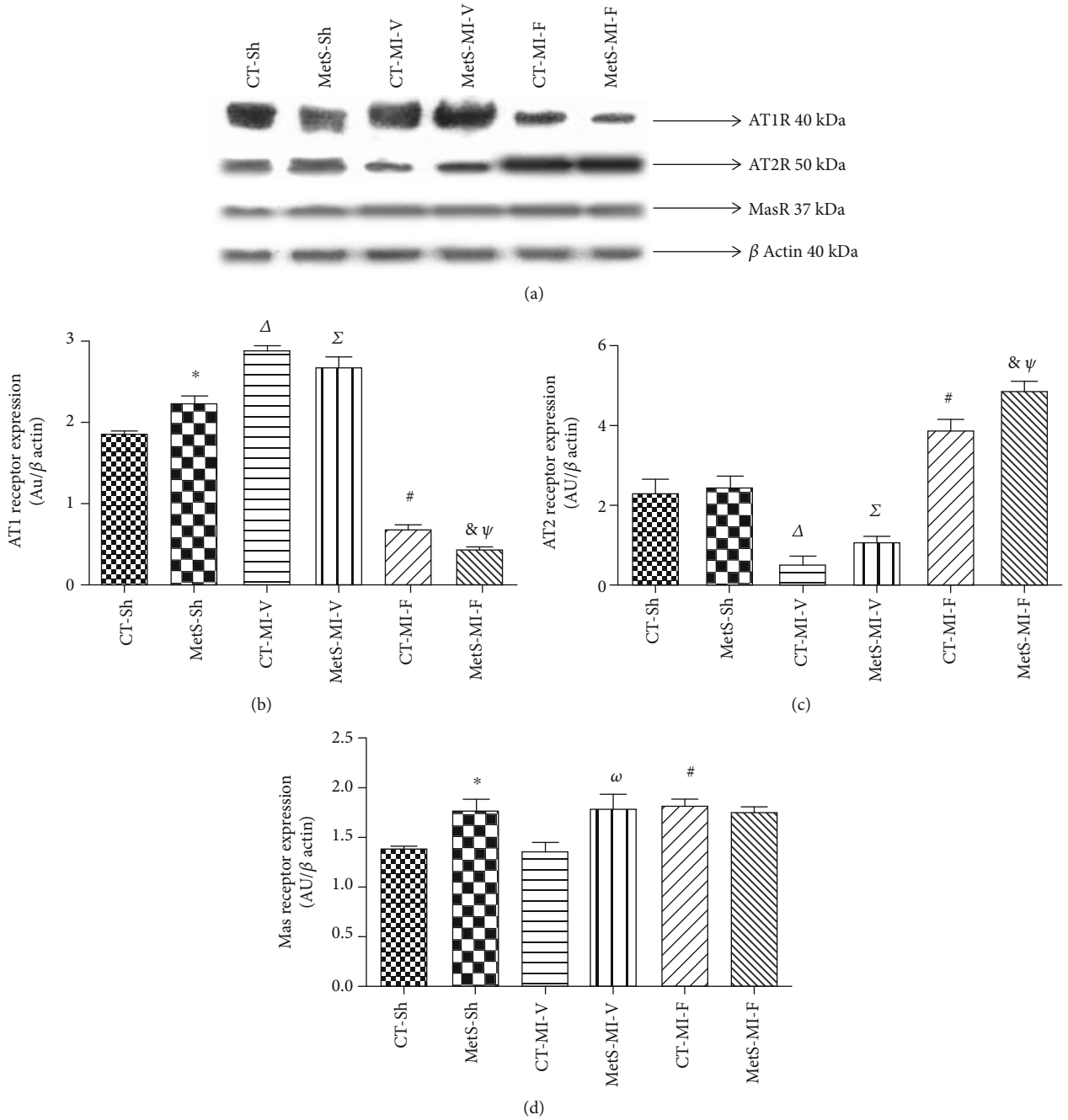

Figure 3: Expression of cardiac angiotensin receptors. The proteins were evaluated in the left ventricles from the control (CT) and metabolic syndrome (MetS) rats subjected to sham (Sh) or myocardial infarction (MI) and treated for two weeks with either vehicle (V) or fenofibrate (F). (a) Representative immunoblot. (b) Angiotensin II-type 1 receptor (AT1R) protein expression. (c) Angiotensin II-type 2 receptor (AT2R) protein expression. (d) MasR protein expression. The values show the mean ± SEM ($n = 5$ per group). $^{*}p < 0.05$ vs. CT-Sh; $^{\Delta}p < 0.05$ vs. CT-Sh; $^{\Sigma}p < 0.05$ vs. MetS-Sh; $^{\#}p < 0.05$ vs. CT-MI-V; $^{\omega}p < 0.05$ vs. CT-MI-V; $^{\&}p < 0.05$ vs. MetS-MI-V; $^{\Psi}p < 0.05$ vs. CT-MI-F. Analysis of variance-Newman-Keuls.

[1]. On the other hand, an accumulating amount of data signals the importance of an alternative pathway of RAS, such as Ang-(1-7) and its cardioprotective properties. Our data are in line with previous findings; however, there are no reports on the effect of fenofibrate on the important counterparts of the RAS pathways analyzed in this paper as far as we know.

Data in Table 1 show that the fenofibrate treatment reversed the signs of MetS such as dyslipidemia and insulin resistance, and it did not affect the other parameters. These data are in accordance with those previously published [1].

Serum CK activity is well known as a cardiac risk biomarker in human and animal models; however, this parameter is unspecific [21–23]. The results in Table 1 show that CK activity was higher in serum from MetS-MI rats than the CT-MI group treated with vehicle. In addition, we demonstrated that fenofibrate treatment significantly reduced the increase

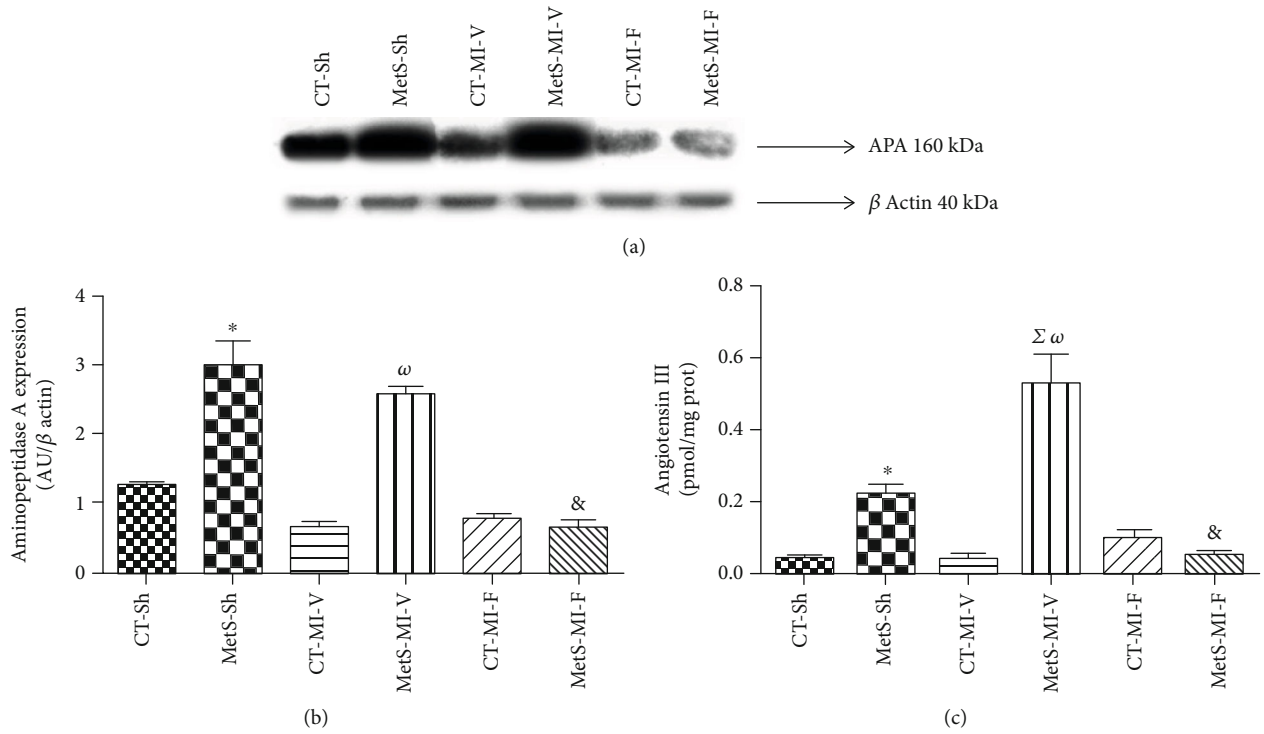

Figure 4: Effect of fenofibrate on the expression of aminopeptidase A (APA) and angiotensin III (Ang III) concentrations in the control (CT) and metabolic syndrome (MetS) rats under ischemic conditions (MI). (a) Representative western blot analysis. (b) APA protein expression. (c) Ang III concentration. Arbitrary units (AU). The values show the mean ± SEM ($n = 5$ per group). $^{*}p < 0.05$ vs. CT-Sh; $^{\Sigma}p < 0.05$ vs. MetS-Sh; $^{\omega}p < 0.05$ vs. CT-MI-V; $^{\&}p < 0.05$ vs. MetS-MI-V. Analysis of variance-Newman-Keuls.

of CK in the serum from both the CT and MetS rats. Nevertheless, this effect was more evident in the CT group. Therefore, our results show that CK activity is a good biomarker of myocardial damage in our experimental model.

In this study, the classical and nonclassical RAS axes were studied. The ACE/Ang II/AT1R axis has been the main RAS pathway studied, and its roles in cardiac damage and therapeutic implications have been extensively reviewed [1]. As expected, the ACE expression and the Ang II concentration were higher (slightly and significantly, respectively) in hearts from MetS animals compared to the CT-Sh group. Ischemic conditions were associated with an increase in the expression of the enzyme and its product (Figures 1(a) and 2(a)). Fenofibrate treatment prevented the increase of ACE expression in both the CT and MetS groups. Consistent with these findings, the Ang II concentration decreased in both experimental groups (Figures 1(b) and 2(a)). As far as we know, there are no reports on the determination of Ang II levels in patients undergoing fenofibrate therapy. There are conflicting data regarding the effect of PPAR agonists on blood pressure in humans, due to heterogeneity of populations, the mechanism underlying the high blood pressure, and differences in concurrent treatments or dietary salt intakes [24]. However, Walker et al. [25] demonstrated a beneficial effect of fenofibrate on vascular endothelial function in humans. Fenofibrate reduces oxidative stress and increases eNOS expression. These effects might be related to the reduction of Ang II concentrations and agree with our previously reported results [1].

On the other hand, ACE2 efficiently hydrolyses Ang II to form Ang-(1-7), a peptide that exerts opposite actions to those of Ang II. Our results show that under basal conditions, the expression of ACE2 was not accompanied by similar changes in Ang-(1-7) concentration. Surprisingly, the ischemic insult promoted an increase in ACE2 expression while the levels of Ang-(1-7) decreased in the MetS group (Figures 1(c) and 2(b)). The increase in ACE2 expression under ischemia conditions suggests a protective role of this enzyme and is in agreement with the data published by other authors in human and animal models [26, 27]. However, the activity of ACE2 should be evaluated to explain the discrepancy between ACE2 expression and Ang-(1-7) concentration. This constitutes a limitation of the present study. The levels of Ang-(1-7) were significantly higher in the ischemic hearts in the presence of fenofibrate in both the CT and MetS animals (Figure 2(b)). Ang-(1-7) decreases hypertension, cardiac hypertrophy, oxidative stress, and insulin resistance [28, 29]. Furthermore, in a previous report, we demonstrated that clofibrate treatment increased Ang-(1-7) concentration in the ischemic myocardium [20].

Figure 3 shows that there is an overexpression of AT1R and MasR in hearts from MetS rats under basal conditions. Under ischemic conditions, AT1R levels increased and AT2R levels decreased in both experimental groups; fenofibrate therapy reversed this effect. The expression of Mas increased only in the CT-MI-F group (Figures 3(a)–3(d)). It has been reported that Ang-(1-7) interacts with both MasR and AT2R [30–32]. Therefore, it is reasonable to suggest that

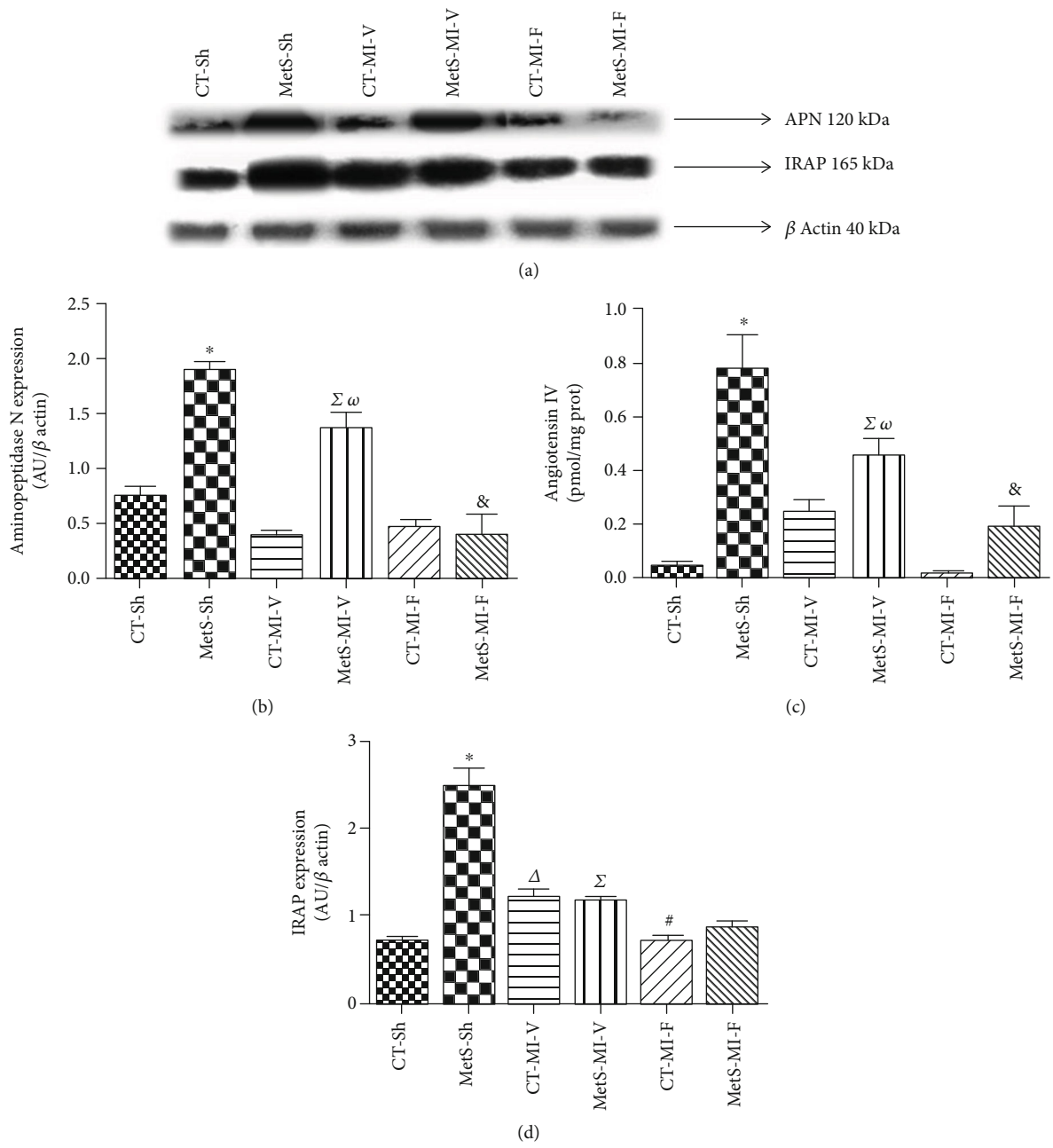

Figure 5: Effect of fenofibrate administration on myocardial aminopeptidase N (APN) expression in myocardial tissue from the control (CT) and metabolic syndrome (MetS) animals. (a) Representative image. (b) Angiotensin IV concentration. (c) Insulin-regulated aminopeptidase (IRAP) protein expression. The values show the mean ± SEM ($n = 5$ per group). $^{*}p < 0.05$ vs. CT-Sh; $^{\Delta}p < 0.05$ vs. CT-Sh; $^{\Sigma}p < 0.05$ vs. MetS-Sh; $^{\#}p < 0.05$ vs. CT-MI-V; $^{\omega}p < 0.05$ vs. CT-MI-V; $^{\&}p < 0.05$ vs. MetS-MI-V. Analysis of variance-Newman-Keuls.

the cardioprotective actions could be mediated through these receptors.

Altogether, our results show that ischemia promotes the activation of the ACE/Ang II/AT1R pathway and that the activation of the Ang-(1-7)/MasR-AT2 signaling pathway is involved in the cardioprotective role of fenofibrate.

Subsequently, we studied the effect of fenofibrate therapy on the nonclassical components of the RAS pathway. Two smaller angiotensin peptides, Ang III and Ang IV, have been reported to have harmful effects via AT1R activation [33, 34]. Ang III and Ang IV levels were increased in the left ventricles in MetS-Sh rats (Figures 4(c) and 5(c)). After the ischemic insult, Ang III concentrations were significantly increased, while Ang IV levels diminished in MetS vehicle-treated hearts. We suggest that this may be a compensatory effect to the ischemic damage. These results were consistent with the expression of APA and APN, respectively (Figures 4(b) and 5(b)). The administration of fenofibrate prevents the rise in the small peptides in MetS rats, while the values remained unchanged in CT animals. Clearly, the decrease in the concentration of the small peptides was directly related to the decrease of its precursor, Ang II; however, our results show

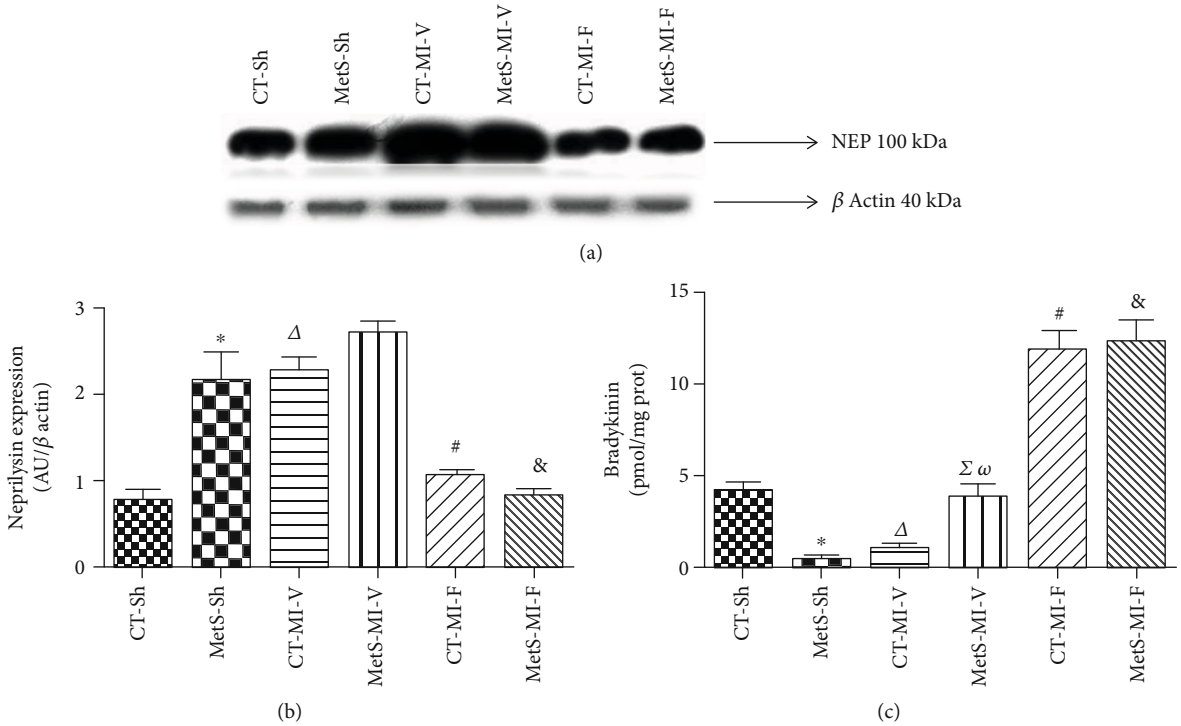

Figure 6: Effect of fenofibrate on the expression of neprilysin (NEP) and bradykinin concentration in control and under ischemic conditions. (a) Representative western blot analysis. (b) NEP protein expression. (c) Bradykinin concentration. The values show the mean ± SEM ($n = 5$ per group). $^{*}p < 0.05$ vs. CT-Sh; $^{\Delta}p < 0.05$ vs. CT-Sh; $^{\Sigma}p < 0.05$ vs. MetS-Sh; $^{\#}p < 0.05$ vs. CT-MI-V; $^{\omega}p < 0.05$ vs. CT-MI-V; $^{\&}p < 0.05$ vs. MetS-MI-V. Analysis of variance-Newman-Keuls.

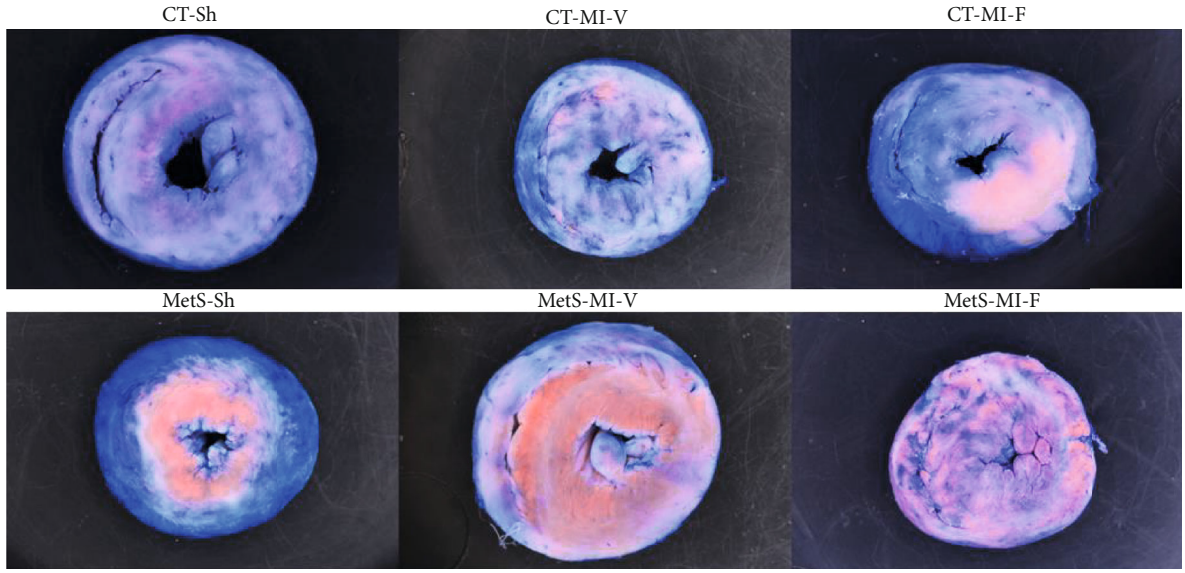

Figure 7: Fenofibrate treatment decreased the area at risk in myocardial infarcted rats. Representative images of TTC staining. Blue areas indicate viable tissue; the red-colored region represents tissue at risk, and the white regions indicate the infarcted myocardium. CT-Sh and MetS-Sh: control and metabolic syndrome sham-operated groups; CT-MI-V: control myocardial infarction vehicle-treated; CT-MI-F: control myocardial infarction fenofibrate-treated; MetS-MI-V: metabolic syndrome myocardial infarction vehicle-treated; MetS-MI-F: metabolic syndrome myocardial infarction fenofibrate-treated.

that the administration of fenofibrate had a direct association with the expression of APA and APN. Moreover, the receptor to Ang IV has been identified in several tissues as an IRAP. The presence of IRAP is important for the translocation of the insulin-stimulated GLUT4 and in the metabolism of oxytocin [33, 35, 36]. MetS and ischemic conditions were

associated with IRAP overexpression, and the therapy with fenofibrate decreased the levels of this protein (Figure 5(d)).

Ang IV is the endogenous inhibitor of the catalytic binding site of IRAP preventing the metabolism of various IRAP substrates, including oxytocin. Oxytocin exerts cardioprotection, either directly or via stimulation of mediators such as the natriuretic peptides and nitric oxide [37]. Furthermore, this hormone enhances glucose uptake via the translocation of GLUT4 to the cell surface [36, 38]. Therefore, we speculate that the Ang IV/AT4R/IRAP axis is also involved in cardiac insulin resistance under ischemic conditions, regulating oxytocin concentrations. Fenofibrate treatment might improve glucose uptake by increasing oxytocin levels as a consequence of the downregulation of the IRAP expression. These suggestions are in agreement with our previous study, in which we showed that ischemia impairs myocardial insulin action and that fibrates reestablish the cardiac insulin signaling pathway [1]. There are few studies reporting that the IRAP deficiency/inhibition protects against cardiac damage; therefore, further studies demonstrating the pathophysiological role of the Ang IV/AT4R/IRAP axis are needed.

We studied whether the administration of fenofibrate had an effect on the expression levels of NEP and bradykinin, due to the interaction between the RAS and the NEP system and the role of peptides, such as bradykinin, in heart homeostasis. We observed that MetS and ischemic conditions were accompanied by a NEP overexpression with the consequent reduction in the concentration of bradykinin (Figures 6(b) and 6(c)). Fenofibrate treatment favored the production of bradykinin by suppressing NEP expression in hearts from both the CT and MetS rats. Our findings suggest the involvement of NEP in the cardioprotective effect of fenofibrate, and this effect could be mediated by genomic actions through the previously reported PPAR activation [39]. Thus, the increase in bradykinin levels might mediate several cardiac functions, as has been previously reported by other authors [40, 41]. Further studies are needed to prove the effect of the pretreatment with fenofibrate on the production of other hormones metabolized by NEP during heart failure, such as natriuretic peptides.

Finally, in order to evaluate the efficacy of our treatment, we analyzed the ischemic size by the TTC staining analysis. Evans blue dye has been used extensively to stain hearts, and it accurately reflects the extent of viable areas and irreversible myocardial ischemic damage. Figure 7 shows that hearts from MetS-Sh rats present a larger area at risk when compared to the CT group. Our results are in line with experimental and clinical trial evidence which suggests that MetS is associated with myocardial infarction [42]. After MI insult, the MetS heart had a larger area at risk and infarcted area when compared to the heart from CT rats. Fenofibrate treatment was able to attenuate MI-induced damage evidenced by the reduction of the area at risk and ischemic area (red- and white-colored regions). This effect is more evident in the CT group. The results of our work are in agreement with those of Mo et al. [22], who showed that fenofibrate reduced the myocardial infarct size.

Cardiac myocytes in the ischemic zone die by apoptosis and necrosis during a myocardial infarction; nevertheless, the magnitudes of each form of cell death remain unclear. Krijnen et al. [43] described that upon permanent occlusion of a coronary vessel in rats, apoptosis occurred in the ischemic region, in the area immediately bordering the ischemic region, and in remote regions from ischemia. Therefore, apoptosis is the major determinant of infarct size. Necrosis occurred less often and was seen only in the ischemic region.

Nevertheless, we did not perform an analysis of cell necrosis and apoptosis in the present study. In a previous report of our group, we found that PPAR-α stimulation with clofibrate augmented the expression of antiapoptotic proteins Bcl-2 and 14-3-3ε and decreased the expression of proapoptotic proteins Bax and the phosphorylation of Bad [44]. Moreover, oxidative stress coexists with apoptosis after myocardial infarction [43]. Our model also presents oxidative stress [1], and therefore, we cannot exclude an effect similar to the one previously reported by our group.

5. Conclusion

Overall, our results show that PPAR-alpha activation by fenofibrate prevents damage due to ischemia in MetS rats by changing the angiotensin metabolites and their receptor profiles. It favors the Ang-(1-7)/AT2 axis and inhibits the Ang III/Ang IV/IRAP signaling pathway. In addition, PPAR-alpha signaling downregulates the expression of NEP and increases the production of bradykinin. Thus, the regulation of the nonclassical axis of RAS is a novel protective effect to myocardial ischemia of fenofibrate.

Data Availability

The data in our study are available from the corresponding author upon reasonable request.

Conflicts of Interest

The authors declare no conflict of interest.

Authors' Contributions

M. S-A. and L. I-L. were responsible for planning and performing the experiments and data analysis; L. DV-M. was responsible for performing the electrophoretic analysis; E. S-C. and M. S-A. were responsible for the histochemistry analysis; J.C. T-N. was responsible for performing some physiological experiments; E. C-T. was responsible for serum biochemical analysis; A. S-M. obtained financial support to partly cover expenses and reviewed the manuscript; M.E. R-R. was responsible for planning the experiments, performing the physiological experiments and data analysis, and writing the paper. M. S-A. and L. I-L. contributed equally to this work.

Acknowledgments

The authors would like to thank Biol. Oscar Infante (Departamento de Instrumentación Electromecánica) for his helpful advice and expertise on blood pressure determination. The authors also thank Biol. Armando Zepeda Rodríguez and

Francisco Pasos Nájera for their support in acquiring photos and José Saúl Carreón Cervantes, Mario Pérez, and Jhony Pérez for excellent technical assistance. This work was supported by Consejo Nacional de Ciencia y Tecnología (CONACyT) (Grant numbers 222720 and 280458 to Alicia Sánchez-Mendoza).

References

[1] L. Ibarra-Lara, M. Sánchez-Aguilar, A. Sánchez-Mendoza et al., "Fenofibrate therapy restores antioxidant protection and improves myocardial insulin resistance in a rat model of metabolic syndrome and myocardial ischemia: the role of angiotensin II," *Molecules*, vol. 22, no. 1, p. 31, 2017.

[2] Y. Marcus, G. Shefer, K. Sasson et al., "Angiotensin 1-7 as means to prevent the metabolic syndrome: lessons from the fructose-fed rat model," *Diabetes*, vol. 62, no. 4, pp. 1121–1130, 2013.

[3] R. A. S. Santos, A. J. Ferreira, T. Verano-Braga, and M. Bader, "Angiotensin-converting enzyme 2, angiotensin-(1–7) and Mas: new players of the renin-angiotensin system," *Journal of Endocrinology*, vol. 216, no. 2, pp. R1–R17, 2013.

[4] M. Slamkova, S. Zorad, and K. Krskova, "Alternative renin-angiotensin system pathways in adipose tissue and their role in the pathogenesis of obesity," *Endocrine Regulations*, vol. 50, no. 4, pp. 229–240, 2016.

[5] S. R. Keller, "Role of the insulin-regulated aminopeptidase IRAP in insulin action and diabetes," *Biological and Pharmaceutical Bulletin*, vol. 27, no. 6, pp. 761–764, 2004.

[6] C. A. McCarthy, L. J. Facey, and R. E. Widdop, "The protective arms of the renin-angiontensin system in stroke," *Current Hypertension Reports*, vol. 16, no. 7, p. 440, 2014.

[7] J. Gao, Y. Marc, X. Iturrioz, V. Leroux, F. Balavoine, and C. Llorens-Cortes, "A new strategy for treating hypertension by blocking the activity of the brain renin–angiotensin system with aminopeptidase A inhibitors," *Clinical Science (London)*, vol. 127, no. 3, pp. 135–148, 2014.

[8] V. Esteban, M. Ruperez, E. Sanchez-Lopez et al., "Angiotensin IV activates the nuclear transcription factor-κB and related proinflammatory genes in vascular smooth muscle cells," *Circulation Research*, vol. 96, no. 9, pp. 965–973, 2005.

[9] P. L. Moraes, L. M. Kangussu, L. G. da Silva, C. H. Castro, R. A. S. Santos, and A. J. Ferreira, "Cardiovascular effects of small peptides of the renin angiotensin system," *Physiological Reports*, vol. 5, no. 22, p. e13505, 2017.

[10] B. M. Park, S. A. Cha, S. H. Lee, and S. H. Kim, "Angiotensin IV protects cardiac reperfusion injury by inhibiting apoptosis and inflammation via AT4R in rats," *Peptides*, vol. 79, pp. 66–74, 2016.

[11] S. A. Hubers and N. J. Brown, "Combined angiotensin receptor antagonism and neprilysin inhibition," *Circulation*, vol. 133, no. 11, pp. 1115–11124, 2016.

[12] J. Kim, D. Han, S. H. Byun et al., "Neprilysin facilitates adipogenesis through potentiation of the phosphatidylinositol 3-kinase (PI3K) signaling pathway," *Molecular and Cellular Biochemistry*, vol. 430, no. 1-2, pp. 1–9, 2017.

[13] M. Kassi, B. Hannawi, and B. Trachtenberg, "Recent advances in heart failure," *Current Opinion in Cardiology*, vol. 33, no. 2, pp. 249–256, 2018.

[14] T. Prasad, L. C. W. Roksnoer, P. Zhu et al., "Beneficial effects of combined AT1 receptor/neprilysin inhibition (ARNI) versus AT1 receptor blockade alone in the diabetic eye," *Investigative Ophthalmology & Visual Science*, vol. 57, no. 15, pp. 6722–6730, 2016.

[15] A. T. Owens, S. Brozena, and M. Jessup, "Neprilysin inhibitors: emerging therapy for heart failure," *Annual Review of Medicine*, vol. 68, no. 1, pp. 41–49, 2017.

[16] E. A. Abd El-Haleim, A. K. Bahgat, and S. Saleh, "Resveratrol and fenofibrate ameliorate fructose-induced nonalcoholic steatohepatitis by modulation of genes expression," *World Journal of Gastroenterology*, vol. 22, no. 10, pp. 2931–2948, 2016.

[17] V. H. Oidor-Chan, E. Hong, F. Pérez-Severiano et al., "Fenofibrate plus metformin produces cardioprotection in a type 2 diabetes and acute myocardial infarction model," *PPAR Research*, vol. 2016, Article ID 8237264, 14 pages, 2016.

[18] M. E. Rubio-Ruíz, L. Del Valle-Mondragón, V. Castrejón-Tellez, E. Carreón-Torres, E. Díaz-Díaz, and V. Guarner-Lans, "Angiotensin II and 1-7 during aging in metabolic syndrome rats. Expression of AT1, AT2 and Mas receptors in abdominal white adipose tissue," *Peptides*, vol. 57, pp. 101–108, 2014.

[19] G. Schumann, R. Bonora, F. Ceriotti et al., "IFCC primary reference procedures for the measurement of catalytic activity concentrations of enzymes at 37 degrees C. Part 2. Reference procedure for the measurement of catalytic concentration of creatine kinase," *Clinical Chemistry and Laboratory Medicine*, vol. 40, no. 6, pp. 635–642, 2002.

[20] L. Ibarra-Lara, M. Sánchez-Aguilar, E. Hong et al., "PPARα stimulation modulates myocardial ischemia-induced activation of renin-angiotensin system," *Journal of Cardiovascular Pharmacology*, vol. 65, no. 5, pp. 430–437, 2015.

[21] M. Kurata, T. Iidaka, Y. Sasayama, T. Fukushima, M. Sakimura, and N. Shirai, "Correlation among clinicopathological parameters of myocardial damage in rats treated with isoproterenol," *Experimental Animals*, vol. 56, no. 1, pp. 57–62, 2007.

[22] H. Mo, S. Zhao, J. Luo, and J. Yuan, "PPARα activation by fenofibrate protects against acute myocardial ischemia/reperfusion injury by inhibiting mitochondrial apoptosis," *International Journal of Clinical Experimental Pathology*, vol. 9, no. 11, pp. 10955–10964, 2016.

[23] W. Chen, J. Liang, Y. Fu et al., "Cardioprotection of cortistatin against isoproterenol-induced myocardial injury in rats," *Annals of Translational Medicine*, vol. 8, no. 6, p. 309, 2020.

[24] K. Gilbert, H. Nian, C. Yu, J. M. Luther, and N. J. Brown, "Fenofibrate lowers blood pressure in salt-sensitive but not salt-resistant hypertension," *Journal of Hypertension*, vol. 31, no. 4, pp. 820–829, 2013.

[25] A. E. Walker, R. E. Kaplon, S. M. S. Lucking, M. J. Russell-Nowlan, R. H. Eckel, and D. R. Seals, "Fenofibrate improves vascular endothelial function by reducing oxidative stress while increasing endothelial nitric oxide synthase in healthy normolipidemic older adults," *Hypertension*, vol. 60, no. 6, pp. 1517–1523, 2012.

[26] A. B. Goulter, M. J. Goddard, J. C. Allen, and K. L. Clark, "ACE2 gene expression is up-regulated in the human failing heart," *BMC Medicine*, vol. 2, no. 1, 2004.

[27] S. Keidar, M. Kaplan, and A. Gamliellazarovich, "ACE2 of the heart: from angiotensin I to angiotensin (1-7)," *Cardiovascular Research*, vol. 73, no. 3, pp. 463–469, 2007.

[28] D. . G. Passos-Silva, T. Verano-Braga, and R. . A. S. Santos, "Angiotensin-(1–7): beyond the cardio-renal actions," *Clinical Science (London)*, vol. 124, no. 7, pp. 443–456, 2013.

[29] B. Liang, Y. Li, Z. Han et al., "ACE2-Ang (1-7) axis is induced in pressure overloaded rat model," *International Journal of Clinical and Experimental Pathology*, vol. 8, no. 2, pp. 1443–1450, 2015.

[30] S. Bosnyak, E. S. Jones, A. Christopoulos, M. I. Aguilar, W. G. Thomas, and R. E. Widdop, "Relative affinity of angiotensin peptides and novel ligands at AT1 and AT2 receptors," *Clinical Science (London)*, vol. 121, no. 7, pp. 297–303, 2011.

[31] M. P. Ocaranza and J. E. Jalil, "Protective role of the ACE2/Ang-(1–9) axis in cardiovascular remodeling," *International Journal of Hypertension*, vol. 2012, Article ID 594361, 12 pages, 2012.

[32] E. J. Tassone, A. Sciacqua, F. Andreozzi et al., "Angiotensin (1–7) counteracts the negative effect of angiotensin II on insulin signalling in HUVECs," *Cardiovascular Research*, vol. 99, no. 1, pp. 129–136, 2013.

[33] J. L. Zhuo, F. M. Ferrao, Y. Zheng, and X. C. Li, "New frontiers in the intrarenal renin-angiotensin system: a critical review of classical and new paradigms," *Frontiers in Endocrinology*, vol. 4, 2013.

[34] K. Kramkowski, A. Mogielnicki, and W. Buczko, "The physiological significance of the alternative pathways of angiotensin II production," *Journal of Physiology and Pharmacology*, vol. 57, no. 4, pp. 529–539, 2006.

[35] S. Y. Chai, R. Fernando, G. Peck et al., "What?s new in the renin-angiotensin system?," *Cellular and Molecular Life Sciences*, vol. 61, no. 21, pp. 2728–2737, 2004.

[36] S. Diwakarla, E. Nylander, A. Grönbladh et al., "Binding to and inhibition of insulin-regulated aminopeptidase by macrocyclic disulfides enhances spine density," *Molecular Pharmacology*, vol. 89, no. 4, pp. 413–424, 2016.

[37] M. Jankowski, T. L. Broderick, and J. Gutkowska, "Oxytocin and cardioprotection in diabetes and obesity," *BMC Endocrine Disorders*, vol. 16, no. 1, p. 34, 2016.

[38] M. Florian, M. Jankowski, and J. Gutkowska, "Oxytocin increases glucose uptake in neonatal rat cardiomyocytes," *Endocrinology*, vol. 151, no. 2, pp. 482–491, 2010.

[39] L. Katsouri, C. Parr, N. Bogdanovic, M. Willem, and M. Sastre, "PPARγ co-activator-1α (PGC-1α) reduces amyloid-β generation through a PPARγ-dependent mechanism," *Journal of Alzheimers Disease*, vol. 25, no. 1, pp. 151–162, 2011.

[40] N.-E. Rhaleb, X.-P. Yang, and O. A. Carretero, "The kallikrein-kinin system as a regulator of cardiovascular and renal function," *Comprehensive Physiology*, vol. 1, no. 2, pp. 971–993, 2011.

[41] R. Sharma, P. K. Randhawa, N. Singh, and A. S. Jaggi, "Bradykinin in ischemic conditioning-induced tissue protection: evidences and possible mechanisms," *European Journal of Pharmacology*, vol. 768, pp. 58–70, 2015.

[42] J. D. Tune, A. G. Goodwill, D. J. Sassoon, and K. J. Mather, "Cardiovascular consequences of metabolic syndrome," *Translational Research*, vol. 183, pp. 57–70, 2017.

[43] P. A. J. Krijnen, "Apoptosis in myocardial ischaemia and infarction," *Journal of Clinical Pathology*, vol. 55, no. 11, pp. 801–811, 2002.

[44] L. Ibarra-Lara, M. Sánchez-Aguilar, E. Soria-Castro et al., "Clofibrate treatment decreases inflammation and reverses myocardial infarction-induced remodelation in a rodent experimental model," *Molecules*, vol. 24, no. 2, p. 270, 2019.

Hindawi
PPAR Research
Volume 2020, Article ID 8889612, 7 pages
https://doi.org/10.1155/2020/8889612

Research Article

Nitric Oxide Mediates Inflammation in Type II Diabetes Mellitus through the PPARγ/eNOS Signaling Pathway

Hua Guo,[1] Qinglan Zhang,[2] Haipo Yuan,[3] Lin Zhou,[4] Fang-fang Li,[4] Sheng-Ming Wang,[5] Gang Shi,[6] and Maojuan Wang[7]

[1]*Department of Clinical Laboratory, Hospital of Chengdu University of Traditional Chinese Medicine, Chengdu, China*
[2]*Department of Endocrinology, Chongqing Hospital of Traditional Chinese Medicine, Chongqing, China*
[3]*Department of Endocrinology, Hospital of Chengdu University of Traditional Chinese Medicine, Chengdu, China*
[4]*Department of Ophthalmology, Huai'an Second People's Hospital, The Affiliated Huai'an Hospital of Xuzhou Medical University, Huai'an, Jiangsu Province, China*
[5]*Department of Stomatology, Huai'an Second People's Hospital, The Affiliated Huai'an Hospital of Xuzhou Medical University, Huai'an, Jiangsu Province, China*
[6]*Department of Pharmacy Services, Hospital of Chengdu University of Traditional Chinese Medicine, Chengdu, China*
[7]*Department of Outpatient, Hospital of Chengdu University of Traditional Chinese Medicine, Chengdu, China*

Correspondence should be addressed to Gang Shi; shigangctu@163.com and Maojuan Wang; wmjlxc1029@163.com

Received 15 September 2020; Revised 12 October 2020; Accepted 12 November 2020; Published 27 November 2020

Academic Editor: Xiao-Jie Lu

Inflammation accounts for the process of type II diabetes mellitus (T2DM), the specific mechanism of which is still to be elucidated yet. Nitric oxide (NO), a critical inflammation regulator, the role of which is the inflammation of T2DM, is rarely reported. Therefore, our study is aimed at exploring the effect of NO on the inflammation in T2DM and the corresponding mechanism. We analyzed the NO levels in plasma samples from T2DM patients and paired healthy adults by Nitric Oxide Analyzer then measured the expression of inflammatory cytokines (C-reactive protein, heptoglobin, IL-1β, TNF-α, IL-6) in insulin-induced HepG2 cells treated with NO donor or NO scavenger, and the PPARγ, eNOS, C-reactive protein, heptoglobin, IL-1β, TNF-α, and IL-6 levels were detected by RT-PCR and western blot in insulin-induced HepG2 cells transfected with si-PPARγ. The results showed that excess NO increased the inflammation marker levels in T2DM, which is activated by the PPARγ/eNOS pathway. These findings will strengthen the understanding of NO in T2DM and provide a new target for the treatment of T2DM.

1. Introduction

Type II diabetes mellitus (T2DM) is a common chronic metabolic and endocrine disease characterized by insulin resistance and β-cell dysfunction. The high prevalence of T2DM is a serious public health event over the world [1]. According to the latest data given by the Chinese Diabetes Society (CDS), the incidence of T2DM in adults over the age of 18 in China is increasing annually and up to 10.4% by 2019 [2]. Studies have shown that the onset of T2DM is associated with a complex interaction between environmental and genetic factors [3, 4], and the specific pathogenesis of the disease has yet to be elucidated. It has been reported that chronic inflammatory responses may be involved in the process of insulin resistance and β-cell dysfunction, which adds the risk of developing T2DM [5, 6]. C-reactive protein can lead to insulin resistance and is an important indicator of the level of inflammation in T2DM [5, 7]. Haptoglobin is an important indicator of liver inflammation, and it is shown that the haptoglobin 2-2 genotype might increase the risk of cardiovascular disease in diabetic patients [8, 9]. Inflammatory factors such as TNF-α, IL-1β, and IL-6 have been clarified to cause insulin resistance by inhibiting insulin signaling [10, 11]. Therefore, actively exploring the mechanisms of

inflammation in T2DM can provide new ideas for the treatment of the disease.

PPARγ belongs to a family of peroxisome proliferator-activated nuclear receptors that regulate the expression of multiple genes involved in the regulation of lipid/glucose/amino acid metabolism, cell proliferation/differentiation, and inflammation, suggesting that it may play important roles in many diseases [12]. Thiazolidinedione, a target drug of PPARγ, has potent insulin-sensitizing effects and is used to treat T2DM, but the drug will produce side effects such as weight gain, liver damage, and cardiovascular risk and is gradually declining in clinical use [13, 14]. Thus, it is extremely important to clarify the mechanism of PPARγ in T2DM. In recent years, studies have told that PPARγ regulates the expression of inflammatory pathways. For example, GMG-43AC antagonist can be applied to treat acne because it activates PPARγ to inhibit inflammation [12]. PPARγ-mediated upregulation of CD36 is involved in the regulation of microglial activation and phenotype and promotes phagocyte-cell proliferation of apoptotic cells, thereby promoting the recovery of postischemic inflammation [15]. Moreover, PPARγ activation is essential in the suppression of intestinal inflammatory response [16]. In T2DM, the detailed mechanism by which PPARγ regulates inflammation remains to be refined.

Nitric oxide (NO), a free radical molecule with pathophysiological functions, is extensively studied in inflammation. NO has anti-inflammatory and proinflammatory effects, which are correlated with its concentration [17]. Excess NO will damage cells and organs and interacts with intermediate components of reactive oxygen species in cells to induce inflammation [18]. Studies have indicated that the NO/inflammatory signaling pathway is associated with the development of depression [19], colon cancer [20], lung squamous cell carcinoma [18], and diabetes [21]. Endothelial nitric oxide synthase (eNOS) is a kind of nitric oxide synthase that induces NO production, occupying the dominant role in regulating NO activity [22]. Previous studies have shown that the PPARγ/eNOS pathway regulates hypertension [23], ischemia/reperfusion-induced acute kidney injury [24], steatohepatitis [25], ischemia/reperfusion-induced liver injury [26], and so on. However, it is not clear whether the PPAR-γ/eNOS pathway mediates the inflammatory process in T2DM.

Therefore, we put forward the hypothesis that NO may regulate inflammation in T2DM through the PPARγ/eNOS pathway and validated in the present study. Our findings may provide a new treatment target for T2DM.

2. Materials and Methods

2.1. Blood Collection from T2DM Patients. The study was approved by the ethics committee of Huai'an Second People's Hospital and Hospital of Chengdu University of Traditional Chinese Medicine. Fifty-five T2DM patients and fifty healthy adults in this study signed informed consent forms and began to sample blood at 8:30 am in the morning under a fasting state (no food and water absorption for at least 8 h before sampling). The whole blood samples were collected and placed in a heparin anticoagulation tube (BD, USA), then centrifuged at 3500 g at 4°C for 10 min. The achieved uppermost layer is the plasma layer, which should be stored at -80°C for subsequent testing.

2.2. Cell Culture. HepG2 cells were purchased from the Cell Bank of the Chinese Academy of Sciences (Shanghai, China); they were cultured in 96-well plates in RPMI1640 medium (Gibco, NY, USA) with 10% fetal bovine serum (Gibco, USA) and 1% penicillin-streptomycin (Gibco, NY, USA) and allowed to grow to logarithmic growth phase for subsequent studies after a successful recovery. To construct a cell model of T2DM, insulin (Gibco, NY, USA) was first diluted in RPMI1640 complete medium to a final concentration of 10^{-6} mol/L. 200 μL of insulin preparation solution was added to each well in the model group, and an equal amount of RPMI1640 complete medium was added to each well in the control group; all cells were cultured for 48 h [27]. In the process of cultivation, cells were incubated in an incubator (37°C, 5% CO_2).

2.3. RNA Interference. HepG2 cells were transfected with 100 pmol PPARγsiRNA (sense, 5′-UAAAUGUCAGUACU GUCGGUUU-3′, antisense, 5′-CCGACAGUACUGACAU UUAUU-3′) by using the Amaxa Lonza Cell Line Nucleofector® Kit (Lonza, Germany) according to the manufacturer's instructions, and an equal amount of nonspecific siRNA (sense, 5′-UUCUCCGAACGUGUCACGU-3′; antisense, 5′-(ACGUGACACGUUCGGAGAA-3′) was transfected with HepG2 cells as a negative control. After incubation for 24 h, they were used for western blot analysis.

2.4. The Measurement of Nitric Oxide. Due to the fact that NO has a short half-life and is not easy to directly detect, the concentration of its stable metabolites nitrite and nitrate can represent the levels of NO [28]. In the present study, nitrite and nitrate in plasma and cells were measured using the Nitric Oxide Analyzer 280i (GE, USA), and there is no need for pretreatment samples before testing. Each sample was tested 3 times.

2.5. ELISA Assay. The levels of IL-1β, TNF-α, and IL-6 in HepG2 cells were detected using an ELISA kit (SPI-BIO, Bertin Pharma, France), and each experiment was performed 3 times according to the manufacturer's instructions.

2.6. Real-Time Quantitative PCR. Total RNA was isolated from cells using TRIzol reagent (Life Technologies, NY, USA) then reverse transcribed into single-stranded cDNA using a Prime ScriptTMRT kit (Takara, Dalian, China). Real-time PCR equipment (7500 Real-Time PCR System, USA) was to detect the expression of C-reactive protein, haptoglobin, eNOS, and PPARγ. The expression levels were analyzed by the -$\Delta\Delta$2Ct method, and GADPH (5′-AGGTCG GAGTCAACGGATTT-3′ (forward) and 5′-TAGTTGAGG TCAATGAAGGG-3′ (reverse)) expression levels were used as the reference standard.

Table 1: Clinical data in the T2DM group and control group.

	T2DM ($n = 55$)			Control ($n = 50$)		p
Age (yrs)	34-50			32-51		
Gender (M/F)	34/21			30/20		
Plasma nitrite (μM)	0.9728 ± 0.6274			0.3779 ± 0.2579		<0.0001
Plasma nitrate (μM)	33.1243 ± 10.7757			19.3209 ± 6.8687		<0.0001
	M	F	p	M	F	p
Plasma nitrite (μM)	1.0454 ± 0.6776	0.8551 ± 0.5305	0.2785	0.3951 ± 0.2680	0.3521 ± 0.2465	0.5689
Plasma nitrate (μM)	32.4212 ± 10.7574	34.2627 ± 10.9713	0.5431	19.8127 ± 6.8145	18.5833 ± 7.0596	0.5408

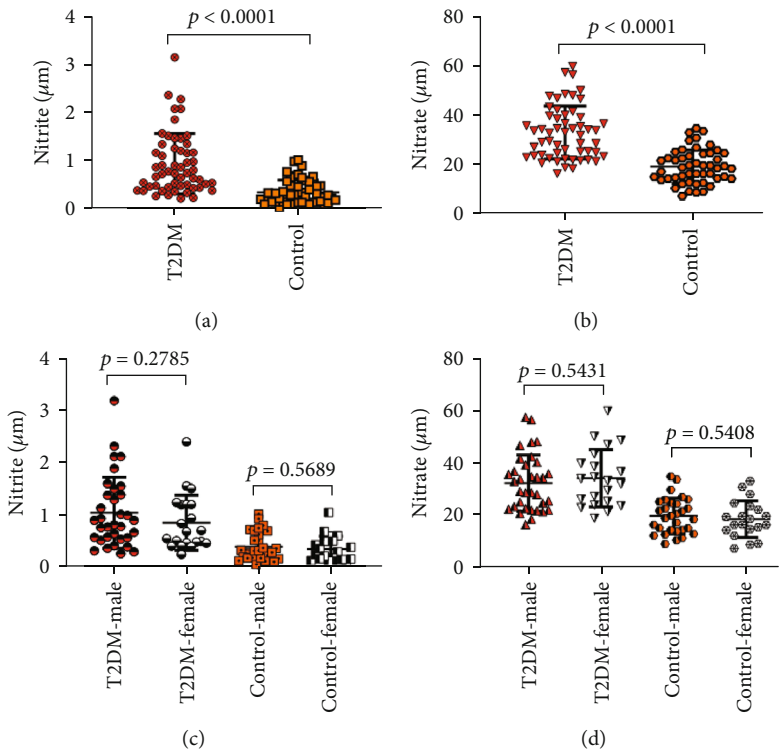

Figure 1: The nitrite and nitrate levels in plasma in the T2DM group and control group.

2.7. Western Blot. After HepG2 cells were treated with RIPA lysis buffer (Sigma, USA), 30 μg of total protein was isolated on 12% SDS-PAGE and transferred to PVDF membranes. Membrane blotting was first blocked with 5% bovine serum albumin (Sigma, USA) for 1 h then incubated with primary antibody (anti-C-reactive protein, antihaptoglobin, antie-NOS, anti-PPARγ) overnight at 4°C, followed by incubation with horseradish peroxidase for 2 h at room temperature. The relative protein expression levels were normalized to GAPDH.

2.8. Data Analysis. All statistics were analyzed using GraphPad Prism 7.0 software (USA), and all experimental data were expressed as mean ± SD. Whether the expression of nitrite, nitrate, and NO differed between the different groups was obtained by t-test analysis. And $p < 0.05$ indicates statistical significance.

Table 2: The TNF-α, IL-1β, and IL-6 contents in insulin-stimulated HepG2 cells.

Cytokines (ng/mL)	Insulin-stimulated HepG2 cells	Insulin-stimulated HepG2 cells+NO donor	Insulin-stimulated HepG2 cells+NO scavenger
TNF-α	0.30 ± 0.06	0.48 ± 0.09	0.18 ± 0.04
IL-1β	0.05 ± 0.01	0.09 ± 0.02	0.03 ± 0.01
IL-6	0.28 ± 0.06	0.53 ± 0.70	0.14 ± 0.05

3. Results

3.1. High NO Production in Plasma in T2DM Patients. To evaluate the effect of NO in the T2DM, we firstly examined the levels of nitrite and nitrate in plasma between 55 T2DM

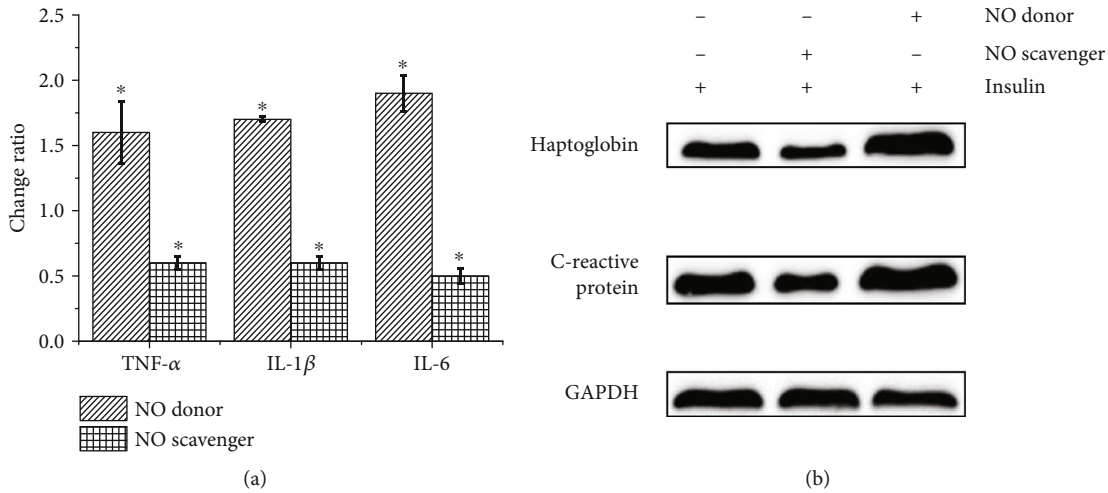

Figure 2: The inflammatory factor levels in HepG2 cells. (a) The ratio of TNF-α, IL-1β, and IL-6 contents in insulin-induced HepG2 cells treated with NO donor or NO scavenger and TNF-α, IL-1β, and IL-6 contents in untreated insulin-induced HepG2 cells. (b) Western blot detects the C-reactive protein and heptoglobin expression in insulin-induced HepG2 cells after different treatments.

patients and paired 50 healthy adults (control group). The clinical data of volunteers in the study is shown in Table 1.

The concentration of plasma nitrite in the T2DM group was significantly higher than the concentration of plasma nitrate in the control group ($p < 0.0001$), and the plasma nitrate levels between the T2DM group and control group were evidently different ($p < 0.0001$), which was found in Figures 1(a) and 1(b). Else, as shown in Figures 1(c) and 1(d), we also found that there were no significant gender differences in plasma nitrite or nitrate contents in the T2DM group and control group. This status revealed the abnormal NO expression in T2DM patients.

3.2. NO Promoted Inflammation in Insulin-Induced HepG2 Cells. NO regulates inflammation, and inflammation promotes the development of T2DM. To investigate whether NO is involved in inflammation in T2DM, we first stimulated HepG2 cells with insulin in vitro to obtain a cell model of T2DM in this study. The cells were then treated with the NO donor DEA (Sigma, USA) and NO scavenger 2-(4-carboxyphenyl)-4, 4, 5, 5-tetramethylimidazoline-1-oxyl-3-oxide (Sigma, USA), respectively. The concentration of IL-1β, TNF-α, and IL-6 is expressed in Table 2. Compared with insulin-induced HepG2 cells, the levels of the inflammatory factors IL-1β, TNF-α, IL-6, C-reactive protein, and heptoglobin in the cells supplied with NO donor were significantly increased, while the levels of these inflammatory factors were significantly decreased in cells treated with NO scavenger, as shown in Figure 2. The above results indicate that the level of NO correlates with the degree of T2DM inflammation.

3.3. PPARγ/eNOS/NO Signaling Is Associated with Inflammation in T2DM. To investigate the mechanism of the development of inflammation in T2DM, we detected the expression of eNOS and NO in vitro. As shown in Figures 3(a) and 3(b), the expression of eNOS and NO was significantly reduced in insulin-treated HepG2 cells after the addition of the NOS inhibitor L-NAME (Cayman, USA), which suggested that the abnormal expression of NO in T2DM might be related to the abnormal expression of eNOS. Considering that PPARγ can modulate the level of diabetic inflammation, the PPARγ/eNOS pathway plays an important role in several diseases. In the present study, insulin-induced HepG2 cells transfected with PPARγ siRNA were found to significantly decrease the expression of PPARγ, eNOS, and NO in Figures 3(b) and 3(c). In addition, Figures 3(c) and 3(d) showed that the inhibition of the PPARγ expression in HepG2 cells prompted a significant decrease in the expression levels of IL-1β, TNF-α, IL-6, C-reactive protein, and heptoglobin. These results suggest that inflammation in T2DM may be associated with the PPARγ/eNOS/NO pathway.

4. Discussion

The inflammatory response can drive the pathological process of T2DM by leading to deleterious effects on tissue function and insulin resistance [10, 29], so exploring the mechanisms of inflammation in T2DM may be extremely important for the treatment of T2DM that currently lacks an effective cure. NO plays significant roles in the inflammatory process and is a potential target for the treatment of inflammatory diseases [30]. In this study, plasma samples collected from 55 T2DM patients were analyzed by Nitric Oxide Analyzer for the first time, and the sample numbers were higher than the previous publications; the results showed higher levels of nitrite and nitrate in the plasma of the T2DM patients. Similarly, it also showed that abnormal levels of nitrogen oxides in plasma, serum and urine samples of T2DM patients before [31, 32]. It suggests that NO may play an important effect in the pathogenesis of T2DM.

In vitro experiment revealed that the concentration of inflammatory factors (C-reactive protein, heptoglobin, IL-1β, TNF-α, IL-6) was significantly increased in insulin-induced HepG2 cells after NO donor treatment, while the levels of inflammatory factors were decreased in insulin-induced HepG2 cells stimulated with NO scavenger. The

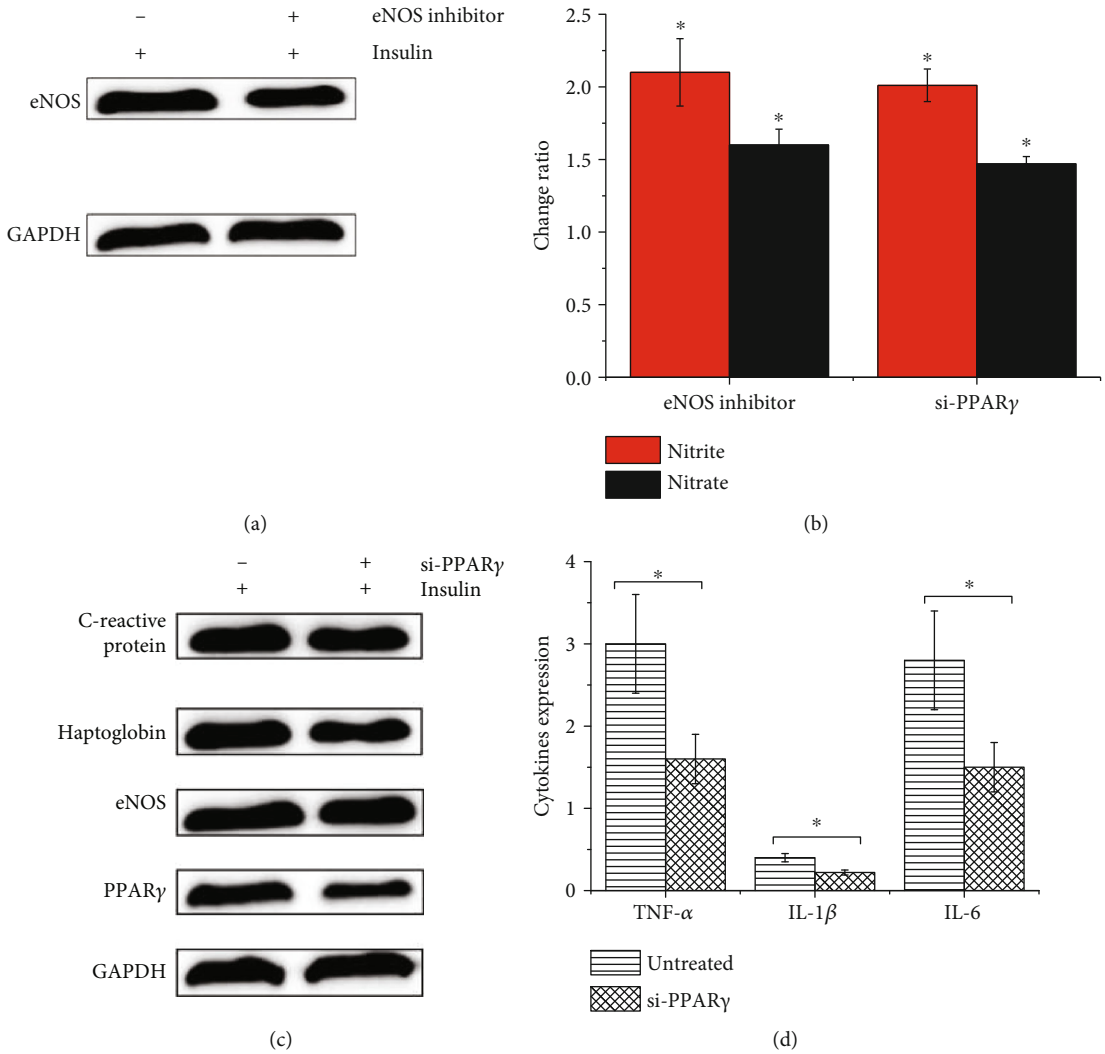

Figure 3: The eNOS, NO, PPARγ, inflammatory factors levels in HepG2 cells. (a) The expression of eNOS in insulin-induced HepG2 cells. (b) The change of nitrite and nitrate in insulin-induced HepG2 cells treated with eNOS inhibitor or si-PPARγ. (c) The effect of PPARγ inhibition on the expression of eNOS, PPARγ, C-reactive protein, and heptoglobin expression in insulin-induced HepG2 cells. (d) The IL-1β, TNF-α, and IL-6 levels in insulin-induced HepG2 cells and insulin-induced HepG2 cells transfected with si-PPARγ.

results support that NO may take part in the inflammatory process in T2DM patients. To investigate the mechanism of NO on inflammation in T2DM, we investigated and conducted further studies. Previous studies have shown that PPARγ hyperglycosylation modification induces endothelial insulin resistance and dysfunction associated with diabetic vascular complications by regulating the eNOS-NO pathway [33]. PPARγ provides assistance to the expression of eNOS [24], which induces NO production. However, whether NO can regulate T2DM inflammation through the PPARγ-eNOS signaling pathway is currently unclear.

To test the hypothesis, this study detected the expression of eNOS and PPARγ in vitro and found that the expression of eNOS and NO decreased after the treatment of insulin-induced HepG2 cells with NOS inhibitor. Inhibiting the expression of PPARγ in insulin-induced HepG2 cells significantly decreased the levels of PPARγ, eNOS, and NO, and the levels of C-reactive protein, heptoglobin, IL-1β, TNF-α, and IL-6 were significantly reduced. Therefore, the expression of T2DM inflammation may be regulated through the PPAR-γ/eNOS pathway-mediated expression of NO.

In summary, this study explored the link between NO and inflammation through insulin-induced HepG2 cells, which provides a potential therapeutic target for the possible treatment of T2DM.

Data Availability

All data are available upon request.

Conflicts of Interest

The authors declare that they have no conflicts of interest.

Authors' Contributions

Hua Guo, Qinglan Zhang, and Haipo Yuan are co-first authors.

References

[1] D. Rahelić, "SEDMO IZDANJE IDF DIJABETES ATLASA–POZIV NA TRENUTNU AKCIJU [7TH edition of IDF diabetes atlas–CALL for immediate action]," *Liječnički Vjesnik*, vol. 138, no. 1-2, pp. 57-58, 2016.

[2] W. Jia, J. Weng, D. Zhu et al., "Standards of medical care for type 2 diabetes in China 2019," *Diabetes/Metabolism Research and Reviews*, vol. 35, no. 6, article e3158, 2019.

[3] R. E. Soccio, E. R. Chen, S. R. Rajapurkar et al., "Genetic variation determines PPARγ function and anti-diabetic drug response in vivo," *Cell*, vol. 162, no. 1, pp. 33–44, 2015.

[4] A. Desiderio, R. Spinelli, M. Ciccarelli et al., "Epigenetics: spotlight on type 2 diabetes and obesity," *Journal of Endocrinological Investigation*, vol. 39, no. 10, pp. 1095–1103, 2016.

[5] P. H. Black, "The inflammatory response is an integral part of the stress response: implications for atherosclerosis, insulin resistance, type II diabetes and metabolic syndrome X," *Brain, Behavior, and Immunity*, vol. 17, no. 5, pp. 350–364, 2003.

[6] H. Blaser, C. Dostert, T. W. Mak, and D. Brenner, "TNF and ROS crosstalk in inflammation," *Trends in Cell Biology*, vol. 26, no. 4, pp. 249–261, 2016.

[7] T. Reinehr, B. Karges, T. Meissner et al., "Inflammatory markers in obese adolescents with type 2 diabetes and their relationship to hepatokines and adipokines," *The Journal of Pediatrics*, vol. 173, pp. 131–135, 2016.

[8] I. Hochberg, E. M. Berinstein, U. Milman, C. Shapira, and A. P. Levy, "Interaction between the haptoglobin genotype and vitamin E on cardiovascular disease in diabetes," *Current Diabetes Reports*, vol. 17, no. 6, p. 42, 2017.

[9] R. Dalan and G. Liuh Ling, "The protean role of haptoglobin and haptoglobin genotypes on vascular complications in diabetes mellitus," *European Journal of Preventive Cardiology*, vol. 25, no. 14, pp. 1502–1519, 2018.

[10] M. Y. Donath and S. E. Shoelson, "Type 2 diabetes as an inflammatory disease," *Nature Reviews Immunology*, vol. 11, no. 2, pp. 98–107, 2011.

[11] T. Reinehr and C. L. Roth, "Inflammation markers in type 2 diabetes and the metabolic syndrome in the pediatric population," *Current Diabetes Reports*, vol. 18, no. 12, p. 131, 2018.

[12] A. Mastrofrancesco, M. Ottaviani, G. Cardinali et al., "Pharmacological PPARγ modulation regulates sebogenesis and inflammation in SZ95 human sebocytes," *Biochemical Pharmacology*, vol. 138, pp. 96–106, 2017.

[13] R. E. Soccio, E. R. Chen, and M. A. Lazar, "Thiazolidinediones and the promise of insulin sensitization in type 2 diabetes," *Cell Metabolism*, vol. 20, no. 4, pp. 573–591, 2014.

[14] B. Gross, M. Pawlak, P. Lefebvre, and B. Staels, "PPARs in obesity-induced T2DM, dyslipidaemia and NAFLD," *Nature Reviews Endocrinology*, vol. 13, no. 1, pp. 36–49, 2017.

[15] I. Ballesteros, M. I. Cuartero, J. M. Pradillo et al., "Rosiglitazone-induced CD36 up-regulation resolves inflammation by PPARγ and 5-LO-dependent pathways," *Journal of Leukocyte Biology*, vol. 95, no. 4, pp. 587–598, 2014.

[16] D. Serra, L. M. Almeida, and T. C. P. Dinis, "Anti-inflammatory protection afforded by cyanidin-3-glucoside and resveratrol in human intestinal cells via Nrf2 and PPAR-γ: comparison with 5-aminosalicylic acid," *Chemico-Biological Interactions*, vol. 260, pp. 102–109, 2016.

[17] N. B. Janakiram and C. V. Rao, "iNOS-selective inhibitors for cancer prevention: promise and progress," *Future Medicinal Chemistry*, vol. 4, no. 17, pp. 2193–2204, 2012.

[18] Z. Gray, G. Shi, X. Wang, and Y. Hu, "Macrophage inducible nitric oxide synthase promotes the initiation of lung squamous cell carcinoma by maintaining circulated inflammation," *Cell Death & Disease*, vol. 9, no. 6, p. 642, 2018.

[19] M. Ghasemi, "Nitric oxide: antidepressant mechanisms and inflammation," *Advances in Pharmacology*, vol. 86, pp. 121–152, 2019.

[20] N. Stettner, C. Rosen, B. Bernshtein et al., "Induction of nitric-oxide metabolism in enterocytes alleviates colitis and inflammation-associated colon cancer," *Cell Reports*, vol. 23, no. 7, pp. 1962–1976, 2018.

[21] D. Kumar, K. Shankar, S. Patel et al., "Chronic hyperinsulinemia promotes meta-inflammation and extracellular matrix deposition in adipose tissue: implications of nitric oxide," *Molecular and Cellular Endocrinology*, vol. 477, pp. 15–28, 2018.

[22] L. Xu, S. Wang, B. Li, A. Sun, Y. Zou, and J. Ge, "A protective role of ciglitazone in ox-LDL-induced rat microvascular endothelial cells via modulating PPARγ-dependent AMPK/eNOS pathway," *Journal of Cellular and Molecular Medicine*, vol. 19, no. 1, pp. 92–102, 2015.

[23] L. Xiao, J. H. Dong, X. Teng et al., "Hydrogen sulfide improves endothelial dysfunction in hypertension by activating peroxisome proliferator-activated receptor delta/endothelial nitric oxide synthase signaling," *Journal of Hypertension*, vol. 36, no. 3, pp. 651–665, 2018.

[24] A. P. Singh, N. Singh, D. Pathak, and P. M. S. Bedi, "Estradiol attenuates ischemia reperfusion-induced acute kidney injury through PPAR-γ stimulated eNOS activation in rats," *Molecular and Cellular Biochemistry*, vol. 453, no. 1-2, pp. 1–9, 2019.

[25] Y. Yamada, M. Eto, Y. Ito et al., "Suppressive role of PPARγ-regulated endothelial nitric oxide synthase in adipocyte lipolysis," *PLoS One*, vol. 10, no. 8, article e0136597, 2015.

[26] K. K. Kuo, B. N. Wu, E. Y. Chiu et al., "NO donor KMUP-1 improves hepatic ischemia-reperfusion and hypoxic cell injury by inhibiting oxidative stress and pro-inflammatory signaling," *International Journal of Immunopathology and Pharmacology*, vol. 26, no. 1, pp. 93–106, 2013.

[27] Z. J. Mao, M. Lin, X. Zhang, and L. P. Qin, "Combined use of astragalus polysaccharide and berberine attenuates insulin resistance in IR-HepG2 cells *via* regulation of the gluconeogenesis signaling pathway," *Frontiers in Pharmacology*, vol. 10, p. 1508, 2019.

[28] E. Goshi, G. Zhou, and Q. He, "Nitric oxide detection methods *in vitro* and *in vivo*," *Medical Gas Research*, vol. 9, no. 4, pp. 192–207, 2019.

[29] K. Eguchi and R. Nagai, "Islet inflammation in type 2 diabetes and physiology," *The Journal of Clinical Investigation*, vol. 127, no. 1, pp. 14–23, 2017.

[30] Y. Kobayashi, "The regulatory role of nitric oxide in proinflammatory cytokine expression during the induction and resolution of inflammation," *Journal of Leukocyte Biology*, vol. 88, no. 6, pp. 1157–1162, 2010.

[31] N. Jelić-Knezović, S. Galijašević, M. Lovrić, M. Vasilj, S. Selak, and I. Mikulić, "Levels of nitric oxide metabolites and myeloperoxidase in subjects with type 2 diabetes mellitus on metformin therapy," *Experimental and Clinical Endocrinology & Diabetes*, vol. 127, no. 1, pp. 56–61, 2019.

[32] S. Apakkan Aksun, B. Özmen, D. Özmen et al., "Serum and urinary nitric oxide in type 2 diabetes with or without microalbuminuria: relation to glomerular hyperfiltration," *Journal of Diabetes and its Complications*, vol. 17, no. 6, pp. 343–348, 2003.

[33] W. Yuan, C. Ma, Y. Zhou, M. Wang, G. Zeng, and Q. Huang, "Negative regulation of eNOS-NO signaling by over-SUMOylation of PPARγ contributes to insulin resistance and dysfunction of vascular endothelium in rats," *Vascular Pharmacology*, vol. 122-123, article 106597, 2019.

Hindawi
PPAR Research
Volume 2020, Article ID 6527564, 19 pages
https://doi.org/10.1155/2020/6527564

Research Article

The Role of Peroxisome Proliferator-Activated Receptors (PPARs) in Pan-Cancer

Runzhi Huang,[1,2,3] Jiaqi Zhang,[1] Mingxiao Li,[1] Penghui Yan,[1] Huabin Yin,[4] Suna Zhai,[5] Xiaolong Zhu,[1] Peng Hu,[1] Jiaxin Zhang,[1] Ling Huang,[1] Man Li,[1] Zehui Sun,[1] Tong Meng,[4,6] Daoke Yang,[5] and Zongqiang Huang[1]

[1]*Department of Orthopedics, The First Affiliated Hospital of Zhengzhou University, 1 East Jianshe Road, Zhengzhou, China*
[2]*Division of Spine, Department of Orthopedics, Tongji Hospital Affiliated to Tongji University School of Medicine, 389 Xincun Road, Shanghai, China*
[3]*Tongji University School of Medicine, 1239 Siping Road, Shanghai 200092, China*
[4]*Department of Orthopedics, Shanghai General Hospital, School of Medicine, Shanghai Jiaotong University, 100 Haining Road, Shanghai, China*
[5]*Department of Radiotherpy, The First Affiliated Hospital of Zhengzhou University, Zhengzhou 450052, China*
[6]*Tongji University Cancer Center, Shanghai Tenth People's Hospital of Tongji University, School of Medicine, Tongji University, Shanghai, China*

Correspondence should be addressed to Tong Meng; mengtong@medmail.com.cn, Daoke Yang; 15903650068@163.com, and Zongqiang Huang; gzhuangzq@163.com

Received 30 June 2020; Revised 21 July 2020; Accepted 31 July 2020; Published 22 September 2020

Academic Editor: Sainan Li

Peroxisome proliferator-activated receptors (PPARs) are members of nuclear transcription factors. The functions of the PPAR family (PPARA, PPARD, and PPARG) and their coactivators (PPARGC1A and PPARGC1B) in maintenance of lipid and glucose homeostasis have been unveiled. However, the roles of PPARs in cancer development remain elusive. In this work, we made use of 11,057 samples across 33 TCGA tumor types to analyze the relationship between PPAR transcriptional expression and tumorigenesis as well as drug sensitivity. We performed multidimensional analyses on PPARA, PPARG, PPARD, PPARGC1A, and PPARGC1B, including differential expression analysis in pan-cancer, immune subtype analysis, clinical analysis, tumor purity analysis, stemness correlation analysis, and drug responses. PPARs and their coactivators expressed differently in different types of cancers, in different immune subtypes. This analysis reveals various expression patterns of the PPAR family at a level of pan-cancer and provides new clues for the therapeutic strategies of cancer.

1. Introduction

Peroxisome proliferator-activated receptors (PPARs), members of nuclear receptor subfamily, are a series of ligand-activated transcription factors (TFs) that regulate the expression of target genes, which involve in various biological processes, including cellular differentiation, cell proliferation, lipid metabolism, and tumorigenesis [1]. PPARs can be activated by various ligands, such as fatty acids (FAs), eicosanoids, and some targeted drugs [2]. Upon binding to the ligand, PPARs form a heterodimer with retinoid X receptor (RXR), and this PPAR/RXR complex is required for its subsequent binding to specific DNA regions in PPAR response elements (PPREs), the gene promotor region [3]. PPARs then trigger transcription of target genes after recruitment of coactivators and release of corepressors [4]. PPARGC1A and PPARGC1B were peroxisome proliferator-activated receptor gamma coactivators 1 alpha and beta, respectively, playing important roles in the PPAR signaling network [5]. There are mainly three isotypes of PPARs with distinct tissue distribution, metabolic patterns, and ligand specificity: PPARα, PPARγ, and PPARδ [6]. Although the roles of the three

isotypes played in carcinogenesis and chemoprevention have not been clearly characterized [7], some agonists of them have been used in clinical trials for years. There is no conclusions but controversial results regarding the antitumor functions of PPARα and PPARγ [8]. The characteristics of PPARs differ from each other, and different isotypes may have different impacts in different types of cancer. To date, there is no bioinformatics study systematically investigating the transcriptional levels of each PPAR in pan-cancer. Thus, it is of importance to study the PPARs' expression patterns in pan-cancer and exploit the potential of PPAR-targeted drugs when it comes to the treatment of differentially PPAR-expressed tumors.

In this study, we analyzed the expression signatures of PPARA, PPARD, PPARG, PPARGC1AA, and PPARGC1B in pan-cancer. Utilizing multidimensional correlation analysis, we found the associations between transcriptional levels of PPARs and stemness, tumor purity, and drug sensitivity across TCGA cancers.

2. Materials and Methods

2.1. Data Downloading and Preprocessing. On June 23, 2020, the gene expression profiles, phenotype information, and survival data of PARRA, PPARD, PPARG, PPARGC1A, and PPARGC1B in 33 types of TCGA tumor samples and adjacent tissues (a total of 11,057 samples) were downloaded from GDC TCGA sets in the UCSC Xena database (http://xena.ucsc.edu/) in formats of Fragments Per Kilobase per Million (FPKM) and HTSeq-Counts. Meanwhile, demographics, tumor information, and follow-up data of all patients were also extracted from the database.

The 33 types of TCGA tumors and abbreviations were as follows: adrenocortical carcinoma (ACC), Bladder Urothelial Carcinoma (BLCA), breast invasive carcinoma (BRCA), cervical squamous cell carcinoma and endocervical adenocarcinoma (CESC), Cholangiocarcinoma (CHOL), colon adenocarcinoma (COAD), Lymphoid Neoplasm Diffuse Large B-cell Lymphoma (DLBC), esophageal carcinoma (ESCA), glioblastoma multiforme (GBM), head and neck squamous cell carcinoma (HNSC), Kidney Chromophobe (KICH), kidney renal clear cell carcinoma (KIRC), kidney renal papillary cell carcinoma (KIRP), Acute Myeloid Leukemia (LAML), Brain Lower Grade Glioma (LGG), liver hepatocellular carcinoma (LIHC), lung adenocarcinoma (LUAD), lung squamous cell carcinoma (LUSC), Mesothelioma (MESO), ovarian serous cystadenocarcinoma (OV), pancreatic adenocarcinoma (PAAD), Pheochromocytoma and Paraganglioma (PCPG), prostate adenocarcinoma (PRAD), rectum adenocarcinoma (READ), Sarcoma (SARC), Skin Cutaneous Melanoma (SKCM), stomach adenocarcinoma (STAD), Testicular Germ Cell Tumors (TGCT), thyroid carcinoma (THCA), Thymoma (THYM), Uterine Corpus Endometrial Carcinoma (UCEC), Uterine Carcinosarcoma (UCS), and Uveal Melanoma (UVM) from GDC TCGA documents in the UCSC Xena database.

2.2. Differential Expression Analysis and Coexpression Analysis of PPARs between Tumor and Normal Samples. For each and across all TCGA tumor types, we used the "ggpubr" R package to perform differential expression analysis (Wilcox test) between tumor and normal tissues. Only tumor types with more than 3 normal samples were included. The differences in expression of the 5 PPAR family genes in pan-cancer were presented in a form of log2 Fold Change (log2 FC) in a heatmap.

Using corrplot R package, coexpression analysis between PPARA, PPARD, PPARG, PPARGC1B, and PPARGC2B was also done at a transcriptional level, to explore the potential expression pattern between every two PPAR genes. Moreover, a protein-protein interaction network among those genes was constructed by using the STRING database (https://string-db.org/) [9].

2.3. Clinical Correlation Analysis. To analyze the differences in overall survival outcomes between patients expressing high and low levels of PPARs, Kaplan-Meier plots for PPAR genes in pan-cancer were generated by using the R package. Phenotype and survival data for 33 TCGA cancer types were downloaded on June 23, 2020, from GDC TCGA sets in the UCSC Xena database (http://xena.ucsc.edu/). Patients were divided into high- and low- expression groups according to the median expression level of PPARA, PPARD, PPARGC1A, and PPARGC1B, respectively.

In addition, Cox proportional hazard regression was applied to access the hazard ratios of PPARA, PPARD, PPARG, PPARGC1A, and PPARGC1B in each TCGA tumor type. Moreover, differential analysis was also used to detect the differences in the level of PPAR expression signatures in different stages of STAD as an example. The threshold for significance was set as two-paired $p < 0.05$.

2.4. Immune Subtype Analysis. Roles of immune tumor microenvironment (TME) were of therapeutic and prognostic significance in antitumor therapies. Six immune subtypes across TCGA tumor types had been identified by investigators based on five representative immune signatures, which offered a resource for analyzing the TME of some specific tumor. For TCGA tumors, the distribution of immune subtypes varies from each other and each immune subtype presents different biological and clinical features, which determine antitumor therapied to some extent [10]. To access the mRNA expression levels of PPARA, PPARD, PPARG, PPARGC1A, and PPARGC2B in the six different immune subtypes across TGCA tumor types, we performed differential expression analysis with the Kruskal test. Tumors were characterized by immunogenomic features identified by Thorsson et al., including wound healing (C1), IFN-γ dominant (C2), inflammatory (C3), lymphocyte depleted (C4), immunologically quiet (C5), and TGF-β dominant (C6) [10].

2.5. Stemness Indices and TME in Pan-Cancer. More than tumor cells, solid tumor tissues consist of other normal cells, such as stromal cells, immune cells, and vascular cells, which made up TME together. We intended to analyze the correlation between PPAR expression and the fraction of stromal and immune cells in TCGA tumor samples. Methods to access the proportion of these two TME components had been proposed, one of which was ESTIMATE (Estimation

of STormal and Immune cells in MAlignant Tumors using Expression data) [11]. The ESTIMATE score was calculated based on gene expression signatures and could reflect tumor purity with favorable prediction accuracy. Thus, Spearman correlation analysis was performed between the expression level of 5 PPAR genes and stromal score by using the estimate package and limma package.

To further analyze the associations between PPARs and stemness features of pan-cancer, we calculated the stemness indices of TCGA tumor samples by using a one-class logistic regression (OCLR) algorithm and performed Spearman correlation analysis based on gene expression and stemness scores [12]. Stemness indices describe the features of self-renewal and dedifferentiation within tumor cells, which might promote distant metastasis and tumorigenesis. Here, two types of stemness indices were obtained, including the DNA methylation-based stemness index (DNAss) and mRNA expression-based stemness index (RNAss).

For breast invasive carcinoma and liver hepatocellular carcinoma, specifically, we accessed RNAss, DNAss, stromal score, immune score, and ESTIMATE score (the algebraic sum of the stromal score and the immune score) to analyze the correlation relationship with PPAR transcriptional expression.

2.6. Drug Sensitivity Analysis in Pan-Cancer. The data including the RNA-seq profiles of PPAR genes and the drug activity were downloaded from the CellMiner database (https://discover.nci.nih.gov/cellminer/). Impute package from Bioconductor (http://www.bioconductor.org/packages/release/bioc/html/impute.html) was used to preprocess the raw data. CellMiner is a web-based tool with genomic and pharmacologic information for investigators to make use of transcript and drug response data in the NCI-60 cell line sets, which was compiled by the U.S. National Cancer Institute [13]. Transcript expression levels of 22,379 genes, 360 microRNAs, and drug responses of 20,503 compounds are available in the CellMiner website [14]. To explore the correlation between the transcriptional expression of PPAR genes and compound sensitivity, we followed the methods of Dong et al. [15], and Pearson correlation analysis was performed between the two controlled by p value < 0.05.

3. Results

3.1. Differential Expression Analysis and Coexpression Analysis of PPARs between Tumor and Normal Samples. The flowchart of the analysis process is summarized in Figure 1. The gene expression of PPARA, PPARD, PPARG, PPARGC1A, and PPARGC1B was displayed (Figure 2(a)). Differential expression analyses with the Wilcox test were performed on 5 PPAR family genes between tumor and paratumor samples (Figure 2(b)). Those 5 PPAR genes were either down- or upregulated in most types of tumors. PPARA, PPARG, PPARGC1A, and PPARGC1B were seen with low expression in the majority of tumors while PPARD is mainly upregulated.

Specifically, compared to normal tissues, PPARA was observed with low expression in most types of tumors except pan-lung: LUAD and LUSC. It is also obvious that PPARA was the only gene in the PPAR family that was downregulated in CHOL ($p < 0.001$, Figure 2(c)). Interestingly, however, we found significant overexpression of PPARD in CHOL ($p < 0.001$, Figure 2(d)). There was a significantly differential expression of PPARG in BRCA. More than BRCA, both two lung tumors, LUAD and LUSC, expressed low PPARG ($p < 0.001$), which is opposite to PPARA as well as PPARD and different from the other 4 PPAR family genes (Figure 2(e)). Significant overexpression of PPARGC1A was observed in KICH ($p < 0.001$), and downregulation was observed in KIRC and THCA ($p < 0.001$) (Figure 2(f)).

We also queried PPAR protein expressions from the Human Protein Atlas database (https://www.proteinatlas.org), and the PPAR proteins that combined to specific antibodies in both tumor and normal issues were displayed in Figure S1, which tend to follow the same expression patterns as the results of differential expression analysis.

Coexpression analysis revealed a correlation (correlation coefficient = 0.45) between PPARA and PPARGC1A, suggesting a potential positive interaction between those two genes (Figure 2(h)), which was further confirmed by the protein-protein interaction (PPI) network (Figure S2). The coexpression relationship could also be observed between PPARA and PPARG (correlation coefficient = 0.24, $p < 0.001$). By contrast, a different coexpression pattern was seen between PPARGC1A and PPAGC1B with a negative correlation (correlation coefficient = −0.13, $p < 0.001$).

3.2. Clinical Correlation Analysis. We employed Kaplan-Meier analyses on PPARA, PPARD, PPARG, PPARGC1A, and PPARGC1B in 33 TCGA tumors (Figures 3(a)–3(f)). Based on the median gene expression values, patients were divided into high and low groups.

Low expression of PPARA was significantly associated with poor prognosis in patients with KIRC ($p < 0.01$, Figure 3(a)), GBM ($p = 0.026$), and LGG ($p = 0.009$).

By contrast, elevated expression of PPARD was correlated with worse clinical outcomes of patients with LGG ($p = 0.040$), LIHC ($p = 0.018$), and SARC ($p = 0.011$) while elevated PPARD led to better clinical outcomes in BLCA ($p = 0.025$) and UVM ($p = 0.006$).

The higher expression of PPARG and PPARGC1A was associated with better prognostic outcomes in KRIC ($p < 0.001$, Figures 3(c) and 3(d)). Likewise, low expression of PPARGC1B might be a less favorable sign for clinical outcomes in patients of READ ($p = 0.011$, Figure 3(f)), which is consistent with the differentially low expression in READ compared to paratumor samples.

Cox proportional hazard regression was applied to detect the prognostic roles of PPARA, PPARD, PPARG, PPARGC1A, and PPARGC1B in 33 TCGA tumors. Genes with a hazard ratio (HR) > 1 were considered as a prognostic factor. From the forest plot (Figure 3(g)), we found that PPARD and PPARG were of pan-cancer significance with HR > 1 in most cancer types.

Specifically, in STAD, we found that the expression of PPARG ($p = 0.016$) and PPARGC1A ($p = 0.005$) was correlated with TNM stages. The expression level of PPARG was

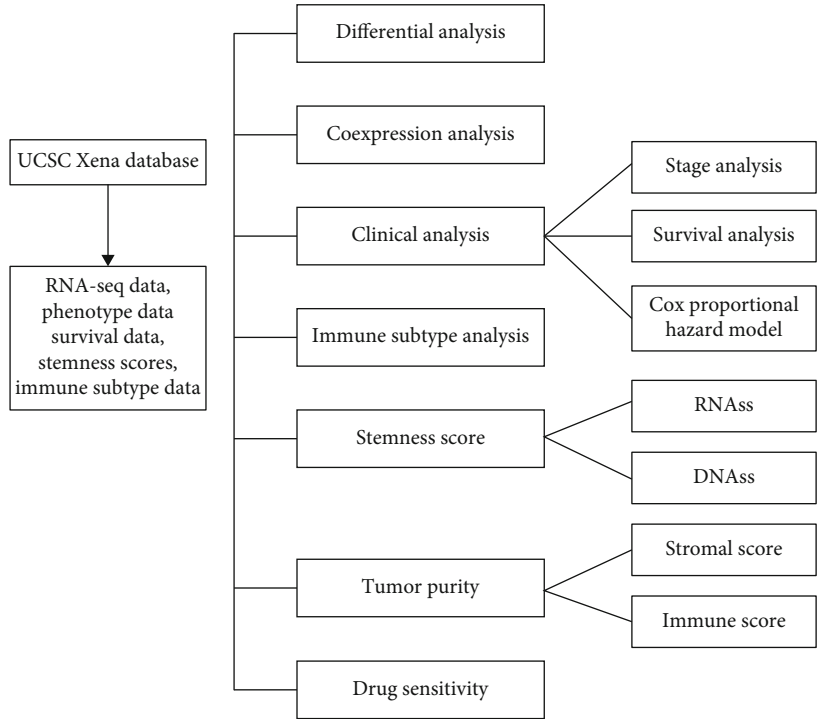

Figure 1: The flowchart of the present study.

comparatively lower in stage III and higher in stage IV. Compared to other TNM stages, the expression level of PPARGC1A was the highest in stage I, followed by stage IV, and was comparatively low in stage II and stage III (Figure 4). The difference in the expression level of PPAR family genes in different TNM stages might serve as predictors of tumor development in clinical applications.

3.3. Immune Subtype Analysis. We applied differential expression analysis with the Kruskal test on the mRNA expression of 5 PPAR genes in the six immune subtypes across 33 TCGA tumor types (Figure 5(a)).

The expression patterns of PPARA ($p < 0.001$), PPARD ($p < 0.001$), PPARG ($p < 0.001$), PPARGC1A ($p < 0.001$), and PPARGC1B ($p < 0.001$) varied in 6 immune subtypes in pan-cancers (Figure 5(a)). Obviously, PPARD ranked the first on the overall expression level in C1-C6.

In addition, different types of tumors displayed variation within immune subtypes. For the C1-C6 immune subtypes of LIHC, there were differences in the expression of PPARA ($p < 0.001$), PPARD ($p < 0.05$), and PPARGC1A ($p < 0.01$) (Figure 5(b)). C6 had the highest expression of PPARA, followed by C4 and C3 while C4 has the lowest expression of PPARD. The expression level of PPARGC1A varied by immune subtypes, with C3, C4, and C6 comparatively high whereas C1 and C2 low.

In BRCA, significant differences were observed in the expression of PPAR family genes in the six immune subtypes (Figure 5(c)). In general, C4 has the lowest expression of PPAR genes. The expression of PPARA ($p < 0.001$), PPARG ($p < 0.001$), PPARGC1A ($p < 0.001$), and PPARGC1B ($p < 0.001$) showed similar patterns in C1-C6, with high expression in C3 and C6 while comparatively low expression in C1, C2, and C4. PPARD, however, expressed higher in C1 and C2 compared to other immune subtypes.

For SARC, C6 had the lowest expression of PPARA ($p < 0.05$) and PPARGC1A ($p < 0.01$), whereas the expression level of PPARG ($p < 0.05$) was the highest among C1, C2, C3, C4, and C6 immune subtypes (Figure 5(d)).

3.4. Stemness Indices and Microtumor Environment in Pan-Cancer. Stromal scores of TCGA cancer samples were calculated by applying the ESTIMATE (Estimation of STromal and Immune cells in MAlignant Tumors using Expression data) algorithm [11]. Spearman correlation analysis was used to describe the correlation between the expression level of PPAR family genes and stromal scores in pan-cancer. As is shown in Figure 6(c), we found a positive correlation between PPARA and stromal scores in TGCT (correlation coefficient = 0.60, $p = 0$). There was likewise a relationship between PPARD and LAML with a correlation coefficient = 0.48, $p < 0.001$. The expression of PPARG was positively correlated with a number of tumor types, including BRCA, DLBC, LGG, MESO, OV, PCPG, PRAD, SARC, and SKCM, suggesting that elevated expression of PPARG was associated with lower tumor purity in many types of tumors. Significant differences were found between PPARGC1A and PPARGC1B towards their relationship with tumor purity. The higher expression of PPARGC1A was correlated with high tumor purity in CHOL, GBM, KIRC, KIRP, and THCA, while with low stromal scores of BLCA, HNSC, LUSC, and TGCT, which was the opposite to the pattern of PPARGC1B.

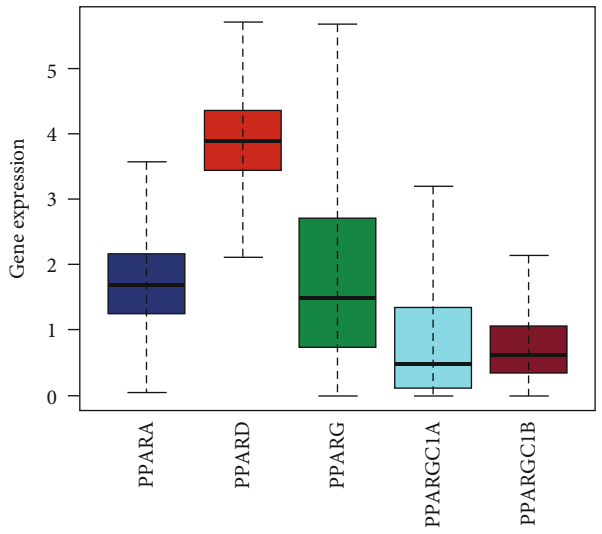

(a)

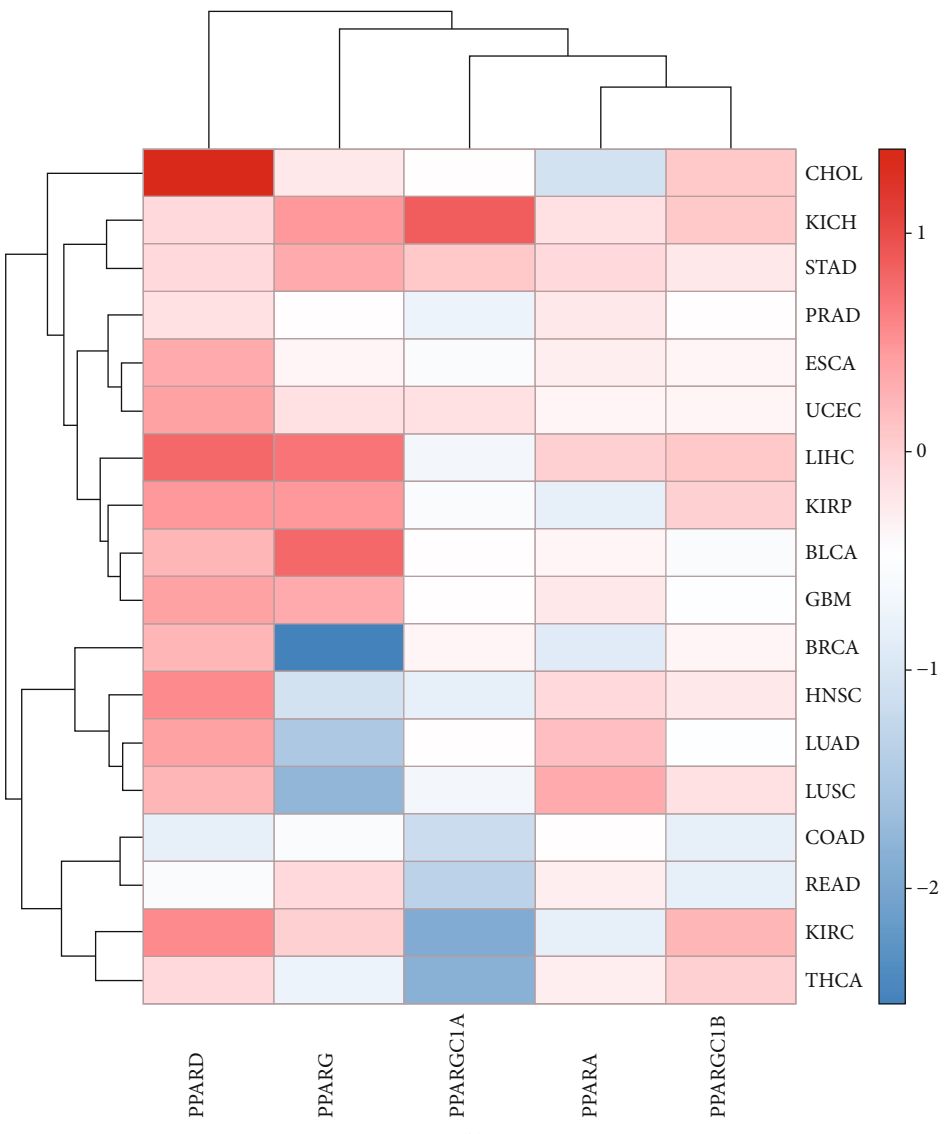

(b)

Figure 2: Continued.

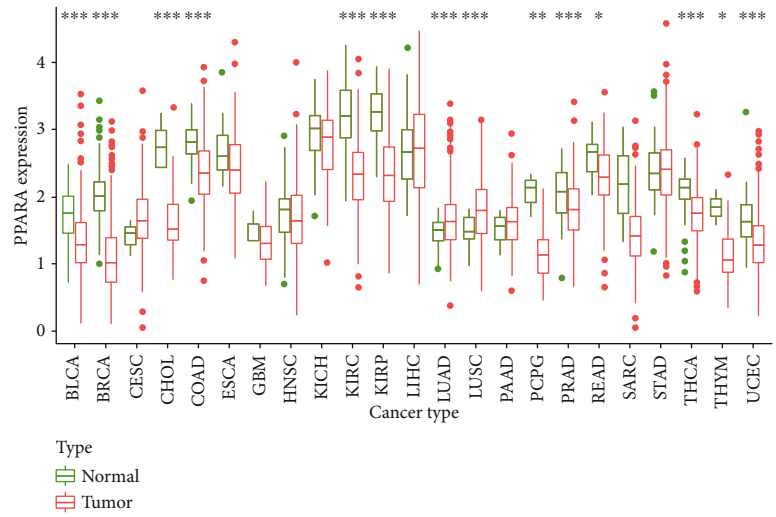

(c)

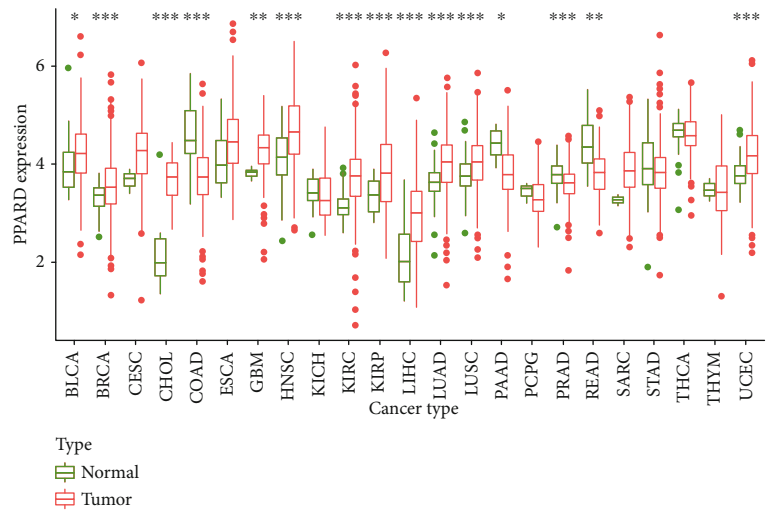

(d)

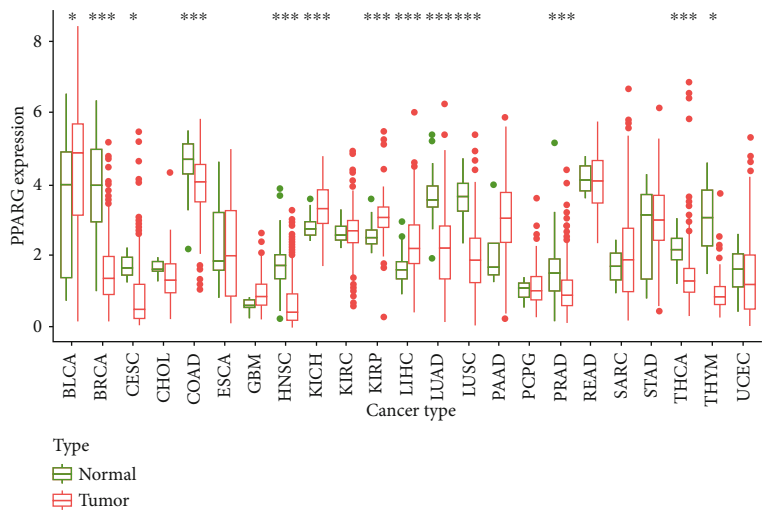

(e)

Figure 2: Continued.

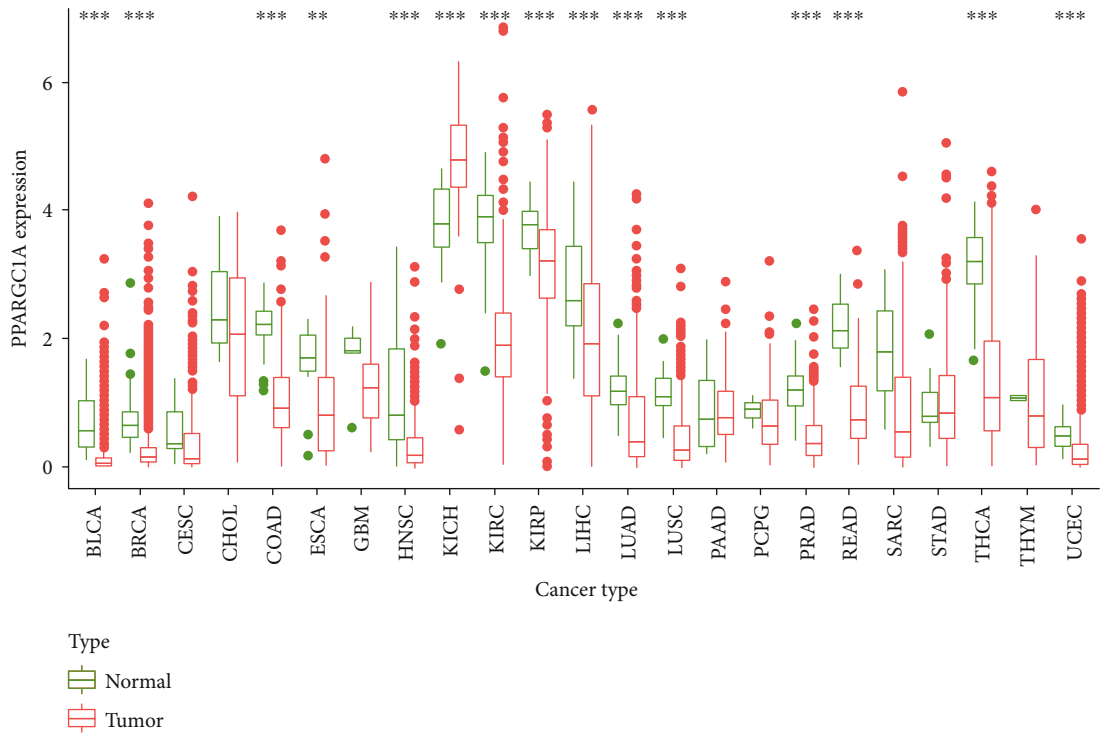

(f)

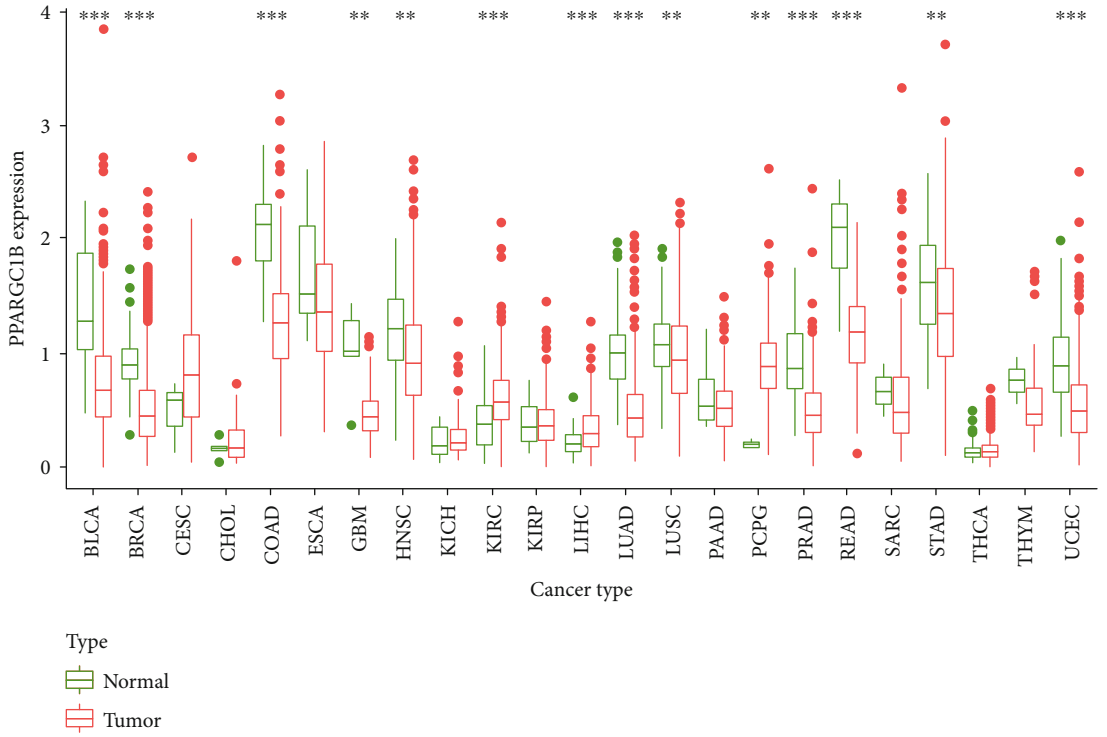

(g)

Figure 2: Continued.

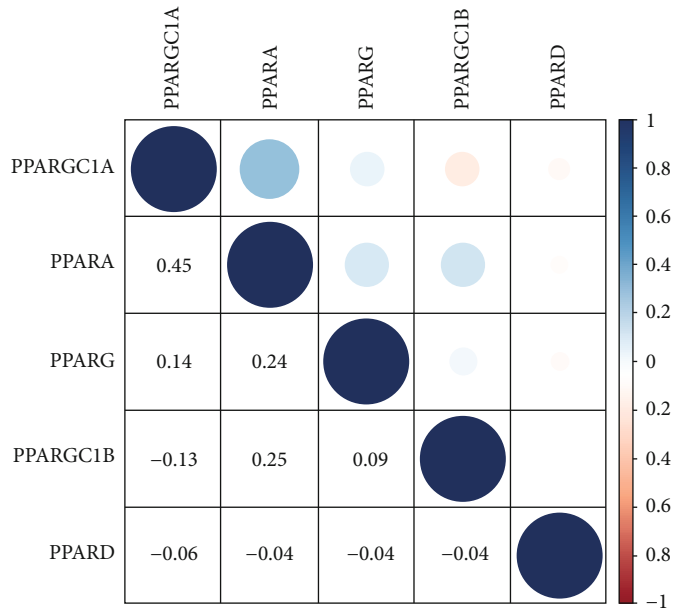

(h)

Figure 2: Differential expression analysis. (a) The box plot showing the transcriptional expression levels of PPARs. (b) The heatmap showing the transcriptional level of PPARs in TCGA tumor types compared to normal tissues; the gradient colors represent the log Fold Change (logFC) value. (c–g) The box plots showing differential expression of PPARs and PPARGC1A and PPARGC1B in normal and tumor tissues ($^{***}p < 0.001$; $^{**}p < 0.01$; $^{*}p < 0.05$); (h) the correlation coefficients by coexpression analysis between every two genes are presented.

To analyze the correlation between PPARs and stemness features of pan-cancer, we calculated the stemness indices of TCGA tumor samples by using a one-class logistic regression (OCLR) algorithm and performed Spearman correlation analysis based on gene expression and stemness scores [12]. Two types of stemness indices were accessed, which included DNA methylation-based stemness index (DNAss) and mRNA expression-based stemness index (RNAss).

There were differences between the two stemness indices on the correlation with the PPAR expression level in TCGA tumors. For DNAss, it is obvious that there were strong correlations between TGCT and PPAR family genes, with positive correlations of PPARD (correlation coefficient = 0.56, $p < 0.001$), PPARG (correlation coefficient = 0.44, $p < 0.001$), and PPARGC1B (correlation coefficient = 0.52, $p < 0.001$) and negative correlations of PPARA (correlation coefficient = −0.59, $p < 0.001$) and PPARGC1A (correlation coefficient = −0.66, $p < 0.001$) (Figure 6(a)).

For RNAss, strong negative correlations were observed between TGCT RNAss and PPARA (correlation coefficient = −0.63, $p < 0.001$), between THYM RNAss and PPARD (correlation coefficient = −0.81, $p < 0.001$), between PCPG RNAss and PPARG (correlation coefficient = −0.53, $p < 0.001$), and between PRAD RNAss and PPARGC1A (correlation coefficient = −0.63, $p < 0.001$) (Figure 6(b)). A positive association between the expression profiles of PPARGC1B and the RNAss of TGCT was detected (correlation coefficient = 0.64, $p < 0.001$), suggesting that PPARGC1B might correlate with the stemness in TGCT.

In BRCA (Figure 7(a)), specifically, the expression profiles of PPARA was positively correlated with BRCA stromal scores (correlation coefficient = 0.14, $p < 0.001$), immune scores (correlation coefficient = 0.21, $p < 0.001$), and ESTIMATE score (correlation coefficient = 0.2, $p < 0.001$). The expression profiles of PPARD were positively correlated with BRCA DNAss (correlation coefficient = 0.19, $p < 0.001$), immune scores (correlation coefficient = 0.27, $p < 0.001$), and ESTIMATE score (correlation coefficient = 0.21, $p < 0.001$). Notably, we found negative correlations between PPARG expression with RNAss (correlation coefficient = −0.45, $p < 0.001$) and DNAss (correlation coefficient = −0.14, $p < 0.001$) while positive correlations with BRCA's stromal score (correlation coefficient = 0.47, $p < 0.001$), immune score (correlation coefficient = 0.34, $p < 0.001$), and ESTIMATE score (correlation coefficient = 0.43, $p < 0.001$). In addition, slight but statistically significant correlations were found between PPARGC1A and stemness indices and tumor purity. There were strong correlations, however, between PPARGC1B and stromal score (correlation coefficient = 0.23, $p < 0.001$), immune score (correlation coefficient = 0.34, $p < 0.001$), and ESTIMATE score (correlation coefficient = 0.32, $p < 0.001$).

For LIHC (Figure 7(b)), however, there were slight correlations between each PPAR family gene and stemness indices and TME except relatively strong associations between PPARA and tumor purity (stromal score: correlation coefficient = −0.17, $p < 0.001$; immune score: correlation coefficient = −0.29, $p < 0.001$; and ESTIMATE score: correlation coefficient = −0.26, $p < 0.001$).

3.5. Drug Sensitivity Analysis in Pan-Cancer. To analyze the potential effects of the PPAR family on drug response, we performed Pearson correlation analysis between the

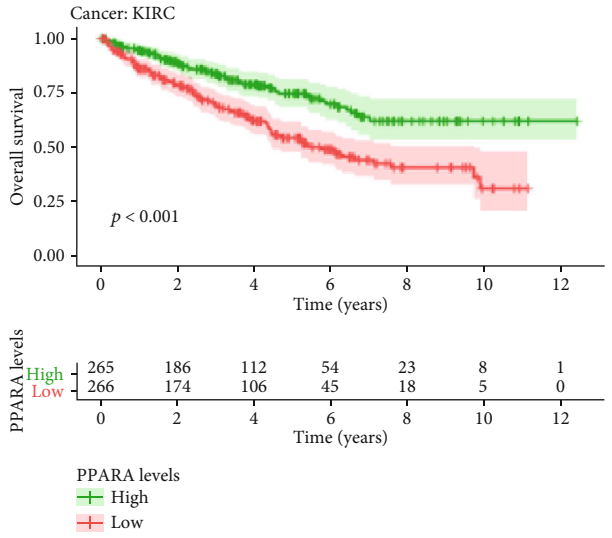

(a)

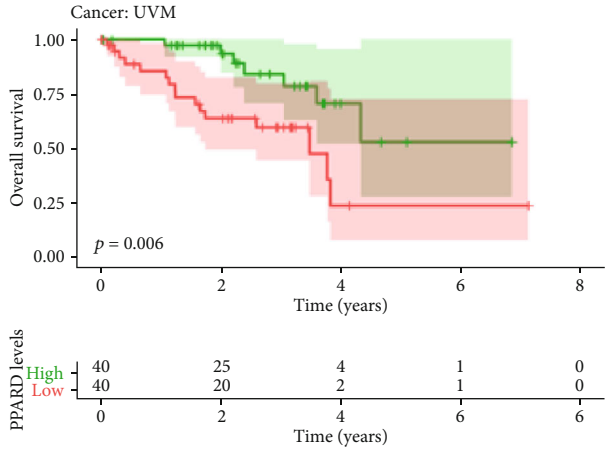

(b)

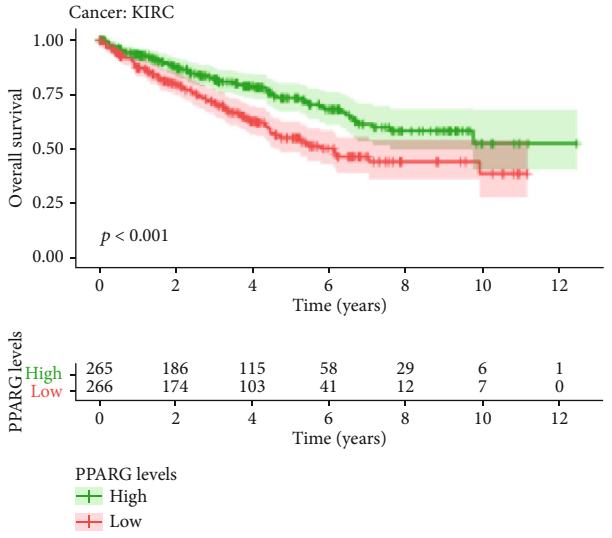

(c)

Figure 3: Continued.

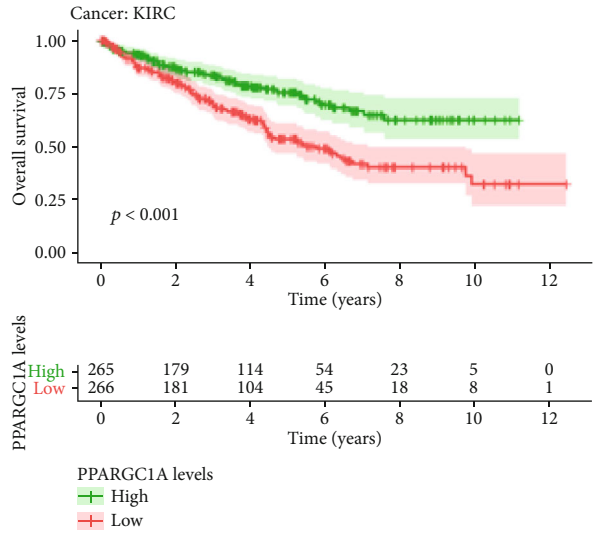

(d)

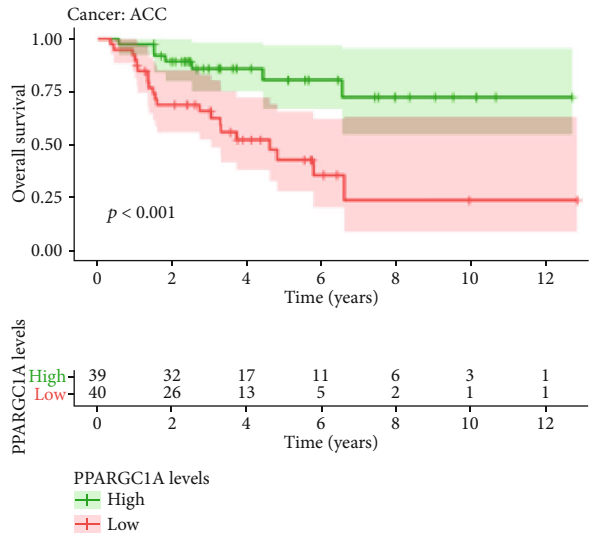

(e)

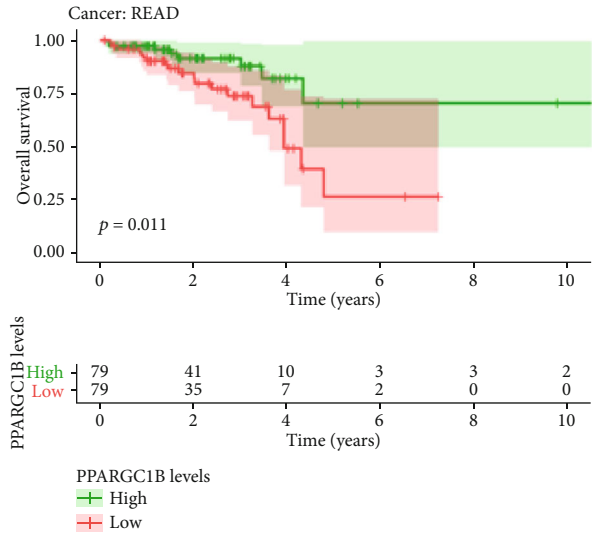

(f)

Figure 3: Continued.

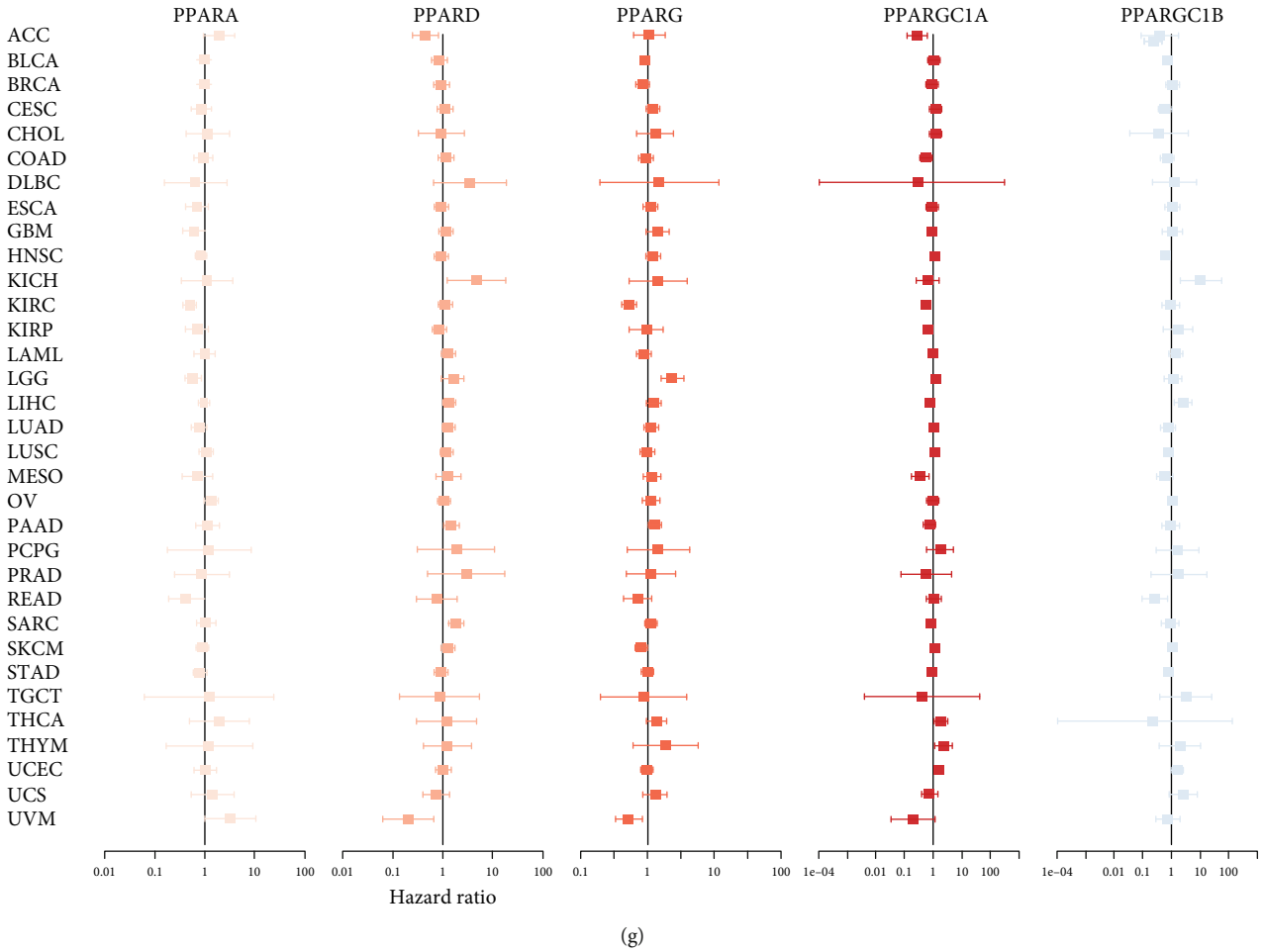

(g)

Figure 3: The results of survival analysis of PPARs in pan-cancer. (a–f) Kaplan-Meier plots of PPARs in pan-cancer showing the differential survival outcomes of high PPAR and low PPAR ($p < 0.05$). (g) Cox proportional hazard analyses illustrating the hazard ratios (HRs) of PPARs in 33 TCGA tumors; those PPARs whose HR > 1 in certain types of cancer were regarded as danger factors of the very type of cancer, which were unfavorable for prognostic outcomes.

transcriptional expression of PPAR family genes in NCI-60 cancer cell lines and drug activity of 263 antineoplastic drugs retrieved from the CellMiner database [16].

The scatter plots that displayed a significant correlation relationship between drug sensitivity and gene expression are presented in Figure 8 and ranked by the p value, selected by $p < 0.05$. Notably, PPARGC1B was positively correlated with the sensitivity of Bafetinib (correlation coefficient = 0.493, $p < 0.001$) and Nilotinib (correlation coefficient = 0.486, $p < 0.001$) and the resistance of staurosporine (correlation coefficient = −0.469, $p < 0.001$). The sensitivity of dabrafenib, a selective inhibitor of mutated forms of BRAF kinase for BRAF-mutated melanoma, thyroid cancer, and non-small-cell lung cancer, was found to be positively associated with PPARGC1A (correlation coefficient = 0.448, $p < 0.001$) and PPARGC1B (correlation coefficient = 0.377, $p = 0.003$). Highly expressed PPARG tumor cells were more resistant to carboplatin (correlation coefficient = −0.422, $p < 0.001$), cisplatin (correlation coefficient = −0.396, $p = 0.002$), arsenic trioxide (correlation coefficient = −0.419, $p < 0.001$), and lomustine (correlation coefficient = −0.410, $p = 0.001$) (Figure 8).

4. Discussion

In the present study, we aimed to explore the correlation of PPAR transcriptional expression with TCGA tumor features, which include TME, clinical significance, immune subtypes, stemness, and drug responses. PPAR isotypes showed distinct effects on tumor development. Using multidimensional analysis, we first performed differential expression analysis on a total of 11,057 samples (10,327 tumor samples and 730 adjacent samples) across 33 TCGA cancer types and found significant difference on the PPARs' expression level in different tumor types. We also applied survival analysis and Cox proportional hazard regression. Statistically significant survival differences were observed between high and low PPAR-expressed patients in some types of cancers, suggesting that PPARs might become potential prognostic indicators for clinical applications.

It is also worth noting that PPARG along with PPARGC1A was found to be differentially expressed in the 4 stages of stomach adenocarcinoma, with highest PPARG in stage IV, which is consistent with the findings of Nagy et al. that PPARG may contribute to STAD carcinogenesis [17]. In

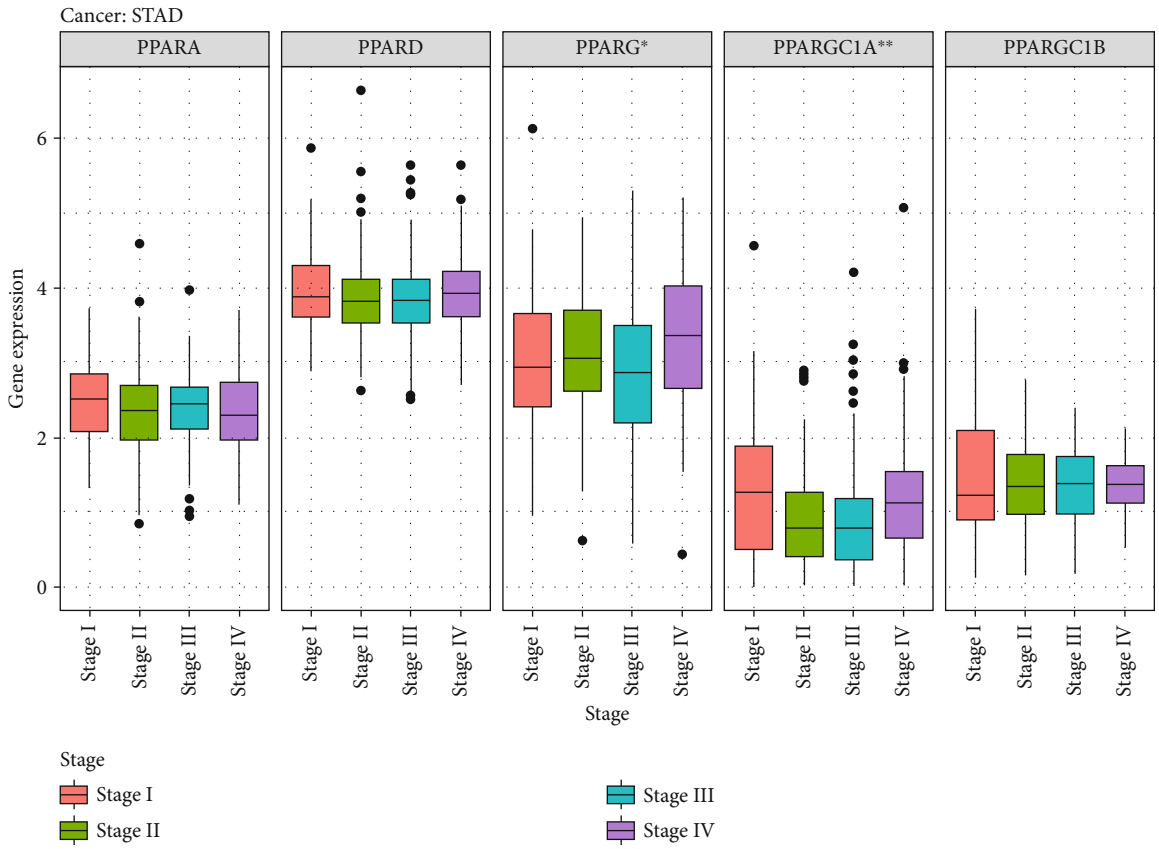

Figure 4: Differential gene expression level of PPARs in different tumor stages in STAD (PPARG: $p < 0.05$; PPARGC1A: $p < 0.01$).

this study, however, PPARG was found to have low expression in the majority of TCGA cancers. Evidence backed for PPARG's antineoplastic actions in inducing cell cycle arrest, terminal differentiation, and anti-inflammatory effect [18]. Troglitazone (TGZ), a PPARG agonist, was reported to induce G2/M cell cycle arrest through activation of p38 mitogen-activated protein kinase in renal cell carcinoma [18, 19], and similar effects were also seen in bladder cancer cells [20]. Another agonist of PPARG, curcumin, was able to eliminate oxidative stress and chronic inflammation via downregulating the WNT/β-catenin pathway, which is observed to have aberrant activation in many cancers [21]. Sporadically, the tumor-promoting side of PPARG was observed in some cancers; it is easy to infer that the precise effects of PPARG and its agonists might depend on types of cancers and tumor environment.

Moreover, according to the C1-C6 immune subtypes previously identified by investigators [10], we classified tumor samples by representative immune signatures and examined the RNA-seq level of PPARA, PPARD, PPARG, PPARGC1A, and PPARGC1B from C1 to C6, which were all seen to have differential expressions. These immune features along with extracellular matrix, tumor vasculature, and tumor cells make up the concept of the tumor microenvironment (TME), the heterogeneity of which highly influences therapeutic response and clinical prognosis [22]. Thus, we further accessed the fractions of stromal cells and immune cells in tumor samples of 33 TCGA cancer types by calculating stromal scores, immune scores, and ESTIMATE scores. Those TME characteristics were correlated with the expression level of PPARA, PPARD, PPARG, PPARGC1A, and PPARGC1B. Unexpectedly, correlations did exist in some types of cancers. In breast invasive carcinoma, particularly, PPARG and PPARGC1B were negatively correlated with tumor purity.

Stemness has been proposed to describe the stem cell-like characteristics of the tumor: self-renewal and dedifferentiation [23]. The acquisition of stem cell-like properties has been reported to be found in many tumor progression [24]. Here, we utilized an OCLR approach to calculate the RNAss score and DNAss score of tumor samples and then correlated it with transcriptional signatures of PPARs. We found an association between PPARs and stemness within tumors, suggesting that PPARs may play a role in stemness maintenance.

This study also found that the transcriptional expression level of PPARs, PPARG1A, and PPARG1B was associated with drug responses. Notably, high expression of PPAGC1B was even more sensitive to Bafetinib and Nilotinib across cancer treatments, which is of clinical significance for selection of antitumor therapies.

The three isotypes of peroxisome proliferator-activated receptors differ in both physiological functions and roles in carcinogenesis. PPARα, encoded by PPARA, mainly enriches in the liver, kidney, and heart, regulating fatty acid metabolism and mitochondrial biosynthesis [25]. In addition to its endogenous ligands (fatty acids), PPARα responds to the PPARα agonists (synthetic fibrates), such

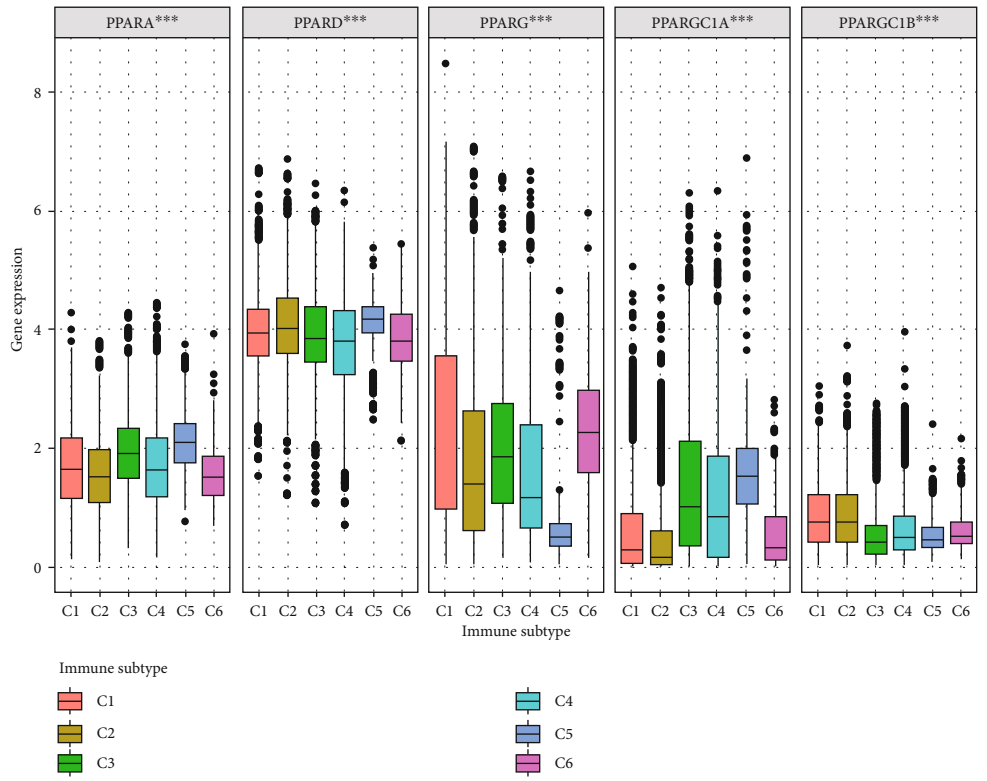

(a)

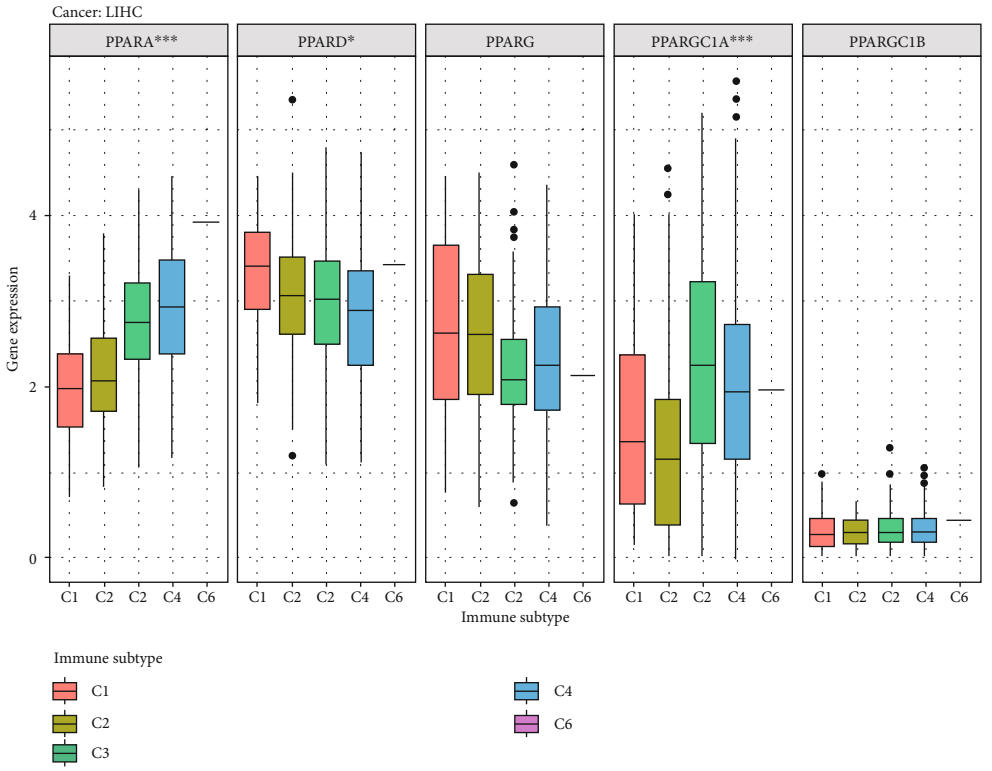

(b)

Figure 5: Continued.

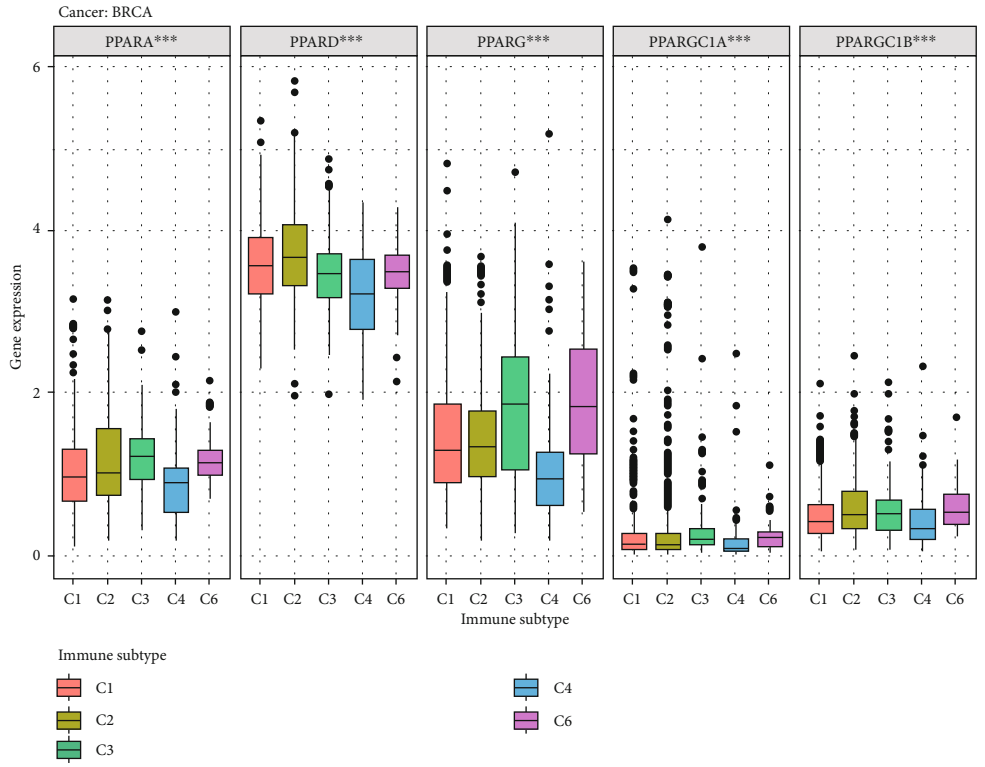

(c)

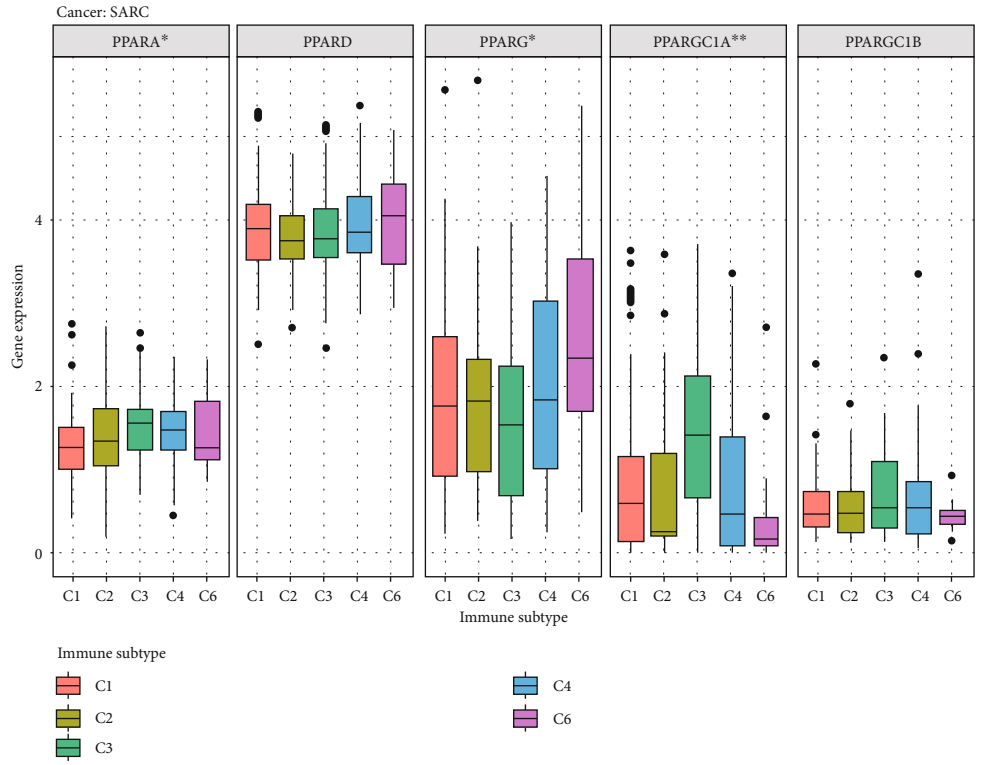

(d)

Figure 5: The results of correlation analysis between members of PPAR and immune subtypes. (a) The transcriptional expression of PPARs in C1-C6 immune subtypes across TCGA cancers. (b–d) Box plots showing the expression level of PPAR immune subtypes in LIHC, BRCA, and SARC, respectively ($^{***}p < 0.001$; $^{**}p < 0.01$; $^{*}p < 0.05$). LIHC: liver hepatocellular carcinoma; BRCA: breast invasive carcinoma; SARC: Sarcoma.

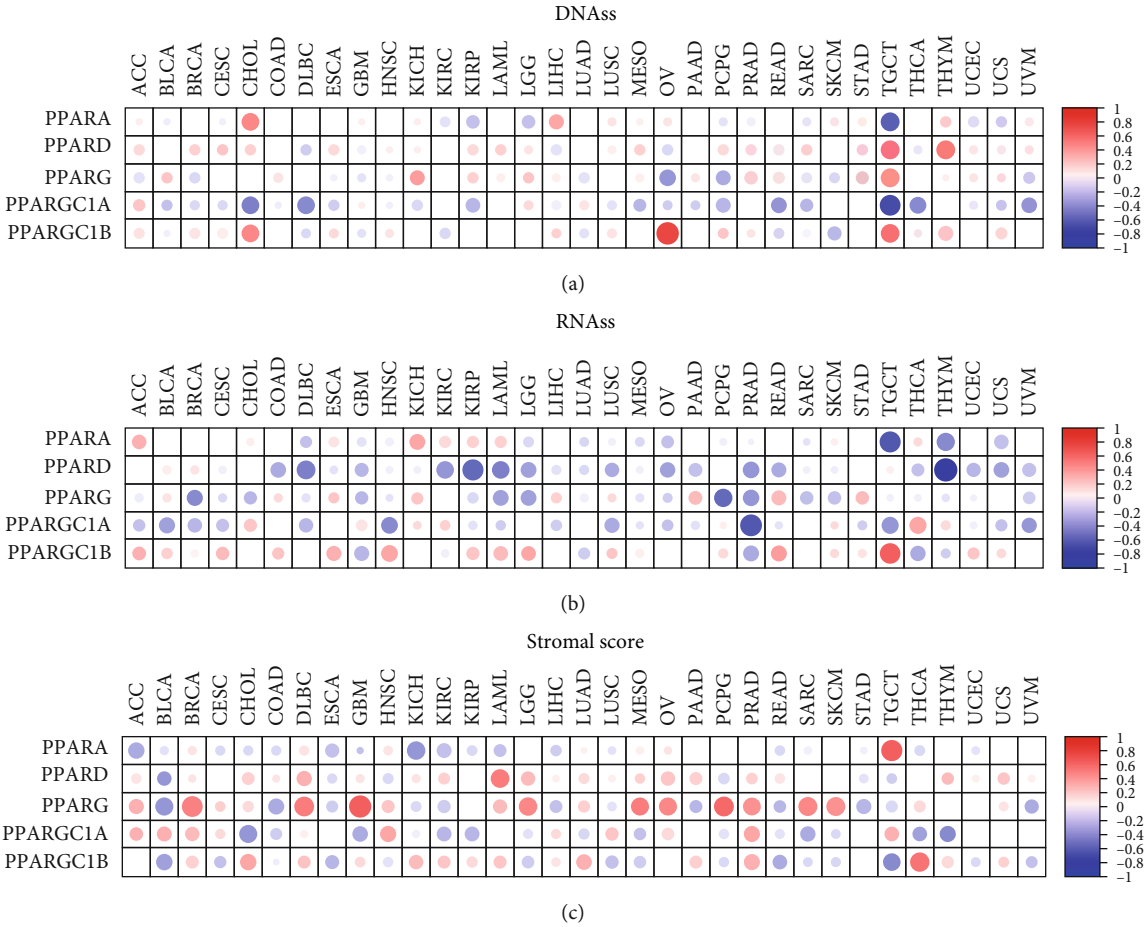

Figure 6: The results of correlation analysis between members of PPAR and stemness indices and microenvironment scores. (a, b) The two heatmaps showing the correlation of the expression level of PPARA, PPARD, PPARG, PPARGC1A, and PPARGC1B and stemness indices (DNAss and RNAss) in 33 TCGA cancer types. DNAss: DNA methylation-based stemness score; RNAss: RNA-based stemness score. (c) The heatmap showing the correlation between stromal scores and the mRNA expression of PPARs (red points represent a positive correlation while blue points represent a negative correlation).

as fenofibrate and gemfibrozil, which have been working well in the treatment for hypolipidemic diseases [26]. Moreover, PPARα agonists have been reported to show antitumor effects in colon carcinogenesis. However, it is still controversial whether the roles of PPARα is cancer-repressing or cancer-promoting [25]. Some studies suggested that long-term activation of PPARα induced hepatocellular carcinoma in mice and was essential for the development of hepatic steatosis [27]. The roles of PPARα in carcinogenesis require further elucidation. PPARG, encoding PPARγ, functions as a key regulator of glucose homeostasis and adipocyte differentiation [28]. Downregulation of PPARγ is associated with decreased terminal differentiation and cell cycle arrest, which induces cell proliferation and leads to tumorigenesis [7, 29]. The potential mechanism was proposed by Drori et al. that the PPARγ-induced differentiation may be mediated by a putative PPARγ coactivator, HIC5, suggesting the importance of coactivators in PPARγ signaling [30]. Peroxisome proliferator-activated receptor coactivators 1 alpha and beta (PPAGC1A and PPARGC1B, respectively) cooperate with PPARPγ, allowing the subsequent interaction between PPARγ and other transcription factors [31, 32]. Pharmacological activators of PPARδ also show controversial effects on the hallmarks of caner, which may depend on the type of PPARδ ligands and target tissues [33, 34].

Although this study is the first one to multidimensionally analyze peroxisome proliferator-activated receptors (PPARs) in pan-cancer, it still possessed some limitations that warrant consideration. Firstly, all the samples involved in this study were from America, and thus, we were not quite sure about the applicability of the prediction model in Europe and Asia. Second, the results of this study have not been verified by other independent databases, and thus, our future work is validating it by our own data and other public database. Third, the potential mechanism in this study is based on bioinformatics analysis and has not been verified by molecular and animal experiments. The analysis of this study focuses on the correlation between the PPAR family and multiple omics data. However, the biostatistical correlation could not elucidate the direct interaction and direct regulation mechanism, which should be the main limitation of this study. Thus, we plan to verify these potential mechanisms via molecular experiments. Further investigations are

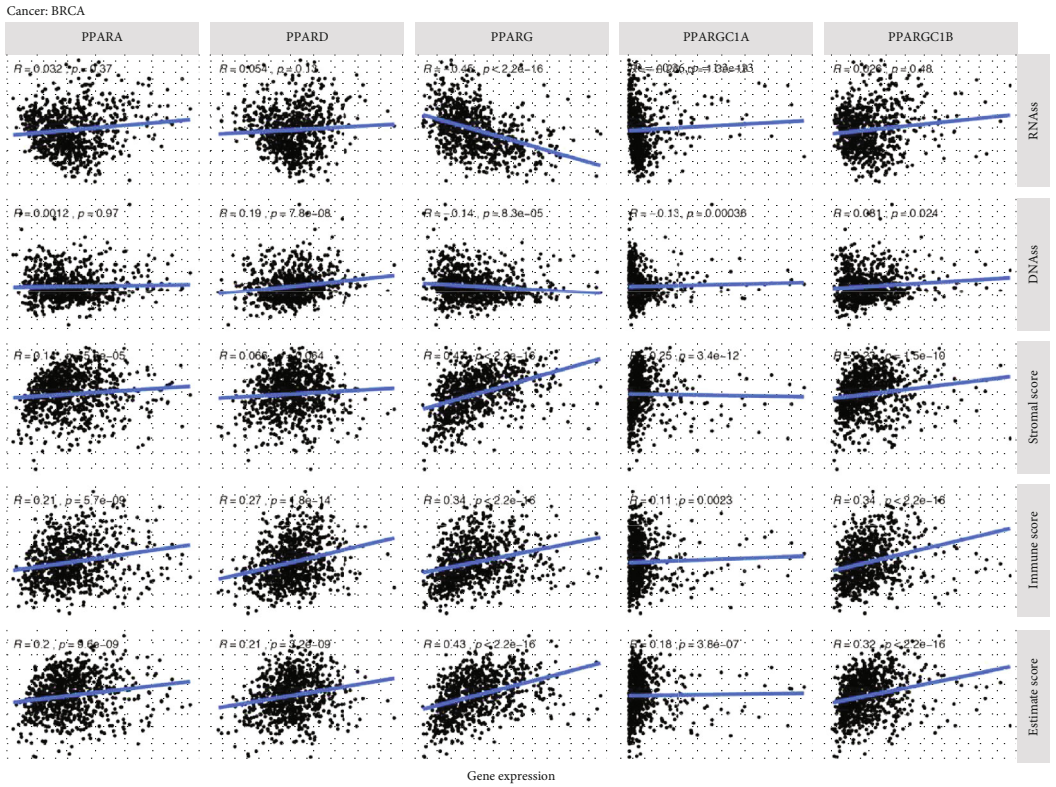

(a)

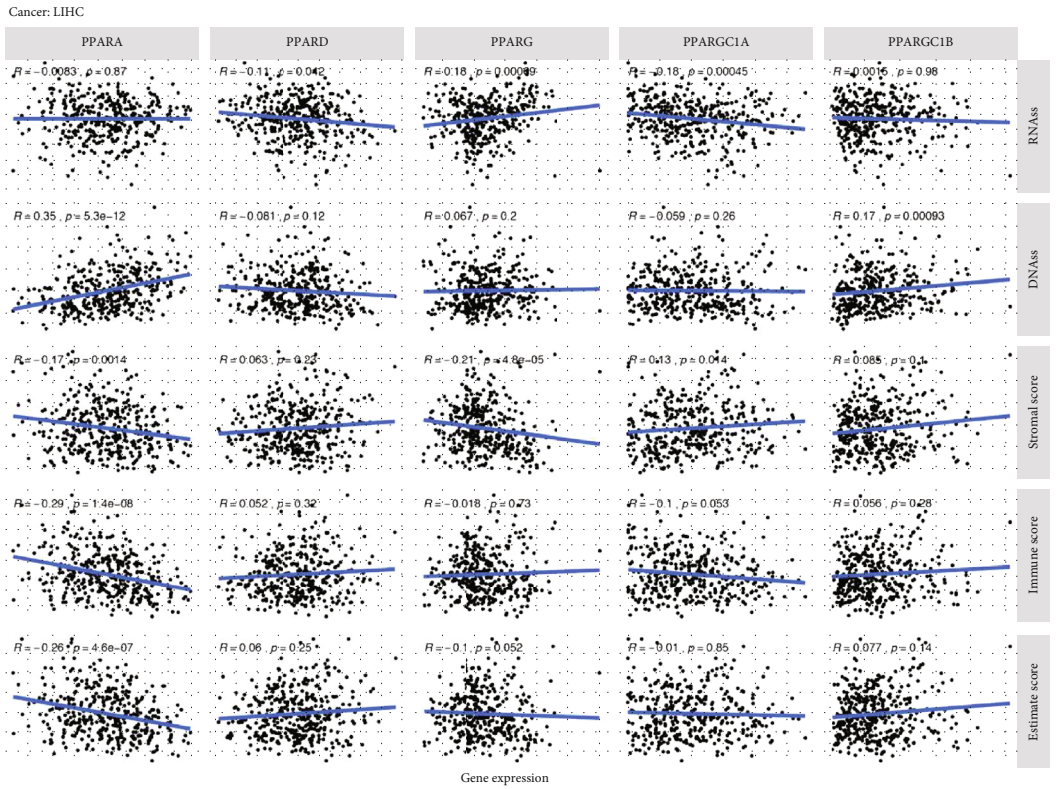

(b)

Figure 7: The correlation between PPARs and their coactivators and stemness scores (RNAss and DNAss), stromal scores, immune scores, and ESTIMATE scores in breast invasive carcinoma (BRCA) and liver hepatocellular carcinoma (LIHC).

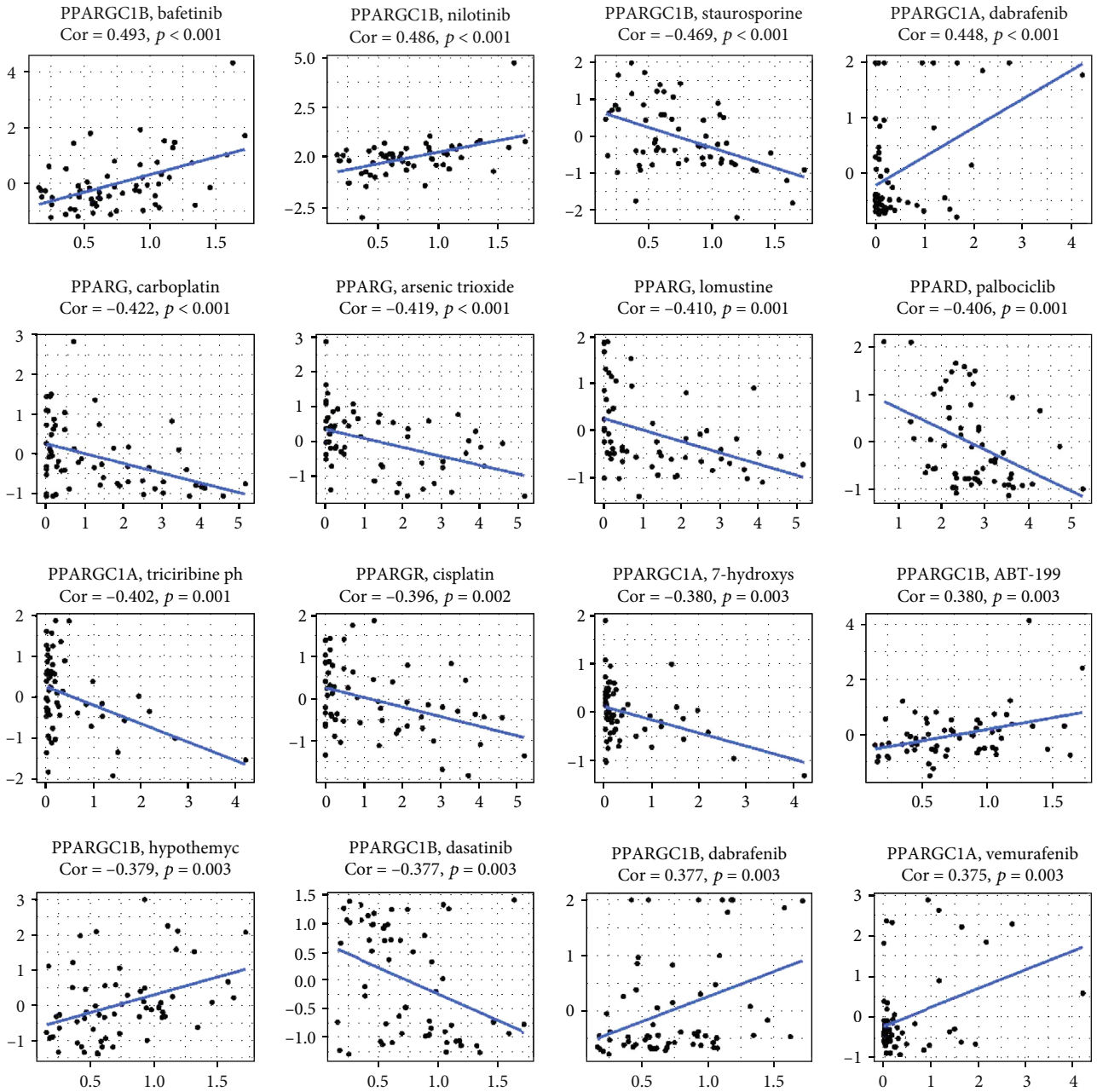

Figure 8: Drug response analysis. The correlation between drug sensitivity and PPARA, PPARD, PPARG, PPARGC1A, and PPARGC1B across TCGA cancers. The scatter plots are ranked by p value.

required to figure out the potentials of PPARs and their coactivators as drug targets for cancer, which makes our study even more important in the contribution to the expression signature analysis of PPARA, PPARD, PPARG, PPARGC1A, and PPARGC1B.

5. Conclusion

We performed multidimensional analyses on PPARA, PPARG, PPARD, PPARGC1A, and PPARGC1B, including differential expression analysis in pan-cancer, immune subtype analysis, clinical analysis, tumor purity analysis, stemness correlation analysis, and drug responses. PPARs and their coactivators expressed differently in different types of cancers, in different immune subtypes. This analysis reveals various expression patterns of the PPAR family at a level of pan-cancer and provides new clues for the therapeutic strategies of cancer.

Data Availability

The datasets generated and/or analyzed during the current study are available in Supplementary Materials and TCGA program (https://portal.gdc.cancer.gov).

Ethical Approval

The study was approved by the Ethics Committee of the First Affiliated Hospital of Zhengzhou University.

Disclosure

The funders had no role in study design, data collection and analysis, decision to publish, or preparation of the manuscript.

Conflicts of Interest

The authors declare that there is no conflict of interests.

Authors' Contributions

Runzhi Huang, Jiaqi Zhang, Peng Hu, Penghui Yan, Huabin Yin, Suna Zhai, Xiaolong Zhu, Jiaxin Zhang, Mingxiao Li, Ling Huang, Man Li, Zehui Sun, Tong Meng, Daoke Yang, and Zongqiang Huang worked on conception/design, collection and/or assembly of data, data analysis and interpretation, manuscript writing, and final approval of manuscript.

Acknowledgments

We thank The Cancer Genome Atlas (TCGA) team for the use of their data. This study was supported in part by the National Natural Science Foundation of China (Grant Nos. 81702659 and 81772856); National Natural Science Foundation of China, joint fund cultivation project (Grant No. U1504822); Youth Fund of Shanghai Municipal Health Planning Commission (No.2017YQ054); Henan Medical Science and Technology research project (No. 201602031); Henan Medical Science and technology research plan, joint project of the Ministry and the province (No. SB201901037); and Henan Provincial Department of science and technology, social development project (No. 142102310055).

Supplementary Materials

Figure S1: PPAR protein expression in cancer (breast cancer, colon adenocarcinoma, and prostate cancer) and normal tissues from the Human Protein Atlas database. Figure S2: the protein-protein interaction (PPI) network constructed among PPARA, PPARD, PPARG, PPARGC1A, PPARGC1B, and their top related genes. *(Supplementary Materials)*

References

[1] V. Dubois, J. Eeckhoute, P. Lefebvre, and B. Staels, "Distinct but complementary contributions of PPAR isotypes to energy homeostasis," *The Journal of Clinical Investigation*, vol. 127, no. 4, pp. 1202–1214, 2017.

[2] J. Youssef and M. Badr, "Peroxisome proliferator-activated receptors and cancer: challenges and opportunities," *British Journal of Pharmacology*, vol. 164, no. 1, pp. 68–82, 2011.

[3] J. D. Brown and J. Plutzky, "Peroxisome proliferator-activated receptors as transcriptional nodal points and therapeutic targets," *Circulation*, vol. 115, no. 4, pp. 518–533, 2007.

[4] C. Pirat, A. Farce, N. Lebègue et al., "Targeting peroxisome proliferator-activated receptors (PPARs): development of modulators," *Journal of Medicinal Chemistry*, vol. 55, no. 9, pp. 4027–4061, 2012.

[5] E. Sahin, S. Colla, M. Liesa et al., "Telomere dysfunction induces metabolic and mitochondrial compromise," *Nature*, vol. 470, no. 7334, pp. 359–365, 2011.

[6] B. Gross, M. Pawlak, P. Lefebvre, and B. Staels, "PPARs in obesity-induced T2DM, dyslipidaemia and NAFLD," *Nature Reviews Endocrinology*, vol. 13, no. 1, pp. 36–49, 2017.

[7] J. M. Peters, Y. M. Shah, and F. J. Gonzalez, "The role of peroxisome proliferator-activated receptors in carcinogenesis and chemoprevention," *Nature Reviews Cancer*, vol. 12, no. 3, pp. 181–195, 2012.

[8] A. Z. Mirza, I. I. Althagafi, and H. Shamshad, "Role of PPAR receptor in different diseases and their ligands: physiological importance and clinical implications," *European Journal of Medicinal Chemistry*, vol. 166, pp. 502–513, 2019.

[9] D. Szklarczyk, A. L. Gable, D. Lyon et al., "STRING v11: protein-protein association networks with increased coverage, supporting functional discovery in genome-wide experimental datasets," *Nucleic Acids Research*, vol. 47, no. D1, pp. D607–D613, 2019.

[10] V. Thorsson, D. L. Gibbs, S. D. Brown et al., "The immune landscape of cancer," *Immunity*, vol. 48, no. 4, pp. 812–830.e14, 2018, e14.

[11] K. Yoshihara, M. Shahmoradgoli, E. Martínez et al., "Inferring tumour purity and stromal and immune cell admixture from expression data," *Nature Communications*, vol. 4, no. 1, 2013.

[12] T. M. Malta, A. Sokolov, A. J. Gentles et al., "Machine learning identifies stemness features associated with oncogenic dedifferentiation," *Cell*, vol. 173, no. 2, pp. 338–354.e15, 2018, e15.

[13] W. C. Reinhold, M. Sunshine, H. Liu et al., "CellMiner: a web-based suite of genomic and pharmacologic tools to explore transcript and drug patterns in the NCI-60 cell line set," *Cancer Research*, vol. 72, no. 14, pp. 3499–3511, 2012.

[14] U. T. Shankavaram, S. Varma, D. Kane et al., "CellMiner: a relational database and query tool for the NCI-60 cancer cell lines," *BMC Genomics*, vol. 10, no. 1, p. 277, 2009.

[15] X. Dong, D. Huang, X. Yi et al., "Diversity spectrum analysis identifies mutation-specific effects of cancer driver genes," *Communications Biology*, vol. 3, no. 1, p. 6, 2020.

[16] A. Puszkiel, G. Noé, A. Bellesoeur et al., "Clinical pharmacokinetics and pharmacodynamics of dabrafenib," *Clinical Pharmacokinetics*, vol. 58, no. 4, pp. 451–467, 2019.

[17] T. A. Nagy, L. E. Wroblewski, D. Wang et al., "β-Catenin and p120 mediate PPARδ-dependent proliferation induced by _Helicobacter pylori_ in human and rodent epithelia," *Gastroenterology*, vol. 141, no. 2, pp. 553–564, 2011.

[18] B. Bandera Merchan, F. J. Tinahones, and M. Macias-Gonzalez, "Commonalities in the association between PPARG and vitamin D related with obesity and carcinogenesis," *PPAR Research*, vol. 2016, Article ID 2308249, 15 pages, 2016.

[19] M. Fujita, T. Yagami, M. Fujio et al., "Cytotoxicity of troglitazone through PPARγ-independent pathway and p38 MAPK pathway in renal cell carcinoma," *Cancer Letters*, vol. 312, no. 2, pp. 219–227, 2011.

[20] M. L. Plissonnier, S. Fauconnet, H. Bittard, and I. Lascombe, "Insights on distinct pathways of thiazolidinediones (PPARγ ligand)-promoted apoptosis in TRAIL-sensitive or -resistant

malignant urothelial cells," *International Journal of Cancer*, vol. 127, no. 8, pp. 1769–1784, 2010.

[21] A. Vallee, Y. Lecarpentier, and J. N. Vallee, "Curcumin: a therapeutic strategy in cancers by inhibiting the canonical WNT/β-catenin pathway," *Journal of Experimental & Clinical Cancer Research*, vol. 38, no. 1, p. 323, 2019.

[22] M. R. Junttila and F. J. de Sauvage, "Influence of tumour micro-environment heterogeneity on therapeutic response," *Nature*, vol. 501, no. 7467, pp. 346–354, 2013.

[23] D. Friedmann-Morvinski and I. M. Verma, "Dedifferentiation and reprogramming: origins of cancer stem cells," *EMBO Reports*, vol. 15, no. 3, pp. 244–253, 2014.

[24] A. Miranda, P. T. Hamilton, A. W. Zhang et al., "Cancer stemness, intratumoral heterogeneity, and immune response across cancers," *Proceedings of the National Academy of Sciences of the United States of America*, vol. 116, no. 18, pp. 9020–9029, 2019.

[25] Y. Luo, C. Xie, C. N. Brocker et al., "Intestinal PPARα protects against colon carcinogenesis via regulation of methyltransferases DNMT1 and PRMT6," *Gastroenterology*, vol. 157, no. 3, pp. 744–759.e4, 2019, e4.

[26] I. Takada and M. Makishima, "Peroxisome proliferator-activated receptor agonists and antagonists: a patent review (2014-present)," *Expert Opinion on Therapeutic Patents*, vol. 30, no. 1, pp. 1–13, 2020.

[27] N. Tanaka, K. Moriya, K. Kiyosawa, K. Koike, F. J. Gonzalez, and T. Aoyama, "PPARalpha activation is essential for HCV core protein-induced hepatic steatosis and hepatocellular carcinoma in mice," *The Journal of Clinical Investigation*, vol. 118, no. 2, pp. 683–694, 2008.

[28] G. T. Robbins and D. Nie, "PPAR gamma, bioactive lipids, and cancer progression," *Frontiers in Bioscience*, vol. 17, no. 1, pp. 1816–1834, 2012.

[29] H. R. Dhaini and Z. Daher, "Genetic polymorphisms of PPAR genes and human cancers: evidence for gene-environment interactions," *Journal of Environmental Science and Health. Part C, Environmental Carcinogenesis & Ecotoxicology Reviews*, vol. 37, no. 3, pp. 146–179, 2019.

[30] S. Drori, "Hic-5 regulates an epithelial program mediated by PPAR," *Genes & Development*, vol. 19, no. 3, pp. 362–375, 2005.

[31] M. Wirtenberger, S. Tchatchou, K. Hemminki et al., "Associations of genetic variants in the estrogen receptor coactivators PPARGC1A, PPARGC1B and EP300 with familial breast cancer," *Carcinogenesis*, vol. 27, no. 11, pp. 2201–2208, 2006.

[32] M. Petr, P. Stastny, A. Zajac, J. Tufano, and A. Maciejewska-Skrendo, "The role of peroxisome proliferator-activated receptors and their transcriptional coactivators gene variations in human trainability: a systematic review," *International Journal of Molecular Sciences*, vol. 19, no. 5, p. 1472, 2018.

[33] K. D. Wagner and N. Wagner, "Peroxisome proliferator-activated receptor beta/delta (PPARβ/δ) acts as regulator of metabolism linked to multiple cellular functions," *Pharmacology & Therapeutics*, vol. 125, no. 3, pp. 423–435, 2010.

[34] N. Wagner and K. D. Wagner, "PPAR beta/delta and the hallmarks of cancer," *Cell*, vol. 9, no. 5, p. 1133, 2020.